Molecular mechanisms controlling μ-opioid receptor activation

Arisbel Batista Gondin

BSc (Hons)

A thesis submitted to Monash University
and the University of Nottingham
for the degree of Doctor of Philosophy

Oct 2018



MONASH University



The University of Nottingham

UNITED KINGDOM · CHINA · MALAYSIA

Copyright Notice

© Arisbel Batista Gondin (2018). Except as provided in the Copyright Act 1968, this thesis may not be reproduced in any form without the written permission of the author.

I certify that I have made all reasonable efforts to secure copyright permissions for third-party content included in this thesis and have not knowingly added copyright content to my work without the owner's permission.

Table of Contents

Abstract ..... **v**

Publications and conference attendance ..... **vii**

Declaration ..... **viii**

Acknowledgements ..... **x**

Abbreviations ..... **xi**

Chapter 1. Introduction **1**

1.1 G protein-coupled receptors **2**

1.1.1 Classification 2

1.1.2 Structural characteristics 3

1.1.3 G protein signalling 7

1.1.4 GPCR regulation 8

1.1.5 G protein-independent signalling 10

1.1.6 Biased agonism 11

1.1.7 Compartmentalised signalling 14

1.2 The opioid system **17**

1.2.1 Opioid-induced analgesia 17

1.2.2 Opioid receptors 19

1.2.3 Opioid ligands 21

1.2.4 Patho-physiology 23

1.3 The μ-opioid receptor **25**

1.3.1 Structures 25

1.3.2 Agonist-induced MOP regulation 28

1.3.3 Agonist-induced MOP signalling 29

1.3.4 Biased agonism at the MOP 31

1.4 Scope of thesis **35**

Chapter 2. Novel BRET biosensors reveal differences in efficacy of various classes of MOP agonists 36

2.1 Abstract 37

2.2 Introduction 38

2.3 Methods 42

2.3.1 Materials 42

2.3.2 Plasmids 42

2.3.3 Cell culture and transfections 42

2.3.4 Enzyme-Linked Immunosorbent Assay (ELISA) 43

2.3.5 Bioluminescence Resonance Energy Transfer (BRET) 43

2.3.6 Data Analysis 44

2.3.7 Statistics 46

2.4 Results 47

2.4.1 Use of Nb33 and mGsi as biosensors to probe MOP activation and G protein coupling 47

2.4.2 Use of Nb33 and mGsi to investigate proximal events to receptor activation in the detection of biased agonism at the MOP 51

2.4.3 MOP-mediated activation of G protein- and β-arrestin2- dependent pathways 55

2.4.4 Calculations of bias factors and MOP agonist relative efficacy 65

2.5 Discussion 74

Chapter 3. GRK mediates MOP plasma membrane reorganisation in an agonist-specific manner 78

3.1 Abstract 79

3.2 Introduction 80

3.3 Methods 83

3.3.1 Materials 83

3.3.2 Plasmids 83

3.3.3 Cell lines generation 84

3.3.4 Cell plating and treatments 84

3.3.5 Fluorescence Correlation Spectroscopy (FCS) 84
3.3.6 Fluorescence Recovery After Photobleaching (FRAP) 86
3.3.7 Anti-pS375 immunocytochemistry 87
3.3.8 Bioluminescence Resonance Energy Transfer (BRET) 87
3.3.9 Statistics 88
3.4 Results 89
3.4.1 Basal plasma membrane organisation of SNAP-MOP detected by FCS and FRAP 89
3.4.2 Ligand-induced changes in the plasma membrane organisation of SNAP-MOP 93
3.4.3 MOP membrane reorganisation is independent of $G_{i/o}$ protein activation 97
3.4.4 Effect of internalisation inhibition on ligand-induced changes in MOP organisation 98
3.4.5 Effect of GRK inhibition on ligand-induced changes in MOP organisation 99
3.4.6 Plasma membrane organisation of phosphorylation-deficient MOP mutants 102
3.5 Discussion 104

Chapter 4. Multisite phosphorylation is required for sustained interaction with GRKs and arrestins during rapid MOP desensitisation 109

Chapter 5. Molecular mechanisms of β-arrestin2 interaction with the MOP 134

5.1 Abstract 135
5.2 Introduction 136
5.3 Methods 139
5.3.1 Materials 139
5.3.2 Plasmids 139
5.3.3 Cell lines 139
5.3.4 Cell culture and transfections 140
5.3.5 Bioluminescence Resonance Energy Transfer (BRET) 140

5.3.6 Data analysis 140

5.4 Results.....141

5.4.1 Agonist-induced Nb33, mGsi and β-arrestin2 recruitment to phosphorylation-deficient MOP mutants 141

5.4.2 Agonist-dependent β-arrestin2 recruitment is partially PTx-sensitive 144

5.4.3 Agonist-induced β-arrestin2 recruitment to MOP in the absence of G proteins 146

5.4.4 Agonist-independent β-arrestin2 recruitment to the plasma membrane 148

5.5 Discussion 150

Chapter 6. General Discussion..... 153

Chapter 7. References..... 165

Appendix 1. Plasma membrane localisation of the μ-opioid receptor controls spatiotemporal signalling..... 189

Appendix 2. Fluorescently Labelled Morphine Derivatives for Bioimaging Studies..... 211

Appendix 3. Table of DNA constructs. 227

Abstract

The μ-opioid receptor (MOP) is a G protein-coupled receptor (GPCR) responsible for mediating the analgesic effects of opioids such as morphine. Despite the numerous adverse effects associated with opioids, the MOP is the main therapeutic target for the treatment of severe and chronic pain. Due to the current 'opioid epidemic crisis' within western societies, extensive research and drug discovery efforts are aiming at the generation of new opioid drugs with improved therapeutic windows. In this context, bias agonism towards the G protein pathway and away from the β-arrestin2 pathway is currently being exploited for the development of safer and more effective MOP-targeted analgesics.

In chapter 2, we characterised a range of opioid ligands, including the most recent G protein-biased MOP agonists (TRV130, PZM21 and SR-17018) using Bioluminescence Resonance Energy Transfer (BRET) tools. In this study, a Venus-tagged nanobody (Nb33-Venus) was developed as a BRET biosensor to quantitatively measure MOP activation. Similarly, we also assessed the recruitment of a modified mini G protein (Venus-mGsi) to measure coupling to G protein. Additionally, we measured different assay endpoints representative of G protein or β-arrestin2 pathways. We found no significant bias for any of the so-called G protein biased agonists. Instead, we found that these ligands displayed lower efficacy than other MOP agonists in pathways proximal to receptor activation. Moreover, we found a strong correlation of efficacies between the G protein- and β-arrestin2- dependent pathways. Thus, we propose that the efficacy of the new generation opioid drugs, widely recognised to be biased ligands, is in fact due to weak partial agonist activity and additional pharmacological properties must be taken into consideration. This is critical information, as some of these new drugs are currently being approved by the FDA.

The work presented in appendix 1 demonstrated that differences in spatiotemporal signalling caused by MOP agonists was due to the redistribution of the MOP at the plasma membrane. Thus, in chapter 3 we extended these observations by studying the dynamics and reorganisation of the MOP at the plasma membrane after agonist stimulation using advanced imaging techniques such as Fluorescence Correlation Spectroscopy (FCS) and Fluorescence Recovery After Photobleaching (FRAP). Our data revealed that DAMGO, a stable analogue of

an endogenous opioid peptide, caused very distinct plasma membrane reorganisation of the MOP compared to the prototypical analgesic, morphine. Interestingly, this study also revealed a novel regulatory role of G protein-coupled receptor kinases (GRKs) in mediating plasma membrane reorganisation of the MOP in an agonist-specific manner and independently of G protein activation and internalisation, providing insights into another molecular event differentially regulated by distinct opioids.

GRKs and β-arrestins are key GPCR regulators in promoting receptor desensitisation and internalisation. Extensive research has shown that different opioid agonists mediate distinct regulatory processes through differential phosphorylation of serine and threonine (S/T) residues. In chapter 4 and 5, we studied the role of specific S/T sites located in the C-terminal tail (Ct) or in the intracellular loops (ICLs) of the MOP. We described that multisite phosphorylation of the ^{375}STANT^{379} motif within the Ct controls the dynamics of GRK and β-arrestin interactions with the MOP and contributes to receptor desensitisation. Our results suggest that other residues outside this motif also participate in the initial and transient recruitment of GRKs and β-arrestins. We described that S/T residues within the ICLs also contribute to G protein coupling and β-arrestin2 recruitment. Moreover, we showed that β-arrestin2 recruitment is partially dependent on G protein activation and that β-arrestin2 can also be translocated to the plasma membrane in an agonist-independent manner by PKC activation. Together, this reveals multiple mechanisms of β-arrestin2 interaction with the MOP. Elucidating these complex receptor-effector interactions represents an essential step toward a mechanistic understanding of MOP function so that effective strategies can be applied for the development of improved opioid drugs.

Publications during enrolment

Research Articles

Gondin AB[†], Miess E[†], Yousuf A[†], Steinborn R, Mösslein N, Yang Y, Göldner M, Ruland JG, Bünemann M, Krasel C, Christie MJ, Halls ML, Schulz S, Canals M. Multisite phosphorylation is required for sustained interaction with GRKs and arrestins during rapid μ-opioid receptor desensitization. *Sci.Signal.* 2018 Jul 17;11(539). doi: 10.1126/scisignal.aas9609.

[†] Shared first author

Lam R, **Gondin AB**, Canals M, Kellam B, Briddon SJ, Graham B, Scammells PJ. Fluorescently Labeled Morphine Derivatives for Bioimaging Studies. *J Med Chem*. 2018 Jan. doi: 10.1021/acs.jmedchem.7b01811

Halls ML, Yeatman HR, Nowell CJ, Thompson GL, **Gondin AB**, Civciristov S, Bunnett NW, Lambert NA, Poole DP, Canals M. Plasma membrane localization of the μ-opioid receptor controls spatiotemporal signaling. *Sci Signal.* 2016 Feb 9;9(414):ra16. doi: 10.1126/scisignal.aac9177

Conference Abstracts

Oral Presentations

Gondin AB, Christie MJ, Halls ML and Canals M. Phosphorylation of the μ-opioid receptor affects its regulation and trafficking. *British Pharmacological Society: Pharmacology 2016*, Dec 2016, London, UK**.**

Poster Presentations

Gondin AB, Halls ML and Canals M. Novel BRET biosensors reveal molecular details of μ-opioid receptor activation. *GPCR Pharmacology: The Next Generation*, Oct 2018, Copenhagen, Denmark**.**

Gondin AB, Halls ML, Canals M and Briddon SJ. Investigating agonist-dependent changes in the membrane organization of the μ-opioid receptor using fluorescence correlation spectroscopy. *GPCR workshop 2017*, Dec 2017, Kona, USA**.**

Gondin AB, Halls ML and Canals M. Phosphorylation-dependent and independent roles of GRK2 in μ-opioid receptor regulation, trafficking and signalling. *Gordon Research Conference*: *Molecular Pharmacology 2017*, March 2017, Lucca, Italy.

Gondin AB, Christie MJ, Halls ML and Canals M. Differential regulation of mu-opioid receptor by distinct agonists. *Joint ASCEPT-MPGPCR Conference 2014*, December 2014, Melbourne, Australia

Declaration

I hereby declare that this thesis contains no material which has been accepted for the award of any other degree or diploma at any university or equivalent institution and that, to the best of my knowledge and belief, this thesis contains no material previously published or written by another person, except where due reference is made in the text of the thesis.

This thesis includes three original papers published in peer reviewed journals. The core theme of the thesis is "molecular mechanisms controlling μ-opioid receptor activation". The ideas, development and writing up of all the papers in the thesis were the principal responsibility of myself, the student, working within the Drug Discovery Biology theme under the supervision of Dr Michelle Halls, Dr Meritxell Canals and Dr Stephen Briddon.

The inclusion of co-authors reflects the fact that the work came from active collaboration between researchers and acknowledges input into team-based research.

In the case of Chapter 4 my contribution to the work involved the following:

Thesis Chapter	Publication Title	Status	Nature and % of student contribution	Co-author name(s) Nature and % of Co-author's contribution
Chapter 4	Multisite phosphorylation is required for sustained interaction with GRKs and arrestins during rapid μ-opioid receptor desensitization	Published	Participated in research design, performed, analysed BRET and ELISA experiments, and interpreted data, wrote and edited the manuscript. (50%)	E.M. and R.S. (30%) performed and analysed β-Gal experiments, and E.M drafted manuscript; A.Y. (8%) performed and analysed electrophysiology experiments; N.M., Y.Y., and M.G. (2%) performed and analysed FRET experiments; J.G.R. (1%) generated FRET constructs; M.B. and C.K. (1%) supervised FRET experiments; M.J.C. (1%) supervised electrophysiology experiments; S.S. (2%) supervised β-Gal experiments; M.L.H. and M.C. (5%) supervised BRET experiments and M.C. edited the manuscript.

Student signature:  **Date:** **08/10/18**

The undersigned hereby certify that the above declaration correctly reflects the nature and extent of the student's and co-authors' contributions to this work. In instances where I am not the responsible author I have consulted with the responsible author to agree on the respective contributions of the authors.

Main Supervisor signature:  **Date:** **08/10/18**

Acknowledgments

My experience as a graduate student has been extraordinary, primarily because of the wonderful people I had the chance to share this journey over the past years. All of the experiences that I encountered have helped shape me into the person I am today, and for that, I am forever grateful. I gratefully acknowledge the financial support that has allowed me to pursue a PhD within the Drug Discovery Biology group at Monash University and the Cell Signalling group at the University of Nottingham and to travel to international conferences which have provided an invaluable opportunity to expand my network and be inspired by outstanding research.

First and foremost, I would like to thank my supervisors Dr Meri Canals and Dr Michelle Halls. For your dedication, support and confidence in me. For allowing me to grow as an independent scientist but being always available when I needed guidance. For reading over all the drafts and always providing invaluable feedback. You have been exceptional role models and contributed immensely to my growth as a scientist. I would like to express my gratitude to my supervisor in Nottingham Dr Steve Briddon, for your guidance and expertise with the microscopes, your kindness, encouragement and understanding.

I would also like to thank my panel members Prof Roger Summers, Prof Federico Mayor and Dr Daniel Poole, as well as Dr Rob Lane who provided essential insight to keep my research in the right direction. Your flexibility and willingness to connect from the most extreme time zones is much appreciated.

I also extend my gratitude to those with whom I worked during my PhD, to all DDB staff and students and the Cell Signalling Research family in Nottingham. For your advice and experimental assistance and making working in the lab such an enjoyable experience.

A special thanks to the many friends I have made along the way: Amy Chen, Carmen Klein-Herenbrink, Thomas Coudrat, Ee Von Moo, Alastair Keen, Quynh Mai, David Sykes, Carl White, Chloe Peach and many others... For the insightful scientific discussions, for inspiring and motivating me to become better. Thanks to my friends outside science, the music debates and dances have balanced it out and help me progress in other fronts.

Finally, I am eternally grateful for the love, care and emotional support of my family and my partner, Peter. Even from the distance, I have always felt your presence. Thanks for believing in me and encouraging me to pursue my dreams.

Abbreviations

β2AR – β2-adrenoceptor

β-FNA – β-funaltrexamine

AC – adenylyl cyclase

AKAP – A-kinase anchoring proteins

AP_2 – adaptin protein subunit 2

ATP – adenosine triphosphate

BRET – Bioluminescence Resonance Energy Transfer

CaMKII – calcium/calmodulin-dependent protein kinase II

cAMP – cyclic adenosine monophosphate

CAMYEL – cAMP sensor using YFP-Epac-RLuc

CHO – Chinese hamster ovary

CNS – central nervous system

Cryo-EM – cryo-electron microscopy

DAG – diacylglycerol

DAMGO – [D-Ala2,N-Me-Phe4,Gly5-ol]-enkephalin

DMEM – Dulbecco's modified Eagle's medium

DOP – δ-opioid receptor

ECL – extracellular loop medium

ELISA – Enzyme-Linked Immunosorbent Assay

ERK – extracellular signal-regulated kinase

Epac – exchange proteins activated by cAMP

FBS – foetal bovine serum

FCS – Fluorescence Correlation Spectroscopy

FDA – Food and Drug Administration

FRAP – Fluorescence Recovery After Photobleaching

GABA - γ aminobutyric acid

GDP – guanosine diphosphate

GIRK – G protein-activated inwardly rectifying potassium channel

GEF – guanine-nucleotide exchange factor

GPCR – G protein-coupled receptor

GRK – G protein-coupled receptor kinase

GTP – guanosine triphosphate

HBSS – Hank's Balanced Salt Solution

HEK – human embryonic kidney

HRP – horseradish peroxidase

ICL – intracellular loop

IP_3 – inositol 1,4,5-triphosphate

JNK – c-Jun N-terminal kinase

KO – knock-out

KOP – κ-opioid receptor

MAPK – mitogen-activated protein kinase

MEK – mitogen-activated protein kinase kinase

mG – mini-G protein

MOP – μ-opioid receptor

Nb – nanobody

NLuc – Nanoluciferase

NMDAR – N-methyl-D-aspartate receptor

NMR – nuclear magnetic resonance

NOP – nociception/orphanin FQ peptide receptor

PAG – periaqueductal grey

PCH – Photon Counting Histogram

PDE – phosphodiesterases

PEI – polyethylenemine

PIP_2 – phosphatidylinositol 4,5-biphosphate

PI3K – phosphoinositide 3 kinase

PKA – protein kinase A

PKC – protein kinase C

PLC – phospholipase C

PNS – peripheral nervous system

PTx – pertussis toxin

RGS – regulators of G protein signalling

RLuc8 – Renilla luciferase

SNPs – single nucleotide polymorphisms

TM – transmembrane

TBS – tris-buffered saline

YFP – yellow fluorescent protein

VGCC – voltage-dependent calcium channel

WT – wild type

Chapter 1

Introduction

1.1 G protein-coupled receptors

1.1.1 Classification

G protein-coupled receptors (GPCRs) are integral membrane proteins that are ubiquitously expressed on the surface of all cells through-out the body. GPCRs represent the third-largest gene family in mammals - over 800 genes within the human genome encode GPCRs (Fredriksson, Lagerstrom, Lundin, & Schioth, 2003). They recognise a wide variety of extracellular stimuli – ranging from photons, ions, odorants, and hormones, to peptides and proteins, and transmit the information across the plasma membrane to inside the cell. This versatility in ligands enables GPCRs to be involved in most fundamental biological processes. Signal transduction occurs mainly through activation of guanine nucleotide binding proteins also known as G proteins. Thus, despite the broad number of GPCRs, ligands and functions, signal transduction converges in the activation of only a few different effector proteins. This implies that the specificity of GPCR signalling is ensured through regulation and tailoring of their signalling responses. Importantly, dysregulation of GPCRs underlies many pathophysiological conditions. For this reason, pharmacological targeting of GPCRs is used to treat a number of clinical disorders including cardiovascular disease, asthma, diabetes, obesity, cancer and pain (Rask-Andersen, Masuram, & Schioth, 2014; Santos et al., 2017). GPCRs are one of the most prominent target classes for drug discovery and embody ~34% of all marketed drugs (Hauser, Attwood, Rask-Andersen, Schioth, & Gloriam, 2017).

GPCRs are classified into five families according to their sequence homology: rhodopsin (family A), secretin (family B), glutamate (family C), frizzled/taste 2 and adhesion (Bjarnadottir et al., 2006; Fredriksson et al., 2003). Although direct coupling to G proteins remains to be shown for the frizzled family (Dijksterhuis, Petersen, & Schulte, 2014), signalling by all five receptor families depends to a certain extent on G protein activation.

The family A is by far the largest GPCR family with the widest variety of ligand types – it comprises 659 receptors in humans, including 388 odorant receptors (Heng, Aubel, & Fussenegger, 2013; Lagerstrom & Schioth, 2008). Family A is further sub-classified depending on the type of ligand to which the receptors bind, and includes the aminergic receptors (e.g.

adrenoceptors, muscarinic, dopamine), peptide receptors (e.g. opioid, tachykinin, relaxin), protein receptors (chemokine), lipid receptors (e.g. free fatty acid, cannabinoid, prostanoid), and nucleotide receptors (adenosine and purinergic) among others. The secretin/family B GPCRs include receptors for glucagon, calcitonin and parathyroid hormone that are critical in endocrinology and regulation of metabolism. Family C includes metabotropic glutamate receptors and γ-aminobutyric acid (GABA) type B receptors that are important in neurobiology. The structure and function of the frizzled and adhesion families are very different and less understood compared to the other GPCR families. Despite belonging to one of the five GPCR families due to their similarity in sequence, ~140 receptors are considered orphan GPCRs because their natural (endogenous) ligands are unknown (Fang, Kenakin, & Liu, 2015).

1.1.2 Structural characteristics

GPCRs possess a conserved structure consisting of an extracellular amino-terminus (N-term), followed by a bundle of seven transmembrane α-helices (TM1-7) joined by alternating intracellular (ICL1-3) and extracellular (ECL1-3) loops, and a cytoplasmic carboxyl-terminus tail (C-term) which, in many GPCRs, contains a small α-helix (helix 8) tethered to the plasma membrane via a palmitoylation moiety (Fig. 1.1).

The GPCR families share over 25% sequence homology in the TM core region with highly conserved residues and motifs (Pierce, Premont, & Lefkowitz, 2002). The 7TM bundle is inserted in the lipid bilayer of the plasma membrane. From the extracellular surface the 7TMs are ordered in an anticlockwise circular arrangement, forming a hydrophobic core impermeable to ions (Mizobe, Maze, Lam, Suryanarayana, & Kobilka, 1996) (Fig. 1.1). For the family A receptors, the binding site for the endogenous ligand, also known as the orthosteric binding pocket, is located deep within the hydrophobic core between the TM domains (Dixon et al., 1987; Tota & Strader, 1990). The residues that make up the orthosteric binding pocket determine the physical and chemical properties of the cavity to ensure ligand specificity.

The extracellular regions diverge between GPCR families in terms of size, structure and function. Family A GPCRs have small extracellular domains that are involved in receptor

folding and assembly into the plasma membrane (Andersson, D'Antona, Kendall, Von Heijne, & Chin, 2003; Cho et al., 2012; Hague et al., 2004). The N-term and ECLs might also serve as a vestibule region for first recognition of ligands before they bind within the buried orthosteric binding pocket (Stanley, Pardo, & Fabritiis, 2016) and can play a role in agonist selectivity (Strasser, Wittmann, & Seifert, 2008) and ligand binding kinetics (Wittmann, Seifert, & Strasser, 2011). In contrast, the family B and family C GPCRs have large extracellular domains involved in ligand binding (O'Hara et al., 1993).

The intracellular domains of all GPCRs serve as the site of interaction with cytosolic signalling proteins. The ICLs and C-term can present variable lengths and contain serine and threonine (S/T) residues that can be differentially phosphorylated by intracellular kinases. Thus, the intracellular region is involved in selectivity of effector coupling, including to the different G protein subtypes and regulatory proteins.

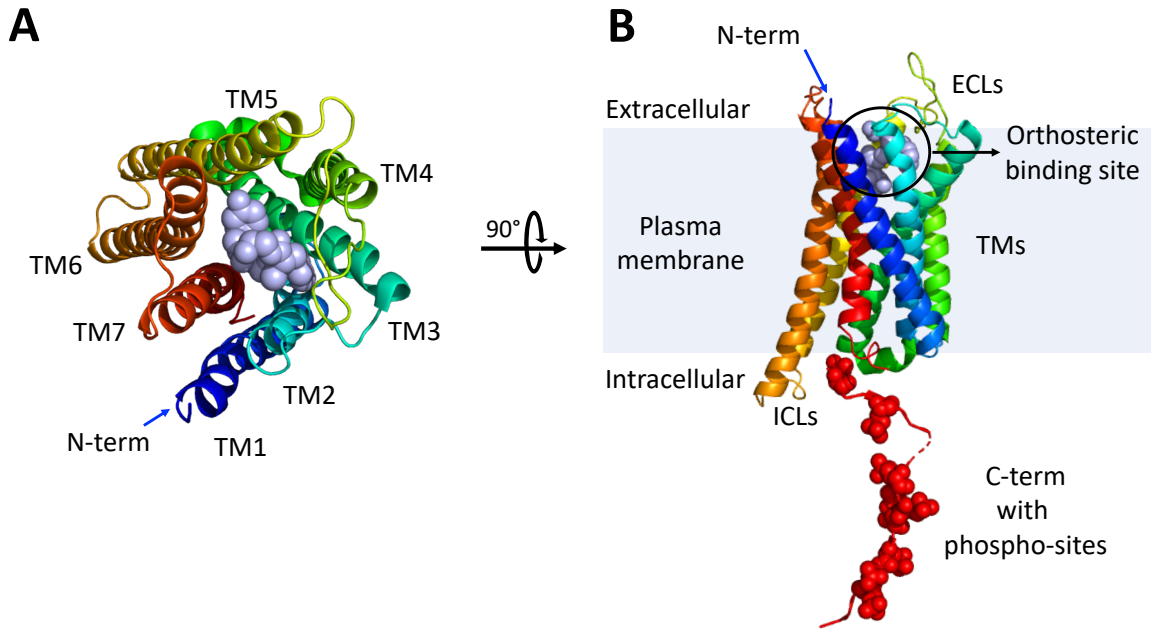


Figure 1.1 Representative structure of a family A GPCR (the μ-opioid receptor) bound to a peptide agonist. Active μ-opioid receptor structure shown as cartoon from PDB 6DDE (Koehl et al., 2018). **(A)** Extracellular view with transmembrane domains (TM1-7) annotated, the position of the N-terminus (N-term) is indicated with a blue arrow. **(B)** Lateral view with extracellular loops (ECLs) and intracellular loops (ICLs) indicated. The C-terminus (C-term) with phosphorylated S/T shown as spheres corresponds to the vasopressin V2 receptor phosphopeptide from PDB 4JQI (Shukla et al., 2013).

The determination of GPCR structures experimentally has been technically challenging due to limitations in protein purification, the conformational heterogeneity in solutions, and the small structured polar surface available for forming crystal lattice contacts. The first GPCR structure was the crystal structure of the bovine rhodopsin receptor (Palczewski et al., 2000). Rhodopsin is a very unique GPCR in that is activated by photons that convert a covalently bound 11-cis-retinal molecule to all-trans-retinal. Despite its distinct mode of activation, a similar arrangement of the 7TM structure was later confirmed for GPCRs that bind to diffusible ligands such as the human β_2-adrenoceptor (β2AR) (Cherezov et al., 2007). Then, the first active-state GPCR structure of ligand free rhodopsin (opsin) followed in 2008 (Scheerer et al., 2008). Since these first structures, extensive research and technology development have facilitated the structural determination of a number of other family A GPCRs including all the members of the opioid receptor family (Granier et al., 2012; Manglik et al., 2012; A. A. Thompson et al., 2012; Wu et al., 2012). Moreover, crystal structures of receptors within the secretin/family B (Siu et al., 2013), glutamate/family C (Dore et al., 2014) and frizzled families (Wang et al., 2013) have also been obtained. High-resolution structures provide insights into the atomic interactions between ligands and the residues that constitute the orthosteric binding pocket and enable rational chemical drug design through structure-based drug discovery (Congreve, Dias, & Marshall, 2014).

Although crystal structures provide a static snapshot of GPCRs, multiple structures of the same receptor in different conformational states have been obtained, including for the μ-opioid receptor (Fig. 1.2). Inactive structures are those in which the receptor is bound to an antagonist and they typically show an occluded intracellular binding surface that is incapable of coupling to G protein. Active intermediate structures are those in which the receptor is bound to an agonist but shows an occluded intracellular surface that resembles the inactive state; these structures represent one of several steps towards full receptor activation following agonist binding. Active structures are those in which the receptor is bound to an agonist and adopts an intracellular surface that is competent for interaction with heterotrimeric G proteins. These fully active structures have only been obtained in the presence of G protein mimicking nanobodies (Che et al., 2018; Huang et al., 2015; Kruse et al., 2013; Ring et al., 2013) or G protein themselves (Rasmussen et al., 2011). This is because

GPCR active states are stabilised by both the agonist and G protein as described by the current ternary complex model of agonist-receptor-G protein interactions (De Lean, Stadel, & Lefkowitz, 1980; Maguire, Van Arsdale, & Gilman, 1976), where enhancement of agonist affinity is due to a two-way positive cooperativity between agonist and G protein. According to this, ligands are typically classified as full agonist, partial agonist, neutral antagonist or inverse (full or partial) agonist depending on the extent to which they modify the conformational state of the receptor and engage or disengage it from transducer–effector pathways. Thus, it is now clear that GPCRs do not fit a simple on/off receptor switch model (Park, Lodowski, & Palczewski, 2008), instead they are highly dynamic proteins that can exist in a plethora of conformations and intermediate states (Manglik & Kruse, 2017; Thal, Glukhova, Sexton, & Christopoulos, 2018).

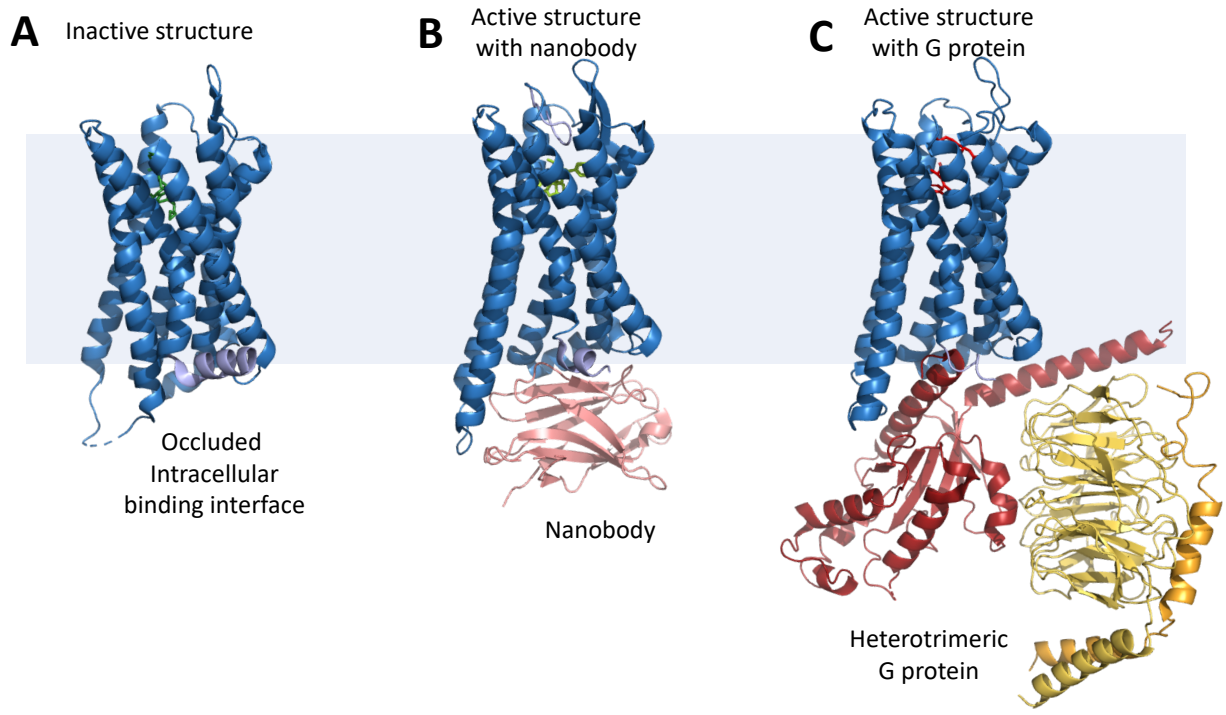


Figure 1.2 Multiple structures of the μ-opioid receptor. (A) Inactive crystal structure of the μ-opioid receptor bound to the irreversible morphinan antagonist β-funaltrexamine from PDB 4DKL (Manglik et al., 2012). **(B)** Active crystal structure of the μ-opioid receptor bound to the morphinan agonist BU72 from PDB 5C1M (Huang et al., 2015). **(C)** Active cryo-EM structure of the μ-opioid receptor bound to the peptide agonist DAMGO from PDB 6DDE (Koehl et al., 2018).

Most recently, advances in cryo-electron microscopy (cryo-EM) have facilitated the study of GPCR signalling complexes including GPCRs in complex with both stimulatory and inhibitory G proteins (Draper-Joyce et al., 2018; Koehl et al., 2018; Y. L. Liang et al., 2017). These GPCR structures in complex with different G proteins have provided further insights regarding how specific ligand-receptor interactions translate into G protein selectivity. However, GPCRs transduce pleiotropic intracellular signals through coupling to different effectors, and the only available structure of a GPCR in complex with another effector is the crystal structure of rhodopsin bound to arrestin (Kang et al., 2015). The structural elucidation of other GPCR-effector complexes would shed light into how distinct ligands might activate different signalling pathways.

1.1.3 G protein signalling

Signal transduction is the biological process by which receptors detect extracellular stimuli and initiate intracellular responses. The family of heterotrimeric G proteins are the canonical transducers for GPCRs. Following ligand binding, GPCRs undergo a conformational change within the TM domains that is allosterically transmitted to the intracellular effector binding site which couples to the G protein.

The signal is then propagated to the intracellular compartment by activation of the G protein. The G protein heterotrimeric complex is composed of alpha (α), beta (β) and gamma (γ) subunits; the latter subunits form a stable dimeric complex known as Gβγ. The Gα subunit binds guanine nucleotides and has GTPase activity. During G protein activation, the inactive Gα subunit releases its bound guanosine diphosphate (GDP) and replaces it with guanosine triphosphate (GTP) which is in excess in the cytoplasm. GTP binding, in turn, stabilises an active form of Gα and promotes its dissociation from the Gβγ complex. The Gα subunit has inherent enzymatic activity and will eventually hydrolyse GTP to GDP, resulting in re-association of the inactive Gαβγ heterotrimer and completing the G protein cycle (Hubbard & Hepler, 2006). GTPase activating proteins, also known as regulators of G protein signalling (RGS), can accelerate termination of G protein signalling by promoting the hydrolysis of GTP (Dohlman & Thorner, 1997). Both Gα and Gβγ can independently regulate downstream effector proteins.

Humans encode 18 different Gα proteins, 5 Gβ proteins and 12 Gγ proteins that modulate diverse physiological functions depending on the targeted cell types, tissues, and organs (Syrovatkina, Alegre, Dey, & Huang, 2016). There are four subtypes of Gα: G_s, $G_{i/o}$, $G_{q/11}$ and $G_{12/13}$ (Wettschureck & Offermanns, 2005). G_s stimulate the enzyme adenylate cyclase (AC) that converts adenosine triphosphate (ATP) to cyclic adenosine monophosphate (cAMP), thereby increasing the production of the second messenger cAMP and activating cAMP-dependent pathways including protein kinase A (PKA) and exchange proteins activated by cAMP (Epac) (Hanoune & Defer, 2001). Conversely, $G_{i/o}$ inhibit AC and result in decreased cAMP production. $G_{q/11}$ activate phospholipase C (PLC), which then cleaves phosphatidylinositol 4,5-bisphosphate (PIP_2) producing two second messengers: inositol 1,4,5-trisphosphate (IP_3) and diacylglycerol (DAG). IP_3 activates calcium (Ca^{2+}) channels allowing the release of intracellular Ca^{2+} from the endoplasmic reticulum. In addition, Ca^{2+} and DAG can together bind to and activate protein kinase C (PKC). $G_{12/13}$ are involved in the activation of Rho guanine-nucleotide exchange factors (Rho GEFs) that regulate actin cytoskeleton remodelling (Dhanasekaran & Dermott, 1996) .

The Gβγ subunit is also involved in the regulation of various effectors such as the activation of G protein receptor kinases (GRKs), modulation of potassium (K^+) and calcium Ca^{2+} channels, as well as certain AC isoforms, PLC, phosphoinositide 3 kinases (PI3Ks) and mitogen-activated protein kinases (MAPKs) (Khan et al., 2013).

Although these descriptions refer to the canonical signalling pathways mediated by the G protein subtypes, each G protein can modulate a range of downstream effectors resulting in the generation of complex signalling networks. Moreover, a single GPCR can couple to multiple Gα proteins further increasing the complexity of GPCR signalling.

1.1.4 GPCR regulation

Upon prolonged or repeated agonist exposure, GPCR signalling can undergo desensitisation. Desensitisation refers to the loss of coupling to G proteins, resulting in reduced receptor signalling. Heterologous desensitisation occurs when activation of second messenger-dependent kinases such as PKC or PKA results in phosphorylation of a receptor

that has not been activated, resulting in the desensitisation of non-activated receptors (Ferguson, 2001). In contrast, homologous desensitisation occurs when only the receptor that is activated by the ligand gets desensitised. Homologous desensitisation is commonly initiated by phosphorylation of the receptor by GRKs that specifically recognise active receptor conformations and phosphorylate intracellular serine/threonine (S/T) sites within the ICLs and the C-term tail of the receptor (Ferguson, 2001). However, specific agonist-activated conformations can undergo different molecular mechanisms of homologous desensitisation (Kelly, Bailey, & Henderson, 2008). There are seven GRKs encoded in the human genome that can be subdivided into three classes based on their kinase sequence and function: GRK1-like (GRK1 and GRK7), GRK2-like (GRK2 and GRK3) and GRK4-like (GRK4, GRK5 and GRK6). The GRK1-like kinases are exclusively expressed in the visual system, whereas the GRK2- and GRK4-like kinases are widely expressed throughout the body (Ribas et al., 2007).

Phosphorylation of the GPCR C-term tail increases the affinity of the receptors for arrestins, which block further interaction with the G protein, resulting in desensitisation and termination of G protein signalling (Tian, Kang, & Benovic, 2014). Similar to GRKs, some arrestin isoforms (arrestin 1 and arrestin 4) are exclusively expressed in the visual system, whereas the other isoforms, arrestin 2 (β-arrestin1) and arrestin 3 (β-arrestin2), are highly expressed through the entire body. Arrestins promote endocytosis of the receptor by interacting with the trafficking machinery (Tian et al., 2014). The mechanism, route and speed of GPCR trafficking is ligand and receptor-dependent, but overall the endocytic process involves the interaction of arrestin with many proteins (Gurevich & Gurevich, 2006) such as the E3 ubiquitin ligase Mdm2 (Shenoy et al., 2009), adaptin protein subunit 2 (AP2) (Laporte, Oakley, Holt, Barak, & Caron, 2000) and the heavy chain of clathrin (Goodman, Krupnick, Gurevich, Benovic, & Keen, 1997) which assembles to form the clathrin-coated pit that initiates receptor internalisation (Le Roy & Wrana, 2005). Dynamin mediates endocytosis by a GTPase activity that constricts the neck of the invaginated vesicle. When the vesicles shed the clathrin coats, they become early endosomes that provide an acidified environment where ligand and receptor dissociate, unbinding of arrestins occurs and cytosolic phosphatases dephosphorylate the receptor. Endosomes represent a major sorting compartment where receptors can be directed to the recycling or degradation pathway.

Recycling endosomes return resensitised receptors to the cell surface for subsequent cycles of activation and signalling, resulting in receptor recovery from desensitisation. Alternatively, the receptor is processed for degradation in lysosomes, resulting in downregulation (reduction in the number of functional receptors) and prolonged attenuation of cellular signalling (Tsao and von Zastrow, 2000). Robust desensitisation generally precedes endocytosis; however, it can also occur independently without further receptor internalisation (Johnson et al., 2006).

1.1.5 G protein-independent signalling

Aside from G proteins, GPCRs also interact with other protein families such as GRKs and arrestins in an activation-dependent manner. Although initially these proteins were only recognised for their regulatory function in mediating desensitisation and internalisation, it is now apparent that they can also act as molecular scaffolds and support noncanonical, G protein-independent signalling (Defea, 2008; Hall, Premont, & Lefkowitz, 1999; Luttrell, 2001; Luttrell & Gesty-Palmer, 2010; Peterson & Luttrell, 2017).

For example, GRKs can regulate cellular processes independent of their kinase activity (Evron, Daigle, & Caron, 2012). In particular, GRK2 interacts with a diverse repertoire of non-GPCR substrates (Ribas et al., 2007). Moreover, β-arrestins can bind to over 20 different protein kinases, serving as signalling adaptors for a number of effector proteins including c-Src, Akt, MAPK, PI3K and c-Jun N-terminal kinase 3 (JNK3) (DeWire, Ahn, Lefkowitz, & Shenoy, 2007; Luttrell et al., 1999; McDonald et al., 2000). β-arrestins bring the signalling effectors in close proximity to the receptor and can therefore target GPCR-mediated signalling to specific subcellular compartments. For example, it has been shown that the β-arrestin-mediated scaffolding of the MAPK cascade leads to retention of the MAPK signalling to the cytosolic compartment (Tohgo, Pierce, Choy, Lefkowitz, & Luttrell, 2002).

Although β-arrestins modulate and scaffold the formation of signalling platforms, it is not yet clear to what extent this is dependent on G protein activation. Recently, it has been shown that arrestin is dispensable for extracellular signal-regulated kinase (ERK) signalling

(O'Hayre et al., 2017) and for many GPCRs ERK signalling first requires functional activation of G proteins (Grundmann et al., 2018).

1.1.6 Biased agonism

GPCRs are highly dynamic proteins that can shift between multiple conformational states and activate various signalling pathways. It is now recognised that different ligands binding to the same receptor do not necessarily have to activate all signalling pathways equally. Biased agonism, or functional selectivity, is the phenomenon by which chemically distinct ligands stabilise a particular active receptor conformation, resulting in the preferential activation of specific signalling pathways. One of the first reports of biased agonism was for the serotonin receptor (Berg et al., 1998), and since then biased drug development programs have pursued the translation of biased agonism for many therapeutically important GPCR targets including the μ- (X.-T. Chen et al., 2013; Manglik et al., 2016) and κ-opioid receptors (Schmid et al., 2013; Zhou et al., 2013).

The intrinsic properties of the ligand (ligand bias) will determine which receptor conformation is stabilised and which particular effector protein is coupled, thus ultimately determining which specific signalling response is activated (Fig. 1.3). However, the signalling response will also be affected by factors such as the stoichiometric ratios of signalling molecules in the cell type where the ligand acts (system bias) (T. Kenakin, 2015) and any changes the system may undergo in disease and/or with treatment (dynamic bias) (Michel, Seifert, & Bond, 2014). Because of the complexity of physiological systems, *in vitro* measurements of signalling bias (i.e. bias factors that indicate the relative agonist potency for each signalling pathway) do not always translate into therapeutic benefits in *in vivo* systems, leaving a translational gap in the application of biased signalling to drug development (T. Kenakin, 2018). Thus, uncovering how effective a drug should be for each signalling pathway in order to achieve a particular therapeutic outcome is one of the biggest challenges in modern day drug discovery (Michel & Charlton, 2018).

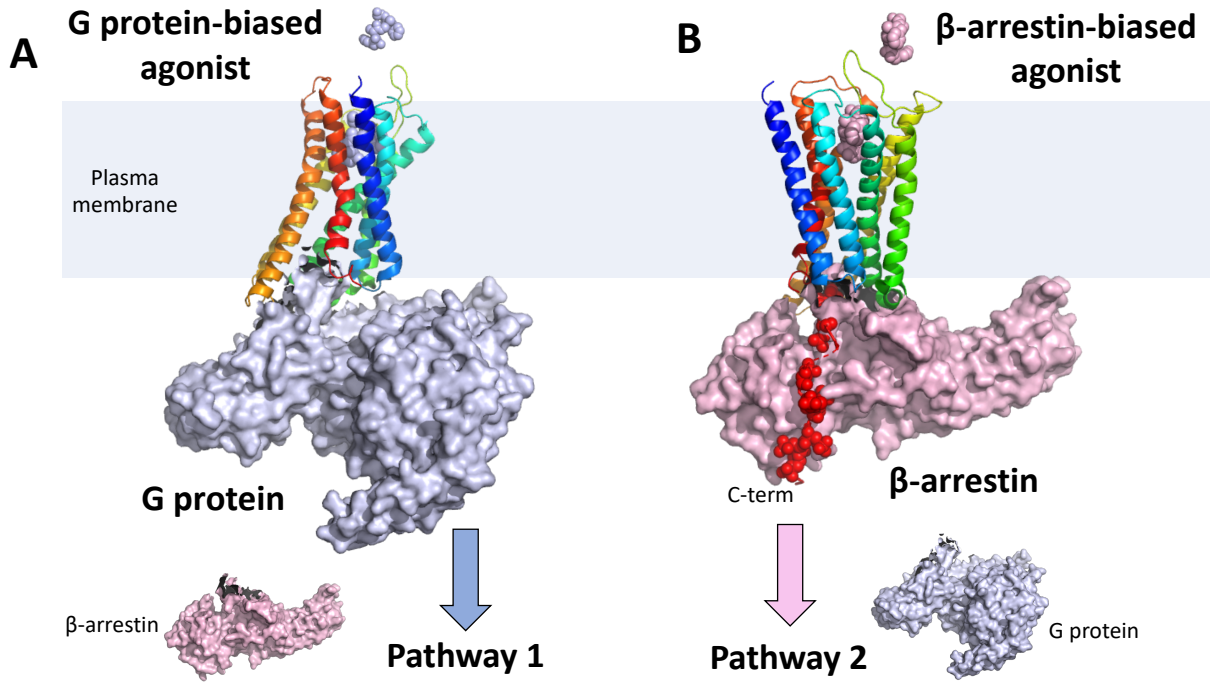


Figure 1.3 Biased agonism at GPCRs is the phenomenon whereby ligands differentially activate downstream signalling events. It has been hypothesised that this occurs by the stabilisation of different receptor conformations each linked to a different functional outcome. **(A)** A G-protein biased agonist will activate a receptor conformation that preferentially couples to G protein over β-arrestin resulting in robust activation of pathway 1. **(B)** A β-arrestin biased agonist will activate a receptor conformation that preferentially couples to β-arrestin over G protein resulting in robust activation of pathway 2.

When the translational gap is bridged, biased agonism may allow the design of drugs that selectively activate signalling pathways that lead to the desired physiological effect (Violin, Crombie, Soergel, & Lark, 2014). As described in (Kenakin, 2017), the promise of improved therapeutics through biased agonism is based on the capability of biased agonists to (1) emphasize beneficial signalling pathways (e.g. β-arrestin biased parathyroid hormone receptor agonists increase bone building capacity for the treatment of osteoporosis (Gesty-Palmer et al., 2013)); (2) de-emphasize harmful signalling pathways (e.g. G protein-biased μ-opioid receptor agonists show less respiratory depression than conventional opioid analgesics (Schmid et al., 2017)); (3) block harmful pathways produced by the endogenous ligand (e.g. G protein-biased angiotensin antagonists lower blood pressure while promoting cardiac performance by β-arrestin-induced signalling (Violin et al., 2010)); and (4) allow pursuit of

previously passed-over drug targets due to unwanted "on-target" side effects (e.g G protein-biased κ-opioid agonists have the potential to treat pain, drug addiction and psychotic disorders without triggering sedation and dysphoric effects mediated by β-arrestin (Brust et al., 2016)).

The first biased drug candidate, TRV120027, targeted the angiotensin II type 1 receptor (AT1R) for congestive heart failure and was designed to be a potent antagonist for G protein activation but an agonist for β-arrestin recruitment and activation of several kinase pathways, including ERK and Src (Violin et al., 2010). Previous AT1R antagonists reduced blood pressure, but unlike the biased antagonist TRV120027, they did not increase cardiac performance. Despite the promising results *in vivo* (Boerrigter, Soergel, Violin, Lark, & Burnett, 2012), TRV120027 did not meet its primary endpoint in a clinical phase II study (Pang et al., 2017). Another promising biased drug is TRV130 (oliceridine or OLINVO), a G protein-biased μ-opioid receptor agonist, which has shown improved analgesia with reduced gastrointestinal and respiratory dysfunction *in vivo* (DeWire et al., 2013). A clinical phase II study confirmed that oliceridine is a potent analgesic drug in patients (Viscusi et al., 2016) with an acceptable safety/tolerability profile and potentially wider therapeutic window than morphine (Singla et al., 2017). For this reason, the Food and Drug Administration (FDA) granted breakthrough therapy status to this drug and has accepted the new drug application for oliceridine injection for review. However, presently available clinical data rely only on short-term administration, which makes it unsuitable to predict whether analgesic tolerance, constipation, and respiratory depression will still occur after chronic treatment with oliceridine, as with traditional opioid drugs.

1.1.7 Compartmentalised signalling

Functionally, GPCRs transduce a wide range of extracellular stimuli into various intracellular signalling pathways via coupling to G proteins or to other effector proteins. Despite the convergence in the signalling pathways activated among different GPCRs, they are capable of regulating a number of physiological effects with great specificity, which suggests a high degree of organisation and regulation of intracellular signalling. Compartmentalised signalling alludes to the spatial and temporal control of the signalling components which provides a mechanism whereby GPCRs can direct the assembly of specialised signalling platforms or 'signalosomes'. These signalling platforms facilitate second messenger production, the organisation and scaffolding of effectors, and co-ordination of regulatory elements. These can now be studied with genetically encoded sensors that allow the measurement of signalling responses with unprecedented temporal and spatial resolution (Halls & Canals, 2018).

In recent years, it has become apparent that GPCRs are highly organised within the plasma membrane and interact with adaptor/scaffolding proteins that facilitate contact of receptors with the signalling components required for fine control of second-messenger cascades (Halls, 2012). For example, for the compartmentalisation of cAMP signalling, GPCRs interact with A-kinase anchoring proteins (AKAPs), which scaffold the formation of high-order signalling domains composed of activators that produce cAMP such as ACs, regulators that break down cAMP such as phosphodiesterases (PDEs) and downstream effectors such as PKA, PKC, Epac and ion channels (Conti, Mika, & Richter, 2014; Dessauer, 2009; Halls & Cooper, 2010; Willoughby, Wong, Schaack, Scott, & Cooper, 2006). Moreover, recent single-molecule studies have revealed plasma membrane "hot spots" at which the β2AR and Gs are transiently immobilized and proposed to couple (Sungkaworn et al., 2017). Indeed, the μ-opioid receptor has been described to signal differently from distinct regions of the plasma membrane (Halls et al., 2016).

In addition to compartmentalised signalling from distinct domains of the plasma membrane, it has now been reported that internalised receptors can remain active and continue to signal from endosomes contributing to the overall amplitude and duration of the

signalling response (Calebiro et al., 2009; DeFea, 2000; Ferrandon et al., 2009; Irannejad et al., 2013; Mullershausen et al., 2009). It has been suggested, for instance, that endosomal signalling mediates sustained pain transmission induced by nociceptive or inflammatory peptides (Cattaruzza et al., 2014; Jensen et al., 2014). Therefore, selective targeting of endosomal signalling may offer a more specific and effective treatment to achieve prolonged analgesia (Jensen et al., 2017; Thomsen, Jensen, Hicks, & Bunnett, 2018; Yarwood et al., 2017). β-arrestins mediate receptor redistribution to endosomes and mediate GPCR signalling from endosomes, however endosomal signalling has also been shown to require G proteins (Godbole, Lyga, Lohse, & Calebiro, 2017; Irannejad et al., 2013). Thus, endosomal signalling seems to require the formation of an alternative GPCR super-complex containing both G protein and β-arrestin (Thomsen et al., 2016).

Moreover, activation of pre-existing pools of intracellular receptors confer additional variety to the signalling repertoire. It has now been reported that GPCRs can be localised to and signal from intracellular compartments such as endoplasmic reticulum (Revankar, Cimino, Sklar, Arterburn, & Prossnitz, 2005), Golgi (Irannejad et al., 2017; Stoeber et al., 2018) and nucleus (Vincent et al., 2016). Ligand lipophilicity and membrane transporters will determine whether a ligand can cross the plasma membrane and access such intracellular receptor pools (Irannejad et al., 2017).

In summary, it is now clear that the particular GPCR and effector subcellular location, both within specific domains of the plasma membrane as well as in intracellular compartments, is important for the spatial and temporal control of cellular responses. Thus, GPCR signalling is a complex process and new paradigms such as G protein-independent signalling, compartmentalised and intracellular signalling continue to emerge (Fig. 1.4). Much remains to be understood about the activation, regulation and functional significance of these processes.

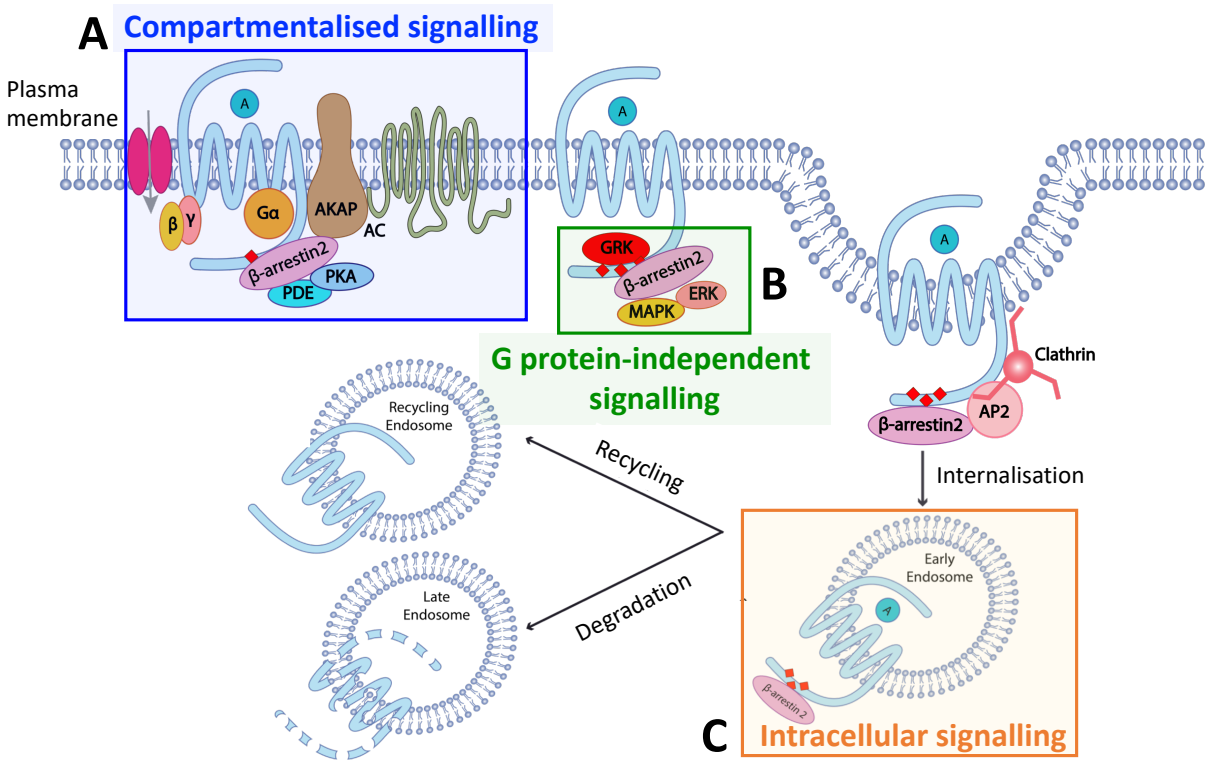


Figure 1.4 New paradigms in GPCR signalling. The 'traditional' view of GPCR signalling was simple – agonist binding initiates GPCR signalling exclusively from the plasma membrane through activation of a single G protein subtype and subsequent receptor regulation mediated by GRK phosphorylation and β-arrestin recruitment which cause uncoupling of the G protein pathway in a process known as desensitisation. After this, the receptor is internalised and sorted into degradation or recycling pathways. However, new paradigms in GPCR signalling continue to emerge – it is now apparent that GPCRs and their signalling effectors are highly organised and compartmentalised within distinct domains of the plasma membrane **(A)**. Additionally, GPCRs are capable of initiating β-arrestin-dependent signalling independently of G protein activation **(B)**. Finally, GPCR signalling can also be initiated from intracellular pools of receptors such as endosomes **(C)**.

1.2 The opioid system

1.2.1 Opioid-induced analgesia

Nociceptive pain is the natural physiological response to a noxious stimulus such as injury or inflammation (Fig. 1.5A). The noxious stimulus is first received by sensory neurons in the periphery. This information is then transmitted through the spinal cord to the central nervous system (CNS). Pro-nociceptive neurotransmitters such as glutamate, calcitonin-gene related peptide or substance P are released in the dorsal horn of the spinal cord and transmit the signal to second-order neurons in the spinal cord. These second-order neurons form the ascending spinothalamic tract that leads to the thalamus, where they synapse with third-order neurons that project to the sensory cortex, where the pain is perceived (Wolkerstorfer, Handler, & Buschmann, 2016).

Pain signals are modulated by the endogenous opioid system. Opioid neuropeptides and their receptors are widely distributed; in the CNS, they modulate various biological processes including pain perception and transmission, euphoria, sedation, respiratory control and reward processing; in sensory nerve fibers of the peripheral nervous system (PNS) where they modulate pain transmission to the CNS and gastrointestinal motility and secretion. Centrally, the periaqueductal grey (PAG), locus coeruleus, rostral ventral medulla and spinal cord show high concentrations of opioid receptors (Pathan & Williams, 2012). Stimulation of the PAG matter of the midbrain activates enkephalin-releasing neurons that project to the raphe nuclei in the brainstem. The dorsal horn of the spinal cord is the major site where analgesia and pain management occur. Here, opioid receptors are distributed at both pre- and post-synaptic nerve terminals, where they restrict the release of pro-inflammatory neurotransmitters and the excitability of pain transmitting neurons (Sprouse-Blum, Smith, Sugai, & Parsa, 2010). Exogenous opioid drugs can also directly activate opioid receptors in brain areas such as PAG, where these receptors are densely expressed, to produce analgesia.

Opioid receptors are mainly coupled to pertussis toxin (PTx)-sensitive heterotrimeric $G\alpha_{i/o}$ proteins and to a lesser extent, to PTx-insensitive $G\alpha_{z}$ (Law, Wong, & Loh, 2000). Activation of the G protein leads to inhibition of AC, reducing intracellular cAMP levels (Raffa,

Martinez, & Connelly, 1994) and the regulation of ion channels. In response to receptor activation, inhibition of voltage-activated calcium channels (VGCC) restricts the release of pro-inflammatory neurotransmitters (Al-Hasani & Bruchas, 2011). Activation of G protein-activated inwardly rectifying potassium (GIRK) channels causes K^+ efflux and neuronal hyperpolarisation which results in attenuation of the transmission of nociceptive electrical currents (Al-Hasani & Bruchas, 2011). In addition, opioid receptors can activate PLC and MAPKs (Law et al., 2000; Standifer & Pasternak, 1997).

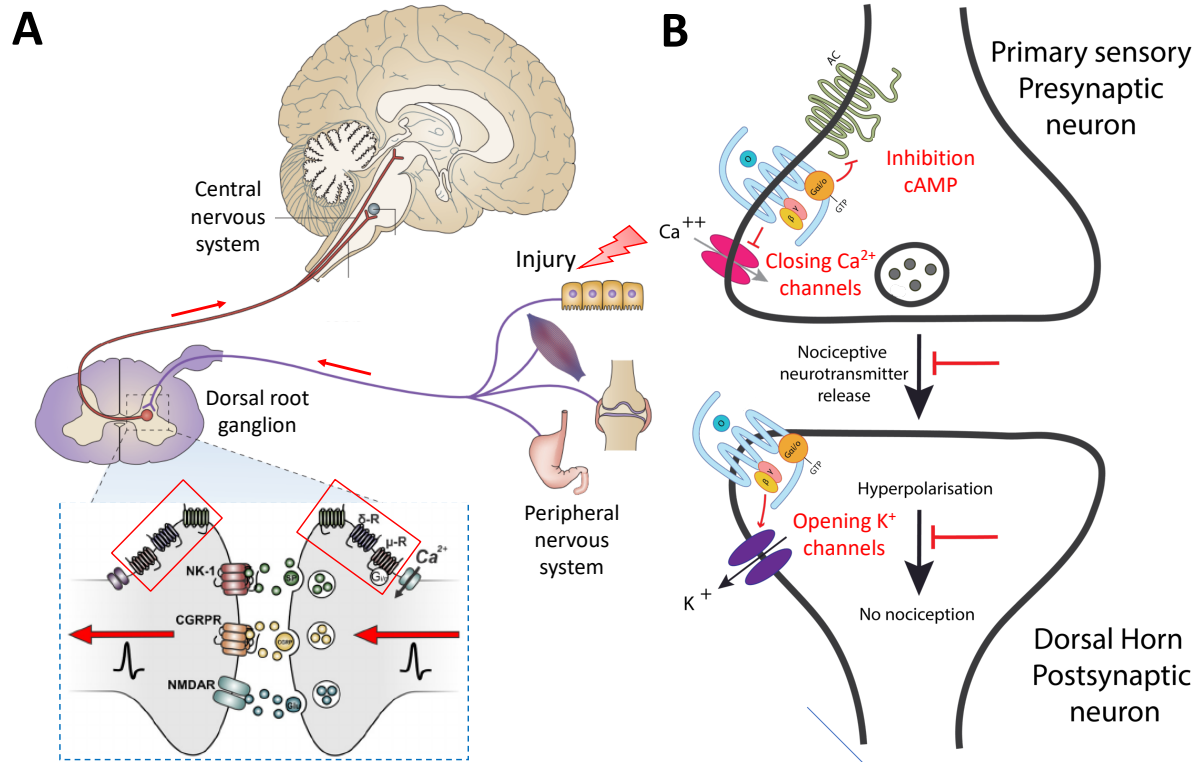


Figure 1.5 Opioid-induced analgesia. (A) In the transmission of pain, the noxious stimulus is received by sensory neurons in the periphery and is transmitted through the spinal cord to the sensory cortex in the central nervous system where the pain is perceived. Pro-nociceptive neurotransmitters bind the corresponding GPCRs such as neurokinin 1 (NK-1), calcitonin-gene related peptide receptor (CGRP) and N-methyl-D-aspartate receptors (NMDAR) in second-order neurons to transmit the nociceptive signal. Opioid receptors (red box) are expressed within the synapse and modulate pain transmission. **(B)** At the presynaptic level, opioid receptors activate inhibitory G proteins resulting in inhibition of cAMP production and closing calcium channels, this restricts the release of proinflammatory neurotransmitters. At the postsynaptic level, opioid receptors open potassium channels, resulting in hyperpolarisation and attenuation of the excitability of neurons.

1.2.2 Opioid receptors

Opioid receptors are members of the family A GPCRs. Three separate genes encode distinct opioid receptor subtypes: *Oprm1* encodes the μ-opioid receptor (MOP), *Oprd1* encodes the δ-opioid receptor (DOP) and *Oprk1* encodes the κ-opioid receptor (KOP) (Dhawan et al., 1996), nomenclature according to (Alexander et al., 2017). Additionally, the 'opioid-related' human nociception/orphanin FQ peptide receptor (NOP) is encoded by *Oprl1.* The first three opioid receptors share the highest sequence homology, at around 70% (Mollereau et al., 1994). The fourth member of the family, NOP, also shares a high degree of structural homology, but its orthosteric binding site and pharmacology are very different from the other members of the family (A. A. Thompson et al., 2012). As a result, NOP recognises different endogenous and synthetic ligands (Reinscheid et al., 1995). Currently there are numerous clinically used opioid drugs, all of which target the MOP which is the focus of this thesis.

Alternative splice transcript variants of the *Oprm1* gene have been described (Pasternak & Pan, 2013). GPCR alternative splicing is widespread and the process includes alternative splice donors and acceptors, novel introns, intron retentions, exon skips and novel exons, all of which diversifies the GPCR superfamily (Einstein et al., 2008). Similar splicing patters are observed for human, mouse and rat MOP. The mouse *Oprm1* gene contains two independent promoter regions (E1 and E11 promoters). The most common mouse MOP isoform uses E1 promoter and contains exons 1, 2 and 3 which encode the 7TM domains followed by exon 4 which encodes the C-term tail. Alternative splicing downstream of exon 3 generates twelve multiple variants that only differ in their C-terminal amino acid sequence (7TM isoforms) (Pan et al., 2005). In addition to this series of functional prototypic 7TM isoforms, transcription from promoter E1 also produces a truncated splice variant that contains only exon 1 which encodes the first TM domain with four variants of the C-term sequence (1TM isoforms). Alternatively, promoter E11 produces a functional truncated variant that contains six TM domains encoded by exons 2 and 3 and three distinct variants in the C-term sequence (6TM isoforms) (Marrone et al., 2016). The different splice variants have distinct subcellular, cellular and tissue distribution and have distinct pharmacological profiles (Xu et al., 2014). For example, the 7TM variant that contains exon 4 is most widely expressed within the spinal cord, striatum, hippocampus, PAG and brainstem but it is poorly expressed

within the prefrontal cortex, thalamus and hypo-thalamus where other 7TM variants predominate (Xu et al., 2014). Interestingly, specific pharmacological targeting of the 6TM isoform by the atypical opioid drug IBNtxA causes strong analgesia with minimal respiratory depression, constipation, sedation, reward and physical dependence compared to morphine stimulation of the 7TM isoform (Lu et al., 2015).

In addition to splice variants, functionally relevant single nucleotide polymorphisms (SNPs) in human MOP have been described (Befort et al., 2001; Oertel et al., 2009). Recent pharmacogenomics studies have shown that the MOP is one of the most variable GPCR drug targets within the human population (Hauser et al., 2018). Specifically, three variants were studied in a G protein activation assay: M153V resulted in partial loss of function; K235N behaved like the wild-type receptor in response to an endogenous peptide agonist but displayed a gain of function for the partial agonist buprenorphine; and V302I exhibited gain of function for full agonists and partial agonists (Hauser et al., 2018). Both gain of function receptor variants maintained G protein signalling when treated with the antagonist naloxone, suggesting that individuals with such variants could have increased risk of overdose due to a loss of efficacy of the antagonist treatment.

Post-translational modifications such as O- and N-glycosylation in the N-term seem to be important for DOP maturation and export to plasma membrane (Petaja-Repo et al., 2001; Petaja-Repo, Hogue, Laperriere, Walker, & Bouvier, 2000), whereas N-glycosylation of MOP does not affect its function (Rostami, Rabbani, & Mir-Mohammad-Sadeghi, 2010). Additionally, the C-term tail contains putative phosphorylation sites (S/T and tyrosine residues) that are involved in receptor regulation; and a conserved cysteine residue usually involved in GPCR palmitoylation. However, mutation of this cysteine has been shown not to affect palmitoylation of the MOP (C. Chen, Shahabi, Xu, & Liu-Chen, 1998).

Altogether, the multiple functional MOP variants generated by alternative splicing, SNPs and post-translational modifications will likely impact opioid pharmacology and could account for clinical differences among individuals in regard to relative analgesia and side effects of opioid drugs.

1.2.3 Opioid ligands

A large family of at least 20 different small peptides constitute the endogenous opioid ligands (Goldstein & Cox, 1977; Guillemin et al., 1977; Hughes et al., 1975). Most of them are generated by proteolytic cleavage of three precursor proteins, pro-opiomelanocortin, pro-enkephalin and pro-dynorphin, which results in the production of three major classes of biologically active endogenous opioid peptides: endorphins, enkephalins and dynorphins, respectively. The peptides range from 5 to 30 amino acids in length and share a common N-terminal tetrapeptide sequence Tyr-Gly-Gly-Phe, with either a Leu or Met in the fifth position (Fig. 1.6A) (Corbett, Henderson, McKnight, & Paterson, 2006). Despite the lack of selectivity for one receptor subtype, these peptides have varying affinities for different opioid receptors: endorphins have greater affinity for MOP, enkephalins for DOP and dynorphins for KOP (Janecka, Fichna, & Janecki, 2004; Mansour, Hoversten, Taylor, Watson, & Akil, 1995). The synthetic opioid peptide DAMGO ([D-Ala2,N-Me-Phe4,Gly5-ol]-enkephalin) is a derivative of enkephalins and has high MOP specificity (Fig. 1.6B). There are also two additional highly selective MOP tetrapeptides, endomorphin-1 and endomorphin-2 (Zadina, Hackler, Ge, & Kastin, 1997), which are structurally unrelated to the typical opioid peptides, but their precursor peptide or encoding gene have not yet been identified (Terskiy et al., 2007). Thus, the status of these peptides as endogenous ligands remains unproven.

Opioid receptors can also be activated by exogenous, natural occurring small molecules found in the opium poppy plant *Pappaver somniferum*. Reports of the earliest use of opium date from 3400 B.C. in Mesopotamia, where it was used as an analgesic and recreational drug. This makes opium one of the oldest drugs in human history (Brownstein, 1993). However, it was not until the 19th century that the individual alkaloid components including morphine (Fig. 1.6C) and codeine were isolated from the opium extract. Another class of natural alkaloids from the plant *Mitragyna speciosa* (“kratom” in Thailand) has been used in Southeast Asia for centuries to treat a variety of ailments, and displays opioid-like effects. Functional characterisation of mitragynine, the primary alkaloid in the plant, as well the potent oxidized analogue 7-hydroxymitragynine, has demonstrated that they act as partial agonists at the MOP and competitive antagonists at the KOP and DOP (Kruegel et al., 2016).

As opioid use increased, the adverse effects including tolerance, physical dependence and addiction became quickly apparent. During the 20th century, semisynthetic opiates of different agonist efficacy such as oxycodone (full), buprenorphine (partial) (Fig. 1.6D) and naloxone (antagonist) were generated (Fig. 1.6E). Fully synthetic opiates such as methadone and fentanyl (Fig. 1.6F) have also been developed in the search for non-addictive opioid substitutes (Rosenblum, Marsch, Joseph, & Portenoy, 2008). A number of different strategies and formulations have been designed in the pursue of opioid analgesics with improved therapeutic profiles. Most of them have focused on enhancing signal transduction at the MOP by designing more potent, efficacious and long-lasting agonists such as methadone and fentanyl. Although successful at causing analgesia, the sustained signalling achieved with these drugs is not favorable for the side effect profile (Berger & Whistler, 2010). Recent emphasis has been placed on the generation of biased opioid agonists. G protein-biased MOP agonists hold promise as improved analgesics with reduced on-target adverse effects due to the lack of arrestin signalling. The three most recent G protein-biased MOP agonists are TRV130, PZM21 and SR-17018 (Fig. 1.6G) and will be discussed further in chapter 2.

In summary, pharmacological targeting of MOP remain the gold standard treatment for pain and is also pursued for the therapeutic treatment of many other conditions including coughing, diarrhoea, as drug replacements to treat addiction and withdrawal symptoms from high abuse substances, as well as to reverse opioid overdose. Currently, drugs targeting the MOP constitute nearly 40 out of the 475 total current FDA-approved drugs (Hauser et al., 2018). Although opioids are effective treatments, 'on-target' adverse effects limit their clinical utility. Moreover, the number of people chronically abusing and/or falling victim to opioid overdose has skyrocketed in recent years, causing the current opioid epidemic crisis (Floyd & Warren, 2018; Manchikanti et al., 2012). Much remains to be understood in order to overcome opioid therapy limitations.

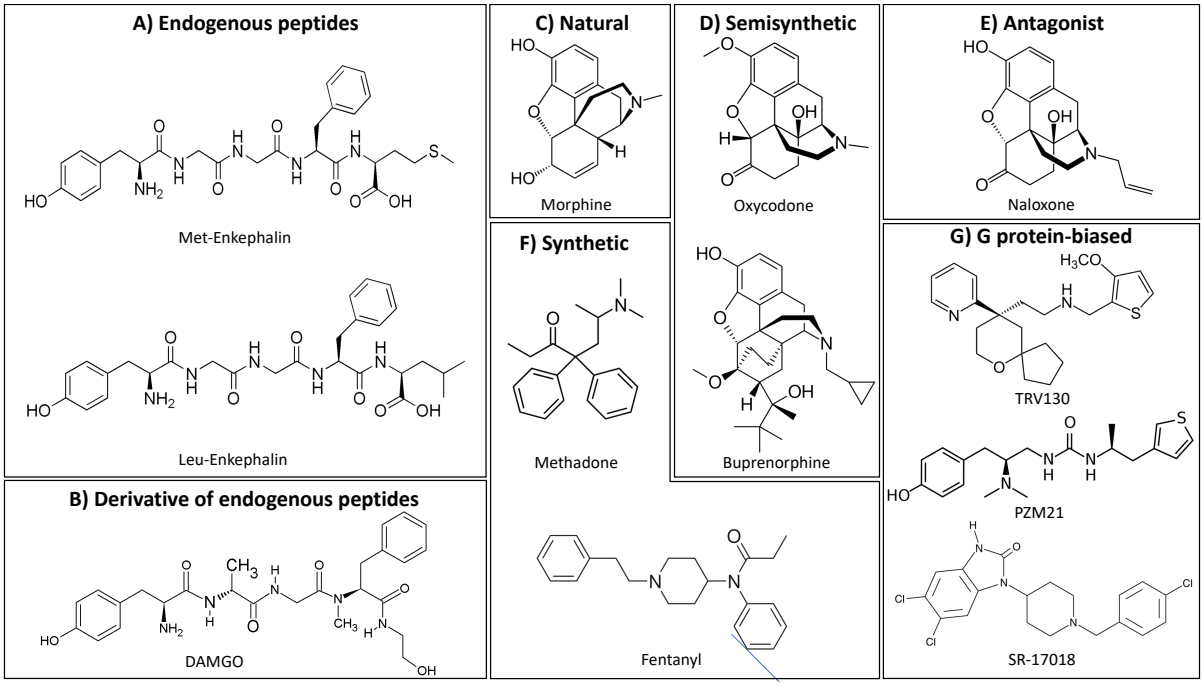


Figure 1.6 Chemical structures of the MOP ligands used in this study. (A) Endogenous peptides: Met-Enkephalin and Leu-Enkephalin. **(B)** Derivative of endogenous peptides: DAMGO. **(C)** Natural agonist: morphine. **(D)** Semisynthetic agonists: oxycodone and buprenorphine. **(E)** Antagonist: naloxone. **(F)** Synthetic agonists: methadone and fentanyl. **(G)** G protein-biased agonists: TRV130, PZM21 and SR-17018.

1.2.4 Patho-physiology

The MOP is the main therapeutic target of current analgesics against acute and severe pain. However, chronic opioid use leads to tolerance, physical dependence, addiction and constipation, all of which severely limit the long-term clinical utility of opioids. Moreover, MOP activation can lead to respiratory depression, which is the major cause for overdose incidents. These 'on-target' adverse effects are due to systemic administration of drugs activating opioid receptors in areas outside of the pain transmission pathway. For example, constipation is caused by activation of opioid receptors within the myenteric plexus of the gastrointestinal tract (Wood & Galligan, 2004), while decreased respiratory function is mediated by activation of opioid receptors within the brainstem (Takita, Herlenius, Lindahl, & Yamamoto, 1997). However, the molecular mechanisms underlying opioid effects are more difficult to pinpoint, thus the specific downstream signalling pathways responsible for analgesia versus adverse effects remain to be determined.

Deletion of the MOP gene abrogates morphine-induced analgesia, tolerance and dependence (Loh et al., 1998; Matthes et al., 1996), indicating that MOP is responsible for both analgesic and undesired effects. Exogenous opioid drugs have a higher liability for inducing tolerance and addiction than the endogenously released native peptide ligands (Whistler, Chuang, Chu, Jan, & von Zastrow, 1999). The main difference is that native opioid peptides are released in a phasic manner at the synaptic terminals of opioidergic neurons and they are rapidly degraded by proteolytic enzymes. In contrast, exogenous opioids are usually administered systemically and remain in the body until complete clearance of the drug. Thus, duration of opioid exposure and systemic administration could be an explanation for the development of opioid tolerance and side effects.

Desensitisation of MOP signalling occurs within seconds to minutes after initiation of exposure to agonists (Williams et al., 2013) and seems to be one of the initial steps for the development of tolerance. Rapid desensitisation in the order of seconds to minutes occurs at the level of ion channels, while desensitisation in the order of tens of minutes occurs at the level of enzymes (e.g. AC, MAPK) and is also affected by other counter-regulatory mechanisms such as receptor internalisation and trafficking (Whistler et al., 1999).

Cellular tolerance is a more complex and multifaceted process by which the receptor response is reduced after chronic exposure to the drug. Tolerance includes mechanisms that involve receptor regulation such as phosphorylation, G protein uncoupling, desensitisation, internalisation and down-regulation (Allouche, Noble, & Marie, 2014), as well as activation of anti-opioid systems (e.g. Neuropeptide FF and NDMA receptors) (Ueda & Ueda, 2009). In addition, cellular and synaptic adaptations occur during the development of opioid tolerance (Williams et al., 2013). For example, chronic opioid use causes microglia and astrocyte activation which have been involved in analgesic tolerance and opioid-induced hyperalgesia (Tumati et al., 2012; Watkins, Hutchinson, Rice, & Maier, 2009). Moreover, activation of MOP in primary afferent nociceptors initiates counter-adaptations to opioids which are responsible for the development of tolerance and opioid-induced hyperalgesia and it is proposed that the combination of opioid agonists with peripheral MOP antagonists will limit such mal-adaptive processes (Corder et al., 2017).

1.3 The μ-opioid receptor

1.3.1 Structures

In recent years, there has been significant progress in the elucidation of the structural characteristics of the MOP. There are inactive (Manglik et al., 2012) and active (Huang et al., 2015) crystal structures, as well as a cryo-EM structure of the MOP in complex with an inhibitory G protein (Koehl et al., 2018) (Fig. 1.2).

The first MOP structure was a 2.8 Å X-ray crystal structure of the *Mus musculus* MOP fused to T4-lysozyme and bound to β-funaltrexamine (β-FNA), an irreversible morphinan antagonist (Fig. 1.2A) (Manglik et al., 2012). This revealed that the orthosteric binding pocket involves contacts between the ligand and TM domains 3, 5, 6, and 7, with the $K233^{5.39}$ (superscript numbers indicating residue position according to Ballesteros-Weinstein (Ballesteros & Weinstein, 1995) side chain being the site of covalent attachment for the ligand β-FNA. Similar to the β2AR, the binding pocket for MOP sits deep within the receptor. However, in contrast to the muscarinic receptors, it is wide and open. The exposed extracellular surface above the ligand may explain why extremely potent opioids present rapid dissociation half-lives (Cassel, Daubert, & DeHaven, 2005). Opioid ligands are composed of two parts according to the message/address model (Portoghese, Sultana, & Takemori, 1990). The 'message' carries the activity of the ligand (agonist or antagonist) and is recognised by deep conserved residues within the binding pocket (Manglik et al., 2012). Whereas the 'address' confers selectivity for the different opioid receptor subtypes and is recognised by divergent residues distal to the binding site (Granier et al., 2012).

Interestingly, in the inactive structure, MOP crystallised as a two-fold symmetric dimer tightly associated through TM5 and TM6 and allosteric modulation between protomers was suggested (Manglik et al., 2012). Despite the non-physiological conditions required for crystallographic studies, additional evidence supports the physiological relevance of both homo- and hetero-dimers involving MOP (Jordan & Devi, 1999). For homodimers, it has been suggested that tolerance to morphine *in vivo* is reduced through the allosteric interaction of one MOP protomer bound to DAMGO or methadone that facilitates endocytosis of an

adjacent protomer bound to morphine (L. He, Fong, von Zastrow, & Whistler, 2002; L. He & Whistler, 2005). For heterodimers, similarly, the allosteric interaction between an antagonist-bound DOP and a morphine-bound MOP protomer improves morphine efficacy (Gomes, Ijzerman, Ye, Maillet, & Devi, 2011). Additionally, disruption of the MOP-DOP heterodimer in the mouse spinal cord, results in an enhancement of morphine analgesia and a reduction in morphine tolerance by preventing DOP-mediated co-degradation (He et al., 2011). However, for MOP at least, dimerisation does not seem to be required for signalling (Kuszak et al., 2009).

Adjacent to the orthosteric binding pocket, a sodium ion interacts with TM2, 3, and 7 and serves as a negative allosteric modulator by stabilising the inactive state of the receptor and decreasing agonist affinity. This effect of sodium was first identified in radioligand binding assays of opioid receptors (Pert, Pasternak, & Snyder, 1973), although it has only recently been described in high-resolution structural detail (Katritch et al., 2014). Pharmacological targeting of this allosteric site with exogenous small molecule allosteric modulators has the potential of enhancing the effects endogenous opioids while avoiding many of the adverse effects seen with exogenous opioid drugs (Livingston & Traynor, 2018).

The active state of MOP has also been studied in a 2.1 Å X-ray crystal structure of the MOP bound to the morphinan agonist BU72 and stabilised by a G protein-mimetic camelid antibody fragment, Nb39 (Fig. 1.2B) (Huang et al., 2015). The agonist BU72 and the antagonist β-FNA occupied a similar pose in the orthosteric binding pocket, thus the structural features within the ligand binding pocket between active and inactive MOP are very similar. The only difference was that in the active state, the extracellular domains formed a lid over the ligand binding pocket. During MOP activation, the ionic lock interaction that normally stabilises TM6 in an inactive conformation is broken and TM6 undergoes a 10 Å outward movement (Huang et al., 2015). The inactive MOP structure identified a dimer interphase that involved TM5 and TM6, however due to steric clash with the outward movement of TM6 in the active state, this dimeric interaction would not be compatible.

The inactive and active crystal structures provide snapshots of two conformational states of MOP, however this does not speak of the intermediate conformational states and

the dynamic sequence of events that lead to receptor activation. Solution-state nuclear magnetic resonance (NMR) has been used to examine the dynamic conformations involved in MOP activation (Sounier et al., 2015). Upon binding of the agonist BU72, the ECL2 containing K209 undergoes a conformational change that initiates the active state of MOP. No change was observed when nanobody 33 (Nb33) alone was present, indicating that the change around K209 was merely due to agonist binding. Co-treatment with both BU72 and Nb33, increased the NMR changes observed for agonist alone. Other spectral changes within ICL1, H8 and the receptor N-term domain were also observed upon binding of BU72 alone. Interestingly, in the active state crystal structure, it was revealed that the receptor N-term folds into the binding pocket and interacts with BU72. This 'closed lid' restricts the dissociation of ligands from the orthosteric pocket and is a result of the allosteric communication between the G protein and ligand binding sites (DeVree et al., 2016).

Remarkably, the effects of the ternary complex were more pronounced in the intracellular part of MOP, with the reposition of lysine residues contained in TM5 and TM6 for the 10Å outward movement of TM6 (Sounier et al., 2015). Additionally, it was proposed that the intracellular regions of ICL1/H8 are the initial point for interaction with the G protein before further docking of the G protein into the receptor core that stabilises TM5 and TM6 in a fully open and active conformation.

The active state MOP coupled to heterotrimeric Gi has also been elucidated in a 3.5 Å cryo-EM structure (Fig. 1.2C) (Koehl et al. 2018). In this structure, the receptor was bound to the agonist peptide DAMGO, despite the larger size and flexibility of the peptide, it occupies the morphinan ligand pocket in a very similar pose. The similarity of this structure with the previous MOP-Nb39 structure revealed that residue changes involved in ligand-mediated activation are not specific to a particular intracellular binder. Although, TM6 was further displaced when MOP was coupled to Gi compared to Nb39, the opening of the G protein cavity was smaller for inhibitory G proteins compared to the structure of β2AR coupled to stimulatory G protein. Additionally, it was shown that the C-terminal α5 of the G protein that interacts with TM5 and TM6 of the receptor contains bulkier residues in Gs than in Gi, revealing some insights into differences for G protein-coupling selectivity.

1.3.2 Agonist-induced MOP regulation

High-resolution structures have provided valuable insights into the structural features underlying MOP ligand binding, receptor activation and G protein coupling. Additionally, decades of research have shown that differential regulation of the MOP contributes to receptor desensitisation and tolerance (Dang & Christie, 2012; Williams et al., 2013).

Endogenous opioid peptides such as Met-enkephalin and its derivative DAMGO, as well as synthetic opioid agonists such as methadone and fentanyl are efficacious at mediating G protein activation, as well as triggering MOP regulatory events such as receptor phosphorylation, β-arrestin recruitment and receptor internalisation and recycling (Keith et al., 1998; Whistler et al., 1999). High-efficacy agonists trigger a hierarchical phosphorylation cascade mediated by GRK2/3 that firstly phosphorylates S375 and then proceeds to phosphorylate the flanking S/T residues within the C-term tail (Y. J. Chen et al., 2013; Lau et al., 2011). As a consequence, this multi-phosphorylation promotes robust β-arrestin1 and β-arrestin2 recruitment and receptor internalisation. DAMGO-induced desensitisation is GRK2- and β-arrestin dependent (Johnson et al., 2006). DAMGO-desensitised receptors are then internalised and recycled back to the plasma membrane in a resensitisation step.

In contrast, morphine induces minimal receptor phosphorylation and limited β-arrestin recruitment, which results in compromised receptor internalisation and resensitisation (Just et al., 2013; Keith et al., 1996). However, overexpression of GRK2 enhances morphine capacity to promote phosphorylation and β-arrestin translocation (Zhang et al., 1998). This is illustrated by the fact that, in striatal neurons, which express high levels of GRK, morphine is able to cause internalisation (Haberstock-Debic et al., 2005). Studies in human embryonic kidney 293 (HEK293) cells as well as *in vivo* evidence have shown that GRK5 phosphorylates the MOP at S375 upon stimulation with morphine (Glück et al., 2014; Just et al., 2013). However, this phosphorylation is not sufficient to cause receptor endocytosis (Just et al., 2013; Yousuf et al., 2015). It has been suggested that the sustained phosphorylation of S375 induced by morphine leads to accumulation of desensitised receptors at the plasma membrane that cannot resensitise in due to the lack of internalisation (Schulz et al., 2004).

GRK2 and GRK5 are expressed in brain regions where the MOP is also abundant such as the hippocampus and locus coeruleus. Interestingly, differential distribution between GRK2 and GRK5 was detected in the periaqueductal gray (PAG). Strong GRK5 mRNA-positive cells were abundantly and uniformly distributed throughout the PAG, whereas only a few GRK2 mRNA-positive cells with lower staining intensity were present in the ventral and dorsal part of PAG (Fan, Zhang, Zhang, Yue, & Ma, 2002). The specific abundance of GRK in MOP-expressing neurons has not yet been established, however, specific GRK expression patterns in different brain regions could influence MOP regulation.

Additional mechanisms have been described to be involved specifically in MOP desensitisation and tolerance to morphine (Bailey et al., 2009). Morphine-induced desensitisation of Ca^{2+} and GIRK channels has been linked to the activation of PKC (Chu, Zheng, Zhang, Loh, & Law, 2010; Johnson et al., 2006). PKC activation leads to MOP phosphorylation at S363 (Feng, Li, & Wang, 2011; Illing, Mann, & Schulz, 2014) and has been implicated in the ability of morphine to induce MOP desensitisation in neurons (Bailey et al., 2009). Moreover, basal phosphorylation at S363 has also been described (Johnson et al., 2006). However, this basal phosphorylation does not lead to constitutive association of arrestin with the receptor (Zhang et al., 1998), in fact mutation of S363 enhances agonist-induced MOP internalisation (El Kouhen et al., 2001). Additionally, basal phosphorylation at T370 by calcium/calmodulin-dependent protein kinase II (CaMKII) has been described (Y. Chen, Yang, & Wang, 2010) and CaMKII activation has also been implicated in morphine tolerance (Tang, Shukla, Wang, & Wang, 2006). Together, this indicates that the activation of agonist-specific kinases could lead to differential regulation and signalling elicited downstream of the same receptor.

1.3.3 Agonist-induced MOP signalling

In regard to signalling, most MOP agonists cause efficient activation of G proteins leading to cAMP inhibition and activation of GIRK channels. However, other downstream signalling pathways are differentially activated by different ligands. It has previously been described that agonists such as morphine and methadone activate ERK via the PKC-dependent pathway, and results in subsequent phosphorylation of p90 ribosomal S6 kinase

which induces the activity of transcription factor cAMP response element-binding protein (Zheng, Loh, & Law, 2008). In contrast, agonists such as etorphine and fentanyl activate ERK in a β-arrestin-dependent manner and the phosphorylated ERK translocates into the nucleus, resulting in the increased gene transcription of GRK2 and β-arrestin2 (Zheng et al., 2008).

Additionally, our group recently expanded on these findings (Appendix 1) by identifying that the distinct spatiotemporal signalling downstream of MOP activation is dictated by the different distribution of the MOP at the plasma membrane (Halls et al., 2016). Activation of the MOP by DAMGO caused a transient increase in both cytosolic and nuclear ERK phosphorylation (Fig. 1.7A), whereas morphine caused sustained activation of PKC at the plasma membrane and ERK phosphorylation only in the cytosol (Fig. 1.7B) (Halls et al., 2016). Interestingly, the distinct signalling profiles elicited by morphine and DAMGO are not dependent on their agonist-selective regulation in terms of internalisation, but instead depend on agonist-induced lateral redistribution of the receptor within the plasma membrane (Halls et al., 2016). Inhibitors of PKC and the Gβγ subunit, as well as disruption of the lipid composition of the plasma membrane, allowed the lateral redistribution of morphine-bound MOP similar to DAMGO, without receptor internalisation (Fig. 1.7C)(Halls et al., 2016). In these conditions, morphine elicited the same spatiotemporal signalling profile as DAMGO (Halls et al., 2016). These results highlight the importance of membrane structure for the compartmentalisation of MOP signalling.

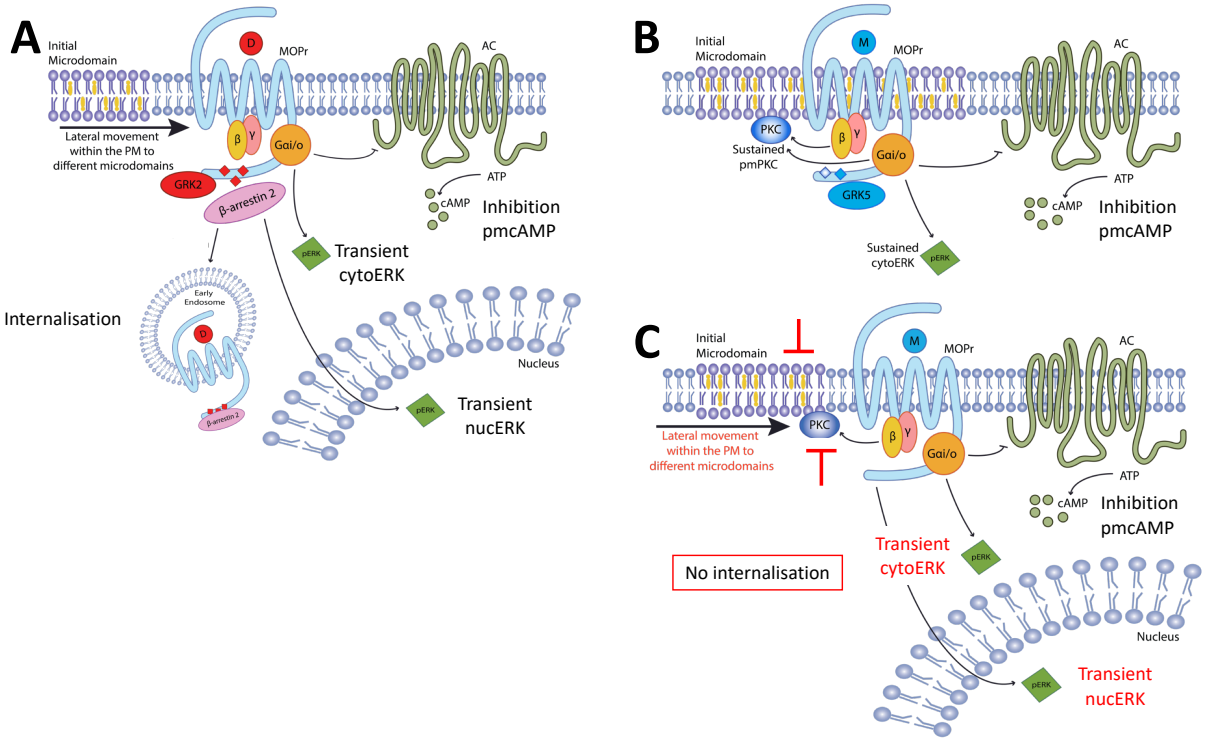


Figure 1.7 Spatiotemporal signalling of the MOP is dictated by its plasma membrane distribution. (A) Activation of the MOP DAMGO causes $G\alpha_{i/o}$-dependent inhibition of cAMP at the plasma membrane and transient increase in cytosolic ERK and a β-arrestin2-mediated transient increase in nuclear ERK phosphorylation. **(B)** Similar to DAMGO, morphine causes $G\alpha_{i/o}$-dependent inhibition of cAMP. However, the increase in ERK phosphorylation is restricted to the cytosol and is sustained. Moreover, morphine causes a Gβγ-mediated PKC activation at the plasma membrane. **(C)** When the Gβγ-PKC axis was inhibited, or cholesterol was depleted, morphine mimicked the signalling of DAMGO without internalisation. Instead morphine caused a receptor distribution at the plasma membrane that was similar to DAMGO.

1.3.4 Biased agonism at the MOP

Theoretically, through biased agonism, GPCRs have the potential to activate a particular signalling pathway over others by stabilising a receptor conformation that is preferential for a particular effector. Opioid ligands have been shown to promote different receptor conformational changes (Morse, Sun, Tran, Levenson, & Fang, 2013), coupling to different Gα subtypes (Masuho et al., 2015) and regulation by RGS proteins (Traynor, 2012). Many studies have also described agonist-specific differences in terms of MOP regulation including desensitisation, phosphorylation, endocytosis and trafficking (Groer, Schmid, Jaeger, & Bohn, 2011; Pradhan, Smith, Kieffer, & Evans, 2012; Raehal, Schmid, Groer, & Bohn,

2011). However, the ligand-specific differences in receptor regulation and signalling could be simply be due to differentially regulated downstream signals rather than bias from the receptor conformation standpoint.

The most well-characterised form of biased agonism for the MOP refers to bias between G protein activation and β-arrestin2 recruitment. Previous studies have shown that a β-arrestin2 gene knockout (KO) mouse showed enhanced and prolonged analgesia with very little morphine tolerance (Bohn et al., 2002). Moreover, coupling to β-arrestin2 has been associated with some of the undesired effects of opioids including respiratory depression and constipation (Raehal et al., 2005). Consequently, biased agonism towards the G protein pathway and away from the β-arrestin2 pathway is currently being exploited to develop safer MOP-targeting analgesics with reduced on-target adverse effects.

The first G protein-biased MOP agonist described was herkinorin, a derivative of salvinorin A that does not promote any β-arrestin2 recruitment and showed long lasting anti-nociception (Groer et al., 2007; Lamb, Tidgewell, Simpson, Bohn, & Prisinzano, 2012). Another G protein-biased MOP agonist is oliceridine (TRV130), which has progressed to clinical trials and shows effective analgesia and less gastrointestinal and respiratory dysfunction compared to morphine (DeWire et al., 2013; Soergel et al., 2014). Moreover, structure-based drug discovery approaches have identified PZM21, as a potent Gαi protein activator with exceptional selectivity for MOP and minimal β-arrestin2 recruitment (Manglik et al., 2016). Another recent study has assessed clinically relevant opioid analgesics for correlation between their bias factor and therapeutic window (Schmid et al., 2017). They found that fentanyl, an opioid drug that is more likely to induce respiratory suppression at weak analgesic doses, appeared to be biased towards β-arrestin2 over the G protein pathway (Schmid et al., 2017). Additionally, they synthesised a range of G protein-biased compounds from which SR-17018 displayed the largest bias away from arrestin and the safest therapeutic window (Schmid et al., 2017). Finally, another G protein-biased agonist, TRV0109101 does not promote opioid-induced mechanical allodynia after chronic administration (Koblish et al., 2017).

Despite the recent efforts in the generation of G protein-MOP biased agonists, the benefits of 'G protein over β-arrestin bias' are far from clear when other studies are considered. For example, some adverse effects are reversed when G protein downstream effectors such as GIRK channels are inhibited (Campbell & Smrcka, 2018; X. Liang, Yong, & Su, 2018). Moreover, endogenous opioid peptides, which do not cause adverse effects to as much extent as exogenous agonists, are 'balanced agonists', meaning that they promote MOP engagement with both G protein and arrestins to a similar extent. In fact, opioid peptides such as endomorphin-1 and endomorphin-2, have been shown to be biased towards β-arrestin recruitment (McPherson et al., 2010; Rivero et al., 2012; Thompson et al., 2015). However, it is very difficult to compare the actions of endogenous peptide agonists with clinical exposure to opioid drugs, since endogenous peptides are released in a pulsatile manner, and thus are subject to a tight temporal regulation that is not present when clinically used opioids are administered.

It has been proposed that ligands such as morphine, that only promote a weak MOP-arrestin interaction not sufficient to cause receptor endocytosis, would cause progressive accumulation of arrestin-bound desensitised receptors at the plasma membrane without significant receptor recycling and resensitisation. Thus, in agreement with the 'G protein over β-arrestin bias' theory, Groer et al. suggest that drugs that activate the receptor without recruiting any arrestins are promising for the development of opiate analgesics that distinguish between agonist activity and receptor regulation (Groer et al., 2007).

On the other hand, if the receptor is not desensitised and remains activated at the membrane, the abnormal prolonged signalling could, in turn, trigger systemic adaptations that manifest in tolerance and physical dependence (Berger & Whistler, 2010). Consistent with this, some studies suggest that ligands like morphine, that promote interactions with G proteins more strongly than they promote interactions with arrestins, show the greatest addictive potential (Molinari et al., 2010). In this line, other studies propose that the β-arrestin-mediated regulation of opioid receptors by endocytosis serves as a protective mechanism in reducing tolerance (Whistler et al., 1999). They indicate that drugs such as methadone and etorphine that induce less tolerance than morphine (Duttaroy & Yoburn,

1995; Mercadante et al., 1998; Rezvani, Huidobro-Toro, Hu, & Way, 1983), present a RAVE (relative activity versus endocytosis) value close to 1 and similar to opioid peptides, whereas morphine presents a RAVE value of 4 due to its poor internalisation (Whistler et al., 1999). They propose that agonists that promote MOP internalisation similar to endogenous ligands would be expected to produce less tolerance (Berger & Whistler, 2010). Additionally, a strong correlation between agonist efficacy and MOP regulation including phosphorylation, β-arrestin recruitment and internalisation has been shown (McPherson et al., 2010; Szekeres, Koenig, & Edwardson, 1998); suggesting that the G protein and arrestin pathways are well interconnected and might not be easy to separate through the stabilisation of different receptor active states.

In conclusion, biased agonism could potentially be an invaluable avenue for the development of better analgesics. However, it is important to elucidate the exact molecular mechanisms underlying MOP pharmacology. A further analysis of G protein-biased agonism at MOP is presented in chapter 2.

1.4 Scope of thesis

The MOP receptor remains the primary target for the treatment of pain, despite the numerous side effects associated with the use of opioid analgesics. Increasing public attention is concentrating in the opioid field because of the current 'opioid epidemic' crisis within western societies. Thus, there is tremendous interest in the generation of new opioid drugs that present improved therapeutic profiles. G protein-biased MOP agonists are emerging as promising drug candidates, and one of them is currently pending approval by the FDA. While some studies demonstrate that G protein-biased MOP agonists retain analgesia without causing constipation or respiratory depression, there are discrepancies with other studies that demonstrate that they are not devoid of such adverse effects. Furthermore, statistical comparison of their bias quantification is usually hampered by their low efficacy in arrestin recruitment and some studies have shown that these ligands display overall low agonist activity at the MOP. Consequently, a more comprehensive and comparative study of such G protein-biased MOP agonists is required to clarify whether biased agonism or low agonist efficacy could be the underlying mechanism behind their improved therapeutic profiles.

Novel mechanisms are increasingly recognised to participate in the regulation of GPCRs. In particular, the plasma membrane organisation of the MOP dictates the differential spatiotemporal signalling elicited by opioid agonists. Furthermore, repeated exposure to opioid drugs results in receptor desensitisation and tolerance. Although the precise molecular mechanisms underlying opioid tolerance have not been fully resolved, receptor phosphorylation by GRKs and arrestin recruitment play an important role in receptor desensitisation.

Accordingly, the aims of the work described in this thesis are:

1. Development of tools to investigate the most recent G protein-biased agonists at pathways proximal to receptor activation (Chapter 2).
2. Assess the plasma membrane organisation of MOP in live cells (Chapter 3).
3. Determine the role of specific phosphorylation sites in MOP regulation and desensitisation (Chapters 4 and 5).

Chapter 2

Novel BRET biosensors reveal differences in efficacy of various classes of MOP agonists

2.1 Abstract

The μ-opioid receptor (MOP) is the main therapeutic target for the treatment of acute and chronic pain. Opioid drugs mediate their analgesic effects through activation of the MOP in a similar manner to endogenous opioid peptides, but unfortunately, they also mediate many on-target adverse effects. Biased agonism towards the G protein pathway and away from the β-arrestin2 pathway is currently being exploited for the development of safer and more effective MOP-targeted analgesics. However, there are reports suggesting that these biased drugs are not devoid of side effects. Here, we present the use of novel genetically encoded Bioluminescence Resonance Energy Transfer (BRET) biosensors in live cells to measure ligand efficacy at events proximal to receptor activation. Using a wide range of opioid ligands, ranging from endogenous opioid peptides to synthetic opioids and the three most recently described G protein-biased MOP agonists (TRV130, PZM21 and SR-17018), we measured the direct recruitment of nanobody 33 (Nb33-Venus) and a mini G protein variant (mGsi-Venus) to MOP-NanoLuc. Additionally, we used more canonical G protein signalling assays such as $G\alpha_{i2}$ activation and cAMP inhibition, as well as GRK2 and β-arrestin2 recruitment and internalisation assays, in order to compare bias factors and the efficacy of these ligands head-to-head. We did not observe G protein bias for any of the so-called G protein-biased MOP agonists. In contrast, we found a strong correlation between the agonist ability to stabilise an active receptor state and efficacy for G protein and β-arrestin2 pathways. This is in line with the idea that the improved therapeutic profiles observed for the novel agonists might result from an ideal efficacy threshold (i.e. partial agonism) that is sufficient to cause analgesia without triggering adverse effects.

2.2 Introduction

Analgesics targeting the μ-opioid receptor (MOP) are the mainstay treatment for severe acute, perioperative, and chronic pain. However, agonists that activate MOP are also responsible for many on-target adverse effects that severely limit their use in the clinic, including analgesic tolerance and hyperalgesia, nausea and vomiting, constipation and respiratory depression (Inturrisi, 2002). Moreover, the misuse of opioids has increased dramatically, reaching epidemic levels of abuse and overdose globally (Floyd & Warren, 2018; Manchikanti et al., 2012). In the hope to improve the therapeutic window of opioid analgesics, the development of drugs that dissociate the signalling pathways linked to opioid analgesia from those mediating their adverse effects (e.g. biased agonists) is currently being pursued.

Mechanistically, biased agonism has been explained by the stabilisation of distinct receptor conformations by different agonists. The molecular evidence for ligand-specific receptor conformations at the β2-adrenergic receptor has been presented through nuclear magnetic resonance spectroscopy (Liu, Horst, Katritch, Stevens, & Wuthrich, 2012; Manglik et al., 2015), fluorescence spectroscopy (Yao et al., 2006) and single molecule fluorescence resonance energy transfer (Gregorio et al., 2017), as well as by the stabilisation of discrete receptor conformations using allosteric nanobodies (Staus et al., 2016). However, these distinct conformations have not yet been linked to differential activation of signalling pathways. Most recently, the cryo-electron microscopy structure of a biased agonist bound to the glucagon-like peptide-1 receptor in complex with the G protein heterotrimer (Liang et al., 2018) demonstrated that this receptor adopts a very distinct conformation when compared to the structure bound to a non-biased agonist (Jazayeri et al., 2017). Importantly, the structural differences in receptor conformation propagated to the effector protein, resulting in an increased rate of G protein activation (Liang et al., 2018). This study provides evidence that specific ligands can stabilise distinct G protein-coupled receptor (GPCR) conformations causing downstream functional differences in the same signalling pathway. However, structural evidence for ligand-stabilised receptor conformations that preferentially couple to one effector protein over another (i.e. biased agonism) remain to be elucidated.

For most GPCRs, biased agonism is studied by *in vitro* measurement of signalling and in many cases is the comparison of G protein signalling versus β-arrestin2 recruitment. Despite the potential of biased agonism to inform the design of drugs with improved therapeutic windows, *in vitro* signalling bias does not always translate into successful therapeutic strategies, which raises the question as to whether it is too early to start a quest for GPCR biased ligands (Kenakin, 2018; Michel & Charlton, 2018).

In the case of the MOP, coupling to inhibitory G proteins ($G\alpha_{i/o}$) results in analgesia (Raffa, Martinez, & Connelly, 1994) and mice that lack β-arrestin2 show enhanced and prolonged analgesia after chronic morphine treatment (Bohn et al., 1999). Moreover, β-arrestin2 has been associated with some of the undesired effects of opioids including respiratory depression, constipation (Raehal, 2005) and tolerance (Bohn, Lefkowitz, & Caron, 2002). Consequently, recent efforts have aimed to take advantage of biased agonism to promote MOP bias towards the G protein pathway and away from β-arrestin2 to develop more effective opioid analgesics with reduced adverse effects.

The three most recent G protein-biased MOP agonists that have shown improved analgesic profiles are: TRV130 (also known as oliceridine or OLINVO, and currently under clinical development) (DeWire et al., 2013), and the experimental compounds PZM21 (Manglik et al., 2016) and SR-17018 (Schmid et al., 2017). *In vitro*, these agonists cause strong cyclic adenosine monophosphate (cAMP) inhibition with limited β-arrestin2 recruitment (DeWire et al., 2013; Manglik et al., 2016; Schmid et al. 2017). *In vivo*, TRV130 caused more potent analgesia with less gastrointestinal and respiratory dysfunction than morphine (DeWire et al., 2013). However, other groups have shown that while TRV130's antinociception was more resistant to tolerance, acute and repeated administration of TRV130 in rodents caused inhibition of the gastrointestinal function and abuse-related effects similar to morphine (Altarifi et al., 2017), and reinforcing effects similar to oxycodone (Zamarripa et al., 2018). In clinical trials, TRV130 had a smaller than anticipated improvement in tolerability in relation to nausea, vomiting and respiratory function at equi-effective doses to morphine (Singla et al., 2017; Soergel et al., 2014; Viscusi et al., 2016). Nevertheless, the improvement in side effect profile was enough that in 2016 the Food and Drug Administration (FDA) granted

a breakthrough therapy designation to oliceridine injection for the management of moderate-to-severe acute pain and oliceridine is currently pending approval as a new drug application.

Concurrently, Schmid et al. described that the degree of bias away from β-arrestin2 recruitment improves the therapeutic window by separating analgesia from respiratory depression. They discovered SR-17018, a highly G protein-biased agonist that displayed the least decrease in respiration (Schmid et al., 2017). Another structure-based discovery program identified PZM21, a G protein-biased MOP agonist which specifically blocked the affective component of pain, while retaining reflexive behaviours, and was devoid of both respiratory depression and morphine-like reinforcing activity in mice at equi-analgesic doses to morphine (Manglik et al., 2016). However, recent reports reassessing the effects of PZM21, suggest that it still causes respiratory depression and antinociceptive tolerance in a similar manner to morphine (Hill et al., 2018).

In addition, Hill et al. showed that PZM21 has low MOP agonist efficacy for both G protein activation and β-arrestin2 recruitment, suggesting that it is a low efficacy partial agonist. Interestingly, buprenorphine is a high affinity MOP partial agonist (Volpe et al., 2011), and it is considered a safer opioid due to its low intrinsic efficacy which causes a 'ceiling effect' for inducing respiratory depression (Dahan et al., 2006). Thus, careful characterisation of novel MOP agonists is necessary to distinguish ligands that have very low agonist efficacy from those that are truly biased. This is important as understanding the mechanism by which ligands result in safer profiles will help future drug discovery efforts.

To address this systematically, we aimed to: i) develop approaches to quantitively assess MOP activation and, ii) investigate the relationship between ligands with different efficacies in receptor activation, G protein activation, the recruitment of GRK2 and β-arrestin2 and internalisation. Here, we developed a C-terminally Venus-tagged nanobody 33 (Nb33-Venus) as a Bioluminescence Resonance Energy Transfer (BRET) biosensor to quantitatively measure ligand-induced MOP activation in live cells. Additionally, we employed a variant of the previously characterised mini-G proteins (Nehme et al., 2017) with an N-terminal Venus-tag (Venus-mGsi) (Wan et al., 2018) to probe direct coupling of MOP to $G\alpha_i$.

We found that TRV130, PZM21 and SR-17018 showed very low efficacy in Nb33 and mGsi recruitment to a similar extent to buprenorphine. We then measured G protein-mediated and arrestin-mediated pathways at different endpoints. Despite the lower efficacy of the so-called G protein-biased ligands for GRK2, β-arrestin2 recruitment and internalisation, only buprenorphine displayed significant bias when comparing all the G protein pathways against the β-arrestin2 pathway. Moreover, G protein bias was only detectable under low GRK2 expression levels, highlighting that the protein content within the system can determine the *in vitro* signalling bias profile. Finally, we found a correlation between the agonist efficacy to stabilise an active MOP conformation and efficacy for activation of all G protein and β-arrestin2 pathways. These data support previous observations that agonist efficacy in G protein activation correlates with the level of MOP phosphorylation, arrestin recruitment and internalisation (McPherson et al., 2010). Altogether, our study suggests that the improved therapeutic window observed with new biased agonists could be due to their lower intrinsic efficacy so that they fall within an "ideal efficacy threshold" that is enough to cause analgesia without triggering adverse effects.

2.3 Methods

2.3.1 Materials

Dulbecco's modified Eagle's medium (DMEM) was purchased from Invitrogen (Mulgrave, VIC, Australia). Foetal bovine serum (FBS) was purchased from ThermoTrace (Melbourne, Australia). DAMGO, Met-Enk and Leu-Enk were purchased from Mimotopes (Melbourne, Australia). Morphine HCl was from GlaxoSmithKline (Boronia, Victoria, Australia). SR17018 was acquired from the University of Nottingham (UK). TRV130 was kindly provided by M. Christie (University of Sydney, Australia). Buprenorphine was kindly provided by B. Capuano (Monash University, Australia). Fentanyl, methadone and oxycodone were from the National Measurement Institute (Australia). Naloxone was from Tocris and PZM21 was from MedChemExpress (MCE). Pertussis toxin was from Invitrogen.

2.3.2 Plasmids

Nb33 cDNA was obtained from Mark von Zastrow (Stoeber et al. 2018) and was subcloned into a Clontech pVenus vector resulting in addition of the Venus tag at the C-terminus. Subcloning of Nb33 into the Venus vector was performed by M. Canals. NES-Venus-mGsi (Wan et al. 2018), Rab5-Venus (Lan, Liu, Li, Wu, & Lambert, 2012), Venus155-239-Gβ1, Venus1-155-Gγ2, masGRKct-RLuc8 (Masuho, Martemyanov, & Lambert, 2015) were obtained from Nevin Lambert (University of Georgia, USA). FLAG-MOP-NLuc was generated by cloning FLAG-MOP (Meiss et al. 2018) into a NLuc-vector from Promega. GRK2-Venus was from D. Jensen (Columbia University, New York), β-arrestin2–YFP were provided by M. Caron (Duke University, North Carolina), GRK2 WT was from M. Smit (Vrije Universiteit, Amsterdam). CAMYEL sensor has been previously characterised (Jiang et al., 2007).

2.3.3 Cell culture and transfections

Human embryonic kidney 293 (HEK293) cells were maintained in DMEM supplemented with 5% v/v FBS at 37°C in a humidified atmosphere of 95% air and 5% CO_2. Transient transfections for BRET experiments were performed using linear polyethylenemine (PEI) with a molecular weight of 25kDa (Polysciences) at a DNA:PEI ratio of 1:6 as previously described (Meiss et al. 2018). Cells were transfected in a 10 cm dish with 1 µg of donor (FLAG-

mMOP-NLuc) and 4 μg of acceptor (Nb33-Venus, mGsi-Venus, GRK2-Venus, β-arrestin2-YFP or Rab5a-Venus). For G protein activation assay, cells were transfected with 2 μg of $G\alpha_{i2}$, 1 μg of Venus155-239-Gβ1, 1 μg of Venus1-155-Gγ2 and 1 μg of masGRK3ct-Rluc8. Transfections for the G protein activation assay were performed by J. Sanchez. For cAMP inhibition assays, cells were transfected with the CAMYEL BRET biosensor (2.5 μg of FLAG-mMOP and 2.5 μg of CAMYEL biosensor per dish). For GRK2 overexpression experiments, cells were co-transfected with an additional 2 μg of GRK2 WT. Transfections for the CAMYEL assay were performed by H.Lim. For ELISA, HEK293 cells were transfected with 2 μg FLAG-MOP and 2 μg of Nb33-Venus or Venus-mGsi in 10-cm dishes.

2.3.4 Enzyme-Linked Immunosorbent Assay (ELISA)

Cells were replated into poly-D-lysine–coated 48-well plates 24 h after transfection and allowed to adhere overnight. After 48 h, cells were treated with 10 μM of DAMGO for 30 min to cause internalisation and cells were fixed with 3.7% (v/v) paraformaldehyde in tris-buffered saline (TBS) for 30 min. Surface or total FLAG-MOP receptors were detected in intact or (Nonidet P-40 equivalent)-detergent permeabilised cells, respectively, using the mouse M2–anti-FLAG antibody followed by horseradish peroxidase (HRP)-conjugated goat anti-mouse IgG. For total expression, cells were permeabilised by 30 min incubation with 0.5% (v/v) NP-40 in TBS. Cells were then incubated in blocking buffer containing 1% (w/v) skim milk powder in 0.1 M $NaHCO_3$ for 4 hours at room temperature and incubated with mouse M2–anti-FLAG antibody (1:2000, overnight). After washing three times with TBS, cells were incubated with HRP-conjugated anti-mouse (1:2000) for 2 hours at room temperature. Cells were washed and stained using the SIGMAFAST OPD substrate (Sigma-Aldrich). Absorbance at 490 nm was measured using a FlexStation plate reader (Molecular Devices). Receptor internalisation was quantified as the percentage of residual cell-surface receptors in agonist-treated cells. ELISA experiment was performed by M. Canals.

2.3.5 Bioluminescence Resonance Energy Transfer (BRET)

Cells were replated into poly-D-lysine–coated 96-well plates 24 h after transfection and allowed to adhere overnight. BRET experiments were performed 48 h post-transfection.

Furimazine (Promega) was used for Nanoluciferase (NLuc)-tagged constructs and Coelenterazine h was used for Renilla luciferase (RLuc8)-tagged constructs at a final concentration of 5 µM. Luciferase substrate was added immediately before dual fluorescence/luminescence measurement in a PHERAstar Omega plate reader (BMG LabTech). The BRET signal was calculated as the ratio of light emitted at 530 nm by YFP or Venus over the light emitted at 430 nm by NLuc or Rluc8. Experiments were recorded using kinetic reads; the baseline BRET ratio was measured for 4 cycles prior to addition of the agonists and BRET signal was recorded every 1 min over a total period of 20-30 min of stimulation until addition of 10 µM naloxone to asses reversal of the signal. Concentration-response curves were constructed from the 10 min time point for all pathways except Rab5-Venus for which concentration-response curves were constructed 30 min after stimulation. To measure agonist-induced cAMP inhibition, cells were pre-incubated with agonists for 10 min prior to addition of 10 µM forskolin to induce cAMP production. Average BRET ratio of the baseline points was subtracted from the raw BRET ratio. BRET signal from vehicle-treated cells was subtracted and data were normalised to the 10 µM DAMGO response at 10 min. BRET G protein activation experiments were performed by J. Sanchez. BRET CAMYEL assays were performed by H.Lim.

2.3.6 Data analysis

Data were analysed using Prism 7.0 (GraphPad Software Inc., San Diego, CA). For the determination of maximal responses (E_{max}) and potencies (pEC_{50}), concentration–response curves were fit to the three-parameter logistic equation (1)

(1) $$Y = \text{Bottom} + \frac{(\text{Top}-\text{Bottom})}{1+10^{(\text{Log}EC_{50}-\log[A])}}$$

where Top and Bottom represent the maximal and minimal asymptote of the concentration response curve, [A] is the molar concentration of ligand and EC_{50} is the molar concentration of ligand required to generate a response halfway between Top and Bottom.

For the determination of pK_A, τ values and transduction coefficients ($\log(\tau/K_A)$), concentration–response data were fit to the operational model (Black & Leff, 1983) - partial agonism equation (2)

$$(2)\ \mathrm{Y} = \mathrm{Basal} + \frac{\mathrm{Em}-\mathrm{Basal}}{1+\left(\frac{10^{logK_A}+10^{log[A]}}{10^{log\tau}\ 10^{log[A]}}\right)^n}$$

where E_m is the maximal possible response of the system, Basal is the basal level of response, K_A represents the equilibrium dissociation constant of the agonist (A) and τ is an index of the signaling efficacy of the agonist that is defined as R_T/K_E, where R_T is the total number of receptors and the parameter K_E denotes the intensity of the reaction and the ability of the system to convert a receptor stimulus into a response, and *n* is the slope of the transducer function that links occupancy to response. The analysis assumes that the transduction machinery utilized for a given cellular pathway are the same for all agonists, such that the E_m and transducer slope (*n*) are shared between agonists.

Biased agonism was quantified as previously described (Kenakin, Watson, Muniz-Medina, Christopoulos, & Novick, 2012; Klein Herenbrink et al., 2016). To exclude the impact of cell-dependent and assay-dependent effects on the observed agonism at each pathway, the log(τ/K_A) value of a reference agonist, in this case DAMGO, was subtracted from the log(τ/K_A) value of the agonists of interest to give a ΔLog(τ/K_A) value. The relative bias was then calculated for each agonist at two different signalling pathways by subtracting the Δlog(τ/K_A) of one pathway from the second pathway to give a ΔΔlog(τ/K_A) value, which is a measure of bias. A lack of biased agonism will result in values of ΔΔlog(τ/K_A) not significantly different from 0. When fold changes in bias are described, this was calculated by converting values of ΔΔlog(τ/K_A) to the corresponding antilog value.

For the determination of bias ratios, we applied an 'equiactive comparison' between signaling pathways previously described (Griffin, Figueroa, Liller, & Ehlert, 2007; Rajagopal et al., 2011). Estimates of the intrinsic relative activity (RA_i) for the different pathways were calculated using equation (3). The bias ratio is determined as the ratio of the RA_i between pathways as per Dewire et al. 2013.

$$(3)\ RA_i = \frac{E_{max}\ ref \cdot EC_{50}\ lig}{E_{max}\ lig \cdot EC_{50}\ ref}$$

2.3.7 Statistics

Data are presented as the mean ± SEM of n≥3 independent experiments. In the instances where the n number is variable between groups, this is due to pooling of different data sets with different groups, as some of the ligands were not included in initial experiments. Differences in E_{max}, pEC_{50} and pK_A were assessed using one-way ANOVA followed by Dunnett's multiple comparisons test to compare the mean of each agonist with a control mean (that of the reference agonist DAMGO). Biased agonism was assessed using one-way ANOVA followed by Tukey's multiple comparisons test to compare the $\Delta\log(\tau/K_A)$ mean of every agonist with every other mean. Correlations were computed using Pearson's correlation analysis to assess whether the τ values of each agonist in a particular pathway vary together with the τ values of the same agonist in a different pathway. A strong correlation was reported when $p < 0.05$ and the fraction of the variance that is "shared" between the two variables is reported as r^2.

2.4 Results

2.4.1 Use of Nb33 and mGsi as biosensors to probe MOP activation and G protein coupling

Nanobodies are camelid single domain antibody fragments that can be generated to stabilise different conformational states of GPCRs. An active-state MOP nanobody, Nb33, has recently been used as an imaging biosensor to localise MOP activation within the cell (Stoeber et al., 2018). Here, we generated a C-terminally Venus-tagged variant of Nb33 (Nb33-Venus) (Fig. 2.1A) to use as a BRET acceptor in order to assess the real-time recruitment of this conformationally-selective nanobody to the C-terminally NanoLuc-tagged mouse MOP (MOP-NLuc) upon agonist stimulation. Incubation of cells with DAMGO or morphine induced a concentration-dependent increase in BRET signal between MOP-NLuc and Nb33-Venus. Both agonists showed similar potency (EC_{50} ~ 200 nM), but morphine displayed lower efficacy (76 ± 2% of DAMGO; $p<0.0001$ one-way ANOVA with Dunnett's post hoc test) (Fig. 2.1B). As expected, recruitment of Nb33-Venus was pertussis toxin (PTx)-insensitive (Fig. 2.1B), indicating that recruitment of Nb33 is independent of G protein activation and therefore serves as a measurement of direct MOP activation.

We also assessed the kinetics of Nb33 recruitment upon addition of increasing concentrations of agonist. Nb33 recruitment was very fast with the BRET signal reaching its maximum within 1 min and remaining sustained for 20 min (Fig. 2.1C, D). Addition of the antagonist naloxone (10 μM) completely reversed the BRET signal back to baseline levels within 1 min. This validates recruitment of Nb33 as a real-time measurement tool for MOP activation upstream of G protein activation.

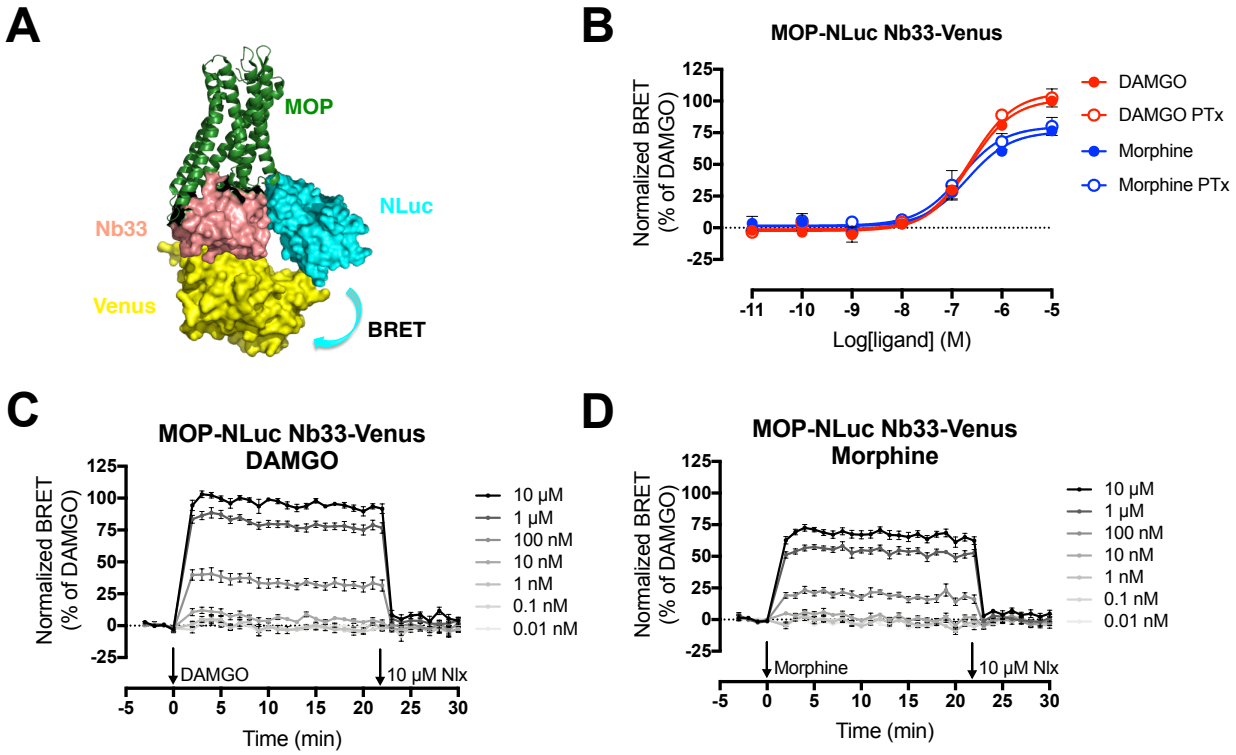


Figure 2.1 Recruitment of Nb33-Venus to MOP-NLuc. (A) Molecular representation of Nb33-Venus (Nb39 from PBD 5C1M combined with Venus form PDB 3AKO) recruited to MOP-NLuc (MOP from PDB 5C1M combined with NLuc form PDB 5IBO). HEK293 cells expressing MOP-NLuc and Nb33-Venus were stimulated with increasing concentrations of DAMGO or morphine in the absence or after pre-treatment with PTx (100ng/ml for 16h). **(B)** Concentration-response curves were constructed from the 10 min timepoint in the kinetic reads. **(C)** Kinetic traces after DAMGO or **(D)** morphine stimulation and following addition of 10 µM naloxone. Raw BRET ratio of vehicle-treated cells was subtracted, and data were normalised to the response of 10 µM DAMGO (0.190 ± 0.055). Data points represent mean ± SEM of n=3-6 independent experiments.

We then employed an N-terminally Venus-tagged variant of the mini G proteins that has been recently developed (Venus-mGsi) (Fig. 2.2A) to probe direct coupling of MOP to Gαi (Wan et al., 2018). Mini G (mG) proteins are Gα subunits that have been engineered to contain only the GTPase domain; in particular, the mGsi variant incorporates mutations at the GPCR-G protein interface to maintain the receptor coupling specificity of the Gα subunit family Gi/o (Wan et al., 2018). Incubation of cells with DAMGO or morphine induced a concentration-dependent increase in BRET signal between MOP-NLuc and Venus-mGsi. Both agonists showed similar potency (EC_{50} ~ 100 nM), but in this case both DAMGO and morphine reached a similar maximal response (100 ± 2% for DAMGO; 95 ± 6% for morphine, p>0.05

one-way ANOVA with Dunnett's post hoc test) (Fig. 2.2B). The similar maximal effect and increased potency of the ligands in this assay compared to Nb33 recruitment suggests a level of amplification and/or more effective coupling that masks the lower intrinsic efficacy of morphine. Amplification within this assay may arise from two different effects; i) translocation of the mGsi to the plasma membrane in close proximity to MOP-NLuc would generate a BRET signal that is not necessarily due to mGsi-MOP interaction but due to bystander BRET; and ii) mGsi has a fast dissociation from the receptor, suggesting that multiple mGsi will be able to reach MOP within the measurement.

As expected, recruitment of mGsi was PTx-sensitive (46 ± 16% for DAMGO and 39 ± 8% for morphine in PTx-pretreated conditions, $p<0.001$ compared to untreated one-way ANOVA with Dunnett's post hoc test) (Fig. 2.2B), thus this assay reflects MOP coupling to the $G\alpha_{i/o}$-PTx sensitive family. mGsi recruitment was also very fast, the BRET signal reached a maximum within 1 min after addition of the agonists and remained sustained for 20 min (Fig. 2.2C, D). Addition of the antagonist naloxone (10 µM) reversed the response within 1 min. This validates the recruitment of mGsi as a real-time measurement of MOP coupling to $G\alpha_i$.

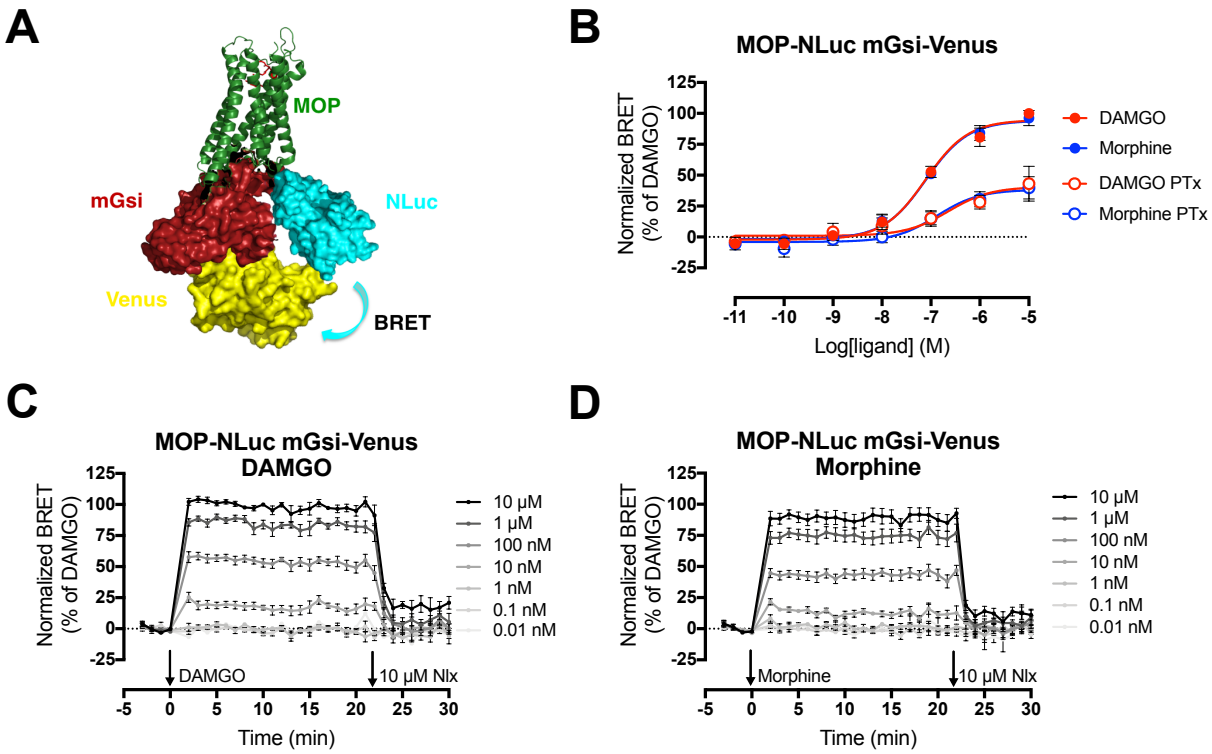


Figure 2.2 Recruitment of Venus-mGsi to MOP-NLuc. (A) Molecular representation of Venus-mGsi (mGo from PBD 6G79 combined with Venus form PDB 3AKO) recruited to MOP-NLuc (MOP from PDB 6DDE combined with NLuc form PDB 5IBO). HEK293 cells expressing MOP-NLuc and mGsi-Venus were stimulated with increasing concentrations of DAMGO or morphine in the absence or after pre-treatment with pertussis toxin (100ng/ml PTx, 16h). **(B)** Concentration-response curves were constructed from the 10 min timepoint in the kinetic reads. **(C)** Kinetic traces after DAMGO or **(D)** morphine stimulation and following addition of 10 µM naloxone. Raw BRET ratio of vehicle-treated cells was subtracted, and data were normalised to the response of 10 µM DAMGO (0.118 ± 0.024). Data points represent mean ± SEM of n=3-6 independent experiments.

A potential caveat of conformational biosensors such as Nb33 or mGsi is that they can "lock" the receptor in an active state and/or alter receptor function. To evaluate whether this was the case, we assessed the effect of overexpression of Nb33-Venus or Venus-mGsi in DAMGO-induced internalisation using anti-FLAG ELISA in cells expressing FLAG-MOP. In agreement with previous reports, expression of Nb33-Venus or Venus-mGsi had minimal perturbation of MOP function as it had no effect on MOP internalisation induced by DAMGO (Fig 2.3).

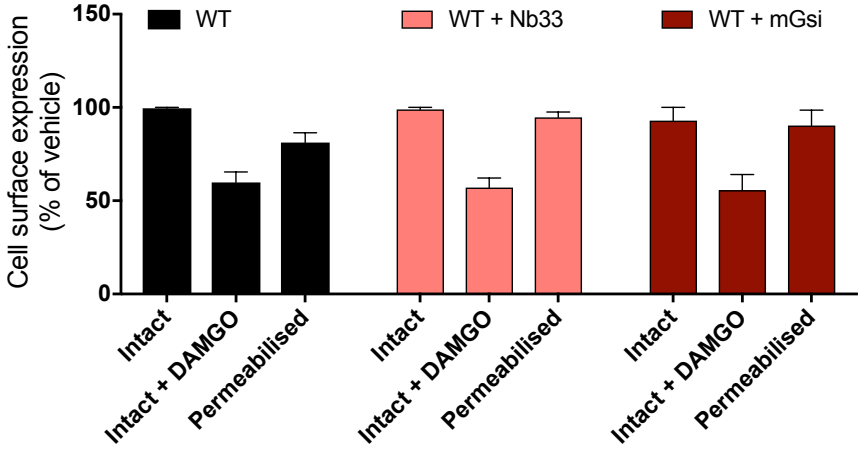


Figure 2.3 Effect of Nb33 and mGsi overexpression in MOP internalisation. Values are expressed as % of vehicle-treated cells; mean ± SEM from n = 3 independent experiments. No significant differences were observed ($p<0.05$) in DAMGO-induced internalisation between the MOP wild-type (WT) and +Nb33 or +mGsi by a two-way ANOVA, Dunnett's post-hoc test.

2.4.2 Use of Nb33 and mGsi to investigate proximal events to receptor activation in the detection of biased agonism at the MOP

Classically, most biased agonism descriptions at MOP have compared cAMP inhibition responses to β-arrestin2 recruitment, which represent different levels of amplification and coupling, and are subject to different steps of regulation. Thus, we aimed to include the biosensors to measure MOP activation (Nb33) and G protein coupling (mGsi) to measure steps more proximal to receptor activation and G protein coupling, and at a similar level to the typical measurement of arrestin recruitment. We assessed the efficacy of a range of opioid ligands including the endogenous peptide agonists Met-enkephalin (Met-Enk) and Leu-enkephalin (Leu-Enk), a MOP-selective synthetic analogue H-Tyr-d-Ala-Gly-N(Me)Phe-Gly-OH (DAMGO), natural and synthetic opioids (morphine, fentanyl, methadone, oxycodone, buprenorphine) and the three recently described biased ligands (TRV130, PZM21, SR-17018) (DeWire et al., 2013; Manglik et al., 2016; Schmid et al. 2017). Responses were normalised to the prototypical MOP agonist DAMGO. From the concentration-response curves, we determined the maximal responses (E_{max}) and potencies (EC_{50}) of each ligand. Additionally, we applied the approach based on the Black and Leff operational model of agonism (Kenakin et al., 2012) to determine transduction coefficients ($\log(\tau/K_A)$) which are required for the quantification of bias. The transduction coefficient is a parameter that is comprised of both agonist efficacy (τ) and functional affinity of the receptor when coupled to a specific signalling pathway (K_A) (Kenakin et al., 2012). The statistical analysis of efficacy (τ) and transduction coefficients ($\log(\tau/K_A)$) will be assessed in the following sections.

In Nb33 recruitment (Table 2.1 and Fig. 2.4), Met-Enk, Leu-Enk and fentanyl were full agonists and displayed similar efficacy to DAMGO. This was followed by methadone that displayed ~80% of the DAMGO response, and morphine and oxycodone which displayed ~70% of the DAMGO response. The biased agonists were next in the following rank order of efficacy: TRV130 and PZM21 displayed ~35% of the maximal response and SR-17018 displayed ~20% of the maximal response. The low efficacy displayed by biased agonists could be indicative of them stabilising a unique receptor conformation that is distinct from that of the MOP bound to high efficacy agonists. However, the partial agonist buprenorphine also displayed very

limited Nb33 recruitment (~25%). All the biased agonists reached a maximal response at 10 µM in G protein pathways; thus, a higher concentration point was not included in succeeding analysis because there were apparent solubility issues in particular with SR-17018 and we were concerned about the specificity of the response at 100 µM. In terms of potencies, that of fentanyl was higher than DAMGO, which translated to a higher functional affinity for Nb33 recruitment. Interestingly, despite their low efficacy, the biased agonists and also buprenorphine displayed higher functional affinity (pK_A) for Nb33.

In mGsi recruitment (Table 2.2 and Fig. 2.5), the overall rank order of efficacies observed in Nb33 recruitment was maintained, although most ligands including methadone, morphine and oxycodone reached a similar E_{max} to that of DAMGO. This suggests that coupling of MOP to mGsi was more amplified than coupling to Nb33. The only agonists that displayed partial mGsi recruitment were TRV130, PZM21, SR-17018 (all ~50%) and buprenorphine (~35%). In contrast to Nb33, only buprenorphine displayed higher functional affinity (pK_A) to mGsi.

Table 2.1 Determination of the maximal responses (E_{max}), potencies (pEC_{50}), functional affinities (pK_A), efficacies (τ) and transduction coefficients ($\log(\tau/K_A)$) of selected agonists to recruit Nb33 to the MOP. Values are expressed as mean ± SEM from n = 4-8 separate experiments. * indicates p<0.05; ** indicates p<0.01; *** indicates p<0.001; **** indicates p<0.001 versus DAMGO in a one-way ANOVA with Dunnett's post hoc test.

Ligand	E_{max} % of DAMGO	pEC_{50}	pK_A	τ	$\log(\tau/K_A)$
DAMGO	101 ± 1	6.74 ± 0.08	5.86 ± 0.09	5.47 ± 0.26	6.69 ± 0.07
Met-Enk	111 ± 3	7.09 ± 0.08	6.24 ± 0.13	7.83 ± 1.14	7.18 ± 0.08
Leu-Enk	102 ± 4	6.55 ± 0.13	5.71 ± 0.13	6.12 ± 1.03	6.49 ± 0.11
Fentanyl	91 ± 10	7.56 ± 0.11**	6.95 ± 0.14**	2.68 ± 0.93	7.44 ± 0.11
Methadone	79 ± 3 **	6.62 ± 0.04	5.99 ± 0.11	2.06 ± 0.30	6.40 ± 0.10
Morphine	68 ± 4 ****	6.63 ± 0.05	6.13 ± 0.08	1.36 ± 0.15	6.36 ± 0.07
Oxycodone	68 ± 4 ****	5.72 ± 0.05***	5.26 ± 0.08	1.38 ± 0.24	5.45 ± 0.04
TRV130	36 ± 3 ****	7.33 ± 0.13*	7.03 ± 0.11****	0.40 ± 0.05	6.73 ± 0.11
PZM21	37 ± 4 ****	6.51 ± 0.15	7.36 ± 0.34****	0.38 ± 0.06	7.01 ± 0.30
SR17018	19 ± 7 ****	7.57 ± 0.41**	7.26 ± 0.30****	0.22 ± 0.07	6.66 ± 0.35
Buprenorphine	26 ± 2 ****	8.20 ± 0.28****	8.12 ± 0.14****	0.24 ± 0.03	7.59 ± 0.14

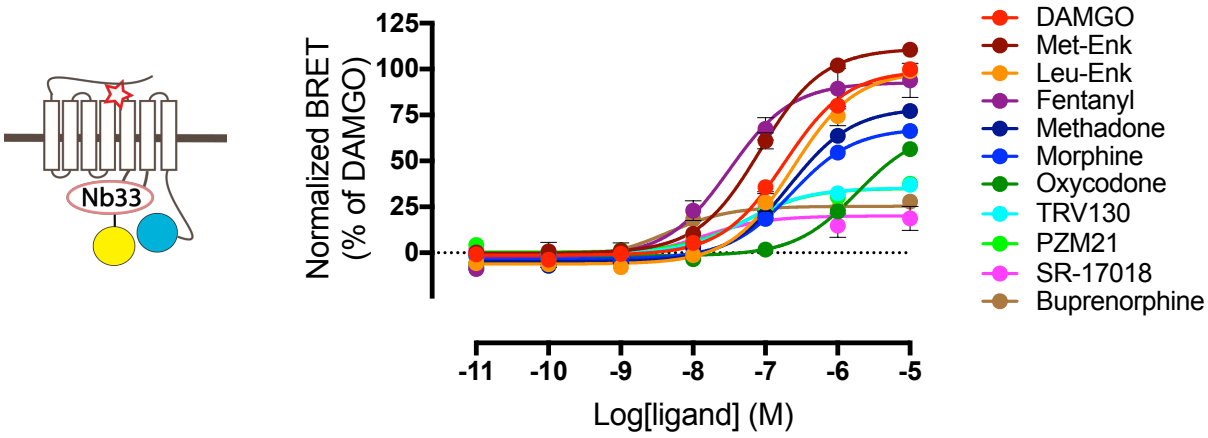


Figure 2.4 The ability of increasing concentrations of selected agonists to recruit Nb33 to the MOP. Concentration-response curves were constructed 10 min after agonist stimulation. Raw BRET ratio of vehicle-treated cells was subtracted, and data were normalised to the response of 10 µM DAMGO (0.167 ± 0.073). Values are expressed as mean ± SEM from n=4-8 separate experiments.

Table 2.2 Determination of the maximal responses (E_{max}), potencies (pEC_{50}), functional affinities (pK_A), efficacies (τ) and transduction coefficients ($\log(\tau/K_A)$) of selected agonists to recruit mGsi to the MOP. Values are expressed as mean ± SEM from n=4-7 separate experiments. ** indicates p<0.01; *** indicates p<0.001; **** indicates p<0.001 versus DAMGO in a one-way ANOVA with Dunnett's post hoc test.

Ligand	E_{max} % of DAMGO	pEC_{50}	pK_A	τ	$\log(\tau/K_A)$
DAMGO	97 ± 2	7.16 ± 0.11	5.88 ± 0.21	5.20 ± 0.94	6.69 ± 0.16
Met-Enk	110 ± 5	7.40 ± 0.11	6.44 ± 0.12	5.13 ± 0.92	7.25 ± 0.13
Leu-Enk	106 ± 5	7.04 ± 0.15	5.96 ± 0.15	6.70 ± 1.86	6.84 ± 0.18
Fentanyl	109 ± 9	7.71 ± 0.07	6.72 ± 0.07	3.47 ± 0.94	7.60 ± 0.15
Methadone	114 ± 10	6.94 ± 0.04	5.74 ± 0.25	4.52 ± 1.89	6.79 ± 0.18
Morphine	83 ± 7	6.95 ± 0.08	6.12 ± 0.11	1.78 ± 0.54	6.46 ± 0.09
Oxycodone	86 ± 9	6.15 ± 0.08	5.39 ± 0.18	1.73 ± 0.54	5.75 ± 0.11
TRV130	52 ± 9***	7.76 ± 0.11	7.12 ± 0.18	0.76 ± 0.23	7.04 ± 0.16
PZM21	53 ± 6***	7.69 ± 0.12	6.82 ± 0.25	0.58 ± 0.21	6.61 ± 0.33
SR17018	51 ± 8***	6.06 ± 0.95	6.19 ± 0.87	0.55 ± 0.25	6.25 ± 0.68
Buprenorphine	33 ± 5****	8.83 ± 0.07*	8.23 ± 0.11**	0.15 ± 0.06	7.51 ± 0.14

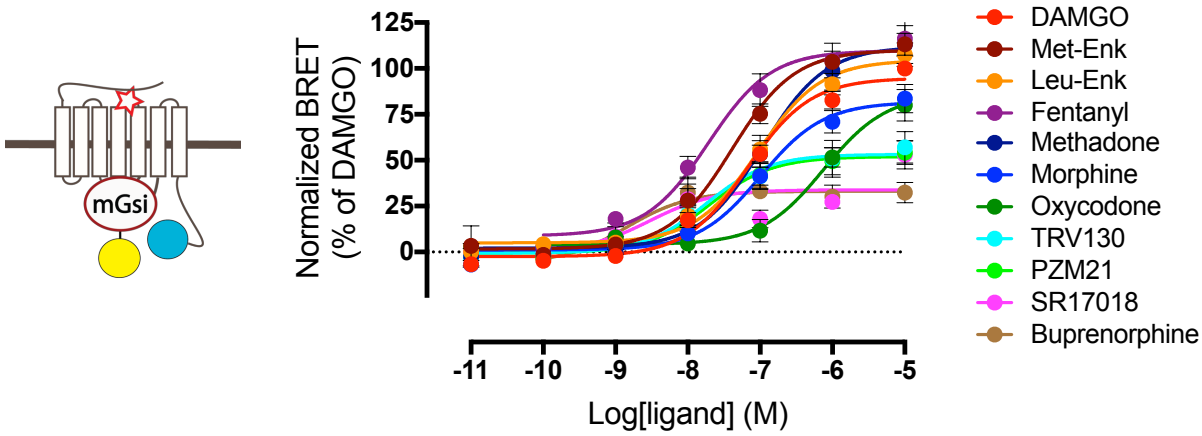


Figure 2.5 The ability of increasing concentrations of selected agonists to recruit mGsi to the MOP. Concentration-response curves were constructed 10 min after agonist stimulation. Raw BRET ratio of vehicle-treated cells was subtracted, and data were normalised to the response of 10 µM DAMGO (0.099 ± 0.016). Values are expressed as mean ± SEM from n=4-7 separate experiments.

We also assessed the kinetics for Nb33 and mGsi recruitment for the ligands that displayed partial responses (Fig. 2.6). While TRV130 and PZM21 showed fast recruitment similar to the most efficacious agonists, SR-17018 and buprenorphine displayed slower recruitment, reaching a maximal response 5-10 min and 2-5 min after addition, respectively. Of note, while the response of all the biased ligands was reversed by naloxone, the response to buprenorphine was the only one that did not reverse back to baseline (Fig. 2.6D, H), reflecting its slow dissociation rate from the receptor (Virk, Arttamangkul, Birdsong, & Williams, 2009).

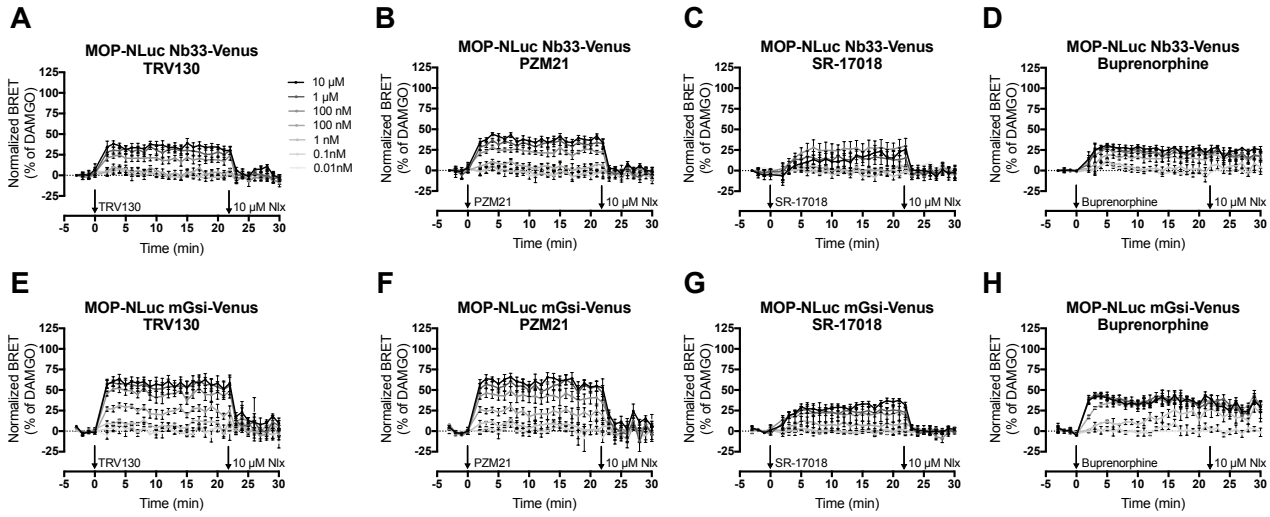


Figure 2.6 Kinetic traces for the recruitment of Nb33 (A-D) or mGsi (E-F) to the MOP. Increasing concentrations of TRV130 **(A, E)**, PZM21 **(B, F)**, SR-17018 **(C, G)** or buprenorphine **(D, H)** stimulation followed by addition of 10 µM naloxone. Raw BRET ratio of vehicle-treated cells was subtracted, and data were normalised to the response of 10 µM DAMGO (0.198 ± 0.072). Values are expressed as mean ± SEM from n=3-7 separate experiments.

2.4.3 MOP-mediated activation of G protein- and β-arrestin2- dependent pathways

The MOP is primarily coupled to inhibitory $G\alpha_i$ proteins (Connor & Christie, 1999). Activation of the Gα subunit results in inhibition of adenylyl cyclase activity, leading to decreased cAMP accumulation. While the Gβγ subunits modulate downstream effectors such as G protein–dependent inward rectifying potassium (GIRK) (North & Williams, 1985) and voltage-dependent calcium channels (Seward, Hammond, & Henderson, 1991), they also mediate the recruitment of GPCR kinases (GRKs). Phosphorylation of MOP by GRKs facilitates β-arrestin2 recruitment, which in turn causes receptor internalisation towards Rab5 positive early endosomes. Here, we assessed the efficacy of opioid ligands in assays reflective of different endpoints of the G protein and β-arrestin2 pathways.

As shown above, Nb33 recruitment is indicative of MOP activation. In the G protein pathway, mGsi represents G protein coupling, the $G\alpha_{i2}$ protein activation assay measures the release of the Gβγ subunits towards an effector and the cAMP sensor using YFP-Epac-RLuc (CAMYEL) measures cAMP accumulation and can serve to measure MOP-mediated inhibition of forskolin-induced cAMP accumulation. As expected, in the $G\alpha_{i2}$ protein activation assay (Table 2.3 and Fig. 2.7) and cAMP inhibition assay (Table 2.4 and Fig 2.8), which are downstream of Nb33 and mGsi recruitment, all agonists displayed higher potencies (~10 nM for $G\alpha_{i2}$ activation and ~1 nM for cAMP inhibition) and most agonists displayed an E_{max} similar to DAMGO, indicative of increased signal amplification and more effective coupling for these endpoints. Only SR-17018 and buprenorphine displayed an E_{max} that was significantly lower than that of DAMGO, at ~50% and ~70%, respectively. Oxycodone displayed lower potency than DAMGO, which resulted in significantly lower pK_A in both assays. Conversely, buprenorphine displayed significantly higher pK_A in both assays.

Table 2.3 Determination of the maximal responses (E_{max}), potencies (pEC_{50}), functional affinities (pK_A), efficacies (τ) and transduction coefficients ($\log(\tau/K_A)$) of selected agonists to activate $G\alpha_{i2}$ via the MOP. Values are expressed as mean ± SEM from n=3 separate experiments. * indicates p<0.05; ** indicates p<0.01 versus DAMGO in a one-way ANOVA with Dunnett's post hoc test.

Ligand	E_{max} % of DAMGO	pEC_{50}	pK_A	τ	$\log(\tau/K_A)$
DAMGO	101 ± 1	7.83 ± 0.27	6.96 ± 0.25	7.46 ± 0.44	7.83 ± 0.27
Met-Enk	102 ± 4	8.32 ± 0.29	7.28 ± 0.24	7.27 ± 3.1	8.28 ± 0.33
Leu-Enk	99 ± 3	7.73 ± 0.31	6.79 ± 0.22	7.76 ± 2.22	7.65 ± 0.33
Fentanyl	105 ± 3	8.51 ± 0.24	7.42 ± 0.21	14.2 ± 3.81	8.53 ± 0.27
Methadone	105 ± 1	7.82 ± 0.24	6.73 ± 0.26	11.5 ± 1.13	7.78 ± 0.24
Morphine	99 ± 9	7.61 ± 0.21	6.68 ± 0.18	4.55 ± 1.94	7.55 ± 0.25
Oxycodone	100 ± 5	6.69 ± 0.33*	5.76 ± 0.12**	4.90 ± 0.99	6.69 ± 0.31
TRV130	83 ± 8	7.73 ± 0.08	7.65 ± 0.09	0.98 ± 0.09	7.64 ± 0.07
PZM21	80 ± 9	8.04 ± 0.30	7.46 ± 0.21	2.91 ± 1.11	7.85 ± 0.36
SR17018	51 ± 20**	7.58 ± 0.28	7.33 ± 0.50	1.56 ± 1.17	7.25 ± 0.23
Buprenorphine	68 ± 1*	8.82 ± 0.10	8.40 ± 0.06*	1.53 ± 0.05	8.58 ± 0.07

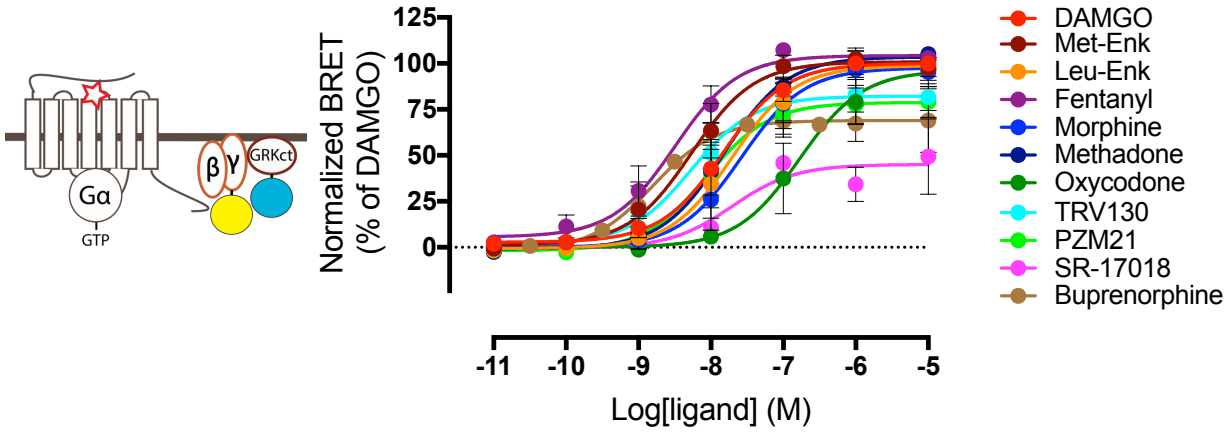


Figure 2.7 The ability of increasing concentrations of selected agonists to activate $G\alpha_{i2}$ via the MOP. Concentration-response curves were constructed 10 min after agonist stimulation. Raw BRET ratio of vehicle-treated cells was subtracted, and data were normalised to the response of 10 µM DAMGO (0.121 ± 0.013). Values are expressed as mean ± SEM from n=3 separate experiments.

Table 2.4 Determination of the maximal responses (E_{max}), potencies (pEC_{50}), functional affinities (pK_A), efficacies (τ) and transduction coefficients ($\log(\tau/K_A)$) of selected agonists to inhibit forskolin-induced cAMP production via the MOP. Values are expressed as mean ± SEM from n=3-7 separate experiments. * indicates p<0.05; ** indicates p<0.01; *** indicates p<0.001; **** indicates p<0.0001 versus DAMGO in a one-way ANOVA with Dunnett's post hoc test.

Ligand	E_{max} % of DAMGO	pEC_{50}	pK_A	τ	$\log(\tau/K_A)$
DAMGO	99 ± 2	8.65 ± 0.31	7.90 ± 0.31	4.79 ± 0.34	8.58 ± 0.30
Met-Enk	104 ± 3	8.27 ± 0.32	7.41 ± 0.26	6.70 ± 1.60	8.22 ± 0.33
Leu-Enk	104 ± 4	8.25 ± 0.30	7.35 ± 0.31	5.63 ± 0.85	8.15 ± 0.29
Fentanyl	101 ± 5	9.16 ± 0.31	8.30 ± 0.30	7.31 ± 1.91	9.08 ± 0.32
Methadone	107 ± 3	8.13 ± 0.20	7.09 ± 0.20	6.79 ± 0.78	8.05 ± 0.20
Morphine	98 ± 6	8.15 ± 0.28	7.33 ± 0.29	4.42 ± 1.15	8.05 ± 0.30
Oxycodone	101 ± 8	7.08 ± 0.24**	6.09 ± 0.27**	3.45 ± 0.79	7.00 ± 0.26
TRV130	87 ± 5	8.60 ± 0.19	7.98 ± 0.15	3.02 ± 0.64	8.41 ± 0.22
PZM21	85 ± 7	8.27 ± 0.33	7.67 ± 0.26	2.88 ± 0.75	8.10 ± 0.37
SR17018	45 ± 11****	7.80 ± 0.21	7.56 ± 0.32	1.00 ± 0.58	7.33 ± 0.18
Buprenorphine	72 ± 10*	9.46 ± 0.74	9.58 ± 0.68***	1.37 ± 0.53	9.77 ± 0.73

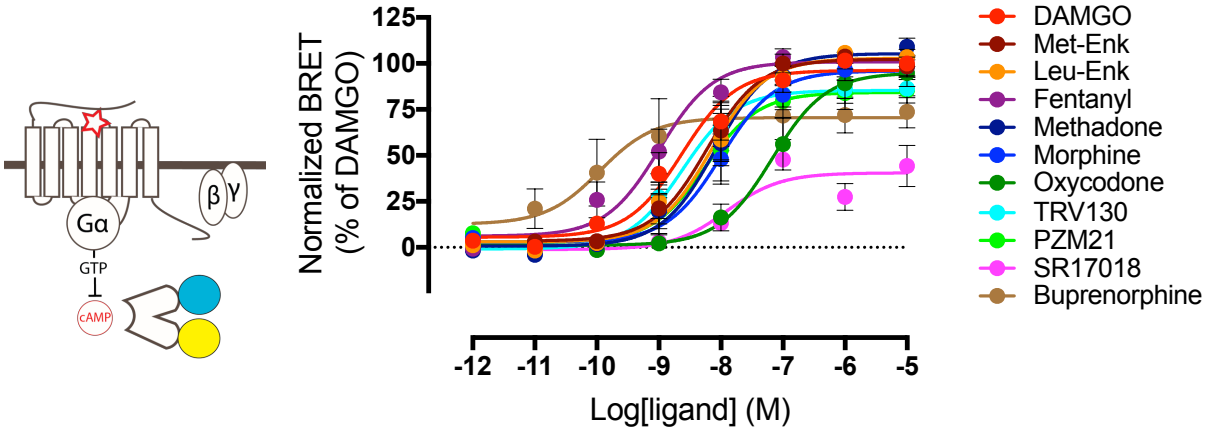


Figure 2.8 The ability of increasing concentrations of selected agonists to inhibit forskolin-induced cAMP production via the MOP. Concentration-response curves were constructed after 10 min of agonist stimulation followed by stimulation with 10 µM forskolin to increase cAMP production. Raw BRET ratio of vehicle-treated cells was subtracted, and data were normalised to the response of 10 µM DAMGO (0.112 ± 0.006). Values are expressed as mean ± SEM from n=3-7 separate experiments.

As mentioned above, the differential recruitment of β-arrestin2 and subsequent receptor internalisation has been used as a guide for the discovery of MOP biased ligands. We systematically assessed the ability of the different agonists to promote different steps of the arrestin pathway. First, we assessed the recruitment of GRK2-Venus to MOP-NLuc. Since we, and others, have shown that GRK2 overexpression enhances the ability of opioids to induce regulatory processes (Miess et al., 2018), and because assessing GRK2 recruitment requires GRK2 overexpression, we performed the β-arrestin2-YFP recruitment assay and the receptor internalisation assay at endogenous levels of GRK2 as well as with GRK2 overexpression.

All agonists induced GRK2 recruitment (Table 2.5 and Fig. 2.9) with potencies similar to those of the proximal MOP activation assays (i.e Nb33 and mGsi). All agonists that showed low efficacy for MOP activation, also had significantly lower efficacy compared to DAMGO for recruiting GRK2: morphine and oxycodone (~60%) and SR-17018, TRV130, PZM21 and buprenorphine (~20-40%). Thus, so far, potency and efficacy for MOP activation (Nb33) corresponds with potency and efficacy for mGsi recruitment and also GRK2 recruitment.

In contrast, β-arrestin2 recruitment displayed overall lower potency under endogenous GRK2 expression levels (Table 2.6 and Fig. 2.10), and in these conditions the low efficacy agonists (morphine, oxycodone, TRV130, PZM21, SR-17018 and buprenorphine) showed a very limited ability to recruit β-arrestin2 compared to DAMGO. In the MOP internalisation assay, that detects MOP-NLuc trafficking to Rab5-Venus containing endosomes, this low efficacy was even more evident and only morphine and oxycodone among the low efficacy agonists elicited a measurable response (Table 2.7 and Fig. 2.11).

Overexpression of GRK2 allowed for the measurement of β-arrestin2 recruitment (Table 2.8 and Fig. 2.12) and MOP internalisation (Table 2.9 and Fig. 2.13) for all the low efficacy ligands without affecting their ability to inhibit cAMP (Table 2.10 and Fig. 2.14). Although the increased efficacy at β-arrestin2 recruitment and MOP internalisation is indicative of effective GRK2 overexpression, protein expression levels need to be quantified.

Table 2.5 Determination of the maximal responses (E_{max}), potencies (pEC_{50}), functional affinities (pK_A), efficacies (τ) and transduction coefficients ($\log(\tau/K_A)$) of selected agonists to recruit GRK2 to the MOP. Values are expressed as mean ± SEM from n=3 separate experiments. * indicates p<0.05; ** indicates p<0.01; **** indicates p<0.0001 versus DAMGO in a one-way ANOVA with Dunnett's post hoc test.

Ligand	E_{max} % of DAMGO	pEC_{50}	pK_A	τ	$\log(\tau/K_A)$
DAMGO	102 ± 2	7.04 ± 0.16	5.98 ± 0.13	7.18 ± 0.87	6.95 ± 0.16
Met-Enk	118 ± 5	7.05 ± 0.03	5.42 ± 0.25	-	7.13 ± 0.16
Leu-Enk	101 ± 3	6.74 ± 0.19	5.38 ± 0.17	-	6.48 ± 0.09
Fentanyl	91 ± 2	7.50 ± 0.17	6.42 ± 0.22	2.90 ± 0.01	7.24 ± 0.08
Methadone	113 ± 7	6.78 ± 0.12	5.04 ± 0.49	6.43 ± 0.00	6.77 ± 0.19
Morphine	62 ± 7**	6.71 ± 0.14	6.15 ± 0.11	0.97 ± 0.32	6.23 ± 0.14
Oxycodone	71 ± 7*	6.08 ± 0.58	6.80 ± 0.00	0.67 ± 0.00	5.56 ± 0.61
TRV130	29 ± 3****	8.15 ± 0.54	7.36 ± 0.46	0.16 ± 0.04	6.72 ± 0.37
PZM21	28 ± 13****	7.03 ± 0.82	7.02 ± 0.79	0.17 ± 0.09	6.16 ± 0.74
SR17018	37± 11****	7.73 ± 0.10	7.18 ± 0.13	0.34 ± 0.17	6.72 ± 0.33
Buprenorphine	20 ± 4****	7.81 ± 0.39	7.63 ± 0.31*	0.08 ± 0.02	6.65 ± 0.33

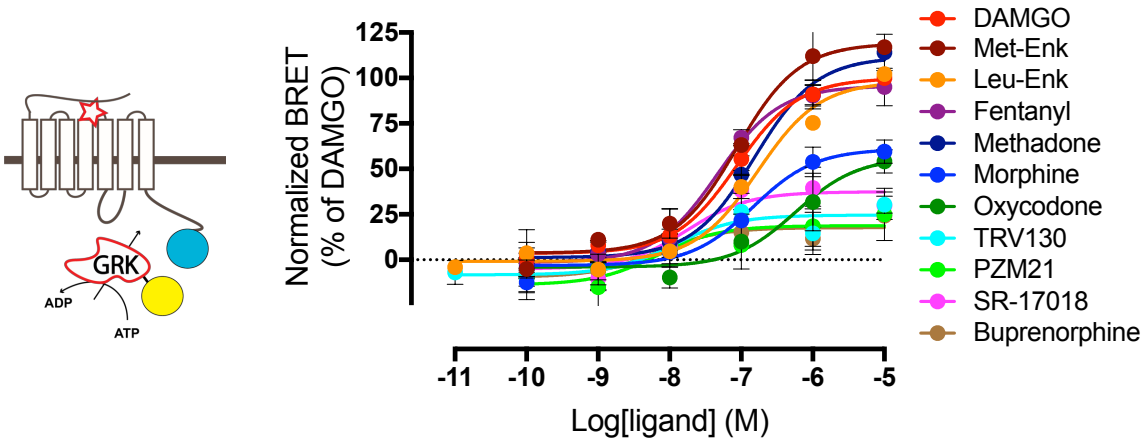


Figure 2.9 The ability of increasing concentrations of selected agonists to recruit GRK2 to MOP. Concentration-response curves were constructed after 10 min of agonist stimulation. Raw BRET ratio of vehicle-treated cells was subtracted, and data were normalised to the response of 10 µM DAMGO (0.036 ± 0.008). Values are expressed as mean ± SEM from n=3 separate experiments.

Table 2.6 Determination of the maximal responses (E_{max}), potencies (pEC_{50}), functional affinities (pK_A), efficacies (τ) and transduction coefficients ($\log(\tau/K_A)$) of selected agonists to recruit β-arrestin2 to the MOP at endogenous GRK2 levels. Values are expressed as mean ± SEM from n=4-12 separate experiments. * indicates p<0.05; **** indicates p<0.0001 versus DAMGO in a one-way ANOVA with Dunnett's post hoc test.

Ligand	E_{max} % of DAMGO	pEC_{50}	pK_A	τ	$\log(\tau/K_A)$
DAMGO	117 ± 5	6.18 ± 0.10	5.68 ± 0.14	3.72 ± 0.95	6.26 ± 0.10
Met-Enk	129 ± 12	6.67 ± 0.09	6.17 ± 0.05	2.54 ± 0.29	6.70 ± 0.07
Leu-Enk	115 ± 9	5.65 ± 0.13	5.37 ± 0.23	1.73 ± 0.12	5.69 ± 0.13
Fentanyl	81 ± 5	7.02 ± 0.11	6.71 ± 0.14*	1.37 ± 0.21	6.93 ± 0.11
Methadone	96 ± 7	6.19 ± 0.05	5.78 ± 0.07	2.00 ± 0.39	6.13 ± 0.05
Morphine	37 ± 5****	6.17 ± 0.23	6.15 ± 0.19	0.37 ± 0.06	5.85 ± 0.16
Oxycodone	34 ± 4****	5.62 ± 0.45	5.38 ± 0.40	0.34 ± 0.05	5.06 ± 0.34
TRV130	16 ± 1****	6.58 ± 0.48	6.45 ± 0.45	0.13 ± 0.01	5.77 ± 0.45
PZM21	15 ± 4****	6.04 ± 0.46	5.37 ± 0.36	0.17 ± 0.05	4.97 ± 0.27
SR17018	46 ± 16****	5.99 ± 0.98	5.06 ± 0.84	0.63 ± 0.18	5.61 ± 0.80
Buprenorphine	17 ± 3****	5.33 ± 0.18	5.40 ± 0.22	0.16 ± 0.04	4.64 ± 0.17

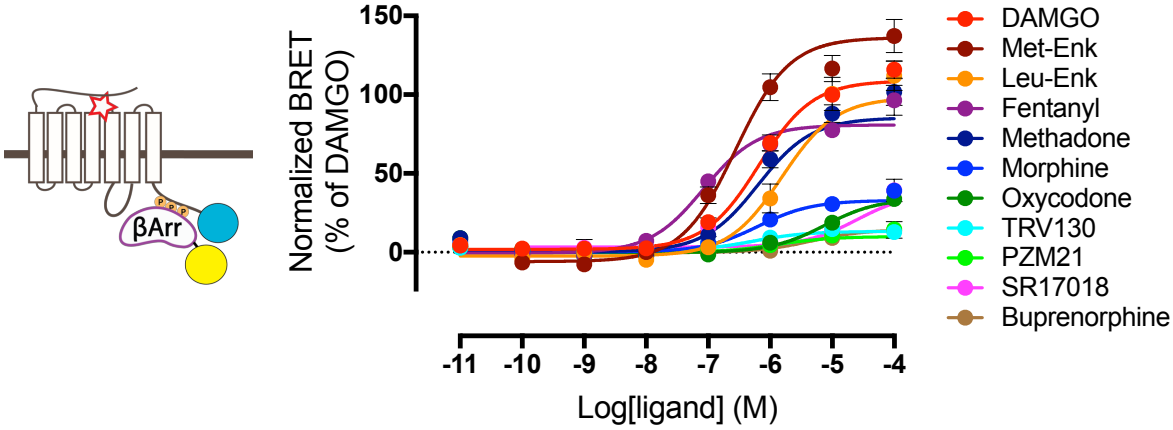


Figure 2.10 The ability of increasing concentrations of selected agonists to recruit β-arrestin2 to MOP at endogenous GRK2 levels. Concentration-response curves were constructed after 10 min of agonist stimulation. Raw BRET ratio of vehicle-treated cells was subtracted, and data were normalised to the response of 10 μM DAMGO (0.080 ± 0.005). Values are expressed as mean ± SEM from n=4-12 separate experiments.

Table 2.7 Determination of the maximal responses (E_{max}), potencies (pEC_{50}), functional affinities (pK_A), efficacies (τ) and transduction coefficients ($\log(\tau/K_A)$) of selected agonists to cause MOP internalisation to Rab5 endosomes at endogenous GRK2 levels. Values are expressed as mean ± SEM from n=4-10 separate experiments. *** indicates p<0.001; **** indicates p<0.0001 versus DAMGO in a one-way ANOVA with Dunnett's post hoc test.
– indicates lack of a measurable response.

Ligand	E_{max} % of DAMGO	pEC_{50}	pK_A	τ	$\log(\tau/K_A)$
DAMGO	132 ± 8	5.98 ± 0.21	5.28 ± 0.26	2.17 ± 0.48	5.75 ± 0.17
Met-Enk	122 ± 17	6.07 ± 0.65	5.44 ± 0.74	1.94 ± 0.72	5.84 ± 0.58
Leu-Enk	134 ± 8	5.56 ± 0.10	4.73 ± 0.11	2.48 ± 0.43	5.27 ± 0.13
Fentanyl	103 ± 7	6.36 ± 0.27	5.87 ± 0.37	1.23 ± 0.33	6.03 ± 0.29
Methadone	108 ± 9	5.97 ± 0.22	5.60 ± 0.42	1.05 ± 0.27	5.67 ± 0.41
Morphine	51 ± 7****	5.47 ± 0.32	5.33 ± 0.19	0.19 ± 0.05	4.44 ± 0.37
Oxycodone	69 ± 17***	4.86 ± 0.32	4.20 ± 0.80	0.28 ± 0.16	4.56 ± 0.87
TRV130	-	-	-	-	-
PZM21	-	-	-	-	-
SR17018	-	-	-	-	-
Buprenorphine	-	-	-	-	-

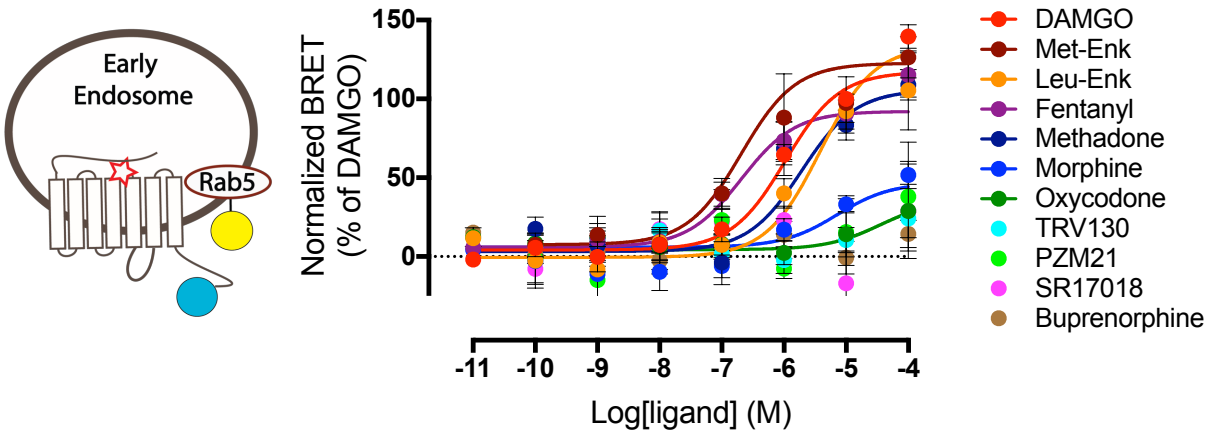


Figure 2.11 The ability of increasing concentrations of selected agonists to cause MOP internalisation at endogenous GRK2 levels. Concentration-response curves were constructed after 30 min of agonist stimulation. Raw BRET ratio of vehicle-treated cells was subtracted, and data were normalised to the response of 10 µM DAMGO (0.071 ± 0.003). Values are expressed as mean ± SEM from n=4-10 separate experiments.

Table 2.8 Determination of the maximal responses (E_{max}), potencies (pEC_{50}), functional affinities (pK_A), efficacies (τ) and transduction coefficients ($\log(\tau/K_A)$) of selected agonists to recruit β-arrestin2 to the MOP with GRK2 overexpression. Values are expressed as mean ± SEM from n = 4-12 separate experiments. * indicates p<0.05; ** indicates p<0.01; *** indicates p<0.001; **** indicates p<0.0001 versus DAMGO in a one-way ANOVA with Dunnett's post hoc test.

Ligand	E_{max} % of DAMGO	pEC_{50}	pK_A	τ	$\log(\tau/K_A)$
DAMGO	95 ± 3	7.61 ± 0.10	7.07 ± 0.12	3.84 ± 0.35	7.64 ± 0.10
Met-Enk	101 ± 3	7.65 ± 0.08	7.00 ± 0.10	5.64 ± 1.09	7.68 ± 0.06
Leu-Enk	84 ± 7	6.91 ± 0.16**	6.45 ± 0.16	3.31 ± 0.81	6.89 ± 0.14
Fentanyl	86 ± 4	8.18 ± 0.08*	7.82 ± 0.08	2.45 ± 0.25	8.18 ± 0.07
Methadone	93 ± 4	7.14 ± 0.12	6.64 ± 0.14	3.41 ± 0.64	7.14 ± 0.12
Morphine	68 ± 4****	7.35 ± 0.16	7.11 ± 0.18	1.47 ± 0.15	7.26 ± 0.15
Oxycodone	69 ± 6***	6.16 ± 0.05****	5.88 ± 0.06*	1.40 ± 0.19	6.07 ± 0.05
TRV130	55 ± 3****	7.73 ± 0.08	7.65 ± 0.09	0.98 ± 0.09	7.64 ± 0.07
PZM21	57 ± 6****	7.56 ± 0.11	7.41 ± 0.13	1.10 ± 0.19	7.43 ± 0.10
SR17018	62 ± 10***	7.23 ± 0.54	6.98 ± 0.48	0.95 ± 0.09	7.09 ± 0.53
Buprenorphine	32 ± 3****	8.53 ± 0.26***	8.83 ± 0.08***	0.56 ± 0.05	8.51 ± 0.06

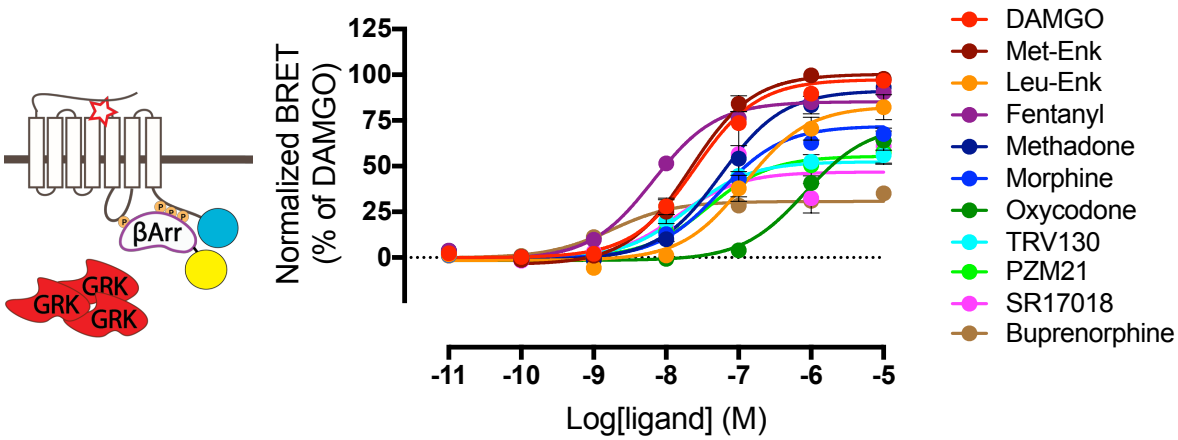


Figure 2.12 The ability of increasing concentrations of selected agonists to recruit β-arrestin2 to the MOP with GRK2 overexpression. Concentration-response curves were constructed after 10 min of agonist stimulation. Raw BRET ratio of vehicle-treated cells was subtracted, and data were normalised to the response of 10 μM DAMGO (0.150 ± 0.007). Values are expressed as mean ± SEM from n=4-12 separate experiments.

Table 2.9. Determination of the maximal responses (E_{max}), potencies (pEC_{50}), efficacies (τ), functional affinities (pK_A), and transduction coefficients ($\log(\tau/K_A)$) of selected agonists to cause MOP internalisation to Rab5 endosomes with GRK2 overexpression. Values are expressed as mean ± SEM from n=4-10 separate experiments. * indicates p<0.05; ** indicates p<0.01; *** indicates p<0.001; **** indicates p<0.0001 versus DAMGO in a one-way ANOVA with Dunnett's post hoc test.

Ligand	E_{max} % of DAMGO	pEC_{50}	pK_A	τ	$\log(\tau/K_A)$
DAMGO	104 ± 2	7.87 ± 0.16	7.37 ± 0.17	1.01 ± 0.09	7.76 ± 0.15
Met-Enk	97 ± 12	8.50 ± 0.34	7.81 ± 0.29	0.84 ± 0.19	8.09 ± 0.23
Leu-Enk	123 ± 11	7.09 ± 0.25	6.60 ± 0.23	1.18 ± 0.15	7.20 ± 0.17
Fentanyl	94 ± 5	8.82 ± 0.11*	8.43 ± 0.11**	0.76 ± 0.08	8.68 ± 0.13
Methadone	97 ± 8	7.70 ± 0.12	7.21 ± 0.14	0.97 ± 0.19	7.53 ± 0.12
Morphine	82 ± 9	7.63 ± 0.18	6.83 ± 0.30	1.00 ± 0.44	7.17 ± 0.15
Oxycodone	83 ± 4	6.67 ± 0.23**	6.19 ± 0.20**	0.60 ± 0.05	6.35 ± 0.18
TRV130	50 ± 9	7.77 ± 0.32	7.64 ± 0.35	0.32 ± 0.09	7.46 ± 0.35
PZM21	71 ± 15	6.52 ± 0.45*	7.13 ± 0.78	0.31 ± 0.07	6.98 ± 0.74
SR17018	73 ± 13	6.71 ± 0.63*	8.07 ± 0.22	0.40 ± 0.11	7.52 ± 0.46
Buprenorphine	32 ± 6****	6.28 ± 0.39***	5.68 ± 0.27**	0.14 ± 0.05	5.27 ± 0.15

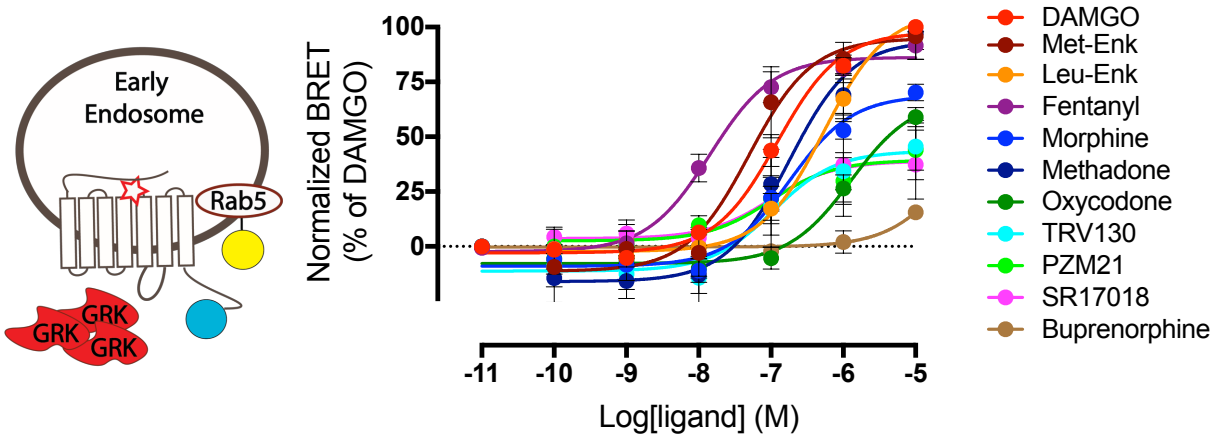


Figure 2.13 The ability of increasing concentrations of selected agonists to cause MOP internalisation with GRK2 overexpression. Concentration-response curves were constructed after 30 min of agonist stimulation. Raw BRET ratio of vehicle-treated cells was subtracted, and data were normalised to the response of 10 μM DAMGO (0.089 ± 0.003). Values are expressed as mean ± SEM from n=4-10 separate experiments.

Table 2.10 Determination of the maximal responses (E_{max}), potencies (pEC_{50}), efficacies (τ), functional affinities (pK_A), and transduction coefficients ($\log(\tau/K_A)$) of selected agonists to inhibit forskolin-induced cAMP production via the MOP with GRK2 overexpression. Values are expressed as mean ± SEM from n=3-4 separate experiments. * indicates p<0.05 versus DAMGO in a one-way ANOVA with Dunnett's post hoc test. ND: not determined

Ligand	E_{max} % of DAMGO	pEC_{50}	τ	pK_A	$\log(\tau/K_A)$
DAMGO	104 ± 6	9.33 ± 0.37	2.13 ± 0.43	8.95 ± 0.33	9.25 ± 0.40
Met-Enk	ND	ND	ND	ND	ND
Leu-Enk	105 ± 7	8.90 ± 0.07	2.07 ± 0.35	8.52 ± 0.01	8.82 ± 0.06
Fentanyl	124 ± 12	9.90 ± 0.02	2.46 ± 0.55	9.27 ± 0.24	10.0 ± 0.13
Methadone	114 ± 12	8.93 ± 0.07	1.93 ± 0.21	8.47 ± 0.11	8.47 ± 0.11
Morphine	119 ± 10	8.58 ± 0.30	2.70 ± 0.84	7.85 ± 0.06	8.55 ± 0.32
Oxycodone	128 ± 12	7.63 ± 0.06*	2.65 ± 0.21	7.13 ± 0.01*	7.62 ± 0.07
TRV130	114 ± 15	9.00 ± 0.24	2.42 ± 0.94	8.45 ± 0.23	8.94 ± 0.28
PZM21	131	9.04	-	8.38	9.04
SR17018	ND	ND	ND	ND	ND
Buprenorphine	100 ± 16	9.93 ± 0.72	1.40 ± 0.35	9.50 ± 0.63	9.80 ± 0.76

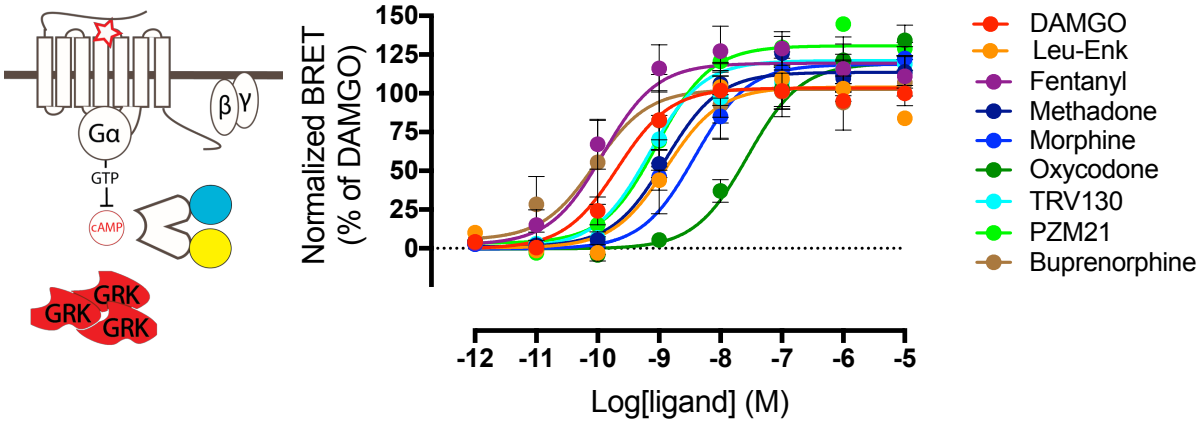


Figure 2.14 The ability of increasing concentrations of selected agonists to inhibit forskolin-induced cAMP production via the MOP with GRK2 overexpression. Concentration-response curves were constructed after 10 min of agonist stimulation followed by stimulation with 10 µM forskolin to stimulate cAMP production. Raw BRET ratio of vehicle-treated cells was subtracted, and data were normalised to the response of 10 µM DAMGO (0.077 ± 0.004). Values are expressed as mean ± SEM from n=3-4 separate experiments.

2.4.4 Calculation of bias factors and MOP agonist relative efficacy

The systematic analysis of eleven opioid agonists in seven activation/signalling assays allowed us to compare the extent of biased agonism displayed by these ligands as well as to investigate whether there is a correlation between signalling responses and intrinsic efficacies of these agonists. Analysis of the above data using an approach based on the operational model of agonism allowed us to estimate transduction coefficient values ($\log(\tau/K_A)$) (Kenakin et al., 2012) (Tables 2.1-10). This method removes the bias of the system, i.e. the difference in stimulus coupling efficiency between two pathways, by normalising the transduction coefficient to a reference agonist, in this case DAMGO. The obtained $\Delta\log(\tau/K_A)$ value is then compared across two different pathways to give a $\Delta\Delta\log(\tau/K_A)$ value as a measurement of biased agonism. In this study we compared the pathways representative of receptor activation (Nb33) and G protein activation (mGsi, $G\alpha_{i2}$, cAMP) against arrestin pathways (GRK2, β-arrestin2 recruitment and internalisation) (Tables 2.11-14). For an accurate quantification of signalling bias, a concentration-dependent response curve is needed. However, the low efficacy agonists (TRV130, PZM21, SR17018 and buprenorphine) displayed limited or no measurable signal in assays where signalling coupling was less efficient (i.e. β-arrestin2 recruitment and internalisation under endogenous GRK2 expression levels), thus a comparison with β-arrestin2 recruitment and internalisation in GRK2 overexpressing conditions was also performed.

G protein bias was detected for buprenorphine when comparing all G protein pathways against β-arrestin2 recruitment at endogenous GRK2 levels (Tables 2.12) or internalisation in GRK2 overexpressing conditions (Table 2.14). However, this bias was not detected when GRK2 was overexpressed in the β-arrestin2 recruitment assay (Table 2.13). PZM21 also displayed a small bias between Nb33 and β-arrestin2 recruitment (Tables 2.12), but again this was lost when comparing against β-arrestin2 recruitment with GRK2 overexpression (Table 2.13). These results support previous data suggesting that bias is highly dependent on the cellular context and expression levels of effector proteins. However, no bias towards G protein was detected for the so-called biased ligands (TRV130, PZM21 or SR-17018) and no bias towards β-arrestin2 was detected for fentanyl.

Table 2.11 Calculation of biased agonism (ΔΔLog(τ/K_A)) of the selected ligands between the indicated pathway and GRK2 recruitment. Biased agonism was calculated utilizing the difference in transduction coefficient (log(τ/K_A). DAMGO was used as the reference agonist. Values are expressed as mean ± SEM from n=3-12 separate experiments.

Pathway	Met-Enk	Leu-Enk	Fentanyl	Methadone	Morphine	Oxycodone
Nb33	0.305 ± 0.250	0.271 ± 0.224	0.454 ± 0.216	-0.110 ± 0.275	0.382 ± 0.236	0.148 ± 0.632
mGsi	0.374 ± 0.303	0.615 ± 0.300	0.619 ± 0.283	0.274 ± 0.343	0.486 ± 0.281	0.445 ± 0.657
$G\alpha_{i2}$	0.260 ± 0.481	0.281 ± 0.459	0.398 ± 0.416	0.123 ± 0.439	0.423 ± 0.427	0.236 ± 0.751
cAMP	-0.552 ± 0.498	0.035 ± 0.452	0.209 ± 0.467	-0.349 ± 0.435	0.184 ± 0.474	-0.190 ± 0.742

Pathway	TRV130	PZM21	SR17018	Buprenorphine
Nb33	0.269 ± 0.426	1.107 ± 0.816	0.201 ± 0.508	1.199 ± 0.401
mGsi	0.578 ± 0.464	0.704 ± 0.840	-0.219 ± 0.787	1.113 ± 0.424
$G\alpha_{i2}$	0.555 ± 0.611	0.805 ± 0.880	-0.363 ± 0.509	1.042 ± 0.461
cAMP	0.059 ± 0.548	0.307 ± 0.892	-1.030 ± 0.504	1.487 ± 0.871

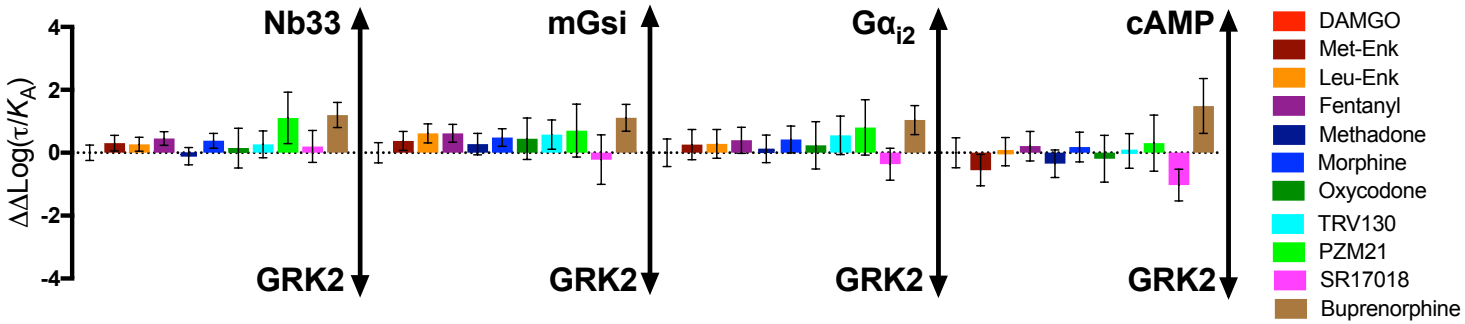


Table 2.12 Calculation of biased agonism (ΔΔLog(τ/K_A)) of the selected ligands between the indicated pathway and β-arrestin2 recruitment. Biased agonism was calculated utilizing the difference in transduction coefficient (log(τ/K_A). DAMGO was used as the reference agonist. Values are expressed as mean ± SEM from n=3-12 separate experiments. ** indicates p<0.01; **** indicates p<0.0001 between pathways in a one-way ANOVA with Tukey's post hoc test.

Pathway	Met-Enk	Leu-Enk	Fentanyl	Methadone	Morphine	Oxycodone
Nb33	0.047 ± 0.162	0.367 ± 0.207	0.077 ± 0.194	-0.161 ± 0.164	0.073 ± 0.215	-0.037 ± 0.367
mGsi	0.115 ± 0.237	0.712 ± 0.288	0.242 ± 0.266	0.223 ± 0.262	0.177 ± 0.264	0.261 ± 0.409
$G\alpha_{i2}$	0.001 ± 0.442	0.378 ± 0.452	0.021 ± 0.404	0.071 ± 0.379	0.114 ± 0.416	0.051 ± 0.547
cAMP	-0.810 ± 0.460	0.131 ± 0.444	-0.168 ± 0.457	-0.400 ± 0.375	-0.125 ± 0.463	-0.374 ± 0.534

Pathway	TRV130	PZM21	SR17018	Buprenorphine
Nb33	0.532 ± 0.475	1.607 ± 0.422**	0.622 ± 0.878	2.518 ± 0.251****
mGsi	0.841 ± 0.509	1.205 ± 0.466	0.202 ± 1.064	2.431 ± 0.287****
$G\alpha_{i2}$	0.818 ± 0.647	1.306 ± 0.536	0.058 ± 0.878	2.360 ± 0.338****
cAMP	0.322 ± 0.587	0.807 ± 0.555	-0.609 ± 0.875	2.806 ± 0.813****

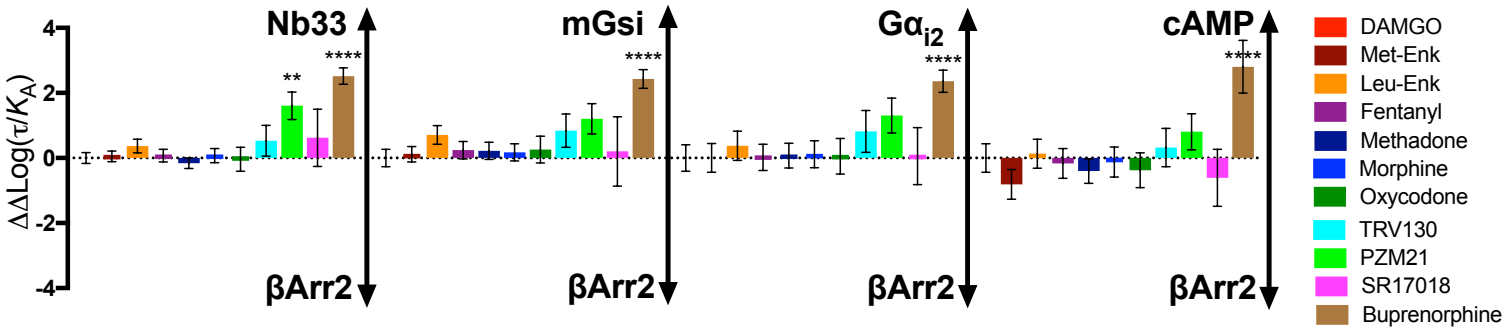


Table 2.13 Calculation of biased agonism (ΔΔLog(τ/K_A)) of the selected ligands between the indicated pathway and β-arrestin2 recruitment with GRK2 overexpression. Biased agonism was calculated utilizing the difference in transduction coefficient (log(τ/K_A). DAMGO was used as the reference agonist. Values are expressed as mean ± SEM from n=3-12 separate experiments.

Pathway	Met-Enk	Leu-Enk	Fentanyl	Methadone	Morphine	Oxycodone
Nb33	0.456 ± 0.156	0.554 ± 0.212	0.215 ± 0.175	0.219 ± 0.194	0.049 ± 0.205	0.338 ± 0.133
mGsi	0.525 ± 0.233	0.898 ± 0.291	0.379 ± 0.253	0.602 ± 0.282	0.153 ± 0.256	0.635 ± 0.223
$G\alpha_{i2}$	0.411 ± 0.440	0.564 ± 0.454	0.159 ± 0.396	0.451 ± 0.393	0.090 ± 0.411	0.426 ± 0.427
cAMP (GRK2)	ND	0.319 ± 0.439	0.233 ± 0.439	0.166 ± 0.435	-0.322 ± 0.545	-0.054 ± 0.421

Pathway	TRV130	PZM21	SR17018	Buprenorphine
Nb33	0.044 ± 0.176	0.530 ± 0.338	0.529 ± 0.642	0.035 ± 0.195
mGsi	0.353 ± 0.254	0.127 ± 0.392	0.110 ± 0.880	-0.052 ± 0.239
$G\alpha_{i2}$	0.331 ± 0.473	0.228 ± 0.473	-0.035 ± 0.643	-0.123 ± 0.299
cAMP (GRK2)	-0.311 ± 0.504	0.002 ± 0.425	ND	-0.318 ± 0.867

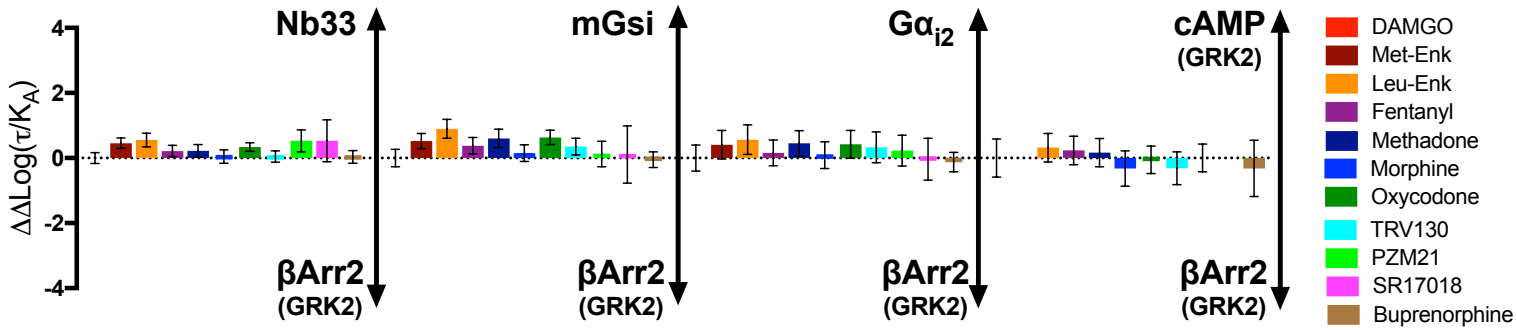
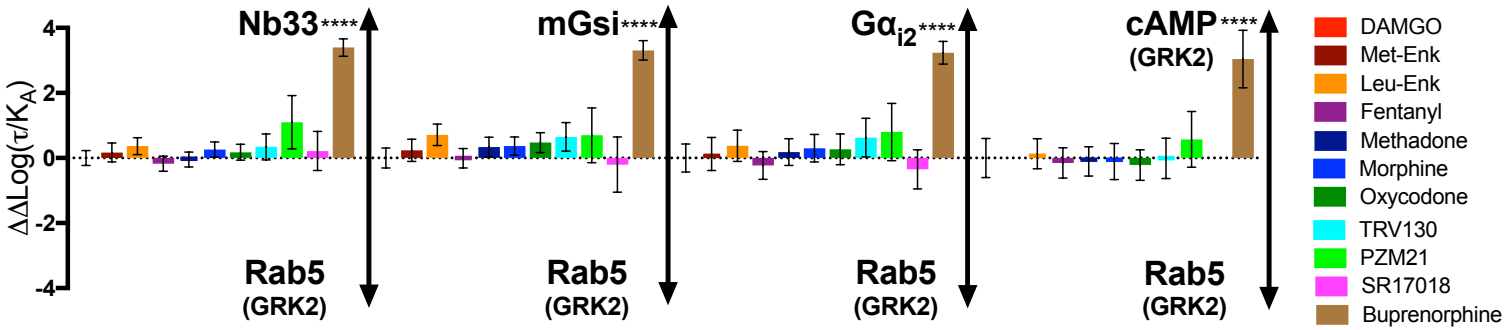


Table 2.14 Calculation of biased agonism (ΔΔLog(τ/K_A)) of the selected ligands between the indicated pathway and MOP internalisation towards Rab5 positive endosomes with GRK2 overexpression. Biased agonism was calculated utilizing the difference in transduction coefficient (log(τ/K_A). DAMGO was used as the reference agonist. Values are expressed as mean ± SEM from n=3-12 separate experiments. **** indicates p<0.0001 between pathways in a one-way ANOVA with Tukey's post hoc test.

Pathway	Met-Enk	Leu-Enk	Fentanyl	Methadone	Morphine	Oxycodone
Nb33	0.170 ± 0.292	0.367 ± 0.260	-0.171 ± 0.233	-0.049 ± 0.228	0.261 ± 0.234	0.177 ± 0.245
mGsi	0.238 ± 0.339	0.711 ± 0.328	-0.007 ± 0.296	0.335 ± 0.306	0.365 ± 0.279	0.474 ± 0.304
$G\alpha_{i2}$	0.124 ± 0.504	0.377 ± 0.478	-0.228 ± 0.425	0.183 ± 0.411	0.302 ± 0.426	0.265 ± 0.474
cAMP (GRK2)	ND	0.131 ± 0.464	-0.153 ± 0.465	-0.102 ± 0.451	-0.110 ± 0.556	-0.216 ± 0.469

Pathway	TRV130	PZM21	SR17018	Buprenorphine
Nb33	0.341 ± 0.401	1.101 ± 0.818	0.217 ± 0.601	3.395 ± 0.264****
mGsi	0.650 ± 0.441	0.698 ± 0.842	-0.203 ± 0.851	3.309 ± 0.298****
$G\alpha_{i2}$	0.628 ± 0.595	0.799 ± 0.883	-0.347 ± 0.602	3.238 ± 0.348****
cAMP (GRK2)	-0.014 ± 0.620	0.573 ± 0.858	ND	3.043 ± 0.885****



We were surprised to see that our determination of bias did not align with previously published reports. However, as we detected very low efficacy for all the so-called G protein-biased MOP agonists, we analysed whether there was a correlation in the intrinsic efficacy of these ligands between pathways. Analysis with the operational model also allows for the estimation of the relative efficacy (τ) of partial agonists. In agreement with the literature, DAMGO, Met-enk, Leu-enk, fentanyl and methadone displayed full agonism in all assays (Tables 2.1-10). Similarly, the lower intrinsic efficacy of morphine, oxycodone, TRV130, PZM21, SR-17018 and buprenorphine was demonstrated by their partial response in most assays except for those where signal amplification is more apparent (i.e $G\alpha_{i2}$ activation and cAMP inhibition). Their estimated relative efficacy (τ) reflects this accordingly.

We then investigated the relationship between the efficacies for MOP activation (τ Nb33) with the efficacies for the G protein pathways (τ mGsi, τ $G\alpha_{i2}$, τ cAMP) (Fig. 2.15). A strong linear correlation was obtained between the MOP activation (Nb33) and all G protein pathways. We also investigated the relationship between the efficacies for MOP activation (τ Nb33) with the efficacies for the arrestin pathways (τ GRK2, τ β-arrestin2, τ Rab5) (Fig. 2.16). However, since the partial agonists did not display a measurable response in some of these pathways at endogenous GRK2 expression levels, we compared the Nb33 assay with the arrestin pathways in which GRK2 was overexpressed. Similar to the correlation between MOP activation and the G protein pathway, a strong linear correlation was obtained between MOP activation and all the arrestin pathways with GRK2 overexpression (Fig. 2.16). Interestingly, we also found a correlation between cAMP inhibition and β-arrestin2 recruitment with GRK2 overexpression (Fig. 2.17). Together, these correlations indicate that the intrinsic efficacy for receptor activation is associated with the extent to which the MOP activates the G protein as well as the β-arrestin2 pathways. Interestingly, while PZM21 and TRV-130 displayed similar relative efficacy in all assays, the τ value estimated for SR-17018 was consistently lower and closer to buprenorphine.

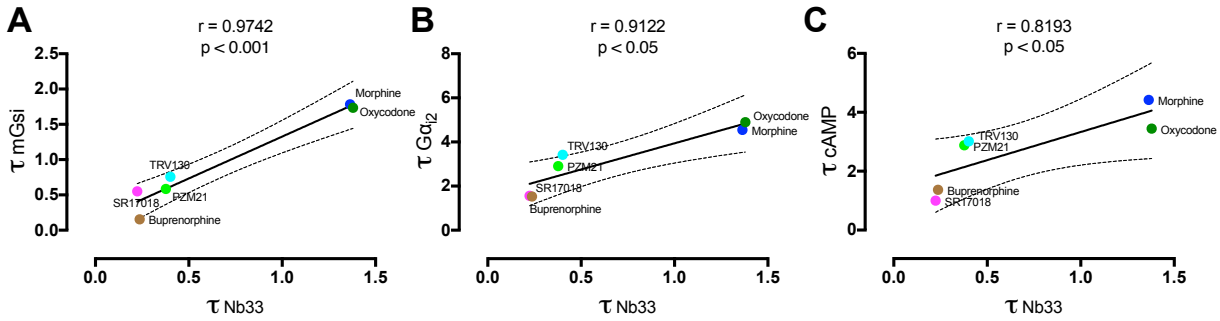


Figure 2.15 Correlation of τ efficacy values between Nb33 and G protein pathways. τ values of partial agonists for Nb33 recruitment (Table 2.1) were correlated to their corresponding τ values for mGsi recruitment (Table 2.2) **(A)**, $G\alpha_{i2}$ protein activation (Table 2.3) **(B)** and cAMP inhibition (Table 2.4) **(C)**. Person r and p values are denoted.

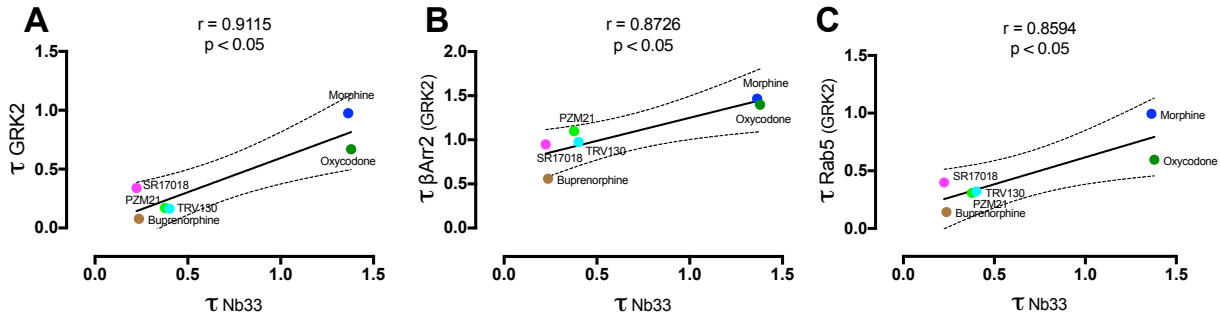


Figure 2.16 Correlation of τ efficacy values between Nb33 and β-arrestin2 pathways. τ values of partial agonists for Nb33 recruitment (Table 2.1) were correlated to their corresponding τ values for GRK2 recruitment (Table 2.5) **(A)**, β-arrestin2 recruitment (Table 2.8) **(B)** and Rab5 internalisation (Table 2.9) **(C)**. Person r and p values are denoted.

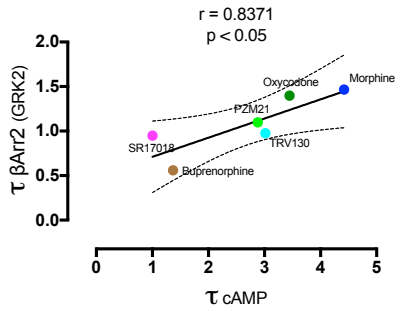


Figure 2.17 Correlation of τ efficacy values between cAMP inhibition and β-arrestin2 recruitment. τ values of partial agonists for cAMP inhibition (Table 2.4) were correlated to their corresponding τ values for β-arrestin2 recruitment (Table 2.8). Person r and p values are denoted.

Finally, we constructed 'bias plots' in which the response in β-arrestin2 recruitment was expressed as a function of the corresponding response for cAMP inhibition. However, bias plots incorporate all three types of bias: system bias (stoichiometric ratios between signalling effectors in a specific cellular background) (Kenakin, 2015), observational bias (assay conditions) (Rajagopal et al. 2011), as well as ligand bias (intrinsic properties of the ligand) (Kenakin 2017). Thus, representation of the agonist responses in such 'bias plots' would provide a qualitatively representation of the influence of changing the system upon overexpression of GRK2. Overall, all ligands follow the same trend which indicates that rather than a ligand-specific bias, the restricted ability for β-arrestin2 recruitment to MOP is due to a system bias that prioritizes G protein signalling over β-arrestin2 recruitment (Fig. 2.18A). Additionally, the system bias is shifted favouring β-arrestin2 recruitment when GRK2 is overexpressed (Fig. 2.18B). This seemed more prominent for morphine compared to buprenorphine, TRV130 and PZM21, thus we calculated bias ratios following the 'equiactive comparison' method that was used for the determination of a bias ratio of 3 for TRV130 (DeWire et al. 2013). Estimates of the intrinsic relative activity (RA_i) for cAMP inhibition or β-arrestin2 recruitment were calculated and the bias ratio reported is the ratio of the RA_i in cAMP inhibition versus the RA_i in β-arrestin2 recruitment (Table 2.15). However, no significantly different bias ratio towards G protein was found for any of the ligands at either endogenous or overexpressing GRK2 levels.

Altogether, these results suggest that the biased agonists described to date are also agonists with very low efficacy at all signalling pathways and thus, the improved therapeutic profiles observed with these agonists might be a result of the agonists having an ideal efficacy threshold that is enough to cause analgesia without triggering adverse effects.

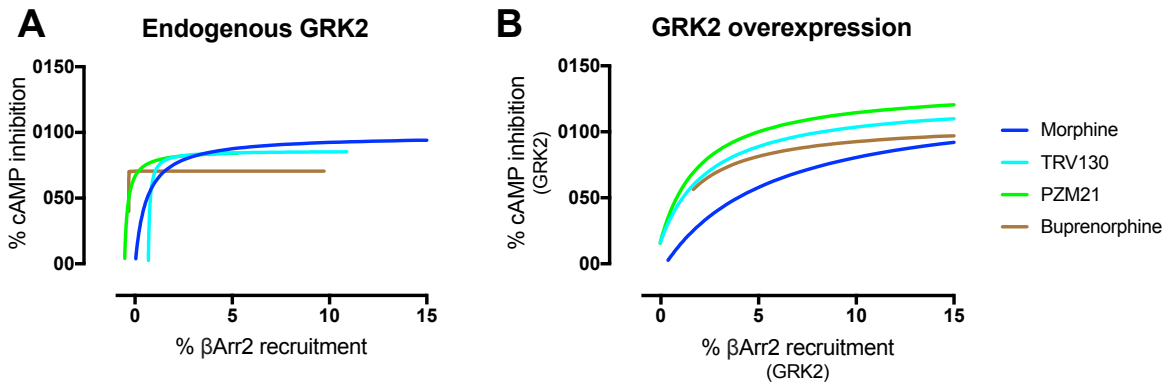


Figure 2.18 Equimolar comparison of cAMP inhibition and β-arrestin2 recruitment. Under endogenous GRK2 levels **(A)** or with overexpression of GRK2 **(B)**. Shown are the generated functions of selected agonists from the cAMP inhibition assay (Fig. 2.4) and β-arrestin2 recruitment (Fig. 2.6) under endogenous GRK2 levels **(A)** or cAMP inhibition assay (Fig. 2.10) and β-arrestin2 recruitment (Fig. 2.8) after GRK2 overexpression **(B)**.

Table 2.15 Quantification of bias ratios following 'equiactive comparison'. Intrinsic relative activity (RA_i) were calculated with morphine as the reference ligand. Bias ratio is the ratio between cAMP inhibition and β-arrestin2 recruitment.

	cAMP			β-arrestin2			
Ligand	**E_{max}**	**pEC_{50}**	**RA_i**	**E_{max}**	**pEC_{50}**	**RA_i**	**Bias Ratio**
Morphine	98	8.15	1	37	6.17	1	1
TRV130	87	8.6	1.19	16	6.58	2.47	0.48
PZM21	85	8.27	1.17	15	6.04	2.41	0.48
SR17018	45	7.8	2.08	46	5.99	0.78	2.67
Buprenorphine	72	9.46	1.58	17	5.33	1.88	0.84

	cAMP (GRK2)			β-arrestin2 (GRK2)			
Ligand	**E_{max}**	**pEC_{50}**	**RA_i**	**E_{max}**	**pEC_{50}**	**RA_i**	**Bias Ratio**
Morphine	119	8.58	1	68	7.35	1	1
TRV130	114	9	1.09	55	7.73	1.30	0.84
PZM21	131	9.04	0.96	57	7.56	1.23	0.78
SR17018	ND	ND	ND	62	7.23	1.08	ND
Buprenorphine	100	9.93	1.38	32	8.53	2.47	0.56

2.5 Discussion

Substantial effort has recently been devoted to generating G protein-biased MOP agonists as improved analgesics that lack the on-target adverse effects that traditional opiates typically present. Although the three most recent G protein-biased MOP agonists display an improved therapeutic window due to reduced side effects, a head-to-head comparison of the *in vitro* signalling bias of these ligands has not been done to date. This comparison is important since the quantification of biased agonism is affected by several confounding factors and has been shown to be dependent on cell background, protein content and kinetics (Klein Herenbrink et al., 2016). Moreover, controversial reports indicating that PZM21 still causes respiratory depression and is a partial agonist (Hill et al. 2018), motivated us to explore MOP function at events more proximal to receptor activation so that we could assess the intrinsic efficacy of such ligands in assays where there is less amplification.

For this, we repurposed tools previously used for structural studies (i.e. nanobody and mini G protein) to interrogate key questions about MOP pharmacology. We developed a conformationally-selective Nb33-Venus BRET biosensor to provide quantitative measurement of MOP activation. Additionally, we used mGsi-Venus as a quantitative measure of MOP coupling to the $G\alpha_{i/o}$-PTx sensitive family. The three most recent MOP G protein-biased agonists: TRV130, PZM21 and SR-17018 displayed a very partial response in Nb33 and mGsi recruitment assays. This suggested that these agonists stabilise a receptor conformation that is distinct of that of high efficacy agonists stabilised by Nb33. Moreover, these ligands displayed a very similar response to that of the partial agonist buprenorphine, suggesting that they too have lower intrinsic efficacy. This agrees with recent studies showing that PZM21 is a low efficacy agonist in a G protein activation assay that measures the separation of $G\alpha_{i1}$ and $G\beta\gamma$ (Hill et al. 2018). Evaluating activation of the G protein pathway at different endpoints (recruitment of mGsi, $G\alpha_{i2}$ activation and cAMP inhibition) revealed signal amplification downstream from receptor activation (Nb33). This was reflected by an increase in agonist potency and efficacy globally, which masked the partial agonism of the so-called G protein-biased MOP agonists. This highlights the value of measuring efficacy at events more proximal to, or representative of receptor activation such as nanobody recruitment so that agonist intrinsic efficacy can be assessed (Livingston et al. 2018).

We performed all our assays in HEK293 cells, the model cell line that has been traditionally used for most MOP-mediated cAMP inhibition measurements *in vitro* (Chen et al 2013, DeWire et al. 2013, Manglik et al. 2016). Importantly, different to previous studies that compared cAMP in HEK293 to β-arrestin2 recruitment in U2OS cells (Schmid et al. 2017) or CHO cells (Manglik et al. 2016); or internalisation in U2OS cells (DeWire et al. 2013; Manglik et al. 2016), we maintained the same cellular background for all assays. This is important because the signalling response measured depends on a combination of factors: the intrinsic properties of the ligand (ligand bias), but also the stoichiometric ratios between signalling effectors in a specific cellular background (system bias) (Kenakin, 2015) and the assay conditions (observational bias) (Rajagopal et al. 2011). All these confounding factors might account for discrepancies between studies. For instance, Schmid et al. reported that fentanyl is biased towards β-arrestin2 and this bias is correlated with its tendency to cause respiratory suppression (Schmid et al., 2017). In our study, fentanyl displayed significantly higher functional affinity pK_A and pEC_{50} in the β-arrestin2 recruitment assays (Tables 2.6 and 2.8), but it failed to show any significant bias towards β-arrestin2 recruitment. The discrepancy with Schmid et al. regarding fentanyl could be due to different assay conditions. Within the same study, when β-arrestin2 recruitment was compared against a GTPγS assay in membranes, fentanyl was β-arrestin2-biased; however, when compared against cAMP inhibition in whole cells, they did not detect any bias (Schmid et al., 2017). This highlights the importance of maintaining the same system (e.g. membrane versus whole cell) and cellular background across the different signalling assays measured, since changes in expression levels of signalling effectors can affect the determination of biased agonism.

In this line, we found that the protein content of cells, such as GRK expression levels, contributes dramatically to bias observed for MOP. In our studies, GRK2 overexpression completely abolished all bias between cAMP inhibition and β-arrestin 2 recruitment. A similar observation was made when PZM21 was first characterised; PZM21 exhibited robust cAMP inhibition with lower efficacy and potency than DAMGO, but higher potency than morphine and TRV130 without eliciting a measurable β-arrestin2 recruitment under endogenous GRK2 expression levels (Manglik et al., 2016). However, bias calculation by the operational model requires a measurable response, and for this they overexpressed GRK2. Despite the lower

efficacy for arrestin recruitment observed for morphine, TRV130 and PZM21 compared to DAMGO, the degree of bias towards the G protein pathway was not significant (Manglik et al., 2016).

Although limited β-arrestin2 recruitment has been shown for the three most recent G protein-biased MOP agonists (TRV130, PZM21 and SR-17018), quantification of this bias has not been easy to demonstrate. As mentioned previously, bias quantification for PZM21 failed to show any significance (Manglik et al., 2016). A small bias ratio of 3 has been reported for TRV130 at the human MOP through comparison between the relative activity in cAMP inhibition versus β-arrestin2 (DeWire et al., 2013). SR-17018 is the MOP biased agonist with the biggest G protein bias factor reported to date (Schmid al., 2017). However, it needs to be noted that SR-17018 did not elicit a measurable response in the β-arrestin2 recruitment assay in U2OS cells which are known to express very low levels of GRKs, a lot lower than brain regions such as the cerebellum and frontal lobe (Nickolls, 2013). In this study GRK was not overexpressed, instead a potency value higher than 10 μM was set for its bias quantification, because SR-17018 was not able to compete an EC_{50} concentration of the DAMGO-induced β-arrestin2 response (Schmid al., 2017). Moreover, the magnitude of bias factors reported for SR-17018 range between 30 and 102 and differ within the same study when assessing different assay conditions and cell backgrounds (e.g. GTPγS (in CHO membranes or brainstems) or cAMP inhibition (in CHO cells) versus arrestin imaging quantification or Pathhunter (in U2OS cells)) (Schmid al., 2017).

Of note, although TRV130 exhibited limited arrestin recruitment (14% of morphine) and receptor internalisation at the human MOP, it initiated greater arrestin recruitment (74% of morphine) at the mouse MOP (DeWire et al., 2013), which was the species used in our study. Species differences might account for disparities between rodent animal models and effects observed during clinical trials. Thus, during the drug development process species differences need to be considered for better translation of bias agonism into clinical effects.

In our study, none of the so-called G protein biased MOP agonists displayed any significant bias in HEK293 cells. Despite them showing significantly higher functional affinity (pK_A) for Nb33 recruitment compared to DAMGO (Table 2.1), the preferential activation of

the MOP did not translate into preferential coupling to either G protein or β-arrestin2 pathways. TRV130, PZM21 and SR-17018 displayed low efficacy at GRK2 and β-arrestin2 recruitment and internalisation assays but they also displayed low efficacy in the G protein pathways upstream of cAMP inhibition (e.g. mGsi as presented in Table 2.2 and Fig. 2.5), which might indicate that they have lower agonist efficacy overall. Moreover, the head-to-head comparison with buprenorphine, which is a partial agonist with higher affinity for the MOP, demonstrated that in the quantification of bias at the MOP, high potency and low efficacy translates into detection of "G protein bias" due to the lack of coupling efficiency of the system for β-arrestin2 recruitment.

Further characterisation of these novel MOP agonists requires assessment of additional downstream signalling pathways (e.g. GIRK channel activation and ERK signalling). In a recent study that quantified bias at the KOP over a number of G protein pathways (GTPγS, cAMP, GIRK and Ca^{2+}) versus arrestin, bias was only found between the arrestin and the GTPγS and GIRK assays, but not between arrestin and cAMP or Ca^{2+} (Ho et al. 2018). Since G proteins activate different downstream effectors, specific G protein-dependent pathways should be taken into consideration when it comes to comparing bias against arrestin. This is particularly important if we consider that different physiological events might be mediated by specific G protein- or arrestin-dependent pathways. For example, MOP inhibits the exercise pressor reflex by closing Ca^{2+} channels but not by opening GIRK channels (Estrada & Kaufman, 2018). While the current dogma is that MOP agonists mediate respiratory depression through activation of arrestin signalling (Madariaga-Mazón et al., 2017; Raehal, Walker, & Bohn, 2005), respiratory depression induced by DAMGO and fentanyl was attenuated in GIRK knock-out mice (Montandon et al., 2016). Thus, a more comprehensive analysis of different downstream signalling pathways at the MOP is required for a better determination of its bias signalling features.

Finally, we inferred τ efficacy values for partial agonists from the operational model. Buprenorphine, TRV130, PZM21 and SR-17018 showed lower intrinsic efficacy in comparison to the other partial agonists (morphine and oxycodone). We found that efficacy for MOP activation (Nb33) correlates with efficacy for both G protein and arrestin coupling. Notably

SR-17018, the agonist with the safest therapeutic window (Schmid et al. 2017), and buprenorphine, a partial agonist that has been shown not to cause respiratory depression at doses that achieve similar analgesia to morphine (Davis, 2012; Pergolizzi et al., 2010), are the two agonists at the lower end of these correlations.

While TRV130, PZM21 and SR17018 appear to be partial agonists similar to buprenorphine, they could still be more efficacious therapeutically compared to buprenorphine due to their distinct binding kinetics. We considered the kinetics for receptor activation and receptor-effector coupling by measuring the response over a 20 min stimulation period and we did not detect any changes in potency or efficacy over time, indicating that, different to other GPCRs (Klein-Herenbrink et al. 2016), the duration of drug exposure might not affect biased agonism at the MOP. Although activation of the MOP occurred very fast, in a similar timescale as previously reported (Lohse, Maiellaro, & Calebiro, 2014) and reached equilibrium rapidly for most ligands, the slow dissociation rate of buprenorphine (Virk et al. 2009) was manifested in the lack of reversal of Nb33 recruitment after 10 min of addition of naloxone (Fig. 2.6). The slow dissociation rate of buprenorphine may be a liability in cases where treatment with other opiate agonists or antagonists is required (i.e. in the case of overdose), as it cannot be displaced. In contrast, MOP activation in response to TRV130, PZM21 and SR-17018 reversed back to baseline immediately after the addition of naloxone (Fig. 2.6), suggesting that their dissociation kinetics are comparable to that of endogenous peptides.

In addition to ligand binding kinetics, recent reports suggest that drug lipophilicity is also an important factor in assessing therapeutic efficacy at MOP since opioid alkaloids can cross the plasma membrane and activate the receptor in intracellular compartments (Stoeber et al. 2018). Morphine was found to activate MOP in the Golgi, where the authors propose that it may generate aberrant signalling that does not occur in response to the cell impermeable endogenous opioid neuropeptides (Stoeber et al. 2018). Altogether, we conclude that many pharmacological properties including intrinsic efficacy, ligand binding kinetics and location bias, in addition to or instead of signalling bias, could contribute to the physiological responses of opioid drugs.

Chapter 3

GRK mediates MOP plasma membrane reorganisation in an agonist-specific manner

3.1 Abstract

Differential regulation of the μ-opioid receptor (MOP) has been linked to the development of opioid tolerance and dependence which both limit the clinical use of opioid analgesics. At a cellular level, MOP regulation occurs via receptor phosphorylation, desensitisation, plasma membrane redistribution and internalisation. Here, we used fluorescence correlation spectroscopy (FCS) and fluorescence recovery after photobleaching (FRAP) to quantify ligand-dependent changes in the plasma membrane organisation of MOP. The poor internalising agonist morphine and the antagonist naloxone did not alter the constitutive MOP plasma membrane organisation. In contrast, the internalising agonist DAMGO changed MOP plasma membrane organisation in a pertussis toxin-insensitive manner and by two distinct mechanisms. DAMGO slowed MOP diffusion in a manner that was independent of internalisation but dependent on GRK2/3. Additionally, DAMGO reduced the surface receptor number and the proportion of mobile receptors, and increased receptor clustering in a manner that was dependent on clathrin-mediated endocytosis. Overall, these results suggest the existence of distinct sequential MOP reorganisation events at the plasma membrane that may differentiate internalising versus non-internalising opioids.

3.2 Introduction

The μ-opioid receptor (MOP) is the G protein-coupled receptor (GPCR) that mediates the analgesic effects of opioids such as morphine. Despite opioids being the mainstay analgesics for the treatment of acute pain, their clinical use for the sustained treatment of inflammatory and chronic pain is severely limited by on target adverse effects including tolerance and dependence. Furthermore, opioid prescription, abuse and overdose deaths have reached record levels globally (Floyd & Warren, 2018; Rudd et al., 2016). As evidenced by the current opioid epidemic, the development of safer and more effective analgesics remains an unmet medical challenge. Differential regulation of MOP by morphine compared to synthetic opioids or opioid peptides, has been linked to its increased liability for the development of tolerance and dependence (Duttaroy & Yoburn, 1995; Morgan & Christie, 2011; Williams et al., 2013). Therefore, a better understanding of the molecular mechanisms governing such regulatory processes and their role in MOP function is an important step to improving the therapeutic profiles of opioid analgesics.

As with other members of the GPCR family, MOP-mediated signalling is initiated at the plasma membrane via protein–protein interactions between the receptor and its effectors. A new paradigm is emerging in which GPCR-mediated signalling can be elicited by effectors separately from the receptor in distinct domains of the plasma membrane (Eichel et al., 2018). As such, compartmentalisation of receptor and signalling effectors within specific subcellular locations or micro-domains of the plasma membrane plays a key role in the signalling outcome following receptor activation (Sungkaworn et al., 2017; Yanagawa et al., 2018). The concept that differential organisation of receptors at the plasma membrane may dictate specific cellular responses is particularly relevant in the context of MOP signalling.

An increasing number of studies demonstrate that different opioid agonists have distinct outcomes on the regulation and downstream signalling responses of MOP. For instance, the peptide agonist DAMGO ([D-Ala^2,N-Me-Phe^4,Gly^5-ol]-enkephalin) causes multi-site phosphorylation at the MOP mediated by GRK2/3, robust arrestin recruitment and internalisation, whereas the alkaloid agonist morphine causes minimal MOP regulation and

internalisation (Doll et al., 2011; Just et al., 2013; Lau et al., 2011; Miess et al., 2018). The localisation of MOP into lipid rafts has also been investigated and MOP dynamics have been shown to contribute to the specific signalling response elicited by different opioid ligands (Gaibelet et al., 2008; Huang et al., 2007; Zheng et al., 2008). In addition, we have previously reported that DAMGO and morphine elicit different spatiotemporal signalling profiles, and these are dictated by the lateral redistribution of MOP within the plasma membrane, rather than internalisation (Halls et al., 2016).

Live cell advanced imaging techniques such as fluorescence correlation spectroscopy (FCS) and fluorescence recovery after photobleaching (FRAP) can provide greater temporal resolution to determine how ligands can affect the dynamics of MOP organisation at the membrane. FCS is a highly sensitive confocal technique that can be used to quantify the diffusion and number of fluorescent species in small areas of living cells (Briddon, Kilpatrick & Hill, 2018; Diekmann & Hoischen, 2014). In FCS, fluorescent particles are excited as they pass through a small, defined confocal volume (~ 0.2 fL) and the emitted photons are detected by a single photon counting avalanche photodiode in a time-dependent manner. This leads to a series of time-dependent fluctuations in the detected fluorescence intensity during the FCS read; statistical analysis of these fluctuations using autocorrelation (AC) or photon counting histogram (PCH) analysis allows to determine the concentration, diffusion and oligomeric state of fluorescent proteins to be determined in a small defined area (~ 0.2 μm^2) of the plasma membrane. FRAP can be used in conjunction with FCS to measure diffusion properties over a larger membrane area and, unlike FCS, can provide an indication of the proportion of mobile and immobile proteins (Haustein & Schwille, 2004; Pucadyil, Mukherjee & Chattopadhyay, 2007).

Opioid receptors have been described to be constitutively distributed into different nanoscale domains at the plasma membrane and cholesterol depletion dynamically regulates the lateral organisation of these receptors (Rogacki et al., 2018). Additionally, FCS studies have described that ethanol alters MOP mobility, surface density and the dynamics of plasma membrane lipids; and that pre-treatment with MOP antagonists mitigates the effects of ethanol (Vukojevic, Ming, D'Addario, Rigler, Johansson & Terenius, 2008). Previous FRAP

studies at variable spot radius have demonstrated that the domain diffusion area of MOP depends on the activating agonist (Sauliere-Nzeh Ndong, Millot, Corbani, Mazeres, Lopez & Salome, 2010). More recently, it was also demonstrated that MOP agonists differentially modulate the rate of receptor diffusion as well as MOP-G protein coupling, and that ligand effects depend on the membrane cholesterol content (Melkes, Hejnova & Novotny, 2016). Together, these studies suggest that agonists that promote distinct functional states of MOP can also affect the dynamic organisation of receptors within the plasma membrane.

Here, we used FCS and FRAP as complementary imaging techniques to investigate the organisation and dynamics of MOP at the plasma membrane upon stimulation with different ligands. We used FCS measurements to quantify changes in the movement (diffusion coefficient; D_{FCS}), number (particle number; N) and clustering (molecular brightness; ε) of a fluorescently labelled SNAP-tagged MOP within small micro-domains of the membrane. Additionally, we performed FRAP measurements to determine the diffusion coefficient (D_{FRAP}) and proportion of mobile (M) receptors over a larger membrane area. We show that the internalising agonist DAMGO slowed MOP diffusion in a time- and concentration-dependent manner, increased receptor clustering and the proportion of immobile MOP and reduced surface receptor number in a pertussis toxin (Ptx)-insensitive manner. These effects were not observed with the antagonist naloxone or the poorly internalising agonist morphine. Notably, by analysing complementary parameters, we were able to determine the regulatory mechanisms underlying the ligand-dependent effects on MOP plasma membrane reorganisation. DAMGO-induced clustering, reduction in surface receptors and decreased proportion of mobile MOP were dependent on clathrin-mediated endocytosis. In contrast, the DAMGO-induced slowing in diffusion was independent of internalisation but dependent on GRK2/3 activity. Our study provides further insights into the specific protein interactions that control MOP plasma membrane organisation and reveals that GRKs act as agonist-specific regulators of MOP micro-diffusion.

3.3 Methods

3.3.1 Materials

DAMGO was obtained from Mimotopes. Morphine, Rhodamine 6G and M2-anti-FLAG were from Sigma-Aldrich (Gillingham, Dorset, U.K.). Naloxone was from Tocris. SNAP-Surface 488 was from New England Biolabs (Ipswich, MA, USA). The phosphosite-specific antibody anti-pS375 was from Cell Signalling. Secondary antibodies (raised in donkey) conjugated to Alexa-Fluor 488 or 647 were from Jackson ImmunoResearch. Coelenterazine h was from NanoLight. Furimazine was from Promega. Compound 101 was from HelloBio. Pitstop2 was from Abcam. Pertussis toxin was from Millipore.

3.3.2 Plasmids

To create the SNAP-MOP constructs, the full coding sequence for the human MOP (hMOP) or the mouse MOP wild-type (WT) (mMOP) or phosphorylation-deficient mutants S363A or S375A (Miess et al., 2018) were ligated into a pcDNA3.1(+) vector containing the 5-HT receptor membrane localisation signal sequence (sig) and the SNAP-tag (New England Biolabs, Ipswich, MA, USA) (Gherbi, May, Baker, Briddon & Hill, 2015) and containing neomycin resistance gene. Initial site-directed mutagenesis was required to remove the internal BamHI site in the MOP receptor while maintaining the amino acid sequence. Additional site-directed mutagenesis was performed to mutate the start codon (Met to Leu) on the MOP cDNAs. These were then ligated to the C-terminus of SNAP using BamHI and XhoI restriction enzymes. The resulting fusion protein contained a Gly-Ser linker between the SNAP open reading frame (ORF) and the MOP.

To create the FLAG-MOP-NLuc, the NLuc sequence (Soave, Stoddart, Brown, Woolard & Hill, 2016) was ligated immediately after the C-terminus of FLAG-mMOP cDNA without stop codon (Miess et al., 2018) with XhoI and XbaI restriction enzymes in a pcDNA3.1 vector. All sequences were confirmed by DNA sequencing.

GRK2-Venus was from D. Jensen (Columbia University, New York), CAMYEL sensor has been previously characterised (Jiang et al., 2007).

3.3.3 Cell lines generation

HEK293 cells (ATCC, Middlesex, UK) were grown in Dulbecco's modified Eagle's medium (DMEM) supplemented with 10% (v/v) fetal calf serum and maintained at 37°C in a humidified incubator containing 5% CO_2. Cells were transfected with the pcDNA3.1+ vector containing SNAP-MOP constructs using Fugene HD (Promega) as transfection reagent according to the manufacturer's instructions. 24 hours post transfection, the medium was supplemented with 1 mg/ml G418-selective pressure for 2 weeks for the generation of stable mixed population HEK293 SNAP-hMOP, SNAP-mMOP WT, SNAP-mMOP S363A or SNAP-mMOP S375A cell lines.

3.3.4 Cell plating and treatments

For experiments, stable mixed population cell lines were plated onto poly-D-lysine–coated 8-well Labtek No.1.5 borosilicate chambered coverglasses (Nunc Nalgene International, Fisher Scientific). On the day of the experiment, SNAP tag labelling was performed by incubating cells with 200 nM (or as otherwise indicated) SNAP-Surface Alexa Fluor® 488 (BG-488) dye in fresh cell culture media for 30 min at 37°C. Cells were washed in pre-warmed HEPES-buffered saline solution (HBSS) containing 4.5 mM D-glucose and pre-treated with inhibitors for 30 min at 37°C, except for pertussis toxin (PTx; 16 h pre-treatment). Inhibitors were used at the following concentrations: 30 µM Pitstop2, 30 µM Cmpd101 or 100 ng/ml PTx. Cells were then stimulated for 20 min (or as otherwise indicated) at 37°C with vehicle (0.3% v/v DMSO), 10 µM DAMGO, 30 µM morphine, 30 µM naloxone or 10 µM DAMGO after pre-treatment for 30 min at 37°C with 30 µM naloxone.

3.3.5 Fluorescence Correlation Spectroscopy (FCS)

Cells were equilibrated to room temperature (22±2°C) to minimise artifacts from temperature-induced plasma membrane fluctuations. FCS measurements were taken at room temperature on a Zeiss LSM510NLO ConfoCor 3 inverted confocal microscope using a 40× c-Apochromat 1.2 NA water-immersion objective (Carl Zeiss, Jena, Germany) as previously described (Ayling et al., 2012). The confocal volume was calibrated on the day of each experiment using 20 nM Rhodamine 6G (R6G; $D = 2.8 \times 10^{-10}\,m^2/s$). The measurement

volume was positioned in x and y over a flat portion of a healthy cell using a live confocal image, then approximately on the upper membrane in z. Precise z-positioning on the upper plasma membrane peak was performed using an intensity z-scan at 0.25µm intervals for ±2µm. Samples were excited using a 488nm argon laser with power set to 50% AOTF (~1.5 kW/cm^2 at the objective). Fluorescence fluctuations were then collected through a BP505-610IR emission filter for 1×30 seconds.

Autocorrelation (AC) and Photon Counting Histogram (PCH) analysis were performed using Zen2010 Black software (Carl Zeiss, Jena, Germany). The dimensions and volume of the detection volume as well as the structure parameter (ratio of volume height to diameter) were determined from a calibration FCS read using 20 nM Rhodamine 6G, fitted to a single 3D diffusion component with a triplet state pre-exponential, as previously described (Briddon et al., 2004). Prior to AC/PCH analysis, the initial 5-10s of data were removed where bleaching was present (indicated by a rapid decrease in the average count rate) in order to ensure that AC functions reached an asymptote at G(0)=1. Average MOP dwell times (τ_D) and particle number (N) were obtained from fitting of autocorrelation (AC) curves to a two-component diffusion model incorporating a pre-exponential component to account for fluorophore triple state (as per Ayling et al., 2012). This allows for a three-dimensional component (τ_{D1}) representative of the diffusion in solution of free SNAP BG-488 label to account for any remaining SNAP label, and a two-dimensional component (τ_{D2}) representative of the plasma membrane diffusion of SNAP BG-488-labelled SNAP-MOP itself (Fig. 3.3A). The average dwell time of free SNAP Surface 488 (τ_{D1}) was fixed to 32µs in the fitting process, having been measured directly using 20nM SNAP-AF488 in HBSS. The structure parameter was also fixed to the value determined in the calibration fit. All other parameters were allowed to vary in the fitting process. Free SNAP BG-488 concentration (% τ_{D1} contribution to the AC amplitude was consistently between 10 and 15% of the total amplitude).

Average dwell time of the SNAP-MOP allowed calculation of the MOP diffusion coefficient (D_{FCS}) using the equation $D=\omega_0^2/4.\tau_D$, where ω_0 is the radius of the beam waist of the detection volume and τ_D is the average dwell time of SNAP-MOP in the volume as determined by autocorrelation analysis. Particle number (N) was calculated from the

fractional contribution of the SNAP-MOP diffusing component (τ_{D2}) to the total particle number (N) as determined by the G(0) value of the autocorrelation curve. This was subsequently expressed in particles per μm^2 ($N/\mu m^2$), by normalising to the area of the detection volume as projected onto a flat 2D membrane ($N/\pi\omega_0^2$).

Molecular brightness (ε) was determined using photon counting histogram (PCH) analysis of the same fluctuation data. For PCH, the first-order correction was obtained from fitting of the R6G calibration data binned at 20 µs, and fixed to this value in subsequent fitting. Data from SNAP-MOP cells were fitted using a bin time of 100 µs. Data were fitted to either a one or two component PCH based on the goodness of fit at high photon counts per bin, visualized on a linear-log scale (Fig. 3.3B).

3.3.6 Fluorescence Recovery After Photobleaching (FRAP)

FRAP measurements were performed at room temperature on a Zeiss LSM510NLO ConfoCor 3 inverted confocal microscope using a 40× c-Apochromat 1.2 NA water-immersion objective using the Zeiss AIM3.5 software (Carl Zeiss, Jena, Germany). After manually focusing on the basal membrane of SNAP-MOP HEK293 cells, images were scanned using 488 nm excitation, with emission collected through a BP505-610IR filter, with pinhole set at 1 Airy unit and gain and offset adjusted to fit the linear response of the photomultiplier (PMT) detectors. Images (512x512 pixels) were acquired continually with no averaging on zoom 2 at a rate of ~1 frame/second. Ten pre-bleach frames were acquired before bleaching (100 ms, 100% power during 30 iterations) a circular region of interest (ROI) of 2.14 µm radius (area = 14.8 μm^2) and fluorescence recovery was followed for a further 120 seconds.

Data were analysed using the FRAP Wizard in Zen2010 Black software (Carl Zeiss, Germany). Fluorescence intensity within the bleached ROI of the bottom membrane was quantified over the time course of the experiment. This was background corrected using a similar sized ROI in an area of the image and for bleaching during scan using an ROI in a non-bleached cell. Pre-bleach frames were averaged and used as a baseline to normalise all post-bleach frames. Recovery curves were fitted to a simple exponential recovery curve to obtain

a half time of recovery ($t_{1/2}$) and a recovery plateau (Fig. 3.4). The mobile fraction (MF) is defined as the intensity of this plateau as a percentage of the pre-bleach control, whilst the immobile fraction (IF) is the percentage difference between intensity of the recovery plateau and the pre-bleach intensity. Diffusion coefficient (D_{FRAP}) was calculated by using the equation $D=\omega^2/4.\tau_{1/2}$, where ω (μm) is the radius of the bleached area and $\tau_{1/2}$ (s) is the half-time recovery from the fitted curve in Zen2010.

3.3.7 Anti-pS375 immunocytochemistry

HEK293 cells transiently expressing FLAG-mMOP WT, S363A or S375A were grown in a 96-well clear bottom plate (PerkinElmer). Cells were serum starved for at least 30 min and then incubated with vehicle or an EC_{50} concentration of DAMGO (1 μM) at 37°C for 5 min. Cells were then fixed in -30°C methanol for 10 min on ice. Antigen retrieval buffer was then applied, cells were heated in PBS supplemented with 10 mM sodium citrate and 0.05% Tween-20 (pH 6.0) at 95°C for 20 min. Cells were then washed in PBS and incubated in blocking solution, 10% goat serum in PBS at room temperature for 30 min. Anti-FLAG mouse antibody and anti-phospho S375 rabbit antibody were diluted in blocking solution (1:1000 and 1:200 respectively) and added to cells for incubation overnight at room temperature. Cells were washed with PBS and incubated with AlexaFluor 488 (AF488) anti-mouse IgG and AlexaFluor 647 (AF647) anti-rabbit goat IgG secondary antibodies (1:1000 in blocking solution) at room temperature for 1h. Cells were washed and imaged on the Operetta High Content Imaging System capturing AF488 and AF647 channels using a 20× objective. The mean fluorescence intensity of each channel was quantified from the raw 16-bit images using the Operetta analysis software and levels of phosphorylation were expressed as a ratio of pS375 (AF647) /FLAG (AF488) immunostaining and normalised to vehicle treatment in control conditions.

3.3.8 Bioluminescence Resonance Energy Transfer (BRET)

HEK293 cells were transiently transfected in a 10 cm dish. For CAMYEL, cells were transfected with 2.5 μg of SNAP-MOP and 2.5 μg of CAMYEL biosensor. For GRK2 recruitment assay, cells were transfected with 1 μg FLAG-MOP-NLuc and 4 μg GRK2-Venus. After 24 h,

cells were re-plated into poly-D-lysine-coated white opaque 96-well plates (CulturPlate, PerkinElmer) and allowed to adhere overnight. BRET experiments were performed 48 h post-transfection. Cells were washed with HBSS and equilibrated for 30 min at 37°C prior to the experiment. Coelenterazine h or Furimazine was added to a final concentration of 5 µM before dual fluorescence/luminescence measurement in a LUMIstar Omega plate reader (BMG LabTech). The BRET signal was calculated as the ratio of light emitted at 530 nm by Venus over the light emitted at 430 nm by Renilla luciferase 8 (RLuc8) or Nano luciferase (NLuc).

For CAMYEL assay, vehicle or DAMGO (at the indicated concentration) was added to control or PTx-pretreated cells for 10 min and baseline was measured for 4 cycles, then 10 µM forskolin was added to induce cAMP production and the BRET signal was measured for 30min. CAMYEL concentration response curve was constructed with the data point at 10min after cAMP stimulation by forskolin. Data were normalised to 0% inhibition (forskolin-induced cAMP production) and 100% inhibition (vehicle only without forskolin-induced cAMP production). For GRK2 recruitment kinetic experiment, the baseline BRET ratio was measured for 4 cycles, then either vehicle (0.01% v/v DMSO) or 10 µM DAMGO was added to control or Cmpd101-pretreated cells, and the BRET signal was measured for 30 minutes.

3.3.9 Statistics

Data representation and statistical analysis were performed using GraphPad Prism v7. FCS and FRAP data are presented as the mean ± SEM of the indicated individual cell measurements. The BRET data was quantified as indicated and represent the mean ± SEM of at least three individual experiments. Quantification of high content imaging was performed as indicated and data represent the mean ± SEM or representative images of at least three individual experiments. Statistical significance was determined by one-way ANOVA ($p<0.05$ considered significant).

3.4 Results

3.4.1 Basal plasma membrane organisation of SNAP-MOP detected by FCS and FRAP

To study the organisation of MOP within living cell membranes, we performed FCS measurements on HEK293 cells stably expressing N-terminally SNAP-tagged human MOP (SNAP-MOP). Addition of the SNAP-tag at the N-terminus of the MOP did not alter its function as shown by its ability to inhibit forskolin-induced cAMP production in a similar way as a previously characterised FLAG-tagged MOP (Fig. 3.1).

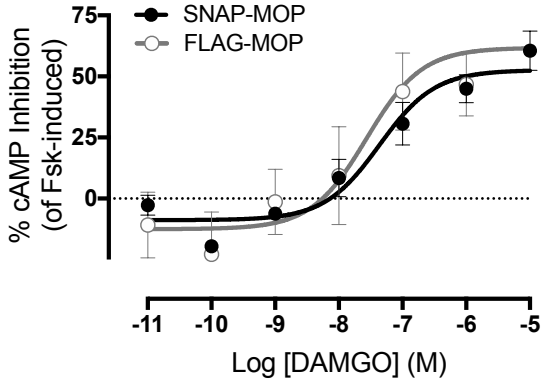


Figure 3.1 Inhibition of forskolin-induced cAMP accumulation with increasing concentrations of DAMGO at the SNAP-MOP (black symbols) or FLAG-MOP (open grey symbols) in a CAMYEL BRET assay (n=4). Data are shown as percentage of inhibition of cAMP induced by 10 µM forskolin (Fsk) and represent mean ± SEM.

Use of a SNAP-MOP fusion allowed specific labelling of cell surface MOP using a cell membrane impermeable SNAP-Surface® 488 (BG-488) dye that specifically and covalently binds to SNAP-tagged receptors present at the cell surface. FCS measurements were performed on SNAP-MOP cells by positioning the confocal volume in x-y over the cell cytoplasm, and subsequently on the upper membrane at the peak intensity of a z scan (Fig. 3.2).

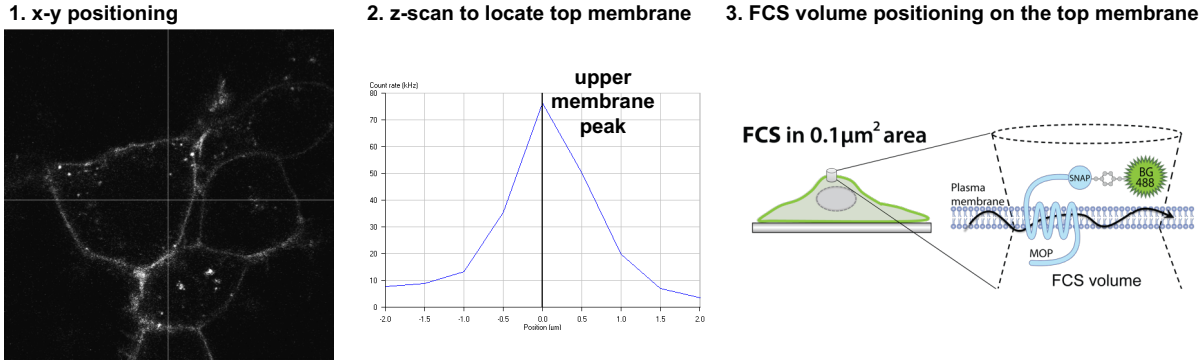


Figure 3.2. Positioning of the confocal volume on the membrane for FCS. FCS measurement volume was positioned on the upper membrane using a live confocal image and an intensity scan in z. Schematic representation of Fluorescence Correlation Spectroscopy (FCS) measurements on the membrane of HEK293 SNAP-MOP cells labelled with SNAP-Surface 488 (BG-488) dye.

FCS fluorescence fluctuation traces were recorded for 30s. The autocorrelation (AC) analysis yielded the average dwell time (τ_{D2}) and particle number (N) of the SNAP-MOP within the detection volume, from which the diffusion coefficient (D_{FCS}; $\mu m^2/s$) and receptor density ($N/\mu m^2$) were calculated (Fig. 3.3A and Materials and Methods). These measurements showed that under basal conditions, D_{FCS} for the SNAP-MOP was 0.146 ± 0.016 $\mu m^2/s$ with a receptor density (N) of 157 ± 19 particles/μm^2 (n = 14 cells) (Fig. 3.3A). Analysis of the same fluorescence fluctuations using photon counting histogram (PCH) analysis yielded average molecular brightness (ε; kHz) of the fluorescent species (Fig. 3.3B and Materials and Methods), providing an indication of the extent of SNAP-MOP clustering. Under basal conditions PCH analysis of reads from the majority (79%) of cells fitted to one brightness component with an average ε of 41.7 ± 3.8 kHz (n = 21 cells) (Fig. 3.3B). Interestingly, in 19% of the cells analysed, a second brighter component (average ε = 90.8 ± 14.1 kHz) was detected (Fig. 3.4C), indicating the presence of higher-order oligomeric forms of SNAP-MOP in basal conditions. Of note, the brighter component was always less abundant relative to the dimmer component.

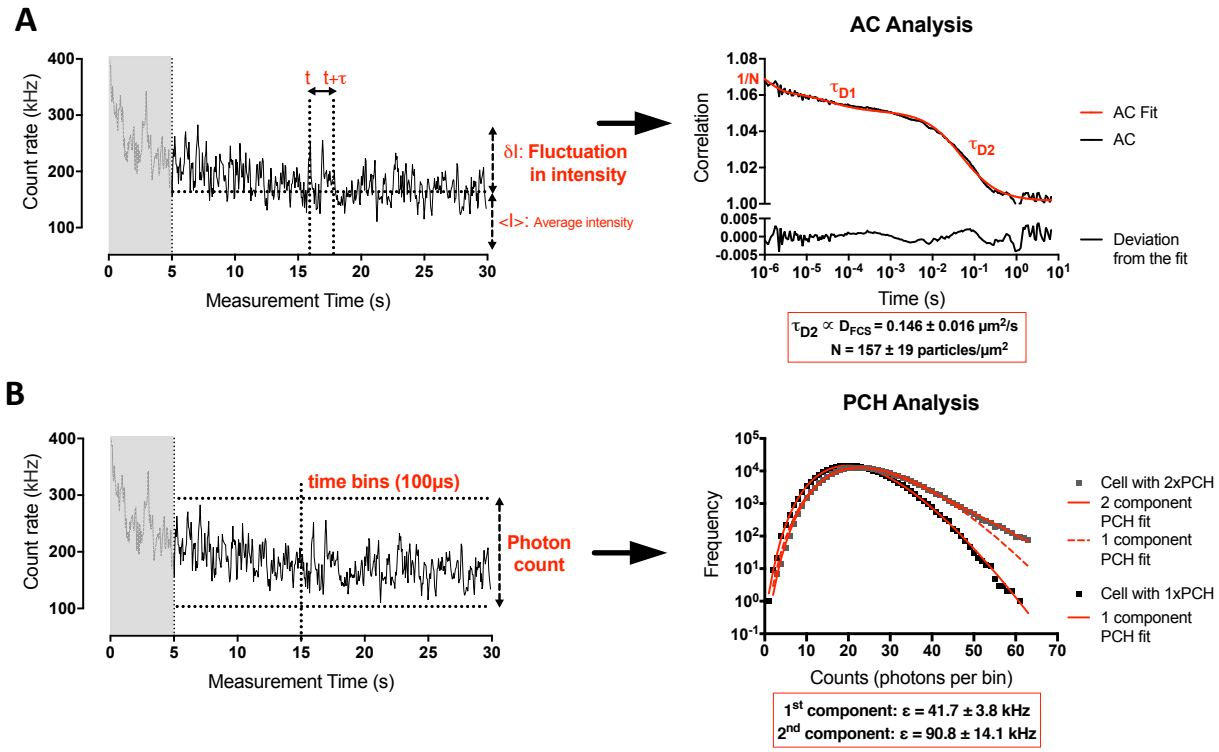


Figure 3.3. FCS Analysis. (A) Representative FCS trace in basal conditions for autocorrelation (AC) analysis in which fluctuations in intensity (δI) from the intensity mean (<I>) are calculated at two time points (t and t+τ) for all t and a range of τ values to generate an autocorrelation function that provides the average dwell time (τ_D) and particle number (N). τ_{D1} represents the average dwell time of free BG-488 and was set to 32 μs; τ_{D2} represents the average dwell time of BG-488 bound to SNAP-MOP from which the receptor diffusion coefficient (D_{FCS}; $\mu m^2/s$) was calculated. N represents the number of particles and was used to calculate surface particle concentration ($N/\mu m^2$). Parameters from Fig 3.4A are noted. **(B)** Representative fluctuation trace in basal conditions and subsequent photon counting histogram (PCH) analysis in which the amplitude of the fluctuations can be analysed by quantifying the photons in defined time bins (100 μs). Super-Poissonian statistical analysis of the resulting frequency histogram allows the molecular brightness (ε) of SNAP-MOP containing particles to be determined. Two representative cell measurements under basal conditions are shown with the fit (solid red line) to one component (black squares) or two components (grey squares) accordingly. The poor 1 component fit (dotted red line) for the cell trace represented in grey squares is also shown. Parameters from Fig. 3.4C are noted.

In order to ensure that accurate diffusion coefficients were obtained excitation laser power was optimised to give a maximum signal to noise ratio (highest ε) with minimal spot photobleaching (indicated by no increase in D_{FCS} or decrease in N) (Fig. 3.4A). On the basis of these data, subsequent experiments used 50% laser power. FCS measurements were also conducted on cells labelled with a range of SNAP-Surface® 488 (BG-488) concentrations to

ensure that all of the cell surface receptors had been labelled (saturated N) whilst minimising the amount of free BG-488 label left after washing. At concentrations of BG-488 above 50 nM, the particle number (N) (Fig. 3.4B) and molecular brightness (ε) remained constant (Fig. 3.4C), indicating all receptor was labelled. On the basis of these data, subsequent experiments used 200 nM BG-488 label. It was also noted that as the concentration of BG-488 label increased, the number of cells that require a second component for the PCH fit also increased (Fig. 3.4C).

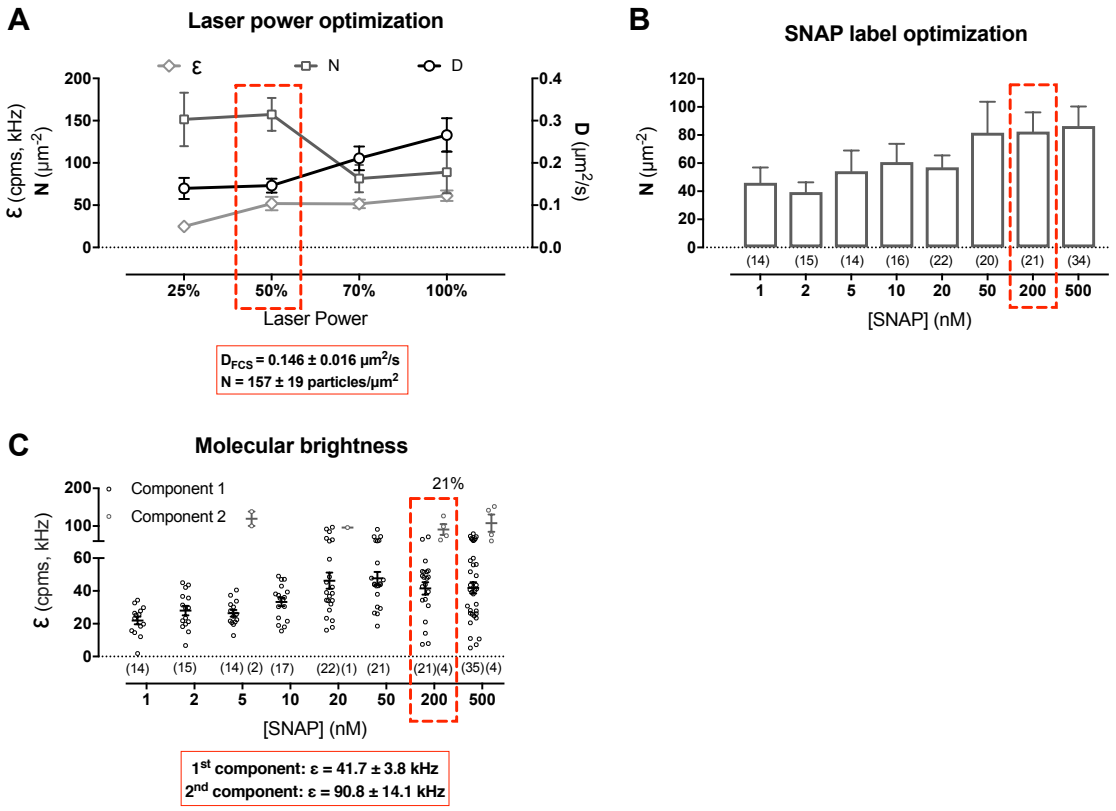


Figure 3.4. Optimisation SNAP-MOP for FCS. (**A)** Plot of FCS parameters with increasing laser power. Molecular brightness (ε represented as diamonds) increases with increasing laser power. A decrease in particle number (N represented as squares) correlated with an increase in diffusion coefficient (D represented as circles) are indicative of photobleaching at high laser powers. The laser power chosen for subsequent experiments was 50% at which D and N remain consistent (n=3). Average parameters at the chosen conditions are noted. (**B)** Particle number (N) with increasing concentrations of SNAP-Surface® 488 (BG-488) dye (n=3-6). The concentration chosen was 200 nM BG-488 since at this concentration, the particle number plateaued, indicating maximum labelling of SNAP-MOP. (**C)** Molecular brightness (ε) with increasing concentrations of SNAP-Surface® 488 (BG-488) dye (n=3-6). At high SNAP label concentrations, a second bright component was necessary for an appropriate PCH fit. Average parameters at the chosen conditions are noted.

Since FCS only measures mobile receptor population, FRAP was also performed over a larger area of the lower cell membrane of adherent cells to allow a macro diffusion coefficient (D_{FRAP}) to be determined, as well as the proportions of mobile (MF) and immobile (IF) receptors (Fig. 3.5). Using a circular bleach area with radius of 2.2 µm (area ~ 15 µm^2), FRAP measurements showed that under basal conditions 67 ± 4% of the receptor population is mobile over this area with a diffusion rate (D_{FRAP}) of 0.084 ± 0.008 µm^2/s which was slower than that seen for D_{FCS}.

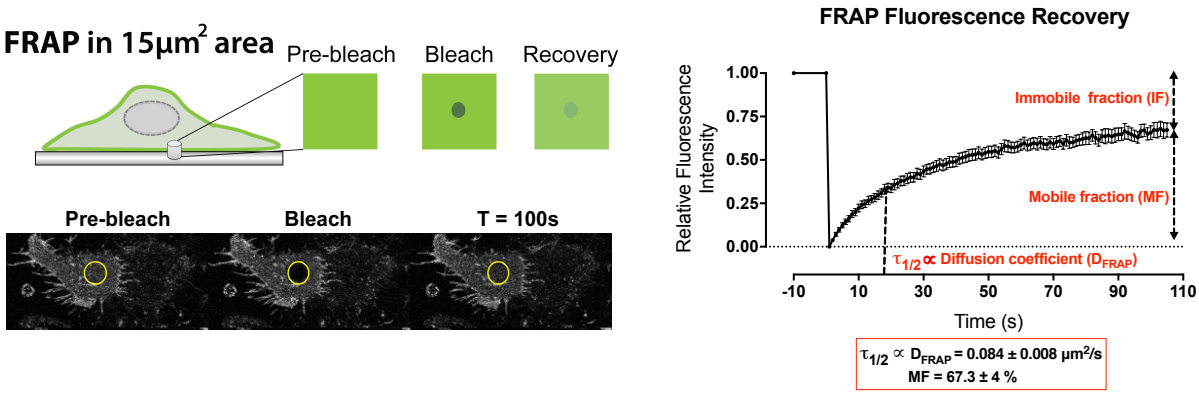


Figure 3.5 Schematic representation of Fluorescence Recovery After Photobleaching (FRAP) method and representative image of a cell in basal conditions during the bleaching protocol. Fluorescence recovery average trace of SNAP-MOP in basal conditions that provides a half-time ($\tau_{1/2}$) from which we can infer diffusion coefficient (D_{FRAP}; µm^2/s), and mobile and immobile fractions (MF and IF respectively). Parameters are noted.

3.4.2 Ligand-induced changes in the plasma membrane organisation of SNAP-MOP

The effect of ligand stimulation on SNAP-MOP membrane organisation was then assessed using FCS and FRAP. Substantial fluorescence was detected at the plasma membrane after stimulation with saturating concentrations of the poorly internalising agonist morphine (30 µM) or the internalising agonist DAMGO (10 µM) for 20 min (Fig. 3.6). This is not surprising since internalisation happens at a later timescale, we have previously shown that DAMGO-induced internalisation reaches maximum 1 hr after agonist stimulation (Halls et al., 2016; Miess et al., 2018). We then recorded FCS fluctuation traces of SNAP-MOP following exposure to each ligand and performed AC and PCH analysis (Fig. 3.7).

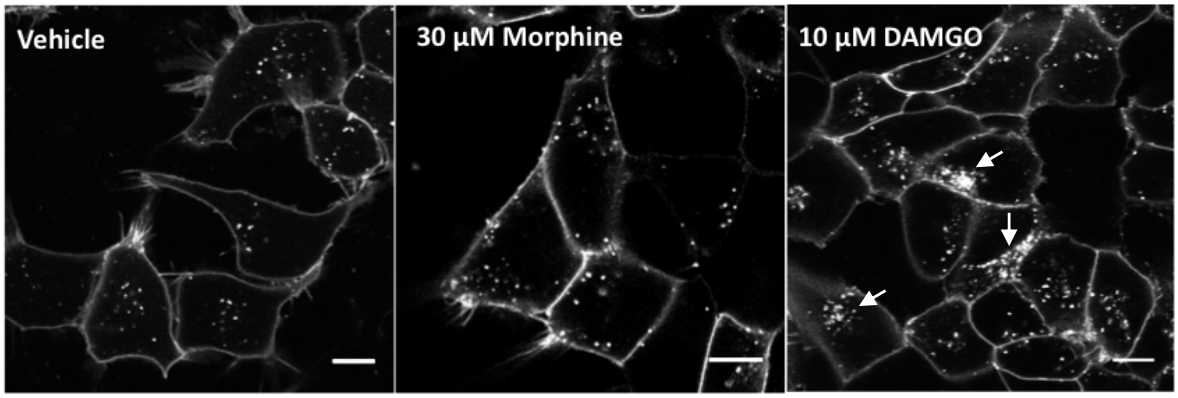


Figure 3.6 HEK293 SNAP-MOP cells labelled with SNAP-Surface 488 (BG-488) dye after stimulation with vehicle, 30 µM morphine or 10 µM DAMGO for 20min. Representative images from cells under the indicated conditions. Scale bar 10µm; arrows represent MOP that is trafficking from the cell surface.

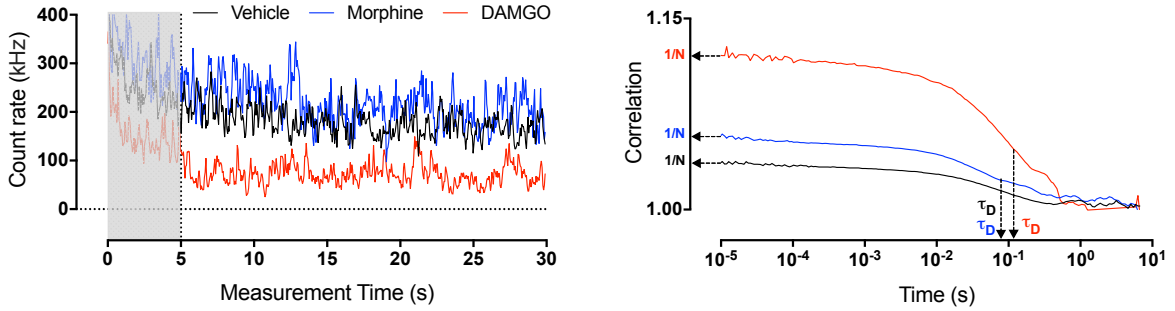


Figure 3.7 FCS measurements in HEK293 SNAP-MOP cells following ligand stimulation. Representative FCS traces from a single HEK293 SNAP-MOP cell after stimulation with vehicle, 30 µM morphine or 10 µM DAMGO for 20min (grey area indicates the initial 5s of data that were removed from the analysis because bleaching was present) and their corresponding AC fit indicating N and τ_D of SNAP-MOP.

Stimulation with DAMGO (10 µM) caused a significant decrease in diffusion (D_{FCS}) (Fig. 3.8A, Table 1), a decrease in particle number (N) (Fig. 3.8B, Table 1); and in the PCH analysis DAMGO stimulation increased the percentage of cells (from 17% in vehicle to 38% in DAMGO-treated cells) with a bright second component, suggesting that DAMGO stimulation induces clustering of SNAP-MOP (Fig. 3.8C, Table 1). These changes were mediated by receptor activation, since they were not present in cells which were pre-treated with the MOP antagonist naloxone (10 µM). The slowing in diffusion caused by DAMGO was concentration- (Fig. 3.9A) and time-dependent (Fig. 3.9B), presenting a significant decrease in D_{FCS} from 1 µM

DAMGO, which matches its EC_{50} for recruitment of regulatory proteins (Miess et al., 2018) and after 20 min of stimulation, which is prior to internalisation (Miess et al., 2018).

In contrast to DAMGO, stimulation with increasing concentrations of morphine (up to 30 µM) or naloxone (30 µM) alone did not cause any significant changes in D_{FCS} or clustering compared to vehicle treatment, indicating that changes in MOP plasma membrane organisation are agonist-specific. Of note, stimulation with naloxone significantly increased the particle number (N) compared to vehicle treatment (Fig. 3.8B) this increase might indicate that naloxone prevents constitutive internalisation observed in vehicle (Fig. 3.6), resulting in an increase in surface receptor number.

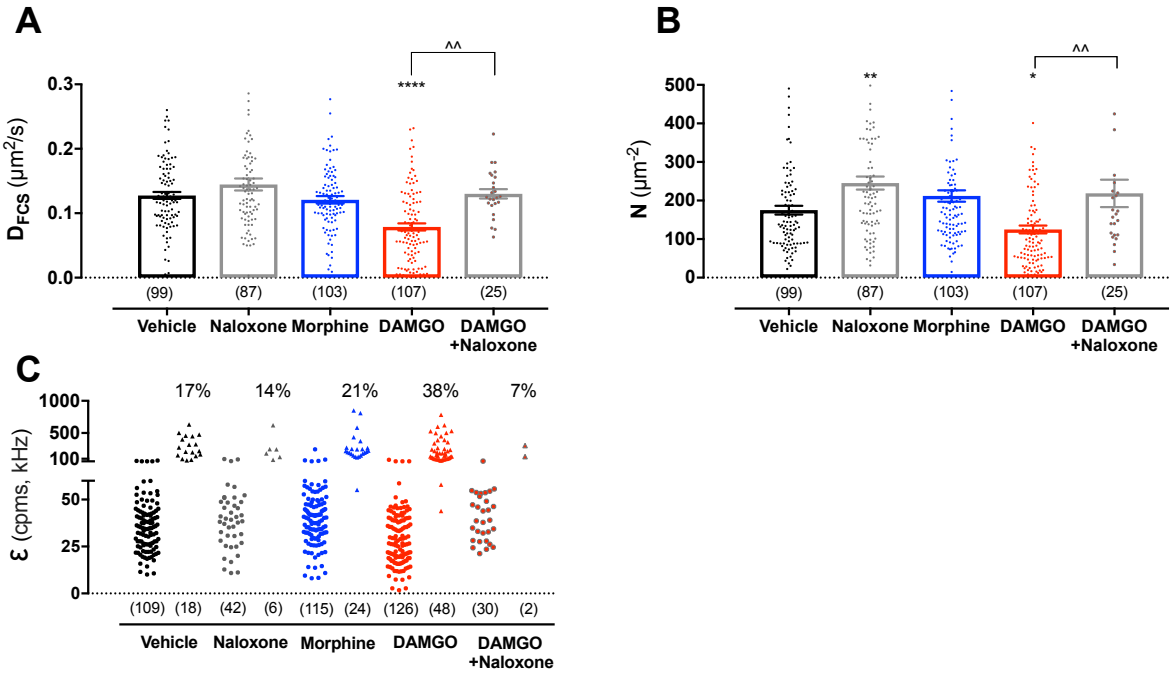


Figure 3.8 FCS and PCH measurements in HEK293 SNAP-MOP cells following ligand stimulation. (A) Diffusion coefficient of SNAP-MOP upon stimulation with 30 µM naloxone, 30 µM morphine, 10 µM DAMGO (20 min, 37°C) or 10 µM DAMGO after pre-treatment with 30 µM naloxone (30 min, 37°C) (n=25-107 cells from 5-23 independent experiments). **(B)** Particle number of SNAP-MOP upon stimulation with 30 µM naloxone, 30 µM morphine, 10 µM DAMGO (20 min, 37°C) or 10 µM DAMGO after pre-treatment with 30 µM naloxone (30 min, 37°C) (n=25-107 cells from 5-23 independent experiments). **C)** Molecular brightness of SNAP-MOP after stimulation with 30 µM naloxone, 30 µM morphine, 10 µM DAMGO or 10 µM DAMGO after pre-treatment with 30 µM naloxone. For each condition, brightness values for the first (left) and second (right) component are shown, with the number of cells requiring a two-component fit indicated as percentage. Each data point on the scatter plots represents

a measurement from an individual cell (number of cells within parenthesis) and column plots represent mean ± SEM of the indicated number of cells. * denotes significance versus vehicle treatment and ^ denotes significance versus DAMGO control in one-way ANOVA with Sidak's multiple comparisons test (* p<0.05; ** p<0.01, **** p<0.0001).

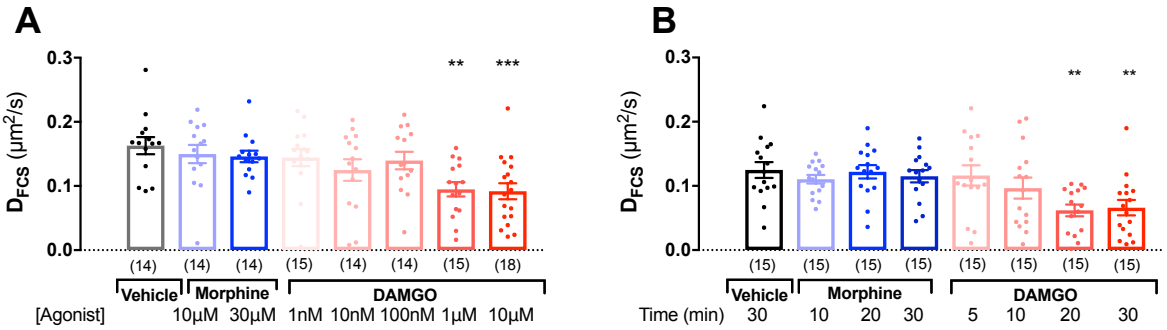


Figure 3.9 Concentration- and time- dependency of FCS diffusion parameter. (A) Diffusion coefficient of SNAP-MOP upon increasing concentration of morphine or DAMGO after 20min incubation (n=14-18 cells from 3 independent experiments). **(B)** Diffusion coefficient of SNAP-MOP upon stimulation with 30 µM morphine or 10 µM DAMGO with increasing time incubation periods (n=15 from 3 independent experiments). Each data point on the scatter plots represents a measurement from an individual cell (number of cells within parenthesis) and column plots represent mean ± SEM of the indicated number of cells. * denotes significance versus vehicle treatment in one-way ANOVA with Sidak's multiple comparisons test (** p<0.01, *** p<0.001).

Since FCS can only determine the properties of mobile receptors, we also used FRAP to assess whether ligand stimulation changes the proportion of mobile vs immobile receptors (Fig. 3.10A). Following exposure of cells to 10 µM DAMGO, the immobile fraction (IF) of MOP was significantly increased from 34 ± 3% in vehicle-treated cells to 52 ± 4% in DAMGO-treated conditions (P<0.0001, Fig. 3.10B). In contrast, treatment with morphine or naloxone showed no change in mobile fraction compared to vehicle. Contrary to the decrease in D_{FCS} induced by DAMGO, D_{FRAP} remained unchanged upon stimulation with any of the ligands (Fig. 3.10C).

Initial data therefore indicate ligand-specific changes in MOP membrane organisation, with DAMGO stimulation slowing MOP diffusion, reducing surface receptor number, increasing receptor clustering and the proportion of immobile receptors. While these effects were prevented by naloxone, none of these changes were observed following stimulation with morphine. A saturating concentration of naloxone was used to antagonise the effects of

DAMGO, as a confirmation of receptor-mediated events. Although this is a very high concentration, the work presented here used HEK293 cells expressing MOP, and no other opioid receptor, thus, lack of selectivity in this system would not be an issue. Nevertheless, it is important to consider this high concentration effect when moving to more physiological systems (expressing multiple opioid receptor subtypes) or responses such as ion channel activation.

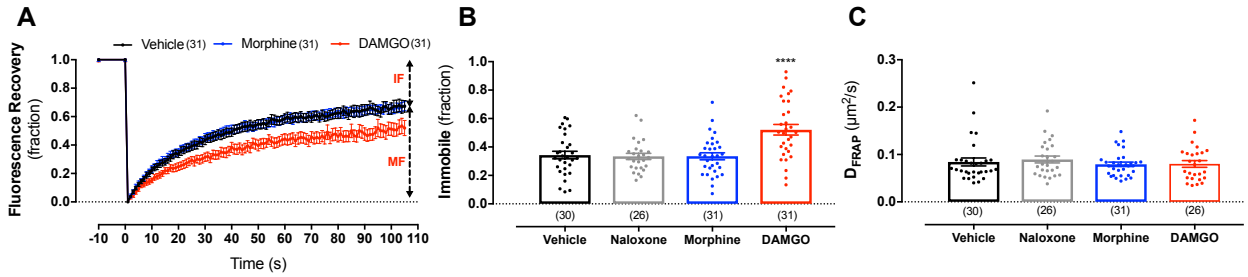


Figure 3.10 FRAP measurements on the lower membrane of HEK293 SNAP-MOP cells following ligand stimulation. (A) Fluorescence recovery curves of HEK293 SNAP-MOP cells during FRAP experiments under control conditions and following stimulation with 30 µM morphine or 10 µM DAMGO for 20 minutes at 37°C (n=26-31 from 6 independent experiments). (**B)** Immobile fraction and **C)** diffusion coefficient of SNAP-MOP as determined by FRAP (D_{FRAP}) analysis following stimulation with 30 µM naloxone, 30 µM morphine or 10 µM DAMGO (n=26-31 from 6 independent experiments). Each data point of the scatter plots represents an individual cell measurement (number of cells within parenthesis) and column plots represent mean ± SEM of the indicated number of cells. * denotes significance versus vehicle treatment in one-way ANOVA with Sidak's multiple comparisons test (**** p<0.0001).

3.4.3 MOP membrane reorganisation is independent of $G_{i/o}$ protein activation

The dependence of MOP reorganisation on G protein activation was then investigated using pertussis toxin (PTx) as a $G\alpha_{i/o}$ inhibitor (100 ng/ml, overnight treatment). Consistent with previous data (Halls et al., 2016), inhibition of $G\alpha_{i/o}$ activation did not prevent DAMGO-induced MOP internalisation (Fig. 3.11A) at a PTx concentration that was effective at preventing agonist-induced cAMP inhibition (Fig. 3.11B). PTx treatment did not affect DAMGO-induced clustering (Fig. 3.11C; Table 1) or slowing in diffusion (Fig. 3.11D, Table 1). Altogether, this indicates that G protein activation is not necessary for the changes in MOP membrane organisation induced by DAMGO.

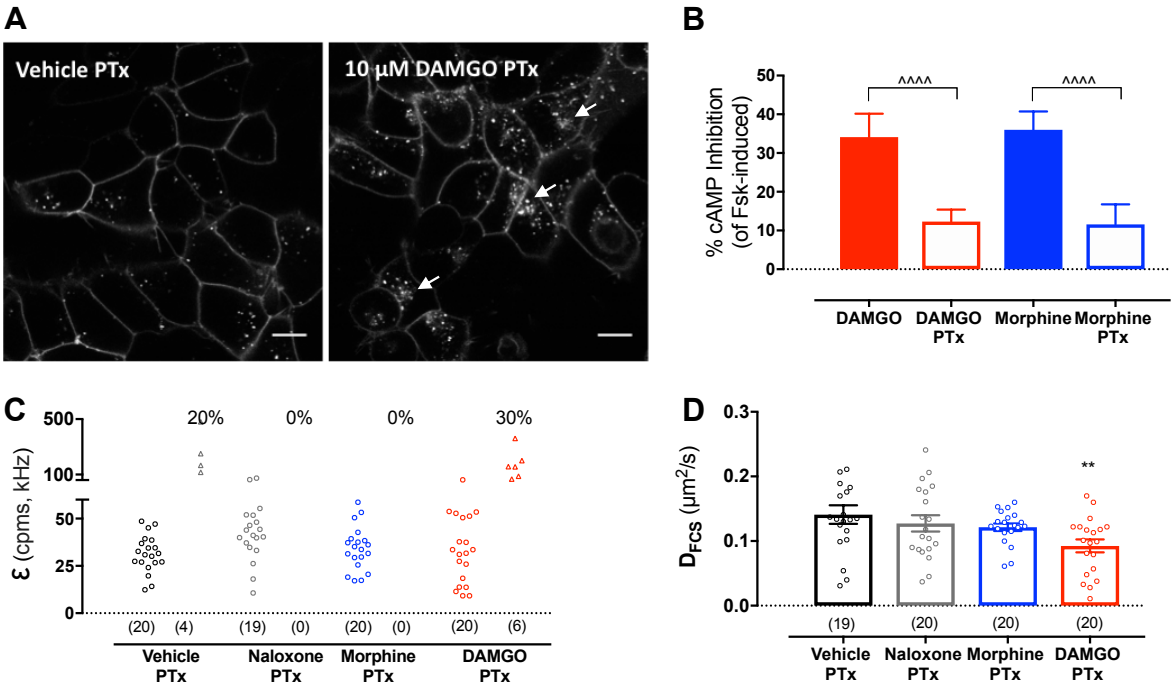


Figure 3.11 Effect of pertussis toxin pre-treatment on SNAP-MOP membrane function and organisation. HEK293 SNAP-MOP cells were exposed to pertussis toxin (PTx) (100 ng/ml overnight, 37°C). **(A)** Representative images of PTx pre-treated HEK293 SNAP-MOP cells after stimulation with vehicle or 10 µM DAMGO. Scale bar 10µm; arrows represent agonist-induced internalisation. **(B)** Agonist-mediated inhibition of forskolin-induced cAMP accumulation upon stimulation with 10 µM DAMGO or 10 µM morphine in control (closed bars) or PTx pre-treated cells (open bars) in a CAMYEL BRET assay. Data are shown as percentage of inhibition of cAMP induced by 10 µM forskolin and represent mean ± SEM of 3 independent experiments. **(C)** Molecular brightness and **D)** diffusion coefficients from FCS measurements of SNAP-MOP after stimulation with 30 µM naloxone, 30 µM morphine or 10 µM DAMGO in PTx pre-treated cells (n=19-20 cells from 4 independent experiments). For each condition, brightness values for the first (left) and second (right) component are shown, with the number of cells requiring a two-component fit indicated as percentage. Each data point on the scatter plots represents a measurement from an individual cell (number of cells within parenthesis) and column plots represent mean ± SEM of the indicated number of cells. * denotes significance versus vehicle treatment in one-way ANOVA with Sidak's multiple comparisons test (** $p<0.01$).

3.4.4 Effect of internalisation inhibition on ligand-induced changes in MOP organisation

To investigate whether the DAMGO-mediated changes in MOP organisation were related to MOP internalisation, we used an inhibitor of clathrin-dependent internalisation, Pitstop2 (30 µM, 30 min pre-treatment) as it has previously been shown to block DAMGO-induced MOP endocytosis (Halls et al., 2016). In FCS experiments, Pitstop2 prevented

DAMGO-induced receptor clustering as indicated by the reduction in the percentage of cells that showed the second brighter PCH component (Fig. 3.12A) and presenting an immobile fraction that was not significantly different from vehicle-treated cells (Table 1). However, inhibiting internalisation did not significantly affect the DAMGO-induced slowing in diffusion measured by FCS (Fig. 3.12B, Table 1). These data suggest that MOP moves laterally in the plasma membrane, clustering and immobilising in clathrin-coated pits prior to internalisation. Some MOP organisation events such as clustering are dependent on clathrin-mediated endocytosis. However, Pitstop2 was not able to prevent the DAMGO-induced slowness in D_{FCS}, highlighting that a different molecular mechanism must be underlying this micro-diffusion event.

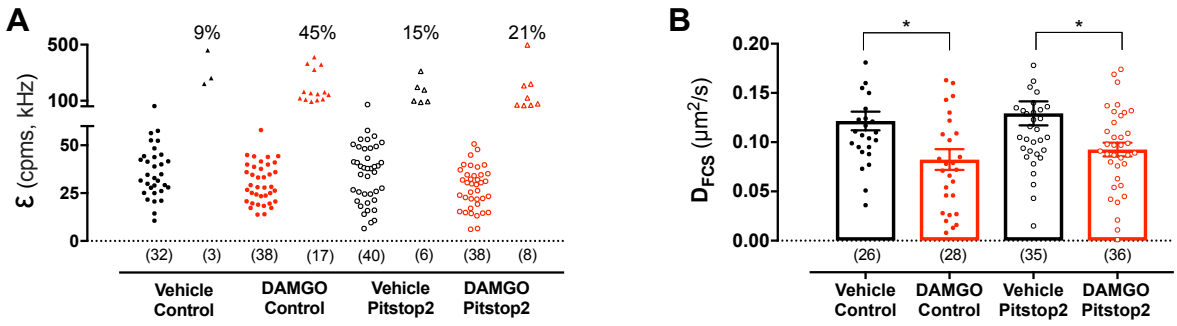


Figure 3.12 Effect of internalisation inhibitor Pitstop2 on SNAP-MOP membrane organisation. HEK293 SNAP-MOP cells were exposed to the internalisation inhibitor Pitstop2 (30 µM, 30 min, 37°C). (**A)** Molecular brightness of SNAP-MOP after stimulation with vehicle or 10 µM DAMGO in control or Pitstop2 pre-treated cells (n=32-40 cells from 6-8 independent experiments). For each condition of the molecular brightness data, brightness values for the first (left) and second (right) component are shown, with the number of cells requiring a two-component fit indicated as percentage. **(B)** Diffusion coefficient of SNAP-MOP upon stimulation with vehicle or 10 µM DAMGO in control or Pitstop2 pre-treated cells (n=26-36 from 6-8 independent experiments). Each data point on the scatter plots represents a measurement from an individual cell (number of cells within parenthesis) and column plots represent mean ± SEM of the indicated number of cells or individual experiments. * denotes significance versus vehicle treatment in one-way ANOVA with Sidak's multiple comparisons test (* $p<0.05$).

3.4.5 Effect of GRK inhibition on ligand-induced changes in MOP organisation

We then investigated a potential role for GRKs in MOP reorganisation since interaction with and phosphorylation by these proteins rapidly occurs after receptor activation and prior to internalisation in an agonist-dependent manner (Miess et al., 2018). As expected from an

event that precedes internalisation, inhibition of GRK2/3 with Cmpd101 (30 µM, 30 min pre-treatment) prevented DAMGO-induced clustering (Fig. 3.13A, Table 1) and the increase in immobile fraction (Table 1). Remarkably, unlike PitStop2, Cmpd101 also prevented the DAMGO-induced slowing as measured by decrease in D_{FCS} (Fig. 3.13B, Table 1). Inhibition of GRKs by Cmpd101 occurs under these conditions since Cmpd101 treatment significantly reduced GRK2-Venus recruitment to FLAG-MOP-NLuc (Fig. 3.13C) and phosphorylation at one of the key C-terminal phosphorylation residues S375 (Fig. 3.13D), indicating that Cmpd101 prevents both recruitment and subsequent activity of GRK2 at the MOP. These data suggest the existence of a GRK-dependent mechanism, either the GRK scaffolding or phosphorylation function, as the driving cause for the agonist-stimulated slowing in diffusion in response to DAMGO, which precedes receptor clustering and internalisation.

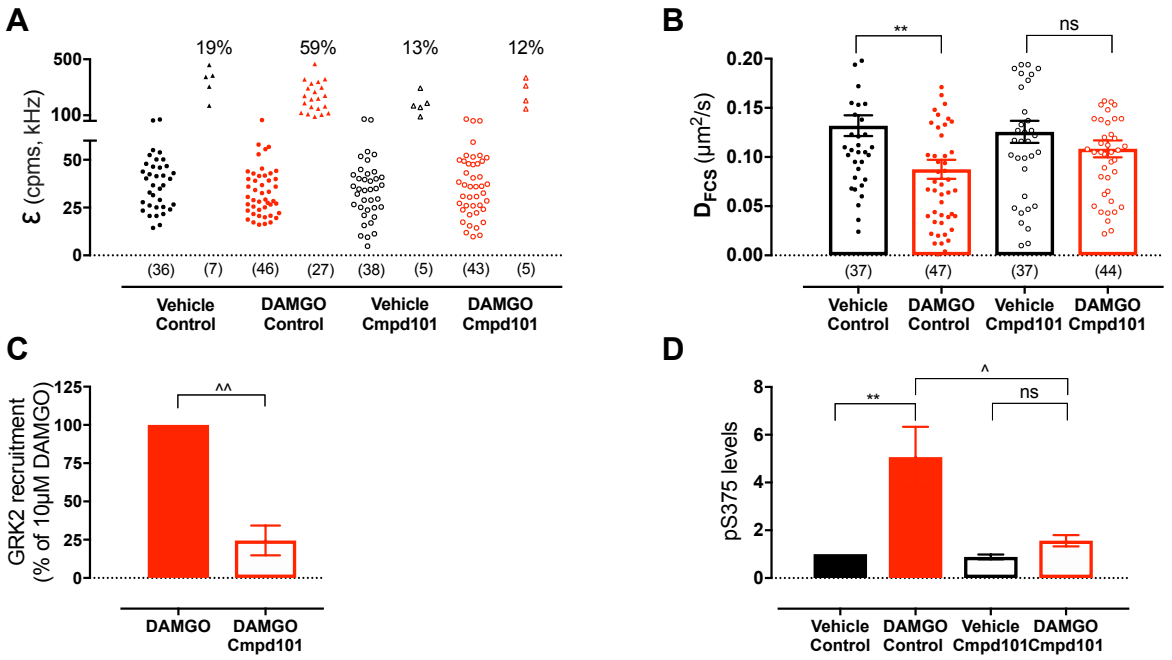


Figure 3.13 Effect of GRK2/3 inhibitor Cmpd101 on SNAP-MOP membrane organisation. HEK293 SNAP-MOP cells were exposed to the GRK2/3 inhibitor Cmpd101 (30 µM, 30 min, 37°C)**. (A)** Molecular brightness of SNAP-MOP after stimulation with vehicle or 10 µM DAMGO in control or Cmpd101 pre-treated cells (n=36-46 cells from 6-8 independent experiments). For each condition of the molecular brightness data, brightness values for the first (left) and second (right) component are shown, with the number of cells requiring a two-component fit indicated as percentage. **(B)** Diffusion coefficient of SNAP-MOP upon stimulation with vehicle or 10 µM DAMGO in control or Cmpd101 pre-treated cells (n=37-47 cells from 6-8 independent experiments). Each data point on the scatter plots represents a measurement from an individual cell (number of cells within parenthesis) and column plots represent mean

± SEM of the indicated number of cells or individual experiments. **(C)** HEK293 were transiently transfected with FLAG-MOP-NLuc and GRK2-Venus to measure GRK2 recruitment in a BRET assay after stimulation with 10 µM DAMGO in control or Cmpd101 pre-treated cells (n=3 independent experiments). The BRET ratio of vehicle-treated cells was subtracted, data represent mean ± SEM normalised to control condition. (**D)** Immunocytochemistry of FLAG-MOP upon stimulation with vehicle or 1 µM DAMGO in control or Cmpd101 pre-treated cells. Quantification of pS375 levels were calculated as a ratio of anti-phosphoS375 (pS375) MOP site antibody immunostaining divided by FLAG immunostaining and normalised to vehicle of the control condition (n=3 independent experiments). * denotes significance versus vehicle treatment and ^ denotes significance versus DAMGO control in one-way ANOVA with Sidak's multiple comparisons test (ns p>0.05, * p<0.05, ** p<0.01).

Table 1. Diffusion coefficient (D_{FCS}), particle concentration (N) and clustering measured by FCS and diffusion coefficient (D_{FRAP}) and immobile fraction (IF) measured by FRAP of SNAP-MOP expressing cells under different treatment conditions.

Treatment conditions		FCS			FRAP	
		D_{FCS} ($\mu m^2/s$)	N (particles/μm^2)	Clustering (% cells)	D_{FRAP} ($\mu m^2/s$)	IF (%)
Control	Vehicle	0.128 ± 0.005	175 ± 11	17	0.084 ± 0.008	34 ± 3
	Naloxone	0.145 ± 0.009	245 ± 17 **	14	0.089 ± 0.007	33 ± 2
	Morphine	0.121 ± 0.006	212 ± 15	21	0.079 ± 0.005	33 ± 3
	DAMGO	0.079 ± 0.006 ****	125 ± 10 *	38	0.080 ± 0.007	52 ± 4 ****
	DAMGO + Naloxone	0.130 ± 0.007 ^^	219 ± 35 ^^	7	ND	ND
PTx	Vehicle	0.132 ± 0.012	155 ± 23.1	20	ND	ND
	Naloxone	0.127 ± 0.013	241 ± 25.3	0	ND	ND
	Morphine	0.122 ± 0.006	236 ± 20.1	0	ND	ND
	DAMGO	0.093 ± 0.010 #	170 ± 17.8	30	ND	ND
Pitstop2	Vehicle	0.129 ± 0.012	112 ± 8.95	15	0.105 ± 0.014	45 ± 4
	Naloxone	0.120 ± 0.024	189 ± 67.7	ND	ND	ND
	Morphine	0.126 ± 0.011	204 ± 18.5	14	0.132 ± 0.027	24 ± 3 #
	DAMGO	0.082 ± 0.010 #	143 ± 16.4	21	0.113 ± 0.031	48 ± 4
Cmpd101	Vehicle	0.126 ± 0.011	180 ± 18.9	13	0.102 ± 0.013	40 ± 5
	Naloxone	0.115 ± 0.012	277 ± 46.3	NA	NA	NA
	Morphine	0.118 ± 0.010	217 ± 23.2	10	0.085 ± 0.009	28 ± 3
	DAMGO	0.106 ± 0.008	243 ± 26.1	16	0.084 ± 0.012	30 ± 4

* denotes significance versus vehicle control (* p<0.05, ** p<0.01, *** p<0.001, **** p<0.0001) in one-way ANOVA with Sidak's multiple comparisons test.
^ denotes significance versus DAMGO control (^ p<0.05, ^^ p<0.01, ^^^ p<0.001, ^^^^ p<0.0001) in one-way ANOVA with Sidak's multiple comparisons test.
# denotes significance versus vehicle in the same inhibitor pre-treatment condition (# p<0.05, ## p<0.01, ### p<0.001, #### p<0.0001) in one-way ANOVA with Sidak's multiple comparisons test.

3.4.6 Plasma membrane organisation of phosphorylation-deficient MOP mutants

Finally, we were interested in discriminating whether the GRK-dependent slowing in MOP diffusion was due to the scaffolding function of GRK through direct interaction with MOP or due to GRK-mediated phosphorylation of MOP. For this, we studied the plasma membrane organisation of different phosphorylation-deficient MOP mutants.

Both S363 and S375 are located within the C-terminus of the MOP. S363 has been described to be constitutively phosphorylated by PKC (Feng, Li & Wang, 2011; Illing, Mann & Schulz, 2014), whereas S375 is the main site for agonist-induced phosphorylation by GRK2/3 (Doll, Konietzko, Poll, Koch, Hollt & Schulz, 2011). Mutation of S363A did not affect DAMGO-induced phosphorylation at S375 (Fig. 3.14A) but presented increased clustering in vehicle to a similar extent than DAMGO-stimulated conditions (Fig. 3.14B) and presented DAMGO-induced slowing in D_{FCS} similar to WT (Fig. 3.14C). In contrast, mutation of S375A prevented DAMGO-induced clustering (Fig. 3.14B) and slowing in diffusion (Fig. 3.14C). This indicates that mutation S363A does not affect DAMGO-induced MOP reorganisation but might have an effect on the constitutive plasma membrane organisation of the MOP, whereas the phosphorylation site S375 is essential for agonist-induced reorganisation. This highlights that different phosphorylation sites might have different roles in the plasma membrane organisation of receptors.

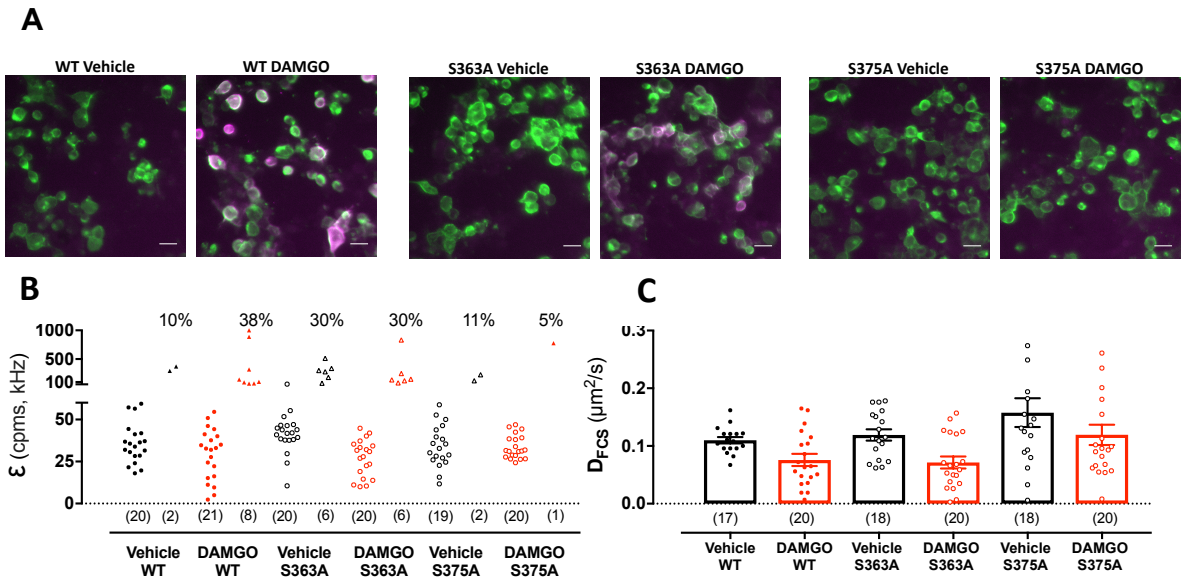


Figure 3.14 Membrane organisation of SNAP-MOP phosphorylation deficient mutants. (A) Anti-pS375 immunocytochemistry of FLAG-MOP WT, S363A or S375A after stimulation with vehicle or 1 µM DAMGO. Representative merged images of total FLAG staining (green) and pS375 (magenta) of n=3 independent experiments in duplicates. Scale bar 20µm. **(B)** Molecular brightness of SNAP-MOP WT, S363A or S375A after stimulation with vehicle or 10 µM DAMGO (n=19-20 cells from 4 independent experiments). For each condition, brightness values for the first (left) and second (right) component are shown, with the number of cells requiring a two-component fit indicated as percentage. **(C)** Diffusion coefficient of SNAP-MOP WT, S363A or S375A after stimulation with vehicle or 10 µM DAMGO (n=17-20 cells from 4 independent experiments). Each data point on the scatter plots represents a measurement from an individual cell (number of cells within parenthesis) and column plots represent mean ± SEM of the indicated number of cells.

3.5 Discussion

The formation of highly dynamic organised signalling complexes at the plasma membrane of the cell is key for the generation of specific cellular responses to extracellular stimuli. Stimulation of transmembrane proteins such as GPCRs can alter the composition of these organised signalling platforms to generate a tailored signalling profile. This is illustrated, for example, by the process of receptor internalisation, where prolonged stimulation of a GPCR by an agonist leads to phosphorylation of its intracellular domains which results in the recruitment of a myriad of regulatory proteins (including β-arrestins, AP-2, clathrin). These proteins facilitate receptor accumulation in clathrin coated pits and trafficking of the receptor to intracellular compartments. While receptor endocytosis represents a macroscopic change in receptor reorganisation, reorganisation of adaptor proteins at the microscopic scale have been suggested to occur prior to internalisation (Rappoport, Kemal, Benmerah & Simon, 2006). Recent advances in quantitative live cell imaging techniques and receptor labelling have been instrumental in providing further information on these dynamic micro-changes in receptor organisation that occur at the plasma membrane prior to receptor accumulation into intracellular compartments (Sungkaworn et al., 2017; Yanagawa et al., 2018). In addition to receptor organisation, previous FCS and FRAP studies have also demonstrated that effector proteins such as adenylyl cyclase redistribute and reorganise its micro-environment which originates highly specialized signalling hubs (Ayling et al., 2012).

Understanding such microdomain level diffusion events is of particular relevance for the MOP, since activation of MOP by different ligands results in distinct regulatory profiles. While endogenous opioid peptides and their analogues induce robust receptor internalisation, other opioid ligands such as morphine are very weak at driving MOP internalisation (Keith et al., 1996; Whistler & von Zastrow, 1998). Moreover, we have recently shown that differential activation of MOP also results in distinct spatiotemporal signalling profiles that are controlled by a change in distribution of the receptor within the plasma membrane (Halls et al., 2016). In this study we have used complementary imaging techniques (FCS and FRAP) to gain further understanding of the changes in plasma membrane MOP distribution that occur following receptor activation with DAMGO (a Met-enkephalin

derivative that causes robust MOP internalisation) compared to morphine (a poor internalising agonist).

Our data shows that only DAMGO, but not morphine, can change the organisation of the MOP from basal conditions in a concentration and time-dependent manner, prior to its movement to clathrin-coated pits and internalisation. We detected significant DAMGO-induced slowing in diffusion at 1 μM after 20 min of stimulation and we have previously shown that 1 μM DAMGO induces internalisation in a later timescale only reaching a maximum after 1h of stimulation (Halls et al., 2016). For this reason, we anticipate that this slowing in diffusion alludes to an event prior to internalisation. DAMGO-induced reorganisation occurs on both the micro- (i.e. diffusion coefficient) and macro- (i.e. surface receptor number, clustering and immobile fraction) scale. Additionally, we showed that this plasma membrane reorganisation was independent of G protein activation and that further changes in MOP clustering are mediated by clathrin-dependent endocytosis. Interestingly, the initial slowing of the MOP was prevented by Cmpd101, a GRK2/3 inhibitor, but was independent of (or occurs prior to) clathrin-mediated endocytosis. The large-scale changes induced by internalisation such as the decrease in particle number and the increase in molecular brightness might represent clustering into coated pits where the receptor is immobilised within the clathrin lattice. We propose that reorganisation of the MOP occurs at the plasma membrane prior to internalisation and is responsible for distinct agonist-specific signalling patterns (as per Halls et al., 2016), and that this is followed by a larger scale reorganisation of the MOP into clathrin-coated pits resulting in clustering and endocytosis (Fig. 3.15). Future studies should address how the GRK-mediated lateral diffusion of MOP identified here in model cell systems relate to endogenous MOP in a primary cell system. To perform similar FCS experiments in primary neurones would require the endogenous MOP to be fluorescently labelled either by the generation of genetically modified animals or with the use of fluorescently-labelled ligands.

GRKs are typically recognized for their catalytic activity in mediating agonist-induced phosphorylation during GPCR internalisation, however new roles indicate that regulatory proteins can signal separately from the agonist-receptor complex in distinct domains of the

plasma membrane (Eichel et al., 2018). Multi-color cross-correlation studies of the MOP bound to fluorescent agonists such as fluorescently labelled morphine (Lam et al., 2018) or a fluorescent opioid peptide (Arttamangkul, Alvarez-Maubecin, Thomas, Williams & Grandy, 2000) together with a fluorescently-tagged GRK protein would be informative to decipher whether the individual components of the agonist-receptor-effector complex diffuse together or separately. Additionally, scaffolding roles for GRK2 have also been described (Penela, Murga, Ribas, Lafarga & Mayor, 2010). The exact GRK-dependent mechanism (i.e. phosphorylation or scaffolding) underlying this micro-diffusion event remains to be elucidated. However, we identified here that specific phosphorylation sites have different roles in DAMGO-mediated MOP reorganisation with S375 being important in retaining agonist-induced changes in diffusion and receptor clustering. DAMGO-induced slowing in MOP diffusion could be caused by a change in the molecular composition of the receptor complex (i.e. direct interaction with GRKs, although interaction with other phosphorylation-dependent proteins cannot be dismissed) soon after receptor activation and prior to its accumulation in clathrin-coated pits. A change in the composition of the MOP complex on this timescale would be consistent with our previous observations of a DAMGO-induced receptor redistribution to control transient activation of cytosolic and nuclear ERK (Halls et al., 2016). Therefore, not only is the differential recruitment of GRK2 by DAMGO versus morphine important for MOP regulation (Miess et al., 2018), it also plays an essential role in MOP diffusion events that facilitate activation of compartmentalised signalling, revealing a novel role of GRKs as agonist-specific regulators of MOP plasma membrane organisation.

Previous FRAP studies using fluorescently labelled receptor and variable spot radius have demonstrated that the domain diffusion size is agonist dependent and that DAMGO-induced changes in diffusion are dependent on the formation of clathrin-coated pits (Sauliere-Nzeh Ndong, Millot, Corbani, Mazeres, Lopez & Salome, 2010). While we did not assess the effect of different radius size in our FRAP experiments, we also confirmed that the long-range changes induced by DAMGO in parameters measured by FRAP (i.e. immobile fraction) were dependent on clathrin-dependent internalisation. Additionally, the use of FCS over a small domain area ~0.1 μm^2, uncovered that at the micro-domain level, DAMGO also induced a GRK-dependent slowing in diffusion.

Another study described that the diffusion rate measured by FRAP increases in response to agonists (Melkes, Hejnova & Novotny, 2016). Although the bleaching region was of comparable size to our FRAP experiments, we did not detect any agonist-induced changes in long-range FRAP diffusion rates. Divergent results concerning the influence of agonists on the lateral mobility of MOP can, however, be attributed to different experimental conditions. For instance, the two studies assessed the diffusion of different fusion proteins. We studied the diffusion of cell surface labelled SNAP-MOP, whereas a C-terminally tagged yellow fluorescent protein MOP (MOP-YFP) was used in the other study. The attachment of a fluorescent protein tag to the receptor does not allow to distinguish between receptors that are already at the cell surface at the time of stimulation and newly synthesized receptors that are subsequently incorporated into the plasma membrane from the intracellular compartment, thus properties from different receptor pools might have been incorporated in Melkes et al. 2016. Moreover, addition of the fluorescent protein within the C-terminus could interfere with complex formation and could affect the diffusion rates measured.

The same study also reported that cholesterol depletion differentially affected the ability of agonists to change receptor mobility (Melkes, Hejnova & Novotny, 2016). Experimental and computational evidence has also highlighted that the membrane organisation of MOP can be influenced by changes in lipid content (Marino, Prada-Gracia, Provasi & Filizola, 2016; Vukojevic et al., 2008). In addition, cholesterol has been shown to promote MOP homodimerisation (Zheng et al., 2012), agonist binding (Gaibelet et al., 2008), coupling with G proteins (Gaibelet et al., 2008; Zheng et al., 2012) and translocation of β-arrestin (Qiu, Wang, Law, Chen & Loh, 2011). Movement between membrane domains with different lipid composition (e.g. cholesterol/non-cholesterol) could account for the slowing in MOP diffusion induced by DAMGO. Thus, this provides a potential mechanism by which the direct interaction of lipids with the receptor or the membrane micro-environment can facilitate interactions with specific signalling effectors and account for the agonist-specific spatiotemporal signalling elicited by the MOP (as per Halls et al. 2016).

In summary, we have described here that the MOP is highly organised at the plasma membrane and stimulation with DAMGO induces lateral reorganisation of the receptor in a G

protein-independent manner. Plasma membrane reorganisation at the micro scale level is only dependent on GRK2/3 and at the macro scale level is dependent on clathrin-dependent internalisation. This study therefore reveals an important and novel role of GRKs in modulating plasma membrane MOP organisation; and provides evidence that the lateral diffusion of MOP represents a molecular event, distinct and prior to internalisation, that is differentially regulated by opioids and controls spatiotemporal signalling.

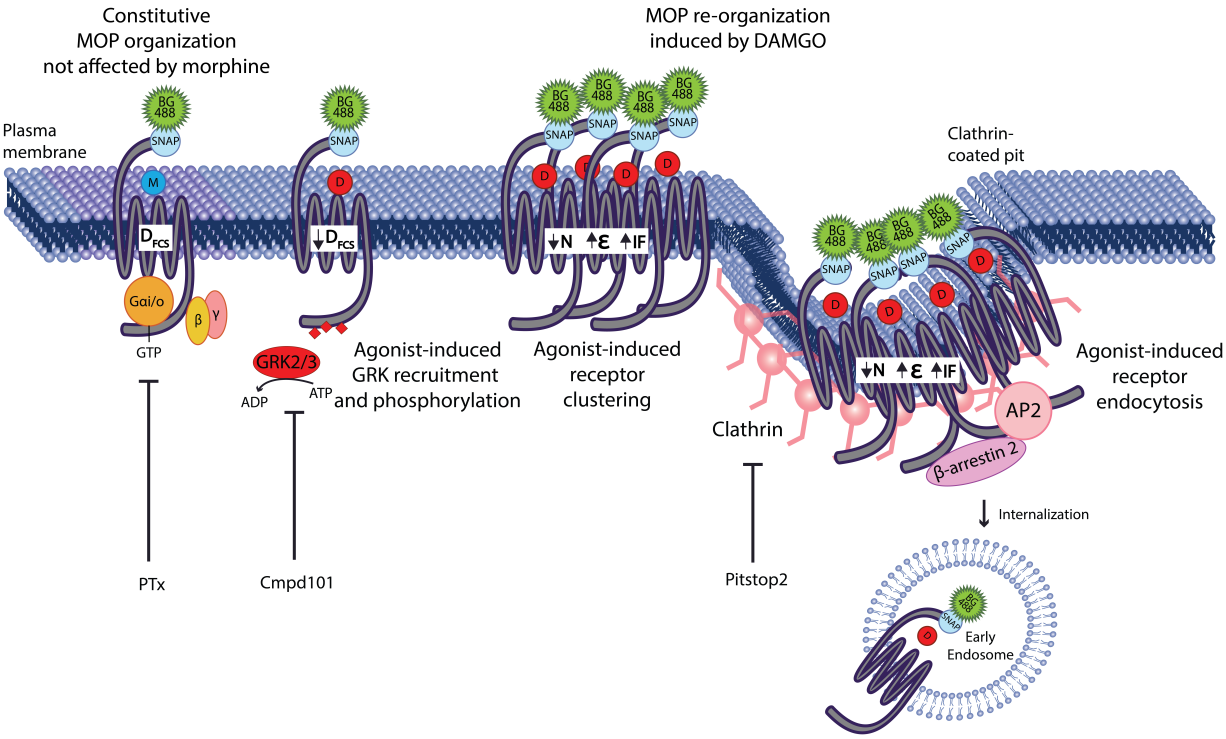


Figure 3.15 Plasma membrane organisation of SNAP-MOP under different treatment conditions. Agonist stimulation of SNAP-MOP with morphine does not alter its constitutive plasma membrane organisation. In contrast, agonist stimulation with DAMGO causes re-organisation of SNAP-MOP indicated by the decrease in diffusion coefficient (D_{FCS}), the decrease in particle concentration (N), the increase in molecular brightness (ε) and the increase in immobile fraction (IF). Different cellular processes and protein interactions underlie these changes. G protein activation is not involved in SNAP-MOP plasma membrane organisation, whereas GRK2/3 activity mediates DAMGO-induced slowing in D_{FCS} independently or prior to clustering and movement of SNAP-MOP into clathrin-coated pits to proceed towards internalisation. The latter events are responsible for changes in macro-scale parameters such as the reduced N, increased ε and IF.

Chapter 4

Multisite phosphorylation is required for sustained interaction with GRKs and arrestins during rapid MOP desensitisation

Arisbel B. Gondin, Elke Miess, Arsalan Yousuf, Ralph Steinborn, Nadja Mösslein, Yunshi Yang, Martin Göldner, Julia G. Ruland, Moritz Bünemann, Cornelius Krasel, MacDonald J. Christie, Michelle L. Halls, Stefan Schulz and Meritxell Canals

Sci. Signal. **11**, eaas9609 (2018) 17 July 2018

SCIENCE SIGNALING | RESEARCH ARTICLE

GPCR SIGNALING

Copyright © 2018 The Authors, some rights reserved; exclusive licensee American Association for the Advancement of Science. No claim to original U.S. Government Works

Multisite phosphorylation is required for sustained interaction with GRKs and arrestins during rapid μ-opioid receptor desensitization

Elke Miess[1]*, Arisbel B. Gondin[2]*, Arsalan Yousuf[3]*, Ralph Steinborn[1], Nadja Mösslein[4], Yunshi Yang[4], Martin Göldner[4], Julia G. Ruland[4], Moritz Bünemann[4], Cornelius Krasel[4], MacDonald J. Christie[3], Michelle L. Halls[2], Stefan Schulz[1†], Meritxell Canals[2†]

G protein receptor kinases (GRKs) and β-arrestins are key regulators of μ-opioid receptor (MOR) signaling and trafficking. We have previously shown that high-efficacy opioids such as DAMGO stimulate a GRK2/3-mediated multisite phosphorylation of conserved C-terminal tail serine and threonine residues, which facilitates internalization of the receptor. In contrast, morphine-induced phosphorylation of MOR is limited to Ser^{375} and is not sufficient to drive substantial receptor internalization. We report how specific multisite phosphorylation controlled the dynamics of GRK and β-arrestin interactions with MOR and show how such phosphorylation mediated receptor desensitization. We showed that GRK2/3 was recruited more quickly than was β-arrestin to a DAMGO-activated MOR. β-Arrestin recruitment required GRK2 activity and MOR phosphorylation, but GRK recruitment also depended on the phosphorylation sites in the C-terminal tail, specifically four serine and threonine residues within the ^{370}TREHPSTANT^{379} motif. Our results also suggested that other residues outside this motif participated in the initial and transient recruitment of GRK and β-arrestins. We identified two components of high-efficacy agonist desensitization of MOR: a sustained component, which required GRK2-mediated phosphorylation and a potential soluble factor, and a rapid component, which was likely mediated by GRK2 but independent of receptor phosphorylation. Elucidating these complex receptor-effector interactions represents an important step toward a mechanistic understanding of MOR desensitization that leads to the development of tolerance and dependence.

INTRODUCTION

Opioids such as morphine are still the mainstay analgesics for the treatment of severe pain. However, the development of tolerance, addiction, and respiratory depression severely limits their utility (*1*). These unwanted effects of opioids are key contributors to opioid-induced overdose deaths, which have drastically increased in the last decade (*2*).

The μ-opioid receptor (MOR) is the G protein–coupled receptor (GPCR) targeted by morphine and most opioid analgesics (*3*). Since the initial observation that morphine elicited less tolerance and decreased side effects in mice lacking β-arrestin2 (*4*, *5*), substantial efforts have focused on the development of opioid ligands that preferentially activate G protein–mediated signals over β-arrestin recruitment. These efforts have resulted in the discovery of several molecules with an improved side effect profile and increased therapeutic window (*6*–*8*). However, the cellular mechanisms whereby opioids mediate analgesia compared to other side effects are still not clear. MOR desensitization is considered to be the initial step for the development of tolerance. Such desensitization entails phosphorylation of the receptor, recruitment of regulatory proteins such as β-arrestins, and receptor internalization (*1*). Together, these regulatory processes result in a reduction of opioid response or sensitivity.

[1]Department of Pharmacology and Toxicology, Jena University Hospital–Friedrich Schiller University Jena, D-07747 Jena, Germany. [2]Drug Discovery Biology Theme, Monash Institute of Pharmaceutical Sciences, Monash University, Victoria 3052, Australia. [3]Discipline of Pharmacology, University of Sydney, New South Wales 2006, Australia. [4]Department of Pharmacology and Toxicology, Philipps-University Marburg, D-35043 Marburg, Germany.
*These authors contributed equally to this work.
†Corresponding author. Email: stefan.schulz@med.uni-jena.de (S.S.); meri.canals@monash.edu (M.C.)

The ligand-dependent and hierarchical nature of MOR phosphorylation and its role in MOR desensitization and internalization have been previously established. Quantitative mass spectrometry and phosphorylation site-specific antibodies have identified two clusters of MOR residues—^{354}TSST^{357} and ^{370}TREHPSTANT^{379} within its C-terminal region—that undergo opioid-induced phosphorylation (*9*–*11*). Agonist-mediated phosphorylation of MOR is initiated at Ser^{375}, but it is the ability of such agonists to induce higher-order phosphorylation on flanking residues that dictates their propensity to internalize MOR. Different opioids produce different phosphorylation patterns; multisite phosphorylation in the C-terminal region of MOR occurs robustly for agonists that induce internalization with less phosphorylation of fewer sites for those that do not (*9*–*11*).

Rapid desensitization of MOR coupling to membrane effectors such as voltage-gated calcium channels (VGCCs) and inwardly rectifying K channels (GIRKs; Kir3.X) also precedes internalization, but its relationship to phosphorylation events and β-arrestin recruitment remains unclear (*1*, *12*). We have previously shown that C-terminal phosphorylation of MOR is necessary for some forms of desensitization, an effect that is also ligand-dependent (*13*). Mutation of all Ser and Thr (S/T) residues within the C-terminal tail of MOR completely abolishes desensitization induced by [Met^5]-enkephalin (ME), but not by morphine. Introduction of an S375A mutation in transgenic mice diminishes the development of tolerance to high-efficacy opioid agonists such as [D-Ala2, N-MePhe4, Gly-ol]-enkephalin (DAMGO) or etonitazene without affecting tolerance to chronic morphine (*14*). Compound 101 (Cmpd101), a small-molecule inhibitor that prevents G protein receptor kinase (GRK) 2/3 activation (*15*), only partially blocked ME-, DAMGO-, and morphine-induced MOR

From Miess, E., Gondin, A. B., Yousuf, A., Steinborn, R., Mosslein, N., Yang, Y., . . . Canals, M. (2018). Multisite phosphorylation is required for sustained interaction with GRKs and arrestins during rapid mu-opioid receptor desensitization. *Sci Signal, 11*(539). doi:10.1126/scisignal.aas960. Reprinted with permission from AAAS.

Downloaded from http://stke.sciencemag.org/ on July 18, 2018

desensitization of GIRKs in rat and mouse locus coeruleus neurons (*16*), suggesting GRK2/3-independent mechanisms of MOR desensitization.

Multisite phosphorylation of MOR induced by high–intrinsic efficacy agonists such as DAMGO or ME requires GRK2/3 (*11*), and activation of MOR by these ligands results in β-arrestin recruitment to the receptor (*17*–*19*). Overexpression of GRK2 also facilitates morphine-induced β-arrestin recruitment and MOR internalization (*20*), supporting a key role of this kinase in MOR regulation. However, it is still unknown what dictates GRK-MOR interactions. Moreover, Raveh *et al.* (*21*) have proposed that GRKs may act to desensitize GIRK channels through a mechanism that is independent of their kinase activity through competition for the βγ subunits of the G protein that activate these channels. Thus, GRKs and arrestins are critical regulatory proteins for which interaction with MOR before internalization has major implications for opioid signaling. However, the molecular determinants that control these interactions are still elusive. How phosphorylation regulates these interactions and what relevance this has for MOR desensitization are questions that remain to be addressed.

In the present study, we systematically assessed how specific multisite phosphorylation controlled the dynamics of GRK and β-arrestin interactions with MOR and showed how such phosphorylation mediates receptor desensitization. Using bioluminescence and Förster resonance energy transfer (BRET and FRET) and β-galactosidase (β-Gal) complementation technology, we showed that the kinetics of GRK2/3 recruitment to a DAMGO-activated MOR were faster than the kinetics of β-arrestin recruitment. β-Arrestin recruitment required GRK2 activity and MOR phosphorylation, whereas GRK recruitment also depended on the integrity of the phosphorylation sites in the C terminus of MOR. Although the ^{370}TREHPSTANT^{379} motif was required for effective recruitment of GRKs and β-arrestins, the ^{354}TSST^{357} region participated in the long-term stability of such interactions. Both GRKs and β-arrestins showed residual recruitment

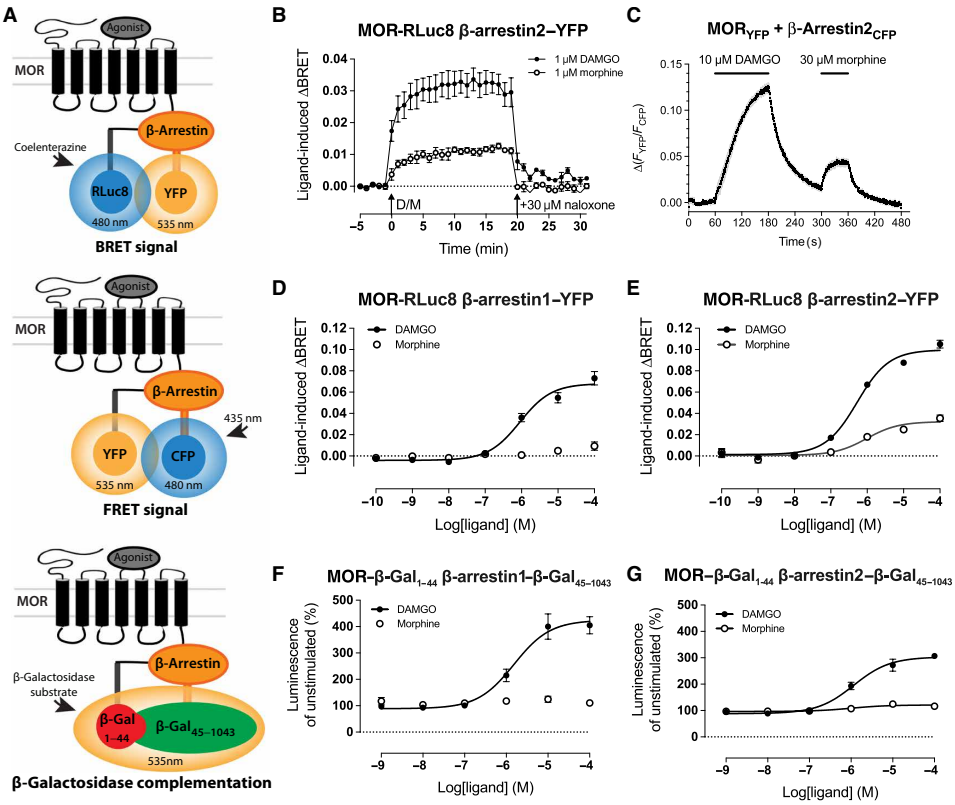


Fig. 1. Agonist-dependent recruitment of β-arrestin1/2 to WT MOR. (**A**) Schematic representation of the approaches used in this study: BRET, FRET, and β-Gal complementation. (**B**) BRET measurements in human embryonic kidney (HEK) 293 cells expressing MOR-RLuc8 and β-arrestin2–YFP and stimulated with 1 μM DAMGO or 1 μM morphine for 20 min before addition of 30 μM naloxone ($n = 4$ independent experiments). (**C**) FRET analysis of HEK293 cells expressing MOR-YFP and β-arrestin2–CFP and stimulated with 10 μM DAMGO or 30 μM morphine for 1 min before agonist washout ($n = 6$ independent experiments). (**D** and **E**) BRET analysis of HEK293 cells expressing MOR-RLuc8 and β-arrestin1/2–YFP and stimulated for 10 min with increasing concentrations of DAMGO (D) or morphine (E) ($n = 6$ independent experiments). (**F** and **G**) β-Gal complementation analysis of HEK293 cells expressing MOR–β-Gal$_{1–44}$ and β-arrestin1/2–β-Gal$_{45–1043}$ and stimulated with increasing concentrations of DAMGO (F) or morphine (G) for 1 hour ($n = 4$ to 6 independent experiments). Raw BRET/FRET ratio of vehicle-treated cells was subtracted, and raw bioluminescence data from β-Gal were normalized to vehicle-treated cells. Data points represent mean ± SEM of the indicated number of experiments.

From Miess, E., Gondin, A. B., Yousuf, A., Steinborn, R., Mosslein, N., Yang, Y., . . . Canals, M. (2018). Multisite phosphorylation is required for sustained interaction with GRKs and arrestins during rapid mu-opioid receptor desensitization. *Sci Signal, 11*(539). doi:10.1126/scisignal.aas960. Reprinted with permission from AAAS.

Downloaded from http://stke.sciencemag.org/ on July 18, 2018

Table 1. Potency (pEC_{50}) and maximal response (E_{max}) of β-arrestin1/2 recruitment to WT and phosphorylation-deficient MOR mutants.
NA, not available.

MOR		β-Arrestin1				β-Arrestin2			
		BRET		β-Gal		BRET		β-Gal	
		pEC_{50}	E_{max} (% of WT DAMGO)	pEC_{50}	E_{max} (% of WT DAMGO)	pEC_{50}	E_{max} (% of WT DAMGO)	pEC_{50}	E_{max} (% of WT DAMGO)
WT	**DAMGO**	6.05 ± 0.06	100	5.82 ± 0.07	100	6.28 ± 0.04	100	5.94 ± 0.03	100
	Morphine	—	—	—	—	6.12 ± 0.05	33.57 ± 2.18	—	—
TSST-4A	**DAMGO**	6.10 ± 0.06	91.59 ± 1.56	5.86 ± 0.05	36.33 ± 6.79^	6.36 ± 0.02	94.08 ± 3.76	5.58 ± 0.05	56.73 ± 7.61^
	Morphine	—	—	—	—	5.85 ± 0.14	29.21 ± 4.11	—	—
S375A	**DAMGO**	5.89 ± 0.07	36.20 ± 6.27^	6.71 ± 0.13	32.20 ± 5.73^	6.30 ± 0.01	71.73 ± 6.47^	6.08 ± 0.18	49.36 ± 16.95^
	Morphine	—	—	—	—	6.37 ± 0.14	17.31 ± 0.90^	—	—
STANT-3A	**DAMGO**	—	—	NA	NA	6.20 ± 0.06	56.26 ± 1.81^	NA	NA
	Morphine	—	—	NA	NA	6.40 ± 0.08	14.76 ± 1.66^	NA	NA
TREHPSTANT-4A	**DAMGO**	—	—	5.95 ± 0.48	28.47 ± 7.18^	NA	NA	5.72 ± 0.05	42.55 ± 6.31^
	Morphine	—	—	—	—	NA	NA	—	—
11S/T-A	**DAMGO**	—	—	8.27 ± 1.74	23.46 ± 2.33^	6.16 ± 0.02	41.90 ± 5.48^	6.08 ± 0.17	43.73 ± 5.16^
	Morphine	—	—	—	—	6.29 ± 0.08	15.92 ± 1.67^	—	—

^Significance compared to WT ($P < 0.01$) by two-way ANOVA with Dunnett's multiple comparison test.

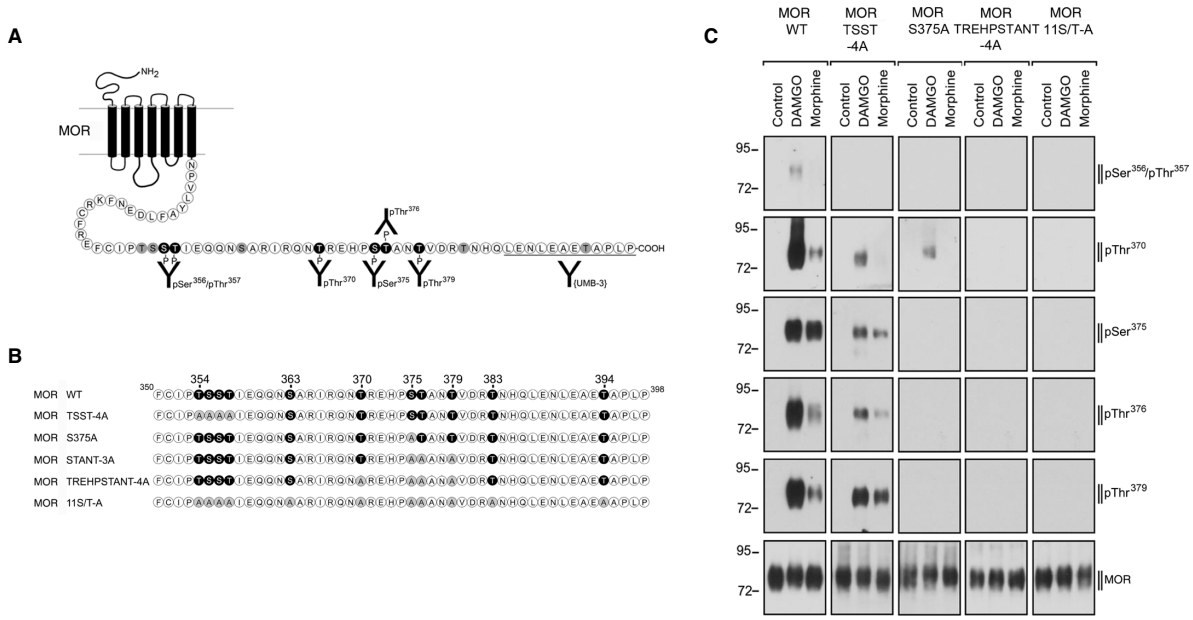


Fig. 2. C-tail phosphorylation of MOR. (**A**) Schematic representation of the C-tail domain of mouse MOR with potential phosphate acceptor sites depicted in gray and phosphosite-specific antibodies against pSer/pThr residues depicted in black ($pSer^{356}$/$pThr^{357}$, $pThr^{370}$, $pSer^{375}$, $pThr^{376}$, and $pThr^{379}$). The epitope recognized by the phospho-independent antibody UMB-3 is underlined. (**B**) C-tail sequences of WT MOR and phosphorylation-deficient MOR mutants are also illustrated. S/T residues depicted in black were mutated to A depicted in gray as shown in each of the mutants. (**C**) Characterization of phosphosite-specific antibodies using Western blot analysis. HEK293 cells stably expressing hemagglutinin (HA)–tagged MOR WT, MOR TSST-4A, MOR S375A, MOR TREHPSTANT-4A, or MOR 11S/T-A were stimulated with 10 μM DAMGO or morphine for 30 min at 37°C. Cells were lysed and immunoblotted with anti-$pSer^{356}$/$pThr^{357}$, anti-$pThr^{370}$, anti-$pSer^{375}$, anti-$pThr^{376}$, or anti-$pThr^{379}$ antibodies. Blots were stripped and reprobed with the phosphorylation-independent MOR antibody UMB-3 or with HA antibody to confirm equal loading ($n = 3$ independent experiments).

From Miess, E., Gondin, A. B., Yousuf, A., Steinborn, R., Mosslein, N., Yang, Y., . . . Canals, M. (2018). Multisite phosphorylation is required for sustained interaction with GRKs and arrestins during rapid mu-opioid receptor desensitization. *Sci Signal, 11*(539). doi:10.1126/scisignal.aas960. Reprinted with permission from AAAS.

Downloaded from http://stke.sciencemag.org/ on July 18, 2018

to a receptor with mutations at all C-terminal phosphosites. Using complementary patch-clamp approaches, we unraveled a fast desensitization event that was independent of MOR phosphorylation and a sustained desensitization component, which required GRK2-mediated phosphorylation of the ^{370}TREHPSTANT^{379} motif and a potential soluble factor. Elucidating these complex receptor-effector interactions represents an important step toward a mechanistic understanding of MOR desensitization that leads to the development of tolerance and dependence.

RESULTS

Agonist-dependent recruitment of β-arrestins to wild-type MOR

We have developed complementary approaches that allow for the systematic investigation of the dynamics and mechanisms of β-arrestin recruitment to MOR. FRET and BRET allow the real-time assessment of the recruitment of a fluorescently tagged β-arrestin [cyan fluorescent protein (CFP) or yellow fluorescent protein (YFP), respectively] to a C-terminally tagged MOR [YFP or *Renilla* luciferase 8 (RLuc8), respectively]. In addition, we have also developed a β-Gal complementation approach to measure steady-state interactions between β-arrestin and MOR. Thus, whereas FRET and BRET provide information about the dynamics of β-arrestin recruitment at early time points, the β-Gal complementation assay provides further insight into the stability of these interactions (Fig. 1A).

The high–intrinsic efficacy agonist DAMGO and the low–intrinsic efficacy opiate morphine (both at 1 μM) increased the BRET signal between MOR-RLuc8 and β-arrestin2–YFP, which peaked within 1 min, although the signal obtained with morphine was smaller than that obtained with DAMGO (Fig. 1B). This signal was blocked by the addition of the antagonist naloxone (30 μM), indicating the specificity and reversibility of the response (Fig. 1B). FRET measurements between MOR-YFP and β-arrestin2–CFP showed similar results (Fig. 1C) (*22*). Activation of MOR with saturating concentrations of DAMGO (10 μM) promoted β-arrestin2 recruitment to the receptor that peaked within 1 min and was reversed after agonist removal. Saturating concentrations of morphine (30 μM) also induced β-arrestin2–CFP recruitment to MOR-YFP, although with a lower FRET signal (Fig. 1C).

We then constructed concentration-response curves for β-arrestin1/2 recruitment using BRET (10-min incubation) or β-Gal complementation assays (1-hour incubation) (Fig. 1, D to G).

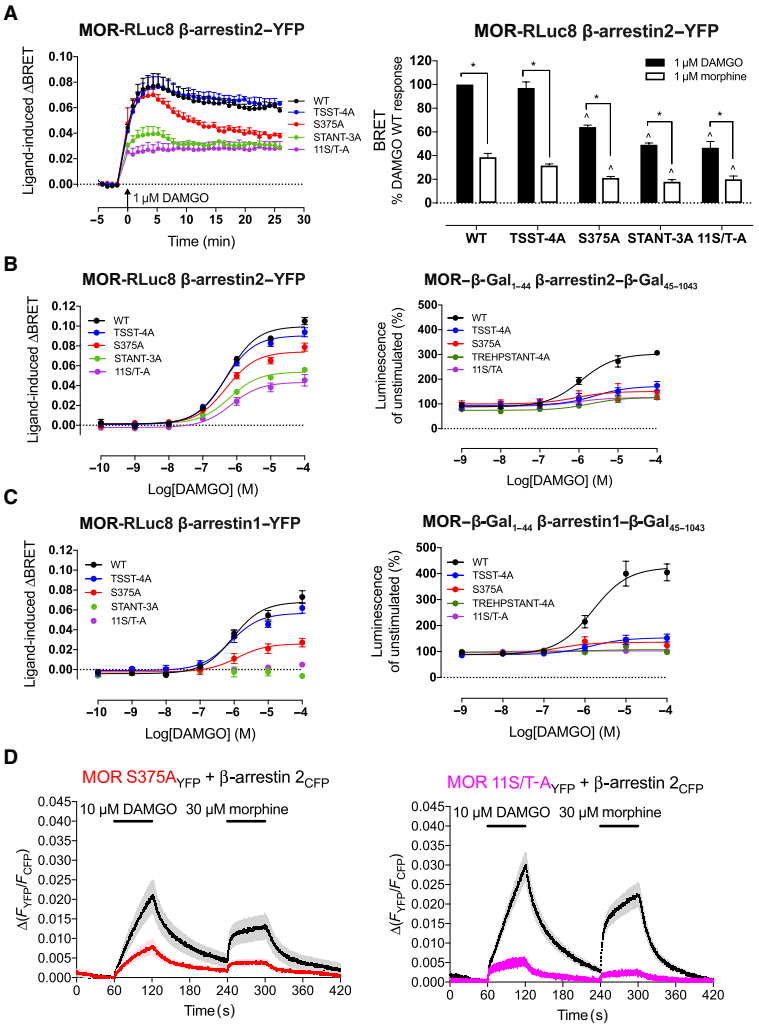


Fig. 3. Recruitment of β-arrestin1/2 to phosphorylation-deficient MOR mutants. (**A**) BRET analysis of HEK293 cells transiently transfected with MOR-RLuc8 WT or phosphorylation-deficient mutants and β-arrestin1/2–YFP and stimulated for 30 min with 1 μM DAMGO (n = 3 to 5 independent experiments). Raw BRET ratio of vehicle-treated cells was subtracted, and data represent mean ± SEM. Area under the curve (AUC) of BRET signal is shown as a percentage of the maximal response to DAMGO in the WT receptor and represents means ± SEM. All responses are significant against vehicle; ^ denotes significance compared to WT ($P < 0.01$) by two-way analysis of variance (ANOVA) with Dunnett's multiple comparison test; * denotes significance of DAMGO compared to morphine ($P < 0.01$) by two-way ANOVA with Sidak's multiple comparison test. (**B**) BRET analysis of HEK293 cells expressing MOR-RLuc8 WT or phosphorylation-deficient mutants and β-arrestin2–YFP or β-Gal complementation analysis of cells expressing MOR–β-Gal$_{1–44}$ WT or phosphorylation-deficient mutants and β-arrestin2–β-Gal$_{45–1043}$. Cells were stimulated with increasing concentrations of DAMGO for 10 min or 1 hour, respectively. Data were normalized to vehicle-treated cells and represent mean ± SEM (n = 3 to 6 independent experiments). (**C**) BRET analysis of HEK293 cells expressing MOR-RLuc8 WT or phosphorylation-deficient mutants and β-arrestin1–YFP or β-Gal complementation analysis of cells expressing MOR–β-Gal$_{1–44}$ WT or phosphorylation-deficient mutants and β-arrestin1–β-Gal$_{45–1043}$. Cells were stimulated with increasing concentrations of DAMGO for 10 min or 1 hour, respectively. Data were normalized to vehicle-treated cells and represent mean ± SEM (n = 3 to 6 independent experiments). (**D**) FRET analysis of HEK293 cells expressing MOR-YFP phosphorylation-deficient mutants and β-arrestin2–CFP and stimulated with 10 μM DAMGO or 30 μM morphine for 1 min before agonist washout (left, n = 14 independent experiments for WT and n = 15 independent experiments for S375A; right, n = 17 independent experiments for WT and 11S/T-A).

From Miess, E., Gondin, A. B., Yousuf, A., Steinborn, R., Mosslein, N., Yang, Y., . . . Canals, M . (2018). Multisite phosphorylation is required for sustained interaction with GRKs and arrestins during rapid mu-opioid receptor desensitization. *Sci Signal, 11*(539). doi:10.1126/scisignal.aas960. Reprinted with permission from AAAS.

Downloaded from http://stke.sciencemag.org/ on July 18, 2018

DAMGO induced a concentration-dependent recruitment of β-arrestin1/2 in both assays with similar potencies (Table 1). In contrast, morphine did not significantly induce β-arrestin1 recruitment and caused only a partial recruitment of β-arrestin2 with similar potency to DAMGO (Table 1). These results are in agreement with previous findings that show a compromised ability of morphine to recruit β-arrestins in the absence of GRK overexpression (*18*, *20*).

Recruitment of β-arrestins to phosphorylation-deficient MOR mutants

To map putative phosphate acceptor sites controlling MOR phosphorylation, we generated phosphorylation-deficient MOR mutants and directly assessed the correlation between phosphorylation and recruitment of regulatory proteins. Receptor phosphorylation at candidate sites was evaluated using phosphosite-specific antibodies (Fig. 2A). Mutations of S/T residues to alanine (A) in different regions of wild-type (WT) MOR generated the following phosphorylation-deficient MOR mutants: TSST-4A (mutations in the ^{354}TSST^{357} cluster), S375A (Ser^{375} mutation), STANT-3A (mutations in the ^{375}STANT^{379} cluster), TREHPSTANT-4A (mutations in the ^{370}TREHPSTANT^{379} motif), and 11S/T-A (mutation of all 11 potential C-terminal S/T phosphorylation sites) (Fig. 2B).

Consistent with earlier observations (*10*, *11*), no constitutive phosphorylation of Ser^{356}/Thr^{357}, Thr^{370}, Ser^{375}, Thr^{376}, or Thr^{379} was observed. Agonist stimulation with morphine resulted in phosphorylation of Ser^{375} and induced only weak phosphorylation of Thr^{370}, Thr^{376}, and Thr^{379}. In contrast, DAMGO resulted in robust MOR phosphorylation at all sites in the ^{370}TREHPSTANT^{379} domain (Fig. 2C) (*10*, *11*). Equivalent receptor loading was confirmed by detecting a distinct nonphosphorylated epitope in the cytoplasmic tail.

Expanding from previous studies, we generated a phosphosite-specific antiserum against Ser^{356} and Thr^{357} of the ^{354}TSST^{357} motif of the MOR C-terminal tail (pSer^{356}/pThr^{357}). DAMGO stimulation induced very weak phosphorylation of these residues, which was abolished in the TSST-4A mutant. Morphine did not promote phosphorylation of any of these residues (Fig. 2C). In addition, mutation of the ^{354}TSST^{357} motif in the TSST-4A mutant produced a modest decrease in the phosphorylation at other S/T sites by both ligands. These data exclude both Ser^{356}/Thr^{357} as prominent initial sites for agonist-induced MOR phosphorylation but highlight the idea that the integrity of the ^{354}TSST^{357} cluster might be important for regulatory events that depend on robust phosphorylation within the ^{370}TREHPSTANT^{379} domain.

Point mutation of Ser^{375} (S375A mutant) within the ^{375}STANT^{379} motif prevented detectable phosphorylation at Ser^{356}/Thr^{357}, Thr^{376}, and Thr^{379}, and also substantially reduced phosphorylation at Thr^{370} (Fig. 2C). This confirms Ser^{375} as the initial residue for agonist-specific hierarchical MOR phosphorylation as previously reported (*10*, *11*). As expected, detection of phosphorylated MOR by any of the phospho-specific antibodies was blocked by mutation of the ^{370}TREHPSTANT^{379} motif or mutation of all S/T residues in the cytoplasmic tail (11S/T-A mutant) (Fig. 2C).

To directly assess the relationship between receptor phosphorylation and the recruitment of β-arrestin1/2, we generated phosphorylation-deficient MOR mutants (Fig. 2A) suitable for BRET, FRET, and β-Gal complementation assay. Correct expression and function of these mutants were evaluated by anti-FLAG enzyme-linked immunosorbent assay (ELISA) and inhibition of forskolin-induced cyclic adenosine monophosphate (cAMP) of FLAG-tagged MOR constructs without C-terminal tags (fig. S1, A and B, and table S1).

Mutation of the ^{354}TSST^{357} cluster (TSST-4A) did not affect DAMGO-induced β-arrestin1/2 recruitment as measured using BRET (Fig. 3, A to C, and Table 1). However, β-Gal complementation showed that deletion of this cluster decreased the absolute recruitment of β-arrestin1/2 (E_{max}) without altering the potency of DAMGO (Fig. 3, B and C, and Table 1). β-Gal complementation requires the two fragments to be in the correct relative orientation to form a functional enzyme, which has been suggested to occur upon "stable" interactions (30 to 90 min). In contrast, for FRET and BRET to occur, the relative orientation between the receptor and β-arrestin is under fewer constraints. Thus, these data suggest that although the initial recruitment of β-arrestins to the receptor may not be affected by mutation of the ^{354}TSST^{357} motif, the stability of this interaction is affected upon mutation of this motif to alanine. Thus, phosphorylation of the ^{354}TSST^{357} region, although not directly involved in β-arrestin recruitment, may participate in the stability of the β-arrestin/MOR complex.

Mutation of the ^{375}STANT^{379} cluster (STANT-3A) or ^{370}TREHPSTANT^{379} affected DAMGO-induced β-arrestin1/2 recruitment to MOR in both BRET and β-Gal complementation assays (Fig. 3, A to C), respectively. Although the potency of DAMGO was unaffected for this mutant, there was a ~50% reduction of the maximal effect of this ligand (Table 1). These results suggest that the ^{375}STANT^{379} motif in conjunction with Thr^{370} constitutes a key region for receptor-arrestin interactions, most likely participating in the initial recruitment of β-arrestin to the activated receptor. Within this region lies Ser^{375}, which drives the hierarchical phosphorylation of MOR, and which affected the dynamics of β-arrestin2 recruitment when mutated. Although the BRET response to DAMGO within the first 5 min after stimulation was similar to the WT receptor, the signal rapidly decayed to levels similar to those measured for the STANT-3A mutant

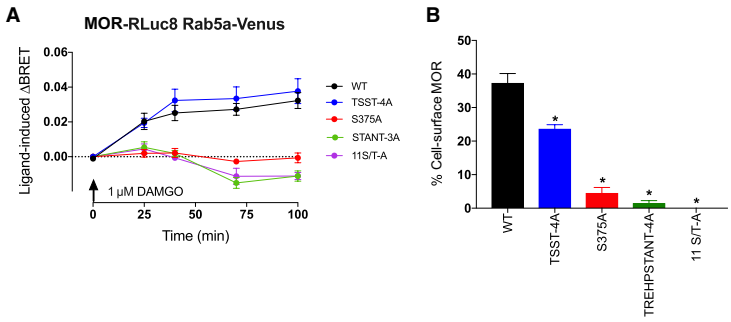


Fig. 4. Internalization of phosphorylation-deficient MOR mutants. (**A**) Internalization BRET assay in HEK293 cells transiently transfected with MOR-RLuc8 WT or phosphorylation-deficient mutants and the early endosome marker Rab5a-Venus and stimulated with 1 μM DAMGO. BRET ratio of vehicle-treated cells was subtracted. Data points represent mean ± SEM (n = 3 to 4 independent experiments). (**B**) HEK293 cells stably expressing the HA-tagged MOR WT, MOR TSST-4A, MOR S375A, MOR TREHPSTANT-4A, or MOR 11S/T-A were preincubated with HA antibody and stimulated with 10 μM DAMGO for 30 min. Receptor sequestration, quantified as the percentage of residual cell-surface receptors on agonist-treated cells, was measured by ELISA (n = 3 independent experiments).

Downloaded from http://stke.sciencemag.org/ on July 18, 2018

From Miess, E., Gondin, A. B., Yousuf, A., Steinborn, R., Mosslein, N., Yang, Y., . . . Canals, M . (2018). Multisite phosphorylation is required for sustained interaction with GRKs and arrestins during rapid mu-opioid receptor desensitization. *Sci Signal, 11*(539). doi:10.1126/scisignal.aas960. Reprinted with permission from AAAS.

(Fig. 3A). Furthermore, although the potency of DAMGO at this mutant was similar to that of the WT receptor, its maximal effect was reduced by 30% (Table 1). As expected, the β-Gal complementation assay revealed that DAMGO-induced recruitment to the MOR S375A mutant was reduced (Fig. 3, B and C, and Table 1). In addition, FRET analysis of MOR S375A-YFP and β-arrestin2–CFP also showed that this mutation substantially attenuated β-arrestin2 recruitment (Fig. 3D). Together, these results not only support the observations that phosphorylation of Ser^{375} serves as an initial residue for multisite phosphorylation but also suggest that this site is key to prolonging the interaction between MOR and β-arrestins. Finally, we assessed β-arrestin2 recruitment to a mutant receptor where all the phosphorylation sites of the C-tail have been mutated to alanine (11S/T-A). As expected, DAMGO-induced β-arrestin1/2 recruitment to this mutant was significantly compromised in all the three assays (Fig. 3, A to D, and Table 1).

We observed that although the DAMGO-induced BRET signal was reduced in the STANT-3A and 11S/T-A mutants, it was not completely abolished and it still increased from basal levels upon addition of the agonist. Addition of the antagonist naloxone (30 μM) reversed the BRET signal to basal levels (fig. S2). A similar effect was observed in the FRET assay after agonist removal (Fig. 3D), although recruitment of β-arrestin2 was not detected for the two phosphorylation-deficient mutants in the β-Gal complementation assay. These data suggest that even in the absence of phosphorylation sites in the C-tail of the MOR, β-arrestins can be transiently recruited to the receptor upon agonist stimulation.

We also investigated the effects of the above mutations on morphine-induced β-arrestin2 recruitment. As observed in the WT receptor, the response induced by morphine was significantly weaker than that induced by DAMGO (Fig. 3A and Table 1). However, the effect of all mutations on morphine's response mirrored those observed for the high-efficacy agonist DAMGO.

Because β-arrestin recruitment precedes MOR internalization (*1*), we assessed the ability of DAMGO to promote endocytosis of MOR phospho-deficient

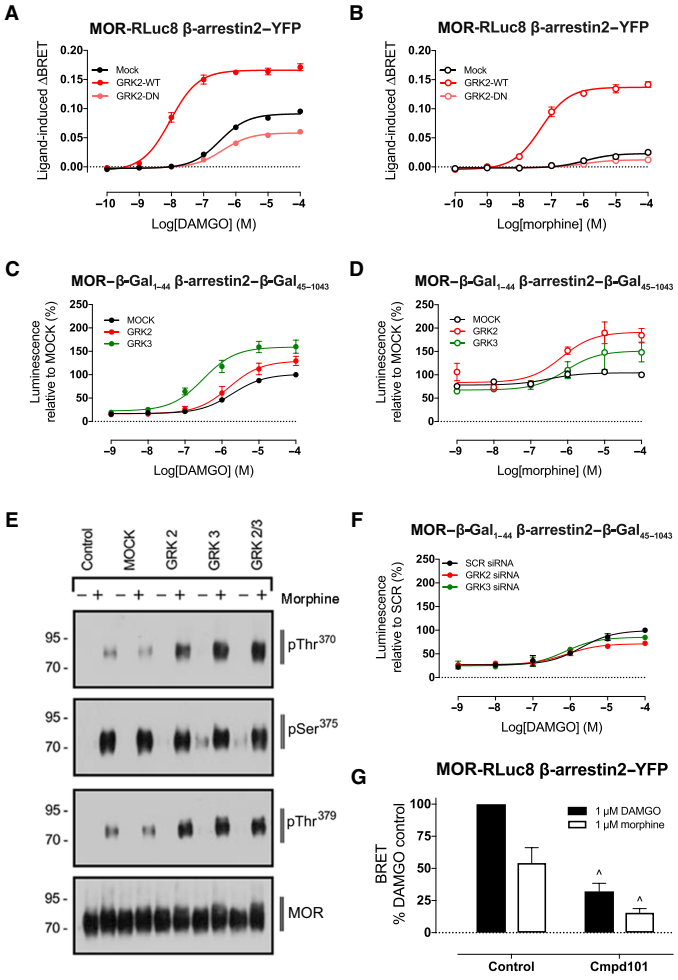


Fig. 5. Role of GRKs in β-arrestin recruitment. (**A** and **B**) BRET analysis of HEK293 cells expressing MOR-RLuc8 and β-arrestin2–YFP; cotransfected with pcDNA3 (mock), GRK2-WT, or GRK2-DN (dominant negative); and stimulated for 10 min with increasing concentrations of DAMGO (A) or morphine (B), and the BRET signal was measured after stimulation ($n = 3$ independent experiments). (**C** and **D**) β-Gal complementation analysis of HEK293 cells expressing MOR–β-$Gal_{1–44}$ and β-arrestin1/2–β-$Gal_{45–1043}$; cotransfected with pcDNA3 (mock), GRK2, or GRK3; and stimulated with increasing concentrations of DAMGO (C) or morphine (D) for 1 hour ($n = 3$ to 6 independent experiments). For BRET, the ratio of vehicle-treated cells was subtracted, and for β-Gal complementation, data were normalized to vehicle-treated cells. Data points represent mean ± SEM. (**E**) HEK293 cells expressing MOR alone (control) or in combination with pcDNA3 (mock), GRK2, GRK3, or both were stimulated with 10 μM morphine for 30 min at 37°C, lysed, and immunoblotted with anti-$pThr^{370}$, anti-$pSer^{375}$, or anti-$pThr^{379}$ antibodies. Blots were stripped and reprobed with the phosphorylation-independent HA antibody to confirm equal loading ($n = 3$ independent experiments). (**F**) β-Gal complementation analysis of HEK293 cells expressing MOR–β-$Gal_{1–44}$ and β-arrestin1/2–β-$Gal_{45–1043}$; cotransfected with scrambled (SCR), GRK2, or GRK3 small interfering RNA (siRNA); and stimulated with increasing concentrations of DAMGO for 1 hour ($n = 4$ independent experiments). The raw BRET ratio of vehicle-treated cells was subtracted, and the raw bioluminescence data from β-Gal were normalized to vehicle-treated cells. (**G**) BRET analysis of HEK293 cells expressing MOR-RLuc8 and β-arrestin2–YFP and pretreated with vehicle or 30 μM Cmpd101 for 30 min before being stimulated with 1 μM DAMGO or 1 μM morphine ($n = 4$ independent experiments). AUC is expressed as a percentage of the maximal response of DAMGO in the control and is shown as the mean ± SEM. ^ denotes significance compared to control ($P < 0.01$) by two-way ANOVA with Dunnett's multiple comparison test.

From Miess, E., Gondin, A. B., Yousuf, A., Steinborn, R., Mosslein, N., Yang, Y., . . . Canals, M . (2018). Multisite phosphorylation is required for sustained interaction with GRKs and arrestins during rapid mu-opioid receptor desensitization. *Sci Signal, 11*(539). doi:10.1126/scisignal.aas960. Reprinted with permission from AAAS.

Downloaded from http://stke.sciencemag.org/ on July 18, 2018

Table 2. Potency (pEC_{50}) and maximal response (E_{max}) of β-arrestin2 recruitment with GRK overexpression (OE) or knockdown (KD).

MOR		BRET		β-Gal	
		pEC_{50}	E_{max} (% of mock DAMGO)	pEC_{50}	E_{max} (% of mock or SCR)
Mock	DAMGO	6.50 ± 0.02	100	5.72 ± 0.02	100
	Morphine	5.95 ± 0.05	25.72 ± 2.10	6.51 ± 0.38	100
GRK2-WT OE	DAMGO	8.03 ± 0.04^	176.43 ± 8.43^	5.81 ± 0.01	128.98 ± 17.03
	Morphine	7.33 ± 0.05^	146.06 ± 6.18^	6.16 ± 0.26	183.99 ± 28.26
GRK2-DN OE	DAMGO	6.41 ± 0.03	62.23 ± 3.18^	—	—
	Morphine	6.55 ± 0.02	12.56 ± 1.66	—	—
GRK3-WT OE	DAMGO	NA	NA	6.51 ± 0.03	157.94 ± 18.66
	Morphine	NA	NA	6.05 ± 0.14	144.58 ± 40.65
SCR	DAMGO	NA	NA	5.71 ± 0.13	100
	Morphine	NA	NA	—	—
GRK2 KD	DAMGO	NA	NA	6.09 ± 0.12	72.39 ± 4.35
	Morphine	NA	NA	—	—
GRK3 KD	DAMGO	NA	NA	6.14 ± 0.15	85.64 ± 2.51
	Morphine	NA	NA	—	—

^Significance compared to WT ($P < 0.01$) by two-way ANOVA with Dunnett's multiple comparison test.

mutants using BRET, cell-surface ELISA, and confocal imaging. Stimulation of the WT receptor with DAMGO, but not with morphine, induced an increase in the BRET signal between MOR-RLuc8 and the early endosome resident protein Rab5a (tagged with Venus) (Fig. 4A and fig. S2B). DAMGO-induced internalization was also observed in cell-surface ELISA assay, which quantifies agonist-induced reduction of cell-surface receptor (Fig. 4B). Confocal imaging of the HA-tagged MOR (fig. S1C) also confirmed the internalization induced by DAMGO. Mutations of the ^{354}TSST^{357} motif had a weak effect on DAMGO-induced MOR internalization (Fig. 4, A and B); however, the S375A, STANT-3A, TREHPSTANT-4A, or 11S/T-A mutations severely impaired receptor endocytosis. These results are consistent with the β-arrestin recruitment data and support the requirement of a strong and sustained MOR–β-arrestin interaction to drive receptor internalization.

Role of GRKs in β-arrestin recruitment

Agonist-induced phosphorylation of MOR is mediated by GRKs. In particular, GRK2 and GRK3 are mainly involved in MOR phosphorylation upon stimulation with high-efficacy agonists, such as DAMGO (*11*). We thus investigated the influence of overexpression, knockdown, and pharmacological inhibition of GRK2/3 on β-arrestin recruitment using BRET and β-Gal complementation approaches. As expected, overexpression of GRK2/3 resulted in increased efficacy and potency of DAMGO- and morphine-induced recruitment of β-arrestin1 (fig. S3A) and β-arrestin2 (Fig. 5, A to D, and Table 2). In addition, and extending a previous study showing that GRK2 overexpression increases morphine-induced phosphorylation of Ser^{375} (*10*), we showed that GRK2/3 overexpression facilitated morphine-induced multisite phosphorylation of Thr^{370} and Thr^{379} in the ^{370}TREHPSTANT^{379} motif (Fig. 5E). Depletion of endogenous GRK2 or GRK3 alone by siRNA (fig. S4E) or by overexpression of a catalytically inactive GRK2 (GRK2 K220R and GRK2-DN) had a small effect in reducing the efficacy of DAMGO and morphine to recruit β-arrestin2 (Fig. 5, A and F, and Table 2). Inhibition by the GRK2/3 inhibitor Cmpd101 (*15*) resulted in inhibition of DAMGO-induced β-arrestin2 recruitment (Fig. 5G). In agreement with the β-arrestin recruitment data and with previous reports, MOR internalization in response to both DAMGO and morphine was enhanced by GRK2 overexpression and abolished by incubation with Cmpd101, as assessed by BRET between MOR-RLuc8 and Rab5a-Venus (fig. S3B). Together, these results illustrate the key role of GRK2/3 in the recruitment of β-arrestins and receptor endocytosis induced by opioid agonists.

GRK recruitment to activated WT and phosphorylation-deficient MOR mutants

To understand the dynamics and mechanisms of GRK recruitment to MOR, we developed FRET, BRET, and β-Gal complementation approaches with the same donor-acceptor pairs used in the β-arrestin assays described above. Real-time measurements of FRET between MOR-YFP and GRK2-mTurquoise or BRET between MOR-RLuc8 and GRK2-Venus showed that GRK2 recruitment to the activated receptor occurs faster than β-arrestin translocation (fig. S4D) and reversed to basal upon agonist removal or addition of 30 μM naloxone (Fig. 6, A and B). Concentration-response curves constructed using BRET or β-Gal complementation assays estimated a potency of 0.6 μM for DAMGO and 0.43 μM for morphine (Fig. 6, C and D, and Table 3). Similar results were obtained for GRK3 in the β-Gal complementation assay (fig. S4, A and B). Cmpd101 prevented GRK2 recruitment to activated MOR (Fig. 6E), suggesting that an active GRK2 is required for its interaction with MOR.

We next sought to understand the role of phosphorylation within MOR C-tail on GRK2 translocation. We obtained similar results to the β-arrestin recruitment data described above. Namely, mutation

From Miess, E., Gondin, A. B., Yousuf, A., Steinborn, R., Mosslein, N., Yang, Y., . . . Canals, M . (2018). Multisite phosphorylation is required for sustained interaction with GRKs and arrestins during rapid mu-opioid receptor desensitization. *Sci Signal, 11*(539). doi:10.1126/scisignal.aas960. Reprinted with permission from AAAS.

Downloaded from http://stke.sciencemag.org/ on July 18, 2018

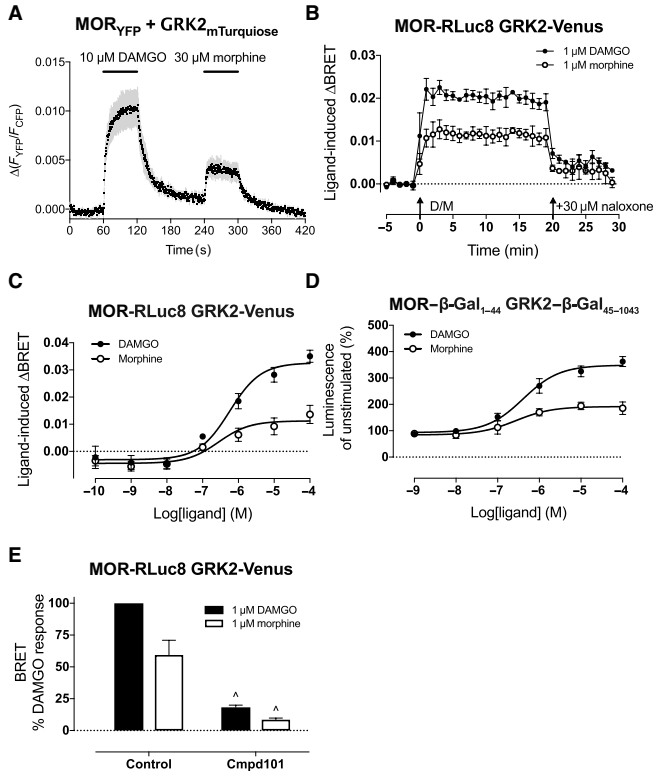


Fig. 6. GRK recruitment to activated WT MOR. (**A**) FRET analysis of HEK293 cells expressing MOR-YFP and GRK2-mTurquoise and stimulated with 10 μM DAMGO or 30 μM morphine for 1 min before agonist washout (n = 6 independent experiments). (**B** and **C**) BRET analysis of HEK293 cells expressing MOR-RLuc8 and GRK2-Venus and stimulated with 1 μM DAMGO or morphine for 20 min before the addition of 30 μM naloxone (B) or for 10 min with increasing concentrations of DAMGO and morphine (C) (both n = 3 independent experiments). (**D**) β-Gal complementation analysis of HEK293 cells expressing MOR–β-Gal$_{1–44}$ and GRK2–β-Gal$_{45–1043}$ and stimulated with increasing concentrations of DAMGO or morphine for 1 hour (n = 4 independent experiments). For BRET or FRET, data from vehicle-treated cells were subtracted, and for β-Gal complementation, the data were normalized to vehicle-treated cells. Data represent mean ± SEM. (**E**) BRET analysis of HEK293 cells expressing MOR-RLuc8 and GRK2-Venus and preincubated with control or 30 μM Cmpd101 for 30 min before stimulation with 1 μM DAMGO or morphine. The 10-min AUC was quantified and is expressed as a percentage of the maximal response of the control-treated DAMGO response (n = 4 independent experiments). Data are expressed as mean ± SEM. ^ denotes significance versus control (P < 0.01) by two-way ANOVA with Dunnett's multiple comparison test.

of the ^{354}TSST^{357} motif (TSST-4A) did not affect early BRET measurements (Fig. 7, A and B, and Table 3), whereas it decreased GRK2 recruitment as measured by β-Gal complementation (Fig. 7C and Table 3). These results again suggest a role of this region in the stability of interactions between the receptor and regulatory proteins. The S375A, STANT-3A, and 11S/T-A mutations all substantially reduced GRK2 recruitment in both assays (Fig. 7, A to C). Similar results were obtained for GRK3 in the β-Gal complementation assay (fig. S4C).

FRET experiments using the S375A and 11S/T-A mutants and GRK2-mTurquoise showed that agonist-induced recruitment of GRK2 to phosphorylation-deficient mutants was reversible after agonist washout (Fig. 7D). Although the BRET signal was reduced for the STANT-3A and 11S/T-A mutants, it was not completely abolished and it still increased from basal levels upon addition of the ligand, and only the addition of the antagonist naloxone returned the BRET signal to basal levels (fig. S4C). These data support the notion that even in the absence of phosphorylation sites at the C-tail of the MOR, GRKs and β-arrestins can be transiently recruited to the receptor upon agonist stimulation.

Desensitization of phosphorylation-deficient MOR mutants

Phosphorylation sites in the vicinity of ^{354}TSST^{357} and ^{375}STANT^{379} play important roles in MOR desensitization. Using conventional whole-cell mode of patch-clamp recording, Birdsong *et al.* (*23*) have shown that the STANT-3A mutation and, more critically, STANT-3A plus TSST-4A impair desensitization by ME in neurons. By contrast, using perforated patch-clamp recording to limit disruption of the cytoplasmic milieu, we have previously reported that mutation of 6 S/T residues, including STANT, abolishes ME-induced internalization but does not inhibit desensitization and that impairment of ME-induced desensitization requires mutation of all 11 S/T residues in the C-tail (*13*). We therefore compared desensitization of the STANT-3A and TSST-4A mutants using both whole-cell and perforated patch-clamp recording. As previously reported (*13*), an initial rapid component of GIRK desensitization (with a time constant of about 2 to 4 s) was observed upon application of ME (10 μM) for both TSST-4A and STANT-3A mutants that was not significantly different from WT MOR (fig. S5, A and C). This rapid component was not observed using a concentration of ME below 100 nM and was less prominent during application of morphine than ME (10 μM; fig. S5C). This effect most likely reflects GIRK regulation by GRK2, which is recruited to the receptor-channel complex by ME but less effectively by morphine, as suggested previously (*21*). However, it should be noted that the potency of ME to induce this rapid desensitization component could not be resolved because the on-rate of ME-activated G_{GIRK} overlapped substantially at low concentrations with the on-rate of the declining component (fig. S5A).

Using perforated patch clamp, both STANT-3A and TSST-4A mutants showed acute desensitization upon exposure to supramaximal concentrations of both ME and morphine (10 μM) similar to WT MOR (Fig. 8, A to D). GIRK conductance acutely declined during the 5-min exposure to both ME and morphine in cells expressing the mutants or WT. As previously reported, the decline in peak GIRK conductance is an insensitive measure of receptor desensitization because of the large receptor reserve present in these cells (*13*, *24*).

From Miess, E., Gondin, A. B., Yousuf, A., Steinborn, R., Mosslein, N., Yang, Y., . . . Canals, M . (2018). Multisite phosphorylation is required for sustained interaction with GRKs and arrestins during rapid mu-opioid receptor desensitization. *Sci Signal, 11*(539). doi:10.1126/scisignal.aas960. Reprinted with permission from AAAS.

Downloaded from http://stke.sciencemag.org/ on July 18, 2018

Table 3. Potency (pEC_{50}) and maximal response (E_{max}) of GRK2 recruitment to phosphorylation-deficient MOR mutants.

MOR		BRET		β-Gal	
		pEC_{50}	E_{max} (% of WT DAMGO)	pEC_{50}	E_{max} (% of WT DAMGO)
WT	DAMGO	6.22 ± 0.14	100	6.39 ± 0.12	100
	Morphine	6.37 ± 0.20	37.88 ± 7.22	6.57 ± 0.36 (0.27)	56.13 ± 9.64
TSST-4A	DAMGO	6.50 ± 0.13	99.02 ± 9.38	5.72 ± 0.11	45.35 ± 1.58^
	Morphine	6.47 ± 0.08	42.72 ± 11.93	—	—
S375A	DAMGO	6.08 ± 0.05	86.02 ± 3.79	5.80 ± 0.09	40.15 ± 7.32^
	Morphine	5.92 ± 0.27	30.36 ± 7.33	—	—
STANT-3A/ TREHPSTANT-4A	DAMGO	5.77 ± 0.15	58.33 ± 6.62^	6.15 ± 0.38	36.73 ± 4.27^
	Morphine	5.63 ± 0.51	26.77 ± 5.45	—	—
11S/T-A	DAMGO	5.77 ± 0.08	53.33 ± 2.48^	6.13 ± 1.46	33.86 ± 3.64^
	Morphine	5.57 ± 0.05	23.20 ± 3.11	—	—

^Significance compared to WT ($P < 0.01$) by two-way ANOVA with Dunnett's multiple comparison test.

Desensitization of the response to a submaximal concentration of ME (10 nM) was significant for TSST-4A, STANT-3A, and WT MOR. As previously reported (*13*), a smaller component of heterologous desensitization of responses to somatostatin acting on somatostatin receptors natively expressed in AtT20 cells was observed in all mutants (fig. S5E). By contrast, desensitization by ME was significantly reduced under whole-cell patch-clamp recording in the STANT-3A mutant but was maintained in TSST-4A and WT MOR (Fig. 8, B and E, and fig. S6, A to E). These results suggest that cytoplasmic desensitization mediators diffuse out of cells during whole-cell but not perforated patch-clamp recording conditions.

We and others have previously reported that inhibition of protein kinase C (PKC) impairs MOR desensitization (*13*, *25*). Moreover, we have previously reported that PKCα causes restricted receptor mobility upon activation by morphine but not DAMGO (*26*). To assess the role of PKC, cells were preincubated with the PKC inhibitor calphostin C and exposed to the inhibitor throughout recordings. Calphostin C (30 nM) did not affect desensitization by ME in WT or TSST-4A MOR but significantly reduced ME-induced desensitization of STANT-3A (Fig. 8, C and F). These data suggest that the ME-induced desensitization by soluble mediators of the STANT-3A mutant is sensitive to PKC inhibition, in a similar manner as previously observed for morphine at the WT MOR (*13*).

DISCUSSION

This study identified the role of multisite phosphorylation of MOR in promoting receptor interactions with GRKs and β-arrestins and mediating rapid receptor desensitization. We systematically mutated the 11 S/T residues present in the C-tail of MOR. The use of complementary approaches to measure protein-protein interactions enabled the assessment of the dynamics of complex formation and provided key information about the roles that different C-terminal motifs play in such dynamic interactions.

The ^{354}TSST^{357} cluster in the proximal region of the C-tail of MOR did not participate in receptor internalization (Fig. 4, A and B) (*9*). However, Birdsong *et al.* (*23*) identified the TSST region as a major mediator of the generation of the high-affinity state of the receptor upon high-efficacy agonist stimulation, suggesting that phosphorylation of this motif can have an allosteric effect on ligand binding. Our data showed that although mutation of the ^{354}TSST^{357}motif (TSST-4A) did not abolish phosphorylation, it did induce a detectable decrease in multisite phosphorylation induced by DAMGO (Fig. 2C). For this mutant, recruitment of GRK2/3 and β-arrestins within the first 30 min remained unaffected (Figs. 3, A to C, and 7, A and B), whereas no detectable recruitment occurred after 1-hour incubation, as observed using the β-Gal complementation approach (Figs. 3, B and C, and 7C). Moreover, desensitization of TSST-4A MOR was indistinguishable from that of the WT receptor (Fig. 8, D to F). Together, these results suggest that the TSST region, by allosterically modulating ligand binding, participates in the stability of the interaction of MOR with regulatory proteins but has no impact on MOR desensitization and internalization.

Our data support previous findings suggesting that Ser^{375} serves as an initial residue that drives hierarchical multisite phosphorylation of MOR (*11*, *27*). As we have previously described, single mutation of this residue severely compromised phosphorylation of other S/T residues (Fig. 2B). Moreover, phosphorylation of Ser^{375} substantially affected the dynamics of recruitment of GRK2 and β-arrestin (Figs. 3A and 7A). The S375A MOR mutant recruited GRK2 and β-arrestin at early time points (5 min); however, the interaction of these proteins with the mutant receptor was transient. Using BRET, we detected a steady decrease in β-arrestin recruitment after 5 min, and the β-Gal complementation assay showed no recruitment after 1-hour incubation (Figs. 3, A to C, and 7, A to C). The use of complementary assays that rely on different stability constraints (β-Gal complementation compared to FRET and BRET) enabled the detection of these different dynamics dictated by receptor phosphorylation. The compromised internalization of S375A also suggests that robust phosphorylation and stable interactions with GRK2 and β-arrestins are required to drive MOR endocytosis. Ser^{375} is the first residue of the ^{375}STANT^{379} motif, which has previously been reported to play a key role in receptor internalization (*9*), although conflicting results have been reported regarding the ability of this mutant to desensitize (*13*, *23*). In the present study, we reconciled

Downloaded from http://stke.sciencemag.org/ on July 18, 2018

From Miess, E., Gondin, A. B., Yousuf, A., Steinborn, R., Mosslein, N., Yang, Y., . . . Canals, M . (2018). Multisite phosphorylation is required for sustained interaction with GRKs and arrestins during rapid mu-opioid receptor desensitization. *Sci Signal, 11*(539). doi:10.1126/scisignal.aas960. Reprinted with permission from AAAS.

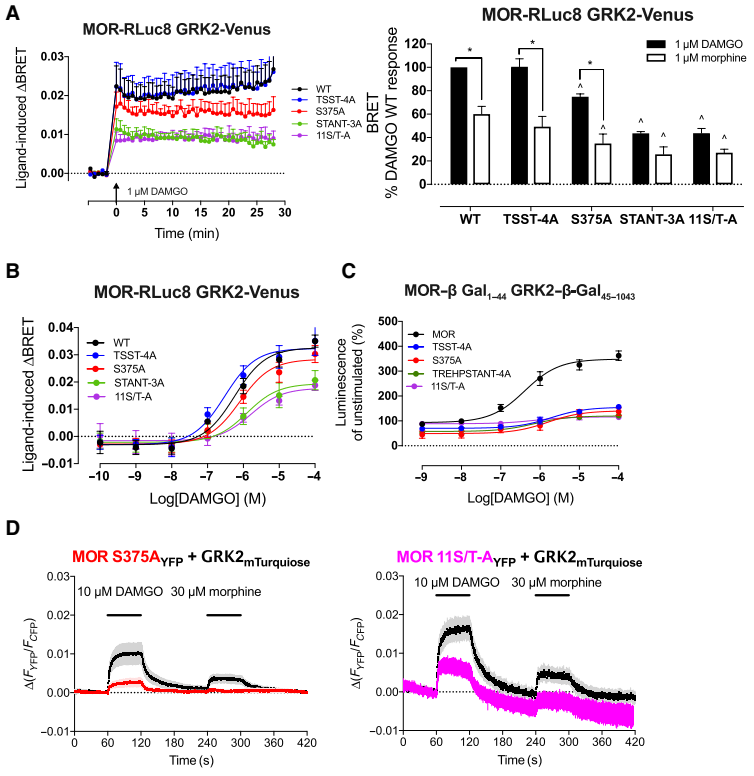


Fig. 7. GRK2 recruitment to phosphorylation-deficient MOR mutants. (**A** and **B**) BRET analysis of HEK293 cells transiently expressing MOR-RLuc8 WT or phosphorylation-deficient mutants and GRK2-Venus and stimulated for 30 min with 1 μM DAMGO (A) or for 10 min with increasing concentrations of DAMGO (B) (both $n = 3$ independent experiments). The BRET ratio of vehicle-treated cells was subtracted, and data represent mean ± SEM. The AUC is expressed as a percentage of the maximal response to DAMGO by the WT receptor and represents mean ± SEM. All responses are significant compared to vehicle; ^ denotes significance compared to WT ($P < 0.01$) by two-way ANOVA with Dunnett's multiple comparison test; * denotes significance of DAMGO compared to morphine ($P < 0.01$) by two-way ANOVA with Sidak's multiple comparison test. (**C**) β-Gal complementation analysis of HEK293 cells expressing MOR–β-Gal$_{1–44}$ WT or phosphorylation-deficient mutants and GRK2–β-Gal$_{45–1043}$ and stimulated with increasing concentrations of DAMGO for 1 hour ($n = 3$ to 4 independent experiments). Data were normalized to vehicle-treated cells and represent the mean ± SEM. (**D**) FRET analysis of HEK293 cells expressing MOR-YFP phosphorylation-deficient mutants and GRK2-mTurquoise and stimulated with 10 μM DAMGO or 30 μM morphine for 1 min before agonist washout (left, $n = 14$ independent experiments for WT and $n = 17$ independent experiments for S375A; right, $n = 14$ independent experiments for WT and $n = 13$ independent experiments for 11S/T-A).

the differences observed with regard to the desensitization of this mutant (Fig. 8, A and B). Our data suggest that the ^{375}STANT^{379} region is crucial for regulating MOR desensitization. High-efficacy agonists like DAMGO and ME regulate MOR desensitization by a GRK2/β-arrestin–mediated mechanism upon phosphorylating crucial sites within this region. Moreover, the observation that the compromised desensitization of the STANT-3A mutant is only detectable when using whole-cell patch clamp further suggests that a soluble (cytosolic) factor mediates this desensitization. In agreement with this notion, we showed that GRK2/3 and β-arrestin recruitment and receptor internalization of the STANT-3A MOR mutant were severely compromised (Figs. 3, A to C; 4, A and B; and 7, A to C). The key role of the ^{375}STANT^{379} region in the regulation of MOR is also illustrated by the results obtained upon mutation of all S/T residues within the C-tail of MOR (11S/T-A) (Figs. 3, A to D; 4, A and B; and 7, A to D).

Because of its limited ability to induce multisite phosphorylation of MOR (Fig. 2B), morphine induced weak recruitment of β-arrestins (Figs. 1, B to G, and 5, B and D). Overexpression of GRK2/3 facilitated phosphorylation of Thr^{370} and Thr^{379} (in addition to Ser^{375}) by morphine, which resulted in both increased β-arrestin recruitment and MOR internalization (Fig. 5E and fig. S3, A and B). These results highlight that the cellular effect of a particular ligand (in this case, morphine) depends on the cellular context and that differences in expression levels of signaling and regulatory proteins will influence the downstream events of receptor activation in a particular cell type. For example, different expression levels of GRK2 may explain why morphine internalizes MOR in striatal neurons (*28*) but not in other neurons (*29*), although this hypothesis remains to be confirmed.

An important finding of the current study is that even when all S/T residues of the C-tail of MOR were mutated to Ala, we detected GRK2 and β-arrestin recruitment using BRET and FRET approaches but not when using the β-Gal complementation assay. These signals were abolished by the addition of the antagonist naloxone or by agonist washout (figs. S2A and 4C). These results suggest that both GRK2 and β-arrestins can be transiently recruited to the activated MOR independently of receptor phosphorylation. Phosphorylation-independent recruitment of β-arrestins has been reported for several GPCRs (*30*, *31*). Moreover, this recruitment of GRK2 is likely to mediate the rapid component of GIRK desensitization (*21*), which still occurred in the STANT-3A mutant (fig. S5C).

GRKs play a key role in GPCR regulation by phosphorylating activated receptors, uncoupling them from G proteins, and facilitating interactions with β-arrestins to promote alternative signaling and/or receptor endocytosis. Our results show that GRK2 activity was required for efficient arrestin recruitment and MOR internalization (Fig. 5, A to G, and fig. S3, A and B). An unexpected result from our studies was that the interaction between GRK2 and the activated MOR also seemed to depend on the integrity of the phosphorylation sites (Fig. 7, A to D). Cmpd101 prevented recruitment of GRK2 to the activated MOR, consequently compromising β-arrestin recruitment and receptor internalization. Binding of Cmpd101 to GRK2 induces small conformational changes that stabilize GRK2 in a nonactive, noncatalytic conformation (*15*). Thus, our results suggest that the unblocked conformation of GRK2/3 is required for the recruitment and interaction of this kinase with MOR.

From Miess, E., Gondin, A. B., Yousuf, A., Steinborn, R., Mosslein, N., Yang, Y., . . . Canals, M . (2018). Multisite phosphorylation is required for sustained interaction with GRKs and arrestins during rapid mu-opioid receptor desensitization. *Sci Signal, 11*(539). doi:10.1126/scisignal.aas960. Reprinted with permission from AAAS.

Downloaded from http://stke.sciencemag.org/ on July 18, 2018

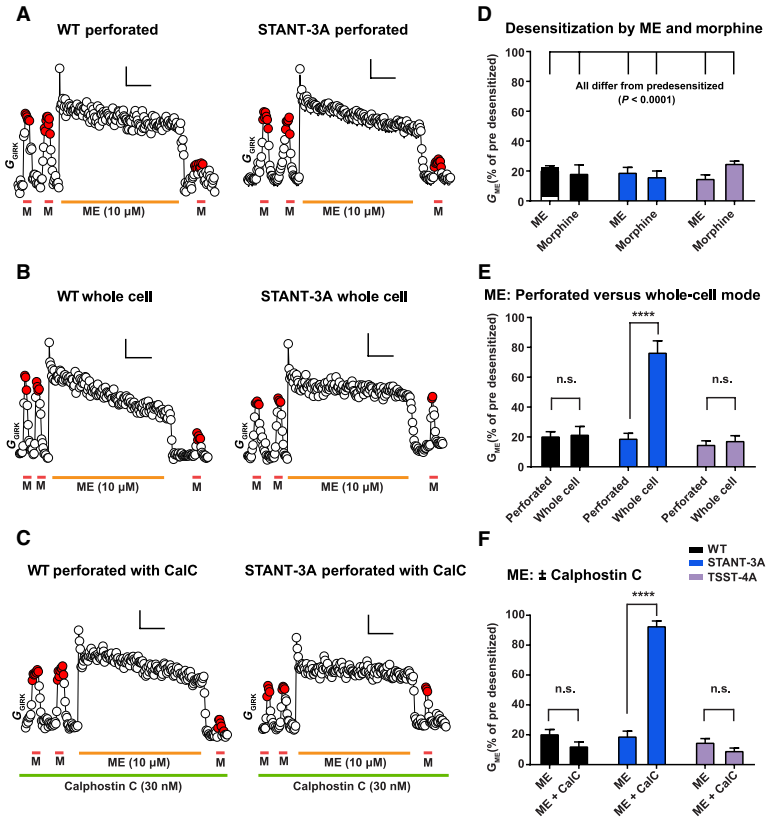


Fig. 8. Acute desensitization in perforated patch-clamp compared to whole-cell patch-clamp recording mode by different MOR mutants. Extent of desensitization was determined by exposure to a submaximal concentration of ME (M; 10 nM, in red) before and after exposure to supramaximal concentrations of ME (10 µM, orange) as shown in (A) to (C). (**A**) Exemplar records of ME-induced desensitization of G_{GIRK} mediated by WT and STANT-3A mutant receptors using perforated patch clamp. (**B** and **C**) Exemplar records of ME-induced desensitization of G_{GIRK} mediated by WT or STANT-3A mutant receptors using whole-cell patch-clamp (B) or perforated patch-clamp mode after pretreatment with 30 nM calphostin C (C). (**D** to **F**) Comparison of acute desensitization using whole-cell and perforated patch-clamp recordings of different mutants (n = 5 times for each group). All scale bars represent 0.2 nS and 1 min. Two-way ANOVAs for (D) to (F) were all significant for main effects. Post hoc comparisons (Bonferroni-corrected) were significant where shown (****P < 0.0001). In (D), postdesensitized compared with predesensitized response (100%) is shown; the main effect of ME compared to morphine was not significant (n.s.; P > 0.05).

Although the molecular mechanisms underlying the development of morphine-induced tolerance remain controversial, MOR desensitization of VGCC and GIRK channels is generally accepted to be an important step. As mentioned above, our results suggest that MOR desensitization by high-efficacy ligands has two components: a sustained component, which requires GRK2-mediated phosphorylation and a potential soluble factor, and a rapid component independent of receptor phosphorylation (Fig. 8, A to D, and fig. S5, C and D). This desensitization component, independent of kinase activity, highlights the potential dual role of GRKs, acting as scaffolding/sequestering proteins in addition to their kinase activity, as earlier suggested by Raveh *et al.* (*21*). In addition to GRKs, PKC has also been suggested to participate in the development of tolerance to morphine (*25*), although the molecular basis of this remains unclear. Our patch-clamp studies suggest that, in the STANT-3A MOR mutant, PKC becomes important in mediating ME desensitization (Fig. 8C). Whether PKC phosphorylates Ser^{363} and/or Thr^{370} as previously suggested (*32*, *33*) or whether PKC is the soluble factor mediating sustained desensitization remains to be investigated.

In summary, our results demonstrate the complex role of MOR phosphorylation in receptor desensitization and in the recruitment of regulatory and scaffolding proteins. These receptor-effector interactions are likely to participate in the control of physiological opioid effects such as tolerance and dependence.

MATERIALS AND METHODS

Reagents

Morphine HCl was from GlaxoSmithKline or Merck Pharma. The rabbit polyclonal phosphosite-specific antibodies anti-$pSer^{356}$/$pThr^{357}$ {4879}, anti-$pThr^{370}$ {3196}, anti-$pSer^{375}$ {2493}, anti-$pThr^{376}$ {3723}, and anti-$pThr^{379}$ {3686} were generated and extensively characterized previously ({numbers} indicate internal inventory numbers) (*10*, *11*, *13*). The phosphorylation-independent rabbit monoclonal anti-MOR antibody {named UMB-3} was obtained from Abcam-Epitomics (*34*). Secondary antibodies (raised in donkey) conjugated to Alexa Fluor 488, 568, or 647 were from Jackson ImmunoResearch. Coelenterazine h was from NanoLight. Cmpd101 was from Hello Bio. DAMGO, ME, calphostin C, amphotericin B, and M2–anti-FLAG were from Sigma-Aldrich.

Plasmids

For BRET experiments, β-arrestin1–YFP and β-arrestin2–YFP were provided by M. Caron (Duke University, North Carolina), GRK2-Venus was from D. Jensen (Columbia University, New York), and Rab5a-Venus has been previously described (*35*). GRK2-WT and GRK2-DN (GRK2-K220R) were from M. Smit (Vrije Universiteit, Amsterdam). The phosphorylation-deficient FLAG-MOR mutants and FLAG-MOR-RLuc8 were purchased from GeneArt. For FRET experiments, GRK2-mTurquoise and GRK2-YFP have been previously described (*36*). β-Arrestin2–mTurquoise was constructed by replacing the CFP coding sequence in β-arrestin2–CFP (*37*) with mTurquoise (*38*). For β-Gal complementation experiments, we adapted the plasmids according to PathHunter (DiscoverX Patent: WO 2010042921 A1, US 20100120063 A1). The plasmids were generated through artificial gene synthesis by Eurofins Genomics and cloned into pcDNA3.1. Briefly, the coding sequence for an N-terminal HA tag was added to the WT MOR and the S/T mutant sequences, whereas the C-terminal end was fused with a Gly-rich linker (GGGGS-GGGGS) and a short β-Gal fragment (1 to 44 amino acids). All acceptor plasmids, GRKs, and β-arrestins had the larger β-Gal synthetic sequence fragment (45 to 1043 amino acids) fused to their C-terminal end.

From Miess, E., Gondin, A. B., Yousuf, A., Steinborn, R., Mosslein, N., Yang, Y., . . . Canals, M . (2018). Multisite phosphorylation is required for sustained interaction with GRKs and arrestins during rapid mu-opioid receptor desensitization. *Sci Signal, 11*(539). doi:10.1126/scisignal.aas960. Reprinted with permission from AAAS.

Downloaded from http://stke.sciencemag.org/ on July 18, 2018

siRNA silencing of gene expression

Double-stranded siRNA duplexes with 3′-dTdT overhangs were obtained from Qiagen for GRK2 (5′-AAGAAAUUCAUUGAGAGCGAU-3′), GRK3 (5′-AAGCAAGCUGUAGAACACGUA-3′), and a nonsilencing RNA duplex (5′-GCUUAGGAGCAUUAGUAAA-3′). HEK293 cells were transfected with 150 nM siRNA for single transfection or with 100 nM of each siRNA for double transfection using HiPerFect (Qiagen). Silencing was quantified after 3 days by performing a GRK β-Gal complementation assay. All experiments showed that the siRNA reduced the target protein levels by ≥80% (fig. S4E).

Cell culture

HEK293 cells were maintained in Dulbecco's modified Eagle's medium (DMEM) supplemented with 5% (v/v) fetal bovine serum (FBS) at 37°C in a humidified atmosphere of 95% air and 5% CO_2. Transient transfections for BRET experiments were performed using linear polyethylenemine (PEI) with a molecular weight of 25,000 (Polysciences) in a DNA/PEI ratio of 1:6 as previously described (*39*). For FRET experiments, transient transfections were performed in 6-cm dishes with Effectene (Qiagen) as previously described (*36*). For transient and stable transfections in β-Gal complementation experiments, TurboFect DNA (Thermo Fisher Scientific) was used. Stably transfected cells were grown in medium supplemented with G418 (400 μg/ml) and/or hygromycin B (100 μg/ml). To increase the total number of HEK293 cells stably expressing MOR or phosphorylation-deficient mutant receptors, we used fluorescence-activated cell sorting (FACS). Trypsinized cells were washed with phosphate-buffered saline (PBS) and transferred into opti-MEM containing an A488-labeled anti-HA antibody at a dilution of 1:1000 (Sigma-Aldrich). After 30-min preincubation at room temperature, cells were centrifuged and the cell pellet was resuspended in FACS buffer [2 mM EDTA, 0.5% (w/v) bovine serum albumin in PBS]. FACS was executed using a BD FACSAria III cell sorter. About 1% of the positive cell population was sorted at an average purity of 85%. Sorted cells were then recultivated. To ensure similar expression levels of WT and mutant receptors, we characterized stable cells using Western blot analysis, cell-surface ELISA assay, and immunocytochemistry.

Patch-clamp experiments were performed in AtT20 cells, which endogenously express GIRK (KirX.3) channels. WT MOR, ^{354}TSST^{357}/A, and ^{375}STANT^{379}/A were all cloned in pcDNA3.0 plasmids with FLAG tag and were expressed stably in AtT20 cells as previously described (*13*). For patch-clamp experiments, AtT20 cells were seeded on 35-mm polystyrene culture dishes (Becton Dickinson Biosciences) in DMEM containing glucose (4.5 g/liter), penicillin-streptomycin (100 μL/ml), G418 (50 mg/ml), and 10% FBS (50 mg/ml). Cell cultures were maintained in a humidified 5% CO_2 atmosphere at 37°C. Cells were ready for recording after 24 hours.

Bioluminescence resonance energy transfer

HEK293 cells were transiently transfected in a 10-cm dish with 1 μg of donor (RLuc8-tagged MOR WT or phosphorylation-deficient mutant) and 4 μg of acceptor (β-arrestin1–YFP, β-arrestin2–YFP, GRK2-Venus, or Rab5a-Venus). For cAMP experiments, cells were transiently transfected with the cAMP sensor using YFP-Epac-RLuc (CAMYEL) BRET biosensor (2.5 μg of FLAG-MOR and 2.5 μg of CAMYEL biosensor per dish). For GRK2 expression experiments, cells were transfected with an additional 2 μg of GRK2-WT, GRK2-DN, or pcDNA3 as a control. After 24 hours, cells were replated into poly-D-lysine–coated white opaque 96-well plates (CulturPlate, PerkinElmer) and allowed to adhere overnight. BRET experiments were performed 48 hours after transfection. Cells were washed with Hanks' balanced salt solution (HBSS) and equilibrated in HBSS for 30 min at 37°C before the experiment. Coelenterazine h was added to a final concentration of 5 μM 10 min before dual-fluorescence/luminescence measurement in a LUMIstar Omega plate reader (BMG LabTech). The BRET signal was calculated as the ratio of light emitted at 530 nm by YFP or Venus over the light emitted at 430 nm by RLuc8. For concentration-response curves, cells were stimulated with DAMGO (10^{-10} to 10^{-4} M) or morphine (10^{-10} to 10^{-4} M) for 10 min before BRET measurements. For short kinetic experiments (β-arrestin and GRK2 recruitment), the baseline BRET ratio was measured for five cycles; then, vehicle [0.01% (v/v) dimethyl sulfoxide (DMSO)], DAMGO (1 μM), or morphine (1 μM) was added to the cells, and the BRET signal was measured for 30 min. For longer kinetic experiments (Rab5a), cells were stimulated with vehicle [0.01% (v/v) DMSO], DAMGO (1 μM), or morphine (1 μM) at different time points as stated over an interval of 100 min.

Förster resonance energy transfer

To measure the interaction between MOR and β-arrestins, HEK293T cells were transfected with 0.8 μg of MOR-YFP (or mutants), 0.4 μg of human GRK2, and 0.8 μg of β-arrestin2–mTurquoise. To measure the interaction between MOR and GRK2, HEK293T cells were transfected with 0.5 μg of MOR-YFP (or mutants), 0.5 μg of rat $G\alpha_{i1}$, 0.5 μg of human $G\beta_1$, 0.4 μg of murine $G\gamma_2$, and 0.5 μg of GRK2-mTurquoise. On the next day, cells were seeded on round 25-mm poly-D-lysine–coated coverslips, and 48 hours after transfection, FRET was measured as previously described (*36*), except that a light-emitting diode (LED) excitation system (pE-2; CoolLED) was used for all experiments. FRET traces were not corrected for bleaching effects.

β-Gal complementation

HEK293 cells stably expressing MOR or mutant MOR constructs C-terminally fused with a β-Gal enzyme fragment ($\beta\text{-Gal}_{1-44}$) and stably or transiently expressing β-arrestins or GRKs fused to an N-terminal deletion mutant of β-Gal ($\beta\text{-Gal}_{45-1043}$) were used (DiscoverX Patent: WO 2010042921 A1, US 20100120063 A1). β-Arrestin or GRK recruitment results in complementation of the two β-Gal fragments that generate an active enzyme. Thus, levels of active enzyme are a direct result of MOR activation and are quantitated using chemiluminescent β-Gal Juice-plus detection reagents (PJK GmbH) containing the β-Gal substrate. The assay was performed as follows: cells were plated into poly-L-lysine–coated 48-well plates at a density of 125,000 cells per well in medium supplemented with G418 (400 μg/ml) and incubated overnight. After 48 hours, test compounds were prepared at each concentration in DMEM and added to the cells. After a 1-hour incubation at 37°C, a cell lysis reagent [1 M $NaH_2PO_4{\cdot}H_2O$, 1 M $Na_2HPO_4{\cdot}2\ H_2O$, and 0.1% (v/v) Triton X-100 (pH 7.4)] was added to each well. Luminescence was measured 1 hour after detection reagent addition (β-Gal Juice-plus) using a FlexStation III (Molecular Devices, 500-ms integration time).

Western blot

Cells were seeded onto poly-L-lysine–coated 60-mm dishes and grown to 80% confluence. After treatment with agonist, cells were lysed in detergent buffer [50 mM tris-HCl (pH 7.4), 150 mM NaCl, 5 mM EDTA, 10 mM NaF, 10 mM disodium pyrophosphate, 1% (v/v) Nonidet P-40, 0.5% (w/v) sodium deoxycholate, and 0.1% (w/v) SDS] in the

Downloaded from http://stke.sciencemag.org/ on July 18, 2018

From Miess, E., Gondin, A. B., Yousuf, A., Steinborn, R., Mosslein, N., Yang, Y., . . . Canals, M . (2018). Multisite phosphorylation is required for sustained interaction with GRKs and arrestins during rapid mu-opioid receptor desensitization. *Sci Signal, 11*(539). doi:10.1126/scisignal.aas960. Reprinted with permission from AAAS.

presence of protease and phosphatase inhibitors (Complete mini and PhosSTOP, Roche Diagnostics). Glycosylated proteins were partially enriched using wheat-germ lectin agarose beads as described (*40*, *41*). Proteins were eluted from the beads using SDS sample buffer for 20 min at 42°C. Samples were split and resolved on 8% SDS–polyacrylamide gels, and after electroblotting, membranes were incubated with anti-pSer^{356}/pThr^{357} {4879}, anti-pThr^{370} {3196}, anti-pSer^{375} {2493}, anti-pThr^{376} {3723}, or anti-pThr^{379} {3686} antibodies followed by detection using an enhanced chemiluminescence detection system (Thermo Fisher Scientific). Blots were stripped and incubated again using the phosphorylation-independent anti-MOR antibody {named UMB-3} (*34*) to ensure equal loading of the gels.

Enzyme-linked immunosorbent assay

HEK293 cells were transfected with 5 μg of DNA (pcDNA3 as a control, FLAG-MOR WT, or phosphorylation-deficient mutants, in 10-cm dishes), replated into poly-D-lysine–coated 48-well plates after 24 h, and allowed to adhere overnight. After 48 hours, cells were fixed with 3.7% (v/v) paraformaldehyde in tris-buffered saline (TBS) for 30 min. For total expression, cells were permeabilized by 30-min incubation with 0.5% (v/v) NP-40 in TBS. Cells were then incubated in blocking buffer [1% (w/v) skim milk powder in 0.1 M $NaHCO_3$] for 4 hours at room temperature and incubated with mouse M2–anti-FLAG antibody (1:2000, overnight at 4°C). After washing three times with TBS, cells were incubated with anti-mouse horseradish peroxidase–conjugated antibody (1:2000) for 2 hours at room temperature. Cells were washed and stained using the SIGMAFAST OPD substrate (Sigma-Aldrich). Absorbance at 490 nm was measured using an EnVision Multilabel Reader (PerkinElmer). Data were normalized to intact HEK293 cells transfected with MOR WT. To measure MOR internalization, HEK293 cells stably expressing the HA-tagged MOR WT, MOR TSST-4A, MOR S375A, MOR TREHPSTANT-4A, or MOR 11S/T-A were preincubated with anti-HA antibody and stimulated with 10 μM DAMGO for 30 min. Receptor sequestration, quantified as the percentage of residual cell-surface receptors in agonist-treated cells, was measured by ELISA as described above.

Confocal imaging and quantitative analysis of MOR internalization

Stably transfected cells were grown on poly-L-lysine–coated coverslips overnight. Cells were then incubated with primary antibody (rabbit anti-HA) in serum-free medium for 2 hours at 4°C. After agonist exposure, cells were fixed with 4% paraformaldehyde and 0.2% picric acid in phosphate buffer (pH 6.9) for 30 min at room temperature and washed several times with PBS. Specimens were permeabilized and then incubated with an Alexa Fluor 488–conjugated goat anti-rabbit antibody (Santa Cruz Biotechnology). Specimens were mounted and examined using a Zeiss LSM 510 META laser scanning confocal microscope. For quantitative internalization assays, cells were seeded onto 24-well plates. On the next day, cells were preincubated with anti-HA antibody for 2 hours at 4°C. Cells were then exposed to agonist at 37°C, fixed, and developed with peroxidase-conjugated secondary antibody as described (*42*, *43*).

Electrophysiology

Patch-clamp recordings were performed as previously described (*13*). Pipettes were pulled from borosilicate glass (A-M Systems) yielding input resistances between 3.5 and 4.5 megohms. For perforated patch-clamp recording, pipettes were filled with internal solution containing 135 mM potassium gluconate, 3 mM $MgCl_2$, and 10 mM Hepes (adjusted to pH 7.4 with KOH). The recording electrodes were first front-filled with this internal solution and then backfilled with the same solution containing amphotericin B (200 μg/ml; in 0.8% DMSO). For whole-cell recording, internal solution contained 135 mM K gluconate, 8 mM NaCl, 8 mM Hepes, 0.5 mM EGTA, 3 mM Mg adenosine 5′-triphosphate, and 0.5 mM Na_2 guanosine 5′-triphosphate (pH 7.3). Cells were initially superfused with external bath solution containing 140 mM NaCl, 3 mM KCl, 1.8 mM $CaCl_2$, 1.2 mM $MgCl_2$, 10 mM Hepes, and 10 mM glucose (pH 7.4). For measuring I_{GIRK}, the KCl concentration in the bath was increased to 20 mM (substituted for NaCl) before the start of the measurements and was maintained throughout the experiments as previously described by Yousuf *et al.* (*13*). Liquid junction potential was calculated to be +16 mV and was adjusted before the start of each recording. Currents were recorded at 37°C in a fully enclosed, temperature-controlled recording chamber using an Axopatch 200B amplifier and pCLAMP 9.2 software and digitized using Digidata 1320 (Axon Instruments, Molecular Devices). Currents were sampled at 100 Hz, low-pass–filtered at 50 Hz, and recorded on hard disk for later analyses. I_{GIRK} was recorded using a 200-ms voltage step to −120 mV from a holding potential of −60 mV delivered every 2 s. Drugs were perfused directly onto cells using a ValveLink 8.2 pressurized pinch valve perfusion system (AutoMate Scientific). In all recorded cells, solution exchange reached steady state within 200 ms (usually within 100 ms), which was confirmed by examination of the current produced at −60 mV by switching from low (3 mM) to high (20 mM) K^+ solution.

All data points are plotted as chord GIRK conductance (G_{GIRK}, nS) using the following calculation: [I_{GIRK} (−60 mV) − I_{GIRK} (−120 mV)] pA/60 mV. The extent of MOR desensitization as a percentage was calculated using the following formula: (Post G_{ME}/Pre G_{ME}) × 100, where "Pre G_{ME}" and "Post G_{ME}" are the G_{GIRK} increase induced by a submaximal probe concentration of ME (10 nM; see fig. S6), averaged for 4 to 5 points during the peak response (colored points in figures), immediately before compared to 1 min after termination of exposure to a supramaximal concentration of agonist (10 μM ME or 10 μM morphine). Desensitization for different MOR mutants was analyzed using a two-factor ANOVA followed by appropriate post hoc tests as indicated.

Statistics

Data are presented as the mean ± SEM of $n \geq 3$ independent experiments. Differences were assessed with GraphPad Prism using one-way or two-way ANOVA followed by Bonferroni-adjusted post hoc tests for multiple comparisons.

SUPPLEMENTARY MATERIALS

www.sciencesignaling.org/cgi/content/full/11/539/eaas9609/DC1

Fig. S1. Expression and function of MOR phosphorylation-deficient mutants.

Fig. S2. Inhibition of β-arrestin2 recruitment upon addition of naloxone and lack of internalization by morphine.

Fig. S3. β-Arrestin1 recruitment and MOR internalization upon overexpression of GRK2 WT or GRK2 DN.

Fig. S4. GRK3 recruitment to MOR WT and mutants, inhibition of GRK2 recruitment upon addition of naloxone, kinetics of GRK recruitment, and siRNA controls.

Fig. S5. Fast desensitization component of MOR.

Fig. S6. Patch-clamp traces for corresponding MOR mutants.

Table S1. Potency and maximal response of MOR mutants in cAMP assay.

From Miess, E., Gondin, A. B., Yousuf, A., Steinborn, R., Mosslein, N., Yang, Y., . . . Canals, M . (2018). Multisite phosphorylation is required for sustained interaction with GRKs and arrestins during rapid mu-opioid receptor desensitization. *Sci Signal, 11*(539). doi:10.1126/scisignal.aas960. Reprinted with permission from AAAS.

Downloaded from http://stke.sciencemag.org/ on July 18, 2018

REFERENCES AND NOTES

1. J. T. Williams, S. L. Ingram, G. Henderson, C. Chavkin, M. von Zastrow, S. Schulz, T. Koch, C. J. Evans, M. J. Christie, Regulation of μ-opioid receptors: Desensitization, phosphorylation, internalization, and tolerance. *Pharmacol. Rev.* **65**, 223–254 (2013).
2. R. A. Rudd, P. Seth, F. David, L. Scholl, Increases in drug and opioid-involved overdose deaths – United States, 2010-2015. *MMWR Morb. Mortal. Wkly Rep.* **65**, 1445–1452 (2016).
3. H. W. D. Matthes, R. Maldonado, F. Simonin, O. Valverde, S. Slowe, I. Kitchen, K. Befort, A. Dierich, M. Le Meur, P. Dollé, E. Tzavara, J. Hanoune, B. P. Roques, B. L. Kieffer, Loss of morphine-induced analgesia, reward effect and withdrawal symptoms in mice lacking the μ-opioid-receptor gene. *Nature* **383**, 819–823 (1996).
4. L. M. Bohn, R. J. Lefkowitz, R. R. Gainetdinov, K. Peppel, M. G. Caron, F. T. Lin, Enhanced morphine analgesia in mice lacking β-arrestin 2. *Science* **286**, 2495–2498 (1999).
5. K. M. Raehal, J. K. L. Walker, L. M. Bohn, Morphine side effects in β-arrestin 2 knockout mice. *J. Pharmacol. Exp. Ther.* **314**, 1195–1201 (2005).
6. S. M. DeWire, D. S. Yamashita, D. H. Rominger, G. Liu, C. L. Cowan, T. M. Graczyk, X. T. Chen, P. M. Pitis, D. Gotchev, C. Yuan, M. Koblish, M. W. Lark, J. D. Violin, A G protein-biased ligand at the μ-opioid receptor is potently analgesic with reduced gastrointestinal and respiratory dysfunction compared with morphine. *J. Pharmacol. Exp. Ther.* **344**, 708–717 (2013).
7. A. Manglik, H. Lin, D. K. Aryal, J. D. McCorvy, D. Dengler, G. Corder, A. Levit, R. C. Kling, V. Bernat, H. Hübner, X.-P. Huang, M. F. Sassano, P. M. Giguere, S. Löber, D. Duan, G. Scherrer, B. K. Kobilka, P. Gmeiner, B. L. Roth, B. K. Shoichet, Structure-based discovery of opioid analgesics with reduced side effects. *Nature* **537**, 185–190 (2016).
8. C. L. Schmid, N. M. Kennedy, N. C. Ross, K. M. Lovell, Z. Yue, J. Morgenweck, M. D. Cameron, T. D. Bannister, L. M. Bohn, Bias factor and therapeutic window correlate to predict safer opioid analgesics. *Cell* **171**, 1165–1170.e13 (2017).
9. E. K. Lau, M. Trester-Zedlitz, J. C. Trinidad, S. J. Kotowski, A. N. Krutchinsky, A. L. Burlingame, M. von Zastrow, Quantitative encoding of the effect of a partial agonist on individual opioid receptors by multisite phosphorylation and threshold detection. *Sci. Signal.* **4**, ra52 (2011).
10. C. Doll, J. Konietzko, F. Pöll, T. Koch, V. Höllt, S. Schulz, Agonist-selective patterns of μ-opioid receptor phosphorylation revealed by phosphosite-specific antibodies. *Br. J. Pharmacol.* **164**, 298–307 (2011).
11. S. Just, S. Illing, M. Trester-Zedlitz, E. K. Lau, S. J. Kotowski, E. Miess, A. Mann, C. Doll, J. C. Trinidad, A. L. Burlingame, M. von Zastrow, S. Schulz, Differentiation of opioid drug effects by hierarchical multi-site phosphorylation. *Mol. Pharmacol.* **83**, 633–639 (2013).
12. V. C. Dang, B. Chieng, Y. Azriel, M. J. Christie, Cellular morphine tolerance produced by βarrestin-2-dependent impairment of μ-opioid receptor resensitization. *J. Neurosci.* **31**, 7122–7130 (2011).
13. A. Yousuf, E. Miess, S. Sianati, Y.-P. Du, S. Schulz, M. J. Christie, The role of phosphorylation sites in desensitization of μ-opioid receptor. *Mol. Pharmacol.* **88**, 825–835 (2015).
14. G. Grecksch, S. Just, C. Pierstorff, A.-K. Imhof, L. Glück, C. Doll, A. Lupp, A. Becker, T. Koch, R. Stumm, V. Höllt, S. Schulz, Analgesic tolerance to high-efficacy agonists but not to morphine is diminished in phosphorylation-deficient S375A μ-opioid receptor knock-in mice. *J. Neurosci.* **31**, 13890–13896 (2011).
15. D. M. Thal, R. Y. Yeow, C. Schoenau, J. Huber, J. J. G. Tesmer, Molecular mechanism of selectivity among G protein-coupled receptor kinase 2 inhibitors. *Mol. Pharmacol.* **80**, 294–303 (2011).
16. J. D. Lowe, H. S. Sanderson, A. E. Cooke, M. Ostovar, E. Tsisanova, S. L. Withey, C. Chavkin, S. M. Husbands, E. Kelly, G. Henderson, C. P. Bailey, Role of G protein–coupled receptor kinases 2 and 3 in μ-opioid receptor desensitization and internalization. *Mol. Pharmacol.* **88**, 347–356 (2015).
17. J. McPherson, G. Rivero, M. Baptist, J. Llorente, S. Al-Sabah, C. Krasel, W. L. Dewey, C. P. Bailey, E. M. Rosethorne, S. J. Charlton, G. Henderson, E. Kelly, μ-Opioid receptors: Correlation of agonist efficacy for signalling with ability to activate internalization. *Mol. Pharmacol.* **78**, 756–766 (2010).
18. P. Molinari, V. Vezzi, M. Sbraccia, C. Grò, D. Riitano, C. Ambrosio, I. Casella, T. Costa, Morphine-like opiates selectively antagonize receptor-arrestin interactions. *J. Biol. Chem.* **285**, 12522–12535 (2010).
19. G. L. Thompson, J. R. Lane, T. Coudrat, P. M. Sexton, A. Christopoulos, M. Canals, Biased agonism of endogenous opioid peptides at the μ-opioid receptor. *Mol. Pharmacol.* **88**, 335–346 (2015).
20. J. Zhang, S. S. G. Ferguson, L. S. Barak, S. R. Bodduluri, S. A. Laporte, P.-Y. Law, M. G. Caron, Role for G protein-coupled receptor kinase in agonist-specific regulation of μ-opioid receptor responsiveness. *Proc. Natl. Acad. Sci. U.S.A.* **95**, 7157–7162 (1998).
21. A. Raveh, A. Cooper, L. Guy-David, E. Reuveny, Nonenzymatic rapid control of GIRK channel function by a G protein-coupled receptor kinase. *Cell* **143**, 750–760 (2010).
22. A. E. Cooke, S. Oldfield, C. Krasel, S. J. Mundell, G. Henderson, E. Kelly, Morphine-induced internalization of the L83I mutant of the rat μ-opioid receptor. *Br. J. Pharmacol.* **172**, 593–605 (2015).
23. W. T. Birdsong, S. Arttamangkul, J. R. Bunzow, J. T. Williams, Agonist binding and desensitization of the μ-opioid receptor is modulated by phosphorylation of the C-terminal tail domain. *Mol. Pharmacol.* **88**, 816–824 (2015).
24. M. Connor, P. B. Osborne, M. J. Christie, μ-Opioid receptor desensitization: Is morphine different? *Br. J. Pharmacol.* **143**, 685–696 (2004).
25. E. A. Johnson, S. Oldfield, E. Braksator, A. Gonzalez-Cuello, D. Couch, K. J. Hall, S. J. Mundell, C. P. Bailey, E. Kelly, G. Henderson, Agonist-selective mechanisms of μ-opioid receptor desensitization in human embryonic kidney 293 cells. *Mol. Pharmacol.* **70**, 676–685 (2006).
26. M. L. Halls, H. R. Yeatman, C. J. Nowell, G. L. Thompson, A. B. Gondin, S. Civciristov, N. W. Bunnett, N. A. Lambert, D. P. Poole, M. Canals, Plasma membrane localization of the μ-opioid receptor controls spatiotemporal signaling. *Sci. Signal.* **9**, ra16 (2016).
27. L. Glück, A. Loktev, L. Moulédous, C. Mollereau, P.-Y. Law, S. Schulz, Loss of morphine reward and dependence in mice lacking G protein–coupled receptor kinase 5. *Biol. Psychiatry* **76**, 767–774 (2014).
28. H. Haberstock-Debic, M. Wein, M. Barrot, E. E. O. Colago, Z. Rahman, R. L. Neve, V. M. Pickel, E. J. Nestler, M. von Zastrow, A. L. Svingos, Morphine acutely regulates opioid receptor trafficking selectively in dendrites of nucleus accumbens neurons. *J. Neurosci.* **23**, 4324–4332 (2003).
29. J. A. Trafton, C. Abbadie, K. Marek, A. I. Basbaum, Postsynaptic signaling via the μ-opioid receptor: Responses of dorsal horn neurons to exogenous opioids and noxious stimulation. *J. Neurosci.* **20**, 8578–8584 (2000).
30. D. Zindel, S. Engel, A. R. Bottrill, J.-P. Pin, L. Prézeau, A. B. Tobin, M. Bünemann, C. Krasel, A. J. Butcher, Identification of key phosphorylation sites in PTH1R that determine arrestin3 binding and fine-tune receptor signaling. *Biochem. J.* **473**, 4173–4192 (2016).
31. L. E. Gimenez, S. Kook, S. A. Vishnivetskiy, M. R. Ahmed, E. V. Gurevich, V. V. Gurevich, Role of receptor-attached phosphates in binding of visual and non-visual arrestins to G protein-coupled receptors. *J. Biol. Chem.* **287**, 9028–9040 (2012).
32. S. Illing, A. Mann, S. Schulz, Heterologous regulation of agonist-independent μ-opioid receptor phosphorylation by protein kinase C. *Br. J. Pharmacol.* **171**, 1330–1340 (2014).
33. A. Mann, S. Illing, E. Miess, S. Schulz, Different mechanisms of homologous and heterologous μ-opioid receptor phosphorylation. *Br. J. Pharmacol.* **172**, 311–316 (2015).
34. A. Lupp, N. Richter, C. Doll, F. Nagel, S. Schulz, UMB-3, a novel rabbit monoclonal antibody, for assessing μ-opioid receptor expression in mouse, rat and human formalin-fixed and paraffin-embedded tissues. *Regul. Pept.* **167**, 9–13 (2011).
35. T.-H. Lan, Q. Liu, C. Li, G. Wu, N. A. Lambert, Sensitive and high resolution localization and tracking of membrane proteins in live cells with BRET. *Traffic* **13**, 1450–1456 (2012).
36. V. Wolters, C. Krasel, J. Brockmann, M. Bünemann, Influence of $G\alpha_q$ on the dynamics of M_3-acetylcholine receptor-G-protein-coupled receptor kinase 2 interaction. *Mol. Pharmacol.* **87**, 9–17 (2015).
37. C. Krasel, M. Bünemann, K. Lorenz, M. J. Lohse, β-Arrestin binding to the β_2-adrenergic receptor requires both receptor phosphorylation and receptor activation. *J. Biol. Chem.* **280**, 9528–9535 (2005).
38. J. Goedhart, L. van Weeren, M. A. Hink, N. O. E. Vischer, K. Jalink, T. W. J. Gadella Jr., Bright cyan fluorescent protein variants identified by fluorescence lifetime screening. *Nat. Methods* **7**, 137–139 (2010).
39. M. L. Halls, D. P. Poole, A. M. Ellisdon, C. J. Nowell, M. Canals, Methods in molecular biology, in *Methods in Molecular Biology* (Springer New York, 2015), vol. 1335, pp. 131–161.
40. S. Schulz, D. Mayer, M. Pfeiffer, R. Stumm, T. Koch, V. Höllt, Morphine induces terminal μ-opioid receptor desensitization by sustained phosphorylation of serine-375. *EMBO J.* **23**, 3282–3289 (2004).
41. T. Koch, S. Schulz, M. Pfeiffer, M. Klutzny, H. Schröder, E. Kahl, V. Höllt, C-terminal splice variants of the mouse μ-opioid receptor differ in morphine-induced internalization and receptor resensitization. *J. Biol. Chem.* **276**, 31408–31414 (2001).
42. S. Lesche, D. Lehmann, F. Nagel, H. A. Schmid, S. Schulz, Differential effects of octreotide and pasireotide on somatostatin receptor internalization and trafficking in vitro. *J. Clin. Endocrinol. Metab.* **94**, 654–661 (2009).
43. F. Pöll, C. Doll, S. Schulz, Rapid dephosphorylation of G protein-coupled receptors by protein phosphatase 1β is required for termination of β-arrestin-dependent signaling. *J. Biol. Chem.* **286**, 32931–32936 (2011).

Acknowledgments: We thank A. Stewart for technical assistance. **Funding:** This work was supported by a Deutsche Forschungsgemeinschaft grant (SFB/TR166-TPC5) to S.S., a Monash Fellowship to M.C., a National Health and Medical Research Council (NHMRC) RD Wright Fellowship to M.L.H. (1061687), and an NHMRC project grant (1121029) to M.C. and M.L.H.
Author contributions: E.M. performed and analyzed the data of β-Gal experiments; A.B.G.

Downloaded from http://stke.sciencemag.org/ on July 18, 2018

From Miess, E., Gondin, A. B., Yousuf, A., Steinborn, R., Mosslein, N., Yang, Y., . . . Canals, M . (2018). Multisite phosphorylation is required for sustained interaction with GRKs and arrestins during rapid mu-opioid receptor desensitization. *Sci Signal, 11*(539). doi:10.1126/scisignal.aas960. Reprinted with permission from AAAS.

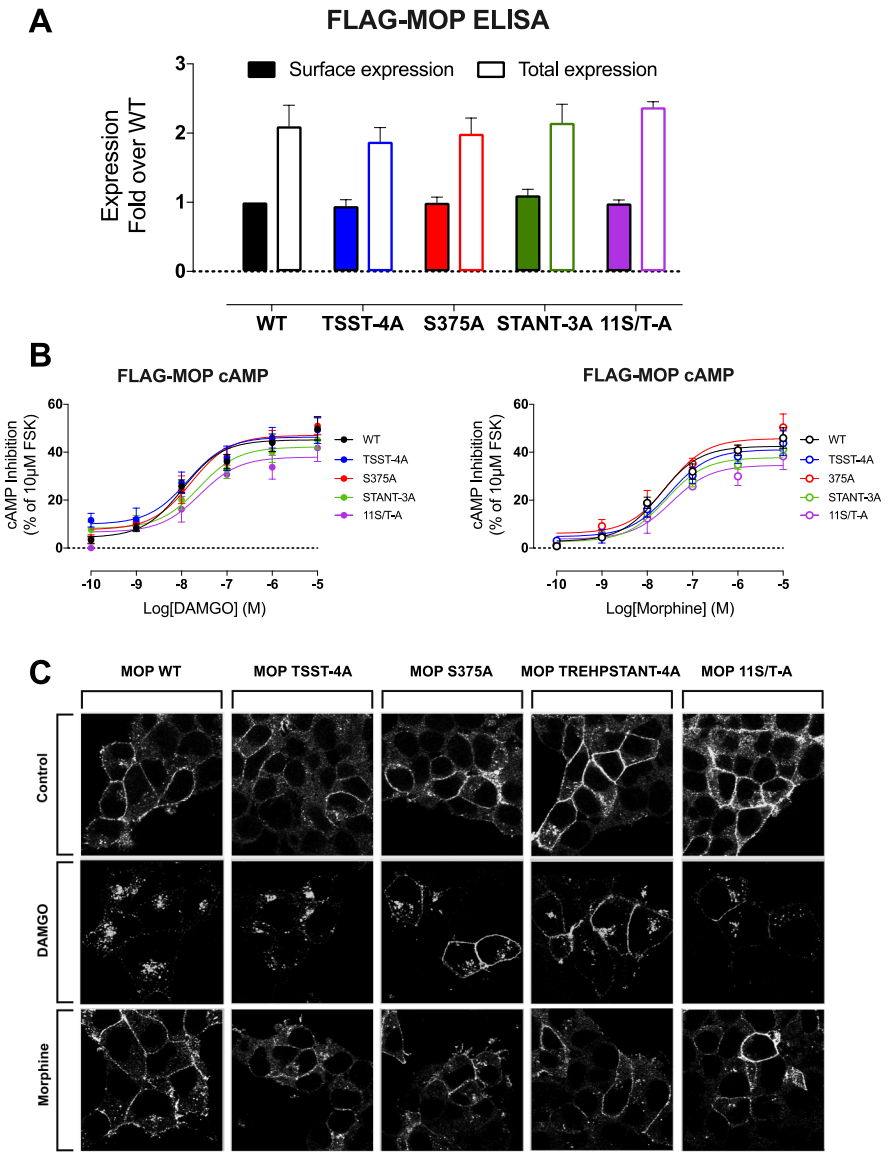
performed and analyzed the data of BRET experiments; A.Y. performed and analyzed electrophysiology experiments; R.S. performed and analyzed the data of some β-Gal experiments; N.M., Y.Y., and M.G. performed and analyzed the data of FRET experiments; J.G.R. generated FRET constructs/reagents; M.B. and C.K. supervised FRET experiments; M.J.C. supervised electrophysiology experiments; M.L.H. and M.C. supervised BRET experiments; and S.S. supervised β-Gal experiments. E.M., A.B.G., and M.C. wrote the manuscript. All authors reviewed the manuscript. **Competing interests:** The authors declare that they have no competing interests. **Data and materials availability:** All data needed to evaluate the conclusions in the paper are present in the paper or the Supplementary Materials.

Submitted 10 January 2018
Accepted 29 June 2018
Published 17 July 2018
10.1126/scisignal.aas9609

Citation: E. Miess, A. B. Gondin, A. Yousuf, R. Steinborn, N. Mösslein, Y. Yang, M. Göldner, J. G. Ruland, M. Bünemann, C. Krasel, M. J. Christie, M. L. Halls, S. Schulz, M. Canals, Multisite phosphorylation is required for sustained interaction with GRKs and arrestins during rapid μ-opioid receptor desensitization. *Sci. Signal.* **11**, eaas9609 (2018).

Downloaded from http://stke.sciencemag.org/ on July 18, 2018

From Miess, E., Gondin, A. B., Yousuf, A., Steinborn, R., Mosslein, N., Yang, Y., . . . Canals, M . (2018). Multisite phosphorylation is required for sustained interaction with GRKs and arrestins during rapid mu-opioid receptor desensitization. *Sci Signal, 11*(539). doi:10.1126/scisignal.aas960. Reprinted with permission from AAAS.



Supplemental Figure 1

Fig. S1. Expression and function of MOR phosphorylation-deficient mutants. (A) Expression levels of FLAG-MOR WT or phosphorylation-deficient mutants measured by ELISA FLAG expression at the surface (non-permeabilised cells) or total expression (permeabilised cells). Data are shown as fold change over surface WT expression and represent mean±SEM (n=3 independent experiments). **(B)** Forskolin-induced cAMP inhibition of MOR WT or phosphorylation-deficient mutants in a CAMYEL BRET assay. Data are

From Miess, E., Gondin, A. B., Yousuf, A., Steinborn, R., Mosslein, N., Yang, Y., . . . Canals, M . (2018). Multisite phosphorylation is required for sustained interaction with GRKs and arrestins during rapid mu-opioid receptor desensitization. *Sci Signal, 11*(539). doi:10.1126/scisignal.aas960. Reprinted with permission from AAAS.

shown as percentage of cAMP induction by 10 μM forskolin (FSK) and represent mean±SEM from at least three independent experiments (n=3 independent experiments). **(C)** HEK293 cells stably expressing the HA-tagged MOR WT, MOR TSST-4A, MOR S375A, MOR TREHPSTANT-4A or MOR 11S/T-A were preincubated with HA antibody and stimulated with 10 μM DAMGO or morphine for 30 min. Cells were then fixed, stained and examined using confocal microscopy. Images are representative of three independent experiments. Scale bar, 20 μm.

From Miess, E., Gondin, A. B., Yousuf, A., Steinborn, R., Mosslein, N., Yang, Y., . . . Canals, M . (2018). Multisite phosphorylation is required for sustained interaction with GRKs and arrestins during rapid mu-opioid receptor desensitization. *Sci Signal, 11*(539). doi:10.1126/scisignal.aas960. Reprinted with permission from AAAS.

Supplemental Figure 2

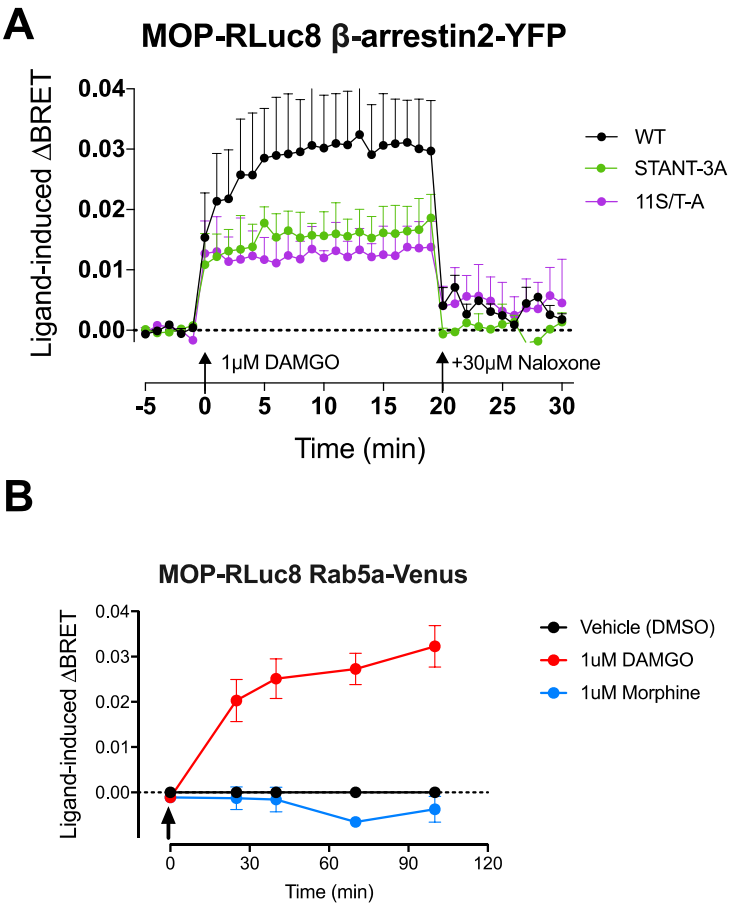
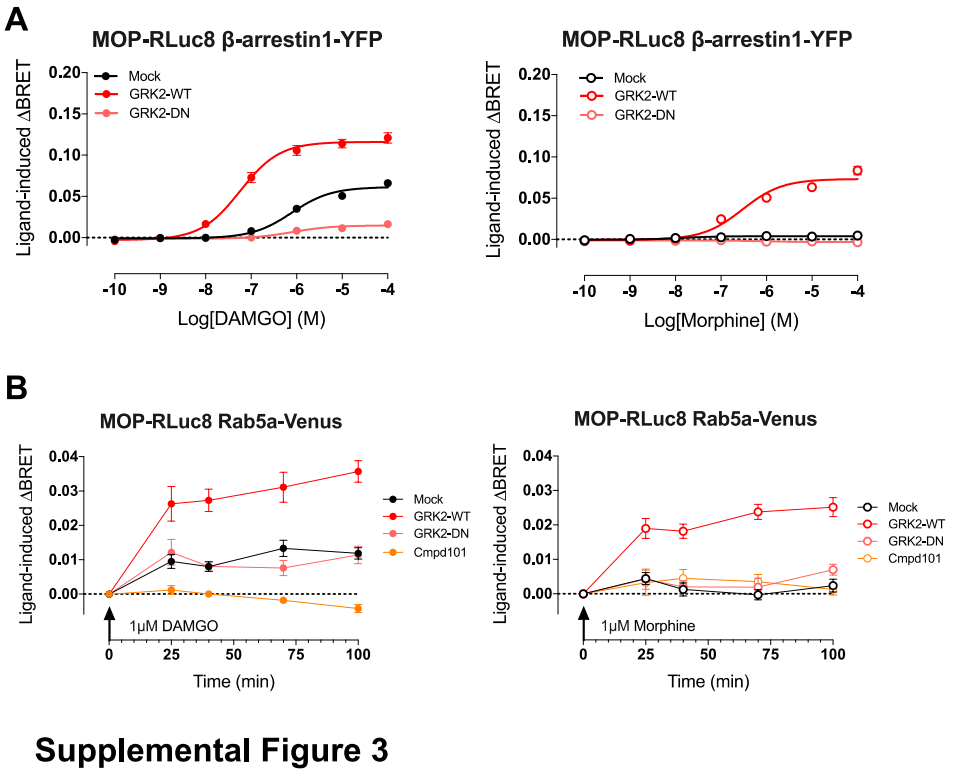


Fig. S2. Inhibition of β-arrestin2 recruitment upon addition of naloxone and lack of internalization by morphine. (**A**) BRET analysis of HEK 293 cells expressing MOR-RLuc8 WT or phosphorylation-deficient mutants and β-arrestin2-YFP and stimulated with 1 μM DAMGO for 20 min before the addition of 30 μM naloxone. The BRET ratio of vehicle-treated cells was subtracted. Data are means ± SEM of three independent experiments. (**B**) HEK 293 cells were transiently transfected with MOR-RLuc8 and the early endosome marker Rab5a-Venus and stimulated with 1 μM DAMGO or morphine. The BRET ratio of vehicle-treated cells was subtracted. Data are means ± SEM of three independent experiments.

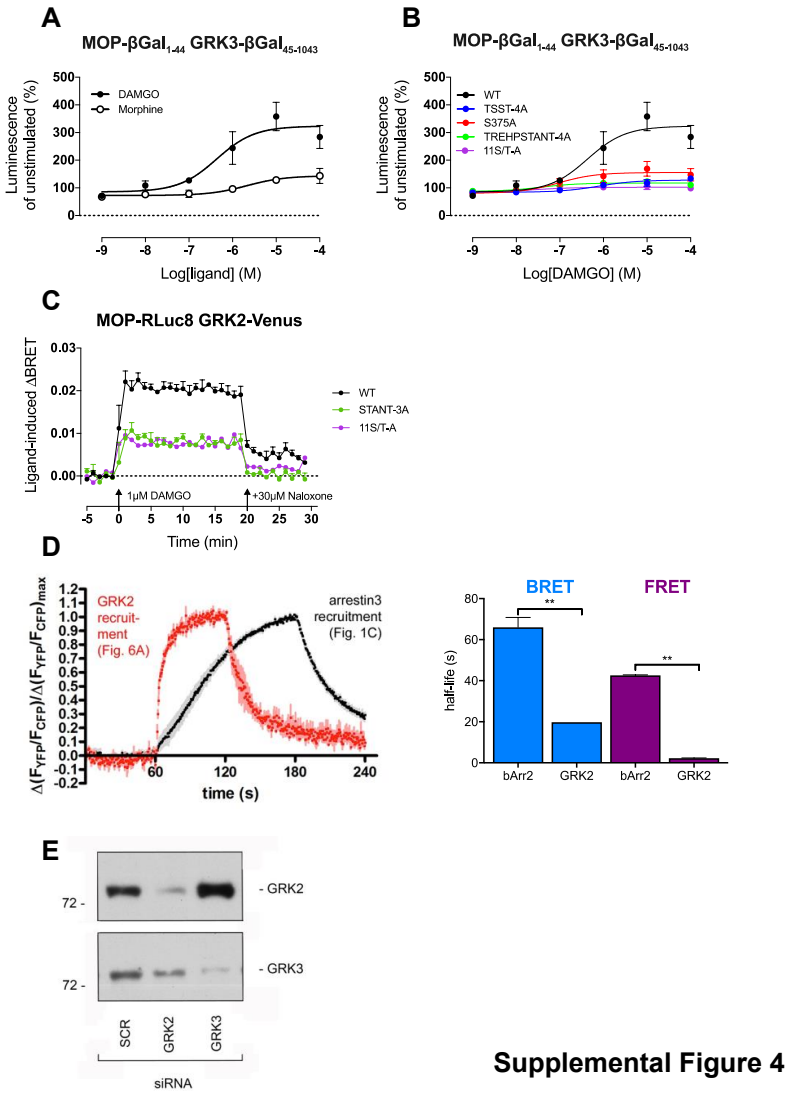
From Miess, E., Gondin, A. B., Yousuf, A., Steinborn, R., Mosslein, N., Yang, Y., . . . Canals, M . (2018). Multisite phosphorylation is required for sustained interaction with GRKs and arrestins during rapid mu-opioid receptor desensitization. *Sci Signal, 11*(539). doi:10.1126/scisignal.aas960. Reprinted with permission from AAAS.



Supplemental Figure 3

Fig. S3. β-Arrestin1 recruitment and MOR internalization upon overexpression of GRK2 WT or GRK2 DN. (**A**) HEK293 cells were transiently transfected with MOR-RLuc8 and β-arrestin1-YFP and pcDNA3 (mock), GRK2-WT or GRK2-DN and stimulated for 10 min with increasing concentrations of DAMGO or morphine (n=3-5 independent experiments). (**B**) HEK293 cells were transiently transfected with MOR-RLuc8, the early endosome marker Rab5a-Venus and pcDNA3 (mock), GRK2-WT or GRK2-DN or treated for 30 min the GRK2/3 inhibitor (Cmpd101, 30 μM) and stimulated with 1 μM DAMGO or morphine (n=3-5 independent experiments). The BRET ratio of vehicle-treated cells was subtracted. Data represents mean±SEM.

From Miess, E., Gondin, A. B., Yousuf, A., Steinborn, R., Mosslein, N., Yang, Y., . . . Canals, M . (2018). Multisite phosphorylation is required for sustained interaction with GRKs and arrestins during rapid mu-opioid receptor desensitization. *Sci Signal, 11*(539). doi:10.1126/scisignal.aas960. Reprinted with permission from AAAS.



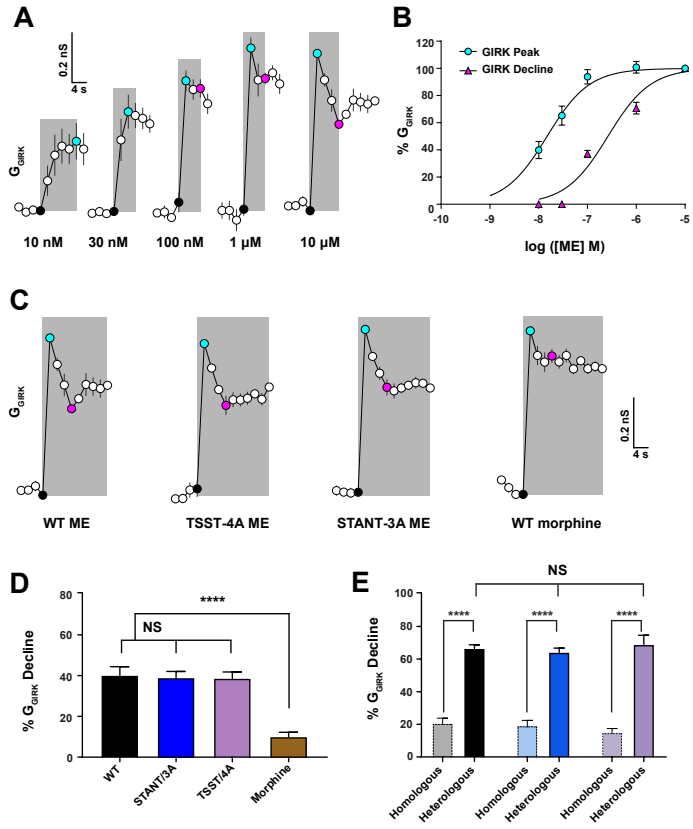
Supplemental Figure 4

Fig. S4. GRK3 recruitment to MOR WT and mutants, inhibition of GRK2 recruitment upon addition of naloxone, kinetics of GRK recruitment, and siRNA controls. (A and B) β-Gal complementation analysis of HEK293 cells expressing MOR-β-Gal1-44 WT (A) or phosphorylation-deficient mutants (B) and GRK3-β-Gal45-1043 and stimulated with increasing concentrations of DAMGO for 1 h (both n=3 independent experiments). Data were normalized to vehicle-treated cells and represent mean±SEM. (**C**) BRET analysis of HEK293 cells expressing MOR-RLuc8 WT or phosphorylation-deficient mutants and GRK2-YFP and

From Miess, E., Gondin, A. B., Yousuf, A., Steinborn, R., Mosslein, N., Yang, Y., . . . Canals, M . (2018). Multisite phosphorylation is required for sustained interaction with GRKs and arrestins during rapid mu-opioid receptor desensitization. *Sci Signal, 11*(539). doi:10.1126/scisignal.aas960. Reprinted with permission from AAAS.

stimulated with 1 μM DAMGO for 20 min prior to the addition of 30 μM naloxone. The BRET ratio of vehicle-treated cells was subtracted (n=3 independent experiments). (D) Comparison between the $t_{1/2}$ of β-arrestin2 and GRK2 recruitment in BRET and FRET assays. **, p<0.005, Mann-Whitney test. (E) Representative Western Blot (of n=3 independent experiments) showing GRK2 and GRK3 protein levels upon transfection of corresponding siRNAs (SCR; scrambled siRNA).

From Miess, E., Gondin, A. B., Yousuf, A., Steinborn, R., Mosslein, N., Yang, Y., . . . Canals, M . (2018). Multisite phosphorylation is required for sustained interaction with GRKs and arrestins during rapid mu-opioid receptor desensitization. *Sci Signal, 11*(539). doi:10.1126/scisignal.aas960. Reprinted with permission from AAAS.

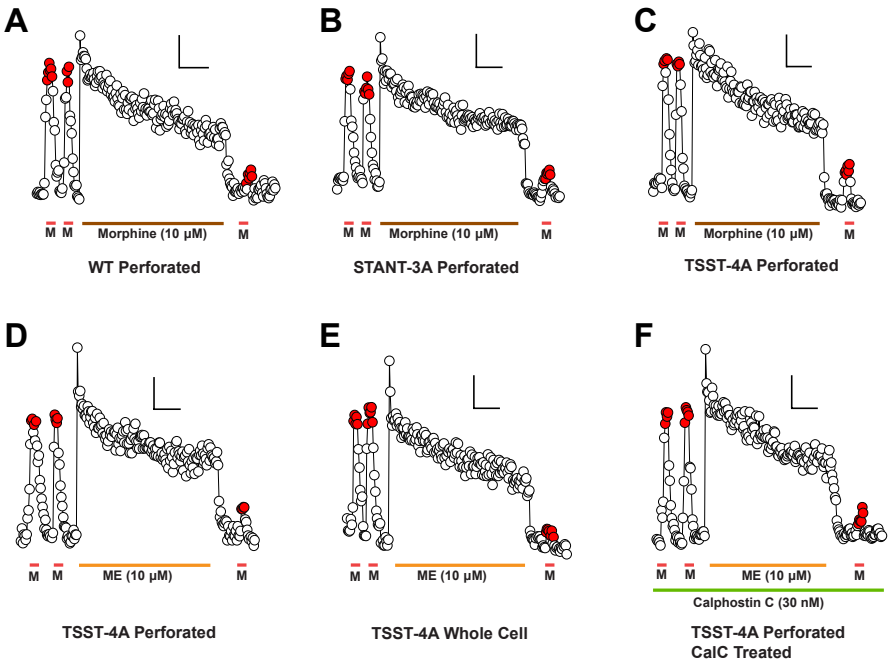


Supplemental Figure 5

Fig. S5. Fast desensitization component of MOR. (**A**) Concentration response of G_{GIRK} in AtT20 cells expressing MOR. ME at concentrations shown was applied for the duration of the shaded area (mean±SEM of 4-5 cells in each example). Pre-drug baseline is marked by black symbols, peak effects by aqua symbols and rapid decline by magenta symbols. (**B**) Peak G_{GIRK} ([aqua – black] %) was normalized to the response in each cell to 10 µM ME and plotted as aqua points. The rapid decline in G_{GIRK} ([aqua – magenta]/[aqua-black] %) was also normalized to the response in each cell to 10 µM ME and plotted as magenta points. (**C**) Rapid decline of G_{GIRK} (mean±SEM of 4-5 cells in each example) during application of ME (10 µM; shaded area) in cells expressing mutants or WT and exposed to morphine (10 µM). (**D**) Magnitude of rapid decline in G_{GIRK} calculated as described for (B) above (**** $P < 0.0001$). (**E**) Extent of

From Miess, E., Gondin, A. B., Yousuf, A., Steinborn, R., Mosslein, N., Yang, Y., . . . Canals, M . (2018). Multisite phosphorylation is required for sustained interaction with GRKs and arrestins during rapid mu-opioid receptor desensitization. *Sci Signal, 11*(539). doi:10.1126/scisignal.aas960. Reprinted with permission from AAAS.

heterologous desensitization as % decline for post compared to pre application of 100 nM somatostatin in each mutant.



Supplemental Figure 6

Fig. S6. Patch-clamp traces for corresponding MOR mutants. Exemplar traces of MOR-mediated G_{GIRK} for morphine-induced desensitization in WT (**A**), STANT-3A (**B**), TSST-4A (**C**) mutants using perforated patch clamp mode and ME-induced desensitization for TSST-4A using perforated patch (**D**), whole cell (**E**) and Calphostin C treatment **(F)**.

From Miess, E., Gondin, A. B., Yousuf, A., Steinborn, R., Mosslein, N., Yang, Y., . . . Canals, M . (2018). Multisite phosphorylation is required for sustained interaction with GRKs and arrestins during rapid mu-opioid receptor desensitization. *Sci Signal, 11*(539). doi:10.1126/scisignal.aas960. Reprinted with permission from AAAS.

Table S1. Potency and maximal response of MOR mutants in cAMP assay. Potency, pEC_{50}. Maximal response, E_{max}.

MOR	DAMGO		Morphine	
	pEC_{50}	E_{max} (% of FSK)	pEC_{50}	E_{max} (% of FSK)
WT	7.88 ± 0.05	45.95 ± 1.49	7.64 ± 0.03	42.95 ± 1.15
TSST-4A	7.84 ± 0.05	46.63 ± 1.95	7.63 ± 0.06	38.85 ± 1.86
S375A	7.67 ± 0.08	48.21 ± 1.47	7.66 ± 0.06	45.35 ± 1.27
STANT-3A	7.59 ± 0.06	42.33 ± 1.38	7.47 ± 0.04	35.86 ± 0.89
11S/T-A	7.71 ± 0.11	37.37 ± 2.31	7.63 ± 0.11	33.71 ± 1.44

From Miess, E., Gondin, A. B., Yousuf, A., Steinborn, R., Mosslein, N., Yang, Y., . . . Canals, M . (2018). Multisite phosphorylation is required for sustained interaction with GRKs and arrestins during rapid mu-opioid receptor desensitization. *Sci Signal, 11*(539). doi:10.1126/scisignal.aas960. Reprinted with permission from AAAS.

Chapter 5

Molecular mechanisms of β-arrestin2 interaction with the MOP

5.1 Abstract

Regulation and desensitisation of the μ-opioid receptor (MOP) contribute to the development of tolerance to opioid analgesics which severely limits their long-term clinical utility. In chapter 4, we showed that high-efficacy agonists trigger multi site phosphorylation within the C-terminal tail (Ct) which facilitates the recruitment of GRKs and β-arrestins to mediate MOP internalisation and desensitisation. However, in a MOP mutant that lacked all phosphorylation sites within the Ct, we still detected a residual component of β-arrestin2 recruitment that did not mediate internalisation. This indicated a potential role for phosphorylation residues outside the Ct and/or for additional phosphorylation-independent mechanisms underlying β-arrestin2 interactions with the MOP. Here, we used the BRET biosensors presented in chapter 2 (Nb33-Venus and Venus-mGsi) and β-arrestin2-YFP to study MOP activation, G protein coupling and β-arrestin2 recruitment, respectively. We generated a new set of phosphorylation-deficient MOP mutants that lack S/T in either the intracellular loops (ICLs), the Ct or both. This study revealed that while deletion of S/T residues does not affect agonist-induced MOP activation, the specific location of such residues in the ICLs or the Ct distinctively dictates the extent of G protein coupling or β-arrestin2 recruitment. Moreover, agonist-induced β-arrestin2 recruitment to MOP is partially dependent on G protein activation. We tested this by pharmacological inhibition with pertussis toxin as well as G protein knock-out cell lines. In addition, we also report that exogenous activation of protein kinase C (PKC) mediates agonist-independent β-arrestin2 recruitment to MOP or the plasma membrane. Together, this study reveals additional molecular mechanisms contributing to β-arrestin2 recruitment to the MOP and suggests that different modes of interaction of β-arrestin2 with specific receptor domains might be involved in distinct functions.

5.2 Introduction

A number of high-resolution arrestin crystal structures (Scheerer & Sommer, 2017), including a rhodopsin–arrestin structure (Kang et al., 2015) and atomic-level computational simulations (Latorraca et al., 2018) have provided major insights into arrestin activation mechanism. In short, arrestin seems to interact with G protein-coupled receptors (GPCRs) in a dual manner: one involving the arrestin N-domain which binds the phosphorylated Ct of GPCRs (Shukla et al., 2013) and/or a second involving the arrestin finger loop region that inserts within the intracellular core of GPCRs (Szczepek et al., 2014).

Moreover, these distinct modes of arrestin interaction have been implicated in different functions (Cahill et al., 2017). The transmembrane GPCR core is involved in interactions with G proteins and has been proposed as a competing region between arrestin and G protein coupling (Szczepek et al., 2014); this region is also implicated in receptor desensitisation (Staus et al., 2018). In addition, the transient association of arrestin with the ICLs of the receptor has been linked to the catalytic activation of arrestin that initiates ERK signalling separately from the receptor in clathrin-coated pits (Eichel et al., 2018). In contrast, the stable and stoichiometric association of arrestin with the phosphorylated Ct is associated with the coordinated movement of receptor-arrestin complexes into clathrin-coated pits to follow internalisation (Cahill et al., 2017) and might be compatible with concomitant GPCR–G protein interactions in endosomes (Thomsen et al., 2016).

The long-term use of opioid analgesics such as morphine is severely limited by the development of antinociceptive tolerance. The cellular mechanisms underlying tolerance are complex and remain unclear. However, it is known that regulation and desensitisation of the μ-opioid receptor (MOP) contribute to the development of tolerance to opioid drugs. Receptor desensitisation starts with phosphorylation of serine and threonine residues (S/T) within the C-tail (Ct), which causes β-arrestin2 recruitment and uncoupling from the canonical G protein signalling. In chapter 4, we showed that MOP desensitisation to high-efficacy agonists requires multisite phosphorylation of S/T within the Ct and the sustained interaction of the receptor with G protein-coupled receptor kinase 2 (GRK2) and β-arrestin2 (Miess et al.,

2018). We also detected a residual component (naloxone-sensitive) of β-arrestin2 recruitment that was present at a MOP mutant that lacked all phosphorylation sites within the Ct, indicating that either other phosphorylation sites outside this domain (i.e. residues in the ICLs) or phosphorylation-independent mechanisms could also participate in β-arrestin2 recruitment to MOP. In addition, morphine induced a small amount of phosphorylation and β-arrestin2 recruitment that was not sufficient to drive receptor internalisation, suggesting additional roles of β-arrestin2 aside from internalisation.

Additional molecular mechanisms might underlie the interaction and function of β-arrestin2 with the MOP. For example, multiple protein kinases can generate distinct receptor phosphorylation patterns that could bind to different conformations of β-arrestin2 to initiate distinct signalling and/or trafficking (DeFea, 2011; Yang et al., 2017). Remarkably, protein kinase C (PKC) has been implicated in desensitisation and tolerance to morphine (Bailey, Kelly, & Henderson, 2004; Bailey, Llorente, et al., 2009; Bailey, Oldfield, et al., 2009).

Previous studies have demonstrated that the ability of most MOP agonists to promote MOP phosphorylation, β-arrestin2 recruitment and internalisation is directly correlated with agonist efficacy for G protein activation (McPherson et al., 2010). Similarly, in chapter 2 we found a strong correlation between efficacy at the G protein and β-arrestin-dependent pathways for the three most recent MOP G protein-biased agonists. Together, these results suggest that G protein activation and β-arrestin2 recruitment are likely to be interlinked for most MOP agonists including the so-called biased ligands.

The design of G protein-biased drugs that present clear separation between G protein signalling and β-arrestin2 recruitment would only be possible if both pathways are truly independent from each other. This is because functional selectivity occurs through stabilisation of ligand-specific receptor conformations that preferentially couple to G protein or β-arrestin2. However, coupling to β-arrestin2 is at least partially dependent on receptor phosphorylation by GRKs, and translocation of cytosolic GRKs such as GRK2 to the plasma membrane occurs following Gβγ subunit release after G protein activation. Thus, it is not surprising to observe a certain degree of correlation between G protein activation and β-

arrestin2 recruitment. Additionally, recent studies have indicated that β-arrestin signalling for some GPCRs requires the presence of functional G proteins (Grundmann et al., 2018). This and other studies have also raised awareness about different strategies to abolish protein function (e.g. inhibitors, mutants, knock-down and knock-out) since some of these approaches are not completely inhibitory and genetic deletions can cause signalling rewiring within the system (Luttrell et al., 2018).

Here, we investigated the molecular mechanisms underlying β-arrestin2 interaction with the MOP. We examined i) agonist-dependent and -independent recruitment, ii) the role of phosphorylation sites located in the Ct versus those in the ICLs and iii) whether G protein activation is required for β-arrestin2 recruitment. We showed that in addition to agonist-induced β-arrestin2 recruitment, agonist-independent activation of PKC by phorbol 12-myristate 13-acetate (PMA) also mediates β-arrestin2 recruitment to the MOP. Both agonist-dependent or -independent β-arrestin2 recruitment required the phosphorylation residues contained within the Ct, and importantly also the ICLs. We then assessed the contribution of G protein activation to β-arrestin2 recruitment through pharmacological inhibition or genetic deletion of G proteins in CRISPR/Cas9 knock-out (KO) cell lines. We obtained similar results using the two different methods, demonstrating that agonist-induced β-arrestin2 recruitment to MOP is only partially dependent on activation of $G\alpha_{i/o}$ isoforms. These data indicate that different molecular mechanisms including phosphorylation of different receptor domains, G protein activation or even agonist-independent activation of PKC can contribute to β-arrestin2 recruitment to MOP.

5.3 Methods

5.3.1 Materials

Dulbecco's modified Eagle's medium (DMEM) was purchased from Invitrogen (Mulgrave, VIC, Australia). Foetal bovine serum (FBS) was purchased from ThermoTrace (Melbourne, Australia). DAMGO was purchased from Mimotopes (Melbourne, Australia). Morphine HCl was from GlaxoSmithKline (Boronia, Victoria, Australia). Naloxone was from Tocris. Pertussis toxin was from Invitrogen.

5.3.2 Plasmids

To generate the C-terminally tagged nanoluciferase (NLuc) MOP constructs, the NLuc sequence (Soave, Stoddart, Brown, Woolard, & Hill, 2016) was ligated immediately after the C-terminus of FLAG-mMOP wild-type (WT) or 11S/T-A (Miess et al., 2018) cDNA without stop codon with XhoI and XbaI restriction enzymes, generating FLAG-MOP-NLuc WT or $\Delta S/T_{Ct}$, which contains mutations of all 11 S/T of the Ct. $\Delta S/T_{ICL}$ (mutations in the ICLs: T97A, T180A, S261A, S266A and S268A) or ΔS/T (mutation of all intracellular S/T) were produced by assembling a synthesized cDNA fragment containing all ICL mutations (Integrated DNA Technologies) into the FLAG-MOP-NLuc WT and $\Delta S/T_{Ct}$, generating FLAG-MOP-NLuc $\Delta S/T_{ICL}$ and ΔS/T, respectively. All sequences were confirmed by DNA sequencing. Nb33-Venus and Venus-mGsi were described in chapter 2 (page 41).

5.3.3 Cell lines

Human embryonic kidney 293 (HEK293) cells were used in this study. Genetically engineered HEK293 cells using CRISPR/Cas9 technology were obtained from A. Inoue (Tohoku University, Sendai, Miyagi, Japan). The cell lines were derived as previously described (O'Hayre et al., 2017). HEK293 ΔGi cell line was generated by simultaneously mutating the GNAI1/2/3, GNAO, GNAZ and GNAT1/2 genes (encoding $G\alpha_{i1}$, $G\alpha_{i2}$, $G\alpha_{i3}$, $G\alpha_{o}$, $G\alpha_{z}$, $G\alpha_{t1}$ and $G\alpha_{t2}$). HEK293 full-ΔG cell line was generated by including the above mutations into previously established ΔGsix cell line (including knockout of Gαq, Gαolf, Gα11, Gαs, Gα12 and Gα13) (Grundmann et al., 2018).

5.3.4 Cell culture and transfections

HEK293 cells were maintained in DMEM supplemented with 5% v/v FBS at 37°C in a humidified atmosphere of 95% air and 5% CO_2. Transient transfections for BRET experiments were performed using linear polyethylenemine (PEI) with a molecular weight of 25 kDa (Polysciences) in a DNA:PEI ratio of 1:6 as previously described (Miess et al., 2018). Cells were transfected in a 10 cm dish with 1 µg of donor (MOP-NLuc WT, ΔS/T_{Ct}, ΔS/T_{ICL} or ΔS/T) and 4 µg of acceptor (Nb33-Venus, mGsi-Venus or β-arrestin2-YFP). For cAMP inhibition assays, cells were transfected with the CAMYEL BRET biosensor (2.5 µg of FLAG-MOP and 2.5 µg of CAMYEL biosensor per dish). Experiments were performed 48 h after transfection.

5.3.5 Bioluminescence Resonance Energy Transfer (BRET)

Furimazine (Promega) or Coelenterazine h were added to a final concentration of 5 µM immediately before dual fluorescence/luminescence measurement in a LUMIstar or PHERAstar Omega plate reader (BMG LabTech). The BRET signal was calculated as the ratio of light emitted at 530 nm by YFP or Venus over the light emitted at 430 nm by NLuc or RLuc8. When experiments were recorded as kinetic reads, the baseline BRET ratio was measured for 4 cycles prior addition of the agonists and BRET signal was recorded every minute over a total period of 20-30 min of stimulation until addition of 10 µM naloxone to asses reversal of the signal. Concentration-response curves were constructed from the 10 min time point for all pathways. For cAMP inhibition, cells were incubated with agonists for 10 min prior to addition of 10 µM forskolin.

5.3.6 Data analysis

Data are presented as the mean ± SEM of n≥3 independent experiments. Significance was assessed using one-way ANOVA followed by Sidak's multiple comparisons test to compare the E*max* and pEC_{50} mean of mutants in a specific agonist treatment, with the WT mean of the same treatment condition.

5.4 Results

5.4.1 Agonist-induced Nb33, mGsi and β-arrestin2 recruitment to phosphorylation deficient MOP mutants

We mutated S/T residues to alanine (A) in different regions of C-terminally NLuc-tagged wild-type (WT) mouse (MOP-NLuc), generating the following phosphorylation-deficient MOP mutants: ΔS/T_{Ct} (contains the 11S/T-A within the Ct, previously described in MOP-RLuc8 11S/T-A (Miess et al., 2018)), ΔS/T_{ICL} (mutations in the ICLs: T97A, T180A, S261A, S266A and S268A), and ΔS/T (mutation of all intracellular S/T residues, ΔS/T_{Ct} and ΔS/T_{ICL} combined). We have previously used Nb33-Venus and Venus-mGsi as BRET biosensors to detect MOP activation and coupling to inhibitory $G\alpha_i$ proteins, respectively (chapter 1). Here, we measured the recruitment of these biosensors to MOP-NLuc WT or the phosphorylation deficient mutants to assess whether mutation of S/T residues affected the overall activity of the mutants or their coupling to G proteins. Additionally, we measured β-arrestin2-YFP recruitment to MOP-NLuc WT or the phosphorylation deficient mutants.

Increasing concentrations of DAMGO (Fig. 5.1A-C) or morphine (Fig. 5.1D-F) generated a concentration-dependent increase in BRET signal for all Nb33, mGsi and β-arrestin2 recruitment assays. Nb33 was recruited to phosphorylation deficient MOP mutants to a similar extent to WT after stimulation with DAMGO or morphine (Fig. 5.1D, Table 5.1), indicating that all mutants can be activated in a similar manner. This also suggests that expression and agonist binding of the mutant receptors are similar to WT, although this needs to be confirmed through ELISA and radioligand binding. However, a significant reduction in E_{max} was found for the response of the ΔS/T_{ICL} and ΔS/T mutants to DAMGO, indicating some ligand-dependent differences in activation of the mutant receptors (Fig. 5.1A, Table 5.1). In the mGsi recruitment assay (Fig. 5.1B,E, Table 5.2), no significant difference between mutants and WT was found. However, there was a clear trend that could show that mutations in the ICLs impair G protein coupling to a greater extent than mutations within the Ct. Further experiments are needed to confirm whether this trend reached biological significance.

Although the mutated residues were chosen for their ability to be phosphorylated, it is not surprising that changes in amino acids within the ICLs of the receptor could impair mGsi recruitment, since the αN helix of Gα is known to interact with the ICLs to accommodate the C-terminal α5 helix of Gα within the transmembrane receptor core. Moreover, G protein coupling does not involve the Ct, thus it was expected that mutations within the Ct would not affect G protein coupling to a great extent. We then measured β-arrestin2 recruitment to MOP phosphorylation deficient mutants (Fig. 5.1C,F, Table 5.3). Mutations within the Ct severely compromised the efficacy of β-arrestin2 recruitment (~25 % of DAMGO WT) as previously reported (Miess et al., 2018). Surprisingly, mutations within the ICLs also compromised the efficacy of β-arrestin2 recruitment to a similar extent. Phosphorylation of S/T residues within the Ct is necessary for agonist-induced β-arrestin2 recruitment to MOP, however, the role of S/T residues within the ICLs has not been explored in detail. Moreover, mutation of S/T residues located within the Ct seemed to affect the DAMGO response to a greater extent than that of morphine (Table 5.3). This is consistent with the multisite phosphorylation of the Ct being fundamental for high-efficacy agonists. In contrast, morphine-induced β-arrestin2 recruitment to MOP seemed to be more affected by mutation of S/T residues located within the ICLs, suggesting that different agonists could promote interactions of distinct arrestin conformations with different regions of the receptor.

Together, these data indicate that the phosphorylation-deficient MOP mutants retain their ability to be activated after agonist addition. The S/T residues contained within the ICLs are important for G protein coupling and β-arrestin2 recruitment, while the S/T residues contained within the Ct are only important for β-arrestin2 recruitment. It is also important to note that mutations in the two different intracellular domains had different effects dependent on the agonist used. This suggests that distinct residues might contribute to agonist-specific stabilised MOP conformations that couple differently to downstream effectors.

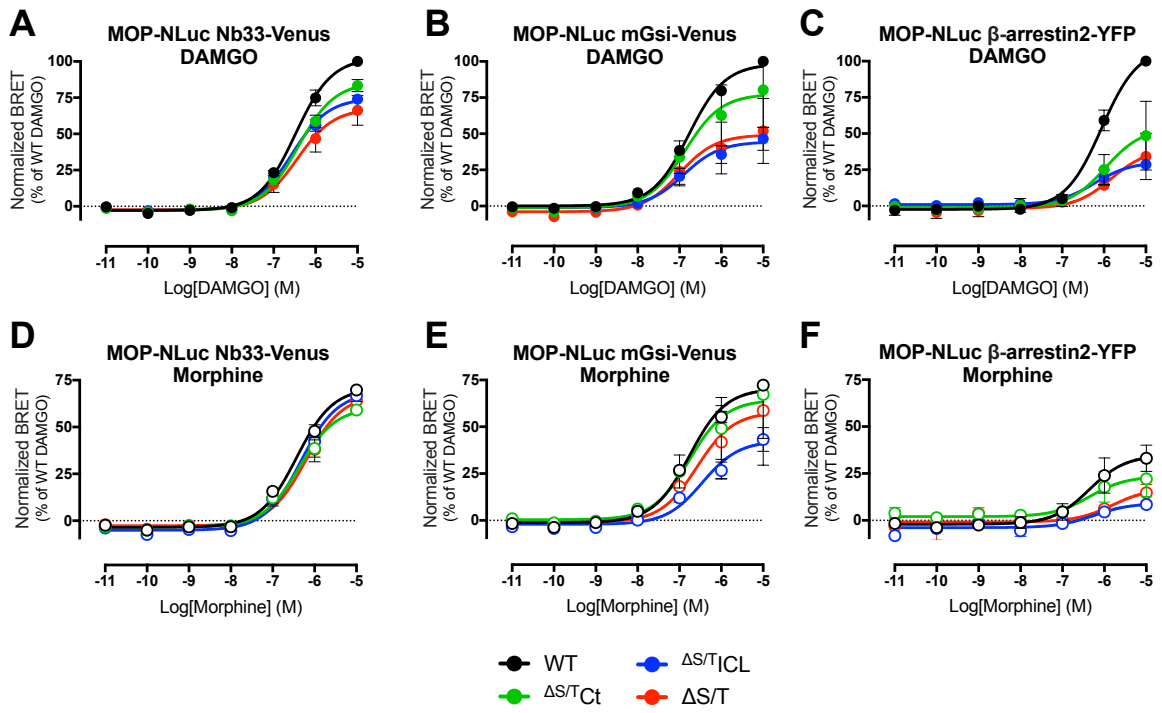


Figure 5.1 Recruitment of Nb33-Venus, mGsi-Venus or β-arrestin2-YFP to MOP-NLuc WT or phosphorylation-deficient mutants. HEK293 cells expressing MOP-NLuc WT, ΔS/T_{Ct}, ΔS/T_{ICL} or ΔS/T and Nb33-Venus **(A, D)**, mGsi-Venus **(B, E)** or β-arrestin2-YFP **(C, F)** were stimulated with increasing concentrations of DAMGO **(A-C)** or morphine **(D-F)**. Concentration-response curves were constructed from the 10 min timepoint of kinetic reads (n=3). Raw BRET ratio of vehicle-treated cells was subtracted and normalised to the response of 10 µM DAMGO in the WT receptor (Nb33-Venus: 0.491 ± 0.054, mGsi-Venus: 0.275 ± 0.129 and β-arrestin2-YFP: 0.225 ± 0.048). Data points represent mean ± SEM of the indicated number of experiments.

Table 5.1. Potency (pEC_{50}) and maximal response (E_{max}) of phosphorylation-deficient MOP mutants in Nb33 recruitment assay. Values are expressed as mean ± SEM from n=3 separate experiments. ** indicates p<0.01; *** indicates p<0.001 between the indicated mutant and the corresponding agonist response in WT in a one-way ANOVA with Sidak's post hoc test.

MOP	DAMGO		Morphine	
	pEC_{50}	E_{max} (% WT)	pEC_{50}	E_{max} (%)
WT	6.47 ± 0.08	103 ± 1	6.42 ± 0.10	71 ± 1
ΔS/T_{Ct}	6.41 ± 0.07	86 ± 4	6.37 ± 0.129	61 ± 2
ΔS/T_{ICL}	6.56 ± 0.11	75 ± 2**	6.32 ± 0.03	69 ± 3
ΔS/T	6.44 ± 0.14	68 ± 10***	6.21 ± 0.10	67 ± 6

Table 5.2. Potency (pEC_{50}) and maximal response (E_{max}) of phosphorylation-deficient MOP mutants in mGsi recruitment assay. Values are expressed as mean ± SEM from n=3 separate experiments. no significance detected between the mutants and the corresponding agonist response in WT in a one-way ANOVA with Sidak's post hoc test.

MOP	DAMGO		Morphine	
	pEC_{50}	E_{max} (%)	pEC_{50}	E_{max} (%)
WT	6.78 ± 0.04	98 ± 1	6.76 ± 0.07	71 ± 1
$\Delta S/T_{Ct}$	6.85 ± 0.04	77 ± 25	6.77 ± 0.01	64 ± 22
$\Delta S/T_{ICL}$	6.85 ± 0.16	45 ± 7	6.42 ± 0.18	43 ± 6
ΔS/T	7.00 ± 0.07	30 ± 16	6.65 ± 0.08	58 ± 29

Table 5.3. Potency (pEC_{50}) and maximal response (E_{max}) of phosphorylation-deficient MOP mutants in β-arrestin2 recruitment assay. ** indicates p<0.01; *** indicates p<0.001 between the indicated mutant and the corresponding agonist response in WT in a one-way ANOVA with Sidak's post hoc test.

MOP	DAMGO		Morphine	
	pEC_{50}	E_{max} (%)	pEC_{50}	E_{max} (%)
WT	6.06 ± 0.12	110 ± 2	6.32 ± 0.15	35 ± 7
$\Delta S/T_{Ct}$	6.17 ± 0.06	44 ± 17**	6.37 ± 0.05	24 ± 10
$\Delta S/T_{ICL}$	6.19 ± 0.20	31 ± 1***	6.13 ± 0.41	11 ± 3
ΔS/T	6.08 ± 0.34	43 ± 23**	6.81 ± 1.33	13 ± 3

5.4.2 Agonist-dependent β-arrestin2 recruitment is partially PTx-sensitive

We have previously shown that activation of the MOP $\Delta S/T_{Ct}$ causes inhibition of cAMP in a similar manner to MOP WT (Miess et al., 2018). This agrees with the data here showing that mutation of S/T within the Ct does not affect G protein coupling. Thus, we wondered whether the residual component of β-arrestin2 recruitment present in the phosphorylation-deficient MOP mutants was due to G protein activation.

We measured the kinetic profile of β-arrestin2 recruitment to MOP WT and phosphorylation-deficient mutants after stimulation with an EC_{50} concentration (1 μM) of

DAMGO (Fig. 5.2A-C) or morphine (Fig. 5.2D-F) under control or pertussis toxin (PTx) treated conditions. From the kinetic traces, agonist-induced β-arrestin2 recruitment to MOP WT and $\Delta S/T_{Ct}$ reversed it back to baseline levels after addition of 10 µM naloxone (Nlx) ($p<0.05$, n=3-9). In contrast, agonist-induced β-arrestin2 recruitment to MOP $\Delta S/T_{ICL}$ and ΔS/T was so limited that further addition of 10 µM Nlx did not reverse it back to baseline.

Additionally, statistical analysis of the area under the curve (AUC) of these traces showed that agonist-induced β-arrestin2 recruitment to MOP WT and $\Delta S/T_{Ct}$ was PTx sensitive (Fig. 5.2C,F). This indicates that the residual β-arrestin2 recruitment present in $\Delta S/T_{Ct}$ is due to activation of G proteins which might require prior engagement with the ICLs of the MOP. Altogether, these data indicate that in addition to the phosphorylation residues contained within the Ct of the MOP, S/T residues within the ICLs are also essential for the interaction of the MOP with β-arrestin2 and could be competing residues for the interaction with G proteins.

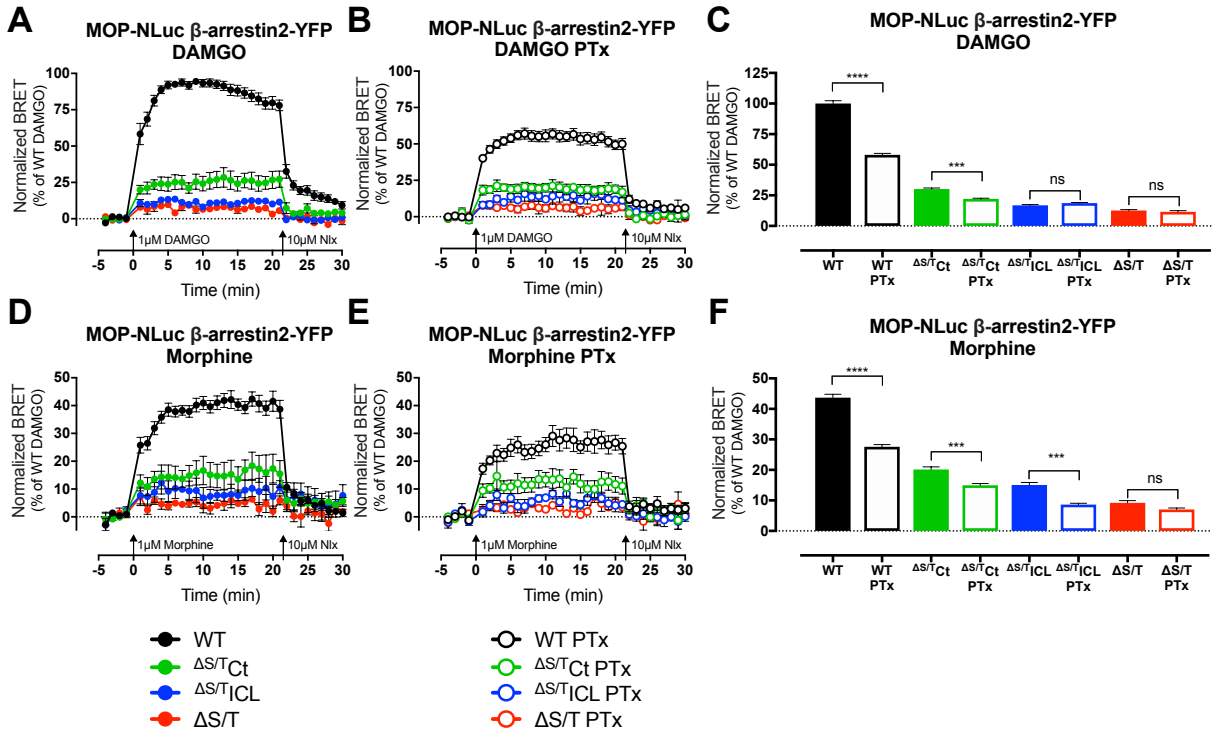


Figure 5.2 Effect of PTx in β-arrestin2 recruitment to MOP WT or phosphorylation-deficient mutants. HEK293 cells expressing MOP-NLuc WT or phosphorylation-deficient mutants and β-arrestin2-YFP were stimulated with 1 µM DAMGO **(A-C)** or 1 µM morphine **(D-F)** prior to addition of 10 µM of the antagonist naloxone (Nlx) (n=3-9). Kinetic traces or quantification of

the area under the curve (AUC) from the total stimulation time in non-pre-treated conditions (solid symbols) or after pre-treatment with pertussis toxin (100 ng/ml PTx; 16 hr) (open symbols). Raw BRET ratio of vehicle-treated cells was subtracted and normalised to the response of DAMGO in MOP WT (0.182 ± 0.030). Data points represent mean ± SEM of the indicated number of experiments. ns indicates not significant; *** indicates p<0.001; **** indicates p<0.0001 between the indicated pair in a one-way ANOVA with Sidak's post hoc test.

5.4.3 Agonist-induced β-arrestin2 recruitment to MOP in the absence of G proteins

$G_{i/o}$ protein inhibition with PTx only caused a partial reduction (~50%) of 1 μM DAMGO-induced β-arrestin2 recruitment to WT MOP (Fig. 5.2C), while restricting completely the ability of 1 μM DAMGO to cause inhibition of forskolin-induced cAMP accumulation (Fig. 5.3A). In order to address whether the remaining 50% of agonist-induced β-arrestin2 recruitment to MOP WT is mediated by PTx-insensitive G proteins, we used HEK293 cell lines with null mutations induced by CRISPR-Cas9 technology: ΔGi (knockout of all G protein isoforms within the Gi family including $G\alpha_{i1}$, $G\alpha_{i2}$, $G\alpha_{i3}$, $G\alpha_{o}$, $G\alpha_{t1}$ and $G\alpha_{t2}$ and $G\alpha_{z}$ [which is PTx insensitive]) and full-ΔG (knockout of all G proteins families including the above ΔGi mutations, plus ΔGs [$G\alpha_{s}$ and $G\alpha_{olf}$], ΔGq [$G\alpha_{q}$ and $G\alpha_{11}$] and ΔG12 [$G\alpha_{12}$ and $G\alpha_{13}$]). We first validated that agonist-induced cAMP inhibition did not occur in these cell lines (Fig. 5.3B). Forskolin-induced cAMP production lowered the BRET ratio detected by the CAMYEL sensor from the vehicle treated condition in ΔGi but this was not reversed in response to DAMGO. In contrast, in the full-ΔG the overall BRET ratio was low and forskolin did not stimulate any cAMP. As expected, we did not detect any agonist-induced inhibition of cAMP in ΔGi or full-ΔG cell lines, indicating that these cells do not encode the G protein isoforms necessary for MOP function. We then assessed β-arrestin2 recruitment in these cell lines (Fig. 5.3A,C). Deletion of the Gi/o/z/t subtypes in the ΔGi reduced the efficacy of the agonists to recruit β-arrestin2 (~50% of the corresponding agonist response in the parental cell line). This was not further reduced with deletion of other G protein subtypes in the full-ΔG. Thus, genetic deletion of the Gi/o/z/t subtypes alone or in combination with all the other subtypes caused a reduction in β-arrestin2 recruitment similar to pharmacological inhibition of the Gi/o subtypes with PTx. This indicates that activation of the $G\alpha_{i/o}$ subfamily accounts only partially for the recruitment of β-arrestin2 to MOP.

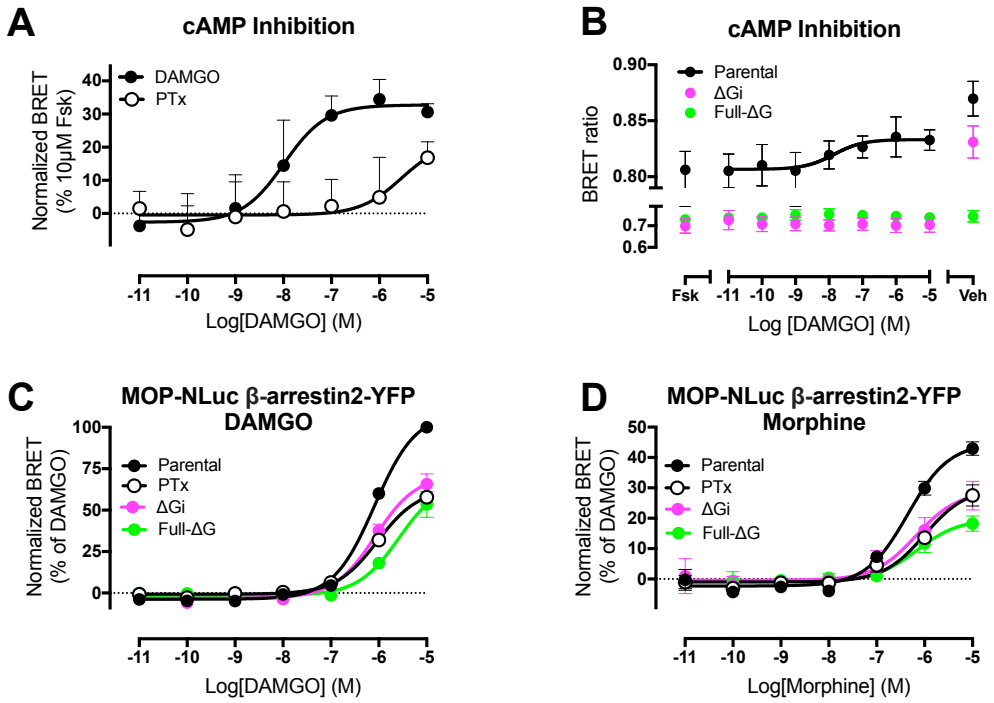


Figure 5.3 Agonist-induced β-arrestin2 recruitment to MOP WT in the absence of G proteins. cAMP inhibition was measured with the CAMYEL BRET sensor after stimulation with increasing concentrations of DAMGO for 10 min followed by stimulation with 10 μM forskolin (Fsk) to stimulate cAMP production under control or PTx pre-treated conditions (n=2) **(A)**. HEK293 parental, ΔGi or full-ΔG cell lines were also assessed in the CAMYEL assay (n=4-5) **(B)**. Raw BRET ratio is presented for comparison of baseline or Fsk-induced cAMP between cell lines. HEK293 parental, ΔGi or full-ΔG cell lines were transiently transfected with MOP-NLuc and β-arrestin2-YFP and stimulated for 10 min with increasing concentrations of DAMGO **(C)** or morphine (n=4-5) **(D)**. Raw BRET ratio of vehicle-treated cells was subtracted and normalised to the response of 10μM DAMGO (0.210 ± 0.074). Data points represent mean ± SEM of the indicated number of experiments.

Table 5.4. Potency (pEC_{50}) and maximal response (E_{max}) of MOP β-arrestin2 recruitment in HEK293 CRISPR/Cas9 cells. * indicates p<0.05; ** indicates p<0.01; *** indicates p<0.001; *** indicates p<0.0001 between the indicated condition and the corresponding agonist response in the parental cell line in a one-way ANOVA with Sidak's post hoc test.

HEK293	DAMGO		Morphine	
	pEC_{50}	E_{max} (%)	pEC_{50}	E_{max} (%)
Parental	6.10 ± 0.04	109 ± 1	6.42 ± 0.09	44 ± 3
PTx	6.04 ± 0.06	63 ± 3****	6.07 ± 0.13	30 ± 5
ΔGi	6.02 ± 0.17	73 ± 9**	6.32 ± 0.18	28 ± 5
Full-ΔG	5.60 ± 0.11	70 ± 12***	6.21 ± 0.18	20 ± 3*

5.4.4 Agonist-independent β-arrestin2 recruitment to the plasma membrane and to MOP WT and phosphorylation-deficient mutants

Agonist-independent β-arrestin2 recruitment was assessed after stimulation with 1 µM phorbol 12-myristate 13-acetate (PMA), a PKC activator. Exogenous activation of PKC caused a gradual increase in the BRET signal between β-arrestin2-YFP and MOP-NLuc (Fig. 5.4A). This signal reached a maximum 10 min after PMA addition and was slower than the agonist-induced β-arrestin2 recruitment that reached a maximum within 5 min (Fig. 5.2A, D). As expected, PMA-induced β-arrestin2 recruitment was PTx insensitive (Fig. 5.4B, C) and was not dependent on the receptor being in an active conformation, since addition of 10 µM Nlx did not reverse it back to baseline. This could indicate that the increase in signal is due to bystander BRET, rather than a direct interaction with the MOP; β-arrestin2-YFP is translocated to the plasma membrane which happens to contain MOP-NLuc. Surprisingly, PMA-induced β-arrestin2 recruitment was reduced in all phosphorylation-deficient MOP mutants. This could indicate that S/T residues contained within the Ct and to a less extent in the ICLs are also important for this agonist-independent PKC-dependent interaction of β-arrestin2 with the MOP (Fig. 5.4C). However, the reduction in signal could also be due to a different location of the mutant receptors within the plasma membrane.

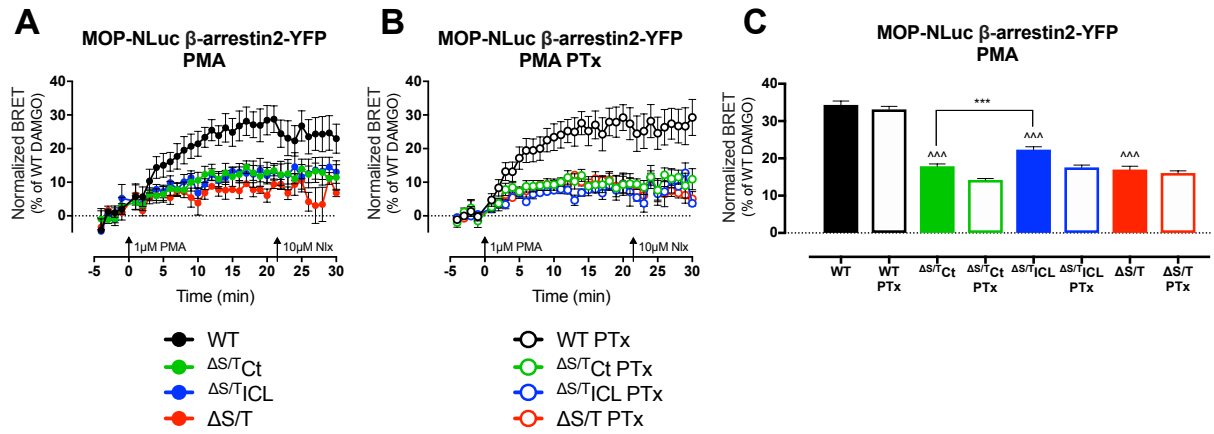


Figure 5.4 Agonist-independent β-arrestin2 recruitment to MOP WT or phosphorylation-deficient mutants. HEK293 cells expressing MOP-NLuc WT or phosphorylation-deficient mutants and β-arrestin2-YFP were stimulated with 1 µM PMA prior to addition of 10 µM of the antagonist naloxone (Nlx) (n=3-9). Kinetic traces or quantification of the area under the curve (AUC) from the total stimulation time in non-pre-treated conditions (solid symbols) or after pre-treatment with pertussis toxin (100 ng/ml PTx; 16 hr) (open symbols). Raw BRET

ratio of vehicle-treated cells was subtracted and normalised to the response of DAMGO in MOP WT (0.182 ± 0.030). Data points represent mean ± SEM of the indicated number of experiments. ^^^ indicates $p<0.001$ versus PMA in the WT; *** indicates $p<0.001$ between the indicated pair in a one-way ANOVA with Sidak's post hoc test.

5.5 Discussion

Currently, the field recognises β-arrestins both as regulatory and signalling molecules with critical importance in GPCR function. It is now accepted that β-arrestins interact with agonist-activated GPCRs to mediate desensitisation, internalisation, and G protein-independent signalling. Moreover, data pointing at specific physiological responses mediated by β-arrestin (Whalen, Rajagopal, & Lefkowitz, 2011), have motivated the design of biased drugs that favour or not the recruitment of β-arrestin (Boerrigter, Soergel, Violin, Lark, & Burnett, 2012; Schmid et al., 2017). However, our understanding of the specific molecular mechanism underlying these arrestin-mediated effects is still limited. For instance, we do not know to what extent the arrestin pathway does indeed require initial G protein activation or can be modulated by canonical G protein-dependent signalling.

Mutant receptors have been generated that do not signal via G proteins but retain β-arrestin recruitment (Donthamsetti et al., 2018), or that lack phosphorylation sites and are hampered in their ability to recruit β-arrestin (Arttamangkul, Heinz, Bunzow, Song, & Williams, 2018; Bradley et al., 2016). However, it is still not clear whether in the wild-type form of a GPCR, the G protein and the arrestin pathways are sufficiently dissociated so that designer drugs can activate one over the other. Recently, a study revealed that arrestin-dependent signalling (ERK phosphorylation) by several GPCRs requires G protein activation (Grundmann et al., 2018). In contrast, arrestin-dependent receptor internalisation can be achieved in the absence of functional G protein (Grundmann et al., 2018). Indeed, arrestin engagement by GPCRs may occur in the absence of receptor activation owing to heterologous phosphorylation by second messenger kinases (Toth et al., 2018), making the picture even more complex.

In this study we investigated the molecular mechanisms that underlie β-arrestin2 recruitment to MOP. We revealed the modes of MOP-β-arrestin2 interaction are varied and complex. Both agonist-dependent phosphorylation and agonist-independent PKC activation can trigger β-arrestin2 recruitment to MOP or the plasma membrane, respectively. This suggests that not only activation of agonist-dependent kinases such as GRKs, but also second

messenger kinases such as PKC can initiate β-arrestin2 recruitment to inactive MOP. Interestingly, activation of several nociceptive GPCRs in neurons, which co-express the MOP, results in activation of PKC second-messenger pathways (Chakraborty, Nepiyushchikh, Davis, Zawieja, & Muthuchamy, 2011; Sun et al., 2004; van der Merwe, Moreau, & MacNaughton, 2009). In this case, PKC activation through the nociceptive pathway could modulate β-arrestin2 recruitment to MOP by crosstalk.

We have previously shown that multi-site phosphorylation of S/T residues located within the Ct is important for β-arrestin2 recruitment to the MOP (chapter 4). In addition to these residues, here we revealed that S/T residues outside the Ct, located within the ICLs are also involved in β-arrestin2 recruitment to the MOP. Moreover, these residues seem to be involved in different functions. The S/T residues located within the Ct domain are involved solely in β-arrestin2 recruitment and are essential for MOP internalisation, whereas the residues within the ICLs are involved in both β-arrestin2 and G protein coupling.

We and others have extensively characterised the role of individual residues contained within the Ct. Multisite phosphorylation is hierarchical and triggered after phosphorylation of S375 which is critical for sustained β-arrestin2 recruitment and internalisation (Miess et al., 2018). Here we simultaneously mutated all S/T residues within the ICL domain, however, it would be interesting to identify the individual residues within the ICLs that are critical for interaction of the MOP with G protein and β-arrestin2 recruitment. In the MOP structure coupled to G protein, T180 (located in the interface of ICL2 with TM4) was an interacting residue with the G protein (Koehl et al., 2018). Moreover, T180 is required for GRK3 and β-arrestin2-mediated MOP desensitisation (Celver, Lowe, Kovoor, Gurevich, & Chavkin, 2001). Mutation of this residue alone could be enough to disrupt G protein coupling and the subsequent β-arrestin2 recruitment.

Additionally, it would be relevant to discern whether phosphorylation of T180 or merely the presence of the residue itself is important for G protein and β-arrestin2 recruitment. This could be investigated by generating phosphosite-specific antibodies against this residue as previously done with residues contained within the MOP Ct domain (Doll et

al., 2011) or indirectly by assessing how inhibition of GRKs might affect G protein and β-arrestin2 recruitment to MOP $\Delta S/T_{Ct}$ which only contains S/T residues within the ICLs. Moreover, GRK2 recruitment to S/T-deficient mutants might also give an indication as to whether ICL residues are necessary/involved in recruitment of the kinase and receptor phosphorylation. An additional experiment investigating agonist-induced phosphorylation (for example with anti-pS375) in the absence of functional G proteins could demonstrate whether agonist-mediated phosphorylation requires G protein activation.

Further investigation of the multiple modes of β-arrestin2 interaction with the MOP will require the study of internalisation and downstream signalling pathways. Arrestin-dependent MOP internalisation can occur regardless of G protein inhibition (Halls et al., 2016), indicating that at least some β-arrestin2 functions are independent from G protein activation. On the other hand, for many GPCRs there are remaining controversies regarding the contribution of G proteins and β-arrestin2 to activation of downstream signalling pathways such as ERK phosphorylation (Grundmann et al., 2018; Luttrell et al., 2018; O'Hayre et al., 2017). Investigation of how G protein and β-arrestin2 genetic deletions affect MOP-mediated ERK signalling remains to be addressed. In addition, future studies should consider the distinct spatial and temporal profile of downstream second messengers, since β-arrestins can scaffold the formation of signalling platforms in different subcellular locations generating specialised compartmentalised signalling hubs. A better understanding of the molecular mechanisms and functional consequences of β-arrestin2 interaction with the MOP is still required in order to advance the development of better opioid analgesics.

Chapter 6

General Discussion

The MOP remains the primary target for the treatment of pain, despite the numerous 'on-target' adverse effects associated with the use of opioid analgesics that target this receptor. Increasing public attention is focussed on the opioid field because of the current ‘opioid epidemic’ crisis within western societies. Thus, there is tremendous interest in the generation of new opioid drugs with improved therapeutic profiles.

Biased agonism presents an invaluable opportunity for designing drugs with fewer 'on-target' adverse effects. For this to be effective, the signalling pathways that produce the desired versus the unwanted physiological effects need to be delineated. For the MOP, reports in the late 90s suggested that β-arrestin2 mediates most of the adverse effects of opioids. The evidence came from β-arrestin2 KO mice, in which morphine displayed stronger analgesia with reduced tolerance, gastrointestinal and respiratory dysfunction (Bohn et al., 1999; Raehal, Walker, & Bohn, 2005). Although the signalling pathways by which β-arrestin2 leads to an opioid's unwanted effects remain unclear, extensive efforts are currently focusing on the generation of G protein-biased agonists that do not promote β-arrestin2 recruitment to the MOP. Some of these drugs have shown improved therapeutic profiles in pre-clinical and clinical studies and seem promising drug candidates. However, this is not without some controversy. Some studies show that a number of the side effects of MOP analgesics, including respiratory depression and inhibition of gastrointestinal motility, are mediated via activation of G protein-mediated signalling pathways in different tissues (Galligan & Akbarali, 2014; Pattinson, 2008). Thus, G protein-biased MOP agonists may not be the ‘holy grail' after all. Moreover, another study has shown that some of the so-called biased ligands are merely MOP agonists with overall lower agonist efficacy and therefore are not completely devoid of side effects (Hill et al., 2018).

In chapter 2, the most recent G protein-biased MOP agonists were compared head-to-head for the first time. We demonstrated that TRV130, PZM21 and SR-17018 present overall lower efficacy at both G protein and β-arrestin2 pathways and that buprenorphine was the only agonist that presented significant G protein bias. However, this was only true under endogenous GRK2 expression levels when agonist efficacy in the β-arrestin2 recruitment assay was very low.

In vitro studies have shown that buprenorphine binds with high affinity to MOP and KOP and relatively lower affinity to DOP (Villiger & Taylor, 1982). Buprenorphine is an extremely lipophilic compound that dissociates very slowly from the MOP (Boas & Villiger, 1985) and is not displaced easily by antagonists, such as naloxone (Eissenberg et al., 1996). This slow receptor dissociation has generally been regarded as the property responsible for the long duration of action of buprenorphine as an analgesic. In this study, we detected low dissociation kinetics and poor displacement with the antagonist naloxone. Additionally, we described that buprenorphine is a G protein biased agonist due to its high potency and limited efficacy at activating the MOP. The fact that buprenorphine activates the MOP in a partial manner translates into minimal arrestin recruitment, thus showing biased agonism away from the arrestin pathway when comparing to G protein activation. This could be the reason why buprenorphine might present a ceiling effect with regards to side effects such as respiration in mice and intestinal motility in rats (Cowan, Doxey, & Harry, 1977). However, it has to be pointed out that arrestin recruitment was very limited for this agonist and concentration response curve fit was not ideal, thus bias quantification might have been hampered by the low efficacy displayed.

Overexpression of GRK2 in both assays (cAMP inhibition and β-arrestin2 recruitment) completely abolished such bias, highlighting that the cellular content of signalling effectors has significant effects on the presentation of biased agonism. This is important when we consider the protein content of different cells within the body, or even the changes of protein complement induced by disease or chronic drug treatment. Although, the abundance of GRK in MOP-expressing neurons has not yet been clearly established, given the importance of GRK levels to morphine-dependent regulation of MOP in model cell systems, it is possible that alterations in GRK2 expression following chronic opioid treatment could contribute to significant reprogramming of opioid regulatory responses. For example, chronic morphine administration regulates expression of a number of genes (Ammon-Treiber & Hollt, 2005), including ∼20% increase in GRK2 protein levels in the rat locus coeruleus (Terwilliger, Ortiz, Guitart, & Nestler, 1994). Similarly, Fan et al. 2002 investigated the potential regulatory effects of acute and chronic morphine administration and withdrawal on GRK2 and GRK5 gene expression in rat brain. It was shown that a single administration of morphine increased

GRK2 and GRK5 mRNA levels in cerebral cortex, hippocampus and thalamus; whereas a significant decrease in GRK5 mRNA levels was observed in periaqueductal gray. In strong contrast, chronic administration of morphine failed to elevate GRK5 mRNA in any of these brain regions, while causing a 60–70% down-regulation of GRK2 expression in cerebral cortex, hippocampus, thalamus, and locus coeruleus. Moreover, morphine withdrawal induced aberrant increase of GRK2 and GRK5 expression. Similarly, an increase in total GRK2 protein was observed in frontal cortex during withdrawal in opiate addicts (Ozaita et al., 1998). Taken together, these results suggest that GRK gene expression can be regulated by opioid treatment.

In this study, we represented the response in cAMP inhibition as a function of the response in β-arrestin2 recruitment in a 'bias plot' that allowed us to qualitatively assess the effect of GRK2 overexpression in the system. This representation incorporates all three types of bias: observation bias (assay), system bias (protein content of cell background) and ligand bias (Kenakin 2017). Although it is unsuitable for determining ligand bias, due to all the confounding factors in the analysis, it demonstrated that limited β-arrestin2 recruitment is due to 'system bias' in which cAMP inhibition is favoured, and that overexpression of GRK2 improves β-arrestin2 recruitment for all the low efficacy ligands. Thus, the reduced β-arrestin2 recruitment observed in response to TRV130, PZM21 and SR-17018 could potentially be attributed to the fact that they are low-efficacy agonists and hence, poorly stimulate signalling pathways when there is low receptor reserve or signal amplification or these pathways are inefficiently coupled.

Additionally, the differences in cellular content are particularly relevant when we take into consideration that bias quantification for some MOP ligands has been performed comparing pathways across different cellular systems. For SR-17018 in Schmid et al. 2016, a bias factor of 40 (the highest so far for MOP agonists) was reported between cAMP inhibition in CHO cells and β-arrestin2 recruitment in U2OS cells which express low levels of GRK2 much lower than those expressed in brain regions (Nickolls, Humphreys, Clark, & McMurray, 2013). Additionally, in the same study fentanyl was reported as a β-arrestin2-biased ligand. In our study, fentanyl did not present any bias, which further supports the fact that cellular

background can account differences in the quantification of biased agonism across different cells. In Manglik et al. 2016, PZM21 did not elicit a measurable response in the arrestin assay in HEK293 with endogenous GRK2 expression levels, and in conditions where GRK2 was overexpressed, similar to our results, a quantitative assessment of bias by the operational model failed to show any significance. In DeWire et al. 2013, TRV130 presented a bias ratio of 3 compared to morphine by comparison of relative intrinsic activities between cAMP inhibition and β-arrestin2 recruitment. We calculated bias ratios using the same approach, but we did not detect any bias towards cAMP inhibition. However, species differences might account for this discrepancy since we used a mouse MOP at which TRV130 had much higher efficacy for β-arrestin2 recruitment compared to the human MOP (DeWire et al. 2013). Our reasons for using the mouse MOP are: i) the phosphorylation sites are conserved across species; ii) most animal models using phosphodeficient mutants are in mice and iii) previous data show that the ligand-dependent differences in arrestin recruitment are maintained in the human MOP.

We also employed novel BRET tools to measure MOP activation (Nb33) and G protein coupling (mGsi) upstream of cAMP inhibition. By measuring endpoints more proximal to receptor activation, we found that the so-called G protein-bias ligands displayed low efficacy in a similar manner to the partial agonist buprenorphine. Thus, these novel ligands present similar characteristics to partial agonists and very distinct from those of high-efficacy agonists such as DAMGO. A complementary method that has been used to evaluate intrinsic efficacy involves depleting the receptor reserve (Kelly, 2013) through the use of an alkylating agent that irreversibly binds to the receptor and lowers the total receptor pool. Although this was not done within the timeline of this thesis, receptor alkylation studies would allow the calculation of efficacy values under conditions with low to none receptor reserve. This would allow us to unequivocally show that TRV130, PZM21 and SR-17018 are partial, and not biased, agonists for the MOP.

As expected, we found a strong correlation between tau efficacy for MOP activation (Nb33 recruitment) and all pathways representative of the G protein pathway (mGsi recruitment, $G\alpha_{i2}$ activation and cAMP inhibition). However, somewhat unexpectedly we also

found a correlation between MOP activation and all pathways representative of the arrestin pathway (GRK2 and β-arrestin2 recruitment and Rab5 internalisation). Consequently, there was also a strong correlation between cAMP inhibition and β-arrestin2 recruitment, which supports previous work by McPherson et al. 2010 that demonstrated that MOP agonist efficacy at G protein activation correlates with the extent of receptor phosphorylation, arrestin recruitment and internalisation. Such correlation raises the question as to what extent the arrestin pathway is associated with G protein activation. Recent reports indicate that arrestin-mediated signalling (but not internalisation) indeed requires the presence of functional G proteins (Grundmann et al., 2018). To investigate this, cells in which G proteins have been knocked out will be very informative (see below).

Interestingly, the two agonists with the lowest overall efficacy (buprenorphine and SR-17018) have been shown to exhibit the safest therapeutic window due to their reduced risk for respiratory depression. Indeed, partial MOP agonists with very low efficacy (much lower than morphine) have been described, and these agonists do not appear to reach the efficacy threshold required to induce respiratory depression. For example, buprenorphine reaches a ceiling effect at doses sufficient to cause analgesia, but insufficient to cause respiratory depression (Davis, 2012; J. Pergolizzi et al., 2010). A more comprehensive analysis of the molecular mechanism underlying the effects of the so-called G protein-biased MOP agonists would provide further insights into whether it is in fact their partial agonism that accounts for their improved tolerability profile and reduced respiratory depression *in vivo*.

G proteins and arrestins modulate a number of downstream effectors, thus additional signalling pathways need to be investigated to pinpoint exactly which pathways are responsible for the physiological effects of opioid drugs. For example, it has been shown that internalisation-dependent ERK signalling contributes to the antinociceptive effect of some (e.g. DAMGO), but not all opioids (e.g. fentanyl) despite their similarities at inducing β-arrestin recruitment and internalisation (Bobeck, Ingram, Hermes, Aicher, & Morgan, 2016). Importantly, we also need to consider that although bias quantification is most commonly measured using signalling assays in recombinant cell lines, the data from these *in vitro* experiments might not translate directly to physiologically relevant tissues that express both

receptor and effectors at endogenous levels. Genetically encoded biosensors, specially FRET sensors have shed light into the compartmentalised signalling pathways activated by endogenous proteins (Halls & Canals, 2018). Technical advancements in this front continue to develop, allowing the detection of multiple signalling pathways (Mehta et al., 2018), thus it is expected that in the future, increasing studies will quantify signalling bias in more than two pathways and in relevant cell systems (e.g. neurons that endogenously express opioid receptors (Ho et al., 2018)), which will hopefully facilitate better translation *in vivo*.

Furthermore, characterisation of the desensitisation profile of these novel ligands is still required to assess whether their long-term use results in the development of tolerance to the analgesic effects as with traditional opioid drugs. Receptor desensitisation after prolonged or repeated exposure to agonists is considered to be the initial step in the development of tolerance. Such desensitisation entails regulatory mechanisms such as receptor phosphorylation, recruitment of GRKs and arrestins, and internalisation. Surprisingly, morphine, which is disproportionally poor at promoting MOP regulation and internalisation, produces more tolerance and dependence liability than other opioids with similar efficacy (Williams et al., 2013). Interestingly, PKC has been shown to play a role in MOP desensitisation and the development of tolerance to morphine (Bailey et al., 2009).

In this line, previous work (presented in appendix 1) described that morphine elicited a unique spatiotemporal signalling profile that involves sustained activation of PKC at the plasma membrane and sustained activation of ERK in the cytosol (Halls et al., 2016). In contrast, activation of the MOP with DAMGO only causes a transient activation of ERK in the cytosol and the nucleus (Halls et al., 2016). Interestingly, this work suggested that the plasma membrane distribution of MOP dictates the agonist differences in signalling profiles. Hence, the focus of chapter 3 was to investigate the effect of agonist stimulation on the plasma membrane organisation of the MOP in live cells.

For this, we developed and validated an N-terminal SNAP-tagged MOP construct and assessed the plasma membrane organisation after agonist stimulation using FCS and FRAP. We reported agonist-specific differences. While naloxone and morphine did not alter the

constitutive MOP organisation, DAMGO caused slowing in diffusion, a reduction in particle number, and an increase in clustering and the proportion of immobile receptors. Moreover, we were able to identify specific molecular mechanisms underlying the distinct events. G protein activation is not involved in MOP reorganisation, however, clathrin-mediated endocytosis only affected macro-parameters such as increased clustering and fraction of immobile receptors, while GRK2/3 mediates the slowing in micro-diffusion that precedes internalisation by DAMGO.

This work thus, has identified a novel role of GRKs in mediating MOP organisation at the plasma membrane in an agonist-specific manner and fits with the recent shift away from the traditional view of GRKs and arrestins as mere regulatory proteins. The identification of novel mechanisms involved in GPCR signal transduction is necessary to fully understand the mechanism of action of the different agonists at the MOP. In this line, arrestin has been identified as a catalytic effector capable of initiating GPCR-mediated signalling from clathrin-coated pits in the absence of the receptor in these domains (Eichel et al., 2018). Future studies should consider the plasma membrane organisation of the ligand, receptor and effector proteins simultaneously to get a comprehensive idea as to whether the individual components move together as a complex or separately. Single-molecule imaging studies of the distribution of GPCRs and their signalling effectors at the plasma membrane (such as chapter 3) are now becoming available (Sungkaworn et al., 2017; Yanagawa et al., 2018). Advanced imaging techniques such as FCS are sensitive enough to detect proteins expressed at endogenous levels, the detection of endogenous proteins is now possible thanks to the generation of fluorescently-labelled agonists such as the one presented in appendix 2 (Lam et al., 2018), as well as with techniques that allow tag labelling of endogenous proteins (White, Vanyai, See, Johnstone, & Pfleger, 2017). Together, these studies will provide greater insights into how agonist stimulation determines receptor organisation and could offer new avenues to selectively and therapeutically target GPCRs.

In chapter 4 and 5 we focused on the role of specific phosphorylation sites in MOP regulation and desensitisation. In chapter 4, we focused on two main phosphorylation clusters (^{354}TSST^{357} and ^{375}STANT^{379}) located in the C-terminal tail (Ct) of the receptor that

contains a total of 11 putative serine and threonine (S/T) residues. In chapter 5, we focused on the S/T residues contained within the intracellular loops (ICLs).

In chapter 4, we employed phosphosite-specific antibodies, phosphorylation-defective mutants and complementary biophysical approaches: BRET, FRET and β-galactosidase complementation. Together, these techniques allowed us to show how specific phosphorylation sites control the dynamics of GRK and β-arrestin interactions with MOP to mediate receptor desensitisation (Miess et al., 2018). Agonist stimulation by DAMGO or morphine causes MOP phosphorylation and regulation by GRK2/3 and β-arrestin1/2 to different extents. Agonist-specific MOP phosphorylation at specific sites had different functions. Mutation of the ^{354}TSST^{357} cluster did not affect internalisation or desensitisation of the MOP, although it contributed to multi-phosphorylation of the ^{375}STANT^{379} cluster and was involved in the long-term stability of the MOP-β-arrestin2 complex. In contrast, phosphorylation of S375 was critical for strong and sustained MOR-β-arrestin2 interactions, which was necessary for internalisation and multi-phosphorylation of adjacent T residues within the ^{375}STANT^{379} cluster. Mutation of the ^{375}STANT^{379} cluster completely abolished the slow desensitisation component measured by whole cell patch clamp. In addition, we found a fast desensitisation component that was independent of phosphorylation within the ^{354}TSST^{357} or the ^{375}STANT^{379} clusters. Moreover, mutation of all phosphorylation residues within the Ct in the 11S/T-A mutant, did not completely prevent GRK2 and β-arrestin2 recruitment, which raised our interest in studying the phosphorylation sites outside the Ct domain.

In chapter 5, we expanded on the role of S/T residues contained within the ICLs and the Ct. We measured the direct recruitment of Nb33, mGsi or β-arrestin2 to MOP wild-type and new phosphorylation-deficient mutants $\Delta S/T_{ICL}$, $\Delta S/T_{Ct}$, $\Delta S/T_{all}$. Removal of phosphorylation sites did not affect receptor activation (Nb33). However, the specific location of such residues (i.e. in ICLs or Ct) distinctively dictates the extent of G protein activation or β-arrestin2 recruitment. Increasing evidence demonstrates that GPCRs interact with arrestins through two distinct domains: the tail and the core. Phosphorylation of the Ct domain is required for the tail conformation, mediates receptor internalisation and has been

extensively investigated for the MOP (Meiss et al., 2018). In contrast, the role of phosphorylation sites within the ICLs of the MOP has been overlooked. In chapter 5, we described that the S/T residues located in the ICLs participate in G protein coupling and β-arrestin2 recruitment. Moreover, β-arrestin2 recruitment is partially dependent on G protein activation (PTx-sensitive). To understand this dependence, we further explored this link in CRISPR/Cas9 knock-out HEK293 cell lines in which all G proteins within the $G_{i/o}$ subfamily have been deleted (ΔGi) or all G proteins have been deleted (full-ΔG). We identified that in ΔGi and full-ΔG (similar to PTx treatment), β-arrestin2 recruitment to MOP was partially reduced. This indicates that pharmacological inhibition of PTx-sensitive G proteins produced a similar effect to the genetic deletion of the entire $G_{i/o}$ subfamily, as well as all G proteins, suggesting that certain component β-arrestin2 recruitment is dependent on G protein activation. This is especially relevant in the context of MOP biased ligands since it might be challenging to find agonists that activate G protein over a downstream effector. It remains to be studied whether MOP internalisation and β-arrestin2-dependent signalling are also dependent on G protein activation.

Additionally, we showed that β-arrestin2 is also recruited to MOP in an agonist-independent manner through activation of PKC. Activation of several other GPCRs that are co-expressed with the MOP in nociceptive neurons results in activation of the PKC pathway. Whether the component of β-arrestin2 recruitment mediated by PKC requires phosphorylation of the receptor remains to be investigated. It has been proposed that S363 is constitutively phosphorylated by PKC.

In conclusion, the studies presented here provide unprecedented details into the molecular mechanisms controlling MOP activation (Fig. 6.1). Agonist-specific activation of the MOP leads to plasma membrane receptor re-organisation, specific phosphorylation patterns and recruitment of regulatory proteins that interact with the receptor in multiple ways and can be involved in different functions. This tight receptor regulation ultimately leads to the spatiotemporal control and fine-tuning of signalling responses elicited by the MOP. Furthermore, the observation that additional pharmacological properties such as intrinsic efficacy might be the underlying cause for some of the promising G protein-biased MOP

agonists, raises the question as to whether a simple consideration of biased agonism between G protein and β-arrestin2 will actually resolve into better opioid analgesics.

Currently, all FDA-approved opioid drugs have agonist activity at the MOP; however, alternative approaches are continually emerging. Drugs with mixed agonism or agonism/antagonism at the different opioid receptor subtypes have shown increased utility (Almatroudi, Ostovar, Bailey, Husbands, & Bailey, 2018; Dietis et al., 2018; Gunther et al., 2018). Additionally, multi-mechanistic opioid drugs that combine MOP activation with an additional non-opioid analgesic component have been proposed as safer analgesic options (Pergolizzi et al., 2018; Raffa, Elling, & Tzschentke, 2018). Finally, the combination of MOP agonists with peripheral MOP antagonists has also been proposed to limit the mal-adaptive signalling processes that lead to analgesic tolerance (Corder et al., 2017). It is clear that the molecular mechanisms underlying MOP pharmacology are diverse and complex, however, once we understand them they also offer new avenues to exploit for the development of improved pharmacological therapies.

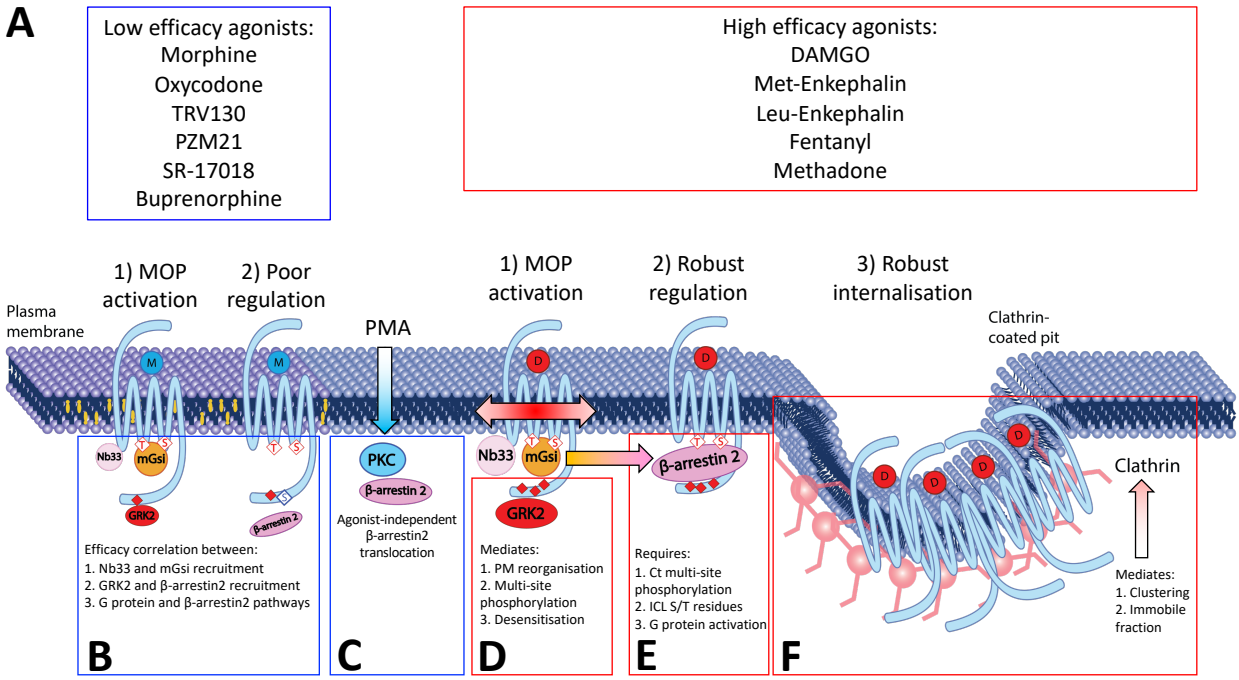


Fig. 6.1 Summary of findings in this study. (A) MOP agonists are classified in low efficacy or high efficacy agonists according to their overall efficacy in pathways proximal to receptor activation: Nb33, mGsi, GRK2 and β-arrestin2 recruitment. **(B)** Low efficacy agonists show correlation of efficacy between Nb33 and mGsi, as well as GRK2 and β-arrestin2 recruitment, thus there is a strong correlation between G protein and β-arrestin2 –mediated pathways. **(C)** Agonist-independent activation of PKC by PMA causes translocation of β-arrestin2 to the plasma membrane. **(D)** Activation of the MOP by DAMGO causes robust GRK2 recruitment which mediates plasma membrane re-organisation, multi-site phosphorylation and desensitisation. **(E)** Subsequently, β-arrestin2 is recruited in a sustained manner due to multi-site phosphorylation within the Ct. However, β-arrestin2 recruitment also depends on S/T residues within the ICLs, as well as G protein activation. **(F)** Then, the receptor clusters within clathrin-coated pits where it is immobilised prior to internalisation.

Chapter 7

References

Al-Hasani, R., & Bruchas, M. R. (2011). Molecular mechanisms of opioid receptor-dependent signaling and behavior. *Anesthesiology, 115*(6), 1363-1381. doi:10.1097/ALN.0b013e318238bba6

Alexander, S. P., Christopoulos, A., Davenport, A. P., Kelly, E., Marrion, N. V., Peters, J. A., . . . Davies, J. A. (2017). THE CONCISE GUIDE TO PHARMACOLOGY 2017/18: G protein-coupled receptors. *Br J Pharmacol, 174 Suppl 1*, S17-s129. doi:10.1111/bph.13878

Allouche, S., Noble, F., & Marie, N. (2014). Opioid receptor desensitization: mechanisms and its link to tolerance. *Front Pharmacol, 5*, 280. doi:10.3389/fphar.2014.00280

Almatroudi, A., Ostovar, M., Bailey, C. P., Husbands, S. M., & Bailey, S. J. (2018). Antidepressant-like effects of BU10119, a novel buprenorphine analogue with mixed kappa/mu receptor antagonist properties, in mice. *Br J Pharmacol, 175*(14), 2869-2880. doi:10.1111/bph.14060

Altarifi, A. A., David, B., Muchhala, K. H., Blough, B. E., Akbarali, H., & Negus, S. S. (2017). Effects of acute and repeated treatment with the biased mu opioid receptor agonist TRV130 (oliceridine) on measures of antinociception, gastrointestinal function, and abuse liability in rodents. *J Psychopharmacol, 31*(6), 730-739. doi:10.1177/0269881116689257

Andersson, H., D'Antona, A. M., Kendall, D. A., Von Heijne, G., & Chin, C. N. (2003). Membrane assembly of the cannabinoid receptor 1: impact of a long N-terminal tail. *Mol Pharmacol, 64*(3), 570-577. doi:10.1124/mol.64.3.570

Arttamangkul, S., Alvarez-Maubecin, V., Thomas, G., Williams, J. T., & Grandy, D. K. (2000). Binding and internalization of fluorescent opioid peptide conjugates in living cells. *Mol Pharmacol, 58*(6), 1570-1580.

Arttamangkul, S., Heinz, D. A., Bunzow, J. R., Song, X., & Williams, J. T. (2018). Cellular tolerance at the μ-opioid receptor is phosphorylation dependent. *eLife, 7*, e34989. doi:10.7554/eLife.34989

Austin Zamarripa, C., Edwards, S. R., Qureshi, H. N., Yi, J. N., Blough, B. E., & Freeman, K. B. (2018). The G-protein biased mu-opioid agonist, TRV130, produces reinforcing and antinociceptive effects that are comparable to oxycodone in rats. *Drug Alcohol Depend, 192*, 158-162. doi:10.1016/j.drugalcdep.2018.08.002

Ayling, L. J., Briddon, S. J., Halls, M. L., Hammond, G. R. V., Vaca, L., Pacheco, J., . . . Cooper, D. M. F. (2012). Adenylyl cyclase AC8 directly controls its micro-environment by recruiting the actin cytoskeleton in a cholesterol-rich milieu. *Journal of Cell Science, 125*(4), 869-886. doi:10.1242/jcs.091090

Bailey, C. P., Kelly, E., & Henderson, G. (2004). Protein kinase C activation enhances morphine-induced rapid desensitization of mu-opioid receptors in mature rat locus ceruleus neurons. *Mol Pharmacol, 66*(6), 1592-1598. doi:10.1124/mol.104.004747

Bailey, C. P., Llorente, J., Gabra, B. H., Smith, F. L., Dewey, W. L., Kelly, E., & Henderson, G. (2009). Role of protein kinase C and mu-opioid receptor (MOPr) desensitization in tolerance to morphine in rat locus coeruleus neurons. *Eur J Neurosci, 29*(2), 307-318. doi:10.1111/j.1460-9568.2008.06573.x

Bailey, C. P., Oldfield, S., Llorente, J., Caunt, C. J., Teschemacher, A. G., Roberts, L., . . . Henderson, G. (2009). Involvement of PKC alpha and G-protein-coupled receptor kinase 2 in agonist-selective desensitization of mu-opioid receptors in mature brain neurons. *Br J Pharmacol, 158*(1), 157-164. doi:10.1111/j.1476-5381.2009.00140.x

Ballesteros, J. A., & Weinstein, H. (1995). [19] Integrated methods for the construction of three-dimensional models and computational probing of structure-function relations

in G protein-coupled receptors. In S. C. Sealfon (Ed.), *Methods in Neurosciences* (Vol. 25, pp. 366-428): Academic Press.

Befort, K., Filliol, D., Decaillot, F. M., Gaveriaux-Ruff, C., Hoehe, M. R., & Kieffer, B. L. (2001). A single nucleotide polymorphic mutation in the human mu-opioid receptor severely impairs receptor signaling. *J Biol Chem, 276*(5), 3130-3137. doi:10.1074/jbc.M006352200

Berg, K. A., Maayani, S., Goldfarb, J., Scaramellini, C., Leff, P., & Clarke, W. P. (1998). Effector pathway-dependent relative efficacy at serotonin type 2A and 2C receptors: evidence for agonist-directed trafficking of receptor stimulus. *Mol Pharmacol, 54*(1), 94-104.

Berger, A. C., & Whistler, J. L. (2010). How to design an opioid drug that causes reduced tolerance and dependence. *Ann Neurol, 67*(5), 559-569. doi:10.1002/ana.22002

Bjarnadottir, T. K., Gloriam, D. E., Hellstrand, S. H., Kristiansson, H., Fredriksson, R., & Schioth, H. B. (2006). Comprehensive repertoire and phylogenetic analysis of the G protein-coupled receptors in human and mouse. *Genomics, 88*(3), 263-273. doi:10.1016/j.ygeno.2006.04.001

Black, J. W., & Leff, P. (1983). Operational models of pharmacological agonism. *Proc R Soc Lond B Biol Sci, 220*(1219), 141-162.

Bobeck, E. N., Ingram, S. L., Hermes, S. M., Aicher, S. A., & Morgan, M. M. (2016). Ligand-biased activation of extracellular signal-regulated kinase 1/2 leads to differences in opioid induced antinociception and tolerance. *Behav Brain Res, 298*(Pt B), 17-24. doi:10.1016/j.bbr.2015.10.032

Boerrigter, G., Soergel, D. G., Violin, J. D., Lark, M. W., & Burnett, J. C., Jr. (2012). TRV120027, a novel beta-arrestin biased ligand at the angiotensin II type I receptor, unloads the heart and maintains renal function when added to furosemide in experimental heart failure. *Circ Heart Fail, 5*(5), 627-634. doi:10.1161/circheartfailure.112.969220

Bohn, L. M., Lefkowitz, R. J., & Caron, M. G. (2002). Differential mechanisms of morphine antinociceptive tolerance revealed in (beta)arrestin-2 knock-out mice. *J Neurosci, 22*(23), 10494-10500.

Bohn, L. M., Lefkowitz, R. J., Gainetdinov, R. R., Peppel, K., Caron, M. G., & Lin, F. T. (1999). Enhanced morphine analgesia in mice lacking beta-arrestin 2. *Science, 286*(5449), 2495-2498.

Bradley, S. J., Wiegman, C. H., Iglesias, M. M., Kong, K. C., Butcher, A. J., Plouffe, B., . . . Tobin, A. B. (2016). Mapping physiological G protein-coupled receptor signaling pathways reveals a role for receptor phosphorylation in airway contraction. *Proc Natl Acad Sci U S A, 113*(16), 4524-4529. doi:10.1073/pnas.1521706113

Briddon, S. J., Kilpatrick, L. E., & Hill, S. J. (2018). Studying GPCR Pharmacology in Membrane Microdomains: Fluorescence Correlation Spectroscopy Comes of Age. *Trends Pharmacol Sci, 39*(2), 158-174. doi:10.1016/j.tips.2017.11.004

Briddon, S. J., Middleton, R. J., Cordeaux, Y., Flavin, F. M., Weinstein, J. A., George, M. W., . . . Hill, S. J. (2004). Quantitative analysis of the formation and diffusion of A1-adenosine receptor-antagonist complexes in single living cells. *Proc Natl Acad Sci U S A, 101*(13), 4673-4678. doi:10.1073/pnas.0400420101

Brownstein, M. J. (1993). A brief history of opiates, opioid peptides, and opioid receptors. *Proc Natl Acad Sci U S A, 90*(12), 5391-5393.

Brust, T. F., Morgenweck, J., Kim, S. A., Rose, J. H., Locke, J. L., Schmid, C. L., . . . Bohn, L. M. (2016). Biased agonists of the kappa opioid receptor suppress pain and itch without causing sedation or dysphoria. *Sci Signal, 9*(456), ra117. doi:10.1126/scisignal.aai8441

Cahill, T. J., Thomsen, A. R. B., Tarrasch, J. T., Plouffe, B., Nguyen, A. H., Yang, F., . . . Lefkowitz, R. J. (2017). Distinct conformations of GPCR–β-arrestin complexes mediate desensitization, signaling, and endocytosis. *Proceedings of the National Academy of Sciences, 114*(10), 2562-2567. doi:10.1073/pnas.1701529114

Calebiro, D., Nikolaev, V. O., Gagliani, M. C., de Filippis, T., Dees, C., Tacchetti, C., . . . Lohse, M. J. (2009). Persistent cAMP-signals triggered by internalized G-protein-coupled receptors. *PLoS Biol, 7*(8), e1000172. doi:10.1371/journal.pbio.1000172

Campbell, A. P., & Smrcka, A. V. (2018). Targeting G protein-coupled receptor signalling by blocking G proteins. *Nat Rev Drug Discov*. doi:10.1038/nrd.2018.135

Cassel, J. A., Daubert, J. D., & DeHaven, R. N. (2005). [(3)H]Alvimopan binding to the micro opioid receptor: comparative binding kinetics of opioid antagonists. *Eur J Pharmacol, 520*(1-3), 29-36. doi:10.1016/j.ejphar.2005.08.008

Cattaruzza, F., Amadesi, S., Carlsson, J. F., Murphy, J. E., Lyo, V., Kirkwood, K., . . . Bunnett, N. W. (2014). Serine proteases and protease-activated receptor 2 mediate the proinflammatory and algesic actions of diverse stimulants. *Br J Pharmacol, 171*(16), 3814-3826. doi:10.1111/bph.12738

Celver, J. P., Lowe, J., Kovoor, A., Gurevich, V. V., & Chavkin, C. (2001). Threonine 180 is required for G-protein-coupled receptor kinase 3- and beta-arrestin 2-mediated desensitization of the mu-opioid receptor in Xenopus oocytes. *J Biol Chem, 276*(7), 4894-4900. doi:10.1074/jbc.M007437200

Chakraborty, S., Nepiyushchikh, Z., Davis, M. J., Zawieja, D. C., & Muthuchamy, M. (2011). Substance P activates both contractile and inflammatory pathways in lymphatics through the neurokinin receptors NK1R and NK3R. *Microcirculation, 18*(1), 24-35. doi:10.1111/j.1549-8719.2010.00064.x

Che, T., Majumdar, S., Zaidi, S. A., Ondachi, P., McCorvy, J. D., Wang, S., . . . Roth, B. L. (2018). Structure of the Nanobody-Stabilized Active State of the Kappa Opioid Receptor. *Cell, 172*(1-2), 55-67.e15. doi:10.1016/j.cell.2017.12.011

Chen, C., Shahabi, V., Xu, W., & Liu-Chen, L. Y. (1998). Palmitoylation of the rat mu opioid receptor. *FEBS Lett, 441*(1), 148-152.

Chen, X.-T., Pitis, P., Liu, G., Yuan, C., Gotchev, D., Cowan, C. L., . . . Yamashita, D. S. (2013). Structure–Activity Relationships and Discovery of a G Protein Biased μ Opioid Receptor Ligand, [(3-Methoxythiophen-2-yl)methyl]({2-[(9R)-9-(pyridin-2-yl)-6-oxaspiro-[4.5]decan-9-yl]ethyl})amine (TRV130), for the Treatment of Acute Severe Pain. *Journal of Medicinal Chemistry, 56*(20), 8019-8031. doi:10.1021/jm4010829

Chen, Y., Yang, C., & Wang, Z. J. (2010). CAMKIIα IS REQUIRED FOR THE INITIATION AND MAINTENANCE OF OPIOID-INDUECED HYPERALGEISA. *The Journal of neuroscience : the official journal of the Society for Neuroscience, 30*(1), 38. doi:10.1523/JNEUROSCI.4346-09.2010

Chen, Y. J., Oldfield, S., Butcher, A. J., Tobin, A. B., Saxena, K., Gurevich, V. V., . . . Kelly, E. (2013). Identification of phosphorylation sites in the COOH-terminal tail of the mu-opioid receptor. *J Neurochem, 124*(2), 189-199. doi:10.1111/jnc.12071

Cherezov, V., Rosenbaum, D. M., Hanson, M. A., Rasmussen, S. G., Thian, F. S., Kobilka, T. S., . . . Stevens, R. C. (2007). High-resolution crystal structure of an engineered human beta2-adrenergic G protein-coupled receptor. *Science, 318*(5854), 1258-1265. doi:10.1126/science.1150577

Cho, D., Min, C., Jung, K., Cheong, S., Zheng, M., Cheong, S., . . . Kim, K. (2012). The N-terminal region of the dopamine D(2) receptor, a rhodopsin-like GPCR, regulates correct

integration into the plasma membrane and endocytic routes. *Br J Pharmacol, 166*(2), 659-675. doi:10.1111/j.1476-5381.2011.01787.x

Chu, J., Zheng, H., Zhang, Y., Loh, H. H., & Law, P. Y. (2010). Agonist-dependent mu-opioid receptor signaling can lead to heterologous desensitization. *Cell Signal, 22*(4), 684-696. doi:10.1016/j.cellsig.2009.12.003

Congreve, M., Dias, J. M., & Marshall, F. H. (2014). Structure-based drug design for G protein-coupled receptors. *Prog Med Chem, 53*, 1-63. doi:10.1016/b978-0-444-63380-4.00001-9

Connor, M., & Christie, M. D. (1999). Opioid receptor signalling mechanisms. *Clin Exp Pharmacol Physiol, 26*(7), 493-499.

Conti, M., Mika, D., & Richter, W. (2014). Cyclic AMP compartments and signaling specificity: Role of cyclic nucleotide phosphodiesterases. *J Gen Physiol, 143*(1), 29-38. doi:10.1085/jgp.201311083

Corbett, A. D., Henderson, G., McKnight, A. T., & Paterson, S. J. (2006). 75 years of opioid research: the exciting but vain quest for the Holy Grail. *Br J Pharmacol, 147 Suppl 1*, S153-162. doi:10.1038/sj.bjp.0706435

Corder, G., Tawfik, V. L., Wang, D., Sypek, E. I., Low, S. A., Dickinson, J. R., . . . Scherrer, G. (2017). Loss of mu opioid receptor signaling in nociceptors, but not microglia, abrogates morphine tolerance without disrupting analgesia. *Nat Med, 23*(2), 164-173. doi:10.1038/nm.4262

Cowan, A., Doxey, J. C., & Harry, E. J. (1977). The animal pharmacology of buprenorphine, an oripavine analgesic agent. *Br J Pharmacol, 60*(4), 547-554.

Dahan, A., Yassen, A., Romberg, R., Sarton, E., Teppema, L., Olofsen, E., & Danhof, M. (2006). Buprenorphine induces ceiling in respiratory depression but not in analgesia. *Br J Anaesth, 96*(5), 627-632. doi:10.1093/bja/ael051

Dang, V. C., & Christie, M. D. J. (2012). Mechanisms of rapid opioid receptor desensitization, resensitization and tolerance in brain neurons. *Br J Pharmacol, 165*(6), 1704-1716. doi:10.1111/j.1476-5381.2011.01482.x

Davis, M. P. (2012). Twelve reasons for considering buprenorphine as a frontline analgesic in the management of pain. *J Support Oncol, 10*(6), 209-219. doi:10.1016/j.suponc.2012.05.002

De Lean, A., Stadel, J. M., & Lefkowitz, R. J. (1980). A ternary complex model explains the agonist-specific binding properties of the adenylate cyclase-coupled beta-adrenergic receptor. *J Biol Chem, 255*(15), 7108-7117.

DeFea, K. (2000). β-Arrestin–Dependent Endocytosis of Proteinase-Activated Receptor 2 Is Required for Intracellular Targeting of Activated Erk1/2. *148*(6), 1267-1282.

Defea, K. (2008). Beta-arrestins and heterotrimeric G-proteins: collaborators and competitors in signal transduction. *Br J Pharmacol, 153 Suppl 1*, S298-309. doi:10.1038/sj.bjp.0707508

DeFea, K. A. (2011). Beta-arrestins as regulators of signal termination and transduction: how do they determine what to scaffold? *Cell Signal, 23*(4), 621-629. doi:10.1016/j.cellsig.2010.10.004

Dessauer, C. W. (2009). Adenylyl Cyclase–A-kinase Anchoring Protein Complexes: The Next Dimension in cAMP Signaling. *Mol Pharmacol, 76*(5), 935-941. doi:10.1124/mol.109.059345

DeVree, B. T., Mahoney, J. P., Velez-Ruiz, G. A., Rasmussen, S. G., Kuszak, A. J., Edwald, E., . . . Sunahara, R. K. (2016). Allosteric coupling from G protein to the agonist-binding pocket in GPCRs. *Nature, 535*(7610), 182-186. doi:10.1038/nature18324

DeWire, S. M., Ahn, S., Lefkowitz, R. J., & Shenoy, S. K. (2007). Beta-arrestins and cell signaling. *Annu Rev Physiol, 69*, 483-510. doi:10.1146/annurev.ph.69.013107.100021

DeWire, S. M., Yamashita, D. S., Rominger, D. H., Liu, G., Cowan, C. L., Graczyk, T. M., . . . Violin, J. D. (2013). A G Protein-Biased Ligand at the -Opioid Receptor Is Potently Analgesic with Reduced Gastrointestinal and Respiratory Dysfunction Compared with Morphine. *Journal of Pharmacology and Experimental Therapeutics, 344*(3), 708-717. doi:10.1124/jpet.112.201616

Dhawan, B. N., Cesselin, F., Raghubir, R., Reisine, T., Bradley, P. B., Portoghese, P. S., & Hamon, M. (1996). International Union of Pharmacology. XII. Classification of opioid receptors. *Pharmacol Rev, 48*(4), 567-592.

Diekmann, S., & Hoischen, C. (2014). Biomolecular dynamics and binding studies in the living cell. *Phys Life Rev, 11*(1), 1-30. doi:10.1016/j.plrev.2013.11.011

Dietis, N., Niwa, H., Tose, R., McDonald, J., Ruggieri, V., Filaferro, M., . . . Lambert, D. G. (2018). In vitro and in vivo characterization of the bifunctional mu and delta opioid receptor ligand UFP-505. *Br J Pharmacol, 175*(14), 2881-2896. doi:10.1111/bph.14199

Dijksterhuis, J. P., Petersen, J., & Schulte, G. (2014). WNT/Frizzled signalling: receptor-ligand selectivity with focus on FZD-G protein signalling and its physiological relevance: IUPHAR Review 3. *Br J Pharmacol, 171*(5), 1195-1209. doi:10.1111/bph.12364

Dixon, R. A., Sigal, I. S., Rands, E., Register, R. B., Candelore, M. R., Blake, A. D., & Strader, C. D. (1987). Ligand binding to the beta-adrenergic receptor involves its rhodopsin-like core. *Nature, 326*(6108), 73-77. doi:10.1038/326073a0

Dohlman, H. G., & Thorner, J. (1997). RGS proteins and signaling by heterotrimeric G proteins. *J Biol Chem, 272*(7), 3871-3874.

Doll, C., Konietzko, J., Poll, F., Koch, T., Hollt, V., & Schulz, S. (2011). Agonist-selective patterns of micro-opioid receptor phosphorylation revealed by phosphosite-specific antibodies. *Br J Pharmacol, 164*(2), 298-307. doi:10.1111/j.1476-5381.2011.01382.x

Donthamsetti, P., Gallo, E. F., Buck, D. C., Stahl, E. L., Zhu, Y., Lane, J. R., . . . Javitch, J. A. (2018). Arrestin recruitment to dopamine D2 receptor mediates locomotion but not incentive motivation. *Molecular Psychiatry*. doi:10.1038/s41380-018-0212-4

Dore, A. S., Okrasa, K., Patel, J. C., Serrano-Vega, M., Bennett, K., Cooke, R. M., . . . Marshall, F. H. (2014). Structure of class C GPCR metabotropic glutamate receptor 5 transmembrane domain. *Nature, 511*(7511), 557-562. doi:10.1038/nature13396

Draper-Joyce, C. J., Khoshouei, M., Thal, D. M., Liang, Y. L., Nguyen, A. T. N., Furness, S. G. B., . . . Christopoulos, A. (2018). Structure of the adenosine-bound human adenosine A1 receptor-Gi complex. *Nature, 558*(7711), 559-563. doi:10.1038/s41586-018-0236-6

Duttaroy, A., & Yoburn, B. C. (1995). The effect of intrinsic efficacy on opioid tolerance. *Anesthesiology, 82*(5), 1226-1236.

Eichel, K., Jullie, D., Barsi-Rhyne, B., Latorraca, N. R., Masureel, M., Sibarita, J. B., . . . von Zastrow, M. (2018). Catalytic activation of beta-arrestin by GPCRs. *Nature, 557*(7705), 381-386. doi:10.1038/s41586-018-0079-1

Eissenberg, T., Greenwald, M. K., Johnson, R. E., Liebson, I. A., Bigelow, G. E., & Stitzer, M. L. (1996). Buprenorphine's physical dependence potential: antagonist-precipitated withdrawal in humans. *J Pharmacol Exp Ther, 276*(2), 449-459.

Einstein, R., Jordan, H., Zhou, W., Brenner, M., Moses, E. G., & Liggett, S. B. (2008). Alternative splicing of the G protein-coupled receptor superfamily in human airway smooth muscle diversifies the complement of receptors. *Proc Natl Acad Sci U S A, 105*(13), 5230-5235. doi:10.1073/pnas.0801319105

El Kouhen, R., Burd, A. L., Erickson-Herbrandson, L. J., Chang, C. Y., Law, P. Y., & Loh, H. H. (2001). Phosphorylation of Ser363, Thr370, and Ser375 residues within the carboxyl tail differentially regulates mu-opioid receptor internalization. *J Biol Chem, 276*(16), 12774-12780. doi:10.1074/jbc.M009571200

Estrada, J. A., & Kaufman, M. P. (2018). micro-Opioid receptors inhibit the exercise pressor reflex by closing N-type calcium channels but not by opening GIRK channels in rats. *Am J Physiol Regul Integr Comp Physiol, 314*(5), R693-R699. doi:10.1152/ajpregu.00380.2017

Evron, T., Daigle, T. L., & Caron, M. G. (2012). GRK2: multiple roles beyond G protein-coupled receptor desensitization. *Trends Pharmacol Sci, 33*(3), 154-164. doi:10.1016/j.tips.2011.12.003

Fan, X., Zhang, J., Zhang, X., Yue, W., & Ma, L. (2002). Acute and chronic morphine treatments and morphine withdrawal differentially regulate GRK2 and GRK5 gene expression in rat brain. *Neuropharmacology, 43*(5), 809-816.

Fang, Y., Kenakin, T., & Liu, C. (2015). Editorial: Orphan GPCRs As Emerging Drug Targets. *Front Pharmacol, 6*. doi:10.3389/fphar.2015.00295

Feng, B., Li, Z., & Wang, J. B. (2011). Protein Kinase C-Mediated Phosphorylation of the -Opioid Receptor and Its Effects on Receptor Signaling. *Mol Pharmacol, 79*(4), 768-775. doi:10.1124/mol.110.069096

Ferguson, S. S. (2001). Evolving concepts in G protein-coupled receptor endocytosis: the role in receptor desensitization and signaling. *Pharmacol Rev, 53*(1), 1-24.

Ferrandon, S., Feinstein, T. N., Castro, M., Wang, B., Bouley, R., Potts, J. T., . . . Vilardaga, J. P. (2009). Sustained cyclic AMP production by parathyroid hormone receptor endocytosis. *Nat Chem Biol, 5*(10), 734-742. doi:10.1038/nchembio.206

Floyd, C. N., & Warren, J. B. (2018). Opioids out of control. *Br J Clin Pharmacol, 84*(5), 813-815. doi:10.1111/bcp.13346

Fredriksson, R., Lagerstrom, M. C., Lundin, L. G., & Schioth, H. B. (2003). The G-protein-coupled receptors in the human genome form five main families. Phylogenetic analysis, paralogon groups, and fingerprints. *Mol Pharmacol, 63*(6), 1256-1272. doi:10.1124/mol.63.6.1256

Gaibelet, G., Millot, C., Lebrun, C., Ravault, S., Saulière, A., André, A., . . . Lopez, A. (2008). Cholesterol content drives distinct pharmacological behaviours of μ-opioid receptor in different microdomains of the CHO plasma membrane. *Molecular Membrane Biology, 25*(5), 423-435. doi:10.1080/09687680802203380

Galligan, J. J., & Akbarali, H. I. (2014). Molecular Physiology of Enteric Opioid Receptors. *Am J Gastroenterol Suppl, 2*(1), 17-21. doi:10.1038/ajgsup.2014.5

Gesty-Palmer, D., Yuan, L., Martin, B., Wood, W. H., 3rd, Lee, M. H., Janech, M. G., . . . Maudsley, S. (2013). beta-arrestin-selective G protein-coupled receptor agonists engender unique biological efficacy in vivo. *Mol Endocrinol, 27*(2), 296-314. doi:10.1210/me.2012-1091

Gherbi, K., May, L. T., Baker, J. G., Briddon, S. J., & Hill, S. J. (2015). Negative cooperativity across β(1)-adrenoceptor homodimers provides insights into the nature of the

secondary low-affinity CGP 12177 β1-adrenoceptor binding conformation. *FASEB J, 29*(7), 2859-2871. doi:10.1096/fj.14-265199

Glück, L., Loktev, A., Moulédous, L., Mollereau, C., Law, P.-Y., & Schulz, S. (2014). Loss of Morphine Reward and Dependence in Mice Lacking G Protein-Coupled Receptor Kinase 5. *Biological psychiatry, 76*(10), 767-774. doi:10.1016/j.biopsych.2014.01.021

Godbole, A., Lyga, S., Lohse, M. J., & Calebiro, D. (2017). Internalized TSH receptors en route to the TGN induce local G(s)-protein signaling and gene transcription. *Nat Commun, 8*. doi:10.1038/s41467-017-00357-2

Goldstein, A., & Cox, B. M. (1977). Opioid peptides (endorphins) in pituitary and brain. *Psychoneuroendocrinology, 2*(1), 11-16. doi:https://doi.org/10.1016/0306-4530(77)90027-0

Gomes, I., Ijzerman, A. P., Ye, K., Maillet, E. L., & Devi, L. A. (2011). G Protein-Coupled Receptor Heteromerization: A Role in Allosteric Modulation of Ligand Binding. *Mol Pharmacol, 79*(6), 1044.

Goodman, O. B., Jr., Krupnick, J. G., Gurevich, V. V., Benovic, J. L., & Keen, J. H. (1997). Arrestin/clathrin interaction. Localization of the arrestin binding locus to the clathrin terminal domain. *J Biol Chem, 272*(23), 15017-15022.

Granier, S., Manglik, A., Kruse, A. C., Kobilka, T. S., Thian, F. S., Weis, W. I., & Kobilka, B. K. (2012). Structure of the delta-opioid receptor bound to naltrindole. *Nature, 485*(7398), 400-404. doi:10.1038/nature11111

Gregorio, G. G., Masureel, M., Hilger, D., Terry, D. S., Juette, M., Zhao, H., . . . Blanchard, S. C. (2017). Single-molecule analysis of ligand efficacy in beta2AR-G-protein activation. *Nature, 547*(7661), 68-73. doi:10.1038/nature22354

Griffin, M. T., Figueroa, K. W., Liller, S., & Ehlert, F. J. (2007). Estimation of agonist activity at G protein-coupled receptors: analysis of M2 muscarinic receptor signaling through Gi/o,Gs, and G15. *J Pharmacol Exp Ther, 321*(3), 1193-1207. doi:10.1124/jpet.107.120857

Groer, C. E., Schmid, C. L., Jaeger, A. M., & Bohn, L. M. (2011). Agonist-directed interactions with specific beta-arrestins determine mu-opioid receptor trafficking, ubiquitination, and dephosphorylation. *J Biol Chem, 286*(36), 31731-31741. doi:10.1074/jbc.M111.248310

Groer, C. E., Tidgewell, K., Moyer, R. A., Harding, W. W., Rothman, R. B., Prisinzano, T. E., & Bohn, L. M. (2007). An opioid agonist that does not induce mu-opioid receptor--arrestin interactions or receptor internalization. *Mol Pharmacol, 71*(2), 549-557. doi:10.1124/mol.106.028258

Grundmann, M., Merten, N., Malfacini, D., Inoue, A., Preis, P., Simon, K., . . . Kostenis, E. (2018). Lack of beta-arrestin signaling in the absence of active G proteins. *Nat Commun, 9*(1), 341. doi:10.1038/s41467-017-02661-3

Guillemin, R., Vargo, T., Rossier, J., Minick, S., Ling, N., Rivier, C., . . . Bloom, F. (1977). beta-Endorphin and adrenocorticotropin are selected concomitantly by the pituitary gland. *Science, 197*(4311), 1367-1369.

Gunther, T., Dasgupta, P., Mann, A., Miess, E., Kliewer, A., Fritzwanker, S., . . . Schulz, S. (2018). Targeting multiple opioid receptors - improved analgesics with reduced side effects? *Br J Pharmacol, 175*(14), 2857-2868. doi:10.1111/bph.13809

Gurevich, V. V., & Gurevich, E. V. (2006). The structural basis of arrestin-mediated regulation of G-protein-coupled receptors. *Pharmacol Ther, 110*(3), 465-502. doi:10.1016/j.pharmthera.2005.09.008

Hague, C., Chen, Z., Pupo, A. S., Schulte, N. A., Toews, M. L., & Minneman, K. P. (2004). The N terminus of the human alpha1D-adrenergic receptor prevents cell surface expression. *J Pharmacol Exp Ther, 309*(1), 388-397. doi:10.1124/jpet.103.060509

Hall, R. A., Premont, R. T., & Lefkowitz, R. J. (1999). Heptahelical Receptor Signaling: Beyond the G Protein Paradigm. *J Cell Biol, 145*(5), 927-932.

Halls, M. L. (2012). Constitutive formation of an RXFP1-signalosome: a novel paradigm in GPCR function and regulation. *Br J Pharmacol, 165*(6), 1644-1658. doi:10.1111/j.1476-5381.2011.01470.x

Halls, M. L., & Canals, M. (2018). Genetically Encoded FRET Biosensors to Illuminate Compartmentalised GPCR Signalling. *Trends Pharmacol Sci, 39*(2), 148-157. doi:10.1016/j.tips.2017.09.005

Halls, M. L., & Cooper, D. M. F. (2010). Sub-picomolar relaxin signalling by a pre-assembled RXFP1, AKAP79, AC2, β-arrestin 2, PDE4D3 complex. *Embo j, 29*(16), 2772-2787. doi:10.1038/emboj.2010.168

Halls, M. L., Yeatman, H. R., Nowell, C. J., Thompson, G. L., Gondin, A. B., Civciristov, S., . . . Canals, M. (2016). Plasma membrane localization of the mu-opioid receptor controls spatiotemporal signaling. *Sci Signal, 9*(414), ra16. doi:10.1126/scisignal.aac9177

Hanoune, J., & Defer, N. (2001). Regulation and role of adenylyl cyclase isoforms. *Annu Rev Pharmacol Toxicol, 41*, 145-174. doi:10.1146/annurev.pharmtox.41.1.145

Hauser, A. S., Attwood, M. M., Rask-Andersen, M., Schioth, H. B., & Gloriam, D. E. (2017). Trends in GPCR drug discovery: new agents, targets and indications. *Nat Rev Drug Discov, 16*(12), 829-842. doi:10.1038/nrd.2017.178

Hauser, A. S., Chavali, S., Masuho, I., Jahn, L. J., Martemyanov, K. A., Gloriam, D. E., & Babu, M. M. (2018). Pharmacogenomics of GPCR Drug Targets. *Cell, 172*(1-2), 41-54 e19. doi:10.1016/j.cell.2017.11.033

Haustein, E., & Schwille, P. (2004). Single-molecule spectroscopic methods. *Curr Opin Struct Biol, 14*(5), 531-540. doi:10.1016/j.sbi.2004.09.004

He, Zhang, Z. N., Guan, J. S., Liu, H. R., Zhao, B., Wang, H. B., . . . Zhang, X. (2011). Facilitation of mu-opioid receptor activity by preventing delta-opioid receptor-mediated codegradation. *Neuron, 69*(1), 120-131. doi:10.1016/j.neuron.2010.12.001

He, L., Fong, J., von Zastrow, M., & Whistler, J. L. (2002). Regulation of opioid receptor trafficking and morphine tolerance by receptor oligomerization. *Cell, 108*(2), 271-282.

He, L., & Whistler, J. L. (2005). An opiate cocktail that reduces morphine tolerance and dependence. *Curr Biol, 15*(11), 1028-1033. doi:10.1016/j.cub.2005.04.052

Heng, B. C., Aubel, D., & Fussenegger, M. (2013). An overview of the diverse roles of G-protein coupled receptors (GPCRs) in the pathophysiology of various human diseases. *Biotechnol Adv, 31*(8), 1676-1694. doi:10.1016/j.biotechadv.2013.08.017

Hill, R., Disney, A., Conibear, A., Sutcliffe, K., Dewey, W., Husbands, S., . . . Henderson, G. (2018). The novel mu-opioid receptor agonist PZM21 depresses respiration and induces tolerance to antinociception. *Br J Pharmacol, 175*(13), 2653-2661. doi:10.1111/bph.14224

Ho, J. H., Stahl, E. L., Schmid, C. L., Scarry, S. M., Aube, J., & Bohn, L. M. (2018). G protein signaling-biased agonism at the kappa-opioid receptor is maintained in striatal neurons. *Sci Signal, 11*(542). doi:10.1126/scisignal.aar4309

Huang, P., Xu, W., Yoon, S. I., Chen, C., Chong, P. L., Unterwald, E. M., & Liu-Chen, L. Y. (2007). Agonist treatment did not affect association of mu opioid receptors with lipid rafts

and cholesterol reduction had opposite effects on the receptor-mediated signaling in rat brain and CHO cells. *Brain Res, 1184*, 46-56. doi:10.1016/j.brainres.2007.09.096

Huang, W., Manglik, A., Venkatakrishnan, A. J., Laeremans, T., Feinberg, E. N., Sanborn, A. L., . . . Kobilka, B. K. (2015). Structural insights into micro-opioid receptor activation. *Nature, 524*(7565), 315-321. doi:10.1038/nature14886

Hubbard, K. B., & Hepler, J. R. (2006). Cell signalling diversity of the Gqalpha family of heterotrimeric G proteins. *Cell Signal, 18*(2), 135-150. doi:10.1016/j.cellsig.2005.08.004

Hughes, J., Smith, T. W., Kosterlitz, H. W., Fothergill, L. A., Morgan, B. A., & Morris, H. R. (1975). Identification of two related pentapeptides from the brain with potent opiate agonist activity. *Nature, 258*(5536), 577-580.

Illing, S., Mann, A., & Schulz, S. (2014a). Heterologous regulation of agonist-independent mu-opioid receptor phosphorylation by protein kinase C. *Br J Pharmacol, 171*(5), 1330-1340. doi:10.1111/bph.12546

Illing, S., Mann, A., & Schulz, S. (2014b). Heterologous regulation of agonist-independent μ-opioid receptor phosphorylation by protein kinase C. *Br J Pharmacol, 171*(5), 1330-1340. doi:10.1111/bph.12546

Inturrisi, C. E. (2002). Clinical pharmacology of opioids for pain. *Clin J Pain, 18*(4 Suppl), S3-13.

Irannejad, R., Pessino, V., Mika, D., Huang, B., Wedegaertner, P. B., Conti, M., & von Zastrow, M. (2017). Functional selectivity of GPCR-directed drug action through location bias. *Nat Chem Biol, 13*(7), 799-806. doi:10.1038/nchembio.2389

Irannejad, R., Tomshine, J. C., Tomshine, J. R., Chevalier, M., Mahoney, J. P., Steyaert, J., . . . von Zastrow, M. (2013). Conformational biosensors reveal GPCR signalling from endosomes. *Nature, 495*(7442), 534-538. doi:10.1038/nature12000

Janecka, A., Fichna, J., & Janecki, T. (2004). Opioid receptors and their ligands. *Curr Top Med Chem, 4*(1), 1-17.

Jazayeri, A., Rappas, M., Brown, A. J. H., Kean, J., Errey, J. C., Robertson, N. J., . . . Marshall, F. H. (2017). Crystal structure of the GLP-1 receptor bound to a peptide agonist. *Nature, 546*(7657), 254-258. doi:10.1038/nature22800

Jensen, D. D., Halls, M. L., Murphy, J. E., Canals, M., Cattaruzza, F., Poole, D. P., . . . Bunnett, N. W. (2014). Endothelin-converting enzyme 1 and beta-arrestins exert spatiotemporal control of substance P-induced inflammatory signals. *J Biol Chem, 289*(29), 20283-20294. doi:10.1074/jbc.M114.578179

Jensen, D. D., Lieu, T., Halls, M. L., Veldhuis, N. A., Imlach, W. L., Mai, Q. N., . . . Bunnett, N. W. (2017). Neurokinin 1 receptor signaling in endosomes mediates sustained nociception and is a viable therapeutic target for prolonged pain relief. *Science Translational Medicine, 9*(392). doi:10.1126/scitranslmed.aal3447

Jiang, L. I., Collins, J., Davis, R., Lin, K. M., DeCamp, D., Roach, T., . . . Sternweis, P. C. (2007). Use of a cAMP BRET Sensor to Characterize a Novel Regulation of cAMP by the Sphingosine 1-Phosphate/G(13) Pathway. *J Biol Chem, 282*(14), 10576-10584. doi:10.1074/jbc.M609695200

Johnson, E. A., Oldfield, S., Braksator, E., Gonzalez-Cuello, A., Couch, D., Hall, K. J., . . . Henderson, G. (2006). Agonist-selective mechanisms of mu-opioid receptor desensitization in human embryonic kidney 293 cells. *Mol Pharmacol, 70*(2), 676-685. doi:10.1124/mol.106.022376

Jordan, B. A., & Devi, L. A. (1999). G-protein-coupled receptor heterodimerization modulates receptor function. *Nature, 399*(6737), 697-700. doi:10.1038/21441

Just, S., Illing, S., Trester-Zedlitz, M., Lau, E. K., Kotowski, S. J., Miess, E., . . . Schulz, S. (2013). Differentiation of opioid drug effects by hierarchical multi-site phosphorylation. *Mol Pharmacol, 83*(3), 633-639. doi:10.1124/mol.112.082875

Kang, Y., Zhou, X. E., Gao, X., He, Y., Liu, W., Ishchenko, A., . . . Xu, H. E. (2015). Crystal structure of rhodopsin bound to arrestin by femtosecond X-ray laser. *Nature, 523*(7562), 561-567. doi:10.1038/nature14656

Kang, Y., Zhou, X. E., Gao, X., He, Y., Liu, W., Ishchenko, A., . . . Xu, H. E. (2015). Crystal structure of rhodopsin bound to arrestin by femtosecond X-ray laser. *Nature, 523*(7562), 561-567. doi:10.1038/nature14656

Katritch, V., Fenalti, G., Abola, E. E., Roth, B. L., Cherezov, V., & Stevens, R. C. (2014). Allosteric sodium in class A GPCR signaling. *Trends in biochemical sciences, 39*(5), 233-244. doi:10.1016/j.tibs.2014.03.002

Keith, D. E., Anton, B., Murray, S. R., Zaki, P. A., Chu, P. C., Lissin, D. V., . . . von Zastrow, M. (1998). mu-Opioid receptor internalization: opiate drugs have differential effects on a conserved endocytic mechanism in vitro and in the mammalian brain. *Mol Pharmacol, 53*(3), 377-384.

Keith, D. E., Murray, S. R., Zaki, P. A., Chu, P. C., Lissin, D. V., Kang, L., . . . von Zastrow, M. (1996). Morphine activates opioid receptors without causing their rapid internalization. *J Biol Chem, 271*(32), 19021-19024.

Kelly, E. (2013). Ligand bias at the mu-opioid receptor. *Biochem Soc Trans, 41*(1), 218-224. doi:10.1042/BST20120331

Kelly, E., Bailey, C. P., & Henderson, G. (2008). Agonist-selective mechanisms of GPCR desensitization. *Br J Pharmacol, 153*(Suppl 1), S379-388. doi:10.1038/sj.bjp.0707604

Kenakin. (2017). Signaling bias in drug discovery. *Expert Opinion on Drug Discovery, 12*(4), 321-333. doi:10.1080/17460441.2017.1297417

Kenakin, T. (2015). The Effective Application of Biased Signaling to New Drug Discovery. *Mol Pharmacol, 88*(6), 1055-1061. doi:10.1124/mol.115.099770

Kenakin, T. (2018). Is the Quest for Signaling Bias Worth the Effort? *Mol Pharmacol, 93*(4), 266-269. doi:10.1124/mol.117.111187

Kenakin, T., Watson, C., Muniz-Medina, V., Christopoulos, A., & Novick, S. (2012). A simple method for quantifying functional selectivity and agonist bias. *ACS Chem Neurosci, 3*(3), 193-203. doi:10.1021/cn200111m

Khan, S. M., Sleno, R., Gora, S., Zylbergold, P., Laverdure, J. P., Labbe, J. C., . . . Hebert, T. E. (2013). The expanding roles of Gbetagamma subunits in G protein-coupled receptor signaling and drug action. *Pharmacol Rev, 65*(2), 545-577. doi:10.1124/pr.111.005603

Klein Herenbrink, C., Sykes, D. A., Donthamsetti, P., Canals, M., Coudrat, T., Shonberg, J., . . . Lane, J. R. (2016). The role of kinetic context in apparent biased agonism at GPCRs. *Nat Commun, 7*, 10842. doi:10.1038/ncomms10842

Koblish, M., Carr, R., 3rd, Siuda, E. R., Rominger, D. H., Gowen-MacDonald, W., Cowan, C. L., . . . Lark, M. W. (2017). TRV0109101, a G Protein-Biased Agonist of the micro-Opioid Receptor, Does Not Promote Opioid-Induced Mechanical Allodynia following Chronic Administration. *J Pharmacol Exp Ther, 362*(2), 254-262. doi:10.1124/jpet.117.241117

Koehl, A., Hu, H., Maeda, S., Zhang, Y., Qu, Q., Paggi, J. M., . . . Kobilka, B. K. (2018). Structure of the micro-opioid receptor-Gi protein complex. *Nature, 558*(7711), 547-552. doi:10.1038/s41586-018-0219-7

Kruegel, A. C., Gassaway, M. M., Kapoor, A., Varadi, A., Majumdar, S., Filizola, M., . . . Sames, D. (2016). Synthetic and Receptor Signaling Explorations of the Mitragyna Alkaloids:

Mitragynine as an Atypical Molecular Framework for Opioid Receptor Modulators. *J Am Chem Soc, 138*(21), 6754-6764. doi:10.1021/jacs.6b00360

Kruse, A. C., Ring, A. M., Manglik, A., Hu, J., Hu, K., Eitel, K., . . . Kobilka, B. K. (2013). Activation and allosteric modulation of a muscarinic acetylcholine receptor. *Nature, 504*(7478), 101-106. doi:10.1038/nature12735

Kuszak, A. J., Pitchiaya, S., Anand, J. P., Mosberg, H. I., Walter, N. G., & Sunahara, R. K. (2009). Purification and functional reconstitution of monomeric mu-opioid receptors: allosteric modulation of agonist binding by Gi2. *J Biol Chem, 284*(39), 26732-26741. doi:10.1074/jbc.M109.026922

Lagerstrom, M. C., & Schioth, H. B. (2008). Structural diversity of G protein-coupled receptors and significance for drug discovery. *Nat Rev Drug Discov, 7*(4), 339-357. doi:10.1038/nrd2518

Lam, R., Gondin, A. B., Canals, M., Kellam, B., Briddon, S. J., Graham, B., & Scammells, P. J. (2018). Fluorescently Labeled Morphine Derivatives for Bioimaging Studies. *J Med Chem, 61*(3), 1316-1329. doi:10.1021/acs.jmedchem.7b01811

Lamb, K., Tidgewell, K., Simpson, D. S., Bohn, L. M., & Prisinzano, T. E. (2012). Antinociceptive effects of herkinorin, a MOP receptor agonist derived from salvinorin A in the formalin test in rats: new concepts in mu opioid receptor pharmacology: from a symposium on new concepts in mu-opioid pharmacology. *Drug Alcohol Depend, 121*(3), 181-188. doi:10.1016/j.drugalcdep.2011.10.026

Lan, T. H., Liu, Q., Li, C., Wu, G., & Lambert, N. A. (2012). Sensitive and high resolution localization and tracking of membrane proteins in live cells with BRET. *Traffic, 13*(11), 1450-1456. doi:10.1111/j.1600-0854.2012.01401.x

Laporte, S. A., Oakley, R. H., Holt, J. A., Barak, L. S., & Caron, M. G. (2000). The interaction of beta-arrestin with the AP-2 adaptor is required for the clustering of beta 2-adrenergic receptor into clathrin-coated pits. *J Biol Chem, 275*(30), 23120-23126. doi:10.1074/jbc.M002581200

Latorraca, N. R., Wang, J. K., Bauer, B., Townshend, R. J. L., Hollingsworth, S. A., Olivieri, J. E., . . . Dror, R. O. (2018). Molecular mechanism of GPCR-mediated arrestin activation. *Nature, 557*(7705), 452-456. doi:10.1038/s41586-018-0077-3

Lau, E. K., Trester-Zedlitz, M., Trinidad, J. C., Kotowski, S. J., Krutchinsky, A. N., Burlingame, A. L., & von Zastrow, M. (2011). Quantitative encoding of the effect of a partial agonist on individual opioid receptors by multisite phosphorylation and threshold detection. *Sci Signal, 4*(185), ra52. doi:10.1126/scisignal.2001748

Law, P. Y., Wong, Y. H., & Loh, H. H. (2000). Molecular mechanisms and regulation of opioid receptor signaling. *Annu Rev Pharmacol Toxicol, 40*, 389-430. doi:10.1146/annurev.pharmtox.40.1.389

Le Roy, C., & Wrana, J. L. (2005). Clathrin- and non-clathrin-mediated endocytic regulation of cell signalling. *Nat Rev Mol Cell Biol, 6*(2), 112-126. doi:10.1038/nrm1571

Liang, X., Yong, Z., & Su, R. (2018). Inhibition of protein kinase A and GIRK channel reverses fentanyl-induced respiratory depression. *Neurosci Lett, 677*, 14-18. doi:10.1016/j.neulet.2018.04.029

Liang, Y. L., Khoshouei, M., Glukhova, A., Furness, S. G. B., Zhao, P., Clydesdale, L., . . . Wootten, D. (2018). Phase-plate cryo-EM structure of a biased agonist-bound human GLP-1 receptor-Gs complex. *Nature, 555*(7694), 121-125. doi:10.1038/nature25773

Liang, Y. L., Khoshouei, M., Radjainia, M., Zhang, Y., Glukhova, A., Tarrasch, J., . . . Sexton, P. M. (2017). Phase-plate cryo-EM structure of a class B GPCR-G-protein complex. *Nature, 546*(7656), 118-123. doi:10.1038/nature22327

Liu, J. J., Horst, R., Katritch, V., Stevens, R. C., & Wuthrich, K. (2012). Biased signaling pathways in beta2-adrenergic receptor characterized by 19F-NMR. *Science, 335*(6072), 1106-1110. doi:10.1126/science.1215802

Livingston, K. E., Mahoney, J. P., Manglik, A., Sunahara, R. K., & Traynor, J. R. (2018). Measuring ligand efficacy at the mu-opioid receptor using a conformational biosensor. *eLife, 7*. doi:10.7554/eLife.32499

Livingston, K. E., & Traynor, J. R. (2018). Allostery at opioid receptors: modulation with small molecule ligands. *Br J Pharmacol, 175*(14), 2846-2856. doi:10.1111/bph.13823

Loh, H. H., Liu, H. C., Cavalli, A., Yang, W., Chen, Y. F., & Wei, L. N. (1998). mu Opioid receptor knockout in mice: effects on ligand-induced analgesia and morphine lethality. *Brain Res Mol Brain Res, 54*(2), 321-326.

Lohse, M. J., Maiellaro, I., & Calebiro, D. (2014). Kinetics and mechanism of G protein-coupled receptor activation. *Curr Opin Cell Biol, 27*, 87-93. doi:10.1016/j.ceb.2013.11.009

Lu, Z., Xu, J., Rossi, G. C., Majumdar, S., Pasternak, G. W., & Pan, Y.-X. (2015). Mediation of opioid analgesia by a truncated 6-transmembrane GPCR. *Journal of Clinical Investigation, 125*(7), 2626-2630. doi:10.1172/jci81070

Luttrell, L. M. (2001). Activation and targeting of extracellular signal-regulated. *98*(5), 2449-2454. doi:10.1073/pnas.041604898

Luttrell, L. M., Ferguson, S. S., Daaka, Y., Miller, W. E., Maudsley, S., Della Rocca, G. J., . . . Lefkowitz, R. J. (1999). Beta-arrestin-dependent formation of beta2 adrenergic receptor-Src protein kinase complexes. *Science, 283*(5402), 655-661.

Luttrell, L. M., & Gesty-Palmer, D. (2010). Beyond Desensitization: Physiological Relevance of Arrestin-Dependent Signaling. *Pharmacol Rev, 62*(2), 305-330. doi:10.1124/pr.109.002436

Luttrell, L. M., Wang, J., Plouffe, B., Smith, J. S., Yamani, L., Kaur, S., . . . Lefkowitz, R. J. (2018). Manifold roles of beta-arrestins in GPCR signaling elucidated with siRNA and CRISPR/Cas9. *Sci Signal, 11*(549). doi:10.1126/scisignal.aat7650

Madariaga-Mazón, A., Marmolejo-Valencia, A. F., Li, Y., Toll, L., Houghten, R. A., & Martinez-Mayorga, K. (2017). Mu-Opioid receptor biased ligands: A safer and painless discovery of analgesics? *Drug Discovery Today, 22*(11), 1719-1729. doi:10.1016/j.drudis.2017.07.002

Maguire, M. E., Van Arsdale, P. M., & Gilman, A. G. (1976). An agonist-specific effect of guanine nucleotides on binding to the beta adrenergic receptor. *Mol Pharmacol, 12*(2), 335-339.

Manchikanti, L., Helm, S., 2nd, Fellows, B., Janata, J. W., Pampati, V., Grider, J. S., & Boswell, M. V. (2012). Opioid epidemic in the United States. *Pain Physician, 15*(3 Suppl), Es9-38.

Manglik, A., Kim, T. H., Masureel, M., Altenbach, C., Yang, Z., Hilger, D., . . . Kobilka, B. K. (2015). Structural Insights into the Dynamic Process of beta2-Adrenergic Receptor Signaling. *Cell, 161*(5), 1101-1111. doi:10.1016/j.cell.2015.04.043

Manglik, A., & Kruse, A. C. (2017). Structural Basis for G Protein-Coupled Receptor Activation. *Biochemistry, 56*(42), 5628-5634. doi:10.1021/acs.biochem.7b00747

Manglik, A., Kruse, A. C., Kobilka, T. S., Thian, F. S., Mathiesen, J. M., Sunahara, R. K., . . . Granier, S. (2012). Crystal structure of the micro-opioid receptor bound to a morphinan antagonist. *Nature, 485*(7398), 321-326. doi:10.1038/nature10954

Manglik, A., Lin, H., Aryal, D. K., McCorvy, J. D., Dengler, D., Corder, G., . . . Shoichet, B. K. (2016). Structure-based discovery of opioid analgesics with reduced side effects. *Nature, 537*(7619), 185-190. doi:10.1038/nature19112

Mansour, A., Hoversten, M. T., Taylor, L. P., Watson, S. J., & Akil, H. (1995). The cloned mu, delta and kappa receptors and their endogenous ligands: evidence for two opioid peptide recognition cores. *Brain Res, 700*(1-2), 89-98.

Marino, K. A., Prada-Gracia, D., Provasi, D., & Filizola, M. (2016). Impact of Lipid Composition and Receptor Conformation on the Spatio-temporal Organization of mu-Opioid Receptors in a Multi-component Plasma Membrane Model. *PLoS Comput Biol, 12*(12), e1005240. doi:10.1371/journal.pcbi.1005240

Marrone, G. F., Grinnell, S. G., Lu, Z., Rossi, G. C., Le Rouzic, V., Xu, J., . . . Pasternak, G. W. (2016). Truncated mu opioid GPCR variant involvement in opioid-dependent and opioid-independent pain modulatory systems within the CNS. *Proc Natl Acad Sci U S A, 113*(13), 3663-3668. doi:10.1073/pnas.1523894113

Masuho, I., Martemyanov, K. A., & Lambert, N. A. (2015). Monitoring G protein activation in cells with BRET. *Methods Mol Biol, 1335*, 107-113. doi:10.1007/978-1-4939-2914-6_8

Masuho, I., Ostrovskaya, O., Kramer, G. M., Jones, C. D., Xie, K., & Martemyanov, K. A. (2015). Distinct profiles of functional discrimination among G proteins determine the actions of G protein-coupled receptors. *Sci Signal, 8*(405), ra123. doi:10.1126/scisignal.aab4068

Matthes, H. W., Maldonado, R., Simonin, F., Valverde, O., Slowe, S., Kitchen, I., . . . Kieffer, B. L. (1996). Loss of morphine-induced analgesia, reward effect and withdrawal symptoms in mice lacking the mu-opioid-receptor gene. *Nature, 383*(6603), 819-823. doi:10.1038/383819a0

McDonald, P. H., Chow, C. W., Miller, W. E., Laporte, S. A., Field, M. E., Lin, F. T., . . . Lefkowitz, R. J. (2000). Beta-arrestin 2: a receptor-regulated MAPK scaffold for the activation of JNK3. *Science, 290*(5496), 1574-1577.

McPherson, J., Rivero, G., Baptist, M., Llorente, J., Al-Sabah, S., Krasel, C., . . . Kelly, E. (2010). mu-opioid receptors: correlation of agonist efficacy for signalling with ability to activate internalization. *Mol Pharmacol, 78*(4), 756-766. doi:10.1124/mol.110.066613

Mehta, S., Zhang, Y., Roth, R. H., Zhang, J. F., Mo, A., Tenner, B., . . . Zhang, J. (2018). Single-fluorophore biosensors for sensitive and multiplexed detection of signalling activities. *Nat Cell Biol, 20*(10), 1215-1225. doi:10.1038/s41556-018-0200-6

Melkes, B., Hejnova, L., & Novotny, J. (2016). Biased mu-opioid receptor agonists diversely regulate lateral mobility and functional coupling of the receptor to its cognate G proteins. *Naunyn Schmiedebergs Arch Pharmacol, 389*(12), 1289-1300. doi:10.1007/s00210-016-1293-8

Mercadante, S., Casuccio, A., Agnello, A., Serretta, R., Calderone, L., & Barresi, L. (1998). Morphine versus methadone in the pain treatment of advanced-cancer patients followed up at home. *J Clin Oncol, 16*(11), 3656-3661. doi:10.1200/jco.1998.16.11.3656

Michel, M. C., & Charlton, S. J. (2018). Biased Agonism in Drug Discovery-Is It Too Soon to Choose a Path? *Mol Pharmacol, 93*(4), 259-265. doi:10.1124/mol.117.110890

Michel, M. C., Seifert, R., & Bond, R. A. (2014). Dynamic bias and its implications for GPCR drug discovery. *Nat Rev Drug Discov, 13*(11), 869. doi:10.1038/nrd3954-c3

Miess, E., Gondin, A. B., Yousuf, A., Steinborn, R., Mosslein, N., Yang, Y., . . . Canals, M. (2018). Multisite phosphorylation is required for sustained interaction with GRKs and arrestins during rapid mu-opioid receptor desensitization. *Sci Signal, 11*(539). doi:10.1126/scisignal.aas9609

Mizobe, T., Maze, M., Lam, V., Suryanarayana, S., & Kobilka, B. K. (1996). Arrangement of transmembrane domains in adrenergic receptors. Similarity to bacteriorhodopsin. *J Biol Chem, 271*(5), 2387-2389.

Molinari, P., Vezzi, V., Sbraccia, M., Gro, C., Riitano, D., Ambrosio, C., . . . Costa, T. (2010). Morphine-like opiates selectively antagonize receptor-arrestin interactions. *J Biol Chem, 285*(17), 12522-12535. doi:10.1074/jbc.M109.059410

Mollereau, C., Parmentier, M., Mailleux, P., Butour, J. L., Moisand, C., Chalon, P., . . . Meunier, J. C. (1994). ORL1, a novel member of the opioid receptor family. Cloning, functional expression and localization. *FEBS Lett, 341*(1), 33-38.

Montandon, G., Ren, J., Victoria, N. C., Liu, H., Wickman, K., Greer, J. J., & Horner, R. L. (2016). G-protein-gated Inwardly Rectifying Potassium Channels Modulate Respiratory Depression by Opioids. *Anesthesiology, 124*(3), 641-650. doi:10.1097/aln.0000000000000984

Morgan, M. M., & Christie, M. D. J. (2011). Analysis of opioid efficacy, tolerance, addiction and dependence from cell culture to human. *Br J Pharmacol, 164*(4), 1322-1334. doi:10.1111/j.1476-5381.2011.01335.x

Morse, M., Sun, H., Tran, E., Levenson, R., & Fang, Y. (2013). Label-free integrative pharmacology on-target of opioid ligands at the opioid receptor family. *BMC Pharmacology and Toxicology, 14*(1), 17. doi:10.1186/2050-6511-14-17

Mullershausen, F., Zecri, F., Cetin, C., Billich, A., Guerini, D., & Seuwen, K. (2009). Persistent signaling induced by FTY720-phosphate is mediated by internalized S1P1 receptors. *Nat Chem Biol, 5*(6), 428-434. doi:10.1038/nchembio.173

Nehme, R., Carpenter, B., Singhal, A., Strege, A., Edwards, P. C., White, C. F., . . . Tate, C. G. (2017). Mini-G proteins: Novel tools for studying GPCRs in their active conformation. *PLoS One, 12*(4), e0175642. doi:10.1371/journal.pone.0175642

Nickolls, S. A. (2013). Co-Expression of GRK2 Reveals a Novel Conformational State of the μ-Opioid Receptor. *8*(12). doi:10.1371/journal.pone.0083691

Nickolls, S. A., Humphreys, S., Clark, M., & McMurray, G. (2013). Co-expression of GRK2 reveals a novel conformational state of the micro-opioid receptor. *PLoS One, 8*(12), e83691. doi:10.1371/journal.pone.0083691

North, R. A., & Williams, J. T. (1985). On the potassium conductance increased by opioids in rat locus coeruleus neurones. *J Physiol, 364*, 265-280.

O'Hara, P. J., Sheppard, P. O., Thogersen, H., Venezia, D., Haldeman, B. A., McGrane, V., . . . Mulvihill, E. R. (1993). The ligand-binding domain in metabotropic glutamate receptors is related to bacterial periplasmic binding proteins. *Neuron, 11*(1), 41-52.

O'Hayre, M., Eichel, K., Avino, S., Zhao, X., Steffen, D. J., Feng, X., . . . Gutkind, J. S. (2017). Genetic evidence that beta-arrestins are dispensable for the initiation of beta2-adrenergic receptor signaling to ERK. *Sci Signal, 10*(484). doi:10.1126/scisignal.aal3395

Oertel, B. G., Kettner, M., Scholich, K., Renne, C., Roskam, B., Geisslinger, G., . . . Lotsch, J. (2009). A common human micro-opioid receptor genetic variant diminishes the

receptor signaling efficacy in brain regions processing the sensory information of pain. *J Biol Chem, 284*(10), 6530-6535. doi:10.1074/jbc.M807030200

Palczewski, K., Kumasaka, T., Hori, T., Behnke, C. A., Motoshima, H., Fox, B. A., . . . Miyano, M. (2000). Crystal structure of rhodopsin: A G protein-coupled receptor. *Science, 289*(5480), 739-745.

Pan, L., Xu, J., Yu, R., Xu, M. M., Pan, Y. X., & Pasternak, G. W. (2005). Identification and characterization of six new alternatively spliced variants of the human mu opioid receptor gene, Oprm. *Neuroscience, 133*(1), 209-220. doi:10.1016/j.neuroscience.2004.12.033

Pang, P. S., Butler, J., Collins, S. P., Cotter, G., Davison, B. A., Ezekowitz, J. A., . . . Felker, G. M. (2017). Biased ligand of the angiotensin II type 1 receptor in patients with acute heart failure: a randomized, double-blind, placebo-controlled, phase IIB, dose ranging trial (BLAST-AHF). *Eur Heart J, 38*(30), 2364-2373. doi:10.1093/eurheartj/ehx196

Park, P. S. H., Lodowski, D. T., & Palczewski, K. (2008). Activation of G Protein–Coupled Receptors: Beyond Two-State Models and Tertiary Conformational Changes. *Annu Rev Pharmacol Toxicol, 48*, 107-141. doi:10.1146/annurev.pharmtox.48.113006.094630

Pasternak, G. W., & Pan, Y. X. (2013). Mu opioids and their receptors: evolution of a concept. *Pharmacol Rev, 65*(4), 1257-1317. doi:10.1124/pr.112.007138

Pathan, H., & Williams, J. (2012). Basic opioid pharmacology: an update. *Br J Pain, 6*(1), 11-16. doi:10.1177/2049463712438493

Pattinson, K. T. (2008). Opioids and the control of respiration. *Br J Anaesth, 100*(6), 747-758. doi:10.1093/bja/aen094

Penela, P., Murga, C., Ribas, C., Lafarga, V., & Mayor, F. (2010). The complex G protein-coupled receptor kinase 2 (GRK2) interactome unveils new physiopathological targets. *Br J Pharmacol, 160*(4), 821-832. doi:10.1111/j.1476-5381.2010.00727.x

Pergolizzi, LeQuang, J. A., Taylor, R., Jr., Ossipov, M. H., Colucci, D., & Raffa, R. B. (2018). Designing safer analgesics: a focus on mu-opioid receptor pathways. *Expert Opin Drug Discov*, 1-8. doi:10.1080/17460441.2018.1511539

Pergolizzi, J., Aloisi, A. M., Dahan, A., Filitz, J., Langford, R., Likar, R., . . . Weinbroum, A. A. (2010). Current knowledge of buprenorphine and its unique pharmacological profile. *Pain Pract, 10*(5), 428-450. doi:10.1111/j.1533-2500.2010.00378.x

Pert, C. B., Pasternak, G., & Snyder, S. H. (1973). Opiate agonists and antagonists discriminated by receptor binding in brain. *Science, 182*(4119), 1359-1361.

Petaja-Repo, U. E., Hogue, M., Laperriere, A., Bhalla, S., Walker, P., & Bouvier, M. (2001). Newly synthesized human delta opioid receptors retained in the endoplasmic reticulum are retrotranslocated to the cytosol, deglycosylated, ubiquitinated, and degraded by the proteasome. *J Biol Chem, 276*(6), 4416-4423. doi:10.1074/jbc.M007151200

Petaja-Repo, U. E., Hogue, M., Laperriere, A., Walker, P., & Bouvier, M. (2000). Export from the endoplasmic reticulum represents the limiting step in the maturation and cell surface expression of the human delta opioid receptor. *J Biol Chem, 275*(18), 13727-13736.

Peterson, Y. K., & Luttrell, L. M. (2017). The Diverse Roles of Arrestin Scaffolds in G Protein–Coupled Receptor Signaling. *Pharmacol Rev, 69*(3), 256-297. doi:10.1124/pr.116.013367

Pierce, K. L., Premont, R. T., & Lefkowitz, R. J. (2002). Seven-transmembrane receptors. *Nat Rev Mol Cell Biol, 3*(9), 639-650. doi:10.1038/nrm908

Portoghese, P. S., Sultana, M., & Takemori, A. E. (1990). Design of peptidomimetic delta opioid receptor antagonists using the message-address concept. *J Med Chem, 33*(6), 1714-1720.

Pradhan, A. A., Smith, M. L., Kieffer, B. L., & Evans, C. J. (2012). Ligand-directed signalling within the opioid receptor family. *Br J Pharmacol, 167*(5), 960-969. doi:10.1111/j.1476-5381.2012.02075.x

Pucadyil, T. J., Mukherjee, S., & Chattopadhyay, A. (2007). Organization and dynamics of NBD-labeled lipids in membranes analyzed by fluorescence recovery after photobleaching. *J Phys Chem B, 111*(8), 1975-1983. doi:10.1021/jp066092h

Qiu, Y., Wang, Y., Law, P. Y., Chen, H. Z., & Loh, H. H. (2011). Cholesterol regulates micro-opioid receptor-induced beta-arrestin 2 translocation to membrane lipid rafts. *Mol Pharmacol, 80*(1), 210-218. doi:10.1124/mol.110.070870

Raehal, K. M. (2005). Morphine Side Effects in -Arrestin 2 Knockout Mice. *Journal of Pharmacology and Experimental Therapeutics, 314*(3), 1195-1201. doi:10.1124/jpet.105.087254

Raehal, K. M., Schmid, C. L., Groer, C. E., & Bohn, L. M. (2011). Functional selectivity at the mu-opioid receptor: implications for understanding opioid analgesia and tolerance. *Pharmacol Rev, 63*(4), 1001-1019. doi:10.1124/pr.111.004598

Raehal, K. M., Walker, J. K., & Bohn, L. M. (2005). Morphine side effects in beta-arrestin 2 knockout mice. *J Pharmacol Exp Ther, 314*(3), 1195-1201. doi:10.1124/jpet.105.087254

Raffa, R. B., Elling, C., & Tzschentke, T. M. (2018). Does 'Strong Analgesic' Equal 'Strong Opioid'? Tapentadol and the Concept of 'μ-Load'. *Advances in Therapy, 35*(10), 1471-1484. doi:10.1007/s12325-018-0778-x

Raffa, R. B., Martinez, R. P., & Connelly, C. D. (1994). G-protein antisense oligodeoxyribonucleotides and mu-opioid supraspinal antinociception. *Eur J Pharmacol, 258*(1-2), R5-7.

Rajagopal, S., Ahn, S., Rominger, D. H., Gowen-MacDonald, W., Lam, C. M., Dewire, S. M., . . . Lefkowitz, R. J. (2011). Quantifying ligand bias at seven-transmembrane receptors. *Mol Pharmacol, 80*(3), 367-377. doi:10.1124/mol.111.072801

Rappoport, J. Z., Kemal, S., Benmerah, A., & Simon, S. M. (2006). Dynamics of clathrin and adaptor proteins during endocytosis. *Am J Physiol Cell Physiol, 291*(5), C1072-1081. doi:10.1152/ajpcell.00160.2006

Rask-Andersen, M., Masuram, S., & Schioth, H. B. (2014). The druggable genome: Evaluation of drug targets in clinical trials suggests major shifts in molecular class and indication. *Annu Rev Pharmacol Toxicol, 54*, 9-26. doi:10.1146/annurev-pharmtox-011613-135943

Rasmussen, S. G., DeVree, B. T., Zou, Y., Kruse, A. C., Chung, K. Y., Kobilka, T. S., . . . Kobilka, B. K. (2011). Crystal structure of the beta2 adrenergic receptor-Gs protein complex. *Nature, 477*(7366), 549-555. doi:10.1038/nature10361

Reinscheid, R. K., Nothacker, H. P., Bourson, A., Ardati, A., Henningsen, R. A., Bunzow, J. R., . . . Civelli, O. (1995). Orphanin FQ: a neuropeptide that activates an opioidlike G protein-coupled receptor. *Science, 270*(5237), 792-794.

Revankar, C. M., Cimino, D. F., Sklar, L. A., Arterburn, J. B., & Prossnitz, E. R. (2005). A transmembrane intracellular estrogen receptor mediates rapid cell signaling. *Science, 307*(5715), 1625-1630. doi:10.1126/science.1106943

Rezvani, A., Huidobro-Toro, J. P., Hu, J., & Way, E. L. (1983). A rapid and simple method for the quantitative determination of tolerance development to opiates in the guinea-pig ileum in vitro. *J Pharmacol Exp Ther, 225*(2), 251-255.

Ribas, C., Penela, P., Murga, C., Salcedo, A., Garcia-Hoz, C., Jurado-Pueyo, M., . . . Mayor, F., Jr. (2007). The G protein-coupled receptor kinase (GRK) interactome: role of GRKs in GPCR regulation and signaling. *Biochim Biophys Acta, 1768*(4), 913-922. doi:10.1016/j.bbamem.2006.09.019

Ring, A. M., Manglik, A., Kruse, A. C., Enos, M. D., Weis, W. I., Garcia, K. C., & Kobilka, B. K. (2013). Adrenaline-activated structure of beta2-adrenoceptor stabilized by an engineered nanobody. *Nature, 502*(7472), 575-579. doi:10.1038/nature12572

Rivero, G., Llorente, J., McPherson, J., Cooke, A., Mundell, S. J., McArdle, C. A., . . . Kelly, E. (2012). Endomorphin-2: a biased agonist at the mu-opioid receptor. *Mol Pharmacol, 82*(2), 178-188. doi:10.1124/mol.112.078659

Rogacki, M. K., Golfetto, O., Tobin, S. J., Li, T., Biswas, S., Jorand, R., . . . Vukojevic, V. (2018). Dynamic lateral organization of opioid receptors (kappa, muwt and muN40D) in the plasma membrane at the nanoscale level. *Traffic*. doi:10.1111/tra.12582

Rosenblum, A., Marsch, L. A., Joseph, H., & Portenoy, R. K. (2008). Opioids and the Treatment of Chronic Pain: Controversies, Current Status, and Future Directions. *Experimental and clinical psychopharmacology, 16*(5), 405-416. doi:10.1037/a0013628

Rostami, A., Rabbani, M., & Mir-Mohammad-Sadeghi, M. (2010). The Role of N53Q Mutation on the Rat μ-Opioid Receptor Function. *J Biomol Tech, 21*(2), 92-96.

Rudd, R. A., Seth, P., David, F., & Scholl, L. (2016). Increases in Drug and Opioid-Involved Overdose Deaths - United States, 2010-2015. *MMWR Morb Mortal Wkly Rep, 65*(5051), 1445-1452. doi:10.15585/mmwr.mm655051e1

Santos, R., Ursu, O., Gaulton, A., Bento, A. P., Donadi, R. S., Bologa, C. G., . . . Overington, J. P. (2017). A comprehensive map of molecular drug targets. *Nat Rev Drug Discov, 16*(1), 19-34. doi:10.1038/nrd.2016.230

Sauliere-Nzeh Ndong, A., Millot, C., Corbani, M., Mazeres, S., Lopez, A., & Salome, L. (2010). Agonist-selective dynamic compartmentalization of human Mu opioid receptor as revealed by resolutive FRAP analysis. *J Biol Chem, 285*(19), 14514-14520. doi:10.1074/jbc.M109.076695

Scheerer, P., Park, J. H., Hildebrand, P. W., Kim, Y. J., Krauss, N., Choe, H. W., . . . Ernst, O. P. (2008). Crystal structure of opsin in its G-protein-interacting conformation. *Nature, 455*(7212), 497-502. doi:10.1038/nature07330

Scheerer, P., & Sommer, M. E. (2017). Structural mechanism of arrestin activation. *Curr Opin Struct Biol, 45*, 160-169. doi:10.1016/j.sbi.2017.05.001

Schmid, C. L., Kennedy, N. M., Ross, N. C., Lovell, K. M., Yue, Z., Morgenweck, J., . . . Bohn, L. M. (2017). Bias Factor and Therapeutic Window Correlate to Predict Safer Opioid Analgesics. *Cell, 171*(5), 1165-1175 e1113. doi:10.1016/j.cell.2017.10.035

Schmid, C. L., Streicher, J. M., Groer, C. E., Munro, T. A., Zhou, L., & Bohn, L. M. (2013). Functional selectivity of 6'-guanidinonaltrindole (6'-GNTI) at kappa-opioid receptors in striatal neurons. *J Biol Chem, 288*(31), 22387-22398. doi:10.1074/jbc.M113.476234

Schulz, S., Mayer, D., Pfeiffer, M., Stumm, R., Koch, T., & Höllt, V. (2004). Morphine induces terminal μ-opioid receptor desensitization by sustained phosphorylation of serine-375. *Embo j, 23*(16), 3282-3289. doi:10.1038/sj.emboj.7600334

Seward, E., Hammond, C., & Henderson, G. (1991). Mu-opioid-receptor-mediated inhibition of the N-type calcium-channel current. *Proc Biol Sci, 244*(1310), 129-135. doi:10.1098/rspb.1991.0061

Shenoy, S. K., Modi, A. S., Shukla, A. K., Xiao, K., Berthouze, M., Ahn, S., . . . Lefkowitz, R. J. (2009). Beta-arrestin-dependent signaling and trafficking of 7-transmembrane receptors is reciprocally regulated by the deubiquitinase USP33 and the E3 ligase Mdm2. *Proc Natl Acad Sci U S A, 106*(16), 6650-6655. doi:10.1073/pnas.0901083106

Shukla, A. K., Manglik, A., Kruse, A. C., Xiao, K., Reis, R. I., Tseng, W. C., . . . Lefkowitz, R. J. (2013). Structure of active beta-arrestin-1 bound to a G-protein-coupled receptor phosphopeptide. *Nature, 497*(7447), 137-141. doi:10.1038/nature12120

Singla, N., Minkowitz, H. S., Soergel, D. G., Burt, D. A., Subach, R. A., Salamea, M. Y., . . . Skobieranda, F. (2017). A randomized, Phase IIb study investigating oliceridine (TRV130), a novel micro-receptor G-protein pathway selective (mu-GPS) modulator, for the management of moderate to severe acute pain following abdominoplasty. *J Pain Res, 10*, 2413-2424. doi:10.2147/JPR.S137952

Siu, F. Y., He, M., de Graaf, C., Han, G. W., Yang, D., Zhang, Z., . . . Stevens, R. C. (2013). Structure of the human glucagon class B G-protein-coupled receptor. *Nature, 499*(7459), 444-449. doi:10.1038/nature12393

Soave, M., Stoddart, L. A., Brown, A., Woolard, J., & Hill, S. J. (2016). Use of a new proximity assay (NanoBRET) to investigate the ligand-binding characteristics of three fluorescent ligands to the human β. *Pharmacol Res Perspect, 4*(5). doi:10.1002/prp2.250

Soergel, D. G., Subach, R. A., Burnham, N., Lark, M. W., James, I. E., Sadler, B. M., . . . Webster, L. R. (2014). Biased agonism of the mu-opioid receptor by TRV130 increases analgesia and reduces on-target adverse effects versus morphine: A randomized, double-blind, placebo-controlled, crossover study in healthy volunteers. *Pain, 155*(9), 1829-1835. doi:10.1016/j.pain.2014.06.011

Soergel, D. G., Subach, R. A., Sadler, B., Connell, J., Marion, A. S., Cowan, C. L., . . . Lark, M. W. (2014). First clinical experience with TRV130: pharmacokinetics and pharmacodynamics in healthy volunteers. *J Clin Pharmacol, 54*(3), 351-357. doi:10.1002/jcph.207

Sounier, R., Mas, C., Steyaert, J., Laeremans, T., Manglik, A., Huang, W., . . . Granier, S. (2015). Propagation of conformational changes during mu-opioid receptor activation. *Nature, 524*(7565), 375-378. doi:10.1038/nature14680

Sprouse-Blum, A. S., Smith, G., Sugai, D., & Parsa, F. D. (2010). Understanding Endorphins and Their Importance in Pain Management. *Hawaii Med J, 69*(3), 70-71.

Standifer, K. M., & Pasternak, G. W. (1997). G proteins and opioid receptor-mediated signalling. *Cell Signal, 9*(3-4), 237-248. doi:10.1016/s0898-6568(96)00174-x

Stanley, N., Pardo, L., & Fabritiis, G. D. (2016). The pathway of ligand entry from the membrane bilayer to a lipid G protein-coupled receptor. *Scientific Reports, 6*, 22639. doi:10.1038/srep22639

Staus, D. P., Strachan, R. T., Manglik, A., Pani, B., Kahsai, A. W., Kim, T. H., . . . Lefkowitz, R. J. (2016). Allosteric nanobodies reveal the dynamic range and diverse mechanisms of G-protein-coupled receptor activation. *Nature, 535*(7612), 448-452. doi:10.1038/nature18636

Staus, D. P., Wingler, L. M., Choi, M., Pani, B., Manglik, A., Kruse, A. C., & Lefkowitz, R. J. (2018). Sortase ligation enables homogeneous GPCR phosphorylation to reveal diversity in

beta-arrestin coupling. *Proc Natl Acad Sci U S A, 115*(15), 3834-3839. doi:10.1073/pnas.1722336115

Stoeber, M., Jullie, D., Lobingier, B. T., Laeremans, T., Steyaert, J., Schiller, P. W., . . . von Zastrow, M. (2018). A Genetically Encoded Biosensor Reveals Location Bias of Opioid Drug Action. *Neuron, 98*(5), 963-976 e965. doi:10.1016/j.neuron.2018.04.021

Strasser, A., Wittmann, H. J., & Seifert, R. (2008). Ligand-specific contribution of the N terminus and E2-loop to pharmacological properties of the histamine H1-receptor. *J Pharmacol Exp Ther, 326*(3), 783-791. doi:10.1124/jpet.108.140913

Sun, R. Q., Tu, Y. J., Lawand, N. B., Yan, J. Y., Lin, Q., & Willis, W. D. (2004). Calcitonin gene-related peptide receptor activation produces PKA- and PKC-dependent mechanical hyperalgesia and central sensitization. *J Neurophysiol, 92*(5), 2859-2866. doi:10.1152/jn.00339.2004

Sungkaworn, T., Jobin, M. L., Burnecki, K., Weron, A., Lohse, M. J., & Calebiro, D. (2017). Single-molecule imaging reveals receptor-G protein interactions at cell surface hot spots. *Nature, 550*(7677), 543-547. doi:10.1038/nature24264

Syrovatkina, V., Alegre, K. O., Dey, R., & Huang, X. Y. (2016). Regulation, Signaling, and Physiological Functions of G-Proteins. *J Mol Biol, 428*(19), 3850-3868. doi:10.1016/j.jmb.2016.08.002

Szczepek, M., Beyrière, F., Hofmann, K. P., Elgeti, M., Kazmin, R., Rose, A., . . . Scheerer, P. (2014). Crystal structure of a common GPCR-binding interface for G protein and arrestin. *Nature Communications, 5*(1). doi:10.1038/ncomms5801

Szekeres, P. G., Koenig, J. A., & Edwardson, J. M. (1998). The relationship between agonist intrinsic activity and the rate of endocytosis of muscarinic receptors in a human neuroblastoma cell line. *Mol Pharmacol, 53*(4), 759-765.

Takita, K., Herlenius, E. A., Lindahl, S. G., & Yamamoto, Y. (1997). Actions of opioids on respiratory activity via activation of brainstem mu-, delta- and kappa-receptors; an in vitro study. *Brain Res, 778*(1), 233-241.

Tang, L., Shukla, P. K., Wang, L. X., & Wang, Z. J. (2006). Reversal of morphine antinociceptive tolerance and dependence by the acute supraspinal inhibition of Ca(2+)/calmodulin-dependent protein kinase II. *J Pharmacol Exp Ther, 317*(2), 901-909. doi:10.1124/jpet.105.097733

Terskiy, A., Wannemacher, K. M., Yadav, P. N., Tsai, M., Tian, B., & Howells, R. D. (2007). Search of the human proteome for endomorphin-1 and endomorphin-2 precursor proteins. *Life Sci, 81*(23-24), 1593-1601. doi:10.1016/j.lfs.2007.09.025

Thal, D. M., Glukhova, A., Sexton, P. M., & Christopoulos, A. (2018). Structural insights into G-protein-coupled receptor allostery. *Nature, 559*(7712), 45-53. doi:10.1038/s41586-018-0259-z

Thompson, Lane, J. R., Coudrat, T., Sexton, P. M., Christopoulos, A., & Canals, M. (2015). Biased Agonism of Endogenous Opioid Peptides at the -Opioid Receptor. *Mol Pharmacol, 88*(2), 335-346. doi:10.1124/mol.115.098848

Thompson, A. A., Liu, W., Chun, E., Katritch, V., Wu, H., Vardy, E., . . . Stevens, R. C. (2012). Structure of the nociceptin/orphanin FQ receptor in complex with a peptide mimetic. *Nature, 485*(7398), 395-399. doi:10.1038/nature11085

Thomsen, A. R. B., Jensen, D. D., Hicks, G. A., & Bunnett, N. W. (2018). Therapeutic Targeting of Endosomal G-Protein-Coupled Receptors. *Trends Pharmacol Sci, 39*(10), 879-891. doi:10.1016/j.tips.2018.08.003

Thomsen, A. R. B., Plouffe, B., Cahill, T. J., 3rd, Shukla, A. K., Tarrasch, J. T., Dosey, A. M., . . . Lefkowitz, R. J. (2016). GPCR-G Protein-beta-Arrestin Super-Complex Mediates Sustained G Protein Signaling. *Cell, 166*(4), 907-919. doi:10.1016/j.cell.2016.07.004

Tian, X., Kang, D. S., & Benovic, J. L. (2014). β-arrestins and G Protein-Coupled Receptor Trafficking. *Handb Exp Pharmacol, 219*, 173-186. doi:10.1007/978-3-642-41199-1_9

Tohgo, A., Pierce, K. L., Choy, E. W., Lefkowitz, R. J., & Luttrell, L. M. (2002). beta-Arrestin scaffolding of the ERK cascade enhances cytosolic ERK activity but inhibits ERK-mediated transcription following angiotensin AT1a receptor stimulation. *J Biol Chem, 277*(11), 9429-9436. doi:10.1074/jbc.M106457200

Tota, M. R., & Strader, C. D. (1990). Characterization of the binding domain of the beta-adrenergic receptor with the fluorescent antagonist carazolol. Evidence for a buried ligand binding site. *J Biol Chem, 265*(28), 16891-16897.

Toth, A. D., Prokop, S., Gyombolai, P., Varnai, P., Balla, A., Gurevich, V. V., . . . Turu, G. (2018). Heterologous phosphorylation-induced formation of a stability lock permits regulation of inactive receptors by beta-arrestins. *J Biol Chem, 293*(3), 876-892. doi:10.1074/jbc.M117.813139

Traynor, J. (2012). μ-Opioid Receptors and Regulators of G protein Signaling (RGS) proteins: From a symposium on new concepts in mu-opioid pharmacology. *Drug and Alcohol Dependence, 121*(3), 173-180. doi:10.1016/j.drugalcdep.2011.10.027

Tumati, S., Largent-Milnes, T. M., Keresztes, A., Ren, J., Roeske, W. R., Vanderah, T. W., & Varga, E. V. (2012). Repeated morphine treatment-mediated hyperalgesia, allodynia and spinal glial activation are blocked by co-administration of a selective cannabinoid receptor type-2 agonist. *Journal of Neuroimmunology, 244*(1-2), 23-31. doi:10.1016/j.jneuroim.2011.12.021

Ueda, H., & Ueda, M. (2009). Mechanisms underlying morphine analgesic tolerance and dependence. *Front Biosci (Landmark Ed), 14*, 5260-5272.

van der Merwe, J. Q., Moreau, F., & MacNaughton, W. K. (2009). Protease-activated receptor-2 stimulates intestinal epithelial chloride transport through activation of PLC and selective PKC isoforms. *Am J Physiol Gastrointest Liver Physiol, 296*(6), G1258-1266. doi:10.1152/ajpgi.90425.2008

Villiger, J. W., & Taylor, K. M. (1982). Buprenorphine: high-affinity binding to dorsal spinal cord. *J Neurochem, 38*(6), 1771-1773.

Vincent, K., Cornea, V. M., Jong, Y.-J. I., Laferrière, A., Kumar, N., Mickeviciute, A., . . . Coderre, T. J. (2016). Intracellular mGluR5 plays a critical role in neuropathic pain. *Nature Communications, 7*. doi:10.1038/ncomms10604

Violin, J. D., Crombie, A. L., Soergel, D. G., & Lark, M. W. (2014). Biased ligands at G-protein-coupled receptors: promise and progress. *Trends Pharmacol Sci, 35*(7), 308-316. doi:10.1016/j.tips.2014.04.007

Violin, J. D., DeWire, S. M., Yamashita, D., Rominger, D. H., Nguyen, L., Schiller, K., . . . Lark, M. W. (2010). Selectively engaging beta-arrestins at the angiotensin II type 1 receptor reduces blood pressure and increases cardiac performance. *J Pharmacol Exp Ther, 335*(3), 572-579. doi:10.1124/jpet.110.173005

Virk, M. S., Arttamangkul, S., Birdsong, W. T., & Williams, J. T. (2009). Buprenorphine is a weak partial agonist that inhibits opioid receptor desensitization. *J Neurosci, 29*(22), 7341-7348. doi:10.1523/jneurosci.3723-08.2009

Viscusi, E. R., Webster, L., Kuss, M., Daniels, S., Bolognese, J. A., Zuckerman, S., . . . Skobieranda, F. (2016). A randomized, phase 2 study investigating TRV130, a biased

ligand of the mu-opioid receptor, for the intravenous treatment of acute pain. *Pain, 157*(1), 264-272. doi:10.1097/j.pain.0000000000000363

Volpe, D. A., Tobin, G. A. M., Mellon, R. D., Katki, A. G., Parker, R. J., Colatsky, T., . . . Verbois, S. L. (2011). Uniform assessment and ranking of opioid Mu receptor binding constants for selected opioid drugs. *Regulatory Toxicology and Pharmacology, 59*(3), 385-390. doi:10.1016/j.yrtph.2010.12.007

Vukojevic, V., Ming, Y., D'Addario, C., Hansen, M., Langel, U., Schulz, R., . . . Terenius, L. (2008). Mu-opioid receptor activation in live cells. *FASEB J, 22*(10), 3537-3548. doi:10.1096/fj.08-108894

Vukojevic, V., Ming, Y., D'Addario, C., Rigler, R., Johansson, B., & Terenius, L. (2008). Ethanol/naltrexone interactions at the mu-opioid receptor. CLSM/FCS study in live cells. *PLoS One, 3*(12), e4008. doi:10.1371/journal.pone.0004008

Wan, Q., Okashah, N., Inoue, A., Nehme, R., Carpenter, B., Tate, C. G., & Lambert, N. A. (2018). Mini G protein probes for active G protein-coupled receptors (GPCRs) in live cells. *J Biol Chem, 293*(19), 7466-7473. doi:10.1074/jbc.RA118.001975

Wang, C., Wu, H., Katritch, V., Han, G. W., Huang, X. P., Liu, W., . . . Stevens, R. C. (2013). Structure of the human smoothened receptor bound to an antitumour agent. *Nature, 497*(7449), 338-343. doi:10.1038/nature12167

Watkins, L. R., Hutchinson, M. R., Rice, K. C., & Maier, S. F. (2009). The "Toll" of Opioid-Induced Glial Activation: Improving the Clinical Efficacy of Opioids by Targeting Glia. *Trends Pharmacol Sci, 30*(11), 581-591. doi:10.1016/j.tips.2009.08.002

Wettschureck, N., & Offermanns, S. (2005). Mammalian G proteins and their cell type specific functions. *Physiol Rev, 85*(4), 1159-1204. doi:10.1152/physrev.00003.2005

Whalen, E. J., Rajagopal, S., & Lefkowitz, R. J. (2011). Therapeutic potential of beta-arrestin- and G protein-biased agonists. *Trends Mol Med, 17*(3), 126-139. doi:10.1016/j.molmed.2010.11.004

Whistler, J. L., Chuang, H. H., Chu, P., Jan, L. Y., & von Zastrow, M. (1999). Functional dissociation of mu opioid receptor signaling and endocytosis: implications for the biology of opiate tolerance and addiction. *Neuron, 23*(4), 737-746.

Whistler, J. L., & von Zastrow, M. (1998). Morphine-activated opioid receptors elude desensitization by β-arrestin. *Proceedings of the National Academy of Sciences, 95*(17), 9914-9919. doi:10.1073/pnas.95.17.9914

White, C. W., Vanyai, H. K., See, H. B., Johnstone, E. K. M., & Pfleger, K. D. G. (2017). Using nanoBRET and CRISPR/Cas9 to monitor proximity to a genome-edited protein in real-time. *Sci Rep, 7*(1), 3187. doi:10.1038/s41598-017-03486-2

Williams, J. T., Ingram, S. L., Henderson, G., Chavkin, C., von Zastrow, M., Schulz, S., . . . Christie, M. J. (2013a). Regulation of -Opioid Receptors: Desensitization, Phosphorylation, Internalization, and Tolerance. *Pharmacol Rev, 65*(1), 223-254. doi:10.1124/pr.112.005942

Williams, J. T., Ingram, S. L., Henderson, G., Chavkin, C., von Zastrow, M., Schulz, S., . . . Christie, M. J. (2013b). Regulation of mu-opioid receptors: desensitization, phosphorylation, internalization, and tolerance. *Pharmacol Rev, 65*(1), 223-254. doi:10.1124/pr.112.005942

Willoughby, D., Wong, W., Schaack, J., Scott, J. D., & Cooper, D. M. F. (2006). An anchored PKA and PDE4 complex regulates subplasmalemmal cAMP dynamics. *Embo j, 25*(10), 2051-2061. doi:10.1038/sj.emboj.7601113

Wittmann, H. J., Seifert, R., & Strasser, A. (2011). Influence of the N-terminus and the E2-loop onto the binding kinetics of the antagonist mepyramine and the partial agonist phenoprodifen to H(1)R. *Biochem Pharmacol, 82*(12), 1910-1918. doi:10.1016/j.bcp.2011.09.005

Wolkerstorfer, A., Handler, N., & Buschmann, H. (2016). New approaches to treating pain. *Bioorg Med Chem Lett, 26*(4), 1103-1119. doi:10.1016/j.bmcl.2015.12.103

Wood, J. D., & Galligan, J. J. (2004). Function of opioids in the enteric nervous system. *Neurogastroenterol Motil, 16 Suppl 2*, 17-28. doi:10.1111/j.1743-3150.2004.00554.x

Wu, H., Wacker, D., Mileni, M., Katritch, V., Han, G. W., Vardy, E., . . . Stevens, R. C. (2012). Structure of the human kappa-opioid receptor in complex with JDTic. *Nature, 485*(7398), 327-332. doi:10.1038/nature10939

Xu, J., Lu, Z., Xu, M., Rossi, G. C., Kest, B., Waxman, A. R., . . . Pan, Y. X. (2014). Differential expressions of the alternatively spliced variant mRNAs of the micro opioid receptor gene, OPRM1, in brain regions of four inbred mouse strains. *PLoS One, 9*(10), e111267. doi:10.1371/journal.pone.0111267

Yanagawa, M., Hiroshima, M., Togashi, Y., Abe, M., Yamashita, T., Shichida, Y., . . . Sako, Y. (2018). doi:10.1101/205161

Yanagawa, M., Hiroshima, M., Togashi, Y., Abe, M., Yamashita, T., Shichida, Y., . . . Sako, Y. (2018). Single-molecule diffusion-based estimation of ligand effects on G protein-coupled receptors. *Sci Signal, 11*(548). doi:10.1126/scisignal.aao1917

Yang, Z., Yang, F., Zhang, D., Liu, Z., Lin, A., Liu, C., . . . Sun, J. P. (2017). Phosphorylation of G Protein-Coupled Receptors: From the Barcode Hypothesis to the Flute Model. *Mol Pharmacol, 92*(3), 201-210. doi:10.1124/mol.116.107839

Yao, X., Parnot, C., Deupi, X., Ratnala, V. R., Swaminath, G., Farrens, D., & Kobilka, B. (2006). Coupling ligand structure to specific conformational switches in the beta2-adrenoceptor. *Nat Chem Biol, 2*(8), 417-422. doi:10.1038/nchembio801

Yarwood, R. E., Imlach, W. L., Lieu, T., Veldhuis, N. A., Jensen, D. D., Klein Herenbrink, C., . . . Bunnett, N. W. (2017). Endosomal signaling of the receptor for calcitonin gene-related peptide mediates pain transmission. *Proc Natl Acad Sci U S A, 114*(46), 12309-12314. doi:10.1073/pnas.1706656114

Yousuf, A., Miess, E., Sianati, S., Du, Y. P., Schulz, S., & Christie, M. J. (2015). Role of Phosphorylation Sites in Desensitization of micro-Opioid Receptor. *Mol Pharmacol, 88*(4), 825-835. doi:10.1124/mol.115.098244

Zadina, J. E., Hackler, L., Ge, L. J., & Kastin, A. J. (1997). A potent and selective endogenous agonist for the mu-opiate receptor. *Nature, 386*(6624), 499-502. doi:10.1038/386499a0

Zamarripa, A. C., Edwards, S. R., Qureshi, H. N., Yi, J. N., Blough, B. E., & Freeman, K. B. (2018). The G-protein biased mu-opioid agonist, TRV130, produces reinforcing and antinociceptive effects that are comparable to oxycodone in rats. *Drug Alcohol Depend, 192*, 158-162. doi:10.1016/j.drugalcdep.2018.08.002

Zhang, J., Ferguson, S. S., Barak, L. S., Bodduluri, S. R., Laporte, S. A., Law, P. Y., & Caron, M. G. (1998). Role for G protein-coupled receptor kinase in agonist-specific regulation of mu-opioid receptor responsiveness. *Proc Natl Acad Sci U S A, 95*(12), 7157-7162.

Zheng, H., Chu, J., Qiu, Y., Loh, H. H., & Law, P. Y. (2008). Agonist-selective signaling is determined by the receptor location within the membrane domains. *Proc Natl Acad Sci U S A, 105*(27), 9421-9426. doi:10.1073/pnas.0802253105

Zheng, H., Loh, H. H., & Law, P.-Y. (2008). β-Arrestin-Dependent μ-Opioid Receptor-Activated Extracellular Signal-Regulated Kinases (ERKs) Translocate to Nucleus in Contrast to G Protein-Dependent ERK Activation. *Mol Pharmacol, 73*(1), 178-190. doi:10.1124/mol.107.039842

Zheng, H., Pearsall, E. A., Hurst, D. P., Zhang, Y., Chu, J., Zhou, Y., . . . Law, P. Y. (2012). Palmitoylation and membrane cholesterol stabilize mu-opioid receptor homodimerization and G protein coupling. *BMC Cell Biol, 13*, 6. doi:10.1186/1471-2121-13-6

Zhou, L., Lovell, K. M., Frankowski, K. J., Slauson, S. R., Phillips, A. M., Streicher, J. M., . . . Bohn, L. M. (2013). Development of functionally selective, small molecule agonists at kappa opioid receptors. *J Biol Chem, 288*(51), 36703-36716. doi:10.1074/jbc.M113.504381

Appendix 1

Plasma membrane localisation of the MOP controls spatiotemporal signalling

Michelle L. Halls, Holly R. Yeatman, Cameron J. Nowell, Georgina L. Thompson, Arisbel B. Gondin, Srgjan Civciristov, Nigel W. Bunnett, Nevin A. Lambert, Daniel P. Poole, Meritxell Canals

Sci. Signal. **9** (414), ra16. 9 Feb 2016

RESEARCH ARTICLE

GPCR SIGNALING

Plasma membrane localization of the μ-opioid receptor controls spatiotemporal signaling

Michelle L. Halls,[1]* Holly R. Yeatman,[1] Cameron J. Nowell,[1] Georgina L. Thompson,[1] Arisbel Batista Gondin,[1] Srgjan Civciristov,[1] Nigel W. Bunnett,[1,2,3,4] Nevin A. Lambert,[5] Daniel P. Poole,[1,6] Meritxell Canals[1,2]*

Differential regulation of the μ-opioid receptor (MOR), a G protein (heterotrimeric guanine nucleotide–binding protein)–coupled receptor, contributes to the clinically limiting effects of opioid analgesics, such as morphine. We used biophysical approaches to quantify spatiotemporal MOR signaling in response to different ligands. In human embryonic kidney (HEK) 293 cells overexpressing MOR, morphine caused a Gβγ-dependent increase in plasma membrane–localized protein kinase C (PKC) activity, which resulted in a restricted distribution of MOR within the plasma membrane and induced sustained cytosolic extracellular signal–regulated kinase (ERK) signaling. In contrast, the synthetic opioid peptide DAMGO ([D-Ala^2,N-Me-Phe^4, Gly^5-ol]-enkephalin) enabled receptor redistribution within the plasma membrane, resulting in transient increases in cytosolic and nuclear ERK activity, and, subsequently, receptor internalization. When Gβγ subunits or PKCα activity was inhibited or when the carboxyl-terminal phosphorylation sites of MOR were mutated, morphine-activated MOR was released from its restricted plasma membrane localization and stimulated a transient increase in cytosolic and nuclear ERK activity in the absence of receptor internalization. Thus, these data suggest that the ligand-induced redistribution of MOR within the plasma membrane, and not its internalization, controls its spatiotemporal signaling.

INTRODUCTION

Heterotrimeric guanine nucleotide–binding protein (G protein)–coupled receptors (GPCRs) are the largest family of cell surface signaling proteins encoded by the human genome. These receptors enable cells to respond to structurally diverse endogenous and environmental signals, and they are the targets of more than 30% of marketed drugs. It is increasingly recognized that the uniform increase in the abundance of second messengers throughout the cell cannot explain the diversity of GPCR-mediated effects. Rather, spatial (location) and temporal (duration) control of signaling play an important role (*1*, *2*). Spatial compartmentalization of signaling can be achieved by the formation of GPCR-dependent protein complexes, which restrict the diffusion of second messengers to induce extremely localized signals (*3*). In addition, multiple regulatory mechanisms (including receptor phosphorylation, desensitization, and internalization) control the duration of GPCR activation. Therefore, the spatial and temporal distribution of both receptors and signaling effectors are critical for the generation of distinct and highly specialized GPCR-mediated responses.

The μ-opioid receptor (MOR) has been extensively studied because of its physiological importance in mediating the effects of endogenous opioids as well as its prominence as the target of opioid analgesics, such as morphine. However, chronic use of opioid analgesics is still clinically limited by the development of tolerance, addiction, constipation, and respiratory depression (*4*). At the cellular level, stimulation of MOR by all opioids activates the same G protein–dependent signaling pathways. MOR activates $G\alpha_{i/o}$ proteins, leading to inhibition of cyclic adenosine monophosphate (cAMP) generation, increased extracellular signal–regulated kinase (ERK) phosphorylation and activation, activation of G protein–regulated inwardly rectifying potassium channels (GIRKs), and inhibition of voltage-gated calcium channels (*5*). However, different MOR agonists induce distinct patterns of receptor regulation and internalization. In particular, morphine causes limited receptor phosphorylation and recruitment of the scaffolding protein β-arrestin, which results in compromised receptor internalization and resensitization (*6*–*10*). These observations have prompted intensive studies of the ability of MOR ligands to differentially activate G proteins and β-arrestins in an effort to explain their divergent biological effects (*11*–*13*).

It is now apparent that the spatiotemporal characteristics of a signal can specify the outcome of receptor activation (*1*, *2*). Most opioids, including morphine, result in the phosphorylation and activation of cytosolic ERK (*14*–*16*); however, unlike other opioids, morphine is unable to promote nuclear ERK activation (*15*). Together with its impaired ability to induce the internalization of MOR, this finding suggests that morphine may stimulate a spatiotemporal cellular response distinct from those induced by other opioids. To investigate this hypothesis, we used complimentary biophysical techniques and superresolution microscopy. We report that morphine and DAMGO activated distinct spatial and temporal signaling profiles that were controlled by the plasma membrane localization of MOR induced by the two ligands. Subcellular targeted Förster resonance energy transfer (FRET) biosensors showed that only morphine-dependent stimulation of MOR induced sustained cytosolic ERK phosphorylation and plasma membrane–localized protein kinase C (PKC) activation, which restricted the localization of MOR. In contrast, DAMGO caused the redistribution of MOR within the plasma membrane as well as the transient activation of both cytosolic and nuclear ERK. Thus, not only did morphine and DAMGO stimulate different signaling pathways, but they also activated signals in distinct subcellular compartments with distinct temporal profiles. Furthermore, we altered the spatiotemporal signaling profile of morphine to

[1]Drug Discovery Biology Theme, Monash Institute of Pharmaceutical Sciences, Monash University, Parkville, Victoria 3052, Australia. [2]ARC Centre of Excellence in Convergent Bio-Nano Science and Technology, Monash Institute of Pharmaceutical Sciences, Monash University, Parkville, Victoria 3052, Australia. [3]Department of Anesthesia and Perioperative Medicine, Monash University, Melbourne, Victoria 3004, Australia. [4]Department of Pharmacology, The University of Melbourne, Parkville, Victoria 3052, Australia. [5]Department of Toxicology and Pharmacology, Georgia Regents University, Augusta, GA 30912, USA. [6]Department of Anatomy and Neuroscience, The University of Melbourne, Parkville, Victoria 3052, Australia.
*Corresponding author. E-mail: michelle.halls@monash.edu (M.L.H.); meri.canals@monash.edu (M.C.)

Downloaded from http://stke.sciencemag.org/ on February 9, 2016

From M. L. Halls, H. R. Yeatman, C. J. Nowell, G. L. Thompson, A. B. Gondin, S. Civciristov, N. W. Bunnett, N. A. Lambert, D. P. Poole, M. Canals. Plasma membrane localization of the m-opioid receptor controls spatiotemporal signaling. Sci. Signal. 9, ra16 (2016). Reprinted with permission from AAAS.

RESEARCH ARTICLE

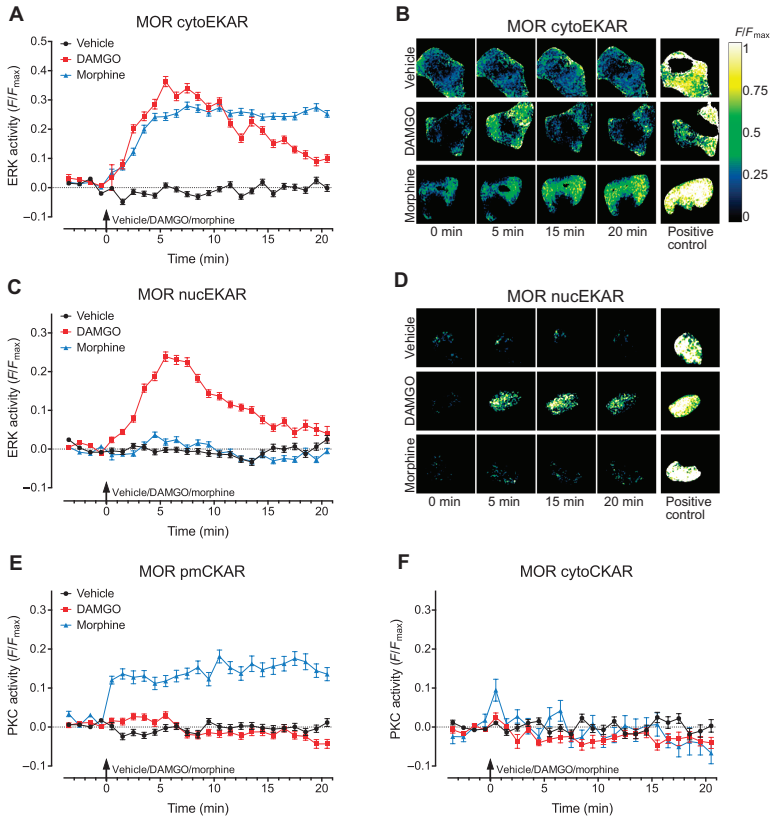


Fig. 1. Ligand-dependent spatiotemporal signaling of MOR. (A to D) Spatiotemporal activation of ERK in transfected HEK 293 cells treated with vehicle, DAMGO, or morphine for the indicated times. (A) Analysis of cytosolic ERK activity. Data are means ± SEM of 416 to 606 cells from five experiments. (B) Representative pseudocolor ratiometric images of cytoEKAR. (C) Analysis of nuclear ERK activity. Data are means ± SEM of 561 to 810 cells from five experiments. (D) Representative pseudocolor ratiometric images of nucEKAR. Pseudocolor scale as in (B). (E and F) Spatiotemporal activation of PKC in transfected HEK 293 cells after treatment with vehicle, DAMGO, or morphine for the indicated times. (E) Analysis of plasma membrane–localized PKC activity. Data are means ± SEM of 155 to 220 cells from three experiments. (F) Analysis of cytosolic PKC activity. Data are means ± SEM of 45 to 115 cells from three experiments.

mimic that of DAMGO by enabling the redistribution of MOR within the plasma membrane in the absence of β-arrestin recruitment or receptor internalization. Thus, these data suggest that receptor localization within the plasma membrane determines the spatiotemporal signals activated by MOR in response to different ligands.

RESULTS

Ligand-dependent spatiotemporal signaling of MOR

To gain spatial and temporal resolution of MOR signaling in live cells, we used FRET biosensors for ERK and PKC (EKAR and CKAR, respectively), which localized to different subcellular compartments (*17*, *18*). In human embryonic kidney (HEK) 293 cells cotransfected with plasmids encoding MOR and either a cytosolic or a nuclear ERK biosensor (cytoEKAR and nucEKAR, respectively), DAMGO and morphine at EC_{50} concentrations (concentration that provokes 50% of the maximal response of the receptor; 10 nM DAMGO and 100 nM morphine, fig. S1A) caused distinct temporal profiles of ERK activation, shown as changes in the corresponding FRET signal. Whereas DAMGO caused a transient increase in cytosolic ERK activity, morphine induced a sustained increase (Fig. 1, A and B). Moreover, only DAMGO caused a transient increase in nuclear ERK activity (Fig. 1, C and D). Ligand-dependent responses were also observed when assessing the direct activation of PKC. In cells cotransfected with plasmids encoding MOR and a plasma membrane–localized biosensor of PKC activity (pmCKAR), only morphine caused a sustained increase in PKC activity (Fig. 1E). DAMGO did not affect the activity of plasma membrane–localized PKC, even at maximal concentrations (1 μM, fig. S1B), and neither ligand stimulated the activity of cytosolic PKC (Fig. 1F).

The distinct internalization profiles of MOR in response to DAMGO and morphine (*6*, *10*) were quantified with a bioluminescence resonance energy transfer (BRET) assay that detects the proximity between BRET partners in defined subcellular compartments in live cells (*19*, *20*). Consistent with previous reports, incubation of HEK 293 cells with 1 μM DAMGO (concentration corresponding to its EC_{50} of β-arrestin recruitment using BRET; fig. S2A) induced MOR internalization, as shown by the increase in the BRET signal between a *Renilla* luciferase–tagged MOR (MOR-RLuc) and a Venus-tagged marker of early endosomes (Rab5a-Venus) (Fig. 2A). In contrast, morphine produced no substantial change in BRET (Fig. 2A and fig. S2B). These results were validated by automated, high-content image analysis (fig. S2C). DAMGO-mediated MOR endocytosis was unaffected by the inhibition of $G\alpha_{i/o}$ activity with NF023 or pertussis toxin (PTx) (*21*, *22*) but was abolished by the clathrin-dependent endocytosis inhibitor PitStop2 (*23*), by the expression of a dominant-negative dynamin mutant (K44E) (*24*), or by knockdown of β-arrestins [combined small interfering RNAs (siRNAs) specific for β-arrestin-1 and β-arrestin-2] (Fig. 2, A and B, and fig. S2, D to H). These data suggest that β-arrestin recruitment and MOR endocytosis are independent of $G\alpha_{i/o}$ coupling.

Previous studies have linked PKC activation to cytosolic ERK activity and β-arrestin activation to increased nuclear ERK activity to conclude that G protein– and β-arrestin–dependent pathways activate distinct modes of ERK signaling (*15*). By inhibiting $G\alpha_{i/o}$ proteins, we demonstrated that cytosolic ERK activation in response to DAMGO and morphine was dependent on $G\alpha_{i/o}$ (Fig. 2C). In agreement with previous studies, cytosolic ERK activity was unaffected by knockdown of β-arrestins (Fig. 2C). However, inhibition of receptor endocytosis by PitStop2 or by expression of the dynamin K44E mutant transformed the profile of DAMGO-induced cytosolic

Downloaded from http://stke.sciencemag.org/ on February 9, 2016

From M. L. Halls, H. R. Yeatman, C. J. Nowell, G. L. Thompson, A. B. Gondin, S. Civciristov, N. W. Bunnett, N. A. Lambert, D. P. Poole, M. Canals. Plasma membrane localization of the mu-opioid receptor controls spatiotemporal signaling. Sci. Signal. 9, ra16 (2016). Reprinted with permission from AAAS.

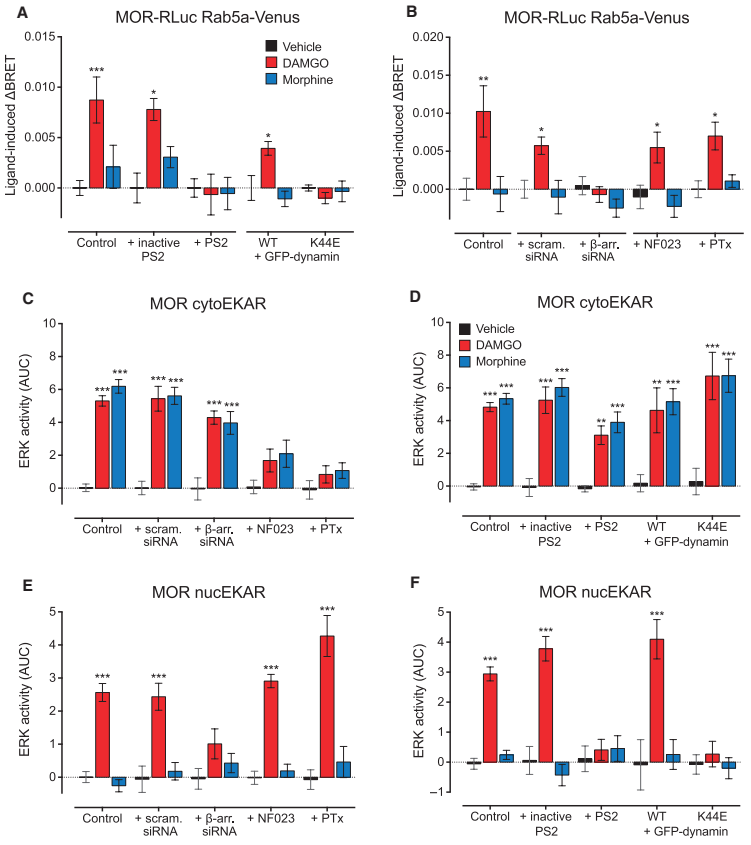


Fig. 2. Effect of $G\alpha_{i/o}$ protein inhibition, β-arrestin knockdown, or inhibition of endocytosis on MOR-stimulated cytosolic and nuclear ERK activities. (A and B) The trafficking of MOR to early endosomes in transfected HEK 293 cells in response to treatment with vehicle, DAMGO, or morphine for 30 min was determined by BRET analysis between MOR-RLuc and Rab5a-Venus. (A) Cells were treated with the clathrin-mediated endocytosis inhibitor PitStop2 (PS2) or its inactive control, or transfected to express wild-type (WT) dynamin or a dominant-negative dynamin K44E mutant. (B) Cells were treated with or without siRNAs specific for β-arrestins or were preincubated with the indicated $G\alpha_{i/o}$ protein inhibitors. Data are means ± SEM from five experiments. (C to F) Analysis of the spatial activation of ERK in HEK 293 cells in response to vehicle, DAMGO, or morphine in the presence or absence of β-arrestin–specific siRNA, $G\alpha_{i/o}$ protein inhibitors, PitStop2 or its inactive control, or upon expression of WT or K44E mutant dynamin. (C) Analysis of cytosolic ERK activity. Data are means ± SEM of 96 to 168 cells from three experiments. (D) Analysis of cytosolic ERK activity in cells in which endocytosis was inhibited. Data are means ± SEM of 35 to 606 cells from three experiments. (E) Analysis of nuclear ERK activity in cells treated with $G\alpha_{i/o}$ protein inhibitors or β-arrestin–specific siRNAs. Data are means ± SEM of 52 to 258 cells from three experiments. (F) Analysis of nuclear ERK activity in cells in which endocytosis was inhibited. Data are means ± SEM of 51 to 306 cells from three experiments. $^*P < 0.05$, $^{**}P < 0.01$, and $^{***}P < 0.001$ versus vehicle control. Data were analyzed by two-way analysis of variance (ANOVA) with Tukey's multiple comparison test. AUC, area under the curve; scram., scrambled.

ERK activity from a transient to a sustained signal, consistent with the retention of MOR at the plasma membrane (Fig. 2D and fig. S2, I and J). As expected, the increase in nuclear ERK activity in response to DAMGO was dependent on β-arrestins and receptor internalization (Fig. 2, E and F). Thus, our results suggest that $G\alpha_{i/o}$ activation by MOR mediates increases in cytosolic ERK activity in response to DAMGO and morphine, and confirm that the increases in nuclear ERK activity in response to DAMGO are dependent on β-arrestins and receptor endocytosis.

Role of PKC activation in the spatiotemporal profile of ERK in response to morphine

Inhibition of the activity of $G\alpha_{i/o}$ subunits (with NF023 or PTx) or of Gβγ subunits [with the cell-permeable N-myristoylated Gβγ-selective peptide mSIRK or by expression of βARKct, a GPCR kinase 2 (GRK2) C-terminal peptide that interferes with Gβγ function] (*25*, *26*) abolished the response of plasma membrane–localized PKC to morphine (Fig. 3A); however, knockdown of β-arrestins and negative controls (inactive mSIRK L9A and scrambled siRNA) had no such effects (Fig. 3A and fig. S3A). Thus, the sustained increase in plasma membrane–localized PKC activity that was stimulated by morphine was mediated by $G\alpha_{i/o}$ and Gβγ subunits.

Previous studies reported that PKC activity mediates the increased activity of cytosolic ERK in response to morphine (*15*). We therefore investigated whether the $G\alpha_{i/o}$-Gβγ-PKC pathway influenced the distinct ERK spatiotemporal signaling profiles of MOR. Rather than decreasing ERK activity, and in contrast to previous reports, inhibition of Gβγ subunits or of PKC (with GF109203X or Gö6983) (*27*, *28*) transformed the temporal profile of morphine-stimulated cytosolic ERK activity to resemble the transient response induced by DAMGO (Fig. 3B and fig. S3, B and C). Moreover, inhibition of the Gβγ-PKC pathway also enabled morphine to increase the activity of nuclear ERK (Fig. 3, C and D). Previous studies implicated PKCα, PKCγ, and PKCε as the PKC isoforms that contribute to morphine signaling and to the development of morphine tolerance (*16*, *29*–*32*). Of these, only the mRNAs of PKCα and PKCε were present in our HEK 293 cell line (fig. S3D). Inhibition of PKCα (with Gö6976, which targets PKCα and $PKC\beta_1$) (*33*), but not PKCε (with iPKCε, a cell-permeable PKCε inhibitory peptide) (*34*), transformed the temporal profile of morphine-stimulated cytosolic ERK activity from being sustained to be being transient and also facilitated an increase in nuclear ERK activity (fig. S3, E and F). There were no effects of inactive controls or these inhibitors on the responses of cells to DAMGO (Fig. 3, B to D, and fig. S3, C and F).

As expected, the inhibition of Gβγ subunits or PKC did not substantially affect the recruitment of β-arrestin-2 or MOR internalization in response to DAMGO, as determined by BRET analysis and high-content imaging (Fig. 3E and fig. S3, G to I). In contrast, upon inhibition of Gβγ subunits or PKC,

Downloaded from http://stke.sciencemag.org/ on February 9, 2016

From M. L. Halls, H. R. Yeatman, C. J. Nowell, G. L. Thompson, A. B. Gondin, S. Civciristov, N. W. Bunnett, N. A. Lambert, D. P. Poole, M. Canals. Plasma membrane localization of the mu-opioid receptor controls spatiotemporal signaling. Sci. Signal. 9, ra16 (2016). Reprinted with permission from AAAS.

RESEARCH ARTICLE

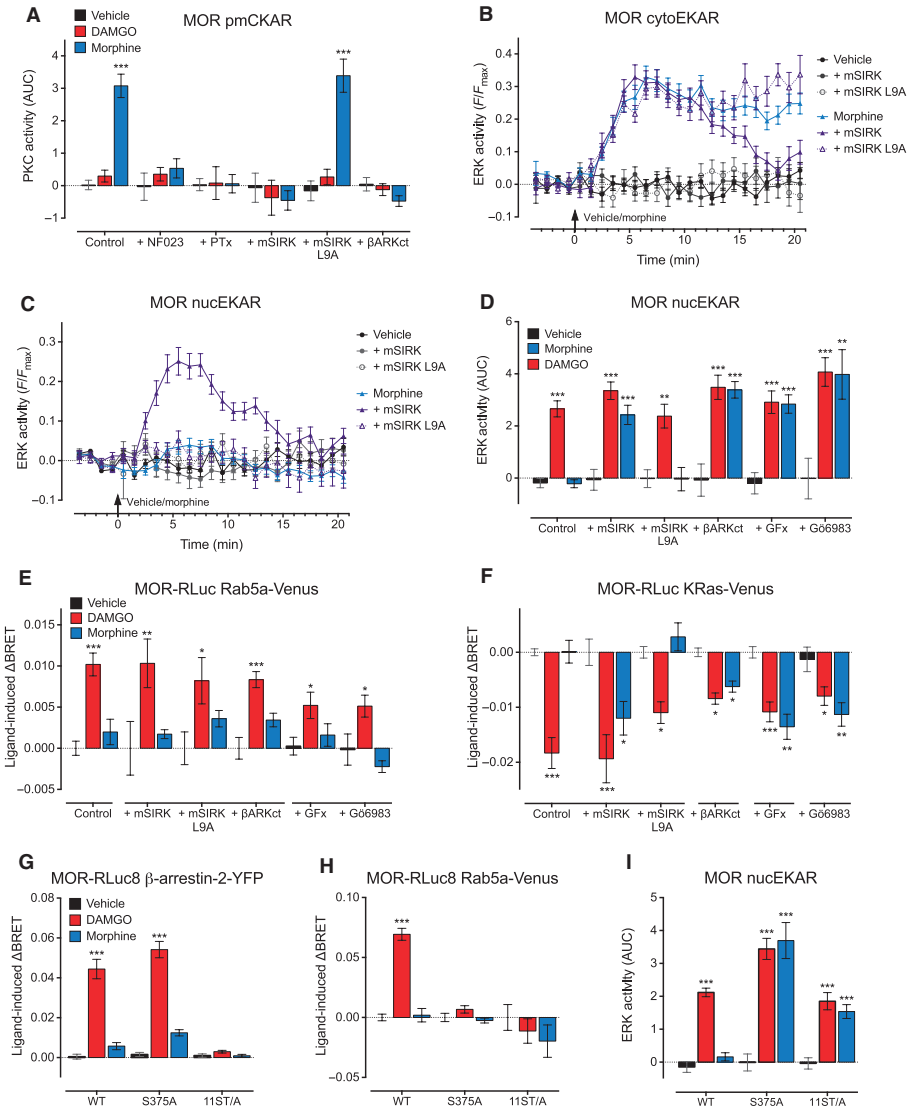


Fig. 3. The role of PKC activation by morphine in the spatiotemporal control of ERK activity. (**A**) The effects of the indicated G protein inhibitors or inactive controls on plasma membrane PKC activity in HEK 293 cells treated with vehicle, DAMGO, or morphine were determined with the pmCKAR FRET biosensor. Data are means ± SEM of 39 to 229 cells from three experiments. (**B** to **D**) Analysis of the MOR-stimulated spatiotemporal activation of ERK in response to vehicle, DAMGO, or morphine in cells in which Gβγ or PKC signaling was inhibited. (B) Analysis of cytosolic ERK activity over time. Data are means ± SEM of 31 to 101 cells from three experiments. (C) Analysis of nuclear ERK activity over time. Data are means ± SEM of 74 to 126 cells from three experiments. (D) Nuclear ERK activity was analyzed as the AUC. Data are means ± SEM of 22 to 360 cells from three experiments. (**E** and **F**) MOR trafficking in response to vehicle, DAMGO, or morphine was monitored in HEK 293 cells in the presence or absence of the indicated Gβγ and PKC inhibitors. (E) Analysis of BRET between MOR-RLuc and Rab5a-Venus. Data are means ± SEM of three to seven experiments. (F) Analysis of BRET between MOR-RLuc and KRas-Venus. Data are means ± SEM of three to seven experiments. (**G** to **I**) Effect of the indicated phosphorylation site mutations on MOR trafficking and nuclear ERK activity. (G) Analysis of BRET between MOR-RLuc8 and β-arrestin-2–YFP (yellow fluorescent protein). Data are means ± SEM of three to seven experiments. (H) Analysis of BRET between MOR-RLuc8 and Rab5a-Venus. Data are means ± SEM of three or four experiments. (I) Analysis of nuclear ERK activity over time. Data are means ± SEM of 87 to 359 cells from three to five experiments. **P* < 0.05, ***P* < 0.01, and ****P* < 0.001 versus vehicle control. Data were analyzed by two-way ANOVA with Tukey's (A and D) or Dunnett's (E to I) multiple comparison tests. GFx, GF109203X.

From M. L. Halls, H. R. Yeatman, C. J. Nowell, G. L. Thompson, A. B. Gondin, S. Civciristov, N. W. Bunnett, N. A. Lambert, D. P. Poole, M. Canals. Plasma membrane localization of the m-opioid receptor controls spatiotemporal signaling. Sci. Signal. 9, ra16 (2016). Reprinted with permission from AAAS.

Downloaded from http://stke.sciencemag.org/ on February 9, 2016

the activation of MOR by morphine resulted in a decrease in BRET between MOR-RLuc and the plasma membrane marker KRas-Venus (Fig. 3F), which suggested that there was an increase in the distance between these two proteins. In the absence of MOR internalization (Fig. 3E and fig. S3, G and H), the morphine-stimulated change in BRET between MOR and KRas may indicate a movement of the receptor away from KRas within the plasma membrane. Thus, the transient activation of cytosolic and nuclear ERK elicited by morphine did not require MOR internalization but may instead depend on the translocation of MOR within the plasma membrane.

The importance of the localization of MOR within the plasma membrane for the control of spatiotemporal signaling was also supported by the effects of the expression of a phosphorylation-deficient MOR mutant (S375A) (*35*). DAMGO still induced the recruitment of β-arrestin-2 to MOR S375A; however, the receptor was not internalized as determined by high-content imaging or analysis of BRET between the receptor and Rab5a (Fig. 3, G and H, and fig. S3, G and H). There was no change in the BRET between MOR S375A and KRas in response to DAMGO or morphine (fig. S3J); however, stimulation of MOR S375A by either DAMGO or morphine induced transient increases in cytosolic and nuclear ERK activity (Fig. 3I and fig. S3K).

To confirm that receptor phosphorylation was key for the control of the plasma membrane localization of MOR and its spatiotemporal signaling, we used a phosphorylation-deficient MOR mutant in which all of the C-terminal serine and threonine residues were mutated to alanines (11ST/A) (*9*). Consistent with previous reports, MOR 11ST/A was not internalized, as determined by measurement of BRET with Rab5a, nor did it recruit β-arrestin-2 in response to DAMGO (Fig. 3, G and H). However, stimulation of MOR 11ST/A by either DAMGO or morphine induced a transient increase in nuclear ERK activity, with no accompanying change in BRET between the receptor and KRas (Fig. 3I and fig. S3J). Phosphorylation of Ser^{375} therefore appears to be critical for the control of the spatiotemporal signaling by MOR in response to morphine. Together, these data suggest that the impaired trafficking of MOR mutants results in an altered signaling profile and support the hypothesis that the plasma membrane localization of MOR, and not β-arrestin recruitment or receptor internalization, plays a key role in the spatiotemporal control of receptor signaling.

Ligand-dependent redistribution of MOR within the plasma membrane

To investigate the changes in MOR distribution elicited by morphine upon inhibition of the Gβγ-PKCα pathway, we assessed receptor localization at the plasma membrane by confocal microscopy and subcellular fractionation. After 10 min of stimulation of the MOR (when all signaling pathways are activated), there was no substantial colocalization between the receptor and immunolabeled clathrin as determined by confocal microscopy analysis under any condition tested (fig. S4, A and B). However, 60 min of stimulation with DAMGO, but not morphine, caused substantial colocalization between MOR and clathrin (fig. S4C). In contrast, activation of the fast internalizing β_2-adrenergic receptor (β_2AR) by isoprenaline caused substantial receptor-clathrin colocalization after only 10 min of stimulation (fig. S4, A to C). Similarly, there was no effect of DAMGO or morphine on the location of FLAG-tagged MOR (FLAG-MOR) within non–lipid-rich (that is, Triton X-100–soluble) plasma membrane domains through basic lipid fractionation analysis (fig. S4D). Therefore, the distinct spatiotemporal signaling profiles of morphine and DAMGO do not reflect either ligand-dependent MOR clustering in clathrin-coated pits or translocation of the receptor to different lipid domains.

To investigate the localization of MOR within the plasma membrane with increased resolution, we used ground-state depletion (GSD) super-resolution microscopy in total internal reflection fluorescence (TIRF) mode. GSD-TIRF enables the detection of events within the plane of the plasma membrane to an axial resolution of 100 nm. This approach can measure the distance between an event (for example, a receptor or receptor clusters) and its nearest neighbor across a population. Stimulation of FLAG-MOR with DAMGO for 10 min increased the average distance between detected events (Fig. 4, A and B), which suggested the redistribution of MOR within the plasma membrane. This increase in distance occurred before, and was independent of, receptor internalization, because the dominant-negative dynamin K44E mutant had no effect (fig. S4, E and F).

The stimulation of cells expressing FLAG-MOR with morphine for 10 min did not change the average distance between events (Fig. 4, A and B); however, after the inhibition of Gβγ subunits, morphine increased the distance between detected MOR events (Fig. 4, C and D, and fig. S4, E and G), suggesting that activation of this pathway by morphine normally restricts MOR localization. Furthermore, the distance between MOR events under basal conditions in cells expressing MOR S375A was also increased when compared to that in cells expressing the wild-type receptor (Fig. 4, E and F). This increase in distance between events was not a result of decreased receptor abundance at the plasma membrane (MOR S375A 510,000 sites per cell, MOR wild-type 121,000 sites per cell measured by whole-cell [^{3}H]diprenorphine binding; table S1), confirming that MOR S375A was differentially distributed compared to the wild-type receptor.

Thus, our results suggest that the activation of MOR by morphine restricts receptor localization, whereas DAMGO stimulates the redistribution of MOR within the plasma membrane. Disruption of the Gβγ-PKCα pathway enabled morphine to stimulate a DAMGO-like redistribution of MOR but did not result in receptor internalization. Receptor redistribution preceded endocytosis (in the case of DAMGO) or occurred independently of endocytosis (in the case of morphine), and it appeared to control the ability of MOR to transiently activate cytosolic and nuclear ERK.

Effect of plasma membrane organization on MOR spatiotemporal signaling

To confirm the importance of membrane organization in the control of compartmentalized MOR signaling, we depleted cholesterol from the plasma membrane with methyl-β-cyclodextrin (MβCD) (*36*) or filipin III (*37*). Neither reagent had any substantial effect on MOR internalization, as determined by high-content imaging (fig. S5, A and B); however, both MβCD and filipin III abolished the distinct spatiotemporal signaling profiles of morphine and DAMGO (Fig. 5 and fig. S5). Upon cholesterol depletion, both morphine and DAMGO increased PKC activity at the plasma membrane and caused a transient increase in both cytosolic and nuclear ERK activity (Fig. 5 and fig. S5, C to F). Indeed, replenishment of membrane cholesterol by incubation of the cells with MβCD-cholesterol complexes completely restored the original spatiotemporal signaling profiles of DAMGO and morphine (Fig. 5 and fig. S5). Thus, disruption of membrane organization altered the spatiotemporal signaling profiles of MOR, with no change in the ability of the receptor to be internalized, suggesting that the plasma membrane localization of MOR plays an important role in determining its spatiotemporal signaling.

MOR compartmentalized signaling in dorsal root ganglion neurons

To confirm the physiological relevance of the spatiotemporal signaling patterns of MOR that we determined in HEK 293 cells, we used nucleofection to transfect isolated neurons from mouse dorsal root ganglions (DRGs) with the FRET biosensors. DRG neurons are the principal mediators of nociception from the periphery to the spinal cord, and activation of endogenous MOR in these neurons partially mediates the analgesic actions of opioids (*38*).

Downloaded from http://stke.sciencemag.org/ on February 9, 2016

From M. L. Halls, H. R. Yeatman, C. J. Nowell, G. L. Thompson, A. B. Gondin, S. Civciristov, N. W. Bunnett, N. A. Lambert, D. P. Poole, M. Canals. Plasma membrane localization of the mu-opioid receptor controls spatiotemporal signaling. Sci. Signal. 9, ra16 (2016). Reprinted with permission from AAAS.

RESEARCH ARTICLE

Activation of MOR in DRG neurons stimulated ERK and PKC activity with spatiotemporal profiles that were identical to those observed in HEK 293 cells. DAMGO caused a transient increase in both cytosolic and nuclear ERK activities, whereas morphine elicited a sustained increase in the activities of cytosolic ERK and plasma membrane–localized PKC (Fig. 6, A to C). Inhibition of PKC decreased the percentage of neurons (from 75 to 49%) that exhibited sustained cytosolic ERK activity in response to morphine and increased the percentage of neurons (from 25 to 51%) that exhibited a transient increase in cytosolic ERK activity (Fig. 6, D and E). There was no effect of PKC inhibition on the temporal profile of cytosolic ERK activity after stimulation with DAMGO (Fig. 6, D and E). As was observed in HEK 293 cells, inhibition of PKC enabled morphine to stimulate nuclear ERK activity in DRG neurons (Fig. 6F).

We also assessed the distribution of endogenous MOR at the plasma membrane of DRG neurons by GSD-TIRF microscopy (Fig. 6G). As was observed in HEK 293 cells, stimulation of endogenous MOR in DRG neurons with DAMGO increased the distance between detected events at the plasma membrane (Fig. 6, H and I). In contrast, there was no change in the distance between MOR events in response to morphine. Thus, in DRG neurons, as in HEK 293 cells, receptor redistribution at the plasma membrane correlated with transient increases in cytosolic and nuclear ERK activities in response to DAMGO. Moreover, inhibition of PKC enabled morphine to cause transient increases in cytosolic and nuclear ERK activities. As such, the spatiotemporal regulation of MOR activation and signaling identified in recombinant expression systems also occurred in DRG neurons endogenously expressing this receptor.

DISCUSSION

The use of biophysical approaches to assess MOR signaling in real time and in live cells revealed a previously uncharacterized mechanism that contributes to the control of differential MOR activation. Here, we showed that the activation of MOR by DAMGO stimulated the translocation of the receptor within the plasma membrane. This translocation preceded receptor trafficking to clathrin-containing domains and internalization, and is likely dependent on receptor phosphorylation (Fig. 7A). This translocation, but

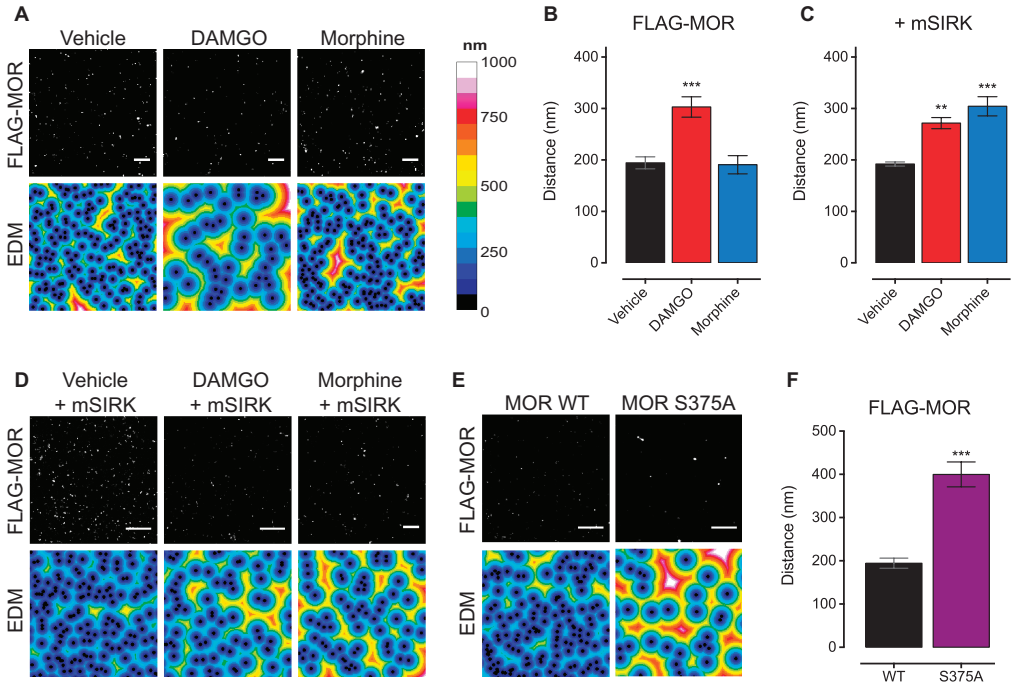


Fig. 4. DAMGO induces a distinct MOR distribution at the plasma membrane. GSD-TIRF microscopy was used to monitor the plasma membrane distribution of FLAG-MOR in HEK 293 cells in response to treatment with vehicle, DAMGO, or morphine for 10 min. (**A**) Representative GSD-TIRF images and Euclidean distance maps (EDMs) from cells under the indicated conditions. Scale bars, 1 μm. (**B**) Average distances to nearest neighbors in the cells shown in (A). Data are means ± SEM of three to nine experiments. (**C**) Average distances to nearest neighbors in cells subjected to Gβγ inhibition by preincubation with mSIRK and then treated with vehicle, DAMGO, or morphine. Data are means ± SEM of three to nine experiments. (**D**) Representative GSD-TIRF images and EDMs from cells preincubated with mSIRK to inhibit Gβγ and then subjected to the indicated treatments. Scale bars, 1 μm. Pseudocolor scale is as described in (A). (**E**) Representative GSD-TIRF images and EDMs of unstimulated cells expressing either WT MOR or the MOR S375A mutant. Scale bars, 1 μm. Pseudocolor scale is as described in (A). (**F**) Average distances to nearest neighbors in the cells shown in (E). Data are means ± SEM of three to nine experiments. $^{**}P < 0.01$ and $^{***}P < 0.001$ versus vehicle control. Data were analyzed by one-way ANOVA with Dunnett's multiple comparison test (B and C) or unpaired *t* test (E).

Downloaded from http://stke.sciencemag.org/ on February 9, 2016

From M. L. Halls, H. R. Yeatman, C. J. Nowell, G. L. Thompson, A. B. Gondin, S. Civciristov, N. W. Bunnett, N. A. Lambert, D. P. Poole, M. Canals. Plasma membrane localization of the m-opioid receptor controls spatiotemporal signaling. Sci. Signal. 9, ra16 (2016). Reprinted with permission from AAAS.

not internalization, of MOR determined the transient cytosolic ERK activity profile and the activation of nuclear ERK (Fig. 7A). In contrast, morphine activated plasma membrane–localized PKCα through Gβγ subunits, which prevented receptor translocation within the plasma membrane. This resulted in the sustained activity of cytosolic ERK, but not nuclear ERK (Fig. 7B). Inhibition of this Gβγ-PKCα pathway enabled the morphine-activated MOR to translocate within the plasma membrane, thus transforming its spatiotemporal signaling profile (Fig. 7B). Furthermore, this altered signaling profile mimicked that of the internalizing ligand DAMGO (that is, it was characterized by transient cytosolic and nuclear ERK activity) but occurred in the absence of β-arrestin-2 recruitment and receptor internalization.

These results add details to previous descriptions of ligand-dependent differences in ERK signaling (*14*–*16*). Previous studies used Western blotting analysis to show that etorphine-induced ERK phosphorylation was dependent on β-arrestins, whereas morphine activated ERK through a PKC-dependent pathway (*15*). However, we showed that upon PKC inhibition, morphine stimulated ERK phosphorylation, although this signal had different temporal dynamics and occurred in both the cytosol and the nucleus (Figs. 3 and 7B). Therefore, the activation of cytosolic ERK by morphine is not PKC-dependent, but rather PKC, by controlling the localization of MOR, likely determines the dynamics and location of this response. It is interesting to consider that in the context of a whole cell after its solubilization (with a relatively greater contribution of cytosolic compared to nuclear ERK), this altered temporal profile could appear as an apparent decrease in morphine-stimulated ERK activity. This illustrates the extra mechanistic detail that can be obtained by resolving spatial and temporal signaling dynamics in live cells. We therefore propose that the plasma membrane organization of MOR, and not just the recruitment of β-arrestin and subsequent receptor internalization, determines the spatiotemporal outcome of receptor activation. Furthermore, these mechanisms appear to operate in nociceptive neurons and may thus contribute to the analgesic actions of opioids.

The ability of DAMGO, but not morphine, to cause receptor redistribution may relate to differential patterns of MOR phosphorylation. Although all opioids cause the phosphorylation of MOR at Ser^{375}, this event is mediated by different kinases depending on the ligand (*9*, *39*). Previous studies showed that the DAMGO-activated MOR is phosphorylated by GRK2 and GRK3 and that internalizing ligands stimulate the higher-order phosphorylation of flanking residues, which results in efficient β-arrestin recruitment and receptor internalization (*9*). Here, we showed that the recruitment of β-arrestin-2, translocation of MOR, and activation of nuclear ERK in response to DAMGO preceded receptor internalization. As such, we hypothesize that the differential recruitment of regulatory proteins (including GRKs and β-arrestins) to MOR

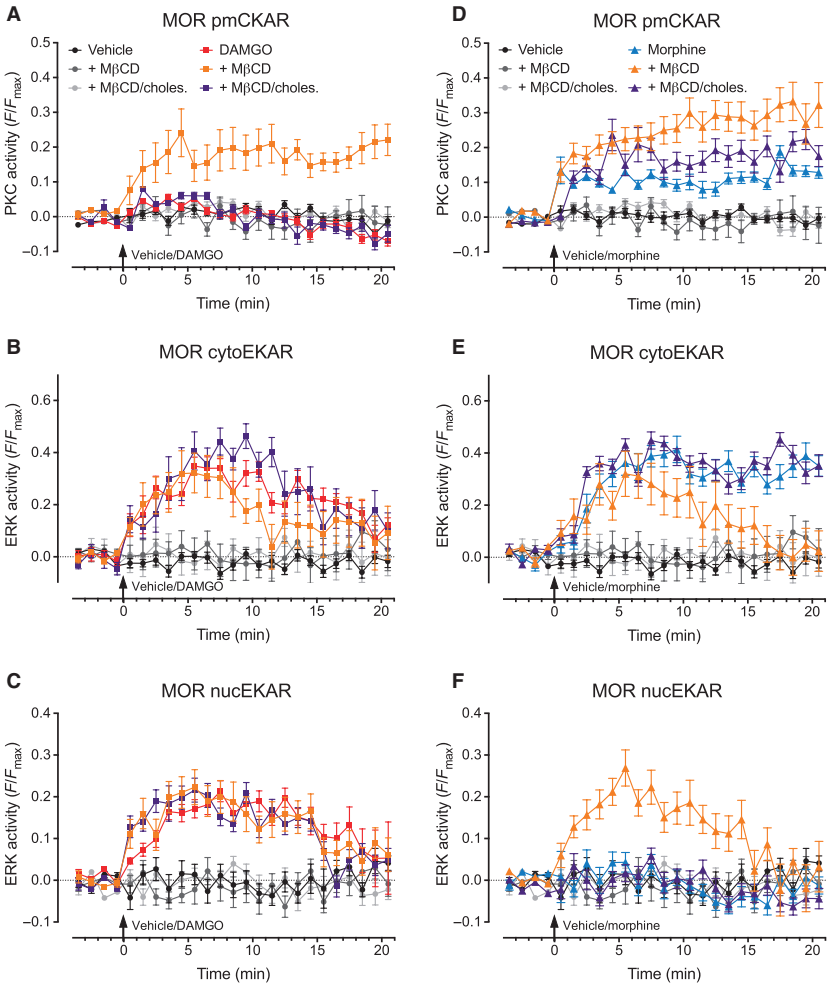


Fig. 5. Disruption of membrane architecture alters MOR signaling profiles. (A to F) HEK 293 cells were pretreated with vehicle, MβCD, or MβCD-cholesterol complexes (MβCD/choles.) before being treated with vehicle, DAMGO, or morphine. The spatiotemporal activation of plasma membrane–localized PKC and either cytoplasmic or nuclear ERK was then measured. (A) Plasma membrane–localized PKC activity in response to DAMGO. Data are means ± SEM of 40 to 174 cells from three experiments. (B) Cytosolic ERK activity in response to DAMGO. Data are means ± SEM of 30 to 167 cells from three experiments. (C) Nuclear ERK activity in response to DAMGO. Data are means ± SEM of 68 to 230 cells from three experiments. (D) Plasma membrane–localized PKC activity in response to morphine. Data are means ± SEM of 41 to 195 cells from three experiments. (E) Cytosolic ERK activity in response to morphine. Data are means ± SEM of 32 to 194 cells from three experiments. (F) Nuclear ERK activity in response to morphine. Data are means ± SEM of 80 to 217 cells from three experiments.

Downloaded from http://stke.sciencemag.org/ on February 9, 2016

From M. L. Halls, H. R. Yeatman, C. J. Nowell, G. L. Thompson, A. B. Gondin, S. Civciristov, N. W. Bunnett, N. A. Lambert, D. P. Poole, M. Canals. Plasma membrane localization of the mu-opioid receptor controls spatiotemporal signaling. Sci. Signal. 9, ra16 (2016). Reprinted with permission from AAAS.

RESEARCH ARTICLE

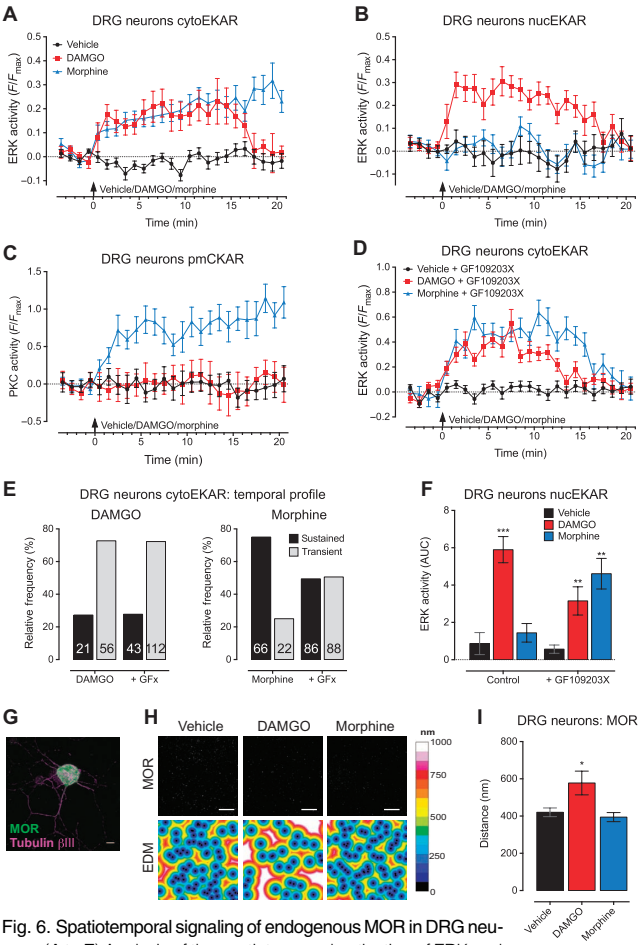


Fig. 6. Spatiotemporal signaling of endogenous MOR in DRG neurons. (A to F) Analysis of the spatiotemporal activation of ERK and PKC in DRG neurons treated with vehicle, DAMGO, or morphine. (A) Cytosolic ERK activity. Data are means ± SEM of 56 to 120 neurons from three experiments. (B) Nuclear ERK activity. Data are means ± SEM of 45 to 64 neurons from three experiments. (C) Plasma membrane–localized PKC activity. Data are means ± SEM of 40 to 55 neurons from three experiments. (D) Effect of PKC inhibition on cytosolic ERK activity. Data are means ± SEM of 86 to 99 neurons from three experiments. (E) Population analysis of the temporal profile of cytosolic ERK activity. The numbers of neurons in each group are indicated. (F) Effect of PKC inhibition on nuclear ERK activity. Data are means ± SEM of 25 to 73 neurons from three experiments. (G to I) GSD-TRIF–based analysis of the plasma membrane distribution of endogenous MOR in DRG neurons in response to treatment with vehicle, DAMGO, or morphine for 10 min. Data are means ± SEM of 9 to 15 cells from three experiments. (G) Isolated DRG neuron immunostained for MOR (green) and tubulin βIII (magenta). Scale bar, 10 μm. (H) Representative GSD-TIRF images and EDMs of DRG neurons under the indicated conditions. Scale bars, 1 μm. (I) Average distances to nearest neighbors. Data are means ± SEM of 9 to 15 cells from three experiments. *$P < 0.05$, **$P < 0.01$, and ***$P < 0.001$ versus vehicle control. Data were analyzed by two-way ANOVA with Tukey's multiple comparison test (F) or one-way ANOVA with Dunnett's multiple comparison test (I).

may underlie receptor redistribution at the plasma membrane, and thus indirectly control spatiotemporal signaling. This hypothesis is supported by the finding that mutation of the key hierarchical phosphorylation site of MOR (to generate the MOR S375A mutant) affected the localization of the receptor within the plasma membrane and its spatiotemporal signaling. In this context, β-arrestins are increasingly recognized as scaffolding proteins for signaling complexes, in addition to their traditional roles in the regulation of receptor desensitization and internalization (*40*). Furthermore, evidence suggests that GRKs can also have important scaffolding functions, particularly in the control of ERK activation (*41*, *42*). We hypothesize that the differential assembly of receptor kinases and other signaling mediators in response to morphine versus DAMGO determines MOR redistribution, transient signaling profiles, and the activation of nuclear ERK. Furthermore, this hypothesis entails that the responses of opioid ligands will be highly dependent on the specific protein content of opioid-responsive cells (*6*, *7*, *43*, *44*).

Our results also highlight the importance of PKCα in governing the spatiotemporal signaling profiles of MOR. Previous studies showed that the phosphorylation and desensitization of MOR after stimulation with morphine is partially dependent on PKC (*39*, *45*, *46*). Moreover, there are indications that PKC plays a substantial role in the initiation and maintenance of tolerance to morphine analgesia (*47*, *48*). To date, evidence for morphine-induced activation of PKC comes from coimmunoprecipitation studies showing the recruitment of overexpressed PKCε to MOR (*16*) and increased PKC activity in cell lysates (*49*). By measuring endogenous PKC activity at the subcellular level, we demonstrated that morphine, but not DAMGO, stimulated the sustained activation of PKC at the plasma membrane. Whereas PKC can phosphorylate MOR directly (*32*, *50*), it can also phosphorylate proteins that participate in MOR signaling, such as $G\alpha_i$ (*51*) or GRK2 (*52*), and could therefore restrict receptor redistribution by modulating the function, association, or both of such signaling and scaffolding proteins with MOR.

It is clear that plasma membrane organization plays a critical role in the control of MOR spatiotemporal signaling. Whether MOR resides within biochemically defined, lipid-rich plasma membrane regions is controversial (*53*–*55*). However, and consistent with our findings, previous studies provided evidence for the restricted plasma membrane localization of the receptor as well as the agonist-regulated diffusion of MOR within the plasma membrane (*56*–*59*). Protein-protein interactions were hypothesized to mediate the restricted and slow diffusion of agonist-stimulated, noninternalizing MOR (*60*). Together with this hypothesis, the results presented here suggest that the dynamic organization of MOR within the plasma membrane, rather than the association of MOR with a predefined lipid-rich domain, may control ligand-dependent receptor redistribution and distinct spatiotemporal signaling profiles. The dependence of MOR signaling on plasma membrane localization extends previous studies that demonstrated distinct control of spatiotemporal signaling by endosomally localized GPCRs (*2*, *61*). In the context of MOR, mechanistic insight into the actions of morphine at the cellular level is of particular therapeutic relevance because of the severe side effects induced by this opiate. Whether chronic exposure to opiates differentially alters the spatiotemporal signaling, plasma membrane distribution, or both of MOR remains to be investigated.

Downloaded from http://stke.sciencemag.org/ on February 9, 2016

From M. L. Halls, H. R. Yeatman, C. J. Nowell, G. L. Thompson, A. B. Gondin, S. Civciristov, N. W. Bunnett, N. A. Lambert, D. P. Poole, M. Canals. Plasma membrane localization of the mu-opioid receptor controls spatiotemporal signaling. Sci. Signal. 9, ra16 (2016). Reprinted with permission from AAAS.

RESEARCH ARTICLE

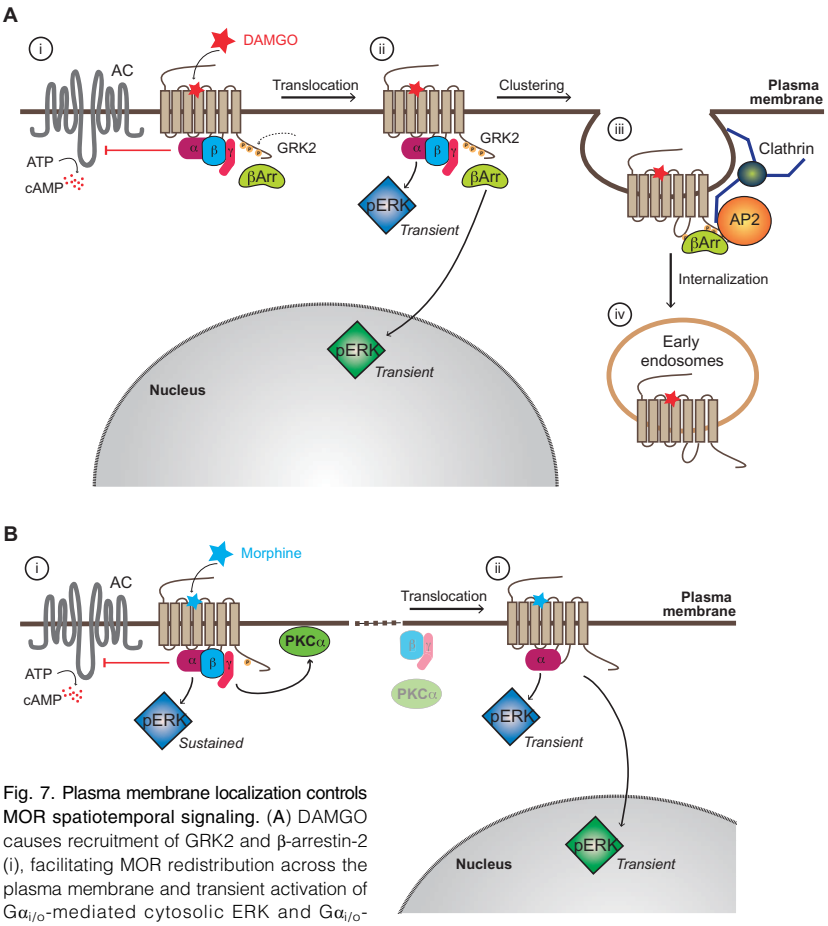


Fig. 7. Plasma membrane localization controls MOR spatiotemporal signaling. (A) DAMGO causes recruitment of GRK2 and β-arrestin-2 (i), facilitating MOR redistribution across the plasma membrane and transient activation of $G\alpha_{i/o}$-mediated cytosolic ERK and $G\alpha_{i/o}$-independent nuclear ERK (ii). Upon prolonged stimulation of MOR, DAMGO stimulates MOR clustering and receptor internalization through clathrin-coated pits (iii) to early endosomes (iv). (B) Morphine stimulates the plasma membrane–localized Gβγ-PKCα pathway, which prevents receptor translocation within the plasma membrane. This causes a sustained activation of $G\alpha_{i/o}$-mediated cytosolic ERK (i). Inhibition of the Gβγ-PKCα pathway or alteration of the organization of the plasma membrane facilitates MOR translocation and the activation of nuclear ERK by morphine (ii) in the absence of receptor internalization.

MATERIALS AND METHODS

Reagents

DAMGO was obtained from Mimotopes. Morphine and anti–FLAG M2 were from Sigma-Aldrich. Coelenterazine h was obtained from Promega. β-Arrestin-1– and β-arrestin-2–specific siRNAs were purchased from GE-Dharmacon. Mouse anti–early endosome antigen 1 was from BD Transduction Laboratories; rabbit anti-MOR (UMB-3) was from Abcam; mouse anti–tubulin βIII isoform for confocal imaging was from Merck Millipore; Alexa Fluor–conjugated goat anti-mouse secondary antibodies were from Jackson ImmunoResearch; anti–caveolin 1, anti–β-actin, and anti–clathrin heavy chain were from Abcam; anti–β-tubulin for Western blotting was from Santa Cruz Biotechnology; antibodies against β-arrestin-1/2 were from Cell Signaling Technology; and fluorescent IRDye–conjugated goat anti-rabbit (800 channel) and anti-mouse (680 channel) secondary antibodies were from LI-COR Biotechnology.

Complementary DNAs

Plasmids encoding KRas-Venus, Rab5a-Venus, green fluorescent protein (GFP)–dynamin, and GFP-dynamin K44E have been previously described (*19*, *61*, *62*). MOR-RLuc was from L. Bohn (Scripps, Jupiter, FL); FLAG-MOR was from M. Christie (University of Sydney, Sydney, New South Wales, Australia); β-arrestin-2–YFP was from M. Caron (University of North Carolina); and FLAG-MOR 11ST/A was from S. Schulz (Friedrich Schiller University, Jena, Germany). The following constructs were obtained from Addgene: cytoEKAR GFP/RFP (plasmid 18680), cytoEKAR Cerulean/Venus (plasmid 18679), nucEKAR GFP/RFP (plasmid 18682) and nucEKAR Cerulean/Venus (plasmid 18681) (*17*), and cytoCKAR (plasmid 14870) and pmCKAR (plasmid 14862) (*18*). MOR S375A has a mutation of the essential site governing hierarchical phosphorylation (human, S377A; mouse, S375A) (*9*) and was generated with the QuikChange site-directed mutagenesis kit. RLuc8-tagged MOR was generated by subcloning MOR into the pcDNA3-RLuc8 vector.

Cell culture and inhibitors

HEK 293 cells were cultured in Dulbecco's modified Eagle's medium (DMEM) supplemented with 5% (v/v) fetal bovine serum (FBS). Cells were transfected with linear polyethyleneimine (*63*). For siRNAs, cells were transfected with scrambled or combined β-arrestin-1 and β-arrestin-2 SMARTpool ON-TARGETplus siRNAs (25 nM) with Lipofectamine 2000, 24 hours before the cells were transfected with plasmids encoding receptor and biosensors. Cells were pretreated with inhibitors for 30 min at 37°C, except for filipin III, MβCD, or MβCD-cholesterol complexes (45-min pretreatment) or PTx (16-hour pretreatment). MβCD-cholesterol complexes were formed as described previously (*64*). Inhibitors were used at the following concentrations: 30 μM PitStop2 or inactive PitStop2, 10 μM NF023, PTx at 100 ng/ml, 5 μM mSIRK or mSIRK L9A, 1 μM GF109203X or Gö6983, 10 nM Gö6976, 10 μM Myr-EAVSLKPT-OH (a PKCε translocation inhibitor peptide), filipin III at 1 μg/ml, 10 mM MβCD, and 2 mM MβCD with 0.2 mM cholesterol (MβCD-cholesterol complexes). All experiments were performed in live cells at 37°C. For all regulation and trafficking experiments, cells were stimulated with an EC_{50} concentration of DAMGO or morphine (both 1 μM) as defined by β-arrestin-2 concentration-response curves (fig. S2A). For all signaling experiments, cells were stimulated with an

Downloaded from http://stke.sciencemag.org/ on February 9, 2016

From M. L. Halls, H. R. Yeatman, C. J. Nowell, G. L. Thompson, A. B. Gondin, S. Civciristov, N. W. Bunnett, N. A. Lambert, D. P. Poole, M. Canals. Plasma membrane localization of the m-opioid receptor controls spatiotemporal signaling. Sci. Signal. 9, ra16 (2016). Reprinted with permission from AAAS.

EC_{50} concentration of DAMGO (10 nM) or morphine (100 nM) as defined by AlphaScreen pERK assays (fig. S1A).

RNA sequencing

RNA was extracted from two passages of HEK 293 cells (P0 and P37) with the RNeasy Mini Kit (Qiagen). Transcriptome sequencing was performed by the Beijing Genomics Institute.

DRG isolation and culture

All procedures involving mice were approved by the Monash Institute of Pharmaceutical Sciences animal ethics committee. DRG neurons were isolated and transfected with 600 ng of cytoEKAR Cerulean/Venus, nucEKAR Cerulean/Venus, or pmCKAR with the Nucleofector system (Lonza). Detailed protocols of DRG isolation and nucleofection were described previously (*63*).

BRET assays

HEK 293 cells were transfected with 1 μg of MOR-RLuc and 4 μg of KRas-Venus, Rab5a-Venus, or β-arrestin-2-YFP. For coexpression, cells were transfected with an additional 2 μg of βARKct, GFP-dynamin, or GFP-dynamin K44E. After 24 hours, cells were plated in poly-D-lysine–coated 96-well plates (CulturPlate, PerkinElmer) and allowed to adhere. Forty-eight hours after transfection, the cells were equilibrated in Hanks' balanced salt solution (HBSS) and then were incubated with vehicle [0.1% dimethyl sulfoxide (DMSO)], DAMGO, or morphine for 30 min. Coelenterazine h (Promega) was added at a final concentration of 5 μM, and the cells were incubated for a further 10 min. BRET measurements were obtained with the PHERAstar Omega microplate reader (BMG Labtech), which enabled sequential integration of the signals detected at 475 ± 30 nm and 535 ± 30 nm with filters with the appropriate band pass. Data were presented as a BRET ratio (calculated as the ratio of the YFP signal to the *Renilla* luciferase signal) corrected for vehicle.

High-content image analysis

HEK 293 cells were plated in poly-D-lysine–coated, black, optically clear 96-well plates (ViewPlate, PerkinElmer) and transfected with plasmid encoding MOR-GFP (20 ng per well). Forty-eight hours after transfection, the cells were incubated with inhibitors and treated with vehicle (0.1% DMSO), DAMGO (1 μM), or morphine (1 μM) for 30 min. Cells were fixed with 4% paraformaldehyde (PFA) and washed three times with phosphate-buffered saline (PBS). Nuclei were stained with Hoechst (1 μg/ml). Images of four fields of view were collected with a GE Healthcare INCell 2000 Analyzer with a Nikon Plan Fluor ELWD 40× [numerical aperture (NA), 0.6] objective. Analysis was performed with the granularity application module in MetaMorph imaging software (v7.8.6, Molecular Devices). Granule detection was set at 4 to 8 μm, nuclei detection was set at 35 to 60 μm, and the total number of cytosolic granules per cell was calculated. The effect of vehicle was subtracted, and the data were expressed relative to the DAMGO-stimulated response (in the absence of inhibitors).

Förster resonance energy transfer

HEK 293 cells were transfected with plasmid encoding MOR (55 ng per well) and with plasmid encoding cytoEKAR GFP/RFP, nucEKAR GFP/RFP, cytoCKAR, or pmCKAR (40 ng per well). For coexpression, cells were transfected with plasmid encoding βARKct, GFP-dynamin, or GFP-dynamin K44E (50 ng per well). Experiments in which GFP-dynamin or GFP-dynamin K44E were coexpressed used the Cerulean-Venus FRET sensors. FRET was measured with a high-content GE Healthcare INCell 2000 Analyzer as described previously (*63*). Briefly, fluorescence imaging was performed with a Nikon Plan Fluor ELWD 40× (NA, 0.6) objective and FRET module. For GFP-RFP emission ratio analysis, cells were sequentially excited with a fluorescein isothiocyanate (FITC) filter (490/20) with emission measured with dsRed (RFP from *Discosoma* sp.) (605/52) and FITC (525/36) filters and a polychroic mirror, optimized for the FITC-dsRed filter pair (Quad4). For cyan fluorescent protein (CFP)–YFP or Cerulean-Venus emission ratio analysis, cells were sequentially excited with a CFP filter (430/24) with emission measured with YFP (535/30) and CFP (470/24) filters and a polychroic mirror, optimized for the CFP-YFP filter pair (Quad3). HEK 293 cells were imaged every 1 min, which enabled image capture at 14 wells/min; DRG neurons were imaged every 1 min with four fields of view per well, which enabled the capture of 3 wells/min. At the end of every experiment, the same cells were stimulated for 10 min with the positive control [200 nM phorbol 12,13-dibutyrate for ERK or 200 nM phorbol 12,13-dibutyrate with phosphatase inhibitor cocktail 2 (Sigma Aldrich) for PKC] to generate a maximal FRET change, and positive emission ratio images were captured for 4 min. Data were analyzed with the FIJI distribution of ImageJ (*65*). The three emission ratio image stacks (baseline, stimulated, and positive) were collated and aligned with the StackCreator script (*63*). Cells were selected, and fluorescence intensity was measured over the combined stack. Background intensity was subtracted, and then the FRET data were plotted as the change in FRET emission ratio relative to the maximal response for each cell [FRET ratio/maximum FRET ratio (F/F_{max})]. For HEK 293 cells, only cells that showed more than a 10% change relative to baseline after stimulation with the positive control were considered for analysis. For DRG neurons, all cells that showed more than a 3% change relative to baseline after stimulation with the positive control were considered for analysis. Ratiometric pseudocolor images were generated as previously described (*66*). The Green Fire Blue LUT was applied, and the brightness and contrast range was set to the minimum and maximum FRET ratios within the image stack (0.13 to 0.23).

GSD-TIRF microscopy

HEK 293 cells and DRG neurons were treated with vehicle (0.1% DMSO), DAMGO, or morphine as indicated in the figure legends; fixed in 4% PFA for 20 min at 4°C; washed for 15 min with PBS; blocked in PBS with 1% normal goat serum and 0.1% saponin for 1 hour at room temperature; and incubated overnight at 4°C with mouse anti-FLAG (at a 1:1000 dilution) for HEK 293 cells or with rabbit anti-MOR (UMB-3, 1:250) and anti–tubulin βIII (1:1000) for DRG neurons. Cells were washed and incubated with Alexa Fluor 568– or Alexa Fluor 647–conjugated goat anti-mouse or anti-rabbit secondary antibodies (1:400; for 2 hours at room temperature). Coverslips were mounted on a concave slide containing 100 mM cysteamine (MEA) and sealed. Cells were observed with a Leica GSD microscope with HCX PL APO 160× (NA, 1.43) objective, SuMo stage, Andor iXon Ultra 897 camera, and LAS AF software. Pumping occurred at 100% laser power until the frame correlation dropped to 0.25. Data were acquired at 50% laser power, and up to 30,000 frames were captured. TIRF penetration was at 110 nm. Only neurons with positive staining for β-tubulin were analyzed. Images were analyzed with FIJI software (*65*). Individual particles were selected with Find Maxima (noise tolerance 5) to generate a binary output of the single points. The average distance between events was calculated by generating a centroid list with the Analyze Particles command and was processed by the Nearest Neighbor Distance (NND) macro (Yuxiong Mao). EDMs were generated from the single-point binary image with the Euclidean distance option.

Whole-cell radioligand binding assays

Cells were plated in a 96-well isoplate (20,000 cells per well; PerkinElmer) and allowed to adhere for 24 hours. The cells were then washed three

Downloaded from http://stke.sciencemag.org/ on February 9, 2016

From M. L. Halls, H. R. Yeatman, C. J. Nowell, G. L. Thompson, A. B. Gondin, S. Civciristov, N. W. Bunnett, N. A. Lambert, D. P. Poole, M. Canals. Plasma membrane localization of the mu-opioid receptor controls spatiotemporal signaling. Sci. Signal. 9, ra16 (2016). Reprinted with permission from AAAS.

times with assay buffer [146 mM NaCl, 10 mM D-glucose, 5 mM KCl, 1 mM $MgSO_4$, 2 mM $CaCl_2$, 1.5 mM $NaHCO_3$, 10 mM Hepes (pH 7.45)] and incubated for 3 hours at 4°C with increasing concentrations of [^{3}H]diprenorphine (specific activity, 36.1 Ci/mmol). Nonspecific binding was determined by the coaddition of 1 μM naloxone. After being washed in cold saline, the cells were solubilized in Optiphase scintillant, and radioactivity was measured in a MicroBeta counter (PerkinElmer).

AlphaScreen pERK signaling assays

ERK1/2 phosphorylation was detected with the AlphaScreen ERK1/2 SureFire protocol (TGR Biosciences). Briefly, cells were seeded in clear 96-well plates (40,000 cells per well) and allowed to adhere for 8 hours. Cells were washed twice with PBS and incubated in serum-free DMEM overnight at 37°C and 5% CO_2. Cells were stimulated for 5 min, and then the medium was replaced with lysis buffer in which the cells were incubated for 5 min at room temperature with agitation. Lysates were transferred to a 384-well white ProxiPlate (PerkinElmer), and then a mixture of activation buffer, reaction buffer, and AlphaScreen beads (100:600:3) was added to generate a final lysate/mixture ratio of 5:8. Plates were incubated for 1.5 hours at 37°C and then were read on a Fusion-α plate reader (PerkinElmer). Data were expressed relative to the responses of cells to vehicle (0%) and 10% (v/v) FBS (100%).

Confirmation of β-arrestin knockdown

Cells were transfected with combined β-arrestin-1– and β-arrestin-2–specific siRNAs or scrambled siRNA (25 nM) in a six-well plate. After 72 hours, cells were washed with ice-cold PBS, harvested by scraping in 1 ml of PBS, and then centrifuged at 500*g* for 5 min at 4°C. Cells were then lysed in 100 μl of lysis buffer [50 mM Tris-HCl (pH 7.4), 150 mM NaCl, 0.1 mM EDTA, 0.6% Tween 20, protease inhibitor cocktail] for 30 min on ice by passing through a 26-gauge needle 10 times. Lysates were then centrifuged at 700*g* for 5 min at 4°C; the supernatants were incubated with 50 U of deoxyribonuclease I for 1 hour at 37°C, and then Laemmli sample buffer was added.

Basic membrane fractionation

Cells transfected with 5 μg of plasmid encoding FLAG-MOR (in confluent 10-cm dishes) were treated with 0.1% DMSO (vehicle), 10 μM DAMGO, or 10 μM morphine for 10 min at 37°C; washed with ice-cold MES buffer [25 mM MES (pH 6.5), 150 mM NaCl]; and then incubated in 1 ml of ice-cold MBS buffer (MES containing 1 mM EDTA and protease inhibitor cocktail) for 10 min on ice. The cells were scraped, centrifuged at 500*g* for 5 min at 4°C, and then resuspended in 0.5 ml of MBS buffer containing 1% Triton X-100. After a 20-min incubation on ice, samples were homogenized with a 2-ml Dounce homogenizer and centrifuged at 16,000*g* for 5 min at 4°C. The supernatants were collected as the Triton X-100–soluble fractions. The pellets (the Triton X-100–insoluble fractions) were resuspended in 225 μl of MBS containing 1% Triton X-100 by sonication three times (30 s, 20% amplitude, 2-mm microprobe) with a Q125 sonicator (Qsonica). Laemmli sample buffer was added, and the samples were incubated at 37°C for 10 min.

Western blotting analysis

Samples were resolved by SDS-PAGE with 10% tris-glycine gels and then were transferred onto 0.45-μm Bio-Rad low-fluorescence polyvinylidene difluoride membranes with a Trans-Blot SD Semi-Dry Transfer Cell (Bio-Rad). Membranes were blocked for 1 hour at room temperature with Odyssey Blocking Buffer (LI-COR Biotechnology) and then were incubated with primary antibody overnight at 4°C. The membranes were washed three times in PBS containing 0.1% Tween 20, incubated with secondary antibody for 1 hour at room temperature, and then were washed three times in PBS containing 0.1% Tween 20. Secondary antibody fluorescence was detected with an Odyssey Classic Infrared Imager (LI-COR Biotechnology) with the intensity setting adjusted to be in the linear range for infrared fluorescence detection. Antibodies were used at the following dilutions: mouse anti–FLAG M2, 1:1000; rabbit anti–caveolin 1, 1:1000; rabbit anti–β-tubulin, 1:5000; rabbit anti–β-arrestin-1/2, 1:2000; mouse anti–β-actin, 1:2000; goat anti-rabbit IRDye800, 1:5000; and goat anti-mouse IRDye680, 1:10,000.

Localization of MOR or β_2AR by confocal microscopy

Cells expressing MOR-GFP were treated with vehicle (0.1% DMSO), DAMGO (1 μM), or morphine (1 μM), whereas cells expressing β_2AR-GFP were treated with vehicle (0.1% ascorbic acid) or 1 μM isoprenaline for the times indicated in the figure legends. After stimulation, the cells were fixed with 4% PFA in PBS for 20 min at 4°C and then were washed for 15 min with PBS. Cells were blocked in PBS containing 1% normal goat serum and 0.1% saponin for 1 hour at room temperature and then were incubated with rabbit anti–clathrin heavy chain (1:1000) overnight at 4°C. Cells were washed and incubated with Alexa Fluor 568–conjugated goat anti-rabbit secondary antibody (1:400) for 2 hours at room temperature. To visualize the colocalization of MOR-GFP or β_2AR-GFP with clathrin in HEK 293 cells or of MOR with β-tubulin in DRG neurons, cells were observed with a Leica SP8 confocal microscope and HCX PL APO 63× CS2 (NA, 1.40) oil objective. Images were collected at a zoom of 1 to 3, and three to five optical sections were taken at intervals of 0.39 μm. Colocalization between receptor and clathrin was quantified with the colocalization threshold command in FIJI (*65*) after background intensity was subtracted from the corresponding images.

SUPPLEMENTARY MATERIALS

www.sciencesignaling.org/cgi/content/full/9/414/ra16/DC1
Fig. S1. Ligand-dependent spatiotemporal signaling of MOR.
Fig. S2. MOR regulation and its effect on cytosolic ERK activity.
Fig. S3. Roles of PKC and receptor phosphorylation on the MOR-dependent spatiotemporal profiles of ERK signaling.
Fig. S4. MOR localization within the plasma membrane is ligand-dependent.
Fig. S5. Effect of membrane disruption on MOR trafficking and spatiotemporal signaling.
Table S1. Expression of wild-type MOR and the MOR S375A mutant.

REFERENCES AND NOTES

1. N. G. Tsvetanova, M. von Zastrow, Spatial encoding of cyclic AMP signaling specificity by GPCR endocytosis. *Nat. Chem. Biol.* **10**, 1061–1065 (2014).
2. D. Calebiro, V. O. Nikolaev, M. C. Gagliani, T. de Filippis, C. Dees, C. Tacchetti, L. Persani, M. J. Lohse, Persistent cAMP-signals triggered by internalized G-protein–coupled receptors. *PLOS Biol.* **7**, e1000172 (2009).
3. V. O. Nikolaev, M. Bünemann, E. Schmitteckert, M. J. Lohse, S. Engelhardt, Cyclic AMP imaging in adult cardiac myocytes reveals far-reaching β_1-adrenergic but locally confined β_2-adrenergic receptor–mediated signaling. *Circ. Res.* **99**, 1084–1091 (2006).
4. K. Ahlbeck, Opioids: A two-faced Janus. *Curr. Med. Res. Opin.* **27**, 439–448 (2011).
5. R. Al-Hasani, M. R. Bruchas, Molecular mechanisms of opioid receptor-dependent signaling and behavior. *Anesthesiology* **115**, 1363–1381 (2011).
6. J. L. Whistler, M. von Zastrow, Morphine-activated opioid receptors elude desensitization by β-arrestin. *Proc. Natl. Acad. Sci. U.S.A.* **95**, 9914–9919 (1998).
7. J. Zhang, S. S. G. Ferguson, L. S. Barak, S. R. Bodduluri, S. A. Laporte, P.-Y. Law, M. G. Caron, Role for G protein-coupled receptor kinase in agonist-specific regulation of μ-opioid receptor responsiveness. *Proc. Natl. Acad. Sci. U.S.A.* **95**, 7157–7162 (1998).
8. N. Quillinan, E. K. Lau, M. Virk, M. von Zastrow, J. T. Williams, Recovery from μ-opioid receptor desensitization after chronic treatment with morphine and methadone. *J. Neurosci.* **31**, 4434–4443 (2011).
9. S. Just, S. Illing, M. Trester-Zedlitz, E. K. Lau, S. J. Kotowski, E. Miess, A. Mann, C. Doll, J. C. Trinidad, A. L. Burlingame, M. von Zastrow, S. Schulz, Differentiation of opioid drug effects by hierarchical multi-site phosphorylation. *Mol. Pharmacol.* **83**, 633–639 (2013).

Downloaded from http://stke.sciencemag.org/ on February 9, 2016

From M. L. Halls, H. R. Yeatman, C. J. Nowell, G. L. Thompson, A. B. Gondin, S. Civciristov, N. W. Bunnett, N. A. Lambert, D. P. Poole, M. Canals. Plasma membrane localization of the m-opioid receptor controls spatiotemporal signaling. Sci. Signal. 9, ra16 (2016). Reprinted with permission from AAAS.

10. D. E. Keith, S. R. Murray, P. A. Zaki, P. C. Chu, D. V. Lissin, L. Kang, C. J. Evans, M. von Zastrow, Morphine activates opioid receptors without causing their rapid internalization. *J. Biol. Chem.* **271**, 19021–19024 (1996).
11. L. M. Bohn, R. J. Lefkowitz, R. R. Gainetdinov, K. Peppel, M. G. Caron, F.-T. Lin, Enhanced morphine analgesia in mice lacking β-arrestin 2. *Science* **286**, 2495–2498 (1999).
12. C. E. Groer, K. Tidgewell, R. A. Moyer, W. W. Harding, R. B. Rothman, T. E. Prisinzano, L. M. Bohn, An opioid agonist that does not induce μ-opioid receptor—Arrestin interactions or receptor internalization. *Mol. Pharmacol.* **71**, 549–557 (2007).
13. S. M. DeWire, D. S. Yamashita, D. H. Rominger, G. Liu, C. L. Cowan, T. M. Graczyk, X.-T. Chen, P. M. Pitis, D. Gotchev, C. Yuan, M. Koblish, M. W. Lark, J. D. Violin, A G protein-biased ligand at the μ-opioid receptor is potently analgesic with reduced gastrointestinal and respiratory dysfunction compared with morphine. *J. Pharmacol. Exp. Ther.* **344**, 708–717 (2013).
14. H. Zheng, J. Chu, Y. Qiu, H. H. Loh, P.-Y. Law, Agonist-selective signaling is determined by the receptor location within the membrane domains. *Proc. Natl. Acad. Sci. U.S.A.* **105**, 9421–9426 (2008).
15. H. Zheng, H. H. Loh, P.-Y. Law, β-Arrestin-dependent μ-opioid receptor-activated extracellular signal-regulated kinases (ERKs) translocate to nucleus in contrast to G protein-dependent ERK activation. *Mol. Pharmacol.* **73**, 178–190 (2008).
16. H. Zheng, J. Chu, Y. Zhang, H. H. Loh, P.-Y. Law, Modulating μ-opioid receptor phosphorylation switches agonist-dependent signaling as reflected in PKCε activation and dendritic spine stability. *J. Biol. Chem.* **286**, 12724–12733 (2011).
17. C. D. Harvey, A. G. Ehrhardt, C. Cellurale, H. Zhong, R. Yasuda, R. J. Davis, K. Svoboda, A genetically encoded fluorescent sensor of ERK activity. *Proc. Natl. Acad. Sci. U.S.A.* **105**, 19264–19269 (2008).
18. J. D. Violin, J. Zhang, R. Y. Tsien, A. C. Newton, A genetically encoded fluorescent reporter reveals oscillatory phosphorylation by protein kinase C. *J. Cell Biol.* **161**, 899–909 (2003).
19. T.-H. Lan, Q. Liu, C. Li, G. Wu, N. A. Lambert, Sensitive and high resolution localization and tracking of membrane proteins in live cells with BRET. *Traffic* **13**, 1450–1456 (2012).
20. D. D. Jensen, C. B. Godfrey, C. Niklas, M. Canals, M. Kocan, D. P. Poole, J. E. Murphy, F. Alemi, G. S. Cottrell, C. Korbmacher, N. A. Lambert, N. W. Bunnett, C. U. Corvera, The bile acid receptor TGR5 does not interact with β-arrestins or traffic to endosomes but transmits sustained signals from plasma membrane rafts. *J. Biol. Chem.* **288**, 22942–22960 (2013).
21. M. Freissmuth, S. Boehm, W. Beindl, P. Nickel, A. P. IJzerman, M. Hohenegger, C. Nanoff, Suramin analogues as subtype-selective G protein inhibitors. *Mol. Pharmacol.* **49**, 602–611 (1996).
22. T. Katada, M. Ui, Direct modification of the membrane adenylate cyclase system by islet-activating protein due to ADP-ribosylation of a membrane protein. *Proc. Natl. Acad. Sci. U.S.A.* **79**, 3129–3133 (1982).
23. L. von Kleist, W. Stahlschmidt, H. Bulut, K. Gromova, D. Puchkov, M. J. Robertson, K. A. MacGregor, N. Tomilin, A. Pechstein, N. Chau, M. Chircop, J. Sakoff, J. P. von Kries, W. Saenger, H.-G. Kräusslich, O. Shupliakov, P. J. Robinson, A. McCluskey, V. Haucke, Role of the clathrin terminal domain in regulating coated pit dynamics revealed by small molecule inhibition. *Cell* **146**, 471–484 (2011).
24. J. S. Herskovits, C. C. Burgess, R. A. Obar, R. B. Vallee, Effects of mutant rat dynamin on endocytosis. *J. Cell Biol.* **122**, 565–578 (1993).
25. J. K. Scott, S.-F. Huang, B. P. Gangadhar, G. M. Samoriski, P. Clapp, R. A. Gross, R. Taussig, A. V. Smrcka, Evidence that a protein-protein interaction "hot spot on heterotrimeric G protein βγ subunits is used for recognition of a subclass of effectors. *EMBO J.* **20**, 767–776 (2001).
26. W. J. Koch, B. E. Hawes, J. Inglese, L. M. Luttrell, R. J. Lefkowitz, Cellular expression of the carboxyl terminus of a G protein-coupled receptor kinase attenuates $G_{\beta\gamma}$-mediated signaling. *J. Biol. Chem.* **269**, 6193–6197 (1994).
27. D. Toullec, P. Pianetti, H. Coste, P. Bellevergue, T. Grand-Perret, M. Ajakane, V. Baudet, P. Boissin, E. Boursier, F. Loriolle, L. Duhamel, D. Charon, J. Kirilovsky, The bisindolylmaleimide GF 109203X is a potent and selective inhibitor of protein kinase C. *J. Biol. Chem.* **266**, 15771–15781 (1991).
28. M. Gschwendt, S. Dieterich, J. Rennecke, W. Kittstein, H.-J. Mueller, F.-J. Johannes, Inhibition of protein kinase C μ by various inhibitors. Inhibition from protein kinase c isoenzymes. *FEBS Lett.* **392**, 77–80 (1996).
29. C. P. Bailey, S. Oldfield, J. Llorente, C. J. Caunt, A. G. Teschemacher, L. Roberts, C. A. McArdle, F. L. Smith, W. L. Dewey, E. Kelly, G. Henderson, Involvement of PKCα and G-protein-coupled receptor kinase 2 in agonist-selective desensitization of μ-opioid receptors in mature brain neurons. *Br. J. Pharmacol.* **158**, 157–164 (2009).
30. M. Inoue, H. Ueda, Protein kinase C-mediated acute tolerance to peripheral μ-opioid analgesia in the bradykinin-nociception test in mice. *J. Pharmacol. Exp. Ther.* **293**, 662–669 (2000).
31. F. L. Smith, B. H. Gabra, P. A. Smith, M. C. Redwood, W. L. Dewey, Determination of the role of conventional, novel and atypical PKC isoforms in the expression of morphine tolerance in mice. *Pain* **127**, 129–139 (2007).
32. S. Illing, A. Mann, S. Schulz, Heterologous regulation of agonist-independent μ-opioid receptor phosphorylation by protein kinase C. *Br. J. Pharmacol.* **171**, 1330–1340 (2014).
33. G. Martiny-Baron, M. G. Kazanietz, H. Mischak, P. M. Blumberg, G. Kochs, H. Hug, D. Marmé, C. Schächtele, Selective inhibition of protein kinase C isozymes by the indolocarbazole Gö 6976. *J. Biol. Chem.* **268**, 9194–9197 (1993).
34. J. A. Johnson, M. O. Gray, C.-H. Chen, D. Mochly-Rosen, A protein kinase C translocation inhibitor as an isozyme-selective antagonist of cardiac function. *J. Biol. Chem.* **271**, 24962–24966 (1996).
35. S. Schulz, D. Mayer, M. Pfeiffer, R. Stumm, T. Koch, V. Höllt, Morphine induces terminal μ-opioid receptor desensitization by sustained phosphorylation of serine-375. *EMBO J.* **23**, 3282–3289 (2004).
36. Y. Ohtani, T. Irie, K. Uekama, K. Fukunaga, J. Pitha, Differential effects of α-, β- and γ-cyclodextrins on human erythrocytes. *Eur. J. Biochem.* **186**, 17–22 (1989).
37. A. W. Norman, R. A. Demel, B. de Kruyff, L. L. M. van Deenen, Studies on the biological properties of polyene antibiotics. Evidence for the direct interaction of filipin with cholesterol. *J. Biol. Chem.* **247**, 1918–1929 (1972).
38. A. I. Basbaum, D. M. Bautista, G. Scherrer, D. Julius, Cellular and molecular mechanisms of pain. *Cell* **139**, 267–284 (2009).
39. C. Doll, J. Konietzko, F. Pöll, T. Koch, V. Höllt, S. Schulz, Agonist-selective patterns of μ-opioid receptor phosphorylation revealed by phosphosite-specific antibodies. *Br. J. Pharmacol.* **164**, 298–307 (2011).
40. K. A. DeFea, β-Arrestins as regulators of signal termination and transduction: How do they determine what to scaffold? *Cell. Signal.* **23**, 621–629 (2011).
41. J. D. Robinson, J. A. Pitcher, G protein-coupled receptor kinase 2 (GRK2) is a Rho-activated scaffold protein for the ERK MAP kinase cascade. *Cell. Signal.* **25**, 2831–2839 (2013).
42. P. Penela, C. Ribas, I. Aymerich, N. Eijkelkamp, O. Barreiro, C. Heijnen, A. Kavelaars, F. Sánchez-Madrid, F. Mayor, G protein-coupled receptor kinase 2 positively regulates epithelial cell migration. *EMBO J.* **27**, 1206–1218 (2008).
43. H. Haberstock-Debic, M. Wein, M. Barrot, E. E. O. Colago, Z. Rahman, R. L. Neve, V. M. Pickel, E. J. Nestler, M. von Zastrow, A. L. Svingos, Morphine acutely regulates opioid receptor trafficking selectively in dendrites of nucleus accumbens neurons. *J. Neurosci.* **23**, 4324–4332 (2003).
44. H. Haberstock-Debic, K.-A. Kim, Y. J. Yu, M. von Zastrow, Morphine promotes rapid, arrestin-dependent endocytosis of μ-opioid receptors in striatal neurons. *J. Neurosci.* **25**, 7847–7857 (2005).
45. C. P. Bailey, F. L. Smith, E. Kelly, W. L. Dewey, G. Henderson, How important is protein kinase C in μ-opioid receptor desensitization and morphine tolerance? *Trends Pharmacol. Sci.* **27**, 558–565 (2006).
46. E. A. Johnson, S. Oldfield, E. Braksator, A. Gonzalez-Cuello, D. Couch, K. J. Hall, S. J. Mundell, C. P. Bailey, E. Kelly, G. Henderson, Agonist-selective mechanisms of μ-opioid receptor desensitization in human embryonic kidney 293 cells. *Mol. Pharmacol.* **70**, 676–685 (2006).
47. X.-Y. Hua, A. Moore, S. Malkmus, S. F. Murray, N. Dean, T. L. Yaksh, M. Butler, Inhibition of spinal protein kinase Cα expression by an antisense oligonucleotide attenuates morphine infusion-induced tolerance. *Neuroscience* **113**, 99–107 (2002).
48. F. L. Smith, A. B. Lohmann, W. L. Dewey, Involvement of phospholipid signal transduction pathways in morphine tolerance in mice. *Br. J. Pharmacol.* **128**, 220–226 (1999).
49. Y. Qiu, W. Zhao, Y. Wang, J.-R. Xu, E. Huie, S. Jiang, Y.-H. Yan, H. H. Loh, H.-Z. Chen, P.-Y. Law, FK506-binding protein 12 modulates μ-opioid receptor phosphorylation and protein kinase Cε–dependent signaling by its direct interaction with the receptor. *Mol. Pharmacol.* **85**, 37–49 (2014).
50. B. Feng, Z. Li, J. B. Wang, Protein kinase C-mediated phosphorylation of the μ-opioid receptor and its effects on receptor signaling. *Mol. Pharmacol.* **79**, 768–775 (2011).
51. J. Chu, H. Zheng, Y. Zhang, H. H. Loh, P.-Y. Law, Agonist-dependent μ-opioid receptor signaling can lead to heterologous desensitization. *Cell. Signal.* **22**, 684–696 (2010).
52. R. Winstel, S. Freund, C. Krasel, E. Hoppe, M. J. Lohse, Protein kinase cross-talk: Membrane targeting of the β-adrenergic receptor kinase by protein kinase C. *Proc. Natl. Acad. Sci. U.S.A.* **93**, 2105–2109 (1996).
53. P. Huang, W. Xu, S.-I. Yoon, C. Chen, P. L.-G. Chong, E. M. Unterwald, L.-Y. Liu-Chen, Agonist treatment did not affect association of mu opioid receptors with lipid rafts and cholesterol reduction had opposite effects on the receptor-mediated signaling in rat brain and CHO cells. *Brain Res.* **1184**, 46–56 (2007).
54. G. Gaibelet, C. Millot, C. Lebrun, S. Ravault, A. Saulière, A. André, B. Lagane, A. Lopez, Cholesterol content drives distinct pharmacological behaviours of μ-opioid receptor in different microdomains of the CHO plasma membrane. *Mol. Membr. Biol.* **25**, 423–435 (2008).
55. L. Moulédous, S. Merker, J. Neasta, B. Roux, J.-M. Zajac, C. Mollereau, Neuropeptide FF-sensitive confinement of mu opioid receptor does not involve lipid rafts in SH-SY5Y cells. *Biochem. Biophys. Res. Commun.* **373**, 80–84 (2008).
56. K. Suzuki, K. Ritchie, E. Kajikawa, T. Fujiwara, A. Kusumi, Rapid hop diffusion of a G protein-coupled receptor in the plasma membrane as revealed by single-molecule techniques. *Biophys. J.* **88**, 3659–3680 (2005).

Downloaded from http://stke.sciencemag.org/ on February 9, 2016

From M. L. Halls, H. R. Yeatman, C. J. Nowell, G. L. Thompson, A. B. Gondin, S. Civciristov, N. W. Bunnett, N. A. Lambert, D. P. Poole, M. Canals. Plasma membrane localization of the mopioid receptor controls spatiotemporal signaling. Sci. Signal. 9, ra16 (2016). Reprinted with permission from AAAS.

57. F. Daumas, N. Destainville, C. Millot, A. Lopez, D. Dean, L. Salomé, Confined diffusion without fences of a G protein-coupled receptor as revealed by single particle tracking. *Biophys. J.* **84**, 356–366 (2003).
58. F. Daumas, N. Destainville, C. Millot, A. Lopez, D. Dean, L. Salomé, Interprotein interactions are responsible for the confined diffusion of a G-protein-coupled receptor at the cell surface. *Biochem. Soc. Trans.* **31**, 1001–1005 (2003).
59. A. Saulière, G. Gaibelet, C. Millot, S. Mazères, A. Lopez, L. Salomé, Diffusion of the mu opioid receptor at the surface of human neuroblastoma SH-SY5Y cells is restricted to permeable domains. *FEBS Lett.* **580**, 5227–5231 (2006).
60. A. Lopez, L. Salomé, Membrane functional organisation and dynamic of μ-opioid receptors. *Cell. Mol. Life Sci.* **66**, 2093–2108 (2009).
61. D. D. Jensen, M. L. Halls, J. E. Murphy, M. Canals, F. Cattaruzza, D. P. Poole, T. Lieu, H.-W. Koon, C. Pothoulakis, N. W. Bunnett, Endothelin-converting enzyme 1 and β-arrestins exert spatiotemporal control of substance P-induced inflammatory signals. *J. Biol. Chem.* **289**, 20283–20294 (2014).
62. F. Schmidlin, O. Déry, K. O. DeFea, L. Slice, S. Patierno, C. Sternini, E. F. Grady, N. W. Bunnett, Dynamin and Rab5a-dependent trafficking and signaling of the neurokinin 1 receptor. *J. Biol. Chem.* **276**, 25427–25437 (2001).
63. M. L. Halls, D. P. Poole, A. M. Ellisdon, C. J. Nowell, M. Canals, in *Methods in Molecular Biology* (Springer, New York, 2015), vol. 1335, pp. 131–161.
64. U. Klein, G. Gimpl, F. Fahrenholz, Alteration of the myometrial plasma membrane cholesterol content with β-cyclodextrin modulates the binding affinity of the oxytocin receptor. *Biochemistry* **34**, 13784–13793 (1995).
65. J. Schindelin, I. Arganda-Carreras, E. Frise, V. Kaynig, M. Longair, T. Pietzsch, S. Preibisch, C. Rueden, S. Saalfeld, B. Schmid, J.-Y. Tinevez, D. J. White, V. Hartenstein, K. Eliceiri, P. Tomancak, A. Cardona, Fiji: An open-source platform for biological-image analysis. *Nat. Methods* **9**, 676–682 (2012).
66. E. Kardash, J. Bandemer, E. Raz, Imaging protein activity in live embryos using fluorescence resonance energy transfer biosensors. *Nat. Protoc.* **6**, 1835–1846 (2011).

Acknowledgments: We thank D. D. Jensen for technical assistance; M. J. Christie for critical discussion; R. J. Summers, J. R. Lane, and A. M. Ellisdon for careful review of this manuscript; and L. Bohn, S. Schulz, and M. Caron for providing DNAs. **Funding:** This work was supported by a Monash Fellowship to M.C.; National Health and Medical Research Council (NHMRC) RD Wright Fellowship to M.L.H. (1061687); NHMRC Australia Fellowship to N.W.B. (63303); NHMRC Project Grants (1011796, 1047633, 1049682, and 1031886) to M.C., M.L.H., and N.W.B.; ARC Centre of Excellence in Convergent Bio-Nano Science and Technology, Monash Institute of Pharmaceutical Sciences Large Grant Support Scheme grants to M.C. and M.L.H.; and Monash University support to N.W.B. G.L.T. is funded by DSTO (Defence Science and Technology Organisation) Australia. **Author contributions:** M.L.H. and M.C. designed the study; M.L.H., H.R.Y., C.J.N., G.L.T., A.B.G., S.C., D.P.P., and M.C. performed the experiments; M.L.H. and M.C. analyzed and interpreted the data; M.L.H. and M.C. drafted and wrote the manuscript; all authors reviewed the manuscript; and N.W.B. and N.A.L. provided reagents. **Competing interests:** The authors declare that they have no competing interests.

Submitted 28 June 2015
Accepted 25 January 2016
Final Publication 9 February 2016
10.1126/scisignal.aac9177
Citation: M. L. Halls, H. R. Yeatman, C. J. Nowell, G. L. Thompson, A. B. Gondin, S. Civciristov, N. W. Bunnett, N. A. Lambert, D. P. Poole, M. Canals, Plasma membrane localization of the μ-opioid receptor controls spatiotemporal signaling. *Sci. Signal.* **9**, ra16 (2016).

Downloaded from http://stke.sciencemag.org/ on February 9, 2016

From M. L. Halls, H. R. Yeatman, C. J. Nowell, G. L. Thompson, A. B. Gondin, S. Civciristov, N. W. Bunnett, N. A. Lambert, D. P. Poole, M. Canals. Plasma membrane localization of the m-opioid receptor controls spatiotemporal signaling. Sci. Signal. 9, ra16 (2016). Reprinted with permission from AAAS.

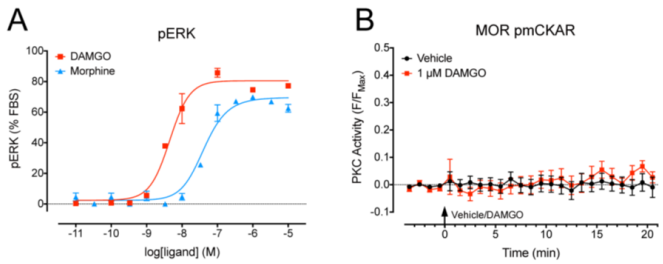


Fig. S1. Ligand-dependent spatiotemporal signaling of MOR. (**A**) Concentration-response curves for the DAMGO- and morphine-dependent activation (phosphorylation) of ERK in HEK 293 cells as determined by the AlphaScreen assay. Data are means ± SEM of three experiments. (**B**) Plasma membrane-localized PKC activity in response to a high concentration of DAMGO. Data are means ± SEM of 71 to 79 cells from three experiments.

From M. L. Halls, H. R. Yeatman, C. J. Nowell, G. L. Thompson, A. B. Gondin, S. Civciristov, N. W. Bunnett, N. A. Lambert, D. P. Poole, M. Canals. Plasma membrane localization of the m-opioid receptor controls spatiotemporal signaling. Sci. Signal. 9, ra16 (2016). Reprinted with permission from AAAS.

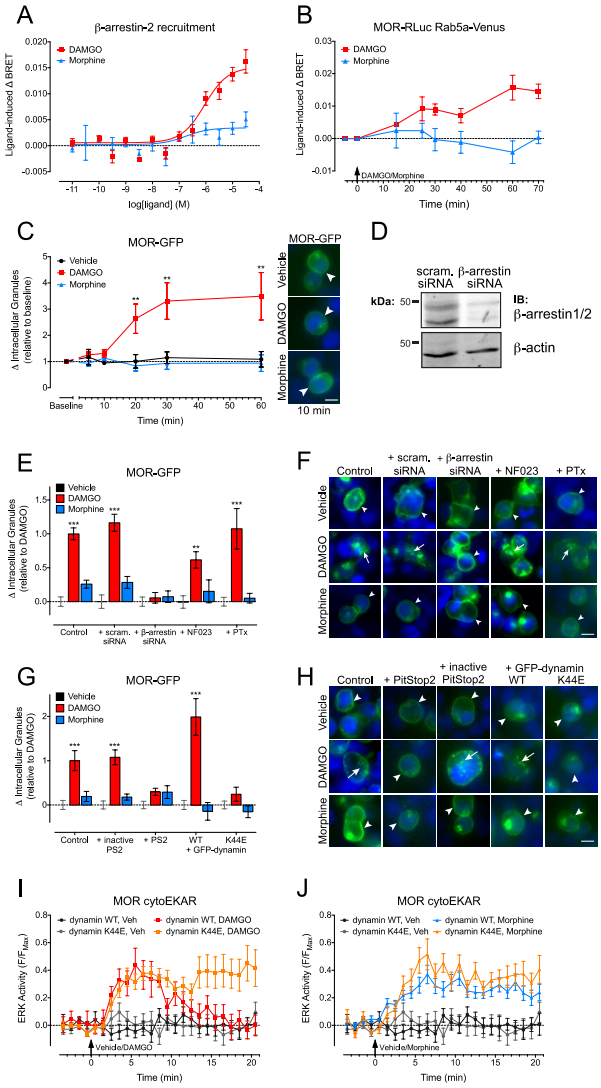


Fig. S2 MOR regulation and its effect on cytosolic ERK activity. (**A**) Concentration-response curves for ligand-dependent β-arrestin-2 recruitment to receptors in HEK 293 cells. Data are means ± SEM of three experiments. (**B**) Time course of BRET between MOR-RLuc and Rab5a-Venus in HEK 293 cells in response to DAMGO or morphine. Data are means ± SEM of three experiments. (**C**) Time course of MOR-GFP internalization in HEK 293 cells. Data are means ± SEM of four to six experiments. Inset: representative images. Scale bar: 10 μm. (**D**) Western blotting (IB) analysis of the knockdown of β-arrestins in HEK 293 cells with siRNA. Blots are representative of three experiments. (**E**) Analysis of the ligand-dependent internalization of MOR-GFP in HEK 293 cells after knockdown of β-arrestins or inhibition of $G\alpha_{i/o}$ protein function. Data are means ± SEM of four to six experiments. (**F**) Representative images from the experiments shown in (E). Scale bar: 10 μm. (**G**) Analysis of the ligand-dependent internalization of MOR-GFP in cells in which endocytosis was inhibited. Data are means ±

From M. L. Halls, H. R. Yeatman, C. J. Nowell, G. L. Thompson, A. B. Gondin, S. Civciristov, N. W. Bunnett, N. A. Lambert, D. P. Poole, M. Canals. Plasma membrane localization of the m-opioid receptor controls spatiotemporal signaling. Sci. Signal. 9, ra16 (2016). Reprinted with permission from AAAS.

SEM of four to twelve experiments. (**H**) Representative images from the experiments shown in (G). Scale bar: 10 μm. (**I**) Effect of inhibition of dynamin on the activation of cytosolic ERK in response to DAMGO. Data are means ± SEM of 22 to 57 cells from three experiments. (**J**) Effect of inhibition of dynamin on the activation of cytosolic ERK in response to morphine. Data are means ± SEM of 22 to 61 cells from three experiments. In (C), (F), and (H), arrowheads indicate cell-surface MORs, whereas arrows indicate intracellular MORs. $^{**}P < 0.01$ and $^{***}P < 0.001$ versus vehicle control. Data were analyzed by two-way ANOVA with Dunnett's (C) or Tukey's (E and G) multiple comparison tests. Scram., scrambled; PS2, PitStop2.

From M. L. Halls, H. R. Yeatman, C. J. Nowell, G. L. Thompson, A. B. Gondin, S. Civciristov, N. W. Bunnett, N. A. Lambert, D. P. Poole, M. Canals. Plasma membrane localization of the m-opioid receptor controls spatiotemporal signaling. Sci. Signal. 9, ra16 (2016). Reprinted with permission from AAAS.

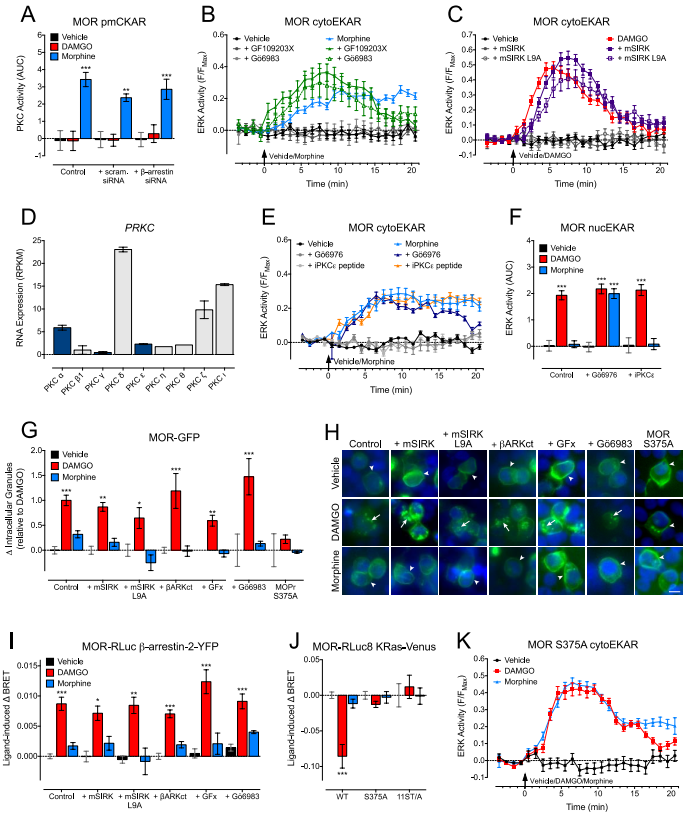


Fig. S3. Roles of PKC and receptor phosphorylation on the MOR-dependent spatiotemporal profiles of ERK signaling. (**A**) Effect of β-arrestin knockdown on plasma membrane PKC activity in HEK 293 cells. Data are means ± SEM of 37 to 86 cells from three experiments. (**B**) Effect of PKC inhibition on the cytosolic ERK response to morphine. Data are means ± SEM of 22 to 108 cells from three experiments. (**C**) Effect of Gβγ inhibition on the cytosolic ERK response to DAMGO. Data are means ± SEM of 26 to 69 cells from three experiments. (**D**) The abundances of mRNAs of the indicated PKC isoforms in HEK 293 cells were determined by qRT-PCR analysis. Data are means ± SEM of three experiments. (**E**) Effect of inhibition of PKCα or PKCε on the activity of cytosolic ERK in response to morphine. Data are means ± SEM of 108 to 188 cells from three experiments. (**F**) Effect of inhibition of PKCα or PKCε inhibition on the activity of nuclear ERK in response to the indicated ligands. Data are means ± SEM of 187 to 284 cells from three experiments. (**G**) Analysis of MOR-GFP internalization in cells in which Gβγ or PKC was inhibited or in which the MOR S375A mutant was overexpressed. Data are means ± SEM of three experiments. (**H**) Representative images from the experiments shown in (G). Scale bar: 10 μm. (**I**) Analysis of BRET between MOR-RLuc and β-arrestin-2-YFP in cells in which Gβγ or PKC was inhibited. Data are means ± SEM of three experiments. (**J**) Analysis of BRET between WT, S375A, or 11ST/1 MOR-RLuc8 and KRas-Venus BRET in response to the indicated ligands. Data are means ± SEM of three to seven experiments. (**K**) Analysis of cytosolic ERK activation by the indicated ligands in cells expressing the MOR S375A mutant. Data are means ± SEM of 63 to 116 cells from three experiments. In (H), arrowheads indicate cell-surface MOR, whereas arrows indicate intracellular MOR. **P* < 0.05, ***P* < 0.01, and ****P* < 0.001 versus vehicle control. Data were analyzed by two-way ANOVA with Tukey's (for A, F, and G) or Dunnett's (for I and J) multiple comparison tests. GFx, GF109203X; iPKCε, inhibitory PKCε peptide.

From M. L. Halls, H. R. Yeatman, C. J. Nowell, G. L. Thompson, A. B. Gondin, S. Civciristov, N. W. Bunnett, N. A. Lambert, D. P. Poole, M. Canals. Plasma membrane localization of the m-opioid receptor controls spatiotemporal signaling. Sci. Signal. 9, ra16 (2016). Reprinted with permission from AAAS.

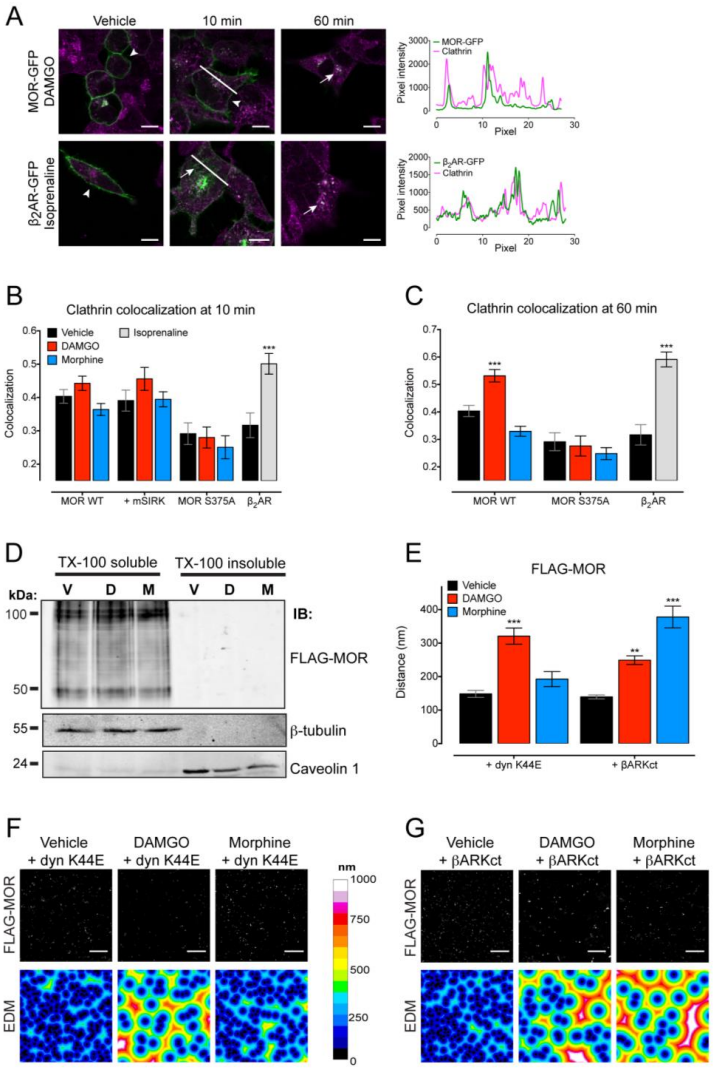


Fig. S4. MOR localization within the plasma membrane is ligand-dependent. (**A**) Representative images showing colocalization of MOR-GFP or β_2AR-GFP (green) with clathrin (purple). Scale bar: 10 μm. Inset: line scan showing pixel intensity across the indicated section after 10 min of stimulation with 1 μM DAMGO or isoprenaline. Data are representative of three experiments. (**B**) Analysis of the colocalization of MOR-GFP or β_2AR-GFP with clathrin after 10 min of stimulation with the indicated ligands. Data are means ± SEM of three experiments. (**C**) Colocalization of MOR-GFP or β_2AR-GFP with clathrin after 60 min of stimulation with the indicated ligands. Data are means ± SEM of three experiments. (**D**) Analysis of FLAG-MOR localization in Triton X-100–soluble or –insoluble membrane domains of HEK 293 cells after fractionation and Western blotting. Caveolin 1 and β-tubulin were used as markers of Triton X-100–insoluble and –soluble domains, respectively. (**E** to **G**) Analysis of the distribution of FLAG-MOR at the plasma membrane with GSD-TIRF. (E) Calculation of the

From M. L. Halls, H. R. Yeatman, C. J. Nowell, G. L. Thompson, A. B. Gondin, S. Civciristov, N. W. Bunnett, N. A. Lambert, D. P. Poole, M. Canals. Plasma membrane localization of the m-opioid receptor controls spatiotemporal signaling. Sci. Signal. 9, ra16 (2016). Reprinted with permission from AAAS.

average distance to nearest neighbor after inhibition of dynamin-dependent endocytosis or Gβγ subunits. Data are means ± SEM of three experiments. (F) Representative GSD-TIRF images and Euclidean Distance maps (EMDs) of HEK 293 cells in which dynamin-dependent endocytosis was inhibited. Scale bar: 1 μm. (G) Representative GSD-TIRF images and EDMs of HEK 293 cells in which Gβγ subunits were inhibited. Scale bar: 1 μm. Pseudocolor scale is as described in (E). In (A), arrowheads indicate cell-surface MORs, whereas arrows indicate intracellular MORs. ***$P < 0.001$ versus vehicle control. Data were analyzed by two-way ANOVA with Dunnett's multiple comparison test. V, vehicle; D, DAMGO; M, morphine; Dyn, dynamin.

From M. L. Halls, H. R. Yeatman, C. J. Nowell, G. L. Thompson, A. B. Gondin, S. Civciristov, N. W. Bunnett, N. A. Lambert, D. P. Poole, M. Canals. Plasma membrane localization of the m-opioid receptor controls spatiotemporal signaling. Sci. Signal. 9, ra16 (2016). Reprinted with permission from AAAS.

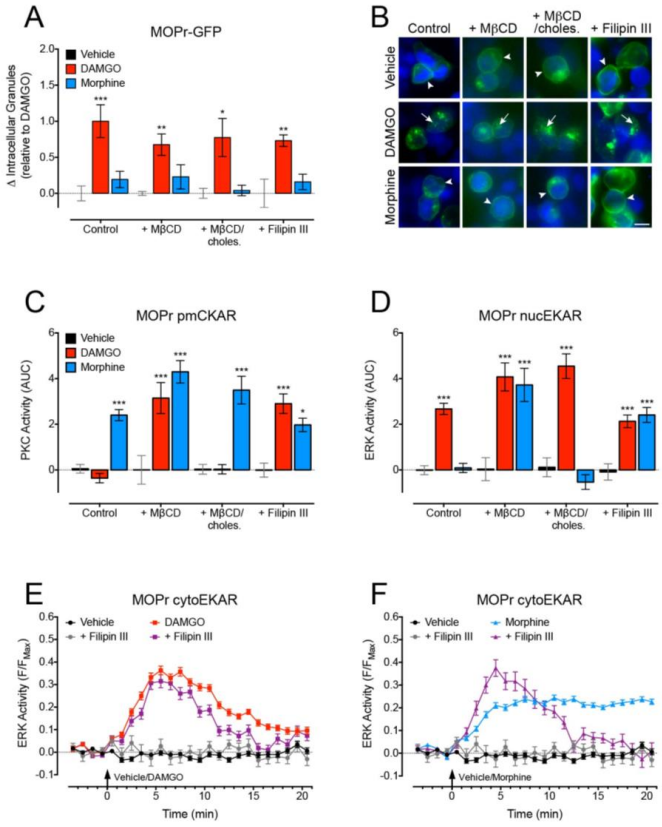


Fig. S5. Effect of membrane disruption on MOR trafficking and spatiotemporal signaling. (**A**) Analysis of MOR-GFP internalization in HEK 293 cells after disruption of the plasma membrane architecture with the indicated reagents. Data are means ± SEM of three experiments. (**B**) Representative images from the experiments shown in (A). Scale bar: 10 μm. (**C**) Analysis of the activation of plasma membrane–localized PKC in HEK 293 cells after disruption of the plasma membrane architecture. Data are means ± SEM of 44 to 192 cells from three experiments. (**D**) Analysis of the activation of nuclear ERK in HEK 293 cells after disruption of the plasma membrane architecture. Data are means ± SEM of 80 to 233 cells from three experiments. (**E**) Analysis of cytosolic ERK activity in response to DAMGO in cells in the presence of Filipin III. Data are means ± SEM of 30 to 167 cells from three experiments. (**F**) Analysis of Cytosolic ERK activity in response to morphine in cells in the presence of Filipin III. Data are means ± SEM of 32 to 194 cells from three experiments. In (B), arrowheads indicate cell surface MORs, whereas arrows indicate intracellular MORs. $*P < 0.05$, $**P < 0.01$, and $***P < 0.001$ versus vehicle control. Data were analyzed by two-way ANOVA with Dunnett's (for A) or Tukey's (for C and D) multiple comparison tests. AUC, area under the curve.

From M. L. Halls, H. R. Yeatman, C. J. Nowell, G. L. Thompson, A. B. Gondin, S. Civciristov, N. W. Bunnett, N. A. Lambert, D. P. Poole, M. Canals. Plasma membrane localization of the m-opioid receptor controls spatiotemporal signaling. Sci. Signal. 9, ra16 (2016). Reprinted with permission from AAAS.

Table S1. Expression of wild-type MOR and the MOR S375A mutant. Whole-cell [^{3}H]diprenorphine saturation binding assays were performed with HEK 293 cells expressing either wild-type (WT) MOR or the MOR S375A mutant. Data are means ± SD of two experiments.

	WT	**S375A**
Bmax (sites/cell)	121000 ± 8700	510000 ± 40800
Kd (nM)	0.32 ± 0.10	0.70 ± 0.22

From M. L. Halls, H. R. Yeatman, C. J. Nowell, G. L. Thompson, A. B. Gondin, S. Civciristov, N. W. Bunnett, N. A. Lambert, D. P. Poole, M. Canals. Plasma membrane localization of the m-opioid receptor controls spatiotemporal signaling. Sci. Signal. 9, ra16 (2016). Reprinted with permission from AAAS.

Appendix 2

Fluorescently labelled morphine derivatives for bioimaging studies

Raymond Lam, Arisbel B. Gondin, Meritxell Canals, Barrie Kellam, Stephen J. Briddon, Bim Graham, and Peter J. Scammells

Journal of Medicinal Chemistry 2018 ***61*** (3), 1316-1329
DOI: 10.1021/acs.jmedchem.7b01811

Journal of Medicinal Chemistry

Article

Cite This: J. Med. Chem. 2018, 61, 1316−1329

pubs.acs.org/jmc

Fluorescently Labeled Morphine Derivatives for Bioimaging Studies

Raymond Lam,[†,§] Arisbel B. Gondin,[‡,#] Meritxell Canals,[‡] Barrie Kellam,[§] Stephen J. Briddon,[#] Bim Graham,[†] and Peter J. Scammells*[,†]

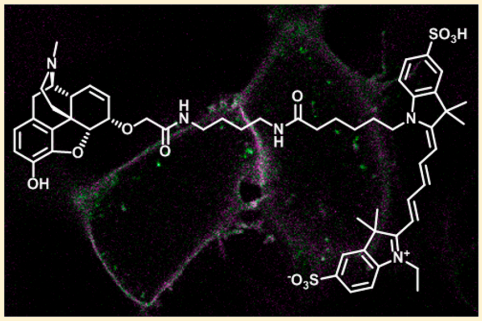
[†]Medicinal Chemistry and [‡]Drug Discovery Biology, Monash Institute of Pharmaceutical Sciences, Monash University, Parkville, Victoria 3052, Australia

[§]School of Pharmacy, Centre for Biomolecular Sciences, University of Nottingham, Nottingham NG7 2RD, U.K.

[#]Cell Signalling Research Group, School of Life Sciences, Queen's Medical Centre, University of Nottingham, Nottingham NG7 2UH, U.K.

Supporting Information

ABSTRACT: Opioids, like morphine, are the mainstay analgesics for the treatment and control of pain. Despite this, they often exhibit severe side effects that limit dose; patients often become tolerant and dependent on these drugs, which remains a major health concern. The analgesic actions of opioids are primarily mediated via the μ-opioid receptor, a member of the G protein-coupled receptor superfamily. Thus far, development of small molecule fluorescent ligands for this receptor has resulted in antagonists, somewhat limiting the use of these probes. Herein, we describe our work on the development of a small molecule fluorescent probe based on the clinically used opiate morphine and initial characterization of its behavior in cell-based assays.



INTRODUCTION

Opioids represent a useful class of drugs for the control and management of pain. Morphine and codeine, the active ingredients in opium from the plant *Papaver somniferum*, have been used for this purpose since early history.[1] More recently, semi-synthetic opioids such as oxycodone have also become important therapeutic agents. Semi-synthetic opioid antagonists such as naloxone and naltrexone are also important therapeutics used to treat opioid overdose. Despite their clinical effectiveness, opioid agonists suffer from significant drawbacks; dose-limiting side effects such as constipation, sedation, and respiratory depression are common.[1] In addition to this, opioid drugs tend to be addictive and require higher doses as the patient develops a tolerance for them, further compounding the problem. In the United States alone, the CDC reported that opioid related deaths accounted for 61% of drug overdose related deaths between 2010 and 2015.[2] Furthermore, the number of incidents has increased dramatically, with death rates tripling during this period compared to 1999.

Opioids act via the three opioid receptor subtypes, namely the μ, κ, and δ opioid receptors (MOR, KOR, and DOR respectively). The more recently discovered nociception/orphanin FQ peptide receptor (NOPr) is another member of the opioid receptor family but does not bind these clinically used morphinan opioids.[3] Herein, we will only discuss the MOR, as this receptor is the primary target of the most commonly used analgesics[4] and therefore holds significant clinical interest for the development of future analgesics.

Binding of an agonist to MOR typically activates $G_{i/o}$ proteins, resulting in inhibition of adenylate cyclase and therefore a reduction in cyclic adenosine monophosphate (cAMP) levels.[1] This results in an influx of K^+ via G protein-mediated K^+ channels, causing neuron hyperpolarization and blockade of voltage-gated Ca^{2+} channels.[5] Hyperpolarization reduces firing potential, and therefore blockade of pain signaling, giving opioids their analgesic effects. Upon prolonged activation, β-arrestin 2 recruitment to the MOR terminates signaling and induces internalization of the receptor.

However, not all opioids recruit arrestin and internalize with the same efficacy and, indeed, β-arrestin biased ligands have been discovered which give different pharmacological outcomes.[6] The prototypical opiate morphine causes very little β-arrestin 2 recruitment following MOR receptor activation while also inducing significant dependency and tolerance in the patient.[7] Herkinorin, like morphine, also provides analgesia with little β-arrestin 2 recruitment but shows very low dependence and tolerance liabilities in animal models.[8] DAMGO, a peptidic agonist, induces β-arrestin 2 recruitment while having reduced dependence and tolerance liabilities.[7] PZM21, a more recent example, appears to be biased toward G_i signaling, lacking any significant β-arrestin 2 recruitment.[6] Analgesia in mice has been demonstrated with fewer side effects compared to morphine. Just from these few examples, it can be seen that different agonists have different pharmacological

Received: December 10, 2017
Published: January 1, 2018

ACS Publications © 2018 American Chemical Society

DOI: 10.1021/acs.jmedchem.7b01811
J. Med. Chem. 2018, 61, 1316−1329

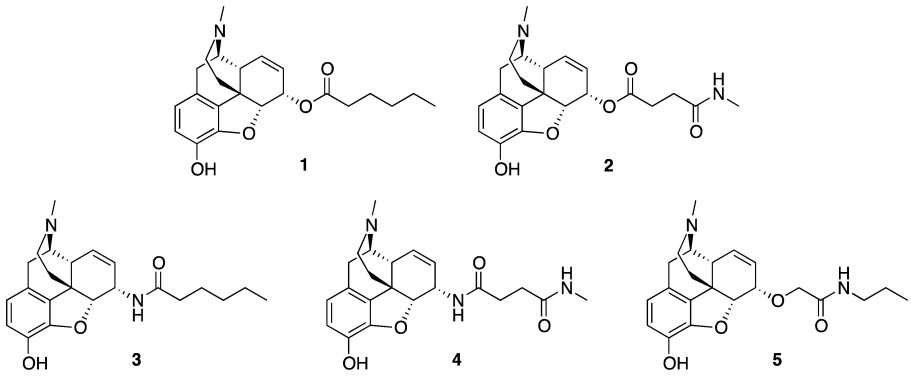
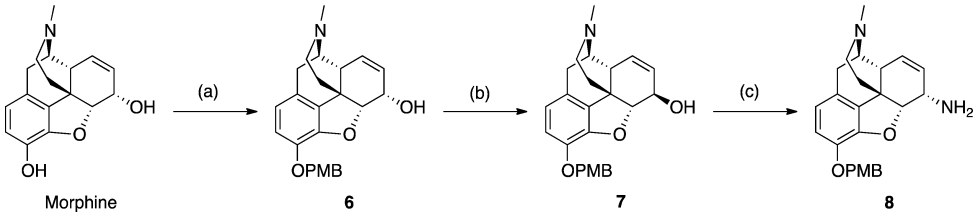


Figure 1. Precongeners synthesized for assessing linker suitability. Note preservation of the C-6 stereocenter.

Scheme 1. Synthesis of C-6 Position Amine[a]



[a]Reagents and conditions: (a) 3 M KOH in MeOH, PMB-Cl, DMF, RT, 4 h, 46%; (b) (i) benzoic acid, PPh_3, DIAD, toluene, 0 °C to RT, 4 h, (ii) 1:1 EtOH/1 M KOH, reflux, 20 min, 78%; (c) (i) phthalimide, PPh_3, DIAD, toluene, 0 °C to RT, 4 h, (ii) EtOH, $N_2H_4{\cdot}H_2O$, reflux, 1 h, 34%.

outcomes despite all acting at MOR. Furthermore, Bohn et al. have demonstrated that tolerance and dependence are not necessarily correlated, as *β*-arrestin 2 knockout mice still develop a dependence toward morphine but lack the expected tolerance.[9]

Understanding the mechanisms behind the different abilities of opioid ligands to promote arrestin recruitment and regulate receptor signaling poses a significant challenge. The development of fluorescent ligands to visualize G protein-coupled receptors (GPCRs) in live cells represents a major advantage that circumvents the use of recombinant cells and allows the study of these receptors in natively expressing systems. One of the earliest examples of a fluorescent opioid is described by Fournie-Zaluski et al., in which enkephalins were conjugated to a fluorescent dansyl sulfonyl group.[10] This particular ligand has seen limited use, perhaps due to the UV excitation maximum and poor quantum yield of the dansyl sulfonyl group not being particularly suitable to modern live cell imaging techniques. The same was true of probes described by Mihara et al., who conjugated enkephalins to the fluorophore L-1-pyrenylalanine.[11] In both cases, introduction of the fluorescent moiety resulted in a reduction in binding affinity compared to the native ligand. More recent variants of these peptidic conjugates have been described by Arttamangkul et al. using more modern fluorophores.[12] These new fluorescent ligands have been used to study MOR internalization, desensitization, and recycling.[13−15]

Small molecule fluorescent opioids have also been described. Kolb et al. described the synthesis of several fluorescent antagonists based on naloxone and naltrexone.[16] Another opioid probe bearing a 7-nitrobenzo-2-oxa-1,3-diazole fluorescent label was described by Archer et al.,[17] quickly followed by another example from Emmerson et al.[18] Most recently, Schembri et al. synthesized a series of orvinols based on the buprenorphine scaffold and conjugated them to a range of fluorophores.[19] However, in all of these cases, the fluorescent probes described were antagonists. Although fluorescent antagonists are still useful to visualize receptors at the plasma membrane and to assess receptor binding, by definition, they do not allow the study of events that follow receptor activation. Herein, we describe our work on the synthesis and evaluation of small molecule fluorescent opioid partial agonists.

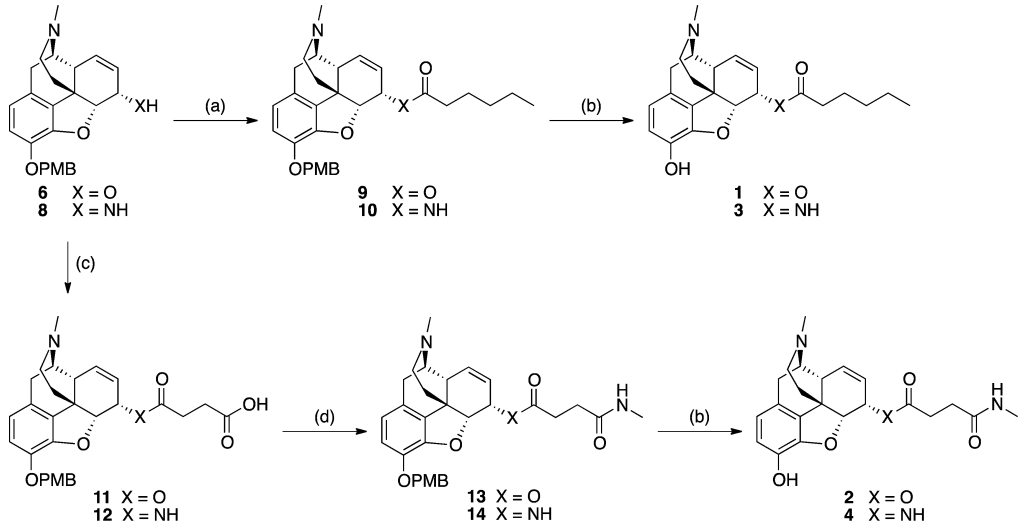
RESULTS

Model Morphine Congeners. Our aim was to develop fluorescent derivatives of morphine, as this clinically used drug is of particular interest. The C-6 position was chosen as our linking point, as the body of prior literature suggests that modifications at this point have minimal effect on ligand activity compared to alternative positions.[20,21] To assess whether our linking modifications would affect ligand activity, we first assessed the proposed structural modifications. To this end, we designed and synthesized model compounds comprising the targeting ligand with short chain linker modifications. Several linking methods were proposed, and these model compounds are illustrated in Figure 1. Importantly, these compounds and their syntheses were designed such that the C-6 stereocenter would be preserved as the native *S* configuration.

Synthesis of our model compounds employed morphine as the starting material. This approach necessitated initial protection of the C-3 phenol, for which we chose the *para*-methoxybenzyl (PMB) group, and this was installed in modest yield to afford **6** (Scheme 1). This material formed the basis for all further synthetic manipulations.

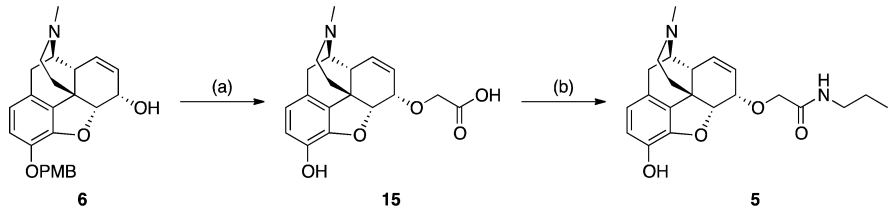
DOI: 10.1021/acs.jmedchem.7b01811
J. Med. Chem. 2018, 61, 1316−1329

Scheme 2. Synthesis of C-6 Position Ester and Amide Precongeners[a]



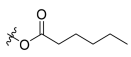
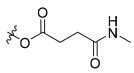
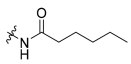
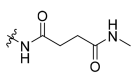
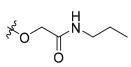
[a]Reagents and conditions: (a) hexanoyl chloride, pyridine, 70 °C, 18 h, 49–80%; (b) triethylsilane, TFA, DCM, RT, 20 min, 16–39%; (c) succinic anhydride, DMAP, TEA, MeCN, 65 °C, 16 h, 28–77%; (d) EDC·HCl, HOBt, TEA, methylamine (2 M in THF), MeCN or DMF, RT, 3 h, 63–84%.

Scheme 3. Synthesis of C-6 Position Ether Precongener[a]



[a]Reagents and conditions: (a) (i) NaH, *tert*-butyl bromoacetate, THF, 0 °C to RT, 1 h, (ii) triethylsilane, TFA, DCM, RT, 1 h, 58%; (b) HCTU, TEA, propylamine, DMF, RT, 19 h, 17%.

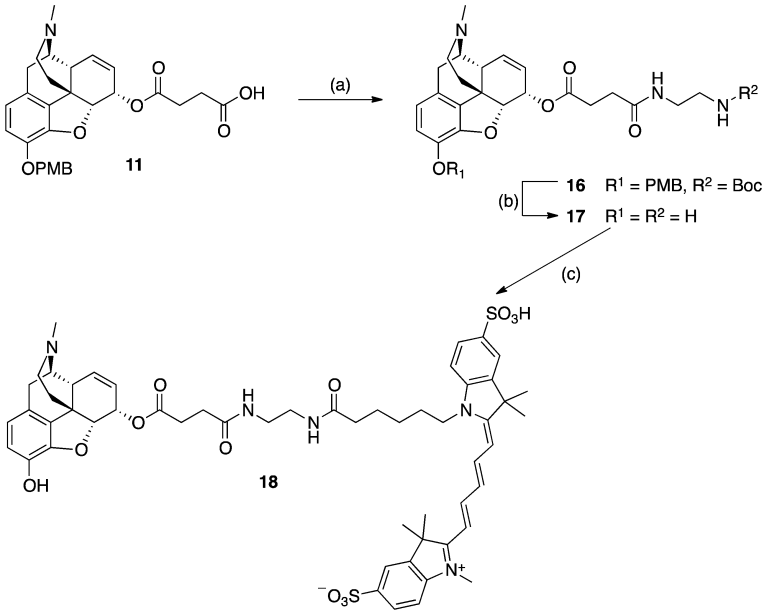
Table 1. pEC_{50} of Model Compounds As Assessed in a cAMP CAMYEL BRET Assay against hMOR

Cpd	6-Substituent	pEC_{50} ± SEM [a]	Relative potency [b]	E_{max} ± SEM [a,c]	Relative efficacy [d]
Morphine	-OH	7.07 ± 0.13	-	35.7 ± 1.7	-
1		6.46 ± 0.11	0.24	37.1 ± 1.9	1.04
2		6.45 ± 0.11	0.24	28.6 ±1.4	0.80
3		5.98 ± 0.11	0.08	28.9 ± 1.9	0.81
4		5.35 ± 0.71	0.02	23.3 ± 11.7	0.65
5		6.81 ± 0.14	0.55	37.5 ± 2.4	1.05

[a]Results presented are the average of 3 independent experiments. [b]Relative to morphine. Relative potency was calculated by dividing EC_{50}(morphine) by EC_{50}(compound). [c]E_{max} is the % inhibition of Forskolin-induced cAMP. [d]Relative to morphine. Relative efficacy was calculated by dividing E_{max}(compound) by E_{max}(morphine).

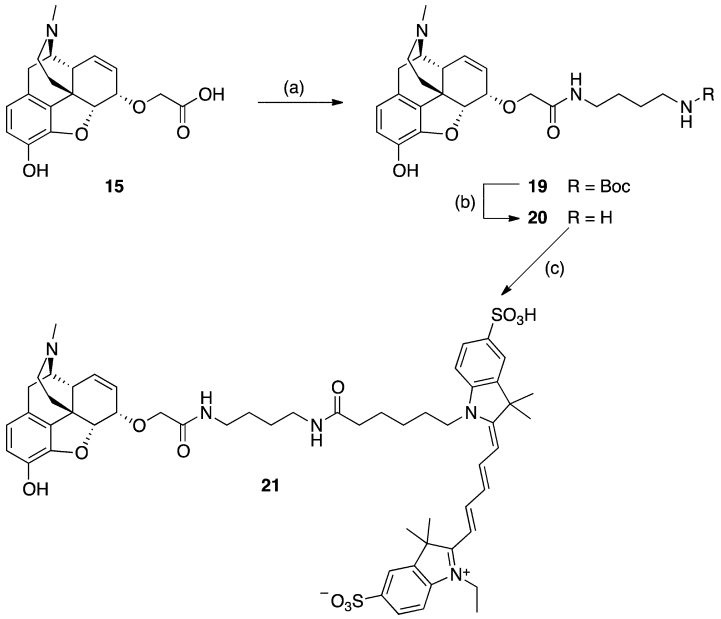
DOI: 10.1021/acs.jmedchem.7b01811
J. Med. Chem. 2018, 61, 1316–1329

Scheme 4. Synthesis of Ester Linked Morphine-Cy5 Probe 18[a]



[a]Reagents and conditions: (a) *N*-Boc-diaminoethane, HCTU, TEA, DMF, RT, 19 h, 83%; (b) triethylsilane, TFA, DCM, RT, 1 h, 51%; (c) sulfo-Cy5 NHS ester (Lumiprobe), HCTU, TEA, DMF, RT, 21 h, 33%.

Scheme 5. Synthesis of Ether Linked Morphine-Cy5 Probe 21[a]



[a]Reagents and conditions: (a) *N*-Boc-diaminobutane, EDC·HCl, HOBt, TEA, DMF, RT, 17 h, 36%; (b) TFA, $CHCl_3$, RT, 1 h, quantitative; (c) sulfo-Cy5, HCTU, TEA, DMF, RT, 18 h, 40%.

An amine moiety was subsequently introduced into the 6-position to provide a point of attachment which retains the capacity to act as a hydrogen bond donor as per the 6-OH of morphine after the linker has been attached. As we also wished to maintain the native stereochemistry of the C-6 position, a double Mitsunobu approach was employed to install this amine, noting that the Mitsunobu reaction has previously been reported to invert this stereocenter in closely related opiates.[22−25] Accordingly, 6-OH was first inverted using benzoic acid under Mitsunobu conditions followed by

DOI: 10.1021/acs.jmedchem.7b01811
J. Med. Chem. 2018, 61, 1316−1329

saponification of the resultant ester to give the 6-isomorphine derivative **7**. A comparison of the NMR spectra of compounds **6** and **7** (Supporting Information, Figure S1) demonstrated stereospecific inversion of this chiral center. Compound **7** was subsequently converted to the desired *S*-stereoisomer via a phthalimide promoted Mitsunobu reaction. Treatment of the phthalimide group with hydrazine hydrate afforded **8**, allowing for linking and elongation to the desired model compounds (Scheme 1).

Two different approaches for ester and amide conjugation were trialed. The first, using an acid chloride, yielded compounds **1** and **3** following phenolic deprotection (Scheme 2). Fluorophore conjugation via acyl chloride chemistry is not a viable synthetic strategy, and we therefore designed a method which would facilitate milder reaction conditions. Ring opening of succinic anhydride via the C-6 amine or alcohol provided a convenient handle for further elongation and subsequent fluorophore conjugation under milder conditions. Methylamine capping of this handle, followed by phenolic deprotection, gave model compounds **2** and **4** (Scheme 2).

As an alternative linking method, an ether linker was also proposed. Using *tert*-butyl bromoacetate to give the C-6 ether, followed by global deprotection, gave **15**, again possessing a convenient handle for further linker elongation. This handle was capped with propylamine to provide the final model amide **5** (Scheme 3).

Model compounds were functionally assessed and compared to morphine using a bioluminescence resonance energy transfer (BRET)-based cAMP sensor using YFP-Epac-RLuc assay (CAMYEL) in HEK293 cells expressing the human MOR (hMOR) and normalized against forskolin (Table 1). All compounds were less potent than morphine, however the ester linked model compounds (**1** and **2**) maintained potencies in the mid nM range, while the amide-linked model compounds (**3** and **4**) showed a significant loss in potency beyond the μM range. The ether linked model compound **5**, however, maintained the same level of maximum activity and was the most potent model congener.

Morphine-Cy5 Conjugates. We then proceeded to synthesize two fluorescent probes based on linker designs **2** and **5**. Sulfo-Cy5 was chosen as the fluorescent tag, as previous work by Schembri et al. suggested that this particular fluorophore had the least potential for inducing nonspecific binding to the cell membrane.[19] The functional handles on **11** and **15** were elongated with a simple Boc-protected diamine chain, followed by global deprotection and chemoselective conjugation to sulfo-Cy5 to give the final fluorescent morphine probes **18** and **21** (Schemes 4 and 5, respectively). In the case of **18**, the coupling reaction with sulfo-Cy5 NHS ester failed to proceed to completion after 7 h. As it was thought this may have resulted from the hydrolysis of the NHS ester to the corresponding carboxylic acid, HCTU was added to drive the reaction to completion (Scheme 4). In the case of **21**, sulfo-Cy5 free acid was used in place of the NHS ester and was installed under standard HCTU coupling conditions (Scheme 5).

Functional assessment of **18** and **21** was conducted in the same manner as the model conjugates (Table 2). Although both sulfo-Cy5 derivatives were still able to activate MOR with potencies in the nM range, they showed a significant loss of efficacy (E_{max}). This loss in activity is consistent with previous literature compounds, where attachment of a fluorescent tag typically results in decreased activity.[12,26] A comparison with DAMGO in the same assay revealed that **21** clearly behaves as a partial agonist, albeit with a lower efficacy compared to the parent compound morphine (Figure 2).

Table 2. pEC_{50} Assessment of Morphine-Cy5 Probes

probe	pEC_{50} ± SEM[a]	relative potency[b]	E_{max} ± SEM[a,c]	relative efficacy[d]
morphine	7.07 ± 0.13		35.7 ± 1.7	
18	7.34 ± 0.37	1.85	10.7 ± 1.2	0.30
21	6.30 ± 0.44	0.17	15.0 ± 3.2	0.42

[a]Results presented are the average of 3 independent experiments. [b]Relative to morphine. Relative potency was calculated by dividing EC_{50}(morphine) by EC_{50}(compound). [c]E_{max} is the % inhibition of Forskolin-induced cAMP. [d]Relative to morphine. Relative efficacy was calculated by dividing E_{max}(compound) by E_{max}(morphine).

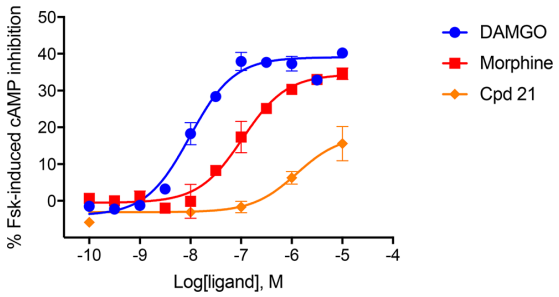


Figure 2. CAMYEL assay comparing DAMGO, morphine and **21**. The probe compound **21** is clearly a partial agonist compared to the full agonist DAMGO. Morphine is known to be a partial agonist but may give differing levels of efficacy depending on the assay used. Results for DAMGO and morphine are consistent with those previously reported.[27,28] Results presented are an average of 3 independent experiments, with error bars representing SEM.

We then assessed whether compounds **18** and **21** were suitable for receptor visualization using confocal microscopy. Initial experiments were conducted to determine whether **18** and **21** bound specifically to the MOR. HEK293 stably expressing SNAP-tagged hMOR (SNAP-hMOR) were pre-incubated with cell impermeable SNAP-Surface 488 (BG-488, New England BioLabs, Figure 3) to label the cell surface

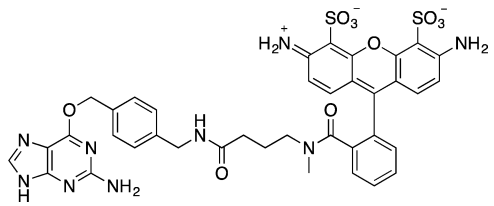


Figure 3. SNAP-Surface 488 (New England BioLabs), a cell impermeable dye targeted to the SNAP domain of SNAP-tagged receptors. This dye enables exclusive labeling of cell surface receptor populations.

SNAP-hMOR, then incubated in the presence or absence of the antagonist naloxone and before exposure to the fluorescent probes. Despite having a higher apparent pEC_{50} value, **18** showed no specific binding to the cell surface receptor population (Figure 4A). On the other hand, **21** was observed to localize at the surface of cells expressing SNAP-hMOR

DOI: 10.1021/acs.jmedchem.7b01811
J. Med. Chem. 2018, 61, 1316−1329

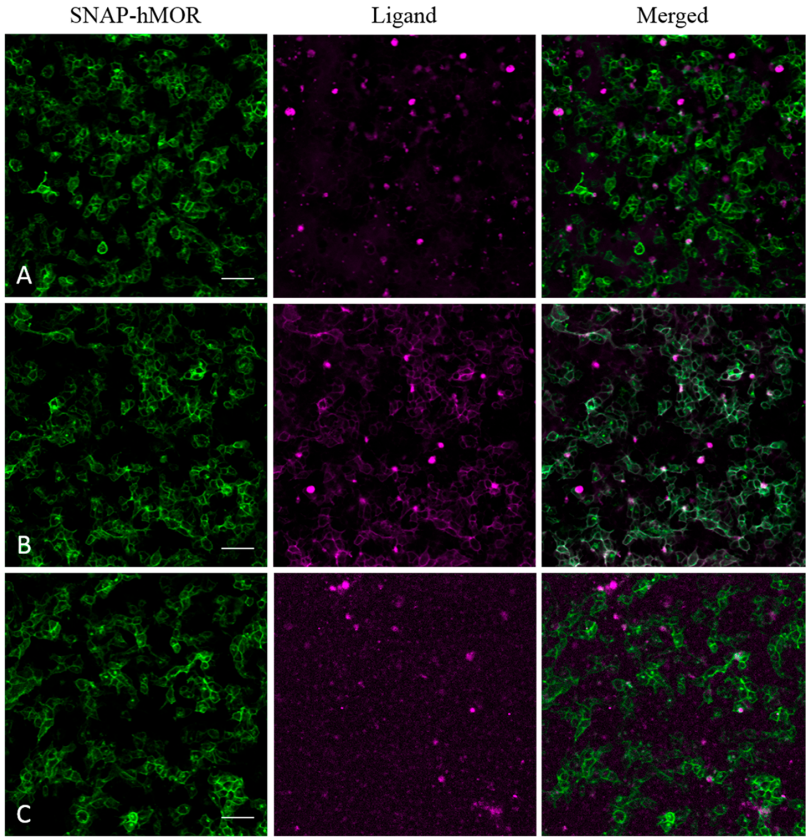


Figure 4. Initial high-content imaging of probes with HEK293 cells expressing SNAP-hMOR. Images are representative of 3 independent experiments. (A) **18** at 3 μM, no specific binding of the probe to the cell surface was observed. (B) **21** at 1 μM, binding of the probe to the cell surface was observed. (C) **21** at 1 μM preincubated with naloxone (1 μM, 30 min, 37 °C), complete blockade of probe binding was observed. Scale bars, 50 μm.

(Figure 4B). **21** binding was abolished by preincubation with naloxone (Figure 4C).

Having demonstrated that **21** could be used to visualize specific binding to the MOR on HEK293 cell membranes, this probe was selected for subsequent study. In HEK293 cells stably expressing SNAP-hMOR and preincubated with BG-488, it was found that **21** co-localized with SNAP-hMOR predominantly on the cell membrane (Figure 5A,B), which was prevented by preincubation with naloxone, confirming the membrane binding of **21** was to the hMOR (Figure 5C). The bulk of the co-localized fluorescence remained at the cell surface. Although some co-localized signals within the cells were present, the signal from intracellular compartments was very weak compared to that at the plasma membrane. These data are in keeping with literature data, which suggests that morphine only poorly induces internalization of the receptor–ligand complex.[7] Because incubation with BG-488 only labels cell surface populations of SNAP-hMOR, any internalized receptor population must therefore have previously been on the cell surface. In keeping with prior literature, it was found that a wash step removed bound ligand (Figure 5D).[19] This is consistent with the fast k_{off} rate of nonpeptide opioids and the known fast k_{off} rate of morphine, so this behavior is not unexpected. In any case, a wash step is typically not included in confocal microscopy experiments, particularly where there is no significant background from extracellular ligand, as in this case.[19,29−31]

In the previous experiments, the EC_{50} concentration of 500 nM was used, thus we wanted to assess the behavior of **21** above this concentration. The use of 10 μM of **21** necessitated a wash step to remove background fluorescence from any excess ligand (Figure 6A). As demonstrated, the level of observed co-localization between **21** and SNAP-hMOR in the intracellular compartment is significantly increased, with minimal cell surface co-localization due to the wash step as expected. Furthermore, this signal could be removed by blockade with naloxone, further demonstrating the lack of nonspecific binding of **21** even at this higher concentration (Figure 6B).

To directly compare, experiments were conducted using the parent compound morphine as the ligand (Figure 7). Obviously, the lack of a fluorescent tag prevents direct visualization of the ligand, but observation of the tagged receptor fluorescence is still of value as it enables visual comparisons to be made between the behavior of our fluorescently tagged probe and its parent compound. A baseline level of receptor internalization was first determined in cells with no ligand present (Figure 7A). These data show that a low constitutive level of receptor internalization is present, even without stimulation. Morphine at 500 nM does not induce any

DOI: 10.1021/acs.jmedchem.7b01811
J. Med. Chem. 2018, 61, 1316−1329

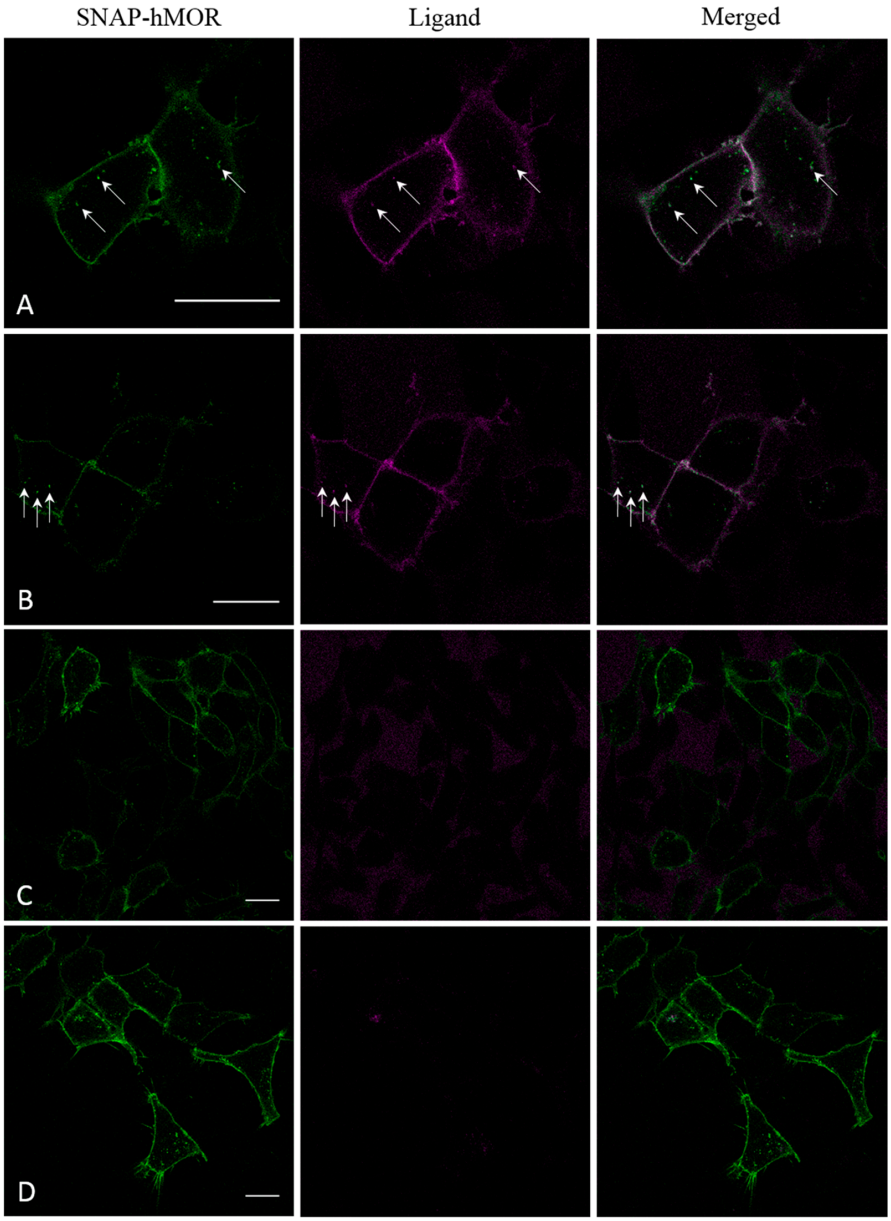


Figure 5. Live cell confocal imaging of **21** in cells expressing SNAP-hMOR. Images are representative of 3 independent experiments. In all cases, **21** was incubated at 500 nM for 30 min at 37 °C following pretreatment (with or without naloxone). (A,B) Typical results obtained from confocal microscopy; the white arrows indicate areas where co-localization of intracellular receptor populations with the fluorescent ligand were observed. (C) **21** following preincubation with naloxone (1 μM, 30 min, 37 °C), indicating specific binding of the probe to hMOR. (D) Loss of ligand signal following a postincubation wash. This is typical of nonpeptide opioids, which tend to have a fast k_{off} rate. Scale bars, 20 μm.

significant receptor internalization, with levels similar to that of the baseline level (Figure 7B). Furthermore, these levels of internalization are similar to when 500 nM of **21** was used (Figure 5A,B). This reinforces the idea that morphine is only weakly able to induce internalization of the MOR. Furthermore, at 10 μM morphine, the level of internalization was comparable to that observed with 10 μM of **21** (Figure 7C compared to Figure 6A). Taken together, these data suggest that our probe behaves very similarly to morphine, which may make it a useful tool in the study of morphine pharmacology.

DISCUSSION AND CONCLUSIONS

Herein, we have described the design and synthesis of a fluorescent partial agonist probe for MOR based on the commonly used analgesic morphine. Our studies have shown that probe compound **21** is able to bind to hMOR on cell membranes and behaves in a similar manner to the parent

DOI: 10.1021/acs.jmedchem.7b01811
J. Med. Chem. 2018, 61, 1316−1329

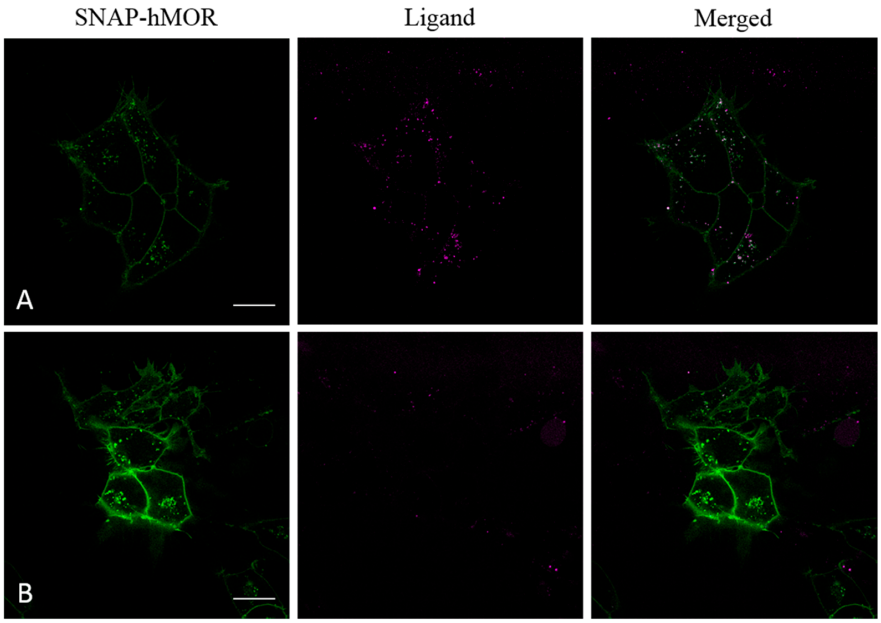


Figure 6. Live cell confocal imaging of **21** at increased concentration in cells expressing SNAP-hMOR. Images are representative of 3 independent experiments. (A) **21** at 10 μM, note the increased level of internalized receptor populations compared to the data presented in Figure 4. (B) **21** at 10 μM following preincubation with naloxone (1 μM, 30 min, 37 °C), demonstrating specific displacement of **21** with little background fluorescence. Scale bars, 20 μm.

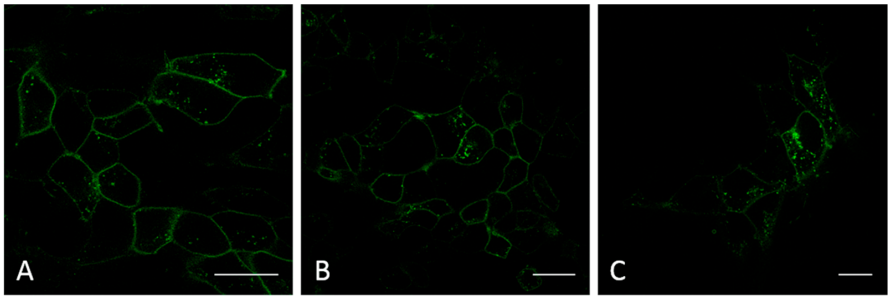


Figure 7. Live cell confocal imaging of SNAP-hMOR in cells exposed to morphine for comparison to **21**. Images are representative of 3 independent experiments. (A) Cells with no stimulation, note the constitutive receptor turnover, even in the absence of any external internalizing stimuli. (B) 500 nM morphine, the level of internalization is similar to that observed when no stimuli is applied, which is in keeping with literature data suggesting morphine's inability to induce internalization. (C) 10 μM morphine, significantly more receptor populations are observed to internalize and therefore can be attributed to the ligand stimulus. Scale bars, 20 μm.

compound morphine. At EC_{50} concentrations, the probe does not induce internalization of the receptor but is present in intracellular compartments at levels consistent with constitutive turnover. At higher concentrations, the probe is able to induce internalization at similar levels to morphine. These data suggest that the probe compound **21** may be used as a tool compound to simulate the behavior of morphine, much in the same way DERM-A594 is used as a tool compound for the study of endogenous opioid peptides.[15] It is clear that morphine has significantly different signaling profile compared to peptides,[23,24] and therefore small molecule-based fluorescent probes may lead to different outcomes compared to studies where fluorescent peptides have been utilized. This new tool compound could also be used in conjunction with the previously described small-molecule fluorescent opioid antagonists to study the differences in ligand–receptor complexes in natively expressing systems rather than in transfected systems.[19]

■ EXPERIMENTAL SECTION

Chemistry. Chemicals and solvents were purchased from standard suppliers and used without further purification. Davisil silica gel (40–63 μm) for flash column chromatography was supplied by Grace Davison Discovery Sciences (Victoria, Australia), and deuterated solvents were purchased from Cambridge Isotope Laboratories, Inc. (USA, distributed by Novachem PTY. Ltd., Victoria, Australia). Davisil reverse phase silica gel (C18, 10–14 μm) for reverse phase flash column chromatography was supplied by Grace Davison Discovery Sciences (Victoria, Australia) and run using the following buffers; buffer A, 0.1% TFA in H_2O; buffer B, 0.1% TFA in MeCN.

Reactions were monitored by thin layer chromatography on commercially available precoated aluminum-backed plates (Merck

DOI: 10.1021/acs.jmedchem.7b01811
J. Med. Chem. 2018, 61, 1316–1329

Kieselgel 60 F_{254}). Visualization was done by examination under UV light (254 and 366 nm). General staining was carried out with $KMnO_4$ or phosphomolybdic acid. Organic solvents were evaporated in vacuo at ≥40 °C (water bath temperature). Purification using preparative layer chromatography (PLC) was carried out on Analtech preparative TLC plates (200 mm × 200 mm × 2 mm).

^{1}H NMR and ^{13}C NMR spectra were recorded on a Bruker Avance Nanobay III 400 MHz Ultrashield Plus spectrometer at 400.13 and 100.62 MHz, respectively. Chemical shifts (δ) are recorded in parts per million (ppm) with reference to the chemical shift of the deuterated solvent. Coupling constants (J) are recorded in Hz and the significant multiplicities described by singlet (s), doublet (d), triplet (t), quadruplet (q), broad (br), multiplet (m), doublet of doublets (dd), and doublet of triplets (dt).

LC-MS were run to verify reaction outcome and purity using an Agilent 6120 series single quad coupled to an Agilent 1260 series HPLC. The following buffers were used; buffer A, 0.1% formic acid in H_2O; buffer B, 0.1% formic acid in MeCN. The following gradient was used with a Poroshell 120 EC-C18 50 mm × 3.0 mm 2.7 μm column and a flow rate of 0.5 mL/min and total run time of 5 min; 0−1 min 95% buffer A and 5% buffer B, from 1 to 2.5 min up to 0% buffer A and 100% buffer B, held at this composition until 3.8 min, 3.8−4 min 95% buffer A and 5% buffer B, and held until 5 min at this composition. Mass spectra were acquired in positive and negative ion mode with a scan range of 100−1000 m/z. UV detection was carried out at 214 and 254 nm.

Preparative HPLC was performed using an Agilent 1260 infinity coupled with a binary preparative pump and Agilent 1260 FC-PS fraction collector, using Agilent OpenLAB CDS software (Rev C.01.04), and an Altima 5 μM C8 22 mm × 250 mm column. The following buffers were used; buffer A, 0.1% TFA in H_2O; buffer B, 0.1% TFA in MeCN, with sample being run at a gradient of 5% buffer B to 100% buffer B over 15 min, at a flow rate of 15 mL/min. All screening compounds were of >95% purity.

High resolution mass spectrometry−time-of-flight (HRMS−TOF) was conducted using an Agilent 6224 TOF LC-MS mass spectrometer coupled to an Agilent 1290 Infinity. Chromatographic separation was performed using an Agilent Zorbax SB-C18 Rapid Resolution HT 2.1 mm × 50 mm, 1.8 μm column using a gradient of 5−100% buffer B in buffer A over 3.5 min at 0.5 mL/min, where buffers are as defined for LC-MS. All mass data was acquired and reference mass corrected via a dual-spray ESI source. Mass spectra were created by averaging scans across each peak and background subtracting against the first 10 s of the total ion count. Acquisition was performed using the Agilent Mass Hunter Data Acquisition software and analysis performed using Mass Hunter Qualitative Analysis software. The mass spectrometer was run using the following conditions: drying gas flow 11 L/min, nebulizer 45 PSI, drying gas temperature 325 °C, capillary voltage 4000 V, fragmentor 160 V, skimmer 65 V, OCT RFV 750 V, scan range acquired 100−150 m/z, internal reference ions positive ion mode = m/z = 121.050873 and 922.009798.

General Deprotection Procedure A. The protected compound was dissolved in dry DCM (typically 5 mL) under an N_2 atmosphere. Triethylsilane (15 equiv) and TFA (20 equiv) were added to the reaction and the vessel purged with N_2. The reaction was allowed to stir for 30−60 min then reduced in vacuo. The resulting residue could then be purified via chromatography.

*6-O-Hexanoylmorphine (**1**).* Compound **9** (67 mg, 0.13 mmol, 1 equiv) was deprotected using general deprotection procedure A. The resulting oil was purified by flash column chromatography (94:5:1 $CHCl_3$/MeOH/TEA), and the resulting yellow oil was further purified by prep-HPLC to give the product as a solid white TFA salt (12 mg, 17%). ^{1}H NMR (DMSO-d_6) δ 10.04 (s, 1H), 9.17 (s, 1H), 6.58 (d, J = 8.1 Hz, 1H), 6.50 (d, J = 8.1 Hz, 1H), 5.71−5.59 (m, 1H), 5.52−5.39 (m, J = 22.7, 9.8 Hz, 1H), 5.26−5.14 (m, 1H), 5.12−5.00 (m, J = 20.5, 6.6 Hz, 1H), 4.13 (s, 1H), 3.31 (d, J = 9.0 Hz, 1H), 3.19 (d, J = 19.7 Hz, 1H), 3.06 (d, J = 4.5 Hz, 1H), 2.98 (s, 1H), 2.92−2.78 (m, J = 41.2 Hz, 3H), 2.71 (dd, J = 20.0, 6.7 Hz, 1H), 2.44−2.29 (m, 2H), 2.21 (td, J = 13.5, 4.6 Hz, 1H), 1.98−1.70 (m, J = 46.3, 12.5 Hz, 1H), 1.64−1.51 (m, 2H), 1.34−1.21 (m, 4H), 0.87 (t, J = 6.9 Hz, 3H). ESI-TOF HRMS m/z [M + H]$^+$ $C_{23}H_{29}NO_4^+$ calcd 384.2169, found 384.2174.

*6-O-(4-Methylamino-4-oxobutanoyl)morphine (**2**).* Compound **13** (26 mg, 0.050 mmol, 1 equiv) was deprotected using general deprotection procedure A. The resulting oil was purified by prep-HPLC to give the product as a solid white TFA salt (4 mg, 16%). ^{1}H NMR (DMSO-d_6) δ 10.04 (s, 1H), 9.23 (s, 1H), 7.85 (d, J = 4.4 Hz, 1H), 6.61−6.56 (m, J = 8.0, 3.1 Hz, 1H), 6.54−6.48 (m, J = 8.1, 4.7 Hz, 1H), 5.65 (d, J = 10.0 Hz, 1H), 5.52−5.39 (m, J = 24.1, 10.0 Hz, 1H), 5.24−5.14 (m, 1H), 5.09−4.99 (m, J = 22.2, 6.7 Hz, 1H), 4.13 (s, 1H), 3.34−3.25 (m, J = 8.5 Hz, 1H), 3.23−3.13 (m, J = 19.7 Hz, 1H), 3.06 (d, J = 4.8 Hz, 1H), 2.98 (s, 1H), 2.89 (d, J = 3.1 Hz, 2H), 2.82−2.67 (m, 2H), 2.62−2.58 (m, J = 6.9, 4.1 Hz, 2H), 2.57−2.55 (m, J = 4.5 Hz, 3H), 2.40 (t, J = 6.9 Hz, 2H), 2.21 (td, J = 13.4, 4.4 Hz, 1H), 1.94−1.74 (m, J = 46.2, 11.8 Hz, 1H). ESI-TOF HRMS m/z [M + H]$^+$ $C_{22}H_{27}N_2O_5^+$ calcd 399.1914, found 399.1922.

*N-((4R,4aR,7S,7aR,12bS)-9-Hydroxy-3-methyl-2,3,4,4a,7,7a-hexahydro-1H-4,12-methanobenzofuro[3,2-e]isoquinolin-7-yl)-hexanamide (**3**).* Compound **10** (39 mg, 0.10 mmol, 1 equiv) was deprotected using general deprotection procedure A. The resulting oil was purified by prep-HPLC to give the product as a solid white TFA salt (12 mg, 31%). $[\alpha]_D^{25}$ −21.4 (c 1.21 mg/mL, MeOH). ^{1}H NMR (DMSO-d_6) δ 10.11−9.88 (m, 1H), 9.28 (s, 1H), 8.20−8.05 (m, J = 25.3, 8.5 Hz, 1H), 5.73 (dt, J = 10.3, 3.1 Hz, 1H), 5.58 (d, J = 10.5 Hz, 1H), 5.16−5.02 (m, J = 25.4 Hz, 1H), 3.85 (t, J = 8.7 Hz, 1H), 3.74 (s, 1H), 3.27−3.20 (m, J = 7.0 Hz, 1H), 3.18 (s, 1H), 3.12−3.02 (m, J = 19.8, 6.3 Hz, 1H), 2.98 (s, 1H), 2.89 (s, 3H), 2.77−2.56 (m, J = 48.6, 9.6 Hz, 2H), 2.40 (d, J = 8.1 Hz, 1H), 2.17−1.97 (m, 3H), 1.87 (d, J = 11.8 Hz, 1H), 1.56−1.43 (m, 2H), 1.31−1.14 (m, 4H), 0.85 (t, J = 7.0 Hz, 3H). ESI-TOF HRMS m/z [M + H]$^+$ $C_{23}H_{31}N_2O_3^+$ calcd 383.2329, found 383.2324.

*N^1-((4R,4aR,7S,7aR,12bS)-9-Hydroxy-3-methyl-2,3,4,4a,7,7a-hexahydro-1H-4,12-methanobenzofuro[3,2-e]isoquinolin-7-yl)-N^4-methylsuccinamide (**4**).* Compound **14** (19 mg, 0.037 mmol, 1 equiv) was deprotected using general deprotection procedure A. The resulting oil was purified by prep-HPLC to give the product as a solid white TFA salt (7 mg, 39%). $[\alpha]_D^{25}$ −21.9 (c 0.78 mg/mL, MeOH). ^{1}H NMR (DMSO-d_6) δ 10.08−9.73 (m, J = 44.4 Hz, 1H), 9.25 (s, 1H), 8.28−8.06 (m, J = 29.6, 9.0 Hz, 1H), 7.79 (d, J = 4.6 Hz, 1H), 5.78−5.68 (m, 1H), 5.65−5.57 (m, 1H), 5.10 (t, J = 13.6 Hz, 1H), 3.94 (d, J = 4.6 Hz, 1H), 3.86 (t, J = 8.5 Hz, 1H), 3.22 (s, 1H), 3.17 (d, J = 19.5 Hz, 1H), 3.10−2.96 (m, 2H), 2.89 (d, J = 4.6 Hz, 2H), 2.79−2.65 (m, 1H), 2.55 (d, J = 4.6 Hz, 3H), 2.43−2.21 (m, 5H), 2.11−1.97 (m, 1H), 1.92−1.67 (m, 1H). ESI-TOF HRMS m/z [M + H]$^+$ $C_{22}H_{28}N_3O_4^+$ calcd 398.2074, found 398.2079.

*6-O-(2-Oxo-2-(propylamino)ethyl)morphine (**5**).* Compound **15** (54 mg, 0.12 mmol, 1 equiv), HCTU (59 mg, 0.14 mmol, 1.2 equiv), and TEA (50 μL, 0.36 mmol, 3 equiv) were dissolved in dry DMF (800 μL) under an N_2 atmosphere and allowed to stir at room temperature for 30 min. A solution of propylamine (12 μL, 0.14 mmol, 1.2 equiv) in DMF (200 μL) was then added and the resulting solution allowed to stir at room temperature for 19 h. The solvent was then removed in vacuo and the residue taken up in buffer B and again reduced in vacuo. The residue was purified by flash column chromatography (74:25:1 MeOH/$CHCl_3$/NH_4OH) and the solvent removed in vacuo and purified again by prep-HPLC to give the product as a solid white TFA salt (10 mg, 17%). $[\alpha]_D^{25}$ −106.1 (c 1.14 mg/mL, MeOH). ^{1}H NMR (DMSO-d_6) δ 9.81 (s, 1H), 9.18 (s, 1H), 7.74 (t, J = 5.7 Hz, 1H), 6.62−6.52 (m, 1H), 6.52−6.43 (m, 1H), 5.82 (d, J = 9.7 Hz, 1H), 5.41−5.24 (m, 1H), 5.18−5.02 (m, 1H), 4.16−3.97 (m, 4H), 3.29 (s, 1H), 3.20 (d, J = 19.8 Hz, 2H), 3.14−3.04 (m, 3H), 2.97 (s, 1H), 2.90 (d, J = 3.9 Hz, 3H), 2.83 (d, J = 16.0 Hz, 2H), 2.74 (dd, J = 19.8, 6.6 Hz, 1H), 2.18 (td, J = 13.8, 4.9 Hz, 1H), 2.03−1.79 (m, 1H), 1.45 (h, J = 7.3 Hz, 2H), 0.84 (t, J = 7.4 Hz, 3H). ESI-TOF HRMS m/z [M + H]$^+$ $C_{22}H_{29}N_2O_4^+$ calcd 385.2122, found 385.2130.

*3-O-(4-Methoxybenzyl)morphine (**6**).* Morphine (394 mg, 1.4 mmol, 1 equiv) was dissolved in DMF (1 mL), and KOH (3 M in MeOH, 552 μL, 1.7 mmol, 1.2 equiv) was added. The resulting mixture was stirred for 10 min, then *para*-methoxybenzyl chloride

DOI: 10.1021/acs.jmedchem.7b01811
J. Med. Chem. 2018, 61, 1316−1329

(215 μL, 1.6 mmol, 1.15 equiv) was added dropwise. After stirring for 4 h at room temperature, aqueous citric acid (1 M, 10 mL) was added. The resulting solution was washed successively with EtOAc (3 × 10 mL), and aqueous NH_4OH (28%, 10 mL) was added to the aqueous phase. The resulting turbid solution was extracted with 3:1 $CHCl_3$/*i*PrOH (5 × 10 mL). The combined organic layers were backwashed with brine, dried over Na_2SO_4, and the solvent removed in vacuo. The resulting yellow oil was purified by flash column chromatography (98:1:1 DCM/MeOH/TEA). The resulting clear oil was redissolved in EtOAc and evaporated again to give the product as a white solid (259 mg, 46%). ^{1}H NMR ($CDCl_3$) δ 7.33 (d, J = 8.4 Hz, 1H), 6.88 (d, J = 8.4 Hz, 1H), 6.71 (d, J = 8.2 Hz, 1H), 6.53 (d, J = 8.1 Hz, 1H), 5.67 (d, J = 9.7 Hz, 1H), 5.27 (d, J = 9.7 Hz, 1H), 5.04 (dd, J = 28.7, 11.4 Hz, 1H), 4.87 (d, J = 6.3 Hz, 1H), 4.15 (d, J = 2.5 Hz, 1H), 3.80 (s, 2H), 3.36 (d, J = 2.4 Hz, 1H), 3.03 (d, J = 18.7 Hz, 1H), 2.86 (s, 1H), 2.69 (s, 1H), 2.61 (dd, J = 11.8, 3.9 Hz, 1H), 2.44 (s, 1H), 2.39 (dd, J = 12.2, 3.1 Hz, 1H), 2.30 (dd, J = 18.6, 6.0 Hz, 1H), 2.08 (td, J = 12.4, 4.8 Hz, 1H), 1.87 (d, J = 11.7 Hz, 1H). ^{13}C NMR (101 MHz, $CDCl_3$) δ 159.5, 147.1, 141.3, 133.6, 131.3, 129.5, 129.4, 128.2, 127.7, 119.7, 116.0, 114.0, 91.3, 71.7, 66.5, 59.0, 55.4, 46.6, 43.1, 42.9, 40.7, 35.8, 20.6. LC-MS m/z $[M + H]^+$ $C_{25}H_{28}NO_4^+$ calcd 406.2, found 406.2.

(4R,4aR,7R,7aR,12bS)-9-((4-Methoxybenzyl)oxy)-3-methyl-2,3,4,4a,7,7a-hexahydro-1H-4,12-methanobenzofuro[3,2-e]-isoquinolin-7-ol ***(7)***. Compound **6** (229 mg, 0.57 mmol, 1 equiv), benzoic acid (104 mg, 0.85 mmol, 1.5 equiv), and triphenylphosphine (223 mg, 0.85 mmol, 1.5 equiv) were dissolved in anhydrous toluene (4 mL) and cooled to 0 °C. DIAD (167 μL, 0.85 mmol, 1.5 equiv) in anhydrous toluene (0.5 mL) were then added dropwise over 2 min. The reaction was then warmed to room temperature and allowed to stir for 4 h, after which the solvent was removed in vacuo. The resulting residue was purified by flash column chromatography (59:40:1 DCM/EtOAc/TEA) to give a white solid and oil mixture. This residue was dissolved in a 1:1 mixture of EtOH and 1 M aqueous KOH (6 mL) and heated to reflux for 20 min. The reaction was then reduced in vacuo, and 1 M citric acid (20 mL) was added to the residue. The aqueous phase was then washed with EtOAc (3 × 20 mL), then neutralized with aqueous NH_4OH (28%, 20 mL). The resulting solution was extracted with 3:1 $CHCl_3$/*i*PrOH (3 × 20 mL). The combined organic layers were backwashed with brine (20 mL), dried over Na_2SO_4, and the solvent removed in vacuo to give a white solid as the pure product (179 mg, 78%). ^{1}H NMR ($CDCl_3$) δ 7.36–7.31 (m, 1H), 6.90–6.85 (m, 1H), 6.70 (d, J = 8.2 Hz, 1H), 6.50 (d, J = 8.2 Hz, 1H), 6.00–5.93 (m, 1H), 5.60 (dd, J = 9.8, 1.9 Hz, 1H), 5.05 (q, J = 11.4 Hz, 1H), 4.79 (s, 1H), 4.20 (d, J = 5.5 Hz, 1H), 3.79 (s, 1H), 3.40 (dd, J = 5.6, 3.2 Hz, 1H), 3.17 (s, 1H), 3.03 (d, J = 18.7 Hz, 1H), 2.66 (dd, J = 12.2, 3.9 Hz, 1H), 2.48 (s, 1H), 2.45–2.33 (m, 1H), 2.18 (td, J = 12.5, 4.9 Hz, 1H), 1.85 (dd, J = 12.7, 2.0 Hz, 1H). ^{13}C NMR ($CDCl_3$) δ 159.5, 146.5, 141.3, 132.8, 131.4, 130.6, 129.6, 129.5, 127.2, 119.0, 116.4, 113.9, 94.2, 71.7, 68.0, 59.3, 55.4, 47.2, 43.9, 42.9, 39.6, 35.5, 20.7. LC-MS m/z $[M + H]^+$ $C_{25}H_{28}NO_4^+$ calcd 406.2, found 406.3.

(4R,4aR,7S,7aR,12bS)-9-((4-Methoxybenzyl)oxy)-3-methyl-2,3,4,4a,7,7a-hexahydro-1H-4,12-methanobenzofuro[3,2-e]-isoquinolin-7-amine ***(8)***. Compound **7** (174 mg, 0.43 mmol, 1 equiv), phthalimide (79 mg, 0.64 mmol, 1.5 equiv), and triphenylphosphine (169 mg, 0.64 mmol, 1.5 equiv) were dissolved in anhydrous toluene (4 mL) and cooled to 0 °C. DIAD (127 μL, 0.64 mmol, 1.5 equiv) in anhydrous toluene (0.5 mL) was then added dropwise over 2 min. The reaction was then warmed to room temperature and allowed to stir for 4 h, after which the solvent was removed in vacuo. The resulting residue was purified by flash column chromatography (59:40:1 DCM/EtOAc/TEA) to give a white solid and oil mixture. To this residue, EtOH (10 mL) and $N_2H_4{\cdot}H_2O$ (0.5 mL) were added and the mixture heated to reflux for 1 h. After cooling, the resulting precipitate was filtered and washed with EtOH. The filtrate was evaporated in vacuo, redissolved in $CHCl_3$, and the resulting precipitate removed. The filtrate was again evaporated in vacuo and the residue purified by flash column chromatography (89:10:1 $CHCl_3$/MeOH/TEA) to give the product as a yellow oil (59 mg, 34%). ^{1}H NMR ($CDCl_3$) δ 7.35–7.30 (m, 1H), 6.89–6.80 (m, 1H), 6.70 (d, J = 8.2 Hz, 1H), 6.55 (d, J = 8.2 Hz, 1H), 5.79–5.60 (m, 1H), 5.13–4.99 (m, 1H), 4.94 (d, J = 2.3 Hz, 1H), 3.78 (s, 2H), 3.59 (d, J = 4.2 Hz, 1H), 3.03 (d, J = 18.7 Hz, 1H), 2.73 (d, J = 9.1 Hz, 1H), 2.55 (dd, J = 12.1, 3.6 Hz, 1H), 2.48–2.37 (m, 2H), 2.29 (td, J = 12.1, 3.7 Hz, 1H), 2.03 (s, 1H), 1.99–1.93 (m, 1H), 1.83–1.77 (m, 1H). ^{13}C NMR ($CDCl_3$) δ 159.4, 145.0, 142.2, 139.3, 130.1, 129.6, 129.5, 127.7, 123.9, 118.9, 116.3, 113.9, 87.4, 71.5, 56.2, 55.3, 49.2, 46.9, 46.3, 43.2, 40.9, 35.5, 20.0. LC-MS m/z $[M + H]^+$ $C_{25}H_{29}N_2O_3^+$ calcd 405.5, found 405.2.

6-O-Hexanoyl-3-O-(4-methoxybenzyl)morphine ***(9)***. Compound **6** (68 mg, 0.17 mmol, 1 equiv) and hexanoyl chloride (70.4 μL, 0.50 mmol, 3 equiv) were dissolved in pyridine (1 mL) and heated at 70 °C in a sealed vessel for 19 h. Water (2 mL) and MeOH (1 mL) were added and the resulting mixture evaporated. MeCN (5 mL) was added, and the mixture was again evaporated to give a yellow oil. Saturated aqueous $NaHCO_3$ (10 mL) was added and the resulting solution extracted with 3:1 $CHCl_3$/*i*PrOH (3 × 10 mL). The combined organic layers were backwashed with brine, dried over Na_2SO_4, and the solvent removed in vacuo to give a yellow oil. Ether was added and the resulting precipitate filtered. The filtrate was evaporated and purified by flash column chromatography (94:5:1 EtOAc/MeOH/TEA) to give the product as a yellow oil (67 mg, 80%). ^{1}H NMR ($CDCl_3$) δ 7.35–7.31 (m, 1H), 6.89–6.84 (m, 1H), 6.67 (d, J = 8.2 Hz, 1H), 6.49 (d, J = 8.2 Hz, 1H), 5.67–5.61 (m, 1H), 5.46–5.39 (m, 1H), 5.19 (ddd, J = 8.1, 5.1, 2.9 Hz, 1H), 5.12 (dd, J = 6.7, 0.8 Hz, 1H), 5.06 (s, 1H), 3.79 (s, 1H), 3.77 (dd, J = 3.6, 2.0 Hz, 1H), 3.40 (dd, J = 5.6, 3.2 Hz, 1H), 3.02 (d, J = 18.7 Hz, 1H), 2.83 (s, 1H), 2.64 (dd, J = 12.0, 3.9 Hz, 1H), 2.47 (s, 2H), 2.42–2.28 (m, 2H), 2.10 (td, J = 12.5, 4.9 Hz, 1H), 1.88 (dd, J = 12.7, 1.8 Hz, 1H), 1.69–1.58 (m, 1H), 1.35–1.20 (m, 3H), 0.92–0.80 (m, 3H). ^{13}C NMR ($CDCl_3$) δ 173.4, 159.4, 147.6, 141.2, 130.9, 129.7, 129.5, 129.2, 128.9, 119.4, 117.3, 113.8, 88.0, 71.8, 68.0, 59.3, 55.3, 43.0, 42.5, 40.4, 35.2, 34.1, 31.4, 24.6, 22.4, 20.7, 14.02. LC-MS m/z $[M + H]^+$ $C_{31}H_{37}NO_5^+$ calcd 504.3, found 504.3.

N-((4R,4aR,7S,7aR,12bS)-9-((4-Methoxybenzyl)oxy)-3-methyl-2,3,4,4a,7,7a-hexahydro-1H-4,12-methanobenzofuro[3,2-e]-isoquinolin-7-yl)hexanamide ***(10)***. Compound **8** (65 mg, 0.16 mmol, 1 equiv) and hexanoyl chloride (67 μL, 0.48 mmol, 3 equiv) were dissolved in pyridine (2 mL) and heated at 70 °C for 18 h. After cooling, the solvent was removed in vacuo, and the resulting residue was purified by flash column chromatography (94:5:1 EtOAc/MeOH/TEA) to give the product as a yellow oil (39 mg, 49%). ^{1}H NMR ($CDCl_3$) δ 7.37–7.30 (m, 2H), 6.89–6.84 (m, 2H), 6.72 (d, J = 8.2 Hz, 1H), 6.59 (d, J = 8.2 Hz, 1H), 5.76 (ddd, J = 10.3, 3.5, 2.8 Hz, 1H), 5.60 (dd, J = 10.3, 1.1 Hz, 1H), 5.40 (d, J = 9.6 Hz, 1H), 5.09–5.00 (m, 2H), 4.94–4.92 (m, 1H), 4.23–4.14 (m, 1H), 3.79 (s, 3H), 3.24 (dd, J = 5.8, 2.7 Hz, 1H), 2.99 (d, J = 18.8 Hz, 1H), 2.73 (dd, J = 18.8, 6.1 Hz, 1H), 2.56–2.49 (m, 1H), 2.39 (s, 3H), 2.27 (td, J = 11.7, 4.5 Hz, 1H), 2.18–2.12 (m, 2H), 2.10 (dd, J = 10.2, 2.8 Hz, 1H), 1.92–1.79 (m, 2H), 1.64–1.56 (m, 2H), 1.36–1.22 (m, 5H), 0.88 (t, J = 7.0 Hz, 3H). ^{13}C NMR ($CDCl_3$) δ 173.1, 159.4, 144.9, 142.2, 134.7, 129.6, 129.5, 129.1, 128.2, 126.2, 119.5, 116.5, 113.9, 86.6, 71.5, 56.7, 55.4, 47.7, 47.0, 44.3, 43.3, 41.1, 36.9, 35.6, 31.5, 25.5, 22.5, 20.0, 14.1. LC-MS m/z $[M + H]^+$ $C_{31}H_{39}N_2O_4^+$ calcd 503.3, found 503.4.

6-O-(3-Carboxypropanoyl)-3-O-(4-methoxybenzyl)morphine ***(11)***. Compound **6** (41 mg, 0.10 mmol, 1 equiv), succinic anhydride (15 mg, 0.15 mmol, 1.5 equiv), DMAP (19 mg, 0.15 mmol, 1.5 equiv), and TEA (29 μL, 0.20 mmol, 2 equiv) were dissolved in dry MeCN (1 mL) under N_2 and heated at 65 °C for 15.5 h. The mixture was then evaporated and the residue purified via flash column chromatography (79:20:1 $CHCl_3$/MeOH/NH_4OH) to give the product as a white foam (40 mg, 77%). ^{1}H NMR ($CDCl_3$) δ 9.98 (brs, 1H), 7.36–7.31 (m, 2H), 6.89–6.84 (m, 2H), 6.68 (d, J = 8.2 Hz, 1H), 6.49 (d, J = 8.2 Hz, 1H), 5.62 (d, J = 10.0 Hz, 1H), 5.34–5.29 (m, 1H), 5.25–5.18 (m, J = 13.8, 9.3, 4.7 Hz, 2H), 5.09 (s, 2H), 3.78 (s, 4H), 3.16 (s, 1H), 3.13–3.05 (m, 1H), 2.99 (d, J = 19.3 Hz, 1H), 2.75 (ddd, J = 17.4, 10.0, 3.8 Hz, 1H), 2.63 (s, 3H), 2.62–2.53 (m, J = 10.5, 5.7 Hz, 3H), 2.49–2.38 (m, 2H), 1.89 (d, J = 11.5 Hz, 1H). ^{13}C NMR ($CDCl_3$) δ 177.6, 172.9, 159.5, 147.8, 141.6, 130.3, 129.7, 129.5, 129.5, 127.6, 124.7, 119.6, 118.3, 113.9, 87.9, 72.0, 67.8, 59.1, 55.4, 46.6, 41.5, 41.1,

DOI: 10.1021/acs.jmedchem.7b01811
J. Med. Chem. 2018, 61, 1316–1329

37.6, 33.1, 30.8, 30.0, 21.3. LC-MS m/z $[M + H]^+$ $C_{29}H_{32}NO_7^+$ calcd 506.2, found 506.2.

*4-(((4R,4aR,7S,7aR,12bS)-9-((4-Methoxybenzyl)oxy)-3-methyl-2,3,4,4a,7,7a-hexahydro-1H-4,12-methanobenzofuro[3,2-e]-isoquinolin-7-yl)amino)-4-oxobutanoic Acid (**12**).* Compound **8** (71 mg, 0.18 mmol, 1 equiv), succinic anhydride (26 mg, 0.26 mmol, 1.5 equiv), DMAP (32 mg, 0.26 mmol, 1.5 equiv), and TEA (49 μL, 0.35 mmol, 2 equiv) were dissolved in MeCN (3 mL) and heated to 70 °C for 18 h. The solvent was then removed in vacuo, and the resulting solid was triturated with EtOAc. The resulting material was suspended in hot EtOH and the resulting precipitate filtered to give the product as a white solid (25 mg, 28%). ^{1}H NMR (DMSO-d_6) δ 7.35−7.29 (m, 2H), 6.95−6.89 (m, 2H), 6.78 (d, J = 8.2 Hz, 1H), 6.61 (d, J = 8.2 Hz, 1H), 5.69−5.63 (m, 1H), 5.56 (dd, J = 10.4, 1.2 Hz, 1H), 5.01−4.96 (m, 3H), 3.74 (s, 3H), 3.16 (s, 1H), 3.13 (dd, J = 5.7, 2.6 Hz, 1H), 2.87 (d, J = 18.7 Hz, 1H), 2.46 (d, J = 7.2 Hz, 1H), 2.44−2.39 (m, 3H), 2.34−2.30 (m, 1H), 2.28 (s, 3H), 2.15 (dd, J = 10.5, 2.7 Hz, 1H), 2.13−2.05 (m, 2H), 1.83 (td, J = 12.3, 4.7 Hz, 1H), 1.60 (d, J = 11.1 Hz, 1H). ^{13}C NMR (101 MHz, DMSO-d_6) δ 174.1, 171.3, 159.0, 147.4, 144.4, 141.6, 136.0, 129.7, 129.4, 129.2, 128.0, 125.0, 118.9, 115.6, 113.7, 106.8, 86.2, 70.2, 55.3, 55.1, 46.2, 43.4, 42.8, 38.8, 34.9, 30.0, 29.7, 29.2, 19.6. LC-MS m/z $[M + H]^+$ $C_{29}H_{33}N_2O_6^+$ calcd 505.2, found 505.3.

*3-O-(4-Methoxybenzyl)-6-O-(4-Methylamino-4-oxobutanoyl)-morphine (**13**).* Compound **11** (40 mg, 0.079 mmol, 1 equiv), EDC·HCl (23 mg, 0.12 mmol, 1.5 equiv), anhydrous HOBt (16 mg, 0.12 mmol, 1.5 equiv), and TEA (22 μL, 0.16 mmol, 2 equiv) were dissolved in MeCN (2 mL) and stirred at room temperature for 1 h. Methylamine (2 M solution in THF, 79.2 μL, 0.1584 mmol, 2 equiv) was then added and stirred for an additional 2 h. The reaction mixture was then evaporated and purified by flash column chromatography (0.5−6% MeOH in $CHCl_3$ with 1% TEA) to give the product as a slightly yellow oil (26 mg, 63%). ^{1}H NMR ($CDCl_3$) δ 7.36−7.28 (m, 2H), 6.90−6.84 (m, 2H), 6.71 (d, J = 8.2 Hz, 1H), 6.52 (d, J = 8.2 Hz, 1H), 5.80 (d, J = 4.0 Hz, 1H), 5.63−5.57 (m, 1H), 5.47−5.38 (m, 1H), 5.17 (ddd, J = 8.9, 5.0, 3.0 Hz, 1H), 5.09 (dd, J = 6.9, 0.8 Hz, 1H), 5.04−4.97 (m, 2H), 3.79 (s, 3H), 3.37 (dd, J = 5.7, 3.2 Hz, 1H), 3.05 (dd, J = 8.8, 5.9 Hz, 1H), 3.02−2.98 (m, 1H), 2.78 (s, 1H), 2.73−2.67 (m, 2H), 2.60 (d, J = 4.8 Hz, 3H), 2.45 (s, 3H), 2.43−2.27 (m, 4H), 2.07 (td, J = 12.4, 5.0 Hz, 1H), 1.86 (dd, J = 12.7, 1.6 Hz, 1H), 1.37 (t, J = 7.3 Hz, 1H). ^{13}C NMR ($CDCl_3$) δ 172.1, 172.1, 159.7, 147.2, 141.2, 130.9, 129.7, 129.4, 129.1, 128.5, 127.7, 119.5, 116.0, 114.0, 87.9, 71.7, 68.0, 59.3, 55.4, 46.8, 45.9, 43.1, 42.5, 40.4, 35.3, 31.5, 30.4, 26.4, 20.5, 9.0. LC-MS m/z $[M + H]^+$ $C_{30}H_{35}N_2O_6^+$ calcd 519.3, found 519.2.

*N^1-((4R,4aR,7S,7aR,12bS)-9-((4-Methoxybenzyl)oxy)-3-methyl-2,3,4,4a,7,7a-hexahydro-1H-4,12-methanobenzofuro[3,2-e]-isoquinolin-7-yl)-N^4-methylsuccinamide (**14**).* Compound **12** (24 mg, 0.48 mmol, 1 equiv), EDC·HCl (14 mg, 0.072 mmol, 1.5 equiv), anhydrous HOBt (10 mg, 0.072 mmol, 1.5 equiv), and TEA (13 μL, 0.096 mmol, 2 equiv) were dissolved in dry DMF (1 mL) and stirred at room temperature for 1 h. Methylamine (2 M in THF, 48 μL, 0.096 mmol, 2 equiv) was then added and the reaction allowed to stir for 19 h. Additional EDC·HCl (18 mg, 0.094 mmol, 2 equiv) and HOBt (11 mg, 0.084 mmol, 1.7 equiv) were added, and following 30 min of stirring, further methylamine (2 M in THF, 48 μL, 0.096 mmol, 2 equiv) was added. The reaction was then allowed to stir at room temperature for a further 24 h and the solvent removed in vacuo. The resulting brown oil was purified by PLC (89:10:1 $CHCl_3$/MeOH/TEA) to give the product as a white solid (21 mg, 84%). ^{1}H NMR ($CDCl_3$) δ 7.35−7.30 (m, 2H), 6.89−6.83 (m, 2H), 6.71 (d, J = 8.2 Hz, 1H), 6.58 (d, J = 8.2 Hz, 1H), 6.30 (d, J = 9.5 Hz, 1H), 6.06 (d, J = 4.2 Hz, 1H), 5.75 (ddd, J = 10.3, 3.5, 2.9 Hz, 1H), 5.59 (dd, J = 10.3, 1.1 Hz, 1H), 5.08−5.00 (m, 2H), 4.95−4.91 (m, 1H), 4.16−4.07 (m, 1H), 3.79 (s, 3H), 3.23 (dd, J = 5.9, 2.7 Hz, 1H), 2.97 (d, J = 18.7 Hz, 1H), 2.76 (d, J = 4.8 Hz, 3H), 2.65 (d, J = 6.1 Hz, 1H), 2.55−2.44 (m, 5H), 2.39 (s, 3H), 2.27 (td, J = 12.0, 3.7 Hz, 1H), 2.17 (dd, J = 10.3, 2.8 Hz, 1H), 1.88 (td, J = 12.2, 4.8 Hz, 1H), 1.84−1.76 (m, 1H). ^{13}C NMR (101 MHz, $CDCl_3$) δ 172.7, 172.4, 159.4, 145.0, 142.3, 134.6, 129.6, 129.5, 129.2, 128.1, 126.1, 119.4, 116.5, 113.9, 86.7, 71.6, 56.5, 55.4, 47.0, 47.0, 46.2, 44.6, 43.2, 41.0, 35.5, 32.0, 31.7, 26.5, 20.1, 10.7. LC-MS m/z $[M + H]^+$ $C_{30}H_{36}N_3O_5^+$ calcd 518.3, found 518.4.

*6-O-Carboxymethylmorphine (**15**).* Compound **6** (93 mg, 0.23 mmol, 1 equiv) was dissolved in dry THF (3 mL) and cooled to 0 °C under an N_2 atmosphere. To this solution, a suspension of prewashed NaH (60%, 37 mg, 0.92 mmol, 4 equiv) in THF (1 mL) was added dropwise. The solution was then allowed to warm to room temperature and stirred for 15 min. A solution of *tert*-butyl bromoacetate in THF (1 mL) was then added dropwise and allowed to stir at room temperature for 1 h. The reaction was then quenched with saturated NH_4Cl (2 mL), and then MeCN (2 mL) was added. The resulting solution was reduced in vacuo, and saturated $NaHCO_3$ (20 mL) was added and extracted with $CHCl_3$ (3 × 20 mL). The combined organic phases were backwashed with brine (20 mL), dried over Na_2SO_4, and the solvent removed in vacuo to give a brown oil. The crude oil was dissolved in DCM (3 mL) under an N_2 atmosphere. Triethylsilane (1.1 mL, 6.9 mmol, 30 equiv) and TFA (1 mL) were then added and the reaction vessel purged with N_2. The reaction was allowed to stir for 1 h, then reduced in vacuo. The resulting oil was purified by prep-HPLC to give the product as a solid white TFA salt (61 mg, 58%). ^{1}H NMR (DMSO-d_6) δ 10.13 (s, 1H), 9.16 (s, 1H), 6.56 (d, J = 8.1 Hz, 1H), 6.46 (d, J = 8.1 Hz, 1H), 5.76 (d, J = 9.9 Hz, 2H), 5.35 (d, J = 9.7 Hz, 2H), 5.14−5.04 (m, 2H), 4.19 (s, 3H), 4.12 (dd, J = 16.4, 3.9 Hz, 3H), 3.30 (d, J = 12.7 Hz, 2H), 3.20 (d, J = 19.8 Hz, 1H), 3.02 (d, J = 26.9 Hz, 2H), 2.89 (s, 3H), 2.82 (s, 2H), 2.74 (dd, J = 19.1, 7.3 Hz, 1H), 2.19 (td, J = 13.6, 4.1 Hz, 1H), 1.95 (d, J = 12.5 Hz, 1H). ^{13}C NMR (DMSO-d_6) δ 171.6, 146.2, 139.3, 131.9, 128.8, 125.9, 121.9, 119.3, 117.2, 87.1, 73.4, 65.4, 59.6, 46.5, 41.4, 40.5, 38.2, 32.8, 20.8. LC-MS m/z $[M + H]^+$ $C_{19}H_{22}NO_5^+$ calcd 344.2, found 344.2.

*3-O-PMB-(6-O-(4-((2-tert-butoxycarbonyl)amino)ethyl)amino-4-oxobutanoyl)morphine (**16**).* Compound **11** (96.5 mg, 0.19 mmol, 1 equiv), HCTU (95 mg, 0.23 mmol, 1.2 equiv), and TEA (54 μL, 0.38 mmol, 2 equiv) were dissolved in dry DMF (1.5 mL) under an N_2 atmosphere and was allowed to stir at room temperature for 30 min. *tert*-Butyl (4-aminoethyl)carbamate (37 mg, 0.23 mmol, 1.2 equiv) was then added as a solution in dry DMF (0.5 mL) and allowed to stir at room temperature for 19 h. EtOAc (20 mL) was then added, and the resulting solution was washed with half-saturated $NaHCO_3$ (3 × 10 mL), saturated $NaHCO_3$ (20 mL), half-saturated brine (2 × 10 mL), and brine (20 mL). The organic phase was then dried over Na_2SO_4 and the solvent removed in vacuo. The resulting residue was purified by flash column chromatography (98:1:1 $CHCl_3$/MeOH/TEA) to give the product as a clear glass (102 mg, 83%). ^{1}H NMR ($CDCl_3$) δ 7.30 (d, J = 8.6 Hz, 2H), 6.86 (d, J = 8.6 Hz, 2H), 6.72 (d, J = 8.2 Hz, 1H), 6.54 (d, J = 8.2 Hz, 1H), 6.31 (t, J = 5.5 Hz, 1H), 5.59 (d, J = 10.1 Hz, 1H), 5.47−5.39 (m, 1H), 5.30 (s, 1H), 5.18−5.08 (m, 2H), 4.98 (s, 2H), 3.77 (s, 3H), 3.33 (dd, J = 5.5, 3.3 Hz, 1H), 3.30−3.23 (m, 1H), 3.11−2.97 (m, 3H), 2.96−2.87 (m, 1H), 2.73 (s, 1H), 2.70−2.61 (m, 2H), 2.57 (dd, J = 12.2, 3.8 Hz, 1H), 2.41 (s, 3H), 2.40−2.34 (m, 1H), 2.29 (ddd, J = 18.1, 9.0, 4.5 Hz, 3H), 2.07−1.97 (m, 1H), 1.84 (d, J = 11.1 Hz, 1H), 1.33 (s, 9H). ^{13}C NMR ($CDCl_3$) δ 171.9, 171.8, 159.8, 156.4, 146.5, 141.2, 130.8, 129.9, 129.5, 128.6, 128.4, 127.7, 119.6, 114.8, 114.0, 87.7, 71.3, 67.7, 59.2, 55.4, 46.8, 43.1, 42.4, 40.6, 40.4, 39.9, 35.2, 31.8, 30.5, 28.4, 20.3. LC-MS m/z $[M + H]^+$ $C_{36}H_{46}N_3O_8^+$ calcd 648.3, found 648.4.

*6-O-(4-((2-Aminoethyl)amino)-4-oxobutanoyl)morphine (**17**).* Compound **16** (102 mg, 0.16 mmol, 1 equiv) was deprotected using general deprotection procedure A. The resulting residue was purified by prep-HPLC to give the product as a solid white mono-TFA salt (43 mg, 51%). ^{1}H NMR (DMSO-d_6) δ 10.01 (s, 1H), 9.22 (s, 1H), 8.10 (t, J = 5.7 Hz, 1H), 7.75 (s, 3H), 6.59 (d, J = 8.1 Hz, 1H), 6.51 (dd, J = 8.0, 4.2 Hz, 1H), 5.65 (d, J = 10.0 Hz, 1H), 5.52−5.39 (m, 1H), 5.25−5.14 (m, 1H), 5.09−4.98 (m, 1H), 4.13 (s, 1H), 3.27 (dd, J = 12.2, 6.2 Hz, 2H), 3.19 (d, J = 19.8 Hz, 1H), 3.06 (d, J = 4.7 Hz, 1H), 2.97 (s, 1H), 2.89 (s, 2H), 2.84 (dd, J = 12.1, 6.0 Hz, 2H), 2.71 (dd, J = 20.0, 6.7 Hz, 1H), 2.65−2.59 (m, 2H), 2.45 (t, J = 6.8 Hz, 2H), 2.20 (dd, J = 13.4, 9.1 Hz, 1H), 1.84 (dd, J = 46.3, 11.7 Hz, 1H). LC-MS m/z $[M + H]^+$ $C_{23}H_{30}N_3O_5^+$ calcd 428.2, found 428.2.

DOI: 10.1021/acs.jmedchem.7b01811
J. Med. Chem. 2018, 61, 1316−1329

*2-((1E,3E,5Z)-5-(1-(6-((2-(4-(((4R,4aR,7S,7aR,12bS)-9-Hydroxy-3-methyl-2,3,4,4a,7,7a-hexahydro-1H-4,12-methanobenzofuro[3,2-e]isoquinolin-7-yl)oxy)-4-oxobutanamido)ethyl)amino)-6-oxohexyl)-3,3-dimethyl-5-sulfoindolin-2-ylidene)penta-1,3-dien-1-yl)-1,3,3-trimethyl-3H-indol-1-ium-5-sulfonate (**18**).* Compound **17** (7.1 mg, 0.013 mmol, 2 equiv), sulfo-Cy5 NHS ester (Lumiprobe, 5 mg, 0.0066 mmol, 1 equiv), and TEA (2.8 μL, 0.020 mmol, 3 equiv) was dissolved in dry DMF (150 μL) under an N_2 atmosphere and allowed to stir at room temperature for 7 h. HCTU (2.7 mg, 0.0066 mmol, 1 equiv) was then added and the reaction stirred for an additional 16 h. Water (20 mL) and MeCN (1 mL) were then added and the solvent removed by freeze-drying. The resulting residue was purified by reverse phase chromatography (5−30% buffer B in buffer A, 1% jump per column volume). Clean fractions were collected and freeze-dried to give the product as a dark-blue solid TFA salt (2.6 mg, 33%). ^{1}H NMR (DMSO-d_6) δ 9.82 (s, 1H), 9.20 (s, 1H), 8.35 (t, *J* = 13.1 Hz, 1H), 7.91 (s, 1H), 7.81 (s, 2H), 7.77 (s, 1H), 7.64 (dd, *J* = 7.6, 3.9 Hz, 2H), 7.31 (d, *J* = 8.4 Hz, 2H), 6.62−6.44 (m, 5H), 6.28 (dd, *J* = 18.3, 13.9 Hz, 2H), 5.59 (d, *J* = 9.9 Hz, 1H), 5.41 (d, *J* = 9.7 Hz, 1H), 5.12−4.93 (m, 2H), 4.08 (s, 4H), 3.59 (s, 2H), 3.16−3.02 (m, 7H), 2.89 (s, 4H), 2.60−2.54 (m, 3H), 2.39 (t, *J* = 6.6 Hz, 3H), 2.03 (t, *J* = 7.1 Hz, 2H), 1.68 (s, 12H), 1.58−1.48 (m, 2H), 1.29 (ddd, *J* = 17.8, 13.8, 8.6 Hz, 5H), 1.17 (t, *J* = 7.3 Hz, 2H). ESI-TOF HRMS *m/z*: [M + H]$^+$ $C_{55}H_{66}N_5O_{12}S_2^+$ calcd 1052.4144, found 1052.4119; [M + 2H]$^{2+}$ $C_{55}H_{67}N_5O_{12}S_2^+$ calcd 526.7108, found 526.7113.

*6-O-((4-((tert-Butoxycarbonyl)amino)butyl)carbamoyl)morphine (**19**).* Compound **15** (130 mg, 0.28 mmol, 1 equiv), anhydrous HOBt (42 mg, 0.31 mmol, 1.1 equiv), EDC·HCl (60 mg, 0.31 mmol, 1.1 equiv), and TEA (119 μL, 85 mmol, 3 equiv) were dissolved in DMF (2 mL) under an N_2 atmosphere and allowed to stir at room temperature for 1 h. *tert*-Butyl (4-aminobutyl)carbamate (64 mg, 0.34 mmol, 1.2 equiv) was then added as a solution in dry DMF (1 mL) and the reaction stirred at room temperature for 17 h. The solvent was then removed in vacuo and the residue purified by reverse phase chromatography (6−35% buffer B in buffer A, 1% jump per column volume). Clean fractions were collected and freeze-dried to give the product as a light-orange solid TFA salt (65 mg, 36%). ^{1}H NMR (MeOD) δ 6.65 (dd, *J* = 8.1, 1.4 Hz, 1H), 6.58 (d, *J* = 8.1 Hz, 1H), 5.92−5.83 (m, 1H), 5.42 (d, *J* = 9.9 Hz, 1H), 5.19−5.12 (m, 1H), 4.91 (s, 9H), 4.28−4.10 (m, 4H), 3.39 (dd, *J* = 13.3, 3.7 Hz, 1H), 3.34 (d, *J* = 6.5 Hz, 1H), 3.26 (d, *J* = 7.3 Hz, 1H), 3.20 (d, *J* = 20.2 Hz, 1H), 3.12−2.94 (m, 7H), 2.87 (dd, *J* = 19.8, 6.8 Hz, 1H), 2.34 (td, *J* = 13.6, 5.0 Hz, 1H), 2.12 (d, *J* = 13.9 Hz, 1H), 1.75−1.62 (m, 3H), 1.60−1.47 (m, 2H), 1.42 (s, 3H). ^{13}C NMR (MeOD) δ 172.6, 147.4, 132.9, 129.9, 126.6, 121.2, 118.7, 89.0, 75.3, 69.8, 69.7, 62.3, 42.9, 41.7, 40.3, 40.0, 39.7, 39.1, 34.3, 28.8, 28.3, 27.7, 27.4, 25.8, 22.2. LC-MS *m/z* [M + H]$^+$ $C_{28}H_{40}N_3O_6^+$ calcd 514.3, found 514.3.

*6-O-((4-Aminobutyl)carbamoyl)morphine (**20**).* Compound **19** (65 mg, 0.10 mmol, 1 equiv) was dissolved in $CHCl_3$ (1 mL) and TFA (0.5 mL) and the resulting solution allowed to stir for 1 h. The solvent was then removed in vacuo and the resulting residue dissolved in buffer A and freeze-dried to give the product as a brown oil TFA salt (60 mg, quantitative). ^{1}H NMR (MeOD) δ 6.65 (d, *J* = 8.1 Hz, 1H), 6.58 (d, *J* = 8.2 Hz, 1H), 5.86 (d, *J* = 10.0 Hz, 1H), 5.41 (d, *J* = 9.8 Hz, 1H), 5.15 (d, *J* = 5.7 Hz, 1H), 4.28−4.10 (m, 4H), 3.38 (dd, *J* = 13.2, 3.8 Hz, 1H), 3.33 (d, *J* = 6.7 Hz, 1H), 3.27 (d, *J* = 20.0 Hz, 1H), 3.18 (d, *J* = 12.0 Hz, 1H), 3.07 (dd, *J* = 13.3, 3.5 Hz, 1H), 3.04−2.93 (m, 6H), 2.87 (dd, *J* = 19.9, 6.7 Hz, 1H), 2.36 (td, *J* = 13.6, 4.6 Hz, 1H), 2.09 (d, *J* = 12.0 Hz, 1H), 1.77−1.58 (m, 4H). ^{13}C NMR (101 MHz, MeOD) δ 172.5, 147.4, 141.0, 132.8, 129.9, 126.7, 123.2, 121.2, 118.7, 89.0, 75.4, 69.7, 62.2, 42.9, 41.7, 40.3, 39.8, 39.1, 34.2, 27.3, 26.8, 25.8, 22.2. LC-MS *m/z* [M + H]$^+$ $C_{23}H_{32}N_3O_4^+$ calcd 414.2, found 414.3.

*1-Ethyl-2-((1E,3E,5Z)-5-(1-(6-((4-(2-(((4R,4aR,7S,7aR,12bS)-9-hydroxy-3-methyl-2,3,4,4a,7,7a-hexahydro-1H-4,12-methanobenzofuro[3,2-e]isoquinolin-7-yl)oxy)acetamido)butyl)-amino)-6-oxohexyl)-3,3-dimethyl-5-sulfoindolin-2-ylidene)penta-1,3-dien-1-yl)-3,3-dimethyl-3H-indol-1-ium-5-sulfonate (**21**).* Sulfo-Cy5 TFA salt (6.0 mg, 7.8 μmol, 1 equiv), HCTU (3.9 mg, 9.3 μmol, 1.2 equiv), and TEA (10 μL) were dissolved in DMF (600 μL) under an N_2 atmosphere and stirred at room temperature for 1 h. Compound **20** (8.2 mg, 16 μmol, 2 equiv) was then added as a solution in DMF (200 μL) and allowed to stir at room temperature for 18 h. Buffer A was added and the resulting solution freeze-dried. The residue was purified by reverse phase chromatography (5−30% buffer B in buffer A, 1% jump per column volume). Clean fractions were collected and freeze-dried to give the product as a dark-blue solid TFA salt (3.6 mg, 40%). ^{1}H NMR (DMSO-d_6) δ 10.22 (s, 1H), 9.19 (s, 1H), 8.35 (t, *J* = 12.6 Hz, 2H), 7.82 (s, 2H), 7.78−7.71 (m, 2H), 7.68−7.61 (m, 2H), 7.34−7.30 (m, 2H), 7.18 (s, 1H), 7.05 (s, 1H), 6.59−6.55 (m, 2H), 6.46 (d, *J* = 8.1 Hz, 1H), 6.30 (d, *J* = 14.0 Hz, 1H), 5.77 (dd, *J* = 10.2, 2.2 Hz, 1H), 5.28 (d, *J* = 10.0 Hz, 1H), 5.07 (d, *J* = 5.9 Hz, 1H), 4.15−3.93 (m, 10H), 3.19 (d, *J* = 19.3 Hz, 1H), 3.14−3.04 (m, 5H), 3.02−2.96 (m, 3H), 2.89 (s, 3H), 2.82 (s, 1H), 2.75−2.66 (m, 1H), 2.23−2.13 (m, 1H), 2.02 (t, *J* = 6.9 Hz, 2H), 1.95−1.89 (m, 1H), 1.58−1.48 (m, 3H), 1.43−1.29 (m, 8H), 1.25 (t, *J* = 7.3 Hz, 6H), 1.17 (t, *J* = 7.3 Hz, 2H). ESI-TOF HRMS *m/z* [M + H]$^+$ $C_{56}H_{70}N_5O_{11}S_2^+$ calcd 1052.4508, found 1052.4545, [M + Na]$^+$ $C_{56}H_{69}N_5O_{11}S_2Na^+$ calcd 1074.4327, found 1074.4338.

Pharmacology. *cAMP BRET CAMYEL Assay.* HEK293 cells were transfected with 2 μg of hMOR pEF5/FRT construct cDNA and 3 μg of CAMYEL sensor cDNA. The cDNA was mixed with 30 μg of polyethylenimine and made up to 250 μL with 0.15 M NaCl, then allowed to incubate for 15−20 min at room temperature. This mixture was then added to the cells dropwise and gently mixed. The cells were then incubated for 24 h in post transfection media (PTM), after which they were resuspended in 15 mL of PTM and replated onto white poly-D-lysine coated plates at 100 μL per well and maintained for 24 h. The media was then aspirated and the cells washed once with 100 μL/well HBSS at 37 °C. HBSS (70 μL/well) was then added back and the cells incubated for 30 min at 37 °C in the absence of CO_2. Coelenterazine H (10 μL, 5 μM final) was added and the cells incubated in the dark for 10 min at 37 °C. The drugs (10 μL) were then added at the desired concentration, followed immediately by forskolin (10 μL, 30 μM final), then incubated for 5 min inside a LUMIstar Omega plate reader set at 37 °C. Luminescence for RLuc8 (480 nm) and fluorescence for YFP (530 nm) were then measured. Baseline and vehicle control values were subtracted, and the BRET signal was normalized as a percentage of forskolin response.

Confocal Microscopy. HEK293 cells stably expressing *N*-terminal SNAP-hMOR were cultured in Dulbecco's Modified Eagle's Medium (DMEM) supplemented with 10% (v/v) fetal calf serum (FCS) and 1 mg/mL G418. Cells were grown in poly-D-lysine-coated 8-well Labtek borosilicate chambered-cover glasses (Nalgene Nunc International, Fisher Scientific). On the day of experimentation, SNAP tag labeling was performed by incubating cells in 500 nM BG-488 in fresh cell culture media for 30 min at 37 °C. Cells were washed in prewarmed HEPES-buffered saline solution (HBS) containing 4.5 mM D-glucose and incubated for 30 min at 37 °C in the presence or absence of 1 μM naloxone prior to addition and incubation with the relevant concentration of **21** for 30 min at 37 °C. Where the concentration of **21** was 10 μM, the cells were washed with HBS prior to imaging. Confocal images were captured using a Zeiss LSM710 laser scanning microscope using a Plan-Apochromat 63 × 1.3NA oil-immersion objective lens (1024 × 1024 pixels, averaging at four frames). The 633 nm HeNe and 488 nm argon lasers were used to excite sulfo-Cy5 and BG-488, respectively. Emission was captured at 638−759 nm and 493−628 nm, respectively. Confocal settings for laser power, offset, and gain were kept constant throughout acquisition. Images were processed in Zeiss Zen 2011, with any linear adjustments made equally cross all images within a data set.

■ ASSOCIATED CONTENT

Supporting Information

The Supporting Information is available free of charge on the ACS Publications website at DOI: 10.1021/acs.jmedchem.7b01811.

Comparison of the NMR spectra of compounds **6** and **7** (PDF)

Molecular formula strings (CSV)

DOI: 10.1021/acs.jmedchem.7b01811
J. Med. Chem. 2018, 61, 1316−1329

AUTHOR INFORMATION

Corresponding Author

*Phone: +61 (0)3 9903 9542. Fax: +61 (0)3 9903 9582. E-mail: peter.scammells@monash.edu.

ORCID

Barrie Kellam: 0000-0003-0030-9908

Peter J. Scammells: 0000-0003-2930-895X

Notes

The authors declare no competing financial interest.

ACKNOWLEDGMENTS

R.L. thanks the Australian Government Research Training Program Scholarship for their financial support. We acknowledge the support of the Monash−Nottingham Joint Doctoral Training Centre program, to which both R.L. and A.B.G. are a part, and has made this work possible. Microscopy work performed at the University of Nottingham was supported by Medical Research Council grant MR/N020081/1. We also acknowledge the assistance and expertise of Dr Luke S. Schembri and Dr Gaik Orbell in opiate chemistry. We acknowledge GSK Australia for providing the morphine used in the synthesis of all our compounds.

ABBREVIATIONS USED

BRET, bioluminescence resonance energy transfer; cAMP, cyclic adenosine monophosphate; DIAD, diisopropyl azodicarboxylate; DMAP, 4-dimethylaminopyridine; DOR, δ opioid receptor; EDC, *N*-(3-(dimethylamino)propyl)-*N*′-ethylcarbodiimide; GPCR, G protein-coupled receptor; HCTU, *O*-(1*H*-6-chlorobenzotriazole-1-yl)-1,1,3,3-tetramethyluronium hexafluorophosphate; KOR, κ opioid receptor; MOR, μ opioid receptor; NOPr, nociception/orphanin FQ peptide receptor; PMB, *para*-methoxybenzyl; NHS, *N*-hydroxysuccinimide; TEA, triethylamine; TFA, trifluoroacetic acid

REFERENCES

(1) Blakemore, P. R.; White, J. D. Morphine, the Proteus of Organic Molecules. *Chem. Commun.* **2002**, 1159−1168.

(2) Rudd, R. A.; Aleshire, N.; Zibbell, J. E.; Gladden, R. M. Increases in Drug and Opioid Overdose Deaths — United States, 2000−2014. *Cent. Dis. Prev. - Morb. Mortal. Wkly. Rep.* **2016**, *64*, 1378−1382.

(3) Thompson, A. A.; Liu, W.; Chun, E.; Katritch, V.; Wu, H.; Vardy, E.; Huang, X.-P.; Trapella, C.; Guerrini, R.; Calo, G.; Roth, B. L.; Cherezov, V.; Stevens, R. C. Structure of the Nociceptin/orphanin FQ Receptor in Complex with a Peptide Mimetic. *Nature* **2012**, *485*, 395−399.

(4) Matthes, H. W. D.; Maldonado, R.; Simonin, F.; Valverde, O.; Slowe, S.; Kitchen, I.; Befort, K.; Dierich, A.; Le Meur, M.; Dollé, P.; Tzavara, E.; Hanoune, J.; Roques, B. P.; Kieffer, B. L. Loss of Morphine-Induced Analgesia, Reward Effect and Withdrawal Symptoms in Mice Lacking the μ-Opioid-Receptor Gene. *Nature* **1996**, *383*, 819−823.

(5) Bodnar, R. J. Endogenous Opiates and Behavior: 2012. *Peptides* **2013**, *50*, 55−95.

(6) Manglik, A.; Lin, H.; Aryal, D. K.; McCorvy, J. D.; Dengler, D.; Corder, G.; Levit, A.; Kling, R. C.; Bernat, V.; Hübner, H.; Huang, X.-P.; Sassano, M. F.; Giguère, P. M.; Löber, S.; Duan, D.; Scherrer, G.; Kobilka, B. K.; Gmeiner, P.; Roth, B. L.; Shoichet, B. K. Structure-Based Discovery of Opioid Analgesics with Reduced Side Effects. *Nature* **2016**, *537*, 185−190.

(7) Connor, M.; Osborne, P. B.; Christie, M. J. Mu-Opioid Receptor Desensitization: Is Morphine Different? *Br. J. Pharmacol.* **2004**, *143*, 685−696.

(8) Lamb, K.; Tidgewell, K.; Simpson, D. S.; Bohn, L. M.; Prisinzano, T. E. Antinociceptive Effects of Herkinorin, a MOP Receptor Agonist Derived from Salvinorin A in the Formalin Test in Rats: New Concepts in Mu Opioid Receptor Pharmacology: from a Symposium on New Concepts in Mu-opioid Pharmacology. *Drug Alcohol Depend.* **2012**, *121*, 181−188.

(9) Bohn, L. M.; Gainetdinov, R. R.; Lin, F. T.; Lefkowitz, R. J.; Caron, M. G. μ-Opioid Receptor Desensitization by β-Arrestin-2 Determines Morphine Tolerance but not Dependence. *Nature* **2000**, *408*, 720−723.

(10) Fournie-Zaluski, M. C.; Gacel, G.; Roques, B. P.; Senault, B.; Lecomte, J. M.; Malfroy, B.; Swerts, J. P.; Schwartz, J. C. Fluorescent Enkephalin Derivatives with Biological Activity. *Biochem. Biophys. Res. Commun.* **1978**, *83*, 300−305.

(11) Mihara, H.; Lee, S.; Shimohigashi, Y.; Aoyagi, H.; Kato, T.; Izumiya, N.; Costa, T. δ and μ Opiate Receptor Probes: Fluorescent Enkephalins with High Receptor Affinity and Specificity. *FEBS Lett.* **1985**, *193*, 35−38.

(12) Arttamangkul, S.; Alvarez-Maubecin, V.; Thomas, G.; Williams, J. T.; Grandy, D. K. Binding and Internalization of Fluorescent Opioid Peptide Conjugates in Living Cells. *Mol. Pharmacol.* **2000**, *58*, 1570−1580.

(13) Arttamangkul, S.; Torrecilla, M.; Kobayashi, K.; Okano, H.; Williams, J. T. Separation of μ-Opioid Receptor Desensitization and Internalization: Endogenous Receptors in Primary Neuronal Cultures. *J. Neurosci.* **2006**, *26*, 4118−4125.

(14) Macey, T. A.; Ingram, S. L.; Bobeck, E. N.; Hegarty, D. M.; Aicher, S. A.; Arttamangkul, S.; Morgan, M. M. Opioid Receptor Internalization Contributes to Dermorphin-mediated Antinociception. *Neuroscience* **2010**, *168*, 543−550.

(15) Macey, T. A.; Bobeck, E. N.; Suchland, K. L.; Morgan, M. M.; Ingram, S. L. Change in Functional Selectivity of Morphine with the Development of Antinociceptive Tolerance. *Br. J. Pharmacol.* **2015**, *172*, 549−561.

(16) Kolb, V. M.; Koman, A.; Terenius, L. Fluorescent Probes for Opioid Receptors. *Life Sci.* **1983**, *33*, 423−426.

(17) Archer, S.; Medzihradsky, F.; Seyed-Mozaffari, A.; Emmerson, P. J. Synthesis and Characterization of 7-Nitrobenzo-2-oxa-1,3-diazole (NBD)-labeled Fluorescent Opioids. *Biochem. Pharmacol.* **1992**, *43*, 301−306.

(18) Emmerson, P. J.; Archer, S.; El-Hamouly, W.; Mansour, A.; Akil, H.; Medzihradsky, F. Synthesis and Characterization of 4,4-Difluoro-4-Bora-3a,4a-Diaza-*s*-Indacene (BODIPY)-Labeled Fluorescent Ligands for the Mu Opioid Receptor. *Biochem. Pharmacol.* **1997**, *54*, 1315−1322.

(19) Schembri, L. S.; Stoddart, L. A.; Briddon, S. J.; Kellam, B.; Canals, M.; Graham, B.; Scammells, P. J. Synthesis, Biological Evaluation, and Utility of Fluorescent Ligands Targeting the μ-Opioid Receptor. *J. Med. Chem.* **2015**, *58*, 9754−9767.

(20) Cunningham, C. W.; Mercer, S. L.; Hassan, H. E.; Traynor, J. R.; Eddington, N. D.; Coop, A. Opioids and Efflux Transporters. Part 2: P-Glycoprotein Substrate Activity of 3- and 6-Substituted Morphine Analogs. *J. Med. Chem.* **2008**, *51*, 2316−2320.

(21) Beale, J. M. J.; Block, J. H. *Wilson and Gisvold's Textbook of Organic Medicinal and Pharmaceutical Chemistry*, 12th ed.; Lippincott Williams & Wilkins: Baltimore, MD, 2011.

(22) Simon, C.; Makleit, S.; Hosztafi, S. Application of the Mitsunobu Reaction for the Preparation of Isomorphine and Isocodeine Derivatives. *Synth. Commun.* **1991**, *21* (3), 407−412.

(23) Simon, C.; Hosztafi, S.; Makleit, U. Stereoselective Synthesis of β-Naltrexol, β-Naloxol, β-Naloxamine, β-Naltrexamine and Related Compounds by the Application of the Mitsunobu Reaction. *Tetrahedron* **1994**, *50* (32), 9757−9768.

(24) Váradi, A.; Hosztafi, S.; Le Rouzic, V.; Tóth, G.; Urai, Á.; Noszál, B.; Pasternak, G. W.; Grinnell, S. G.; Majumdar, S. Novel 6β-Acylaminomorphinans with Analgesic Activity. *Eur. J. Med. Chem.* **2013**, *69*, 786−789.

(25) Urai, A.; Varadi, A.; Szocs, L.; Komjati, B.; Le Rouzic, V.; Hunkele, A.; Pasternak, G. W.; Majumdar, S.; Hosztafi, S. Synthesis

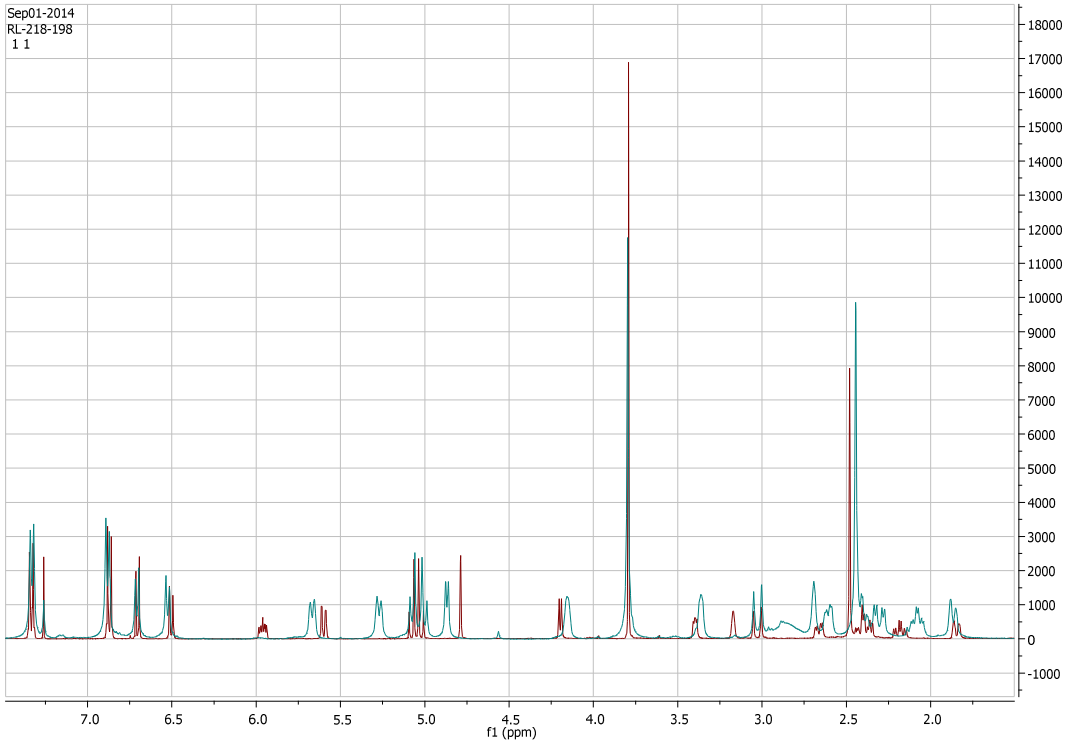
DOI: 10.1021/acs.jmedchem.7b01811
J. Med. Chem. 2018, 61, 1316−1329

and Pharmacological Evaluation of Novel Selective MOR Agonist 6β-Pyridinyl Amidomorphines Exhibiting Long-Lasting Antinociception. *MedChemComm* **2017**, *8* (1), 152−157.
(26) Middleton, R. J.; Briddon, S. J.; Cordeaux, Y.; Yates, A. S.; Dale, L.; George, M. W.; Baker, J. G.; Hill, S. J.; Kellam, B. New Fluorescent Adenosine A_1-Receptor Agonists that Allow Quantification of Ligand − Receptor Interactions in Microdomains of Single Living Cells. *J. Med. Chem.* **2007**, *50*, 782−793.
(27) Thompson, G. L.; Lane, J. R.; Coudrat, T.; Sexton, P. M.; Christopoulos, A.; Canals, M. Biased Agonism of Endogenous Opioid Peptides at the μ-Opioid Receptor. *Mol. Pharmacol.* **2015**, *88* (2), 335−346.
(28) Thompson, G. L.; Lane, J. R.; Coudrat, T.; Sexton, P. M.; Christopoulos, A.; Canals, M. Systematic Analysis of Factors Influencing Observations of Biased Agonism at the Mu-Opioid Receptor. *Biochem. Pharmacol.* **2016**, *113*, 70−87.
(29) Stoddart, L. A.; Vernall, A. J.; Briddon, S. J.; Kellam, B.; Hill, S. J. Direct Visualisation of Internalization of the Adenosine A_3 Receptor and Localization with Arrestin Using a Fluorescent Agonist. *Neuropharmacology* **2015**, *98*, 68−77.
(30) Vernall, A. J.; Stoddart, L. A.; Briddon, S. J.; Hill, S. J.; Kellam, B. Highly Potent and Selective Fluorescent Antagonists of the Human Adenosine A_3 Receptor Based on the 1,2,4-triazolo[4,3-*a*]quinoxalin-1-one Scaffold. *J. Med. Chem.* **2012**, *55* (4), 1771−1782.
(31) Baker, J. G.; Middleton, R.; Adams, L.; May, L. T.; Briddon, S. J.; Kellam, B.; Hill, S. J. Influence of Fluorophore and Linker Composition on the Pharmacology of Fluorescent Adenosine A_1 Receptor Ligands. *Br. J. Pharmacol.* **2010**, *159* (4), 772−786.

DOI: 10.1021/acs.jmedchem.7b01811
J. Med. Chem. 2018, 61, 1316−1329

S2

Figure S1. Comparison between ^{1}H NMR spectra of compounds **6** and **7**.



Compound **6** = teal spectra, compound **7** = red spectra. Note the lack of overlap between spectra other than the peaks associated with ring A and the PMB protecting group in the aromatic region, as well as the PMB methoxy group at 3.79 ppm. Most notably, the peak assigned to the C-6 proton has shifted from 4.15 ppm in compound **6** to 4.20 ppm in compound **7** with no overlap between the two spectra. Furthermore, the C-5 proton has similarly shifted from 4.87 ppm in compound **6** to 4.79 ppm in compound **7**. These data support specific inversion of the C-6 stereocenter under Mitsunobu conditions. All spectra were run in $CDCl_3$ at 400 MHz to enable direct comparison.

Appendix 3. Table of DNA constructs used in this thesis.

Chapter	Construct	Origen	Reference
2, 3, 5	FLAG-MOP-NLuc WT	AB.Gondin	
2, 5	Nb33-Venus	M.Canals	
2, 5	NES-Venus-mGsi	N.Lambert	Wan et al. 2018
2, 3	GRK2-Venus	D. Jensen	
2, 4	β-arrestin2–YFP	M. Caron	
4	β-arrestin1–YFP	M. Caron	
2	Rab5-Venus	N.Lambert	Lan, Liu, Li, Wu, & Lambert, 2012
2, 4	GRK2 WT	M. Smit	
4	GRK2 DN (K220R)	M. Smit	
2	Venus155-239-Gβ1	N.Lambert	Masuho, Martemyanov, & Lambert, 2015
2	Venus1-155-Gγ2	N.Lambert	Masuho, Martemyanov, & Lambert, 2015
2	masGRKct-RLuc8	N.Lambert	Masuho, Martemyanov, & Lambert, 2015
2, 3	CAMYEL		Jiang et al., 2007
4	FLAG-MOP-Rluc8 WT	Purchased from GeneArt	Meiss et al. 2018
4	FLAG-MOP-Rluc8 TSST-4A	Purchased from GeneArt	Meiss et al. 2018
4	FLAG-MOP-Rluc8 S375A	Purchased from GeneArt	Meiss et al. 2018
4	FLAG-MOP-Rluc8 STANT-3A	Purchased from GeneArt	Meiss et al. 2018
4	FLAG-MOP-Rluc8 11S/T-A	Purchased from GeneArt	Meiss et al. 2018
3	SNAP-hMOP	AB.Gondin	
3	SNAP-mMOP WT	AB.Gondin	
3	SNAP-mMOP S375A	AB.Gondin	
3	SNAP-mMOP S363A	AB.Gondin	
5	FLAG-MOP-NLuc ΔS/T_{ICL}	AB.Gondin	
5	FLAG-MOP-NLuc ΔS/T_{Ct}	AB.Gondin	
5	FLAG-MOP-NLuc ΔS/T	AB.Gondin	